BIOCONVERSION AND BIOREFINERY OF C1 COMPOUNDS

EDITED BY: Guodong Luan, Eun Yeol Lee, Fu-Li Li, Yu Wang, Pramod P. Wangikar and Michael Thomas Guarnieri

PUBLISHED IN: Frontiers in Microbiology

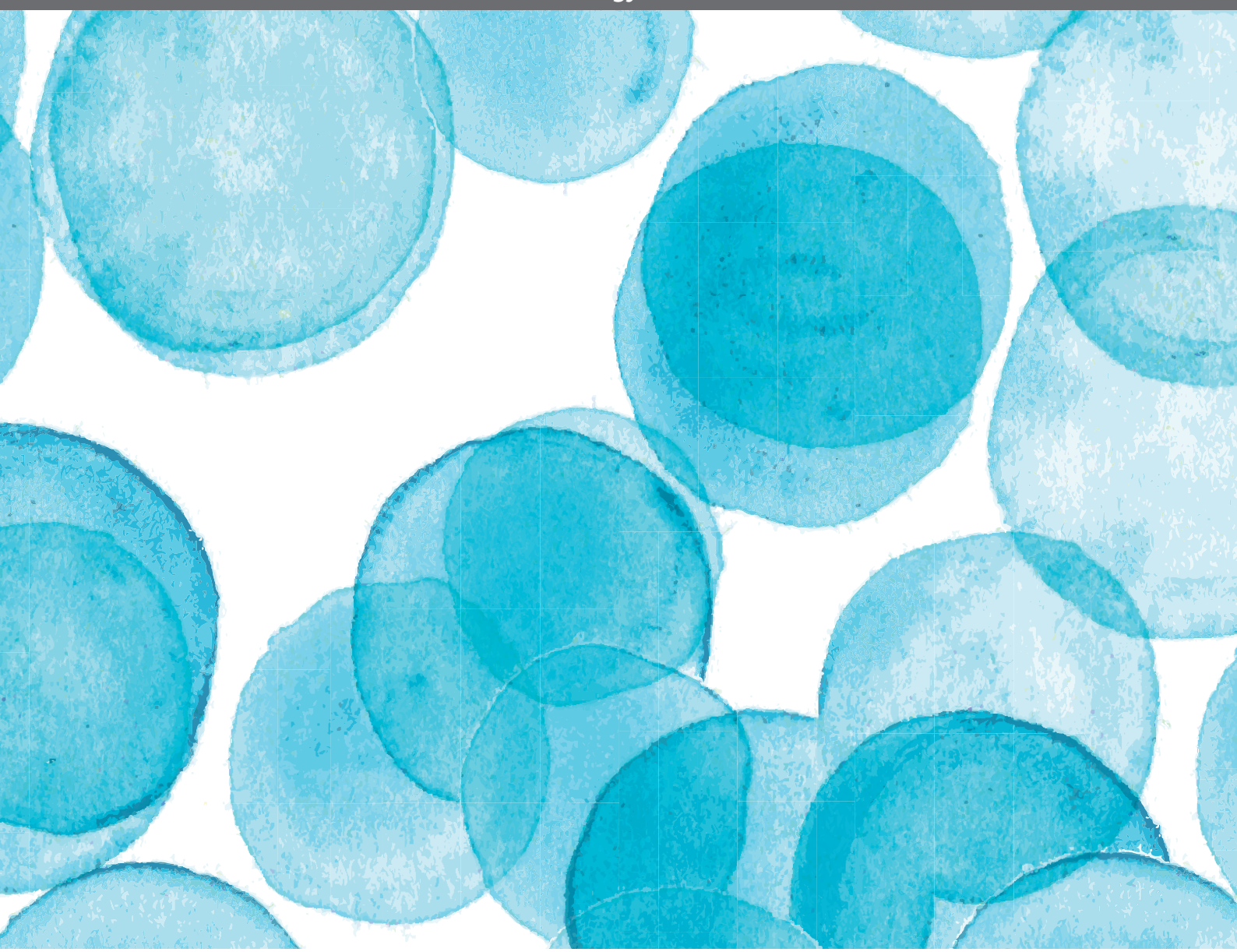

frontiers Research Topics

frontiers

ISSN 1664-8714
ISBN 978-2-88971-906-8
DOI 10.3389/978-2-88971-906-8

About Frontiers

Frontiers is more than just an open-access publisher of scholarly articles: it is a pioneering approach to the world of academia, radically improving the way scholarly research is managed. The grand vision of Frontiers is a world where all people have an equal opportunity to seek, share and generate knowledge. Frontiers provides immediate and permanent online open access to all its publications, but this alone is not enough to realize our grand goals.

Frontiers Journal Series

The Frontiers Journal Series is a multi-tier and interdisciplinary set of open-access, online journals, promising a paradigm shift from the current review, selection and dissemination processes in academic publishing. All Frontiers journals are driven by researchers for researchers; therefore, they constitute a service to the scholarly community. At the same time, the Frontiers Journal Series operates on a revolutionary invention, the tiered publishing system, initially addressing specific communities of scholars, and gradually climbing up to broader public understanding, thus serving the interests of the lay society, too.

Dedication to Quality

Each Frontiers article is a landmark of the highest quality, thanks to genuinely collaborative interactions between authors and review editors, who include some of the world's best academicians. Research must be certified by peers before entering a stream of knowledge that may eventually reach the public - and shape society; therefore, Frontiers only applies the most rigorous and unbiased reviews.
Frontiers revolutionizes research publishing by freely delivering the most outstanding research, evaluated with no bias from both the academic and social point of view. By applying the most advanced information technologies, Frontiers is catapulting scholarly publishing into a new generation.

What are Frontiers Research Topics?

Frontiers Research Topics are very popular trademarks of the Frontiers Journals Series: they are collections of at least ten articles, all centered on a particular subject. With their unique mix of varied contributions from Original Research to Review Articles, Frontiers Research Topics unify the most influential researchers, the latest key findings and historical advances in a hot research area! Find out more on how to host your own Frontiers Research Topic or contribute to one as an author by contacting the Frontiers Editorial Office: frontiersin.org/about/contact

BIOCONVERSION AND BIOREFINERY OF C1 COMPOUNDS

Topic Editors:
Guodong Luan, Qingdao Institute of Bioenergy and Bioprocess Technology, Chinese Academy of Sciences (CAS), China
Eun Yeol Lee, Kyung Hee University, South Korea
Fu-Li Li, Qingdao Institute of Bioenergy and Bioprocess Technology, Chinese Academy of Sciences (CAS), China
Yu Wang, Tianjin Institute of Industrial Biotechnology, Chinese Academy of Sciences, China
Pramod P. Wangikar, Indian Institute of Technology Bombay, India
Michael Thomas Guarnieri, National Renewable Energy Laboratory (DOE), United States

Citation: Luan, G., Lee, E. Y., Li, F.-L., Wang, Y., Wangikar, P. P., Guarnieri, M. T., eds. (2021). Bioconversion and Biorefinery of C1 Compounds.
Lausanne: Frontiers Media SA. doi: 10.3389/978-2-88971-906-8

Table of Contents

frontiers in Microbiology

EDITORIAL
published: 28 October 2021
doi: 10.3389/fmicb.2021.778962

Editorial: Bioconversion and Biorefinery of C1 Compounds

Eun Yeol Lee[1], Fu-Li Li[2], Yu Wang[3], Pramod P. Wangikar[4], Michael Thomas Guarnieri[5] and Guodong Luan[2]**

[1] Department of Chemical Engineering (Integrated Engineering), College of Engineering, Kyung Hee University, Yongin-si, South Korea, [2] Qingdao Institute of Bioenergy and Bioprocess Technology, Chinese Academy of Sciences (CAS), Qingdao, China, [3] Key Laboratory of Systems Microbial Biotechnology, Tianjin Institute of Industrial Biotechnology, Chinese Academy of Sciences (CAS), Tianjin, China, [4] Department of Chemical Engineering, Indian Institute of Technology Bombay, Mumbai, India, [5] National Renewable Energy Laboratory (DOE), Golden, CO, United States

Keywords: C1 compounds, bioconversion, biorefinery, biocatalysts, green economy

Editorial on the Research Topic

Bioconversion and Biorefinery of C1 Compounds

The past decade has seen significant progress in the field of metabolic engineering and synthetic biology. The exponentially growing multi-omics data and technological advances in the development of efficient genetic manipulation tools and techniques have allowed scientists to explore and expand their understanding of microbial metabolisms and further develop sophisticated engineering strategies to realize the use of industrial "workhorses" and non-conventional microorganisms for sustainable bioconversion and biorefinery. There is of great interest for the research community in using C1 compounds (i.e., CO_2, CO/syngas, methane, methanol) as the next generation feedstocks for microbial cell factories and biocatalysts to promote the sustainable development of a green economy (**Figure 1**). Considering lowering input costs is also a main consideration for successful business ventures, the use of inexpensive, abundant, and widely accessible C1 compounds is envisioned as a promising route for the sustainable production of fine chemicals, fuels, and other high-value products. Many C1 compounds are waste gases from industrial activities and may have detrimental effects on climate change upon emission into the atmosphere. Therefore, promoting the use of C1 compounds as renewable carbon feedstocks can greatly contribute to the reduction of anthropogenic emission of air pollutants.

In this Research Topic, a collection of articles including original research articles, reviews and minireviews specialized in C1 bioconversion and biorefining from leading research groups in the field is presented. Each article provides a state-of-the-art view of current metabolic engineering efforts, technical advances on contemporary genetic manipulation tools, and prospects in C1 bioconversion and biorefinery. The Research Topic focuses on the development of acetogens, cyanobacteria, methanotrophs, synthetic autotrophs, and synthetic methylotrophs as cell factories or biocatalysts for valorizing C1 compounds.

Compared to conventional chemical methods, bioconversion of C1 gases to liquids using microorganisms is an attractive approach to capture waste carbon for biorefining. In the current Research Topic, Sahoo et al. provide an overview of the core metabolic pathways of methanotrophs, their advantages, prospects, limitations, and consideration for further improvement. The capability of methanotrophs for bioconversion of methane into methanol at room temperature has been demonstrated before. However, the constant expression of methanol dehydrogenase reduces the yield of methanol bioconversion. To address the issue, Ito et al. developed a methanol dehydrogenase (MxaF) knockout mutant of *Methylosinus trichosporium* OB3b to enable switching between methanol accumulation mode and cell growth. Despite the low conversion efficiency,

Edited by:
Eric Altermann, AgResearch Ltd., New Zealand

Reviewed by:
Sachin Mandavgane, Visvesvaraya National Institute of Technology, India

***Correspondence:**
Eun Yeol Lee
eunylee@khu.ac.kr
Guodong Luan
luangd@qibebt.ac.cn

Specialty section:
This article was submitted to Microbiotechnology, a section of the journal Frontiers in Microbiology

Received: *17 September 2021*
Accepted: *07 October 2021*
Published: *28 October 2021*

Citation:
Lee EY, Li F-L, Wang Y, Wangikar PP, Guarnieri MT and Luan G (2021) Editorial: Bioconversion and Biorefinery of C1 Compounds. Front. Microbiol. 12:778962. doi: 10.3389/fmicb.2021.778962

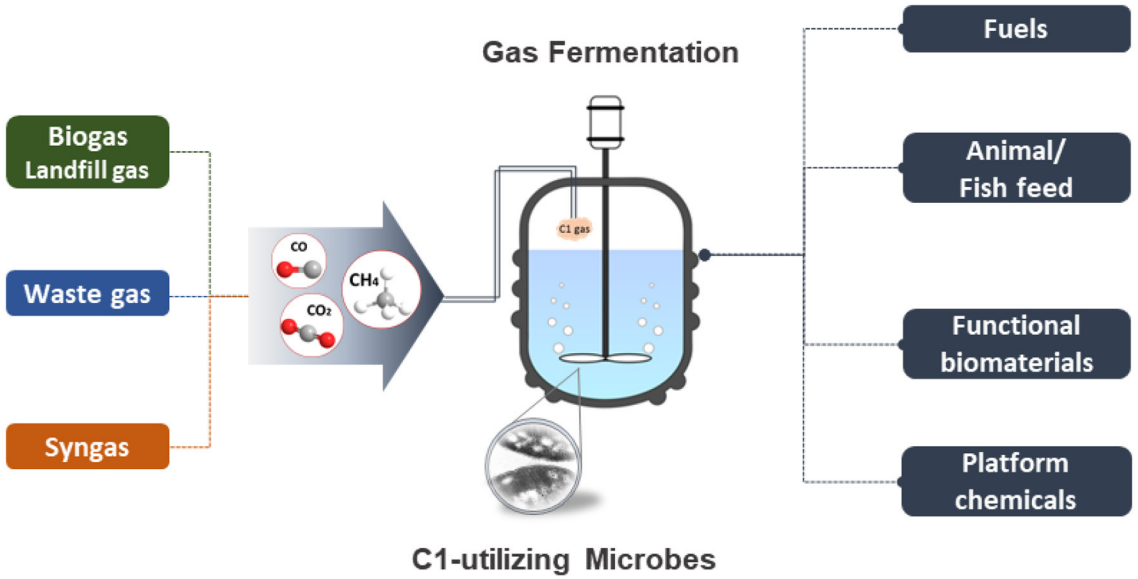

FIGURE 1 | Bioconversion and biorefinery of C1 compounds.

the capability of mutant for methanol accumulation can be maintained longer than wild-type and does not require inhibitors to accumulate methanol. Another recent advance for metabolic engineering of methanotrophs is the development of efficient electroporation systems for chromosomal deletion and integration for heterologous expression. Although genetic manipulation tools for methanotrophs have been explored for a while, Hu et al. have developed and optimized electroporation parameters for gene deletion and heterologous gene expression through electroporation of linear DNA fragments, increasing the maximum electroporation efficiency by 10-fold.

Valorization of CO_2 into high-value products is an important aspect of C1 bioconversion, thus significant efforts have been exerted to improve and expand host organisms and genetic manipulation tools. Cyanobacteria and microalgae are the two groups of hosts commonly employed to produce high-value products from CO_2. Despite being the largest phylum of prokaryotes, only a handful of model cyanobacteria have been studied and employed for biotechnological applications. To further expand the range of available model cyanobacteria, Chenebault et al. have developed a genetic toolbox for the robust unicellular cyanobacterium *Cyanothece* PCC 7425 and further demonstrated the production of limonene in this species. In another study, Gupta and Srivastava highlighted the combinatorial effects of promoters and ribosome binding sites on growth performance and glycogen production of *Synechococcus* sp. PCC 7002 overexpressing a sodium-dependent bicarbonate transporter, SbtA. Host development is also another approach for improving the capabilities of cell factories. For scaling up the production from cyanobacteria for outdoor cultivations, other traits such as high light, high temperature and salt tolerances are desirable. Zhang et al. proposed and demonstrated a convenient and markerless strategy for rapidly improving high light and high temperature tolerances of an important cyanobacterial chassis *S. elongatus* PCC 7942 through an introduction of a point mutation (C252F) in ATP synthase α subunit. Cui et al. have successfully improved salt tolerance of a promising cyanobacterium *S. elongatus* UTEX 2973 by redirecting and enhancing carbon flux toward a glucosylglycerol biosynthetic pathway. Computational analysis is a valuable tool for culture conditions optimization. Vasile et al. constructed a model framework that encompasses multi factors to relay key physiological parameters in the cultivation environment. These studies expand the current strategies to engineer more efficient cyanobacterial chassis cells. In the case of microalgae, owing to their unique properties and high potential applications in nutraceutical and pharmaceutical industries, they have gained considerable interest for commercialization. Yet, the lack of understanding of regulatory networks remains a major obstacle. To tackle this problem, Mariam et al. employed omics analysis and media engineering to gain new insights on the methyl erythritol phosphate (MEP) pathway and crosstalk between different metabolic pathways in *Botryococcus braunii*. The study proposes a new strategy to enhanced production without compromising growth.

Several articles in the current Research Topic focused on improving solventogenesis of acetogens, a group of bacteria capable of utilizing CO, CO_2 and H_2 *via* Wood–Ljungdahl pathway. In a recent study, Han et al. have reported the dramatic effects of a combination of trace metals on the production of higher alcohols in syngas fermentation. The yields obtained from the modified composition were 10-fold higher than the original composition, with the maximum concentrations of accumulated ethanol and butanol reaching 2.0 and 1.0 g/L, respectively. In

another study, He et al. demonstrated the effects of process parameters on the production of bioethanol from H_2/CO_2 by solventogenesis using anaerobic granular sludge. These studies provide important insights on solventogenesis optimization by adjusting operational temperature and trace metal composition.

The recent emergence of synthetic methylotrophs and autotrophs is also of equal importance to facilitate a sustainable bioeconomy. The development of synthetic biology and efficient genetic tools for industrial workhorses have made it possible to introduce complex carbon-fixing modules to heterologous hosts. Furthermore, with a better understanding of the natural carbon fixation pathways of microorganisms, developing efficient designs for synthetic C1 fixation pathways is no longer improbable. In a review article from Liang et al., the recent advances, prospects, and main challenges in developing efficient synthetic autotrophic microorganisms are thoroughly discussed. Novel one-carbon assimilation pathways were investigated in the work of Mao et al.. In this work, a comb-flux balance analysis algorithm was employed to predict novel and carbon-conserving formaldehyde assimilation pathways that are independent of additional energy and/or reducing power. The work demonstrated a systematic approach to design C1 assimilation pathways using artificial aldolases, in which one novel pathway named the glycolaldehyde-allose 6-phosphate assimilation pathway achieved a high carbon yield of 94% *in vitro*. A major challenge for further development of synthetic methylotrophs is the cytotoxicity from substrates and intermediates such as methanol and formaldehyde. While there are reports on successful constructions of synthetic methylotrophs, poor growth rates and biomass accumulation are common observations. Bennett et al. attempted to address this issue by conducting chemical mutagenesis and adaptive laboratory adaptation on an *Escherichia coli* methylotroph. The authors found a connection between common mutations in the 30S ribosomal subunit proteins and methanol tolerance. The findings provide insight into a novel methanol tolerance mechanism for synthetic methylotrophs and further advance the development of this field. However, the improved methanol tolerance is specifically attributed to methanol, not formaldehyde. It remains to be seen how to improve formaldehyde tolerance of synthetic methylotrophs.

Overall, there is no doubt that bioconversion and biorefinery of C1 compounds using metabolically engineered microorganisms present a promising route to promote sustainable development of the bioeconomy in the future. With the development of more efficient C1 biocatalysts, a new range of biotechnical applications and perspectives can be opened. Although there is still a long road ahead, it is our belief that the series of articles in the Research Topic provide a contemporary overview and multiple metabolic engineering strategies that can help to pave the way for industrial applications of C1 compounds in the future.

AUTHOR CONTRIBUTIONS

EL drafted this editorial. F-LL, YW, PW, MG, and GL edited the final text. All authors approved the final version.

FUNDING

The C1 Gas Refinery Program through the National Research Foundation of Korea (NRF) funded by the Ministry of Science and ICT (2015M3D3A1A01064882), the National Key R&D Program of China (2018YFA0901500 and 2018YFA0903600), and the Youth Innovation Promotion Association of Chinese Academy of Sciences (2021177) are appreciated. MG was supported by the US Department of Energy, Office of Energy Efficiency and Renewable Energy under Agreement No. 26680.

ACKNOWLEDGMENTS

The guest editors thank all the authors contributing in this special issue and reviewers and D. M. H. Anh for their kind support.

frontiers in Microbiology

ORIGINAL RESEARCH
published: 18 September 2020
doi: 10.3389/fmicb.2020.586601

A Genetic Toolbox for the New Model Cyanobacterium *Cyanothece* PCC 7425: A Case Study for the Photosynthetic Production of Limonene

Célia Chenebault[1], Encarnación Diaz-Santos[1], Xavier Kammerscheit[1], Sigrid Görgen[1,2], Cristian Ilioaia[1], Simona Streckaite[1], Andrew Gall[1], Bruno Robert[1], Elodie Marcon[3], David-Alexandre Buisson[3], Karim Benzerara[2], Jean-François Sassi[4], Corinne Cassier-Chauvat[1] and Franck Chauvat[1]**

[1] Université Paris-Saclay, CEA, CNRS, Institute for Integrative Biology of the Cell (I2BC), Gif-sur-Yvette, France, [2] Sorbonne Université, Muséum National d'Histoire Naturelle, UMR CNRS 7590, Institut de Minéralogie, de Physique des Matériaux et de Cosmochimie, IMPMC, Paris, France, [3] Université Paris-Saclay, Service de Chimie Bio-organique et Marquage (SCBM), CEA/DRF/JOLIOT, Gif-sur-Yvette, France, [4] Commissariat à l'Énergie Atomique et aux Énergies Alternatives (CEA), Centre de Cadarache, Saint-Paul-lez-Durance, France

OPEN ACCESS

Edited by:
Guodong Luan,
Qingdao Institute of Bioenergy and Bioprocess Technology (CAS), China

Reviewed by:
Tao Sun,
Tianjin University, China
Martin Hagemann,
University of Rostock, Germany

***Correspondence:**
Corinne Cassier-Chauvat
corinne.cassier-chauvat@cea.fr
Franck Chauvat
franck.chauvat@cea.fr

Specialty section:
This article was submitted to Microbiotechnology, a section of the journal Frontiers in Microbiology

Received: 23 July 2020
Accepted: 31 August 2020
Published: 18 September 2020

Citation:
Chenebault C, Diaz-Santos E, Kammerscheit X, Görgen S, Ilioaia C, Streckaite S, Gall A, Robert B, Marcon E, Buisson D-A, Benzerara K, Sassi J-F, Cassier-Chauvat C and Chauvat F (2020) A Genetic Toolbox for the New Model Cyanobacterium Cyanothece PCC 7425: A Case Study for the Photosynthetic Production of Limonene. Front. Microbiol. 11:586601. doi: 10.3389/fmicb.2020.586601

Cyanobacteria, the largest phylum of prokaryotes, perform oxygenic photosynthesis and are regarded as the ancestors of the plant chloroplast and the purveyors of the oxygen and biomass that shaped the biosphere. Nowadays, cyanobacteria are attracting a growing interest in being able to use solar energy, H_2O, CO_2 and minerals to produce biotechnologically interesting chemicals. This often requires the introduction and expression of heterologous genes encoding the enzymes that are not present in natural cyanobacteria. However, only a handful of model strains with a well-established genetic system are being studied so far, leaving the vast biodiversity of cyanobacteria poorly understood and exploited. In this study, we focused on the robust unicellular cyanobacterium *Cyanothece* PCC 7425 that has many interesting attributes, such as large cell size; capacity to fix atmospheric nitrogen (under anaerobiosis) and to grow not only on nitrate but also on urea (a frequent pollutant) as the sole nitrogen source; capacity to form CO_2-sequestrating intracellular calcium carbonate granules and to produce various biotechnologically interesting products. We demonstrate for the first time that RSF1010-derived plasmid vectors can be used for promoter analysis, as well as constitutive or temperature-controlled overproduction of proteins and analysis of their sub-cellular localization in *Cyanothece* PCC 7425. These findings are important because no gene manipulation system had been developed for *Cyanothece* PCC 7425, yet, handicapping its potential to serve as a model host. Furthermore, using this toolbox, we engineered *Cyanothece* PCC 7425 to produce the high-value terpene, limonene which

has applications in biofuels, bioplastics, cosmetics, food and pharmaceutical industries. This is the first report of the engineering of a *Cyanothece* strain for the production of a chemical and the first demonstration that terpene can be produced by an engineered cyanobacterium growing on urea as the sole nitrogen source.

Keywords: conjugation, RSF1010 derivative plasmids, promoter probe vector, temperature-controlled expression vector, sub-cellular localization, growth on urea, terpene production

INTRODUCTION

Cyanobacteria, the oldest and largest phylum of prokaryotes that perform the plant-like photosynthesis (Schirrmeister et al., 2015), are regarded as the ancestors of the plant chloroplast (Ponce-Toledo et al., 2017) and the purveyors of the oxygen that shaped our biosphere (Hamilton et al., 2016). Contemporary cyanobacteria still capture a vast quantity of solar energy to assimilate huge amounts of CO_2 (Dai et al., 2018) and nitrogen (nitrate, ammonium or urea) (Singh et al., 2016; Veaudor et al., 2019) to produce an enormous biomass that sustain most life forms on our planet. In colonizing most waters (fresh, brackish and marine) and soils (even deserts) biotopes, cyanobacteria have developed as widely diverse organisms. Their genomes vary in size (1.44–12.07 Mb) and organization (presence/absence of plasmids and linear chromosomes in addition to their circular chromosome) (Cassier-Chauvat et al., 2016). Furthermore, cyanobacteria display different cell sizes (1–10 μm) and morphologies, ranging from unicellular (cylindrical or spherical) (Koksharova and Wolk, 2002; Mazouni et al., 2004) to complex multi-cellular (filamentous) species (Cassier-Chauvat and Chauvat, 2014; Montgomery, 2015) capable to differentiate specialized cells for nitrogen fixation (Herrero et al., 2016) or survival to harsh environments (Chauvat et al., 1982; Legrand et al., 2019). Thus, cyanobacteria are interesting models to study how cells divide and pass their morphology on to their progeny (Cassier-Chauvat and Chauvat, 2014). Collectively, the disparities of the genome size, cell morphology and metabolism of cyanobacteria should prompt us to analyze a larger number of evolutionary-distant models to better understand and distinguish the common and species-specific aspects of cyanobacteria (Cassier-Chauvat and Chauvat, 2018).

Besides their great interest for basic science (Cassier-Chauvat and Chauvat, 2018), cyanobacteria are also regarded as promising cell factories for the production of chemicals for human health (Cassier-Chauvat et al., 2017; Demay et al., 2019) and industries (Cassier-Chauvat and Chauvat, 2018; Knoot et al., 2018). They capture solar energy at high efficiencies (3–9%) (Ducat et al., 2011) to fix a huge amount of carbon from atmospheric CO_2 (about 25 gigatons annually) into a huge energy-dense biomass (Jansson and Northen, 2010), and they tolerate high CO_2-containing ($\geq$50%) industrial gas (Ducat et al., 2011). So far, only a handful of model strains with a well-established genetic have been engineered, such as *Synechocystis* PCC 6803, *Synechococcus* PCC 7942, or *Synechococcus* PCC 7002, leading to a weak and often transient production (Knoot et al., 2018; Lin and Pakrasi, 2019). Thus, the influence of the large biodiversity of cyanobacteria on the efficiency of the photosynthetic production of chemicals, has been overlooked.

For all the above-mentioned reasons we think that the time has come to enlarge the panel of the model cyanobacteria to better study and exploit their biodiversity for basic and applied research purposes.

In this study, we focused our attention on the poorly studied unicellular cyanobacterium *Cyanothece* PCC 7425 (also designated as *Cyanothece* ATCC 29141), which was isolated in 1972 from a rice paddy in Senegal (Rippka et al., 1979), because it has numerous attractive properties. *Cyanothece* PCC 7425 has larger cells (about 3–4 μm) (Porta et al., 2000; Bandyopadhyay et al., 2011) than the well-studied models *Synechococcus* PCC 7942 (cylindrical shape, 1.5 μm × 0.5 μm, Koksharova and Wolk, 2002) and *Synechocystis* PCC 6803 (1.5 μm in diameter, Mazouni et al., 2004). This feature should facilitate the analysis of the localization of proteins involved in assembly and distribution of the CO_2-fixing carboxysomes and cell division, which are so far mainly studied in *Synechocystis* PCC 6803 and *Synechococcus* PCC 7942 (Cassier-Chauvat and Chauvat, 2014; Sommer et al., 2019; Sun et al., 2019; MacCready et al., 2020). Unlike these models, *Cyanothece* PCC 7425 can fix atmospheric nitrogen in anaerobiosis (Bandyopadhyay et al., 2011). It is also able to form intracellular CO_2-sequestrating calcium carbonate granules, an interesting but as yet poorly studied particularity (Blondeau et al., 2018). *Cyanothece* PCC 7425 can also synthesize various biotechnologically interesting products, such as: (i) cyanophycin, the nitrogen-rich polymer of arginine and aspartate (Klemke et al., 2016); (ii) cyanobactins, a family of cyclic peptides (Houssen et al., 2012); (iii) alkane, sucrose and polyhydroxyalkanoates (biodegradable bioplastics) (Porta et al., 2000; Bandyopadhyay et al., 2011).

Furthermore, the genome of *Cyanothece* PCC 7425 (5.82 Mb) in being much larger than those of the well-studied models *Synechocystis* PCC 6803 (3.95 Mb), *Synechococcus* PCC 7002 (3.40 Mb) and *Synechococcus* PCC 7942 (2.75 Mb), should teach us new lessons about cyanobacteria. For example, *Cyanothece* PCC 7425 has the genes encoding the two (anti-oxidant) super-oxide dismutases SodA (Mn-dependent) and SodB (Fe-dependent), whereas *Synechocystis* PCC 6803, *Synechococcus* PCC 7002 and *Synechococcus* PCC 7942 only have SodB (Veaudor et al., 2019). Similarly, *Cyanothece* PCC 7425 encodes the anti-oxidant glutathione reductase enzyme that is missing in both *Synechocystis* PCC 6803 (Marteyn et al., 2009) and *Synechococcus* PCC 7002 (Narainsamy et al., 2013). *Cyanothece* PCC 7425 has two *radA* DNA-repair genes whereas all three model cyanobacteria have a single-copy *radA* gene (Cassier-Chauvat et al., 2016). Also interestingly, *Cyanothece* PCC 7425 possesses the full panoply of genes coding for urea uptake and catabolism, whereas *Synechococcus* PCC 7942 has no

such genes, and *Synechocystis* PCC 6803 and *Synechococcus* PCC 7002 have no genes for the ureolytic enzymes urea carboxylase and allophanate hydrolase (Veaudor et al., 2019).

So far, only two attempts to manipulate a *Cyanothece* strain have been reported. First, a single-stranded spectinomycin resistance DNA-cassette, which could be introduced (by electro-transformation) and integrated into the genome of *Cyanothece* PCC 7822 cells, yielded no spectinomycin resistant clones when tested with *Cyanothece* PCC 7425 (Min and Sherman, 2010). More recently, Liberton et al. (2019) using DNA methylases to protect the incoming DNA from the *Cyanothece* ATCC 51142 restriction enzymes, could insert a kanamycin resistance cassette into the glycogen-catabolism gene glgX, generating a glycogen-rich mutant. However, this technique was not tested with *Cyanothece* PCC 7425. Thus, no gene manipulation system is yet available for *Cyanothece* PCC 7425, hampering its otherwise interesting potential to serve as a model host.

In this work, we first improved the classical BG-11 mineral medium cyanobacteria (Stanier et al., 1971) for better growth of *Cyanothece* PCC 7425, which appeared capable to grow not only on nitrate, the usual nitrogen source for cyanobacteria cultivated in the laboratory, but also on urea a frequent pollutant. Then, we developed a simple and efficient protocol for the conjugative transfer to *Cyanothece* PCC 7425 of the plasmid vectors derived from the broad-host-range plasmid RSF1010 that we previously constructed for gene manipulation in *Synechocystis* PCC 6803 and *Synechococcus* PCC 7942 (Marraccini et al., 1993; Mermet-Bouvier and Chauvat, 1994; Mazouni et al., 2004). We showed that these vectors replicate autonomously in *Cyanothece* PCC 7425 where they can be used for facile (i) promoter analysis, (ii) high-level, constitutive or temperature-controlled, protein productions, and (iii) analysis of sub-cellular localization of proteins. Finally, using this genetic toolbox we engineered a *Cyanothece* PCC 7425 strain for the stable photosynthetic production of limonene. This high-value terpene serves in cosmetics and food industries (Jongedijk et al., 2016), and it can be used as a fuel additive (Tracy et al., 2009; Chuck and Donnelly, 2014). This is the first report of the engineering of a *Cyanothece* strain for the photosynthetic production of a chemical, and the first demonstration that a terpene can be produced by an engineered cyanobacterium growing on urea as the sole nitrogen source. This suggests that it could be important in the future to couple chemicals productions with water treatment to reduce the costs (Veaudor et al., 2019).

RESULTS AND DISCUSSION

Identification of Effective Conditions for the Growth of *Cyanothece* PCC 7425: Positive Influence of Calcium and Bicarbonate

As *Cyanothece* PCC 7425 has been poorly studied so far, we first analyzed the influence of usually important parameters, such as light fluence, temperature and mineral availability, on its photoautotrophic growth, *Cyanothece* PCC 7425 appeared to grow well (**Figure 1A**) under the conditions defined as standard for *Synechocystis* PCC 6803, e.g., under white light 2000 lux (25.0 $\mu E.m^{-2}.s^{-1}$), at 30°C, in the MM mineral medium (Domain et al., 2004). As *Cyanothece* PCC 7425 possesses the full panoply of genes encoding the uptake and catabolism of urea that frequently occurs in natural waters (Veaudor et al., 2019), we have tested its capability to grow on urea as the sole nitrogen source. The results showed that cells grew well on urea up to 2 mM, whereas higher urea concentrations reduced the duration of healthy growth and production of biomass (**Supplementary Figure S1**). After 7–10 days of cultivation on urea, *Cyanothece* PCC 7425 can turn yellowish, as previously observed in the phylogenetically distant cyanobacteria *Anabaena cylindrica*, *Synechococcus* PCC 7002 (Sakamoto et al., 1998) and *Synechocystis* PCC 6803 growing on urea as the sole nitrogen source (Veaudor et al., 2019). Again as observed in *Synechocystis* PCC 6803 (Veaudor et al., 2018), once installed the chlorosis process decreased the cell viability measured by plating assays on standard growth medium (it contains nitrate, not urea). Interestingly, *Cyanothece* PCC 7425 grew up to increasing cell densities in response to increasing urea quantities, which needed to be supplied not all at once, but as small successive sub-doses along cell growth (**Supplementary Figure S1**). Also interestingly, the maximal growth (biomass production) of *Cyanothece* PCC 7425 was greatly improved by supplementing the MM with both 9.52 mM $NaHCO_3$ and 2.92 mM $CaCl_2$ (**Figure 1A**), in agreement with the previous finding that *Cyanothece* PCC 7425 forms intracellular calcium carbonate granules (De Wever et al., 2019).

Using the presently improved growth medium, hereafter designated as MM_{CaC}, we found that the growth of *Cyanothece* PCC 7425 (doubling time about 24 h) is (i) similar under light intensities ranging from 1500 to 3500 lux (18.75–43.75 $\mu E.m^{-2}.s^{-1}$) (**Figure 1C**); (ii) not stimulated by the addition of vitamin B12 that can be beneficial or essential to cyanobacterial life (**Figure 1B**); and (iii) slightly improved or decreased by increasing the temperature to 34 or 39°C, respectively (**Figure 1D**).

Development of an Effective Protocol for the Conjugative Transfer of RSF1010-Derived Replicative Plasmids to *Cyanothece* PCC 7425

Three decades ago, we contributed to the development of the genetics of the cyanobacteria *Synechocystis* PCC 6803 and *Synechococcus* PCC 7942, in using the broad-host-range plasmid RSF1010 for the construction of pSB2A, the first promoter-probe vector (Marraccini et al., 1993), and pFC1, the first conditional expression vector (Mermet-Bouvier and Chauvat, 1994). These vectors could be transferred by conjugation (or electroporation) from *Escherichia coli*, to these model cyanobacteria, where they stably replicate autonomously, though they contain no cyanobacterial origin of DNA replication (Mermet-Bouvier et al., 1993). Like RSF1010, pSB2A and pFC1 are not self-transmissible. They must be first introduced (by standard transformation)

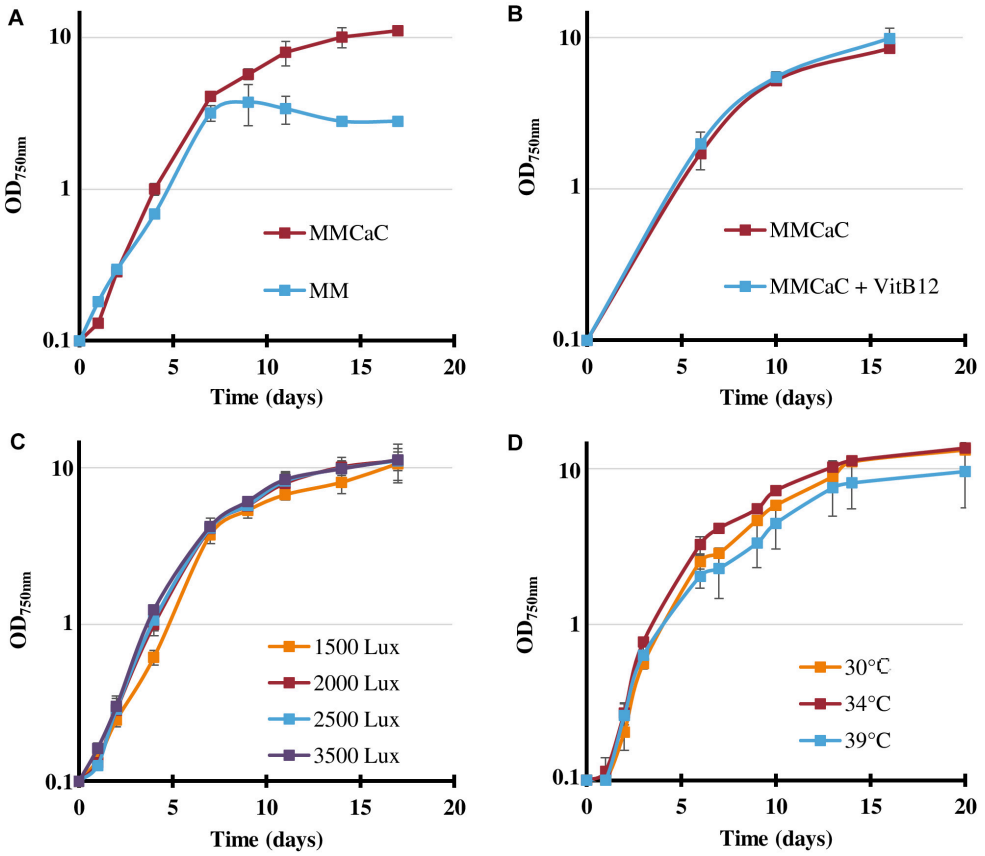

FIGURE 1 | Influence of various conditions on the growth of *Cyanothece* PCC 7425. **(A)** Typical photoautotrophic growth of *Cyanothece* PCC 7425 at 30°C, 2000 lux (25.0 μE.m^{-2}.s^{-1}) in liquid mineral medium (MM) or MM supplemented with 9.52 mM $NaHCO_3$ and 2.92 mM $CaCl_2$ (MM_{CaC}). **(B)** Influence of the addition of vitamin B12 (4 μg.L^{-1}). **(C)** Influence of various light intensities on cell growth at 30°C in liquid MM_{CaC}. **(D)** Influence of various temperatures on cell growth in liquid MM_{CaC} under 2000 lux. Error bars represent standard deviation from three biological replicates.

into an *E. coli* strain that already contains the self-transmissible RP4 plasmid, which cannot replicate in cyanobacteria, but encodes in *trans* the functions promoting the transfer of pSB2A or pFC1 to cyanobacteria. The resulting *E. coli* donor cells possessing both RP4 and pSB2A, or pFC1, are co-incubated with the cyanobacterial recipient cells in liquid medium. Then, the mixture is plated on solid mineral medium for selecting the cyanobacterial conjugants based on their antibiotic resistance encoded by pSB2A or pFC1 (Mermet-Bouvier et al., 1993).

In the present study, the pSB2A and pFC1 plasmids were used to test whether RSF1010-derivatives can be transferred by conjugation from *E. coli* to *Cyanothece* PCC 7425, and whether they can stably replicate autonomously in this cyanobacterium as observed in *Synechocystis* PCC 6803 and *Synechococcus* PCC 7942 (Mermet-Bouvier et al., 1993). For this purpose, a simpler and faster efficient protocol was developed that bypassed the introduction of pSB2A or pFC1 into the RP4-harboring *E. coli* strain that normally precedes and enables their conjugative transfer to cyanobacteria. Instead, the cyanobacterial recipient strain was co-incubated, on plate (not in liquid medium) in order to favor cell-cell interaction, with the two *E. coli* strains, one harboring RP4 and the other one pSB2A or pFC1. Also interestingly, similar high frequencies of conjugation, about 5.10^{-4} per cyanobacterial cell, were obtained when pSB2A or pFC1 were propagated in commonly used (*recA* KO) strains of *E. coli*, such as MC1061, TOP10 or XL1-Blue.

The RSF1010-Derived Plasmid Vector pSB2A Can Serve for Promoter Analysis in *Cyanothece* PCC 7425

In this section we used pSB2A, the first promoter-probe-vector originally developed for *Synechocystis* PCC 6803 and *Synechococcus* PCC 7942 (Marraccini et al., 1993; Dutheil et al., 2012). pSB2A possesses a multiple cloning site for cloning any studied promoter in front of the promoter-less chloramphenicol acetyl transferase (*cat*) reporter gene. When expressed, for example by the strong *E. coli tac* promoter we cloned in pSB2A, yielding pSB2T (**Supplementary Table S1**), *cat* directs the production of the CAT reporter enzyme. The activity of this enzyme can be easily monitored by a spectrophotometric assay (Ferino and Chauvat, 1989) and confers the resistance to chloramphenicol (Marraccini et al., 1993; Dutheil et al., 2012) and references therein.

The presently reported conjugation protocol was used to introduce the Sm^R/Sp^R plasmids pSB2A and pSB2T in *Cyanothece* PCC 7425. Among the large number of Sm^R/Sp^R conjugants obtained, two independent clones were collected, re-streaked on Sm^R/Sp^R plates and analyzed by PCR using relevant oligonucleotides primers (**Supplementary Table S2**). The results showed that pSB2A and pSB2T replicate stably in *Cyanothece* PCC 7425 (**Supplementary Figure S2**). Then, we measured the *cat* activities of the *Cyanothece* PCC 7425 reporter strains propagating pSB2A or pSB2T. As expected, a strong CAT activity was observed in *Cyanothece* PCC 7425 cells propagating pSB2T (**Figure 2A**). In contrast, no CAT activities were detected in *Cyanothece* PCC 7425 WT cells, which have no *cat* gene, and pSB2A-propagating cells, where the *cat* reporter gene is not expressed. Collectively, these results showed that the replicative promoter-probe vector pSB2A can be used for promoter analyses in *Cyanothece* PCC 7425.

The RSF1010-Derived Plasmid Vector pFC1 Can Be Used for Temperature-Controlled Protein Production in *Cyanothece* PCC 7425

In this section, we used pFC1, the first conditional expression vector for cyanobacteria, originally developed for *Synechocystis* PCC 6803 and *Synechococcus* PCC 7942 (Mermet-Bouvier and Chauvat, 1994). pFC1 harbors the lambda-phage cI_{857} gene encoding the temperature-sensitive repressor that tightly controls the activity of the otherwise strong p_R promoter located behind cI_{857} (in opposite direction) (Mermet-Bouvier and Chauvat, 1994). The p_R promoter is followed by a canonical ribosome-binding site (RBS, 5′-AGGA-3′) and a correctly spaced ATG initiation codon embedded within the unique *Nde*I restriction site (5′-CAT**ATG**-3′) for easy cloning and strong conditional expression of the studied protein-coding sequences (Sakr et al., 2013; Ortega-Ramos et al., 2014) and references therein.

The Sm^R/Sp^R plasmids pFC1, and its pPMB13 derivative for temperature-controlled expression of the *E. coli lacZ* gene encoding the beta-galactosidase reporter enzyme (Mermet-Bouvier and Chauvat, 1994), were introduced by conjugation (see above) in *Cyanothece* PCC 7425. Among the large number of Sm^R/Sp^R conjugant clones obtained, two independent clones were collected and re-streaked on Sm^R/Sp^R plates, prior to PCR analyses that showed that pFC1 and pPMB13 replicate stably in *Cyanothece* PCC 7425 (**Supplementary Figure S3**). Then, we measured the beta-galactosidase activities of the *Cyanothece* PCC 7425 reporter strains propagating pFC1 or pPMB13. No beta-galactosidase activities were detected in cells propagating pFC1, which lacks *lacZ*. A weak beta-galactosidase activity was observed in cells propagating pPMB13 grown at 30°C where *lacZ* expression is mostly blocked by the temperature-sensitive repressor CI_{857} produced by pPMB13. Finally, the transfer of pPMB13 reporter cells to higher temperatures increased *lacZ* expression, proportionally to the growth temperature, i.e., moderately at 34°C and massively at 39°C, as expected (**Figure 2B**). These results showed that the autonomously replicating plasmid vector pFC1 can be used for temperature-regulated protein production in *Cyanothece* PCC 7425, as was observed in *Synechocystis* PCC 6803 for many endogenous proteins (Sakr et al., 2013; Ortega-Ramos et al., 2014) and references therein. This system for tight control of (strong) gene expression is very interesting when one wants to produce chemicals that are toxic and prevent cell growth or generates mutations that decrease the production to escape cell death (Cassier-Chauvat et al., 2016). Using such a tightly controlled production system it is possible to first grow the engineered cyanobacterium up to a large cell population, before triggering the production of the toxic product which should thus be more efficient (Cassier-Chauvat et al., 2016).

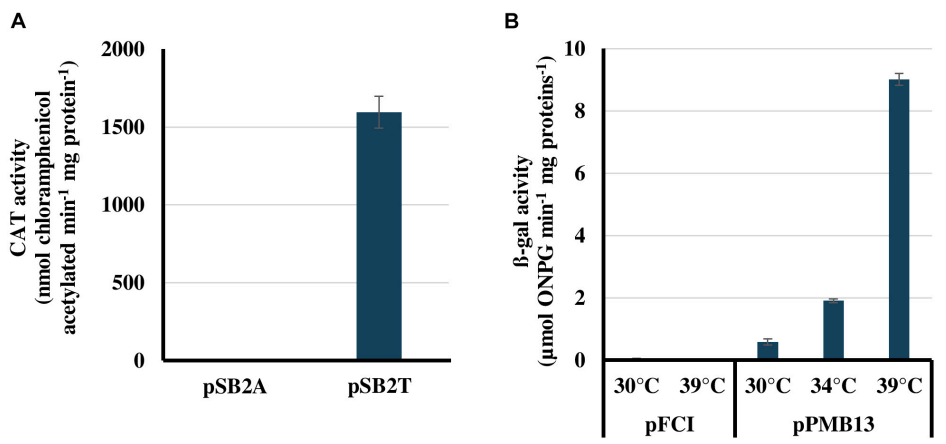

FIGURE 2 | Validation of the pSB2A and pFC1 plasmid vectors for promoter analysis and temperature-controlled protein production in *Cyanothece* PCC 7425, respectively. **(A)** Chloramphenicol acyl transferase (CAT) activities of *Cyanothece* PCC 7425 cells propagating either the promoter probe vector pSB2A, which harbors the promoter-less *cat* reporter gene, or its pSB2T derivative, which expresses the *cat* gene from the strong *E. coli tac* promoter. **(B)** β-galactosidase activities of *Cyanothece* PCC 7425 cells propagating either the temperature-controlled expression vector pFC1 or its pMB13 derivative harboring the *lacZ* protein coding sequence. All activities are the mean values of three measurements performed on two different cellular extracts.

RSF1010-Derived Plasmids and the Green-Fluorescent Reporter Protein Can Be Used to Analyze Protein Localization in *Cyanothece* PCC 7425

In a few model cyanobacteria, such as *Synechocystis* PCC 6803 and *Synechococcus* PCC 7942, translational fusion of studied proteins to the green-fluorescent reporter protein (GFP) proved useful to analyze the sub-cellular localization of proteins involved in cell division (Cassier-Chauvat and Chauvat, 2014) or the biogenesis of the CO_2-fixing carboxysome microcompartment (Cameron et al., 2013).

To test whether the GFP reporter protein can be employed to study protein localization in *Cyanothece* PCC 7425, we tried to conjugate it with our previously constructed plasmids pSB2T-ftsZ-gfp, pSB2T-gfp-ftn6 and pSB2T-gfp-sepF that produce the *Synechocystis* PCC 6803 cytokinetic proteins FtsZ, SepF, and Ftn6 translationally fused to GFP (Mazouni et al., 2004; Marbouty et al., 2009). All attempts were unsuccessful, suggesting that these fusion proteins impair the crucial cytokinetic process of *Cyanothece* PCC 7425.

Consequently, we tried to introduce in *Cyanothece* PCC 7425 the presently constructed pSB2T-derived plasmids pSB2T-ccmk1$_{tsbp1}$-gfp and pSB2T-maf$_{S6803}$-gfp which encode GFP fusions with the presumptive carboxysome protein CcmK1 (Tll0946) of the cyanobacterium *Thermosynechococcus elongatus* BP1 (Cameron et al., 2013) and the *Synechocystis* PCC 6803 presumptive cytokinetic protein (Sll0905) Maf (Hamoen, 2011), respectively (**Supplementary Figure S2**). pSB2T-ccmk1$_{tsbp1}$-gfp was constructed by cloning downstream of the *tac* promoter of pSB2T opened at its unique *Hpa*I restriction site, an *Eco*RV restriction fragment containing the *ccmk1*$_{tsbp1}$-*gfp* fusion gene (synthetized by Genecust; **Supplementary Figure S4**). Similarly, pSB2T-maf$_{S6803}$-gfp harbors the *maf* $_{S6803}$-*gfp* fusion gene downstream of its *tac* promoter (**Supplementary Figures S2, S5**).

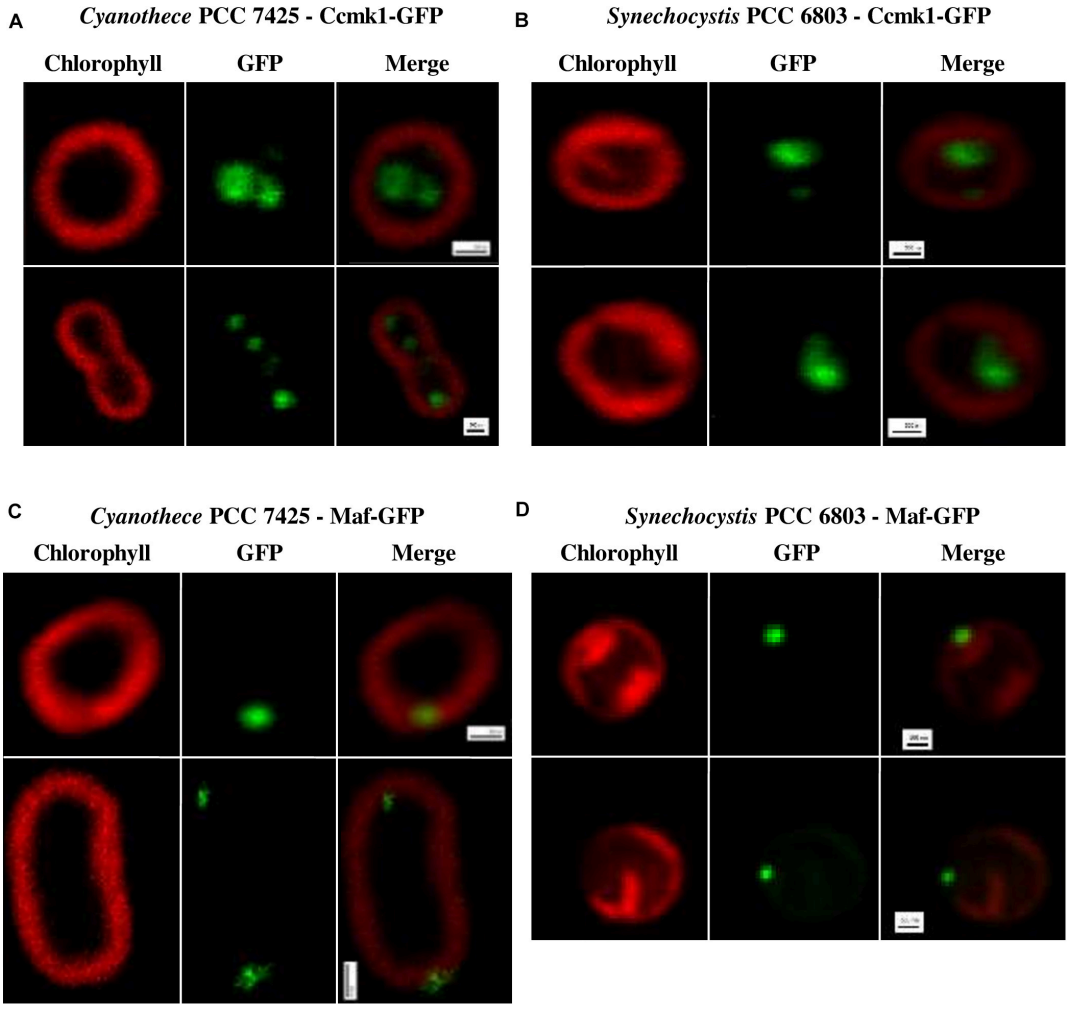

FIGURE 3 | Localization of the fusion proteins Ccmk1$_{tsbp1}$-GFP and Maf$_{S6803}$-GFP in *Cyanothece* PCC 7425 and *Synechocystis* PCC 6803. Fluorescence images (scale bars, 500 nm) of *Cyanothece* PCC 7425 and *Synechocystis* PCC 6803 reporter cells propagating the plasmids pSB2T-ccmk1$_{tsbp1}$-gfp **(A,B)** or pSB2T-maf$_{S6803}$-gfp **(C,D)**, respectively.

These plasmids, along with the previously constructed pSB2T-GFP plasmid encoding the unfused GFP (Mazouni et al., 2004), were transferred by conjugation to *Cyanothece* PCC 7425 and also to *Synechocystis* PCC 6803 as a control strain. Similar high-numbers of conjugant clones were obtained in all cases. PCR analyses showed that all three plasmids appeared to propagate stably in *Synechocystis* PCC 6803 and *Cyanothece* PCC 7425 (**Supplementary Figure S2**). In both hosts, the GFP protein alone displayed no particular localization, as previously observed in *Synechocystis* PCC 6803 (Mazouni et al., 2004). In contrast, the CcmK1$_{tsbp1}$-GFP protein appeared to localize inside the cells of both *Synechocystis* PCC 6803 and *Cyanothece* PCC 7425 (**Figures 3A,B**), likely in their carboxysome as observed with the similar CcmK1$_{S7942}$-GFP fusion protein in *Synechococcus* PCC 7942 (Cameron et al., 2013). The localization of the Maf$_{S6803}$-GFP fusion protein was also similar in both *Synechocystis* PCC 6803 and *Cyanothece* PCC 7425, but this protein was accumulated in one to two spots at the inner periphery of the cells (**Figures 3C,D**), unlike the CcmK1$_{tsbp1}$-GFP protein. Collectively these data show that RSF1010-derived plasmids and the fluorescent GFP reporter protein are useful tools to study protein localization in the interesting cyanobacterium *Cyanothece* PCC 7425 that has larger cells than the models *Synechocystis* PCC 6803 and *Synechococcus* PCC 7942 classically used for analyzing the sub-cellular localization of proteins.

Construction of a *Cyanothece* PCC 7425 Strain Carrying the *Mentha spicata* Limonene Synthase Encoding Transgene Expressed From the Strong Lambda-Phage p_R Promoter of a RSF1010-Derived pC Plasmid Vector

Then we tested whether *Cyanothece* PCC 7425 can be used for the photosynthetic production of high-value chemicals, such as limonene ($C_{10}H_{16}$). This volatile terpene, naturally produced by plants, has applications in biofuels (Tracy et al., 2009; Chuck and Donnelly, 2014), bioplastics, cosmetic and pharmaceutical industries (Jongedijk et al., 2016). We employed the limonene synthase from *Mentha spicata* because it efficiently transforms the geranyl diphosphate metabolite produced by the NAD(P)H-dependent MEP pathway, into limonene of high purity (Colby et al., 1993). Furthermore, this plant enzyme worked well in the model cyanobacteria *Synechococcus* PCC 7002 (Davies et al., 2014), *Synechococcus* PCC 7942 (Wang et al., 2016) and *Synechocystis* PCC 6803 (Lin et al., 2017). Like previous workers, we removed the first 168 bp encoding the chloroplast targeting sequence from the *Mentha spicata* limonene synthase gene (*ls*) and we adapted its coding sequence to the cyanobacterial usage of codon. We chose the codon usage of *Synechocystis* PCC 6803, because it is similar to that of *Cyanothece* PCC 7425 and proteins efficiently produced in *Synechocystis* PCC 6803 are also well produced in *Cyanothece* PCC 7425 (**Figures 2**, **3**). The *ls* nucleotide sequence was synthesized by the Eurofins company as a DNA segment flanked by *Nde*I and *Eco*RI restriction sites at its 5′- and 3′-ends, respectively. After cleavage with both *Nde*I and *Eco*RI, the *ls* gene was cloned downstream of the strong λp_R promoter of the pFC1-derivative pC plasmid for high-level constitutive gene expression (Veaudor et al., 2018), which was opened with the same enzymes (**Supplementary Figures S6, S7**).

The resulting pC-LS plasmid (**Supplementary Figure S6**) was transferred by conjugation to *Cyanothece* PCC 7425. Two independent Sm^R/Sp^R clones were selected and analyzed by PCR and DNA sequencing (**Supplementary Figure S3**), which showed that pC-LS replicates stably in *Cyanothece* PCC 7425. As expected, the presence of the pC-LS plasmid did not adversely affect the photoautotrophic growth of *Cyanothece* PCC 7425 (**Figures 4A,B**), irrespectively of the number of sub-cultivation (regular verifications were performed during 12 months). Because of the volatility of limonene, a dodecane overlay was applied on cultures to collect limonene in the organic layer. As observed with *Synechococcus* PCC 7002 (Davies et al., 2014) and *Synechocystis* PCC 6803 (Lin et al., 2017), the dodecane overlay had little influence on the growth of *Cyanothece* PCC

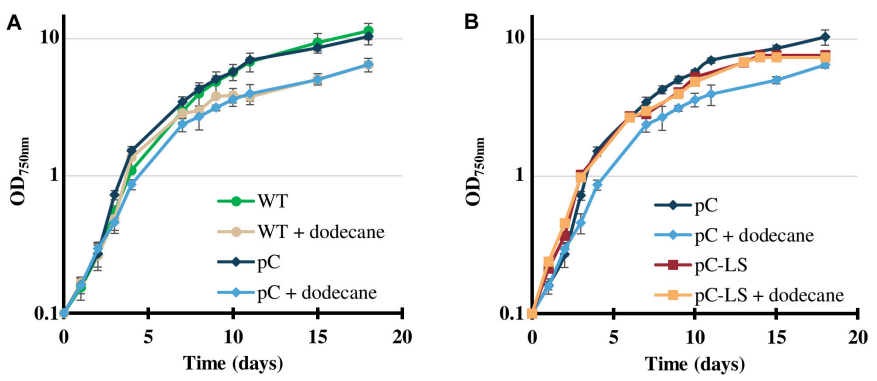

FIGURE 4 | Influence of the pC-LS plasmid expressing the limonene synthase gene on the photoautotrophic growth of *Cyanothece* PCC 7425, in absence or presence of a dodecane overlay. **(A)** Typical photoautotrophic growth of the *Cyanothece* PCC 7425 wild-type strain (WT) and its derivative propagating the pC plasmid, at 30°C, 2000 lux (25.0 μE.m^{-2}.s^{-1}) in liquid MM$_{CaC}$ mineral medium, in the presence or absence of a 20% (vol/vol) dodecane overlay. **(B)** Typical photoautotrophic growth in the same conditions of *Cyanothece* PCC 7425 strains propagating pC or its pC-LS derivative for high-level constitutive expression of the limonene synthase gene. Error bars represent standard deviation from three biological replicates.

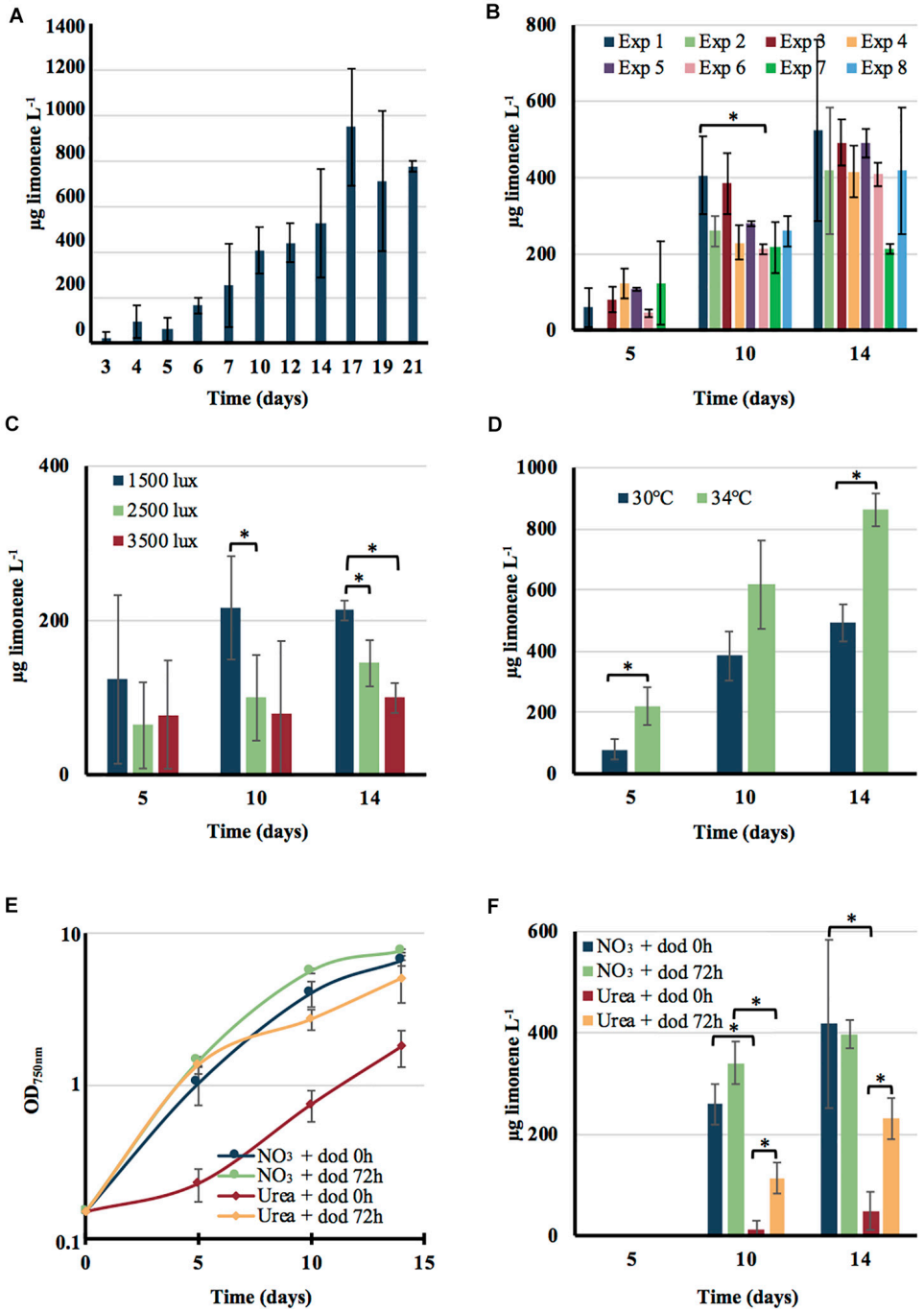

FIGURE 5 | Influence of various growth conditions on the production of limonene by the engineered strain of *Cyanothece* PCC 7425. Cells growing in MM_{CaC} at 30°C under a 1500 lux light (18.75 $\mu E.m^{-2}.s^{-1}$) were inoculated at the initial cell density of 4×10^6 cells mL^{-1} ($OD_{750\ nm}$ = 0.15) and further grown under the indicated conditions. Limonene production was monitored at the indicated time intervals. **(A)** Cells were grown for 21 days under above indicated conditions in the presence of a 20% (vol/vol) dodecane overlay. **(B)** Cells were sub-cultured in standard conditions (absence of dodecane) for variable periods (a few weeks to 9 months) prior to assay limonene production as described above during 14 days periods. **(C)** Cells were grown for 14 days in MM_{CaC} at 30°C under the indicated light intensities: 1500 lux (18.75 $\mu E.m^{-2}.s^{-1}$), 2500 lux (31.25 $\mu E.m^{-2}.s^{-1}$) or 3500 lux (42 $\mu E.m^{-2}.s^{-1}$) in the presence of a 20% (vol/vol) dodecane (dod) overlay prior to test limonene production. **(D)** Cells were grown at 30°C or 34°C in MM_{CaC} under a 1500 lux light (18.75 $\mu E.m^{-2}.s^{-1}$) and a 20% (vol/vol) dodecane overlay. Typical growth **(E)** and limonene production **(F)** of cells incubated at 30°C under 1500 lux (18.75 $\mu E.m^{-2}.s^{-1}$) in a nitrogen-free MM_{CaC} medium (MM_{CaC0N}), which was supplemented at times 0, 4, and 8 days with the same amounts of nitrogen. They were provided as successive additions of either 2 mM nitrate (NO_3; up to 8 mM final) or 1 mM urea [$CO(NH_2)_2$; up to 4 mM final]. The dodecane overlay was added either at the beginning of the experiment (dodecane 0 h) or after 72 h of growth. In all cases, error bars represent standard deviation from three biological replicates. The hooks ⊏ indicate a significant difference between the two compared experiments (*t*-test, $P < 0.05$; symbolized by *).

7425 (**Figures 4A,B**), and the C12 chain length of dodecane ($C_{12}H_{26}$) allowed chromatographic separation from the C10 length of limonene ($C_{10}H_{16}$) (**Supplementary Figure S8**).

The Engineered Strain of *Cyanothece* PCC 7425 Propagating the Limonene Synthase Expression Vector pC-LS Is a Stable Limonene Producer

The rate of limonene biosynthesis during the growth phase of the *Cyanothece* PCC 7425 strains propagating the pC-LS plasmid or the (empty) pC vector, were measured over a 21-days period of cultures with a 20% (v/v) dodecane overlay (**Figure 5A**). GC-MS analysis of dodecane overlay samples from the pC-LS propagating strain showed a prominent peak with a similar retention time to pure commercial standards of *S*-(-)-limonene (6.90 min). This peak, which was not observed in the case of the negative control strain propagating the (empty) pC vector, displays a similar pattern than the *S*-(-)-limonene reference spectra from the NIST Mass Spectral Library (**Supplementary Figure S8**).

The overall limonene production, about 0.6–1.0 mg/L, was unaffected by the duration of sub-cultivation under photoautotrophic conditions (up to 9 months) of the engineered *Cyanothece* PCC 7425 strain, prior to limonene assay (**Figures 5A,B**). This test, rarely presented in articles reporting the engineering of cyanobacteria for chemical production (Knoot et al., 2018; Lin and Pakrasi, 2019), showed that the *Cyanothece* PCC 7425 limonene producer is genetically stable. This finding is interesting since it is known that cyanobacteria engineered for chemical production can be genetically unstable (for a review see Cassier-Chauvat et al., 2016). The level of limonene production by the engineered *Cyanothece* PCC 7425 strain was slightly increased by either decreasing the light down to 1500 lux or shifting the temperature up to 34°C (**Figures 5C,D**). In every cases it was similar to what was reported for *Synechococcus* PCC 7942 (Wang et al., 2016), but lower (about fivefold) than what was reported for the very-well known model cyanobacteria *Synechococcus* PCC 7002 (Davies et al., 2014) and *Synechocystis* PCC 6803 (Lin et al., 2017). However, it is very difficult to meaningfully compare limonene production from different cyanobacteria growing under various conditions in different laboratories. Future work will be required to attempt at increasing limonene production by the engineered *Cyanothece* PCC 7425. This will involve finding better conditions for cell growth and limonene collection, as well as effective metabolic engineering strategies.

The Engineered Strain of *Cyanothece* PCC 7425 Can Photosynthetically Produce Limonene, Using Either Nitrate or Urea as the Sole Nitrogen Source

As we have shown above, *Cyanothece* PCC 7425 can grow not only on nitrate, the usual nitrogen source of cyanobacteria, but also on urea, a frequent and abundant pollutant (Veaudor et al., 2019). Growth on urea occurs when it is supplied not all at once, but as small successive sub-doses along cell growth (**Supplementary Figure S1**). Consequently, we compared the level of limonene production by our engineered strain of *Cyanothece* PCC 7425 growing either on nitrate or urea added in similar small quantities along cell growth. As compared to cells growing on nitrate, cells growing on urea can be affected by the dodecane overlay used for limonene trapping (**Figure 5E**). Both cell growth and limonene production are reduced when the dodecane overlay is applied at the beginning of the culture (when the cell density is very low) (**Figures 5E,F**). The negative influence of dodecane on urea-growing cells is reduced when it is applied after 72 h of growth (when the cell density is higher). Such urea-growing cells produced limonene up to about 50% of the quantity produced by cells growing on nitrate. Future work will be required to find good conditions for the photosynthetic production of limonene by *Cyanothece* PCC 7425 growing either on urea. This objective is important in the future view of using cyanobacteria for the photosynthetic production of chemicals coupled with water treatment to reduce the costs (Veaudor et al., 2019).

CONCLUSION

We have developed a genetic toolbox for the robust unicellular cyanobacterium *Cyanothece* PCC 7425. We first showed that the addition of extra calcium and carbonate to the BG-11 mineral medium, classically used to grow cyanobacteria (Stanier et al., 1971), improved the growth of *Cyanothece* PCC 7425. Then, we showed that *Cyanothece* PCC 7425 can grow, not only on nitrate the standard nitrogen source of cyanobacteria, but also on urea a frequent and abundant pollutant (Veaudor et al., 2019). Then, we developed a simple and efficient protocol for the conjugative transfer to *Cyanothece* PCC 7425 of plasmid vectors derived from the broad-host-range plasmid RSF1010. We previously constructed these vectors for (i) promoter analysis (Marraccini et al., 1993), (ii) constitutive or temperature-controlled protein productions (Mermet-Bouvier and Chauvat, 1994), and (iii) analysis of sub-cellular localization of proteins (Mazouni et al., 2004; Marbouty et al., 2009) in the model cyanobacteria *Synechocystis* PCC 6803 and *Synechococcus* PCC 7942. As expected, these autonomously replicating plasmid vectors appeared to work well in *Cyanothece* PCC 7425.

To emphasize the interest of this genetic toolbox for gene manipulation in *Cyanothece* PCC 7425, we used it to engineer a strain for the photosynthetic production of the high-value chemical limonene. Limonene, a 10-carbons volatile terpene ($C_{10}H_{16}$) normally produced by plants, is commercially used in cosmetics and food industries (Jongedijk et al., 2016), and it can be used as an additive to diesel (Tracy et al., 2009) or jet-fuel (Chuck and Donnelly, 2014; Lin et al., 2017). Finally, we have also shown that our engineered strain of *Cyanothece* PCC 7425 is genetically stable and it can produce limonene in calcium-rich water using either nitrate or urea as the sole nitrogen source. This is the first report of the engineering of a *Cyanothece* strain for the photosynthetic production of a chemical. It is also the first demonstration that a terpene can be produced by an engineered cyanobacterium growing on urea as the sole nitrogen source. This

finding is interesting, because it could be important in the future to couple chemicals productions with wastewater treatment to reduce the costs (Veaudor et al., 2019).

MATERIALS AND METHODS

Bacterial Strains and Growth Condition

Cyanothece PCC 7425 and *Synechocystis* PCC 6803 were grown at 30°C, in the MM mineral medium that corresponds to BG-11 (Stanier et al., 1971) enriched with 3.78 mM Na_2CO_3 (Domain et al., 2004), under continuous agitation (140 rpm, Infors rotary shaker) and cool white light. The intensities were, respectively 1500–2000 lux (18.75–25.00 $\mu E.m^{-2}.s^{-1}$) for *Cyanothece* PCC 7425 and 2500 lux (31.25 $\mu E.m^{-2}.s^{-1}$) for *Synechocystis* PCC 6803. Both of them were also grown on MM solidified with 10% Bacto Agar (Difco). For some experiments performed with *Cyanothece* PCC 7425, MM was supplemented with 9.52 mM $NaHCO_3$ and 2.92 mM $CaCl_2$ (hereafter designated as MM_{CaC}) and/or nitrate was replaced by urea (1–4 mM), as indicated. In these latter cases, nitrate-grown cells were washed twice with nitrate-free medium before resuspension in urea-containing medium.

Escherichia coli strains MC1061 (Casadaban and Cohen, 1980), TOP10 (Invitrogen) or XL1-Blue (Agilent) were used for gene manipulations and/or conjugative transfer (CM404, Mermet-Bouvier et al., 1993) of RSF1010-derived replicative plasmids to *Cyanothece* PCC 7425 and *Synechocystis* PCC 6803 (CM404) (**Supplementary Table S1**). They were grown on LB medium at 30°C (CM404 and all cells harboring pFC1 derivatives) or 37°C (all other strains). Antibiotic selections were as follows for *E. coli*: chloramphenicol (Cm) 34 $\mu g.mL^{-1}$, kanamycin (Km) 50 $\mu g.mL^{-1}$, streptomycin (Sm) 25 $\mu g.mL^{-1}$ and spectinomycin (Sp) 75 $\mu g.mL^{-1}$; for *Cyanothece* PCC 7425: Cm 10 $\mu g.mL^{-1}$, Km 25 $\mu g.mL^{-1}$, Sm 2 $\mu g.mL^{-1}$, and Sp 10 $\mu g.mL^{-1}$; for *Synechocystis* PCC 6803: Km 50 $\mu g.mL^{-1}$, Sp 5 $\mu g.mL^{-1}$, and Sm 5 $\mu g.mL^{-1}$.

Conjugative Transfer of RSF1010-Derived Plasmids to *Cyanothece* PCC 7425 or *Synechocystis* PCC 6803

All plasmids were transferred from *E. coli* to cyanobacterial cells by trans-conjugation (Mermet-Bouvier et al., 1993), using a simplified and more efficient procedure involving a triparental mating and the co-incubation of *E. coli* and recipient cyanobacterial cells on solid medium. Five mL overnight-grown cultures of *E. coli* CM404 harboring the self-transferable mobilization vector (pRK2013, a derivative of RP4, Mermet-Bouvier et al., 1993) and a 5 mL overnight grown culture of *E. coli* strains harboring one of the studied pSB2A- or pFC1-derivative plasmids were washed twice with LB and resuspended separately into 800 µL LB (final concentration of 1.3×10^9 cells.mL^{-1}). Hundred µL *Cyanothece* PCC 7425 mid-log phase culture (about 1.25×10^7 cells) were mixed with 30 µL of a CM404 *E. coli* culture and 30 µL of a culture of an *E. coli* strain harboring a studied plasmid. Then, 30 µL aliquots of the *E. coli* and cyanobacterial mixture were spotted onto non-selective MM agar plates that were incubated at 30°C for 72 h under light (1500 lux, 18.75 $\mu E.m^{-2}.s^{-1}$). Then, 4 spots were resuspended into 200 µL of fresh MM medium. One 50 µL-aliquot was serially diluted in and plated on fresh MM to calculate the number of *Cyanothece* PCC 7425 cells (colony-forming units), while the other three 50 µL-aliquots were plated onto MM containing the selective antibiotics and incubated for 10 days under standard conditions to select the conjugant clones, and calculate the frequency of trans-conjugation. A negative control was realized by spreading onto antibiotic-containing MM plates *Cyanothece* PCC 7425 cells that were not co-incubated with *E. coli* cells to detect possible spontaneous antibiotic resistant mutant cells. Antibiotics resistant conjugant clones were re-streaked onto selective plates, prior to analyzing their plasmid content through PCR and DNA sequencing (Eurofins Genomics, see **Supplementary Table S2** for sequencing primers).

Spectrophotometric Assay of Chloramphenicol Acetyl-Transferase Activity

CAT assays were done basically as described for *Synechocystis* PCC 6803 (Ferino and Chauvat, 1989; Marraccini et al., 1993). *Cyanothece* PCC 7425 strains harboring the pSB2A or pSB2T plasmids were grown in MM_{CaC} at 30°C under 2000 lux (1×10^8 cells.mL^{-1}) washed twice and resuspended into 2 mL of 50 mM Tris-HCl, pH 8.0. Approximately 2.10^9 cells were broken in a chilled Eaton press (250 Mpa). Cell extracts were centrifuged (14,000 rpm, 4°C, 10 min) to remove cell debris and were either stored at −20°C until assay or used directly. 1–40 µL of cells extracts mixed with 200 µL of reaction solution (Tris HCl 100 mM pH 8, DTNB 0.4 mg.mL^{-1} and acetyl CoA 0.1 mM) were loaded into a 96-well plate (Greiner bio-one). Five µL of chloramphenicol at 5 mM was automatically added in each well by a microplate reader (ClarioStar; BMG Labtech). Immediately the absorption at 412 nm of the yellow TNB (5′-thio-2-nitrobenzoic acid) product was measured for 3 min at 30°C. Chloramphenicol acyltransferase activity was defined as the number of nanomoles of chloramphenicol acetylated per minute per mg protein that were quantified by the Bradford assay (Bio-Rad) using bovine serum albumin (0–10 µg BSA) as the standard.

Spectrophotometric Assay of Beta-Galactosidase Activity

β-galactosidase assays were done basically as described for *Synechocystis* PCC 6803 (Mermet-Bouvier and Chauvat, 1994). *Cyanothece* PCC 7425 strains harboring the pFCI or pPMB13 plasmids grown at 30°C in MM_{CaC} under 2000 lux (5×10^7 cells.mL^{-1}) were heat-induced by a fourfold dilution into prewarmed growth medium and then incubated for 168 h at the indicated temperatures (30–39°C). Roughly, 2×10^9 cells were washed, resuspended (in 2 mL Tris-HCl 50 mM pH 8.0), broken and centrifuged as described above. Immediately, 2–10 µL of cells extracts mixed with 200 µL of reaction solution (100 mM Na_2HPO_4/NaH_2PO_4 buffer pH 7.5, 50 mM β-mercaptoethanol)

were loaded into a clear 96-well plate (Greiner bio-one). Then, 40 μL of ONPG (of *o*-nitrophenol-galactoside) 4 mg.mL^{-1} in K_2HPO_4/KH_2PO_4 buffer, pH 7.5) were automatically added in each well with a microplate reader (ClarioStar; BMG Labtech). The reaction was immediately followed by measuring the absorption at 420 nm of the yellow ONP (*o*-nitrophenol) product for 3 min at 30°C. β-galactosidase activity was calculated as the number of micromoles ONPG hydrolyzed per minute per mg proteins, which were quantified by the Bradford assay.

Microscopy

Mid-log phase cultures of *Synechocystis* PCC 6803 and *Cyanothece* PCC 7425 cells harboring the pSB2TΔKm^R-gfp, pSB2T-ccmk1$_{tsbp1}$-gfp and pSB2T-maf$_{S6803}$-gfp plasmids were placed in sandwiches consisting of two glass coverslips (22 mm diameter, Paul Marienfeld GmbH & Co. KG) one of which being coated with a Poly-L-lysine (Sigma-Aldrich) monolayer. These coverslip sandwiches were sealed and placed inside a home-made sample holder, which was mounted on a Nikon Ti-U inverted microscope coupled with an iXon ULTRA 897 CCD camera (Andor Technology), equipped with a 100x oil immersion (NA 1.45) microscope objective. Epifluorescence images were recorded using an excitation provided by a plasma light source (HPLS245 Thorlabs, Inc.) and an excitation filter (MF469-35 Thorlabs, Inc.), while for super-resolution laser scanning images a 488 nm laser (OBIS, Coherent) was used as an excitation source.

Chlorophyll and GFP fluorescence were recorded using ET655LP (Chroma Technology Corporation) and MF525/39 (Thorlabs, Inc.) emission filters, respectively.

Limonene Collection and Quantification/Measurement by Gas Chromatography–Mass Spectrometry

Cyanothece PCC 7425 engineered for limonene production was grown photoautotrophically (1500–3500 lux) in 125- or 250-mL erlenmeyers respectively containing 25 or 50 mL cell suspensions overlaid with 20% (vol/vol) dodecane (analytical grade, Sigma-Aldrich) to trap limonene during the whole experimental time course. At time intervals, aliquots of 300 μL were harvested from the dodecane overlay. One μL samples were injected into a GC-MS [Trace1300 (GC) + ISQ LT (MS), ThermoScientific] equipped with a TG-5MS column (30 m × 0.25 mm × 0.25 μm) and operated with H_2 carrier gas at 1.0 mL.min^{-1}; ionization voltage 70 eV, split ratio of 25:1; transfer line temperature 250°C; ion source temperature 200°C. The oven program was as followed: 50°C (held for 1 min), 50–150°C (10°C min^{-1}), 150–250°C (20°C min^{-1}), and held for 5 min, with a total program of 21 min. Analysis were carried out in the selected ion monitoring mode: m/z = 50–650.

The limonene peak was identified based on its different ion chromatogram and retention time as compared to those of the α-pinene (Supelco 80599, Sigma-Aldrich) used as an internal standard. A standard curve at m/z = 136 was constructed by GC peak integration of serial dilutions of *S*-limonene (Supelco 62128, Sigma-Aldrich) pure standard in dodecane (**Supplementary Figure S9**). The limonene concentration in every dodecane sample was determined using this ratio and by taking-into-account the decrease of the dodecane overlay volume after each sample collection.

DATA AVAILABILITY STATEMENT

All datasets generated for this study are included in the article/**Supplementary Material**.

AUTHOR CONTRIBUTIONS

FC, CC-C, J-FS, and KB conceived the project. FC, CC-C, CC, ED-S, AG, BR, J-FS, and KB conceived the experiments. CC, ED-S, XK, SG, CI, SS, AG, EM, and D-AB performed the experiments. All authors analyzed the data, read and approved the manuscript. FC, CC-C, and CC drafted the manuscript. FC and CC-C wrote the manuscript. FC agreed to serve as the author responsible for contact and ensures communication.

FUNDING

This work was partly supported by the CEA-DRF PTNTE Greenfuels project, the ANR Harley project (ANR-19-CE44-0017-03), and the platform of Biophysics of I2BC supported by French Infrastructure for Integrated Structural Biology (FRISBI) ANR-10-INBS-05-05. ED-S received a post-doctoral fellowship from the CEA (PTNTE project Greenfuels). CC and SG received a Ph.D. fellowship from the CEA (SL-DRF-17-0106) and the MENESR, respectively.

ACKNOWLEDGMENTS

We thank Amélie Goudet for help using GC-MS apparatus.

SUPPLEMENTARY MATERIAL

The Supplementary Material for this article can be found online at: https://www.frontiersin.org/articles/10.3389/fmicb.2020.586601/full#supplementary-material

REFERENCES

Bandyopadhyay, A., Elvitigala, T., Welsh, E., Stöckel, J., Liberton, M., Min, H., et al. (2011). Novel metabolic attributes of the genus *Cyanothece*, comprising a group of unicellular nitrogen-fixing cyanobacteria. *mBio* 2:e00214-11. doi: 10.1128/mBio.00214-11

Blondeau, M., Sachse, M., Boulogne, C., Gillet, C., Guigner, J. M., Skouri-Panet, F., et al. (2018). Amorphous calcium carbonate granules form within an

intracellular compartment in calcifying cyanobacteria. *Front. Microbiol.* 9:1768. doi: 10.3389/fmicb.2018.01768

Cameron, J. C., Wilson, S. C., Bernstein, S. L., and Kerfeld, C. A. (2013). Biogenesis of a bacterial organelle: the carboxysome assembly pathway. *Cell* 155, 1131–1140. doi: 10.1016/j.cell.2013.10.044

Casadaban, M. J., and Cohen, S. N. (1980). Analysis of gene control signals by DNA fusion and cloning in *Escherichia coli*. *J. Mol. Biol.* 138, 179–207. doi: 10.1016/0022-2836(80)90283-1

Cassier-Chauvat, C., and Chauvat, F. (2014). "Cell division in cyanobacteria," in *The Cell Biology of Cyanobacteria*, eds E. Flores and A. Herrero (Norfolk: Caister Academic Press).

Cassier-Chauvat, C., and Chauvat, F. (2018). *Cyanobacteria: Wonderful Microorganisms for Basic and Applied Research*. Hoboken, NJ: John Wiley & Sons Ltd.

Cassier-Chauvat, C., Dive, V., and Chauvat, F. (2017). Cyanobacteria: photosynthetic factories combining biodiversity, radiation resistance, and genetics to facilitate drug discovery. *Appl. Microbiol. Biotechnol.* 101, 1359–1364. doi: 10.1007/s00253-017-8105-z

Cassier-Chauvat, C., Veaudor, T., and Chauvat, F. (2016). Comparative genomics of DNA recombination and repair in cyanobacteria: biotechnological implications. *Front. Microbiol.* 7:1809. doi: 10.3389/fmicb.2016.01809

Chauvat, F., Corre, B., Herdman, M., and Joset-Espardellier, F. (1982). Energetic and metabolic requirements for the germination of akinetes of the cyanobacterium Nostoc PCC 7524. *Arch. Microbiol.* 133, 44–49. doi: 10.1007/BF00943768

Chuck, C. J., and Donnelly, J. (2014). The compatibility of potential bioderived fuels with Jet A-1 aviation kerosene. *Appl. Energy* 118, 83–91. doi: 10.1016/j.apenergy.2013.12.019

Colby, S. M., Alonso, W. R., Katahira, E. J., McGarvey, D. J., and Croteau, R. (1993). 4S-limonene synthase from the oil glands of spearmint (*Mentha spicata*). cDNA isolation, characterization, and bacterial expression of the catalytically active monoterpene cyclase. *J. Biol. Chem.* 263, 23016–23024.

Dai, W., Chen, M., Myers, C., Ludtke, S. J., Pettitt, B. M., King, J. A., et al. (2018). Visualizing individual RuBisCO and its assembly into carboxysomes in marine cyanobacteria by cryo-electron tomography. *J. Mol. Biol.* 430, 4156–4167. doi: 10.1016/j.jmb.2018.08.013

Davies, F. K., Work, V. H., Beliaev, A. S., and Posewitz, M. C. (2014). Engineering limonene and bisabolene production in wild type and a glycogen-deficient mutant of *Synechococcus* sp. PCC 7002. *Front. Bioeng. Biotechnol.* 2:21. doi: 10.3389/fbioe.2014.00021

De Wever, A., Benzerara, K., Coutaud, M., Caumes, G., Poinsot, M., Skouri-Panet, F., et al. (2019). Evidence of high Ca uptake by cyanobacteria forming intracellular CaCO3 and impact on their growth. *Geobiology* 17, 676–690. doi: 10.1111/gbi.12358

Demay, J., Bernard, C., Reinhardt, A., and Marie, B. (2019). Natural products from cyanobacteria: focus on beneficial activities. *Mar. Drugs* 17:320. doi: 10.3390/md17060320

Domain, F., Houot, L., Chauvat, F., and Cassier-Chauvat, C. (2004). Function and regulation of the cyanobacterial genes lexA, recA and ruvB: LexA is critical to the survival of cells facing inorganic carbon starvation. *Mol. Microbiol.* 53, 65–80. doi: 10.1111/j.1365-2958.2004.04100.x

Ducat, D. C., Way, J. C., and Silver, P. A. (2011). Engineering cyanobacteria to generate high-value products. *Trends Biotechnol.* 29, 95–103. doi: 10.1016/j.tibtech.2010.12.003

Dutheil, J., Saenkham, P., Sakr, S., Leplat, C., Ortega-Ramos, M., Bottin, H., et al. (2012). The AbrB2 autorepressor, expressed from an atypical promoter, represses the hydrogenase operon to regulate hydrogen production in *Synechocystis* strain PCC6803. *J. Bacteriol.* 194, 5423–5433. doi: 10.1128/JB.00543-12

Ferino, F., and Chauvat, F. (1989). A promoter-probe vector-host system for the cyanobacterium, *Synechocystis* PCC6803. *Gene* 84, 257–266. doi: 10.1016/0378-1119(89)90499-X

Hamilton, T. L., Bryant, D. A., and Macalady, J. L. (2016). The role of biology in planetary evolution: cyanobacterial primary production in low-oxygen Proterozoic oceans. *Environ. Microbiol.* 18, 325–340. doi: 10.1111/1462-2920.13118

Hamoen, L. W. (2011). Cell division blockage: but this time by a surprisingly conserved protein. *Mol. Microbiol.* 81, 1–3. doi: 10.1111/j.1365-2958.2011.07693.x

Herrero, A., Stavans, J., and Flores, E. (2016). The multicellular nature of filamentous heterocyst-forming cyanobacteria. *FEMS Microbiol. Rev.* 40, 831–854. doi: 10.1093/femsre/fuw029

Houssen, W. E., Koehnke, J., Zollman, D., Vendome, J., Raab, A., Smith, M. C. M., et al. (2012). The discovery of new cyanobactins from *Cyanothece* PCC 7425 defines a new signature for processing of patellamides. *ChemBioChem* 13, 2683–2689. doi: 10.1002/cbic.201200661

Jansson, C., and Northen, T. (2010). Calcifying cyanobacteria-the potential of biomineralization for carbon capture and storage. *Curr. Opin. Biotechnol.* 21, 365–371. doi: 10.1016/j.copbio.2010.03.017

Jongedijk, E., Cankar, K., Buchhaupt, M., Schrader, J., Bouwmeester, H., and Beekwilder, J. (2016). Biotechnological production of limonene in microorganisms. *Appl. Microbiol. Biotechnol.* 100, 2927–2938. doi: 10.1007/s00253-016-7337-7

Klemke, F., Nürnberg, D. J., Ziegler, K., Beyer, G., Kahmann, U., Lockau, W., et al. (2016). CphA2 is a novel type of cyanophycin synthetase in N2-fixing cyanobacteria. *Microbiology* 162, 526–536. doi: 10.1099/mic.0.000241

Knoot, C. J., Ungerer, J., Wangikar, P. P., and Pakrasi, H. B. (2018). Cyanobacteria: Promising biocatalysts for sustainable chemical production. *J. Biol. Chem.* 293, 5044–5052. doi: 10.1074/jbc.R117.815886

Koksharova, O. A., and Wolk, C. P. (2002). A novel gene that bears a DnaJ motif influences cyanobacterial cell division. *J. Bacteriol.* 184, 5524–5528. doi: 10.1128/JB.184.19.5524-5528.2002

Legrand, B., Miras, Y., Beauger, A., Dussauze, M., and Latour, D. (2019). Akinetes and ancient DNA reveal toxic cyanobacterial recurrences and their potential for resurrection in a 6700-year-old core from a eutrophic lake. *Sci. Total Environ.* 687, 1369–1380. doi: 10.1016/j.scitotenv.2019.07.100

Liberton, M., Bandyopadhyay, A., and Pakrasi, H. B. (2019). Enhanced nitrogen fixation in a glgX-deficient strain of *Cyanothece* sp. strain ATCC 51142, a unicellular nitrogen-fixing cyanobacterium. *Appl. Environ. Microbiol.* 85:e02887-18. doi: 10.1128/AEM.02887-18

Lin, P. C., and Pakrasi, H. B. (2019). Engineering cyanobacteria for production of terpenoids. *Planta* 249, 145–154. doi: 10.1007/s00425-018-3047-y

Lin, P.-C., Saha, R., Zhang, F., and Pakrasi, H. B. (2017). Metabolic engineering of the pentose phosphate pathway for enhanced limonene production in the cyanobacterium *Synechocystis* sp. PCC 6803. *Sci. Rep.* 7:17503. doi: 10.1038/s41598-017-17831-y

MacCready, J. S., Basalla, J. L., and Vecchiarelli, A. G. (2020). Origin and evolution of carboxysome positioning systems in cyanobacteria. *Mol. Biol. Evol.* 37, 1434–1451. doi: 10.1093/molbev/msz308

Marbouty, M., Saguez, C., Cassier-Chauvat, C., and Chauvat, F. (2009). Characterization of the FtsZ-interacting septal proteins SepF and Ftn6 in the spherical-celled cyanobacterium *Synechocystis* strain PCC 6803. *J. Bacteriol.* 191, 6178–6185. doi: 10.1128/JB.00723-09

Marraccini, P., Bulteau, S., Cassier-Chauvat, C., Mermet-Bouvier, P., and Chauvat, F. (1993). A conjugative plasmid vector for promoter analysis in several cyanobacteria of the genera *Synechococcus* and *Synechocystis*. *Plant Mol. Biol.* 23, 905–909. doi: 10.1007/BF00021546

Marteyn, B., Domain, F., Legrain, P., Chauvat, F., and Cassier-Chauvat, C. (2009). The thioredoxin reductase-glutaredoxins-ferredoxin crossroad pathway for selenate tolerance in *Synechocystis* PCC6803. *Mol. Microbiol.* 71, 520–532. doi: 10.1111/j.1365-2958.2008.06550.x

Mazouni, K., Domain, F., Cassier-Chauvat, C., and Chauvat, F. (2004). Molecular analysis of the key cytokinetic components of cyanobacteria: FtsZ, ZipN and MinCDE. *Mol. Microbiol.* 52, 1145–1158. doi: 10.1111/j.1365-2958.2004.04042.x

Mermet-Bouvier, P., Cassier-Chauvat, C., Marraccini, P., and Chauvat, F. (1993). Transfer and replication of RSF1010-derived plasmids in several cyanobacteria of the genera *Synechocystis* and *Synechococcus*. *Curr. Microbiol.* 27, 323–327. doi: 10.1007/BF01568955

Mermet-Bouvier, P., and Chauvat, F. (1994). A conditional expression vector for the cyanobacteria *Synechocystis* sp. strains PCC6803 and PCC6714 or

Synechococcus sp. strains PCC7942 and PCC6301. *Curr. Microbiol.* 28, 145–148. doi: 10.1007/BF01571055

Min, H., and Sherman, L. A. (2010). Genetic transformation and mutagenesis via single-stranded DNA in the unicellular, diazotrophic cyanobacteria of the genus *Cyanothece*. *Appl. Environ. Microbiol.* 16, 7641–7645. doi: 10.1128/AEM.01456-10

Montgomery, B. L. (2015). Light-dependent governance of cell shape dimensions in cyanobacteria. *Front. Microbiol.* 6:514. doi: 10.3389/fmicb.2015.00514

Narainsamy, K., Marteyn, B., Sakr, S., Cassier-Chauvat, C., and Chauvat, F. (2013). "Genomics of the Pleïotropic Glutathione System in Cyanobacteria," in *Advances in Botanical Research*, ed. J. A. Callow (Amsterdam: Elsevier), 157–188. doi: 10.1016/b978-0-12-394313-2.00005-6

Ortega-Ramos, M., Jittawuttipoka, T., Saenkham, P., Czarnecka-Kwasiborski, A., Bottin, H., Cassier-Chauvat, C., et al. (2014). Engineering *Synechocystis* PCC6803 for hydrogen production: influence on the tolerance to oxidative and sugar stresses. *PLoS One* 9:e0089372. doi: 10.1371/journal.pone.0089372

Ponce-Toledo, R. I., Deschamps, P., López-García, P., Zivanovic, Y., Benzerara, K., and Moreira, D. (2017). An early-branching freshwater cyanobacterium at the origin of plastids. *Curr. Biol.* 27, 386–391. doi: 10.1016/j.cub.2016.11.056

Porta, D., Rippka, R., and Hernández-Mariné, M. (2000). Unusual ultrastructural features in three strains of *Cyanothece* (cyanobacteria). *Arch. Microbiol.* 173, 154–163. doi: 10.1007/s002039900126

Rippka, R., Deruelles, J., Waterbury, J. B., Herdman, M., and Stanier, R. Y. (1979). Generic assignments, strain histories and properties of pure cultures of cyanobacteria. *J. Gen. Microbiol.* 11, 1–61. doi: 10.1099/00221287-111-1-1

Sakamoto, T., Delgaizo, V. B., and Bryant, D. A. (1998). Growth on urea can trigger death and peroxidation of the cyanobacterium *Synechococcus* sp. strain PCC 7002. *Appl. Environ. Microbiol.* 64, 2361–2366. doi: 10.1128/AEM.64.7.2361-2366.1998

Sakr, S., Dutheil, J., Saenkham, P., Bottin, H., Leplat, C., Ortega-Ramos, M., et al. (2013). The activity of the *Synechocystis* PCC6803 AbrB2 regulator of hydrogen production can be post-translationally controlled through glutathionylation. *Int. J. Hydrogen Energy* 38, 13547–13555. doi: 10.1016/j.ijhydene.2013.07.124

Schirrmeister, B. E., Gugger, M., and Donoghue, P. C. J. (2015). Cyanobacteria and the great oxidation event: evidence from genes and fossils. *Palaeontology* 58, 769–785. doi: 10.1111/pala.12178

Singh, J. S., Kumar, A., Rai, A. N., and Singh, D. P. (2016). Cyanobacteria: a precious bio-resource in agriculture, ecosystem, and environmental sustainability. *Front. Microbiol.* 7:529. doi: 10.3389/fmicb.2016.00529

Sommer, M., Sutter, M., Gupta, S., Kirst, H., Turmo, A., Lechno-Yossef, S., et al. (2019). Heterohexamers formed by CcmK3 and CcmK4 increase the complexity of beta carboxysome shells. *Plant Physiol.* 179, 156–167. doi: 10.1104/pp.18.01190

Stanier, R. Y., Kunisawa, R., Mandel, M., and Cohen-Bazire, G. (1971). Purification and properties of unicellular blue-green algae (order Chroococcales). *Bacteriol. Rev.* 35, 171–205. doi: 10.1128/mmbr.35.2.171-205.1971

Sun, Y., Wollman, A. J. M., Huang, F., Leake, M. C., and Liu, L. N. (2019). Single-organelle quantification reveals stoichiometric and structural variability of carboxysomes dependent on the environment. *Plant Cell* 31, 1648–1664. doi: 10.1105/tpc.18.00787

Tracy, N. I., Chen, D., Crunkleton, D. W., and Price, G. L. (2009). Hydrogenated monoterpenes as diesel fuel additives. *Fuel* 88, 2238–2240. doi: 10.1016/j.fuel.2009.02.002

Veaudor, T., Cassier-Chauvat, C., and Chauvat, F. (2018). Overproduction of the cyanobacterial hydrogenase and selection of a mutant thriving on urea, as a possible step towards the future production of hydrogen coupled with water treatment. *PLoS One* 13:e0198836. doi: 10.1371/journal.pone.0198836

Veaudor, T., Cassier-Chauvat, C., and Chauvat, F. (2019). Genomics of urea transport and catabolism in cyanobacteria: biotechnological implications. *Front. Microbiol.* 10:2052. doi: 10.3389/fmicb.2019.02052

Wang, X., Liu, W., Xin, C., Zheng, Y., Cheng, Y., Sun, S., et al. (2016). Enhanced limonene production in cyanobacteria reveals photosynthesis limitations. *Proc. Natl. Acad. Sci. U.S.A.* 113, 14225–14230. doi: 10.1073/pnas.1613340113

Conflict of Interest: The authors declare that the research was conducted in the absence of any commercial or financial relationships that could be construed as a potential conflict of interest.

frontiers in Microbiology

ORIGINAL RESEARCH
published: 25 September 2020
doi: 10.3389/fmicb.2020.577266

Combination of Trace Metal to Improve Solventogenesis of *Clostridium carboxidivorans* P7 in Syngas Fermentation

Yi-Fan Han[1,2†], Bin-Tao Xie[1,2†], Guang-xun Wu[1,2], Ya-Qiong Guo[1,2], De-Mao Li[1,2] and Zhi-Yong Huang[1,2]*

[1] Tianjin Key Laboratory for Industrial Biological Systems and Bioprocessing Engineering, Tianjin Institute of Industrial Biotechnology, Chinese Academy of Sciences, Tianjin, China, [2] National Technology Innovation Center of Synthetic Biology, Tianjin, China

OPEN ACCESS

Edited by:
Fu-Li Li,
Qingdao Institute of Bioenergy and Bioprocess Technology (CAS), China

Reviewed by:
Yang Tan,
Chinese Academy of Sciences (CAS), China
Yu-Sin Jang,
Gyeongsang National University, South Korea

***Correspondence:**
Zhi-Yong Huang
huang_zy@tib.cas.cn

† These authors have contributed equally to this work

Specialty section:
This article was submitted to Microbiotechnology, a section of the journal Frontiers in Microbiology

Received: *29 June 2020*
Accepted: *04 September 2020*
Published: *25 September 2020*

Citation:
Han Y-F, Xie B-T, Wu G-x, Guo Y-Q, Li D-M and Huang Z-Y (2020) Combination of Trace Metal to Improve Solventogenesis of Clostridium carboxidivorans P7 in Syngas Fermentation. Front. Microbiol. 11:577266. doi: 10.3389/fmicb.2020.577266

Higher alcohols such as butanol (C4 alcohol) and hexanol (C6 alcohol) are superior biofuels compared to ethanol. *Clostridium carboxidivorans* P7 is a typical acetogen capable of producing C4 and C6 alcohols natively. In this study, the composition of trace metals in culture medium was adjusted, and the effects of these adjustments on artificial syngas fermentation by *C. carboxidivorans* P7 were investigated. Nickel and ferrous ions were essential for growth and metabolite synthesis during syngas fermentation by P7. However, a decreased dose of molybdate improved alcohol fermentation performance by stimulating carbon fixation and solventogenesis. In response to the modified trace metal composition, cells grew to a maximum OD_{600nm} of 1.6 and accumulated ethanol and butanol to maximum concentrations of 2.0 and 1.0 g/L, respectively, in serum bottles. These yields were ten-fold higher than the yields generated using the original composition of trace metals. Furthermore, 0.5 g/L of hexanol was detected at the end of fermentation. The results from gene expression experiments examining genes related to carbon fixation and organic acid and solvent synthesis pathways revealed a dramatic up-regulation of the Wood–Ljungdahl pathway (WLP) gene cluster, the *bcs* gene cluster, and a putative CoA transferase and butanol dehydrogenase, thereby indicating that both *de novo* synthesis and acid re-assimilation contributed to the significantly elevated accumulation of higher alcohols. The *bdh35* gene was speculated to be the key target for butanol synthesis during solventogenesis.

Keywords: *Clostridium carboxidivorans* P7, syngas fermentation, higher alcohol, molybdate, solventogenesis regulation

INTRODUCTION

To address the increasing and urgent demand for sustainable and clean energy production, the biosynthesis of alcohols such as ethanol and *n*-butanol using renewable resources has been receiving increased worldwide attention (Babu et al., 2017; Ullah et al., 2018; Kamani et al., 2019). Although the US Department of Energy has proposed that ethanol can be used as a major component for achieving the goals of renewable fuels, higher alcohols such as butanol and hexanol are less

Abbreviations: Ni, nickel; Fe, iron; Mo, molybdenum; ORP, oxidation reduction potential; WLP, Wood–Ljungdahl pathway.

hygroscopic, contain a higher volumetric energy density, and are less water soluble and less volatile, thereby making these alcohols much more promising for use as "drop-in" biofuels (Phillips et al., 2015). Additionally, higher alcohols exhibit much more flexibility compared to that exhibited by ethanol. For example, butanol is also an important precursor used in the paint, polymer, and plastic industries (Kushwaha et al., 2020). Owing to the decreasing price of petroleum, renewable bio-alcohol research has become increasingly focused on higher alcohols rather than on ethanol.

Clostridium carboxidivorans bacteria utilize CO, CO_2, and H_2 via WLP (Kim et al., 2020). Alcohols are the only major end-metabolites produced during the HBE process (Hexanol-Butanol-Ethanol process) in this species (Fernández-Naveira et al., 2017). The bioconversion of the gaseous substrates occurs in two stages that include the acidogenic phase and the solventogenic phase (Gottwald and Gottschalk, 1985; Huang et al., 1985; Duürre, 2005). During acidogenesis, acetate and butyrate are the primary metabolites, and there is a dramatic decrease in pH. To survive in such harsh environments, solventogenic clostridia initiate solventogenesis, during which the acids produced earlier are consumed and alcohols become the main metabolic products.

To maximize product acquisition, considerable relevant research, including global transcriptional, proteomic, and metabolomics research, has focused on HBE fermentation analyses. However, the mechanism underlying the metabolic shift from the acidogenic to the solventogenic phase remains unclear (Janssen et al., 2010; Jang et al., 2014; Cheng et al., 2019; Kim et al., 2020). Another vital problem for traditional ABE fermentation is that this technology uses high-starch feedstocks or molasses as substrates, and these are costly and exert a large impact on the food economy (Jiang et al., 2015; Rezania et al., 2020).

Inorganic nutrients are considered to be one of the four categories of molecules that are required for extant life. These nutrients primarily consist of molecules of only a few atoms such as H_2, N_2, CH_4, CO, and CO_2 that were released from volcanic exhalations in ancient times. Some transition metal ions such as cobalt, nickel, and iron possess centers that contain sulfido, carbonyl, and other ligands are catalytically active and promote the growth of organic superstructures through the process of carbon fixation. This is the theory that describes the chemoautotrophic origin of life (Wächtershäuser, 2006). Based on this theory, it has been speculated that the active-site structures of the enzymes involved in carbon fixation in *C. carboxidivorans* are often reminiscent of minerals. According to previous research, the active sites of bifunctional CO dehydrogenase (CODH)–acetyl–ScoA synthase (ACS), a key enzyme in the WLP of acetogens, contains nickel (Alfano and Cavazza, 2020).

Similar to its autotrophic relatives, the *C. carboxidivorans* strain P7 relies on the WLP to transform CO and CO_2 into acetyl-CoA that can be further metabolized into organic acids and alcohols (Drake et al., 2008; Bengelsdorf et al., 2018). Recently, trace metals have been reported to exert a large impact on cell growth and metabolite synthesis in *C. carboxidivorans* strain P7. Li et al. (2018) investigated the effects of zinc on syngas fermentation by the *C. carboxidivorans* strain P7, and they found that increasing the zinc concentration upregulated the expression of *fdh*II and *bdh* and led to enhanced cell growth and ethanol and butanol production. Using a statistical method, Shen et al. (2017b) found that a combination of trace metals used with variable-temperature cultivation could enhance alcohol synthesis during CO-rich off-gas fermentation by *Clostridium carboxidivorans* P7. In ATCC medium 1754, the optimum concentration of the trace metals was found to be 5-fold Ni^{2+}, Co^{2+}, $SeO_4{}^{2+}$, and $WO_4{}^{2+}$, 3.48-fold Cu^{2+}, 0.55-fold $MoO_4{}^{2+}$, 0.5-fold Zn^{2+} and $(NH_4)(_2)SO_4{\cdot}FeSO_4{\cdot}6H(_2)O$, and 44.32 mu M $FeCl_3{\cdot}6H(_2)O$. The production of alcohol and organic acid changed from 2.16 g/L and 2.37 g/L to 4.40 g/L and 0.50 g/L, respectively, and the alcohol-to-product ratio increased from 47.7% to 89.8%. Shen et al. (2017a) reported that when using an optimized combination of trace metals, the production of alcohol and organic acid changed from 2.16 g/L and 2.37 g/L to 4.40 g/L and 0.50 g/L, respectively, and this increased the alcohol-to-product ratio from 47.7% to 89.8%. The effects of tungsten and selenium on C1 gas bioconversion by an enriched anaerobic sludge and microbial community were also studied by Chakraborty et al. (2020). To date, a number of studies have been have been performed to examine the effects of trace metals on C1 gas fermentation by *Clostridium* spp. Trace metals not only serve as essential metal cofactors for metalloenzymes in the WLP and alcohol synthesis pathways (Chen, 1995; Korkhin et al., 1998; Bender et al., 2011), but they also regulate gene expression to reprogram the intracellular metabolic network in solvent-producing clostridia and acetogens (Matson et al., 2010; Wu et al., 2015). There have been few reports regarding the effects of combined trace metals on regulation of gene expression during C1 gas fermentation.

In this study, *C. carboxidivorans* P7 was fermented under simulated industrial converter gas conditions (50% CO/35% CO_2/15% H_2) in a modified medium. By varying the Ni, Fe, Co, Se, and Mo concentrations, it was revealed that Ni and Fe acted as two vital trace metals required for growth and metabolite synthesis. The concentration of molybdate was the key inhibitor of biomass accumulation and alcohol production. Based on kinetic analysis of product synthesis and CO utilization, we propose that molybdate-restricted CO consumption can hinder acid re-assimilation, ultimately leading to a failure in the transition from acidogenesis to solventogenesis. Furthermore, based on the newly published complete genome sequence of *C. carboxidivorans* P7, we constructed gene expression profiles of the WLP and the ethanol, butanol, acetate, and butyrate synthesis pathways under different fermentation conditions, and our results revealed the regulatory mechanism of molybdate on these pathways and identified a number of potential key genes that are involved in solventogenesis.

MATERIALS AND METHODS

Strain, Medium, and Cultivation

C. carboxidivorans P7 was generously provided by the laboratory of Professor Yang Gu (Li et al., 2015) and was maintained

at −80°C with 20% glycerol for long-term preservation. For cultivation, frozen cells were revived in modified Wilkins Chalgren Anaerobic Medium (ATCC medium no. 2713) for 36 h and then transferred to fresh medium until the $OD_{600\,nm}$ reached 1.0, which served as the seed for gas fermentation. We modified Wilkins Chalgren Anaerobic Medium by replacing 10 g/L of gelatin peptone with 10 g/L of fish peptone. The gas fermentation medium was formulated on the basis of modified standard acetogen medium (Li et al., 2015; Huang et al., 2016). The pH of the medium was adjusted to 6.0 using solid NaOH.

Preparation of Trace Element Solutions

Trace element solutions were prepared by mixing the reagents together in ddH_2O. The concentrations of the trace metals in the original recipe are presented in **Table 1**, and the concentrations are defined as 1x. Additionally, five different trace element solutions that lacked either **Ni**$Cl_2{\cdot}6H_2O$, $(NH_4)_2{\cdot}$**Fe**$SO_4{\cdot}6H_2O$, **Co**$Cl_2{\cdot}6H_2O$, Na_2**Se**O_4, or Na_2**Mo**$O_4{\cdot}2H_2O$ were prepared and have been defined as Ni (0x), Fe (0x), Co (0x), Se (0x), and Mo (0x), respectively. To determine the concentration of molybdate in the medium, the prepared medium was transported to SGS for quantitative analysis of Mo.

Syngas Fermentation in a Serum Bottle and a Bioreactor

A serum bottle (120 mL) containing 20 mL of modified standard acetogen medium was used for gas fermentation. The headspace of the bottle was purged using 99.995% nitrogen for 5 min and then sealed with a rubber stopper. All prepared serum bottles were sterilized at 121°C for 20 min. For gas fermentation, 1 mL of pre-cultured seed liquor was inoculated. The atmosphere within the headspace of the bottle was replaced with a simulated industrial converter gas (50% CO/35% CO_2/15% H_2) and pressurized to 0.2 MPa. Fermentation was performed at 37°C at an agitation speed of 200 rpm. Samples (1.5 mL) of the culture were acquired at 24-h intervals. The cell density, pH, metabolite concentration, and CO consumption were all analyzed. The gas atmosphere was replaced with fresh simulated industrial converter gas after each round of sampling to equalize the pressure. Gas fermentation experiments in serum bottles were performed in two batches. In each batch, three repeats were introduced. A 7-L bioreactor (New Brunswick, Eppendorf, United States) was used to investigate the effects of the novel trace metal composition under continuous gas-fed conditions. A 300-mL culture was inoculated in 3 L of fermentation medium, and fermentation was performed at 37°C with agitation at 200 rpm with a gas flow rate of 400 mL/min. Gas fermentation in the bioreactor was performed in two batches.

TABLE 1 | Concentration of metals in the original medium (1x).

Trace metal	(μM)
$(NH_4)_2{\cdot}$**Fe**$SO_4{\cdot}6H_2O$	20.40
Co$Cl_2{\cdot}6H_2O$	8.41
Zn$SO_4{\cdot}7H_2O$	6.96
Cu$Cl_2{\cdot}2H_2O$	1.49
Ni$Cl_2{\cdot}6H_2O$	0.84
Na_2**Mo**$O_4{\cdot}2H_2O$	0.83
Na_2**Se**O_4	1.06
Na_2**W**$O_4{\cdot}2H_2O$	0.61

Analytical Procedures

The pH was measured using an FE-20 FiveEasy Plus laboratory pH meter (METTLER TOLEDO, United States). The cell density, as represented by the optical density, was monitored using a UV-1800 ultraviolet spectrophotometer (SHIMADZU, Japan) at an OD of 600 nm. The ORP was measured using an S220 SevenCompact^{TM} pH/Ion Meter (METTLER TOLEDO, Switzerland). The fermentation products were measured according to an internal standard method (Huang et al., 2016) using gas chromatography (FULI GC-9790, Wenling, China) equipped with a flame ionization detector and a capillary column (Zebron ZB-WaxPlus, Phenomenex, United States). All samples were prepared by centrifugation at 12,000 × *g* at 4°C for 5 min followed by filtration of the supernatant with 0.22-μm filters. The analysis was performed using the following program: oven temperature, 150°C; injector temperature, 180°C; and detector temperature, 180°C.

The CO concentration in the gas samples was analyzed using another gas chromatograph (Tianmei GC-7900, Shanghai, China) that was equipped with a TDX-01 80/100 mesh column (Techcomp, China) and a thermal conductivity detector. Helium was used as the carrier gas. The injector and detector temperatures were set to 80°C and 180°C, respectively, while the oven temperature was maintained at 150°C. The following equation was used to quantify CO based on the scheme presented in **Figure 1**:

$$n = (V1 + V2) \times C_0$$

where C_0 is the concentration of CO under standard atmospheric pressure as quantified by the standard curve method, $V1$ is the gas volume in the serum bottle as calculated by subtracting the culture volume from the total volume of serum bottle, $P1$ is the

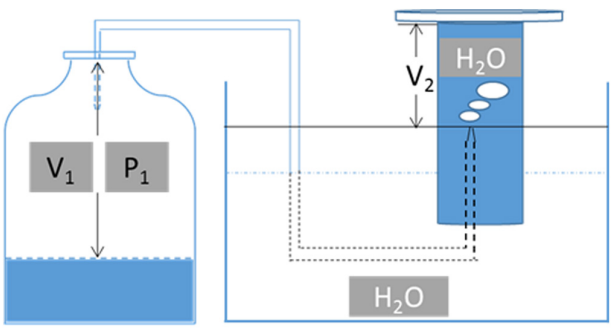

FIGURE 1 | Schematic diagram for gas volume monitoring during fermentation. V1, the gas volume in the serum bottle, calculated by the total volume of the serum bottle minus the culture volume; P1, pressure in the serum bottle during gas fermentation; V2, the volume of H_2O pushed out when transforming P1 into standard atmospheric pressure.

pressure in the serum bottle during gas fermentation, and $V2$ is the volume of H_2O pushed out when transforming $P1$ into standard atmospheric pressure (**Figure 1**).

Relative Gene Expression Profiles Detected by qPCR

Gene expression profiles were constructed for the Mo (0x) and Mo (1x) groups. Bacteria grown to mid-log phase (approximately 36 h of fermentation) were harvested using a Sorvall ST 16R centrifuge at 6,000 × *g* at 4°C for 5 min (Thermo Scientific, United States). The cell pellets were immediately frozen in liquid nitrogen and stored at −80°C. Total RNA was extracted using the Bacteria Total RNA Extraction kit (TIANGEN, Beijing, China) according to the manufacturer's instructions. The RNA concentration and quality were determined using a Biophotometer Plus (Eppendorf, Hamburg, Germany) combined with gel electrophoresis analysis. Primers specific for 16S rDNA were used to test for DNA contamination in the total RNA samples (Metcalf et al., 2010). An aliquot (0.5 μg) of RNA was used to generate cDNA using the RevertAid First Strand cDNA Synthesis Kit (Thermo Scientific, Lithuania, EU) using random primers at 42°C for 30 min. cDNA (3 μL) and 0.3 μL of 20 μM gene-specific primers (**Supplementary Table S1**) were then mixed with the SYBR® Select Master Mix (Applied Biosystems, Austin, TX, United States) to a final volume of 20 μL. The details of the detected genes are listed in **Table 2**, and these details are based on the genome accession number NZ_CP011803.1 (Li et al., 2015) and genomic analysis reported by Bruant et al. (2010). A LightCycler 96 real-time PCR system (Roche Diagnostics, Mannheim, Germany) was used to amplify and quantify the PCR products. The reaction mixtures were incubated for 5 min at 95°C, and this was followed by 40 amplification cycles of 10 s at 95°C and 30 s at 60°C. All reactions were performed in 96-well reaction plates. The transcript abundance of these genes was normalized to the housekeeping gene *guk* (formyl-tetrahydrofolate synthetase) that is constitutively expressed under the tested conditions (unpublished data). The relative transcript abundance levels of the studied genes were calculated using the $2^{-\Delta\Delta CT}$ method (Livak and Schmittgen, 2001). Fold changes of >2 or <0.5 were considered to be significant gene expression changes. Quantitative real-time PCR was performed in triplicate for each sample in every experiment, and the results were confirmed using biological duplicates.

RESULTS

Effect of the Absence of Nickel, Iron, Cobalt, Selenium, and Molybdenum on Cell Growth and Product Synthesis

The maximum OD_{600nm} (1.2) of strain P7 was achieved in medium containing the full level of trace metals (**Figure 2**). The concentrations of the accumulated acetate and butyrate reached their maximum on day 3, and these concentrations were 2.09 g/L and 0.08 g/L, respectively. At the same time, the ethanol and butanol concentrations also reached their highest concentrations, and these were 0.89 g/L and 0.08 g/L, respectively. The hexanol titer was too low to be detected.

In the medium without Ni^{2+}, evident deficiencies in both cell growth and metabolite synthesis were observed. The maximum acetate concentration was only 0.12 g/L, and no butyric acids and alcohols were detected. In the Fe (0x) medium, the values for the cell density and all of the product titers were reduced to approximately half of their values under the original medium conditions.

Without Co^{2+} and SeO_4^{2-} supplementation in the medium, there were no significant effects on growth and product synthesis. In this study, molybdate was a key trigger for gas fermentation by strain P7. The actual concentration of Mo in the medium of Mo (0x) and Mo (1x) was analyzed by SGS test. There was 23ug/L of Mo in the Mo (0x) medium and 55 ug/L of Mo in the Mo (1x) medium (**Supplementary Figures S1, S2**). Of note, the cell density reached a maximum OD_{600nm} of approximately 1.6 Abs in the Mo (0x) medium. Furthermore, the acetate and butyrate concentrations dramatically declined to 0.15 g/L and 0.05 g/L, respectively, while the ethanol and butanol yields were significantly increased to 1.66 g/L and 0.84 g/L, respectively. Additionally, 0.3 g/L of hexanol was produced on day 3, while the other treatments produced no detectable hexanol.

Effect of Molybate on Cell Density, CO Utilization, and Metabolite Synthesis

Syngas fermentation was performed using three biological replicates under a 50% CO/35% CO_2/15% H_2 atmosphere. The response of *C. carboxidivorans* P7 toward molybdate was assessed by comparing cell growth, CO consumption, and metabolite synthesis in the Mo (0x) and Mo (1x) setups.

Both cultures of *C. carboxidivorans* P7 in Mo (0x) and Mo (1x) media entered the stationary phase after two days of cultivation, and the maximum values of OD_{600nm} were approximately 1.5 and 1, respectively (**Figure 3**). In the Mo (1x) group, acetate and butyric acid accumulated throughout the fermentation process and produced ethanol and butanol starting from days 2 and 3, respectively. The highest concentrations of acetate and butyric acid were 2.59 g/L and 0.32 g/L, respectively, at day 5. The accumulation of ethanol and butanol reached maximum levels of 1.19 g/L and 0.18 g/L, respectively, at day 3, and these levels then declined from day 4 to day 5 (**Figure 3A**). In the Mo (0x) group, the concentrations of acetic acid and butyric acid reached maximum levels (0.97 and 0.32 g/L, respectively) on day 1 and day 2, respectively, and these levels then began to decline. Ethanol was produced simultaneously with cell growth, while the synthesis of butanol and hexanol began on days 2 and 3, respectively. The peak concentration of ethanol was 2.17 g/L on day 4, while the maximum titer of butanol was 1.10 g/L on day 3. On day 4, the concentration of hexanol reached its maximum value of 0.43 g/L (**Figure 3B**).

TABLE 2 | Targeted genes and relevant metabolic pathways.

Gene locus	Gene	Function	Pathway
Ccar_00570	*guk*	Guanylate kinase	Reference gene
Ccar_18835	*fhs*	Formate–tetrahydrofolate ligase	WLP gene cluster
Ccar_18790	*acsE*	CODH/ACS complex, methyltransferase subunit	
Ccar_18795	*acsC*	Corrinoid iron-sulfur protein large subunit	
Ccar_18800	*acsD*	Corrinoid iron-sulfur protein small subunit	
Ccar_18805	*CooCI*	Carbon monoxide dehydrogenase	
Ccar_18840	*CooCII*	Carbon monoxide dehydrogenase	
Ccar_18845	*acsA*	CODH/ACS complex, CODH subunit	
Ccar_18785	*acsB*	Acetyl-CoA decarbonylase/synthase complex subunit alpha/beta	
Ccar_18815	*metF*	Methylenetetrahydrofolate reductase	
Ccar_18825	*folD*	Methylene-tetrahydrofolate dehydrogenase/formyltetrahydrofolate cyclohydrolase	
Ccar_01740	*fdhI*	Formate dehydrogenase	CO_2 reduction or formate oxidization
Ccar_16080	*fdhII*	Formate dehydrogenase	
Ccar_03945	*fdhIII*	Formate dehydrogenase	
Ccar_13505	*fdhIV*	Formate dehydrogenase	
Ccar_16050	*fdhV*	Formate dehydrogenase	
Ccar_22795	*bcd*	Butyryl-CoA dehydrogenase	Butyral-CoA synthesis from acetyl-CoA
Ccar_22780	*crt*	Crotonase	
Ccar_22785	*hbd*	3-Hydroxybutyryl-CoA dehydrogenase	
Ccar_22790	*thl*	Acetyl-CoA acetyltransferase	
Ccar_22800	*etfB*	Electron transfer flavoprotein	
Ccar_22805	*etfA*	Electron transfer flavoprotein subunit alpha	
Ccar_00690	*pta*	Phosphate acetyltransferase	Acetate synthesis from acetyl-CoA
Ccar_00695	*ack*	Acetate kinase	
Ccar_19520	*ptb*	Phosphate butyryltransferase	Butyrate synthesis from butyral-CoA
Ccar_19515	*buk*	Butyrate kinase	
Ccar_07995	*adh*	Acetaldehyde dehydrogenase	Alcohol synthesis from acetyl-CoA and butyral-CoA
Ccar_00050	*bdh50*	NAD(P)H-dependent butanol dehydrogenase	
Ccar_04610	*bdh10*	NADPH-dependent butanol dehydrogenase	
Ccar_24835	*bdh35*	NADPH-dependent butanol dehydrogenase	
Ccar_25840	*bdh40*	NADPH-dependent butanol dehydrogenase	
Ccar_01440	*CoAT*	CoA transferase	Acid re-assimilation

To provide more insight into the differences between the two fermentation groups, the consumption of CO was investigated. In both groups, the utilization of CO was observed throughout the entire fermentation period, and the results are shown in **Supplementary Table S2**. The total consumption of CO was 29.06 mmol in the Mo (0x) group and 22.67 mmol in the Mo (1x) group (**Supplementary Table S2**), thereby indicating that more carbon was immobilized in the Mo (0x) group than that in the Mo (1x) group.

Comparison of the Gene Expression Profiles of WLP During Syngas Fermentation Under Different Molybdenum Concentrations

Based on the complete genome sequence information recently published by Li et al. (2015) and the genomic analysis performed by Bruant et al. (2010), the key enzymes responsible for acetyl-CoA synthesis from CO and CO_2 were all recognized in the *C. carboxidivorans* P7 chromosome. We updated and remapped the WLP gene cluster (**Table 2**, and it ranged from Ccar_18775 to _18845 and contained 15 genes (Pierce et al., 2008; Bruant et al., 2010). Formate dehydrogenase (FDH), the enzyme responsible for CO_2 reduction or formate oxidization, is not present in the WLP gene cluster. Five genes scattered throughout the genome were identified as FDH. These genes included Ccar_01740 (fdhI), Ccar_16080 (fdhII), Ccar_03945 (fdhIII), Ccar_13505 (fdhIV), and Ccar_16050 (fdhV), and they encode two selenocysteine-containing formate dehydrogenase H enzymes, a predicted formate dehydrogenase, a formate dehydrogenase accessory protein, and a predicted formate dehydrogenase D, respectively. We observed no significant difference in the expression levels of these five genes in cultures grown under Mo (0x) and Mo (1x) conditions (**Figure 4**). Additionally, we assessed the expression levels of 11 genes in the WLP gene cluster that were annotated and assumed to be functional enzymes in this pathway (Drake et al., 2008; Bruant et al., 2010). Among these genes, the transcripts of Ccar_18845 (cooCII) were nearly undetectable under both conditions. In

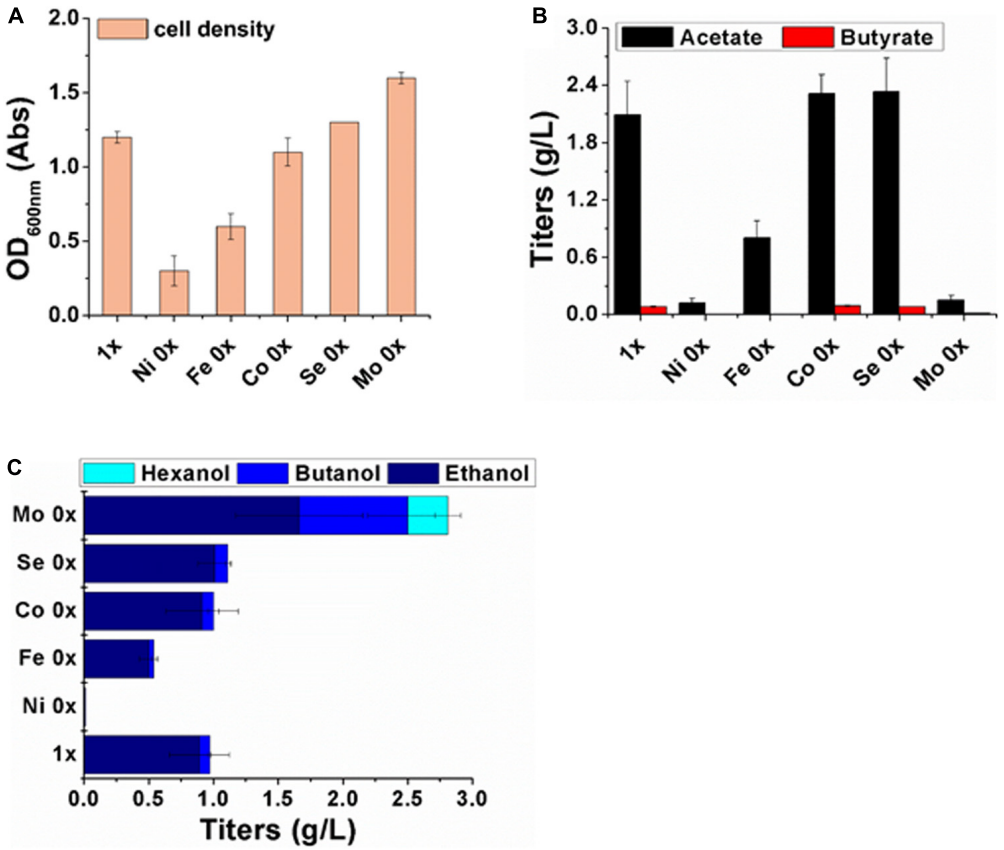

FIGURE 2 | Cell growth and metabolites analysis after 3 days of fermentation with different metal compositions. **(A)** Cell density; **(B)** concentrations of acetate (filled black column) and butyrate (filled red column); **(C)** concentrations of ethanol (filled dark blue), butanol (filled blue) and hexanol (filled light blue).

the absence of Mo, the other 10 genes in the WLP were significantly upregulated compared to those in the presence of Mo (1x) (**Figure 4**).

Comparison of the Gene Expression Profiles of the Metabolite Synthesis Pathways During Syngas Fermentation Under Different Molybdenum Concentrations

To elucidate the contrasting levels of gene expression and metabolite synthesis between the Mo (0x) and Mo (1x) conditions, we selected samples after 36 h of fermentation, as cultures at this point are at a stage of significantly different acid and alcohol syntheses. Based on information from a previous genome analysis (Li et al., 2015), we focused on genes involved in acetate (ack and pta), butyryl-CoA (crt, thl, and bcd), butyric acid (buk and ptb), ethanol (adh), and butanol (bdh) production. The expression levels of the acetate synthesis genes *ack* (Ccar_00695) and *pta* (Ccar_00690) were significantly downregulated in the Mo (0x) group (**Figure 5A**). Similar to the ABE fermentation performed by other Clostridia, *C. carboxidivorans* P7 converts acetyl-CoA into butyryl-CoA, which is the precursor for butyric acid and butanol synthesis, through *thl*, *hbd*, *crt*, *bcd*, *etfA*, and *etfB*. These six genes were clustered together on the chromosome from Ccar_22780 to Ccar_22805 and were all dramatically up-regulated under the Mo (0x) condition compared to levels observed in the Mo (1x) condition (**Figure 5B**). Two adjacent CDSs (Ccar_19515 and Ccar_19520) that encode *buk* and *ptb,* respectively, were involved in the conversion of butyryl-CoA to butyrate, and the expression levels of these genes exhibited no significant changes in response to alteration of the Mo concentration (**Figure 5C**). One CDS (Ccar_07995), present in the chromosome with two adjacent copies, was characterized as being involved in the ethanol and butanol production pathways. This gene encodes a bifunctional alcohol/acetaldehyde dehydrogenase that is involved in the conversion of acetyl-CoA to ethanol and butyryl-CoA to butanol. However, this *adh* gene exhibited no evident response to the change in Mo concentration (**Figure 5D**). In addition to *adh*, four *bdh* genes (*bdh50*, *bdh10*, *bdh40,* and *bdh35*) encoding a NAD(P)H-dependent butanol dehydrogenase and three different NADPH-dependent butanol dehydrogenases were also recognized on the P7 chromosome. Compared to levels in the Mo (0x) group, two of the NADPH-dependent butanol dehydrogenases (*bdh10* and *bdh35*) were significantly upregulated in Mo (1x). In particular, the expression level of *bdh35* exhibited a change of up to 20-fold, while the

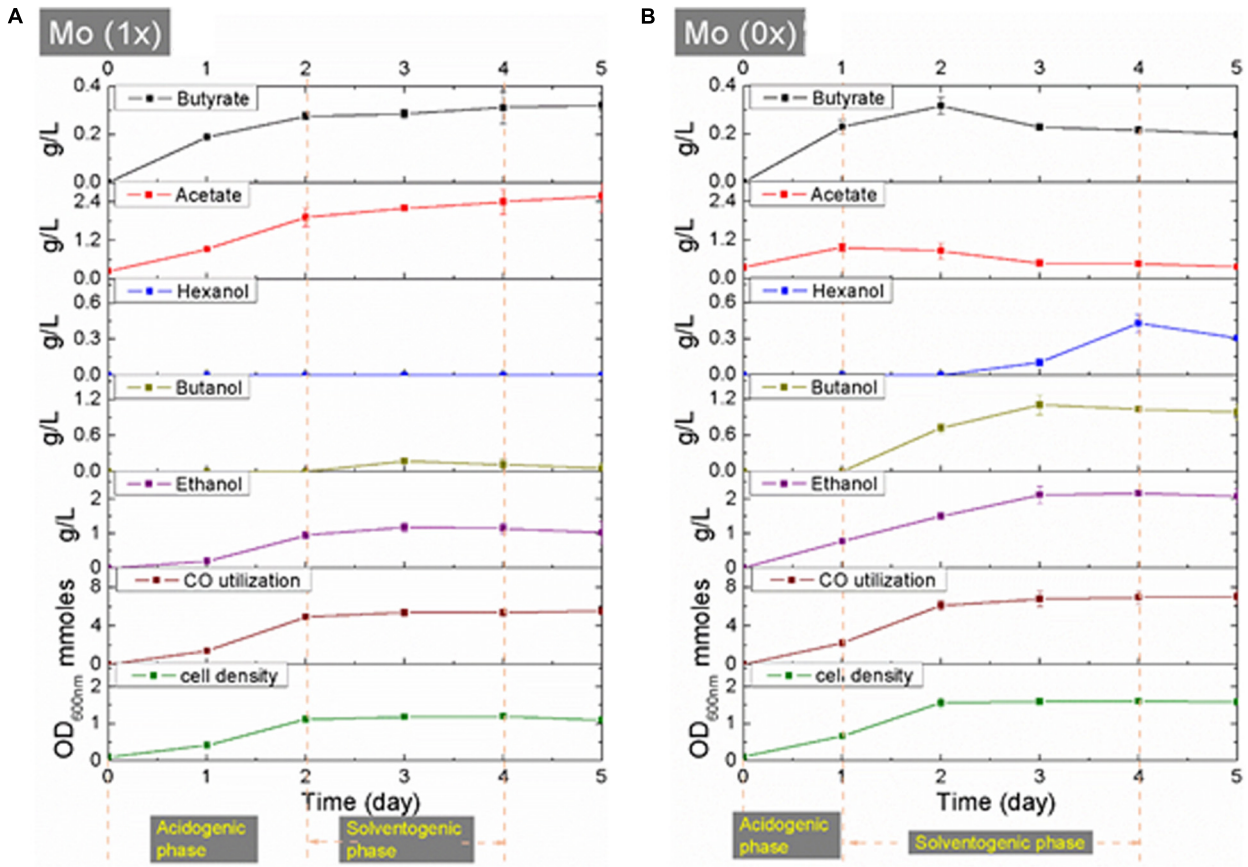

FIGURE 3 | (A,B) CO utilization, cell growth and product synthesis during fermentation under Mo (0x) and Mo (1x).

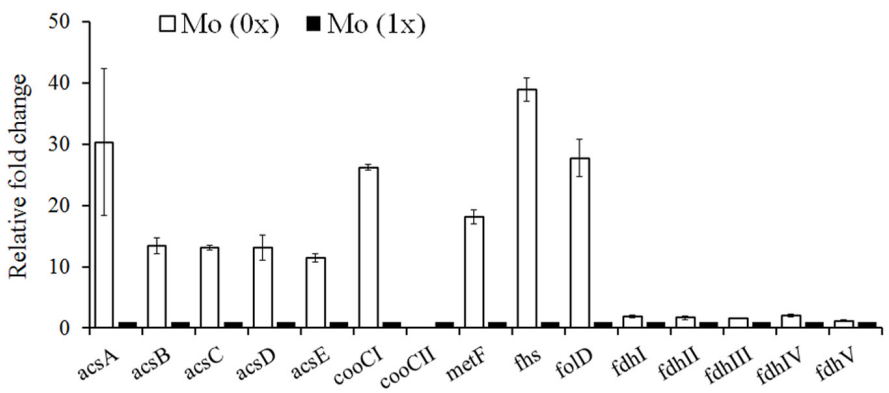

FIGURE 4 | Gene expression profiles of the carbon fixation which was similar with Mo (1x) in this research. In our work, combination of trace metal could improve solvent generation only and shift of acidogenesis to solvent producing in strain p7 was observed. Ratio of solvent to acid was almost 20:1. Regulation of trace metal not only stimulated producing, but also was a trigger of acid reusing in strain p7. Lower concentration of acid in fermenting liquor could benefit downstream operation. acsA, CODH/ACS complex, CODH subunit; acsB, acetyl-CoA decarbonylase/synthase complex subunit alpha/beta; acsC, corrinoid iron-sulfur protein large subunit; acsD, corrinoid iron-sulfur protein small subunit; acsE, CODH/ACS complex, methyltransferase subunit; cooC, carbon monoxide dehydrogenase; fdh, formate dehydrogenase; fhs, formyl-tetrahydrofolate synthase; folD, bifunctional methylene-tetrahydrofolate dehydrogenase/formyl-tetrahydrofolate cyclohydrolase; metF, methylene-tetrahydrofolate reductase.

transcript of *bdh40* was too low to be detected (**Figure 5D**). In contrast, the expression level of the NAD(P)H-dependent butanol dehydrogenase *bdh50* did not change significantly under the Mo (0x) condition. Additionally, the predicted CoA transferase gene *CoAT* (Ccar_01440) that is speculated to be involved in the conversion of acetate and butyrate to acyl-CoA

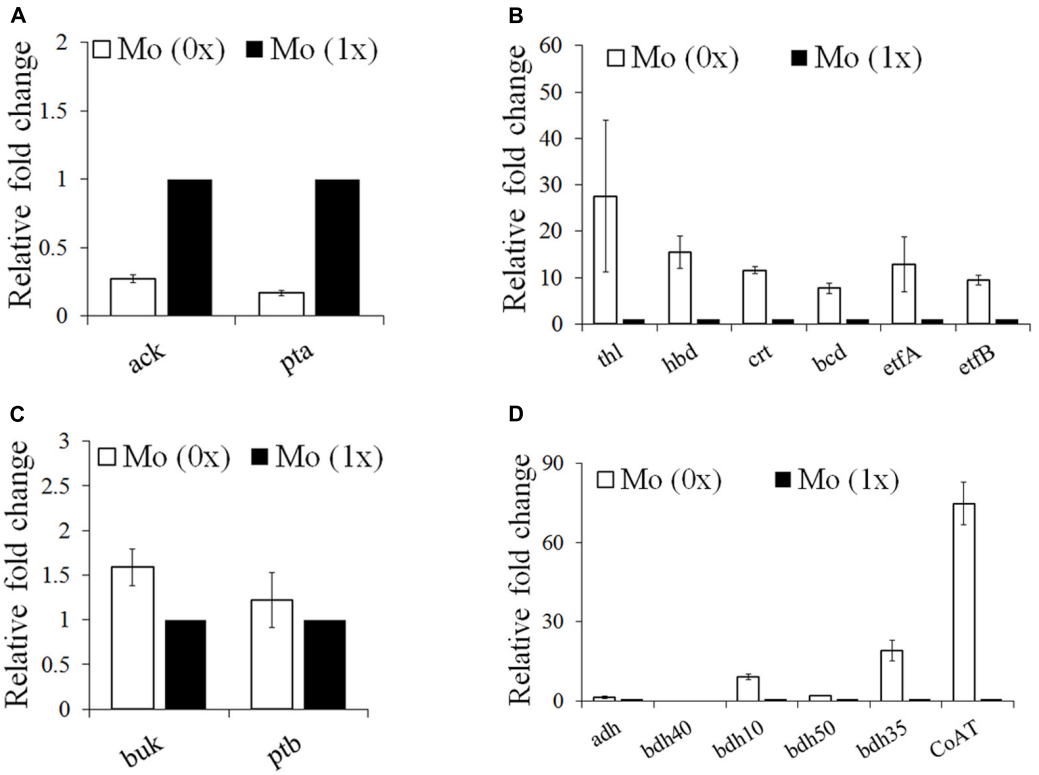

FIGURE 5 | Gene expression profiles of the acids and butyryl-CoA and alcohol synthesis pathways under Mo (0x) and (1x). **(A)** Acetate synthesis from acetyl-CoA; **(B)** butyryl-CoA synthesis from acetyl-CoA; **(C)** butyrate synthesis from butyryl-CoA; **(D)** alcohol synthesis and acid re-assimilation related genes. ack, acetate kinase; adh, bifunctional acetaldehyde/alcohol dehydrogenase; bcd, butyryl-CoA dehydrogenase; bdh, butanol dehydrogenase; buk, butyrate kinase; pta, phosphate acetyltransferase; thl, acetyl-CoA acetyltransferase; hbd, 3-hydroxybutyryl-CoA dehydrogenase; crt, crotonase; etfA, electron transfer flavoprotein subunit alpha; etfB, electron transfer flavoprotein; ptb, phosphate butyryltransferase; CoAT, CoA transferase.

and butyryl-CoA, respectively, was dramatically up-regulated by 70-fold (**Figure 5D**).

Syngas Fermentation in a 7-L Bioreactor With a Medium Containing Mo (0x)

Scaled-up syngas fermentation was performed using biological replicates (**Figure 6**). The highest cell density in the absence of Mo was 1.94. After 3 days of fermentation, bacteria entered the late log phase, and the acid concentration began to decrease until day 7. The pH values declined from day 0 to day 3. The maximum acetate and butyric acid concentrations (2 g/L and 0.3 g/L, respectively) were reached when the pH value was at the lowest point (∼4.6) (**Figure 6**). The alcohol yield increased significantly during the late log phase of growth, and the pH value also began to increase during this period. The highest pH value was 6.2. The highest ethanol, butanol, and hexanol yields were 3.2 g/L, 1 g/L, and 0.6 g/L, respectively (**Figure 6B**).

DISCUSSION

Effects of Specific Trace Metals

In WLP, CODH, FDH, and H2ase that are involved in CO oxidation, CO_2 reduction, and H_2 oxidization, respectively, are all recognized as iron-sulfur proteins (Saxena and Tanner, 2011). Moreover, an iron-nickel-sulfur metal cluster was found to act as a critical component of the active sites of both CODH and ACS, which are responsible for acetyl-CoA synthesis. Oxidization of CO and H_2 is the source of the reducing pool for acetogens under autotrophic conditions, and this process is not only tightly connected to ATP synthesis through the electron bifurcation mechanism or the cytochrome-based electron transport chain, but is also closely related to alcohol production via acetyl-CoA and butyryl-CoA reduction. Hence, the absence of nickel and iron should lead to a decrease in growth and metabolite synthesis, as reported in *C. ragsdalei* (Saxena and Tanner, 2011). However, the total cessation of cell growth under the Ni (0x) condition indicates that nickel is a key element for life in autotrophic solvent-producing clostridia.

Decreasing molybdenum concentrations dramatically promotes cell growth and alcohol synthesis, particularly for C4 and C6 alcohols. This negative regulation of alcohol synthesis by molybdenum is consistent with that mentioned in Shen's report (Li et al., 2018). Moreover, molybdenum exerted no significant effect on cell growth or metabolite synthesis in *C. ragsdalei* (Saxena and Tanner, 2011), thereby indicating that the function of molybdenum was species-specific. In acetogens, Mo and/or tungsten are reported to serve as cofactors of

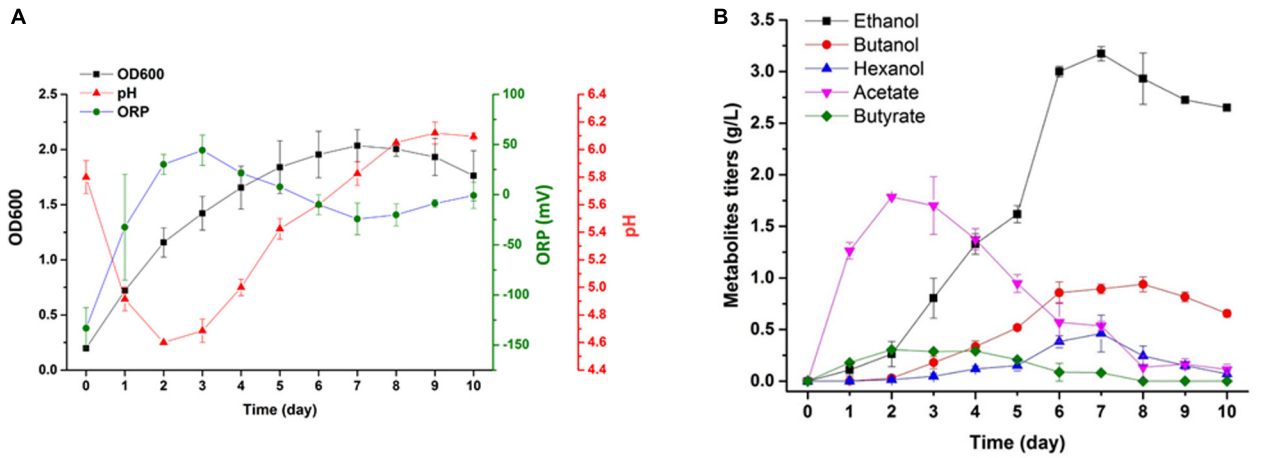

FIGURE 6 | Cell growth, pH, ORP and product monitoring in a 7 L bioreactor under Mo (0x). **(A)** Cell density (filled black square), pH value (red triangle), and ORP value (green circle); **(B)** concentrations of acetate (inverted purple triangle), butyrate (green diamond), ethanol (black square), butanol (red circle) and hexanol (blue triangle).

FDH_H, which is a key enzyme for catalyzing CO_2 to formate conversion in WLP (Zhu and Tan, 2009). There are two types of FDH_H enzymes, including: molybdenum-containing formate dehydrogenase and tungsten-containing formate dehydrogenase. These two enzymes possess similar structures and functions. In strain P7, there might be a tungsten-containing formate dehydrogenase that lost its activity in Mo-supplemented medium (Fontecilla-Camps et al., 2009).

Kinetic Analysis of Syngas Fermentation Under Different Molybdenum Concentrations

In solventogenic clostridia, C4 and C6 alcohols are generally synthesized through *de novo* synthesis and acid re-assimilation. *De novo* synthesis relies on the CoA-dependent Clostridium route (Zhang et al., 2012), while acid re-assimilation occurs via the function of carboxylic acid reductase or CoA transferase (Jones and Woods, 1986; Papoutsakis, 2008; Köpke et al., 2010). Time-course analyses of the acetate and butyrate concentrations revealed that removing molybdenum clearly reduced the acidogenic phase, activated acid re-assimilation, and prolonged the solventogenic phase. Moreover, cell growth and substrate utilization were also considerably increased. These results indicate that molybdenum may play a key role not only in affecting specific enzyme activity, but also in global metabolic networking in the gas fermentation process in *C. carboxidivorans* strain P7 (Alissandratos et al., 2013; Mintmier et al., 2020). In contrast, we expected that the external pH pressure and the concentration of undissolved organic acid would be two important factors for successful acid re-assimilation (Ramio-Pujol et al., 2015; Xie et al., 2015; Shen et al., 2017b). However, in this study, the external pH value was 5.1 when P7 shifted to acid-re-assimilation. This was much higher than the typical shifting point of ∼ 4.8, thereby indicating that the variation of trace metals was essential for metabolic shifting from acidogenesis to solventogenesis. Thus, it can be hypothesized that the intracellular metabolic model can be properly adapted to alcohol production by fine-tuning the trace metals within the medium of *C. carboxidivorans* P7.

In this study, the maximal productivity was 1.25g/L·d of ethanol, 0.47g/L·d of butanol, and 0.34g/L·d of hexanol in a 7-L CTRS bio-reactor. The total productivity of the solvent was 2.06g/L·d. According to previous research examining *C. carboxidivorans*, a maximal productivity of 2.5g/L·d of ethanol was achieved in a CTRS bio-reactor combined with monolithic packs for cell immobilization and 3.5g/L·d of ethanol in a CTRS bio-reactor coupled with a hollow fiber membrane. These accessories could immobilize cells and increase the mass transfer coefficient of gas to liquid. Although the productivity observed in these studies was higher than that reported by our study, 1.25g/L-1·d and 2.8g/L·d of acetate were also produced in their system (Shen et al., 2014a,b). The production of acid and solvent was simultaneous in their study, and this was similar to our observations using Mo (1x) in this study. In our work, a combination of trace metals could improve only solvent generation, and a shift from acidogenesis to solvent production in strain p7 was achieved. The solvent to acid ratio was nearly 20:1. Regulation of molybdenum concentration not only affected fermentation productivity, but also triggered acid reuse in strain p7. A lower concentration of acid in the fermenting liquor was found to benefit downstream operation.

Effect of Different Molybdenum Concentrations on Gene Expression Profiles

We expected molybdenum to act as a cofactor for FDH in a number of clostridia, and we also expected it to bind to tungsten active sites in enzymes. However, the regulatory role of FDH in the intracellular network in autotrophic solvent-producing clostridia remains unknown. Thus, the

gene expression profiles of the WLP, acetate, butyrate, ethanol, and butanol synthesis pathways were examined to elucidate the regulatory role of molybdenum on syngas fermentation of *C. carboxidivorans* P7 and to identify potential key genes responsible for substrate utilization and solventogenesis. Compared to the Mo (1x) medium, the carbon fixation and butyryl-CoA synthesis pathways were significantly up-regulated when Mo was decreased in the Mo (0x) medium (**Figure 6**), and these findings are consistent with improved CO consumption and cell growth. The expression levels of the acetate synthesis genes *ack* (Ccar_00695) and *pta* (Ccar_00690) were found to be significantly downregulated in Mo (0x) medium, and this was consistent with the decrease in the acetate yield during 24 h of syngas fermentation. Among the three NADPH-dependent butanol dehydrogenases that were predicted to be highly related to solventogenesis, only *bdh10* and *bdh35* were significantly upregulated (especially *bdh35*), indicating that these two genes are potential key genes for higher alcohol production in *C. carboxidivorans* P7. Furthermore, expression of the predicted CoA transferase gene *CoAT* (Ccar_01440), that is thought to be involved in the transition from acetate and butyrate to acyl-CoA and butyryl-CoA, was dramatically up-regulated by 70-fold, thereby indicating an evident acid re-assimilation effect in low-concentration molybdenum medium. In summary, we hypothesize that a relatively low concentration of molybdenum leads to up-regulation of the WLP gene cluster, ultimately resulting in improved substrate utilization and acetyl-CoA accumulation. These factors, in combination with the down-regulation of the acetate and butyrate synthesis pathways and the up-regulation of solventogenesis-related genes, ultimately result in improved alcohol production (**Figure 7**).

Elucidation of Carbon Destinations

Cell growth stagnated on day 4. The total amount of CO consumed on day 4 was re-calculated and found to be 22.04 mmol in the Mo (0x) group and 17.12 mmol in the Mo (1x) group. The total amount of carbon in the selected metabolites was 3.951 mmol in the Mo (0x) group and 3.02 mmol in the Mo (1x) group on day 4. The total amount of immobilized carbon was higher in the former; however, the proportion of carbon conversion from CO to metabolites was similar in the two groups, with 17.93% in the Mo (0x) group and 17.64% in the Mo (1x) group. Redundant fixed carbon flowed to form the cellular skeleton or to provide reducing power, and this was supported by data showing a higher cell density and titers of alcohol in the Mo (0x) group compared to the values in the Mo (1x) group. In regard to the converted carbon in the metabolites, approximately 87.12% was converted to produce alcohol in the Mo (0x) group, while only 37.36% was converted in the Mo (1x) group. A high ratio of alcohol in fermenter liquor could reduce the cost of the recovery process.

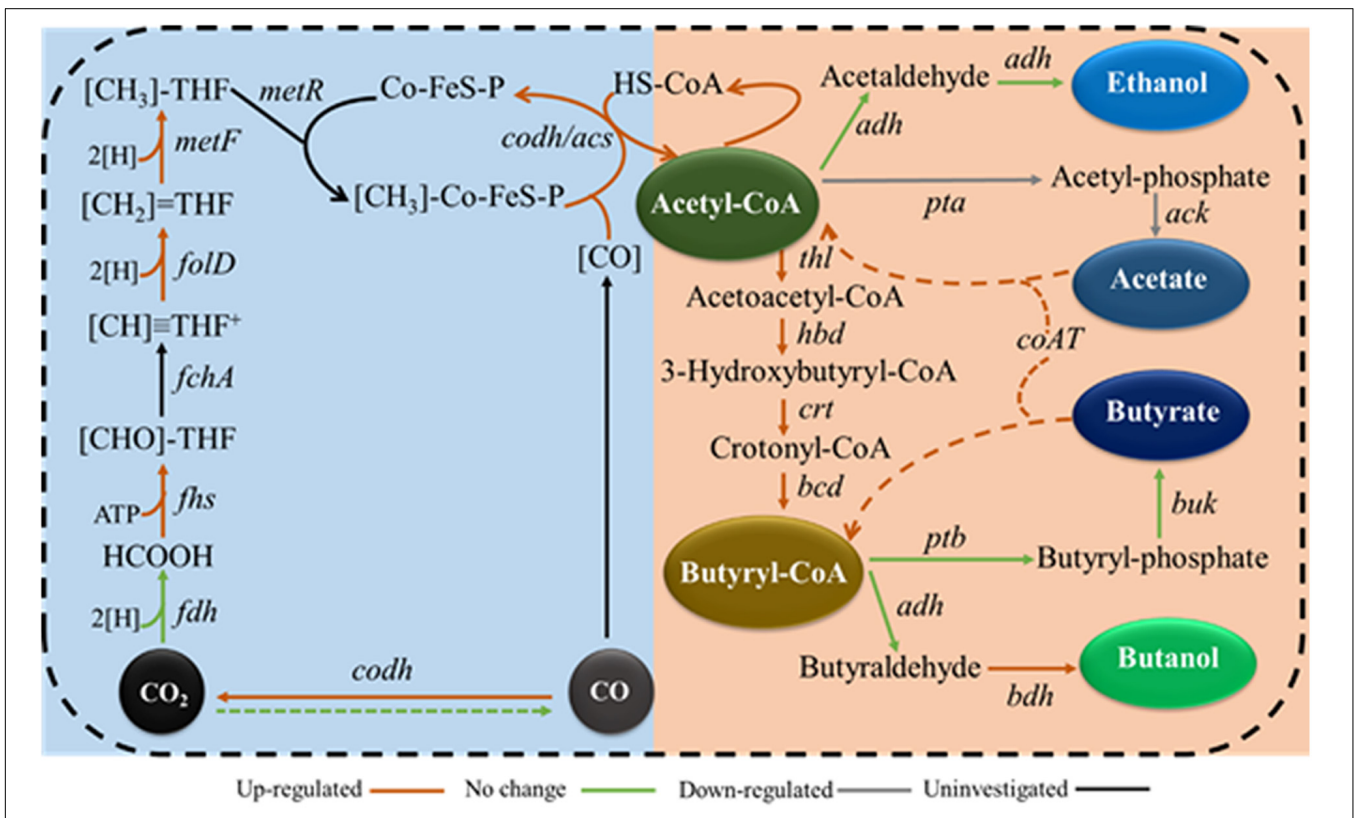

FIGURE 7 | Hypothetical metabolic regulation model of molybdenum in *C. carboxidivorans* P7 during syngas fermentation. *codh*, carbon monoxide dehydrogenase; *fchA*, formimido-tetrahydrofolate cyclodeaminase; *metR*, methyltransferase; [H], from NADH or NADPH.

CONCLUSION

In conclusion, Ni and Fe were found to be two vital metals for the growth of *C. carboxidivorans* P7 during syngas fermentation. Without the addition of these two metals, all product synthesis and biomass accumulation were significantly decreased. The dosage of molybdate was shown to be an important trigger for CO utilization and alcohol production, as this compound reduced the acidogenic phase, advanced the solventogenic phase, and dramatically increased alcohol production, particularly that of butanol and hexanol. Gene expression profiles of key metabolic pathways of *C. carboxidivorans* P7 under different syngas fermentation conditions were also determined in this study, and our results revealed that molybdate at 55 μg/L inhibited WLP and butanol synthesis pathways and the acid re-assimilation pathway. These results indicate that reducing this trace metal promotes alcohol production through both the *de novo* pathway and the acid re-assimilation mechanism.

DATA AVAILABILITY STATEMENT

The raw data supporting the conclusions of this article will be made available by the authors, without undue reservation.

AUTHOR CONTRIBUTIONS

Y-FH assisted in the experiment design, data analysis, and manuscript revising. B-TX designed and performed the experiments, analyzed the data, and drafted the manuscript, whose contributing was equally as first author. G-xW and Y-QG gave a hand in performing the experiments. Z-YH conceived the study and revised the manuscript. D-ML participated in the language editing. All authors read and approved the final manuscript.

FUNDING

The research was financially supported by the Ministry of Science and Technology of the People's Republic of China (2015AA020202), Chinese Academy of Sciences (KSZD-EW-Z-017-1), and National Natural Science Foundation of China (3140020013).

ACKNOWLEDGMENTS

We would like to thank the lab of Professor Yang Gu for the bacterial strain and original cultivation recipe. We would like to thank *Editage* (www.editage.cn) for English language editing.

SUPPLEMENTARY MATERIAL

The Supplementary Material for this article can be found online at: https://www.frontiersin.org/articles/10.3389/fmicb.2020.577266/full#supplementary-material

REFERENCES

Alfano, M., and Cavazza, C. (2020). Structure, function, and biosynthesis of nickel-dependent enzymes. *Protein Sci.* 29, 1071–1089. doi: 10.1002/pro.3836

Alissandratos, A., Kim, H. K., Matthews, H., Hennessy, J. E., Philbrook, A., and Easton, C. J. (2013). *Clostridium carboxidivorans* strain P7T recombinant formate dehydrogenase catalyzes reduction of CO2 to formate. *Appl. Environ. Microbiol.* 79, 741–744. doi: 10.1128/Aem.02886-12

Babu, M. V., Murthy, K. M., and Rao, G. A. P. (2017). Butanol and pentanol: The promising biofuels for CI engines A - review. *Renew. Sustain. Energy Rev.* 78, 1068–1088. doi: 10.1016/j.rser.2017.05.038

Bender, G., Pierce, E., Hill, J. A., Darty, J. E., and Ragsdale, S. W. (2011). Metal centers in the anaerobic microbial metabolism of CO and CO2. *Metallomics* 3, 797–815. doi: 10.1039/c1mt00042j

Bengelsdorf, F. R., Beck, M. H., Erz, C., Hoffmeister, S., Karl, M. M., Riegler, P., et al. (2018). Bacterial anaerobic synthesis gas (Syngas) and CO2+H2 fermentation. *Adv. Appl. Microbiol.* 103, 143–221. doi: 10.1016/bs.aambs.2018.01.002

Bruant, G., Levesque, M. J., Peter, C., Guiot, S. R., and Masson, L. (2010). Genomic analysis of carbon monoxide utilization and butanol production by *Clostridium carboxidivorans* strain P7(T). *PLoS One* 5:e13033. doi: 10.1371/journal.pone.0013033

Chakraborty, S., Rene, E. R., Lens, P. N. L., Rintala, J., Veiga, M. C., and Kennes, C. (2020). Effect of tungsten and selenium on C-1 gas bioconversion by an enriched anaerobic sludge and microbial community analysis. *Chemosphere* 250:126105. doi: 10.1016/j.chemosphere.2020.126105

Chen, J. S. (1995). Alcohol dehydrogenase: multiplicity and relatedness in the solvent-producing clostridia. *FEMS Microbiol. Rev.* 17, 263–273. doi: 10.1111/j.1574-6976.1995.tb00210.x

Cheng, C., Li, W., Lin, M., and Yang, S.-T. (2019). Metabolic engineering of *Clostridium carboxidivorans* for enhanced ethanol and butanol production from syngas and glucose. *Bioresour. Technol.* 284, 415–423. doi: 10.1016/j.biortech.2019.03.145

Drake, H. L., Gossner, A. S., and Daniel, S. L. (2008). Old acetogens, new light. *Ann. N. Y. Acad. Sci.* 1125, 100–128. doi: 10.1196/annals.1419.016

Duürre, P. (2005). *Handbook on Clostridia*. Boca Raton, FL: Taylor & Francis.

Fernández-Naveira, Á, Veiga, M. C., and Kennes, C. (2017). H-B-E (hexanol-butanol-ethanol) fermentation for the production of higher alcohols from syngas/waste gas. *J. Chem. Technol. Biotechnol.* 92, 712–731. doi: 10.1002/jctb.5194

Fontecilla-Camps, J. C., Amara, P., Cavazza, C., Nicolet, Y., and Volbeda, A. (2009). Structure-function relationships of anaerobic gas-processing metalloenzymes. *Nature* 460, 814–822. doi: 10.1038/nature08299

Gottwald, M., and Gottschalk, G. (1985). The Internal-Ph of *Clostridium-acetobutylicum* and its effect on the shift from acid to solvent formation. *Arch. Microbiol.* 143, 42–46. doi: 10.1007/Bf00414766

Huang, H., Chai, C., Li, N., Rowe, P., Minton, N. P., Yang, S., et al. (2016). CRISPR/Cas9-based efficient genome editing in *Clostridium ljungdahlii*, an autotrophic gas-fermenting bacterium. *ACS Synth. Biol.* 5, 1355–1361. doi: 10.1021/acssynbio.6b00044

Huang, L., Gibbins, L. N., and Forsberg, C. W. (1985). Transmembrane Ph gradient and membrane-potential in *Clostridium-acetobutylicum* during growth under acetogenic and solventogenic conditions. *Appl. Environ. Microbiol.* 50, 1043–1047. doi: 10.1128/aem.50.4.1043-1047.1985

Jang, Y. S., Han, M. J., Lee, J., Im, J. A., Lee, Y. H., Papoutsakis, E. T., et al. (2014). Proteomic analyses of the phase transition from acidogenesis to solventogenesis using solventogenic and non-solventogenic *Clostridium acetobutylicum* strains. *Appl. Microbiol. Biotechnol.* 98, 5105–5115. doi: 10.1007/s00253-014-5738-z

Janssen, H., Doring, C., Ehrenreich, A., Voigt, B., Hecker, M., Bahl, H., et al. (2010). A proteomic and transcriptional view of acidogenic and solventogenic steady-state cells of *Clostridium acetobutylicum* in a chemostat culture. *Appl. Microbiol. Biotechnol.* 87, 2209–2226. doi: 10.1007/s00253-010-2741-x

Jiang, Y., Liu, J., Jiang, W., Yang, Y., and Yang, S. (2015). Current status and prospects of industrial bio-production of n-butanol in China. *Biotechnol. Adv.* 33, 1493–1501. doi: 10.1016/j.biotechadv.2014.10.007

Jones, D. T., and Woods, D. R. (1986). Acetone-butanol fermentation revisited. *Microbiol. Rev.* 50, 484–524. doi: 10.1128/mmbr.50.4.484-524.1986

Kamani, M. H., Es, I., Lorenzo, J. M., Remize, F., Rosello-Soto, E., Barba, F. J., et al. (2019). Advances in plant materials, food by-products, and algae conversion into biofuels: use of environmentally friendly technologies. *Green Chem.* 21, 3213–3231. doi: 10.1039/c8gc03860k

Kim, J., Kim, J., Um, Y., and Kim, K. H. (2020). Intracellular metabolite profiling and the evaluation of metabolite extraction solvents for *Clostridium carboxidivorans* fermenting carbon monoxide. *Process Biochem.* 89, 20–28. doi: 10.1016/j.procbio.2019.10.012

Köpke, M., Held, C., Hujer, S., Liesegang, H., Wiezer, A., Wollherr, A., et al. (2010). *Clostridium ljungdahlii* represents a microbial production platform based on syngas. *Proc. Natl. Acad. Sci. U.S.A.* 107, 13087–13092. doi: 10.1073/pnas.1004716107

Korkhin, Y., Kalb, A. J., Peretz, M., Bogin, O., Burstein, Y., and Frolow, F. (1998). NADP-dependent bacterial alcohol dehydrogenases: crystal structure, cofactor-binding and cofactor specificity of the ADHs of *Clostridium beijerinckii* and *Thermoanaerobacter brockii*. *J. Mol. Biol.* 278, 967–981. doi: 10.1006/jmbi.1998.1750

Kushwaha, D., Srivastava, N., Prasad, D., Mishra, P. K., and Upadhyay, S. N. (2020). Biobutanol production from hydrolysates of cyanobacteria *Lyngbya limnetica* and *Oscillatoria obscura*. *Fuel* 271:117583. doi: 10.1016/j.fuel.2020.117583

Li, D. M., Meng, C. X., Wu, G. X., Xie, B. T., Han, Y. F., Guo, Y. Q., et al. (2018). Effects of zinc on the production of alcohol by *Clostridium carboxidivorans* P7 using model syngas. *J. Ind. Microbiol. Biotechnol.* 45, 61–69. doi: 10.1007/s10295-017-1992-2

Li, N., Yang, J., Chai, C., Yang, S., Jiang, W., and Gu, Y. (2015). Complete genome sequence of *Clostridium carboxidivorans* P7(T), a syngas-fermenting bacterium capable of producing long-chain alcohols. *J. Biotechnol.* 211, 44–45. doi: 10.1016/j.jbiotec.2015.06.430

Livak, K. J., and Schmittgen, T. D. (2001) Analysis of relative gene expression data using real-time quantitative PCR and the $2^{-\Delta\Delta C_T}$ method. *Methods* 25, 402–408. doi: 10.1006/meth.2001.1262

Matson, E. G., Zhang, X. N., and Leadbetter, J. R. (2010). Selenium controls transcription of paralogous formate dehydrogenase genes in the termite gut acetogen, *Treponema primitia*. *Environ. Microbiol.* 12, 2245–2258. doi: 10.1111/j.1462-2920.2010.02188.x

Metcalf, D., Sharif, S., and Weese, J. S. (2010). Evaluation of candidate reference genes in *Clostridium* difficile for gene expression normalization. *Anaerobe* 16, 439–443. doi: 10.1016/j.anaerobe.2010.06.007

Mintmier, B., Nassif, S., Stolz, J. F., and Basu, P. (2020). Functional mononuclear molybdenum enzymes: challenges and triumphs in molecular cloning, expression, and isolation. *J. Biol. Inorgan. Chem.* 25, 547–569. doi: 10.1007/s00775-020-01787-y

Papoutsakis, E. T. (2008). Engineering solventogenic clostridia. *Curr. Opin. Biotechnol.* 19, 420–429. doi: 10.1016/j.copbio.2008.08.003

Phillips, J. R., Atiyeh, H. K., Tanner, R. S., Torres, J. R., Saxena, J., Wilkins, M. R., et al. (2015). Butanol and hexanol production in *Clostridium carboxidivorans* syngas fermentation: Medium development and culture techniques. *Bioresour. Technol.* 190, 114–121. doi: 10.1016/j.biortech.2015.04.043

Pierce, E., Xie, G., Barabote, R. D., Saunders, E., Han, C. S., Detter, J. C., et al. (2008). The complete genome sequence of *Moorella thermoacetica* (f. *Clostridium thermoaceticum*). *Environ. Microbiol.* 10, 2550–2573. doi: 10.1111/j.1462-2920.2008.01679.x

Ramio-Pujol, S., Ganigue, R., Baneras, L., and Colprim, J. (2015). Incubation at 25 degrees C prevents acid crash and enhances alcohol production in *Clostridium carboxidivorans* P7. *Bioresour. Technol.* 192, 296–303. doi: 10.1016/j.biortech.2015.05.077

Rezania, S., Oryani, B., Cho, J., Talaiekhozani, A., Sabbagh, F., Hashemi, B., et al. (2020). Different pretreatment technologies of lignocellulosic biomass for bioethanol production: An overview. *Energy* 199:117457. doi: 10.1016/j.energy.2020.117457

Saxena, J., and Tanner, R. S. (2011). Effect of trace metals on ethanol production from synthesis gas by the ethanologenic acetogen, *Clostridium ragsdalei*. *J. Ind. Microbiol. Biotechnol.* 38, 513–521. doi: 10.1007/s10295-010-0794-6

Shen, S.H., Gu, Y., Chai, C., Jiang, W., Zhuang, Y., and Wang, Y. (2017a). Enhanced alcohol titre and ratio in carbon monoxide-rich off-gas fermentation of *Clostridium carboxidivorans* through combination of trace metals optimization with variable-temperature cultivation. *Bioresour. Technol.* 239:236. doi: 10.1016/j.biortech.2017.04.099

Shen, S. H., Gu, Y., Chai, C. S., Jihoang, W. H., Zhuang, Y. P., and Wang, Y. H. (2017b). Enhanced alcohol titre and ratio in carbon monoxide-rich off-gas fermentation of *Clostridium carboxidivorans* through combination of trace metals optimization with variable-temperature cultivation. *Bioresour. Technol.* 239, 236–243. doi: 10.1016/j.biortech.2017.04.099

Shen, Y., Brown, R., and Wen, Z. (2014a). Enhancing mass transfer and ethanol production in syngas fermentation of *Clostridium carboxidivorans* p7 through a monolithic biofilm reactor[J]. *Appl. Energy* 136, 68–76. doi: 10.1016/j.apenergy.2014.08.117

Shen, Y., Brown, R., and Wen, Z. (2014b). Syngas fermentation of *Clostridium carboxidivoran* P7 in a hollow fiber membrane biofilm reactor: Evaluating the mass transfer coefficient and ethanol production performance[J]. *Biochem. Eng. J.* 85, 21–29. doi: 10.1016/j.bej.2014.01.010

Ullah, K., Sharma, V. K., Ahmad, M., Lv, P. M., Krahl, J., Wang, Z. M., et al. (2018). The insight views of advanced technologies and its application in bio-origin fuel synthesis from lignocellulose biomasses waste, a review. *Renew. Sustain. Energy Rev.* 82, 3992–4008. doi: 10.1016/j.rser.2017.10.074

Wächtershäuser, G. (2006). From volcanic origins of chemoautotrophic life to bacteria, archaea and eukarya. *Philos. Trans. R. Soc. Lond. B Biol. Sci.* 361, 1787–1808. doi: 10.1098/rstb.2006.1904

Wu, Y. D., Xue, C., Chen, L. J., Wan, H. H., and Bai, F. W. (2015). Transcriptional analysis of micronutrient zinc-associated response for enhanced carbohydrate utilization and earlier solventogenesis in *Clostridium acetobutylicum*. *Sci. Rep.* 5:16598. doi: 10.1038/srep16598

Xie, B. T., Liu, Z. Y., Tian, L., Li, F. L., and Chen, X. H. (2015). Physiological response of *Clostridium ljungdahlii* DSM 13528 of ethanol production under different fermentation conditions. *Bioresour. Technol.* 177, 302–307. doi: 10.1016/j.biortech.2014.11.101

Zhang, J., Babtie, A., and Stephanopoulos, G. (2012). Metabolic engineering: enabling technology of a bio-based economy. *Curr. Opin. Chem. Eng.* 1, 355–362. doi: 10.1016/j.coche.2012.09.003

Zhu, X. F., and Tan, X. S. (2009). Metalloproteins/metalloenzymes for the synthesis of acetyl-CoA in the Wood-Ljungdahl pathway. *Sci. China Ser. B Chem.* 52, 2071–2082. doi: 10.1007/s11426-009-0082-3

Conflict of Interest: The authors declare that the research was conducted in the absence of any commercial or financial relationships that could be construed as a potential conflict of interest.

frontiers in Microbiology

REVIEW
published: 09 November 2020
doi: 10.3389/fmicb.2020.592631

Recent Advances in Developing Artificial Autotrophic Microorganism for Reinforcing CO_2 Fixation

Bo Liang[1,2]*, *Yukun Zhao*[3] *and Jianming Yang*[1,2]*

[1] *Energy-rich Compounds Production by Photosynthetic Carbon Fixation Research Center, Qingdao Agricultural University, Qingdao, China,* [2] *Shandong Key Lab of Applied Mycology, College of Life Sciences, Qingdao Agricultural University, Qingdao, China,* [3] *Pony Testing International Group, Qingdao, China*

With the goal of achieving carbon sequestration, emission reduction and cleaner production, biological methods have been employed to convert carbon dioxide (CO_2) into fuels and chemicals. However, natural autotrophic organisms are not suitable cell factories due to their poor carbon fixation efficiency and poor growth rate. Heterotrophic microorganisms are promising candidates, since they have been proven to be efficient biofuel and chemical production chassis. This review first briefly summarizes six naturally occurring CO_2 fixation pathways, and then focuses on recent advances in artificially designing efficient CO_2 fixation pathways. Moreover, this review discusses the transformation of heterotrophic microorganisms into hemiautotrophic microorganisms and delves further into fully autotrophic microorganisms (artificial autotrophy) by use of synthetic biological tools and strategies. Rapid developments in artificial autotrophy have laid a solid foundation for the development of efficient carbon fixation cell factories. Finally, this review highlights future directions toward large-scale applications. Artificial autotrophic microbial cell factories need further improvements in terms of CO_2 fixation pathways, reducing power supply, compartmentalization and host selection.

Keywords: CO_2 fixation, autotrophy, heterotrophy, synthetic biology, reducing power, cell factory

OPEN ACCESS

Edited by:
Guodong Luan,
Qingdao Institute of Bioenergy and Bioprocess Technology (CAS), China

Reviewed by:
Lei Chen,
Tianjin University, China
Jian Yu,
University of Hawai'i at Mānoa, United States

***Correspondence:**
Bo Liang
liangboqdnd@163.com
Jianming Yang
yjming888@126.com

Specialty section:
This article was submitted to Microbiotechnology, a section of the journal Frontiers in Microbiology

Received: *07 August 2020*
Accepted: *21 October 2020*
Published: *09 November 2020*

Citation:
Liang B, Zhao Y and Yang J (2020) Recent Advances in Developing Artificial Autotrophic Microorganism for Reinforcing CO_2 Fixation. Front. Microbiol. 11:592631. doi: 10.3389/fmicb.2020.592631

INTRODUCTION

The carbon element is the most important component in all types of living organic matter, accounting for approximately 50% of the dry weight of the organics. In nature, elemental carbon exists in many forms, including carbon dioxide (CO_2) in the atmosphere, CO_2 dissolved in water (H_2CO_3, HCO_3^-, and CO_3^{2-}) and carbon in organics, as well as carbon in rocks and fossil fuels. Currently, combustion of fossil fuels leads to considerable emission of greenhouse CO_2 and causes global warming, which is a major concern for all societies (Irfan et al., 2019). Thus, it is urgent to minimize CO_2 emissions by reducing the consumption of fossil fuels and reinforcing CO_2 fixation (Pacala and Socolow, 2004). Compared to chemical methods, biological carbon sequestration is an attractive option for CO_2 fixation, as it has several advantages, including mild reaction conditions and an eco-friendly approach (Li et al., 2012). Organisms that fix carbon include plants and autotrophic microorganisms. In green plants, carbon flux occurs primarily from CO_2 to biomass driven by solar energy. Autotrophic microorganisms exist in certain special conditions on Earth in which plants cannot live, and they assimilate CO_2 into biomass driven by solar energy or chemical energy produced by oxidizing inorganic substance in a more direct

and rapid way. It is supposed that CO_2 fixation might be more economic and efficient when sustainable bioprocesses producing biofuel and valuable chemicals directly from CO_2 are realized. In this respect, autotrophic microorganisms can be regarded as the most suitable cell factories (Liu et al., 2020).

Autotrophic microorganisms are capable of incorporating CO_2 into biomass via six natural carbon fixation pathways (Bar-Even et al., 2012). Since the discovery of the Calvin-Benson-Bassham (CBB) cycle in the 1940s and 1950s, another five CO_2 assimilation mechanisms have been elucidated, namely, the reductive citric acid cycle (rTCA), the reductive acetyl-CoA pathway (Wood-Ljungdahl pathway), the 3-hydroxypropionate bicycle (3HP bicycle), the 3-hydroxypropionate/4-hydroxybutyrate cycle (3HP/4HB cycle), and dicarboxylate/4-hydroxybutyrate cycle (DC/HB cycle) (Berg, 2011). The CBB cycle is ubiquitous in autotrophic microorganisms, primarily occurring in cyanobacteria. Remarkable progress has been made in producing biofuel and chemicals from CO_2 and solar energy by engineering the native CBB cycle in cyanobacteria, including ethanol, butanol, lactic acid, acetone, isobutyraldehyde, isoprene, and biodiesel (Savakis and Hellingwerf, 2015; Veaudor et al., 2020). However, the titer of target products is unsatisfactory (Hagemann and Hesse, 2018; Luan et al., 2020). The CO_2 capturing rate of ribulose-1,5-bisphosphate carboxylase/oxygenase (Rubisco) (EC 4.1.1.39) in the CBB cycle is an order of magnitude lower than the average of central metabolic enzymes, and efforts to improve Rubisco's kinetic properties have attained only limited success so far (Antonovsky et al., 2017; Liang et al., 2018). Moreover, low levels of growth and CO_2 fixation efficiency, as well as deficient genetic operating platforms have largely limited industrial applications of cyanobacteria (Blankenship et al., 2011; Kushwaha et al., 2018). Hence, there is a need for faster and more efficient bioprocesses for the conversion of CO_2 into the desired products. Generally, heterotrophic microorganisms have the advantage that growth and production yields are typically superior compared to the autotrophic life cycle. Massive and mature genetic manipulation tools make heterotrophy more accessible to a brand-new metabolism and proliferation mode (Nielsen and Keasling, 2016). The considerable advances in synthetic biology allow the engineering of novel functions and *de novo* metabolism networks in heterotrophic microorganisms for industrial biotechnology applications (Chen Y. et al., 2020; Clarke and Kitney, 2020). Previous developments in engineering of CO_2-fixing pathways for improving the efficiency of CO_2 fixation in autotrophic and heterotrophic microorganisms have been addressed in reported reviews (Claassens et al., 2016; Antonovsky et al., 2017; Hu et al., 2018).

In this review, we discuss recent advances in developing artificial autotrophic microorganisms for reinforcing CO_2 fixation (**Figure 1**). Starting from heterotrophs to hemiautotrophs, and finally to complete autotrophs, a variety of natural and artificial synthetic CO_2 fixation pathways have been developed and introduced into heterotrophic chassis. These engineered artificial autotrophs represent very promising candidates for highly efficient CO_2 fixation and sustainable production of biofuels and value-added chemicals.

NATURAL CO_2 FIXATION PATHWAYS

Carbon dioxide assimilation is the process of reducing CO_2 into cellular carbon which requires reducing equivalents and energy provided by ATP hydrolysis. The reductant varies by different microorganisms. In anaerobes, low-potential electron donors bearing more energy are responsible for offering reducing equivalents, such as ferredoxin $E_0' \approx -400$ mV. In contrast, aerobic microbial organisms require more ATP equivalents since high-potential electron donors with less energy are used as electron donors, such as NADPH $E_0' \approx -320$ mV (Berg, 2011). The sensitivity of enzymes toward molecular oxygen decides the distribution of CO_2 fixation pathways in both anaerobic and aerobic microorganisms.

Currently, six autotrophic CO_2-fixing pathways in microorganisms have been elucidated in detail. These pathways are divided into two groups according to the tolerance of key enzymes toward oxygen. The aerobic pathways include the CBB cycle, 3HP bicycle and 3HP/4HB cycle, while the rTCA cycle, Wood-Ljungdahl pathway and DC/HB cycle belong to the anaerobic pathways group since strictly anaerobic enzymes operate in these routes.

For common microorganisms, the CBB cycle is the most important mechanism of autotrophic CO_2 fixation (Bar-Even et al., 2012). The entire cycle is composed of 13 steps and three stages, consisting of carboxylation, reduction and regeneration (Bassham and Calvin, 1962). First, the key enzyme Rubisco catalyzes the carboxylation of CO_2 and ribulose-1,5-bisphosphate (RuBP) to generate 3-phosphoglycerate (3-PGA). Free energy change ($\Delta_rG'm$) is −37.8 kJ/mol. Then this product is reduced to glyceraldehyde-3-phosphate (GAP) consuming ATP and NADPH by 3-phosphoglycerate kinase and GAP dehydrogenase, in which the reaction catalyzed by 3-phosphoglycerate kinase is thermodynamically challenging ($\Delta_rG'm$ = +18.7 kJ/mol). Next, 5-bisphosphate (Ru5P) is regenerated through conversion between C_3, C_4, C_5, C_6, and C_7 sugar. Finally, Ru5P is phosphorylated by phosphoribulokinase to regenerate RuBP ($\Delta_rG'm$ = −24.2 kJ/mol). After one cycle, the CBB cycle can fix three CO_2 molecules and produce one GAP molecule at the cost of nine molecules of ATP and six molecules of NADPH reducing equivalents. The regeneration of energy carrier (ATP) and reducing equivalents (NADPH) in living microbes can be realized by photosystems. Despite the CBB cycle being the most prevalent CO_2 fixation mechanism on Earth, the efficiency of carbon assimilation is unsatisfactory. First, the final product of this cycle is a C3 compound that is inefficient for the synthesis of acetyl-CoA since CO_2 is inevitably lost during the conversion of GAP to acetyl-CoA. Acetyl-CoA is the central precursor for producing value-added multicarbon compounds, such as fatty acids (Blatti et al., 2013). Furthermore, the strong side reaction of Rubisco with oxygen can incur loss of fixed carbon, and the side product 2-phosphoglycolate is toxic to cell (Hagemann and Bauwe, 2016). In addition, large amounts of ATP and NADPH are consumed in this cycle (Berg, 2011).

As the key enzyme in the CBB cycle, Rubisco is the most abundant protein in the biosphere, which fixes $\sim 10^{11}$ tons of CO_2 from the atmosphere per year (Hayer-Hartl and Hartl, 2020).

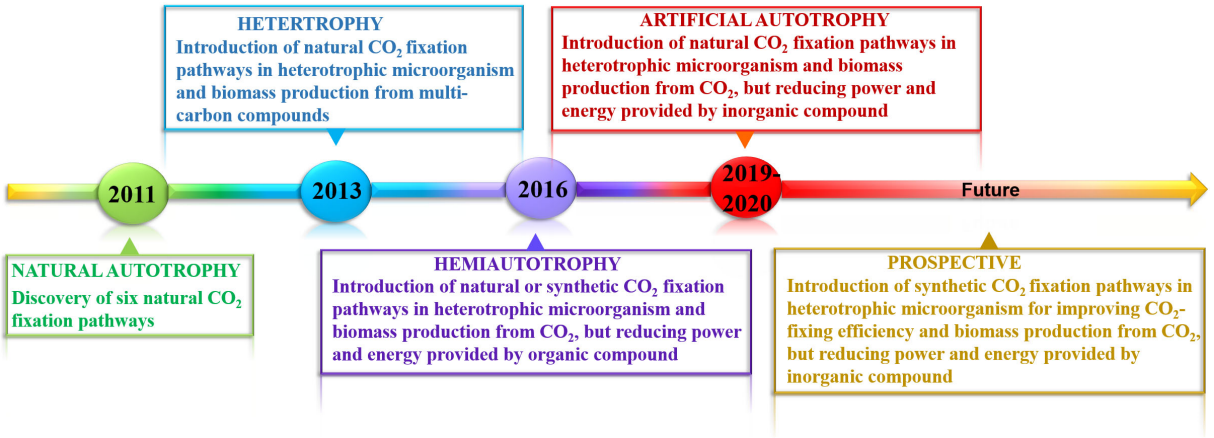

FIGURE 1 | Milestone in developing artificial autotrophy in the last decade. Until 2011, six naturally occurring CO_2 fixation pathways have been identified, some of which were introduced into heterotrophic microorganisms. However, all of biomass was derived from additional multi-carbon compounds, such as glucose. The strong advances in synthetic biology enable the engineering of synthetic CO_2 fixation pathways for improving carbon assimilation efficiency. Since 2016, hemiautotrophy has been successfully constructed by integrating natural or synthetic CO_2 fixation pathways in heterotrophic hosts using organic compound as reducing power and energy source, in which biomass was completely derived from CO_2. In 2019 and 2020, the conversion of heterotrophy to fully autotrophy was realized though integration of natural CO_2 fixation pathways to support cell growth and inorganic compound's oxidation to provide reducing power and energy.

Rubisco is a well-studied enzyme in photosynthetic organism since it provides organic carbon for life (Iniguez et al., 2020). Crystal structures of Rubisco from several origins have been analyzed by X-ray, including *Rhodospirillum rubrum*, *Synechococcus* PCC6301, *Chlorobium tepidum*, *Thermococcus kodakaraensis* KOD1, and so on (Iniguez et al., 2020). Two forms of Rubisco participate in the CBB cycle. Form I exists in all photosynthetic organisms, consisting of eight large-subunits (50–60 kDa) and eight small-subunits (12–18 kDa) that form an L8S8 structure. The tertiary structure of Form I is similar to a barrel, in which the L8 core is formed through the tetramerization of four interactional L2 dimers. Eight small subunits equally divided into two sets separately assemble the L8 core upside and downside. The large subunit harbors catalytic sites, especially amino acid sequences between 169 and 220, as well as 321 and 340. Compared to the small subunits, homology of the large subunits among different species is high. Small subunits have regulatory functions. Form II Rubisco is found in purple nonsulfur photosynthetic bacteria, such as *Rhodospirillum rubrum* and some marine dinoflagellates. This type is composed of two large-subunits (L2). Form I and Form II Rubisco are simultaneously found in several nonsulfur phototropic bacteria, such as *Rhodobacter sphaeroides* and *R. capsulatus*, as well as *Thiobacillus* sp. and *Hydrogenovibrio marinus*. Although Rubisco plays a pivotal role in global carbon fixation, its extremely poor carboxylation activity and competing oxygenase activity greatly hinder high carbon-fixing efficiency in the CBB cycle. CO_2 and O_2 competitively combine in the active site of Rubisco. The competitive efficiency for CO_2 and O_2 is defined as the specificity factor ($\Omega = V_cK_o/V_oK_c$), which is the ratio of the catalytic efficiency (V_{max}/K_M) for the carboxylation and oxygenation reactions. The specificity factor Ω of Form II (Ω = 10 to15) is much lower than that of Form I (Ω = 25 to 75 in bacteria). Significant efforts have been made to improve the value of specificity factor Ω and the efficiency of carbon capturing. In recent years, remarkably improved heterologous expression levels have been realized. However, molecular modification of Rubisco has been challenging owing to its complicated protein structure and intricate nature. *Escherichia coli* has long been the preferred host for the directed evolution of Rubisco for the sake of enhancing carboxylation activity toward CO_2 due to its high transformation efficiency and simple genetic tools (Mueller-Cajar and Whitney, 2008a). Several screening platforms for directed evolution of Rubisco have been developed by coupling cell growth to Rubisco activity (Parikh et al., 2006; Mueller-Cajar et al., 2007; Mueller-Cajar and Whitney, 2008b; Cai et al., 2014; Wilson et al., 2016; Zhou and Whitney, 2019). Unfortunately, affinity and catalytic efficiency toward CO_2 failed to synchronously increase (Kubis and Bar-Even, 2019). Moreover, remarkable kinetic enhancement was not obtained, likely due to an improper library screening platform, such as the host. In addition to model heterotrophs, *Rhodobacter capsulatus* has been used as an autotrophic host for directed evolution and rational design of Rubisco (Satagopan et al., 2019). In the *R. capsulatus* Rubisco deletion strain, complementation of a foreign Rubisco gene allowed the selection of substitutions. These screened mutants exhibited an improved affinity toward CO_2 rather than improved carboxylation activity. For example, the V186I/T327A^L mutant showed a 42% decreased K_c and a 41% increased K_o. These mutant sites are located in the hemiconserved hydrophobic region adjacent to the active site and connect the large-small interface. The above studies related to Rubisco engineering are limited to bacterial Rubisco since prokaryotic hosts cannot form the eukaryotic holoenzyme. By swapping certain residues of the large-subunit's primary structure that are responsible for preventing heterologous eukaryotic holoenzyme formation, Koay et al. (2016) created bacterial and eukaryotic Rubisco hybrids that could express and assemble in *E. coli*. These chimeric Rubisco

proteins serve as targets for directed evolution and rational design in the future work.

The 3HP bicycle was first discovered in 1986 by Helge Holo and primarily exists in photosynthetic green non-sulfur bacteria, such as *Chloroflexus* (Mattozzi et al., 2013). In the first cycle, three HCO_3^- molecules and one acetyl-CoA molecule are converted to glyoxylate via ten steps catalyzed by ten enzymes ($\Delta_rG'm$ = −109.4 kJ/mol). In the second cycle, glyoxylate and propionyl-CoA synthesize acetyl-CoA and pyruvate through five steps ($\Delta_rG'm$ = −55.4 kJ/mol). In addition to the number of steps in this pathway, the energy costs are higher than in the other four natural pathways. 3HP bicycle fixes three CO_2 molecules and produces one pyruvate molecule with the consumption of seven ATP molecules and five molecules of reducing equivalents. A "chimeric" photosynthetic system is used to regenerate ATP and reducing equivalents (Xin et al., 2018).

The 3HP/4HB cycle was first identified in archaea (Berg et al., 2007). In this pathway, acetyl-CoA/propionyl-CoA carboxylase fixes two molecules of HCO_3^- to produce succinyl-CoA ($\Delta_rG'm$ = −61.9 kJ/mol). To regenerate acetyl-CoA, succinyl-CoA is reduced to 4-hydroxybutyrate, which is then activated to 4-hydroxybutyryl-CoA ($\Delta_rG'm$ = −17.0 kJ/mol). Crotonyl-CoA is synthesized by the key enzyme 4-hydroxybutyryl-CoA dehydratase from 4-hydroxybutyryl-CoA ($\Delta_rG'm$ = −7.7 kJ/mol). Finally, crotonyl-CoA is oxidized and subsequently cleaved into acetyl-CoA ($\Delta_rG'm$ = −16.5 kJ/mol). The 3HP/4HB cycle fixes two molecules of HCO_3^- to produce one molecule of acetyl-CoA at the expense of six ATPs and four NAD(P)H reducing equivalents after 16 steps. In this cycle, the hydrolysis of pyrophosphate may provide energy (Berg, 2011).

The rTCA cycle exists in photosynthetic green sulfur bacteria and anaerobic bacteria (Buchanan and Arnon, 1990). This cycle reverses the reactions of the oxidative citric acid cycle (TCA cycle) and forms acetyl-CoA from two molecules of CO_2 at the cost of two molecules of ATP, which is far less than the above three pathways. The regeneration of ATP and reducing equivalents in living microbes can be realized by photosynthetic reaction center type I (Berg, 2011). To reverse the TCA cycle, three irreversible enzymes are required, including fumarate reductase, ferredoxin-dependent 2-oxoglutarate synthase and ATP-citrate lyase, among which ferredoxin-dependent 2-oxoglutarate synthase is strictly anaerobic. Thermodynamically challenging reactions ($\Delta_rG'm$ > 10 kJ/mol) are catalyzed by ATP-citrate lyase, 2-ketoglutarate synthase and isocitrate dehydrogenase in this cycle.

The Wood-Ljungdahl pathway is characterized by high energetic efficiency because in this route two CO_2 molecules are fixed to produce acetyl-CoA with the consumption of only one ATP (Ljungdahl, 1969). In detail, this pathway begins with one CO_2 molecule reduction to formic acid by highly oxygen sensitive formate dehydrogenase (FDH), which is thermodynamically challenging ($\Delta_rG'm$ = +18.0 kJ/mol). Another CO_2 molecule is reduced to carbon monoxide by a nickel atom in the active center of another highly oxygen sensitive CO dehydrogenase, which is also thermodynamically challenging ($\Delta_rG'm$ = +32.6 kJ/mol). Then formic acid is attached to tetrahydrofolate (THF) for further reduction. Finally, the one-carbon unit transfers to nickel-bound CO and forms acetyl-CoA. In acetogens, CO_2 is reduced to acetic acid with H_2 via the Wood-Ljungdahl pathway, in which the ATP required for formate activation is regenerated in the acetate kinase reaction (Mock et al., 2015; Lemaire et al., 2020).

The DC/HB cycle is a another strictly anaerobic CO_2 fixation pathway, in which two molecules of HCO_3^- and acetyl-CoA are converted to succinyl-CoA by two carboxylase pyruvate synthase and phosphoenolpyruvate (PEP) carboxylase (Huber et al., 2008). The regeneration of acetyl-CoA occurs through the same route as in the 3HP/4HB cycle. However, some enzymes and electron carriers, such as pyruvate synthase and ferredoxin, are inactivated by oxygen. Within this cycle, one molecule of HCO_3^- and one molecule of CO_2 are fixed to generate one molecule of acetyl-CoA via 13 steps catalyzed by 10 enzymes with the consumption of five molecules of ATP.

INTRODUCTION OF NATURAL CO_2 FIXATION PATHWAYS INTO HETEROTROPHIC MICROORGANISMS

Although autotrophic organisms are the sponsors to fix CO_2 in nature, low activity of carbon capturing dramatically influences the efficient conversion of CO_2 to biomass. Many efforts have been made to improve CO_2 carboxylation rate during the CBB cycle since Rubisco exhibits an extremely low affinity toward CO_2 and obvious oxygenation side-reactions in conditions of low levels of CO_2 (Ducat and Silver, 2012; Lin et al., 2014). Unfortunately, limited success has been achieved through engineering Rubisco or other related enzymes. Moreover, it is challenging to attempt genetic manipulation of autotrophic microorganisms owing to their unclear genetic background and the absence of genetic tools. Meanwhile, overexpressing new genes responsible for foreign CO_2 fixation pathway in autotrophic microorganisms may exert negative influences on regulatory networks in cells, such as carbon/nitrogen metabolism (Song et al., 2020). As model heterotrophs, *E. coli* and *Saccharomyces cerevisiae* have been widely used to serve as chassis to express natural CO_2 fixation routes (Antonovsky et al., 2017).

E. coli

The 3-HP bi-cycle from *Chloroflexus aurantiacus* has been successfully integrated into *E. coli*. To heterologously express the entire bicycle, a grouping strategy was employed, by which a 16-step enzymatic reaction was divided into four functional subpathways, and each group was independently expressed in a synthetic operon. This study provides evidence for the evolution of bacteria by horizontal gene transfer (Mattozzi et al., 2013). However, the functional co-expression of the overall bicycle in *E. coli* failed to support autotrophic growth.

The possibility of producing sugar for cell proliferation was explored by switching off the inflow of organic carbon into the CBB cycle. In this pioneer work, reconstruction of the fully functional CBB cycle conferred in *E. coli* the capacity to synthesize sugar and other biomass components from CO_2 by implementing a comprehensive approach that involved rational metabolic network construction, heterologous recombination expression and adaptive laboratory evolution

(ALE). To cut off gluconeogenesis, central metabolism was divided into two independent modules by introducing Rubisco from *Synechococcus* sp. PCC 7002 and phosphoribosyl kinase (PRK) from *S. elongatus* PCC 7942, simultaneously deleting the phosphoglycerol mutase gene. The first module included upstream glycolysis, pentose phosphate pathway (PPP) and recombinant CBB cycle enzymes (Rubisco and PRK). Meanwhile, the second module was an energy portion containing downstream glycolysis and TCA cycle, providing ATP and reducing power for carbon fixation of module one. However, the resultant strain could not grow in the presence of CO_2 and pyruvate (In this study, energy and reducing power were supplied by the oxidation of pyruvate). Only addition of a second sugar could support cell growth. The ALE strategy has advanced our ability to rapidly obtain a desired phenotype (Lee and Kim, 2020). The engineered strain was initially grown in a xylose-restricted chemostat, and at last, the evolved strain could grow with pyruvate as the sole carbon source at high CO_2 concentrations. Further mass spectrometry analysis showed that CO_2 was the only carbon source for phospho-sugars synthesis in the evolved strain, including ribose-5 phosphate, sedoheptulose-7 phosphate, fructose-6-phosphate, and glucose-6 phosphate, indicating that the fully functional CBB cycle in *E. coli* can directly synthesize sugar from CO_2. Four molecules of pyruvate were consumed per sugar. After genome-wide sequencing, the *prs* gene, encoding ribose phosphate pyrophosphate kinase, was the only common mutant gene found in three chemostat experiments, which is the primary branching enzyme of the CBB cycle module. This study shows that the functionality of the CBB cycle depends not only on heterologous enzymes (Rubisco and PRK) but also on the endogenous components that interact with them, particularly metabolic enzymes in the circulating carbon pool (Antonovsky et al., 2016). Proper balance of kinetic properties in enzymes at branch point is imperative to maintain a stable metabolism *in vivo* (Barenholz et al., 2017). In this work, three molecules of CO_2 were fixed to one molecule of pyruvate via CBB cycle. However, three molecules of CO_2 were produced during the TCA cycle using pyruvate as substrate. Therefore, the net CO_2 fixation was zero.

S. cerevisiae

Biofuel has been widely regarded as a promising alternative to fossil fuels concerning energy security, renewability, and global warming (Caspeta et al., 2013). Bioethanol is currently the most highly produced biofuel on an industrial scale (Nielsen et al., 2013). *S. cerevisiae* is the most commonly used host for bioethanol fermentation due to its high ethanol productivity and strong ethanol tolerance (Alper et al., 2006). However, during the process of yeast fermentation to produce ethanol, the production of ethanol is accompanied by CO_2 release, causing carbon loss and greenhouse gas emissions. In addition, excessive NADH causes excessive accumulation of the byproduct glycerol. To recycle CO_2, heterologous PRK and Rubisco derived from various origins were introduced into *S. cerevisiae* to construct the CO_2-fixing route. The product of CO_2 fixing by Rubisco is glycerate 3-phosphate (G3P). Ethanol is produced from G3P. At the same time, glycerol can also be formed using GAP as substrate by the actions of glycerol-3-phosphate dehydrogenase and glycerol-3-phosphatase. GAP is produced during xylose fermentation via non-oxidative PPP. This approach increased ethanol production and reduced the accumulation of the byproduct glycerol. For example, researchers co-expressed PRK from *spinach* and Rubisco from *Thiobacillus denitrificans* in *S. cerevisiae*. *T. denitrificans* Rubisco belongs to type II, composed of 8 large subunits. Its active expression requires the assistance of *E. coli* chaperons GroEL and GroES. Compared to the original strain, 90% in the reduction of byproduct glycerol and 10% increase of the production of ethanol were realized when the media was supplemented with glucose and galactose (Guadalupe-Medina et al., 2013). The use of sugarcane and corn starch as raw materials for the production of ethanol has the problem of "competing with people for food" (Tilman et al., 2009). As the second most abundant sugar in hydrolysis products from lignocellulose, xylose is an ideal feedstock to yield bioethanol via the xylose reductase (XR)/xylitol dehydrogenase (XDH) pathway in *S. cerevisiae* (Nogue and Karhumaa, 2015). CO_2 fixation has been achieved by introducing PRK from *Spinacia oleracea* and Rubisco from *Rhodospirillum rubrum* using xylose as substrate. Three molecules of CO_2 were fixed into one molecule of GAP by introducing PRK and Rubisco into yeast. Then, one molecule of ethanol was produced from one molecule of GAP with releasing one molecule of CO_2. And pyruvate was formed from GAP to produce acetyl-CoA for other metabolism to support cell growth with inevitably releasing CO_2. Therefore, the net production of CO_2 was observed in this engineered strain. Note that, results showed that the reduced release of CO_2 was observed during xylose fermentation, suggesting that the CO_2 generated by pyruvate decarboxylase was partially re-assimilated through the synthetic reductive PPP (Xia et al., 2017). Results demonstrated that the net ethanol production of engineered yeast had increased 10%, and the byproducts decreased 11%, demonstrating that the introduction of the PRK-Rubisco route achieved CO_2 recycling (Xia et al., 2017). An improved dual-module system was constructed in *S. cerevisiae* by employing mutants with alternate cofactor preference. Moreover, PRK and Rubisco from *Ralstonia eutropha* H16 were co-expressed in yeast (Li et al., 2017). *R. eutropha* H16 Rubisco belongs to type I, which is composed of 8 large subunits and 8 small subunits. To assist with proper folding of proteins, the endogenous chaperones of *S. cerevisiae* (Hsp60-HSP10) were co-expressed. Results showed that the productivity of ethanol was 15% higher than in the control strain, and the CO_2 fixation rate reached 336.6–436.3 mg CO_2/(L h) with consuming 3.1 g/L total sugar, which was significantly higher than previous natural or engineered microorganisms [5.8–147.0 mg CO_2/(L h)]. Of note, this experiment proves that type I Rubisco has higher carboxylation activity than type II, likely because the small subunit has the ability to enrich CO_2, which increases the concentration of CO_2 at the active site of the enzyme (Li et al., 2017). In the above studies, the introduction of Rubisco and PRK into brewer's yeast to achieve *in situ* fixation of CO_2 in the process of bioethanol production and increase the output of the target product bioethanol has laid the foundation for the production of other fuels and chemicals from lignocellulose.

INTRODUCTION OF SYNTHETIC CO_2 FIXATION PATHWAYS INTO HETEROTROPHIC MICROORGANISM

Despite their naturally existing diversity, the application of CO_2 fixation pathways for biomanufacturing valuable compounds directly from CO_2 has been limited so far. These naturally occurring CO_2 assimilation mechanisms contribute to cell growth rather than to products of interest. Moreover, CO_2-fixing efficiency of these natural or ALE routes is still unsatisfactory and most of them are inactivated in the presence of oxygen. The emerging field of synthetic biology facilitates to creation of artificial synthetic CO_2 fixation pathways.

With the goal of enhancing CO_2 assimilation efficiency, much interest has been devoted to creating stoichiometrically and thermodynamically feasible routes. Starting with CO_2 capturing enzymes, oxygen-insensitive and kinetically superior carboxylases or reductases have been identified, for instance, PEP carboxylase (EC 4.1.1.31) (Durall et al., 2020), pyruvate decarboxylase (EC 6.4.1.1) (Bar-Even et al., 2010), CoA-dependent carboxylase and metal-dependent FDH (Schwander et al., 2016; Cotton et al., 2018). Next, a series of CO_2 fixation pathways were predicted *in silico* by evaluating the stoichiometric and thermodynamic feasibility of theoretical pathways, from which to recruit a route characterized by high energy-efficiency. To sustain the proposed draft, potential enzymes were selected from the natural enzyme pool and then engineered to improve their kinetic profiles through directed evolution or rational design. Finally, a cocktail containing all of these enzymes was developed to investigate the feasibility of the proposed pathways *in vitro*, and further, all of these enzymes were introduced into heterotrophic model microorganisms to create artificial autotrophy. ^{13}C-labeling method is a powerful tool to pinpoint carbon flow. The ultimate aim is to produce biofuels and value-added compounds directed from CO_2 through the developed artificial autotrophy.

The first attempt of *de novo* design of a CO_2 fixation pathway *in vitro* was the crotonyl–coenzyme A (CoA)/ethylmalonyl-CoA/hydroxybutyryl-CoA (CETCH) cycle. Under aerobic condition, one molecule of glyoxylate was generated from two molecules of CO_2 consuming two molecules of ATP and three molecules of NADPH though this completely artificial carbon fixation pathway with 12 core reactions (Schwander et al., 2016). ECRs with high catalytic efficiency toward CO_2 were used as the initial enzyme of the entire cycle ($\Delta_r G'm = -26.1$ kJ/mol). The methylsuccinyl-CoA dehydrogenase (Mcd) was a rate-limiting enzyme, and a protein engineering approach was used to convert Mcd into a methylsuccinyl-CoA oxidase (Mco). A thermodynamically challenging reaction ($\Delta_r G'm \geq 10$ kJ/mol) is catalyzed by 4-hydroxybutyryl-CoA synthetase in this cycle. Compared to other aerobic naturally occurring CO_2 fixation flux, the CETCH process consumed the least amount of ATP. The feasibility of the CETCH cycle *in vitro* is a big breakthrough, demonstrating that more efficient CO_2 assimilation can be realized by rewiring natural elements. However, the final product of this cycle is glyoxylate rather than acetyl-CoA, which hinders the efficient connection between the CETCH cycle and central metabolism. Moreover, it is not economical to employ a complex enzyme assembly to synthesize useful products from CO_2 on a large scale. The challenges of introducing this artificial synthetic pathway into a heterotrophic host involve the complex interplay among these enzymes used in the CETCH cycle and aboriginal enzymes, as well as this route and endogenous metabolism network. Metabolic regulation also influences expression levels of each enzyme. Last but not least, it is crucial to maintain an efficient supply of reducing power for CO_2 fixation.

There are several different strategies to activate CO_2 with specific enzymes in nature. In addition to carboxylation, reduction can also be used to convert CO_2 to formate by another kind of carbon capturing enzyme, which is FDH. It catalyzes the reversible reaction between CO_2 and formate, taking part in various metabolic pathways with a variety of redox partners in different subcellular locations (Maia et al., 2017). Roughly, FDH can be divided into two classes, including NAD-independent and NAD-dependent (Jormakka et al., 2003). NAD-independent FDH is characterized by high activity toward CO_2 and sensitivity to oxygen (Maia et al., 2016; Yu et al., 2017). This class of FDH contains complex redox-active centers harboring different transition metals, such as molybdenum (Mo), tungsten and nonhaemiron, molybdopterin guanine dinucleotide (MGD) and selenocysterine (Niks and Hille, 2019; Lemaire et al., 2020). It has been identified only in prokaryotic organisms. In contrast, NAD-dependent FDH has relatively low activity toward CO_2 and is insensitive to oxygen (Hartmann and Leimkuhler, 2013; Choe et al., 2014; Altas et al., 2017). This kind of FDH has no metal ions or other redox-active centers and is widely distributed in bacteria, yeasts, fungi, and plants (Maia et al., 2017). However, the conversion of CO_2 to formate is unfavorable ($\Delta_r G'm = +18.0$ kJ/mol) (Liu et al., 2020).

After reducing CO_2 to formate, the next stage of carbon fixation can be implemented via natural or synthetic formate assimilation pathways (Bar-Even, 2016). Two well-known natural enzymes are capable of activating formate, oxygen-tolerant formate-tetrahydrofolate ligase (FTL) and oxygen-sensitive pyruvate formate-lyase (PFL) (Zelcbuch et al., 2016; Cotton et al., 2018). Starting from these entry-points, two types of formate assimilation pathways proceed, termed the reductive glycine (rGly) pathway and the PFL-PKT cycle (Cotton et al., 2018). Within the aerobic rGly process, formate is attached to THF to form formyl-THF, which can be subsequently reduced to methylene-THF. Glycine is formed by attaching another CO_2 molecule to methylene-THF via glycine cleavage/synthase system (GCS). Next, serine is generated by adding another methylene-THF molecule. Last, serine is reduced to pyruvate for biomass production. The overall thermodynamics of the pathway starting from formate to serine favor the reductive direction with $\Delta_r G'm = -6$ kJ/mol (Yishai et al., 2018). During the anaerobic PFL-PKT cycle, PFL catalyzes the reaction of acetyl-CoA and formate to yield pyruvate. This intermediate is transformed to sugar-phosphates though gluconeogenic and pentose-phosphate pathways. Phosphoketolase (PKT) catalyzes the generation of acetyl-phosphate (AcP) from xylulose 5-phosphate. Finally, acetyl-CoA is regenerated from AcP by the

action of phosphate acetyltransferase (PTA, EC 2.3.1.8), and the cycle is closed.

As mentioned above, the rGly pathway is an efficient synthetic route for aerobic assimilation of formate. In *E coli*, foreign enzymes required for the rGly process were expressed, including formate-THF ligase, 5,10-methenyl-THF cyclohydrolase (Fch) and 5,10-methylene-THF dehydrogenase (MtdA) from the *Methylobacterium extorquens* GCS. The resultant strain could biosynthesize cellular glycine and C1 compounds derived from formate and CO_2 when cells grown under heterotrophic condition (Yishai et al., 2018). Unlike the CBB cycle, the rGly process has few overlaps with cellular central metabolism, reducing the influence of metabolic regulations. Bang and Lee (2018) introduced this pathway in *E. coli* to realize one-carbon assimilation *in vivo* by overexpressing enzymes related to the rGly pathways as well as NAD-dependent FDH for producing reducing power from formate. After glucose depletion, the engineered strain maintained a slight growth using only formate and CO_2 as substrates, confirming its feasibility for supplying energy and reducing power via NAD-dependent FDH oxidative activity. Based on these pioneer studies, an outstanding work made an attempted to endow *E. coli* grown on formate or methanol and CO_2 without any other organics via the rGly route. Enzymes in rGly pathways, as well as NAD-dependent FDH, were overexpressed in the strain, in which formate was the only source for cell growth. To improve growth rate, a short-term laboratory evolution was performed. After 40 generations of culture, the doubling time of cells was reduced by 6–8-fold. Genome sequence analysis of the initial and evolved strains revealed two mutations involving energy and reducing power supply (Kim et al., 2020). In another study, cell growth was achieved when integrating the formate assimilation pathway and subsequent ALE without FDH supplying NADH. Genomic sequence analysis showed that mutations covered rGly pathway related genes, biofilm formation genes and formate-utilizing genes (Kim et al., 2019). However, in above studies, the net CO_2 emission was inevitable since one molecule of CO_2 was lost during the process of oxidizing formate to supply NADH.

In addition to ethanol, *S. cerevisiae* also has the ability to tolerate high levels of formate in the environment. Moreover, this host harbors necessary genes for the rGly route. Given these unique features, overexpression of rGly route native enzymes in *S. cerevisiae* resulted in net production of glycine using formate as feedstock. However, the addition of sugar instead of formate supported cell growth (de la Cruz et al., 2019). Engineering downstream biomass formation from glycine and subsequent ALE holds promise for use in the development of yeast that are fully autotrophic.

Compared to formate, the more active feature allows formaldehyde easier access to the central metabolism. Therefore, the reduction of formate to formaldehyde coupled with subsequent the natural or synthetic formaldehyde assimilation pathway is an attractive bypass to fix one-carbon compounds. With the goal of shorting the process of one-carbon utilization and accelerating growth starting from formate, an artificial synthetic route was computationally designed, the formolase (FLS) pathway. In this linear route, two natural enzymes with considerable activity toward substrate analogs were identified. Acetyl-CoA synthase (ACS) derived from *E. coli* catalyzes the ATP-dependent conversion of formate into formyl-CoA, and then putative acylating aldehyde dehydrogenase (ACDH) from *Listeria monocytogenes* catalyzes the NADH-dependent reduction of formyl-CoA to formaldehyde. Next, a novel enzyme FLS, which catalyzes the carboligation of three molecules of formaldehyde into one molecule of dihydroxyacetone was created through rational protein design and site-directed mutagenesis based on benzaldehydelyase (BAL) from *Pseudomonas fluorescens biovar I*. Finally, this C3 product can flow into central metabolism. It is speculated by *in silicon* calculations that this completely new synthetic pathway is superior to any natural one-carbon utilization starting from formate pathways due to having the fewest steps and the highest chemical driving force under fully aerobic conditions (the total Gibbs energy change $\Delta_r G'm$ from formaldehyde to acetyl-CoA is −110.2 kJ/mol). However, the low enzymatic activity of FLS resulted in undetectable cell growth with formate as a substrate (Siegel et al., 2015), suggesting the biotransformation of C1 directly to C3 is difficult to achieve. Given these findings, investigators wondered whether it was possible to produce C2 directly from C1. Recently, a synthetic aerobic acetyl-CoA (SACA) pathway was designed and constructed wherein two molecules of formaldehyde were transferred into one molecule of acetyl-CoA through only three steps ($\Delta_r G'm$ is −96.7 kJ/mol). First, formaldehyde was condensed into glycolaldehyde (GALD) by glycolaldehyde synthase (GALS). Then, GALD was converted into AcP by acetyl-phosphate synthase (A EC 4.1.2.9). GALS and ACPS were screened and engineered to enhance their catalytic efficiency toward their new substrates, respectively. Finally, the phosphate group of AcP was replaced with CoA catalyzed by PTA, and acetyl-CoA was successfully produced both *in vitro* and *in vivo* (Bar-Even et al., 2010; Li et al., 2019). Although the SACA process is characterized by carbon-conserved and ATP-independent processes, achieving high-efficiency of the pathway has been challenging, likely due to the toxicity of formaldehyde to cells and kinetic bottlenecks of enzymes. To address this issue, renovating the host and implementing further protein engineering may represent promise solutions.

REDUCTION OF CO_2 LOSS IN MICROORGANISMS

In heterotrophic hosts, fixed carbon flows into the central metabolism for synthesis of metabolites for cell growth, during which carbon inevitably suffers great or small loss. For example, the product dihydroxyacetone of the FLS pathway can be converted into acetyl-CoA via the glycolysis pathway with carbon loss and a theoretical carbon yield of 66.7%. To address this issue, significant efforts have been devoted to designing an artificial bypass to reduce the loss of carbon during acetyl-CoA formation. The nonoxidative glycolysis (NOG) pathway achieved biosynthesis of acetyl-CoA from sugar without carbon loss by rewiring the known carbon rearrangement pathway (Bogorad et al., 2013). In this pathway, bifunctional phosphoketolase

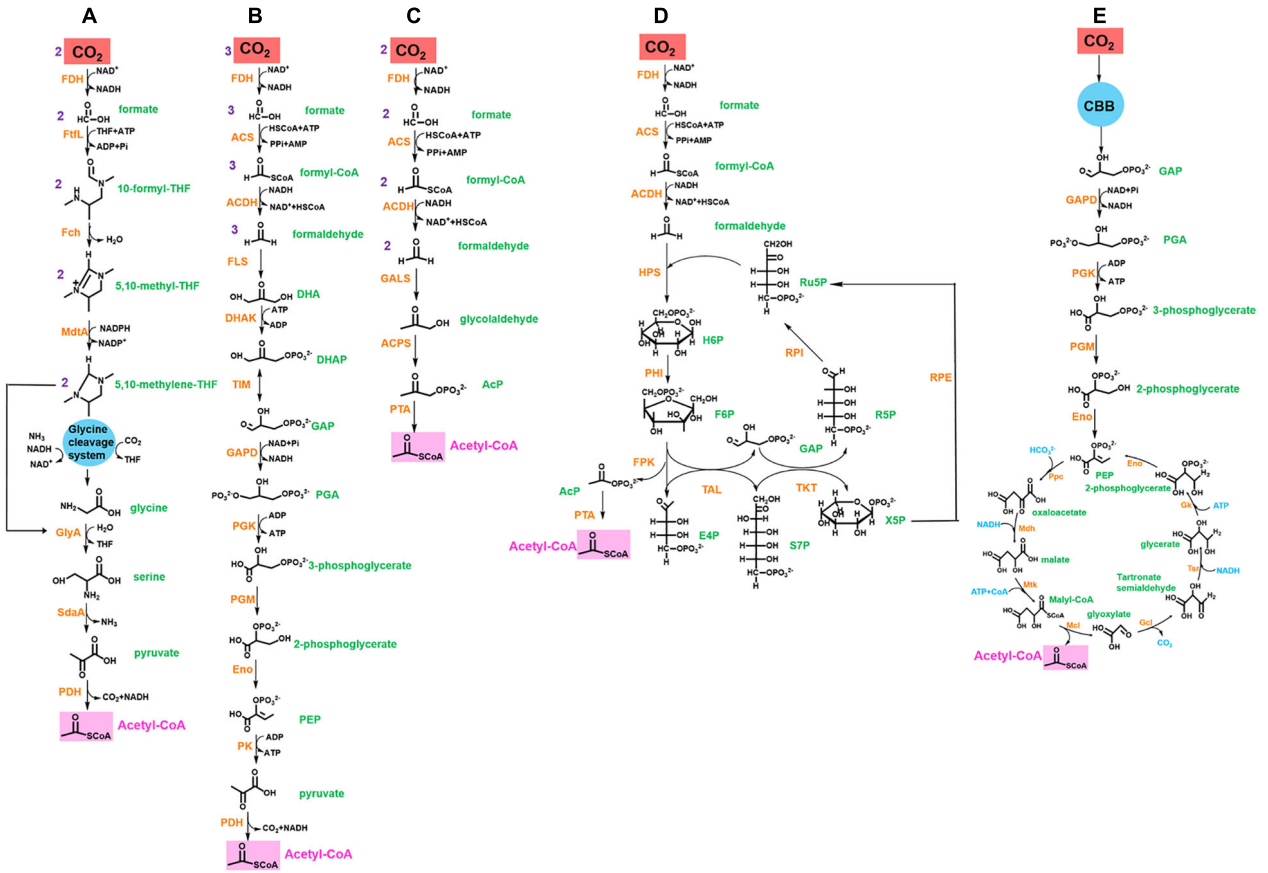

FIGURE 2 | Synthetic CO_2 fixation pathways for acetyl-CoA synthesis. **(A)** rGly pathway coupled FDH. **(B)** Formolase pathway coupled FDH. **(C)** SACA pathway coupled FDH and partial formolase path. **(D)** MCC pathway coupled FDH and partial formolase path. **(E)** MCG cycle coupled CBB cycle. Abbreviation for enzymes (orange in color): FDH, formate dehydrogenase; FtfL, formate-THF ligase; FchA, 5,10-methenyl-THF cyclohydrolase; MtdA, 5,10-methenyl-THF dehydrogenase; GlyA, serine hydroxymethyl-transferase; SdaA, serine deaminase; PDH, pyruvate dehydrogenase; ACS, acetyl-CoA synthase; ACDH, acetaldehyde dehydrogenase; FLS, formolase; DHAK, dihydroxyacetone kinase; TIM, triose phosphate isomerase; GAPD, glyceraldehyde-3-phosphate dehydrogenase; PGK, 3-phosphoglycerate kinase; PGM, phosphoglycerate mutase; Eno, enolase; PK, pyruvate kinase; GLAS, glycolaldehyde synthase; ACPS, acetyl-phosphate synthase; PTA, phosphate acetyltransferase; HPS, hexulose-6-phosphate synthase; PHI, phosphohexulose isomerase; FPK, fructose-6-phosphate phosphoketolase; TAL, transaldolase; TKT, transketolase; RPE, ribulose 5-phosphate epimerase; RPI, ribose-5 phosphate isomerase; Ppc, phosphoenolpyruvate carboxylase; Mdh, malate dehydrogenase; Mtk, malate thiokinase; Mcl, malyl-CoA lyase; Gcl, glyoxylate carboligase; Tsr, tartronate semialdehyde reductase; Gk, glycerate kinase. Abbreviation for metabolites (green in color): DHA, dihydroxyacetone; DHAP, dihydroxyacetone phosphate; GAP, glyceraldehyde 3-phosphate; PGA, 1,3-biphosphoglycerate; PEP, phosphoenolpyruvate; AcP, acetyl phosphate; H6P, hexulose-6-phosphate; Ru5P, ribulose-5 phosphate; F6P, fructose-6-phosphate; R5P, ribose-5 phosphate; E4P, erythrose-4 phosphate; S7P, sedoheptulose-7 phosphate; X5P, xylose-5 phosphate.

(Fxpk) from *Bifidobacterium adolescentis* breaks down three molecules of fructose 6-phosphate (F6P) into three molecules of AcP and three molecules of erythrose 4-phosphate (E4P). The three molecules of E4P regenerate two molecules of F6P through carbon rearrangement. The net reaction includes one molecule of F6P that produces three molecules of AcP without carbon loss. By overexpressing Fxpk and removing succinic acid, lactic acid, ethanol, formic acid, and other competitive pathways, the engineered *E. coli* strain produces acetic acid with a yield of 2.2 mol/mol from xylose, close to the theoretical maximum yield (2.5 mol/mol) and exceeding the maximum theoretical value of producing acetic acid from xylose though the EMP pathway (1.67 mol/mol). However, this pathway itself cannot support the growth of cells in a minimal medium that uses sugar as a carbon source, and requires the assistance of reducing equivalents and metabolites in the EMP pathway. To overcome this challenge, researchers further constructed an *E. coli* strain that does not use EMP for glycocatabolism. The engineered strain, which contained 11 overexpressed genes, 10 deleted genes, and more than 50 gene mutations, including three overall regulatory factors, was obtained through directed evolution. This strain can grow in the medium containing glucose, and the carbon conversion rate of anaerobic fermentation of glucose to acetic acid is close to 100% (Lin et al., 2018). By combining the ribulose monophosphate (RuMP) and NOG pathways, acetyl-CoA was produced from methanol through the methanol condensation cycle (MCC) pathway (Bogorad et al., 2014). The first step in MCC is the oxidation of methanol to formaldehyde. This C1 compound and Ru5P were converted to F6P via upstream of the RuMP pathway. Next,

TABLE 1 | Comparison of synthetic CO_2 fixation pathways with natural ones.

Pathway	Status	Fixed CO_2 or HCO_3^-	Product	ATP consumption	NAD(P)H consumption	CO_2 capturing enzyme	Specific activity μmol/min/mg	References
CBB	Natural	3	Glyceraldehyde-3-phosphate	9	6	Ribulose-1,5-bisphosphate, Carboxylase/oxygenase	3.5	Bar-Even et al., 2010
3HP bicycle	Natural	3	Pyruvate	7	5	Acetyl-CoA carboxylase, propionyl-CoA carboxylase	18, 30	Herter et al., 2001; Bar-Even et al., 2010
3HP/4HB cycle	Natural	2	Acetyl-CoA	6	4	Acetyl-CoA carboxylase, propionyl-CoA carboxylase	18, 30	Berg et al., 2007; Bar-Even et al., 2010
rTCA	Natural	2	Pyruvate	2	5	2-oxoglutarate synthase, isocitrate dehydrogenase	–, 53	Kim et al., 1992; Martinez et al., 2007
Wood-Ljungdahl	Natural	2	Acetyl-CoA	1	4	NAD-independent formate dehydrogenase, CO dehydrogenase/acetyl-CoA synthase	2.34, 0.46	Ragsdale, 1997
DC/HB cycle	Natural	2	Acetyl-CoA	5	4	Pyruvate synthase, PEP carboxylase	–, 35	Huber et al., 2008; Garcia-Gonzalez and De Wever, 2017
CETCH	Synthetic	2	Glyoxylate	1	4	CoA-dependent carboxylase		
rGly	Synthetic	3	Pyruvate	2	3	Glycine cleavage system		
Formolase path	Synthetic	3	Dihydroxyacetone phosphate	4	3	NAD-independent formate dehydrogenase		
Partial formolase path + SACA path	Synthetic	2	Acetyl-CoA	2	2	NAD-independent formate dehydrogenase		
partial formolase path + MCC path	Synthetic	1	Acetyl-CoA	1	1	NAD-independent formate dehydrogenase		
CBB + MCG path	Natural + synthetic	2	Acetyl-CoA	5.5	4	PEP carboxylase, ribulose-1,5-bisphosphate, carboxylase/oxygenase		

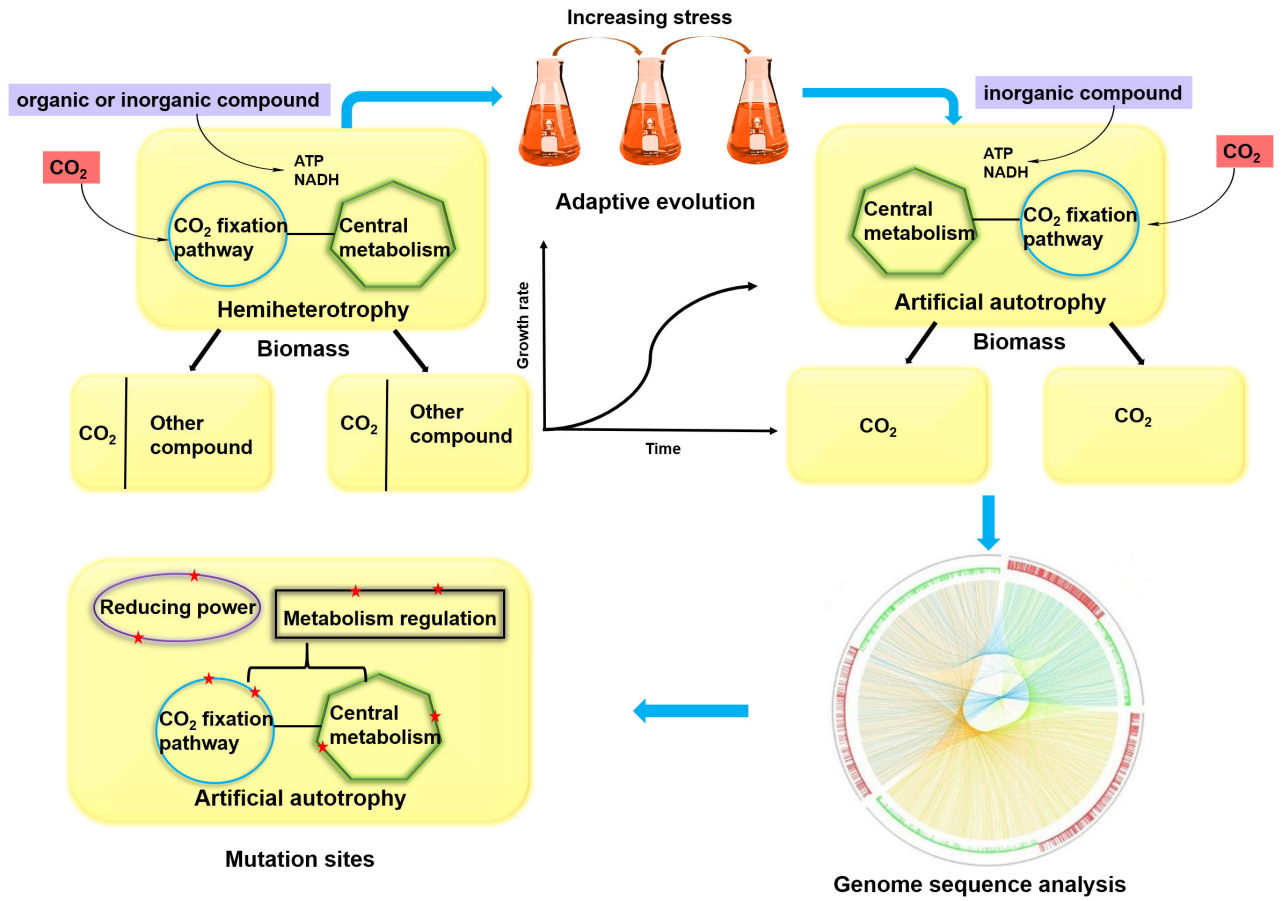

FIGURE 3 | The conversion process of hemiheterotrophy to artificial autotrophy. In hemiheterotrophic microorganism, CO_2 was fixed into organic carbon via introducing CO_2 fixation pathway and organic or inorganic compound provided reducing power and energy. Biomass was derived from CO_2 and another compound. The artificial autotrophic microorganism can be obtained through ALE strategy, in which inorganic compound provided reducing power and energy and biomass was completely derived from CO_2. To understand the genetic basis for adaptation to autotrophy, genomic analysis can be carried out, and mutation sites were related to CO_2 fixation pathway, central metabolism, reducing power and metabolism regulation (depicted by red star).

acetyl-CoA is produced from F6P by downstream of NOG bypass. Meanwhile, Ru5P was regenerated though the RuMP pathway. Throughout the entire pathway, phosphates were conserved, and C1 compounds were assimilated into acetyl-CoA in an ATP-independent manner. However, construction of MCC *in vivo* has not been implemented, and protein engineering of key enzymes is expected to accelerate carbon flux.

In addition to the EMP pathway, a high level of carbon loss also occurs within TCA cycle. In glyoxysome of plants, the glyoxylate shunt (GS) shares several common intermediates with the TCA cycle. GS involves the conversion of fatty acid to sugar, and the net reaction includes two molecules of acetyl-CoA producesing one molecule of succinic acid without carbon loss. It can be assumed that the reverse version of the glyoxylate shunt (rGS) might be used to generate acetyl-CoA to circumvent loss of carbon. Based on the rGS, a synthetic pathway was designed, in which malate and succinate were converted to oxaloacetate and two molecules of acetyl-CoA. However, the driving force of key steps relies on the hydrolysis of ATP, and the growth rate of the resultant strain was relatively slow (Mainguet et al., 2013).

Like the abovementioned C4 metabolites, acetyl-CoA can also be produced from C3 metabolites. A synthetic malonyl-CoA-glycerate (MCG) pathway has been demonstrated to be an efficient way to produce acetyl-CoA (Yu et al., 2018). First, two molecules of PEP were carboxylated into two molecules of oxaloacetate by inputting two molecules of bicarbonate. This reaction was catalyzed by PEP carboxylase, an attractive CO_2 fixing enzyme regarding its robustness and activity. Oxaloacetate was reduced to malate and then activated to malyl-CoA with ATP consumption. Two molecules of malyl-CoA were split into two acetyl-CoAs and two glyoxylates. The latter products were regenerated to PEP via the glyoxylate assimilation route, during which one CO_2 was released. Thus, coupled with the CBB cycle, the MCG pathway can fix two molecules of CO_2 to produce one molecule of acetyl-CoA with the consumption of 5.5 molecules of ATP equivalents and 4 molecules of reducing equivalents. The feasibility of the MCG pathway has been demonstrated both *in vitro* and *in vivo*. Moreover, when coupled with the CBB cycle in cyanobacteria, both acetyl-CoA level and bicarbonate assimilation rate increased one-fold.

TABLE 2 | Essential mutations for adaptation to autotrophy.

Overexpression enzymes	Energy source and reducing power	Mutated genes	Functions	Host	References
Ribulose-1,5-bisphosphate, carboxylase/oxygenase, phosphoribosyl kinase, formate dehydrogenase	Pyruvate	*prs* (ribose-phosphate diphoskinase), *pgi* (glucosephosphate isomerase), *serA* (3-phosphoglycerate dehydrogenase)	CBB cycle	*E. coli*	Herz et al., 2017
		crp (cAMP receptor protein), *ppsR* (PEP synthetase regulatory protein)	Metabolism regulation		
Formate-THF ligase, methenyl-THF cyclohydrolase, methylene-THF dehydrogenase, serine glyoxylate transaminase, serine hydroxymethyltransferase hydroxypyruvate reductase, glycerate kinase	Formate	*metF* (methylenetetrahydrofolate reductase) *purU* (formyltetrahydrofolate deformylase)	Folate metabolism	*E. coli*	Kim et al., 2019
		purT/purN (phosphoribosylglycinamide formyltransferase) *hycA/fnr* (formate hydrogenlyase)	Formate hydrogen lyase regulation		
Ribulose-1,5-bisphosphate, carboxylase/oxygenase, phosphoribosyl kinase, formate dehydrogenase, carbonic anhydrase	Formate	*prs* (ribose-phosphate diphoskinase), *pgi* (glucosephosphate isomerase), *aroH* (2-dehydro-3-deoxyphosphoheptonate aldolase)	CBB cycle	*E. coli*	Gleizer et al., 2019
		fdh (formate dehydrogenase)	Reducing power		
Phosphoribosyl kinase phosphoglycerate kinase glyceraldehyde-3-phosphate dehydrogenase triosephosphate isomerase transketolase	Methanol	*Prk* (phosphoribosyl kinase)	CBB cycle	*P. pastoris*	Gassler et al., 2020
		NMA1 (nicotinic acid mononucleotide adenylyltransferase)	Reducing power		
Formate-THF ligase, methenyl-THF cyclohydrolase, methylene-THF dehydrogenase, glycine cleavage/synthase system, serine hydroxymethyltransferase, serine deaminase, formate dehydrogenase	Formate	*fdh* (formate dehydrogenase), *pntAB* (membrane-bound transhydrogenase)	Reducing power	*E. coli*	Kim et al., 2020

Therefore, the novel synthetic pathway can be designed by coupling CO_2-fixing reactions with the abovementioned carbon loss-reducing pathways to improve CO_2 fixation efficiency (**Figure 2** and **Table 1**). Once a source of reducing power is provided, this pathway could theoretically allow growth with CO_2 as the sole carbon source.

THE CONVERSION OF MICROORGANISMS FROM HEMIAUTOTROPHY INTO FULLY AUTOTROPHS

Challenges in rewiring hemiautotrophy to complete autotrophy for steady-state growth on CO_2 as the sole source of carbon include (1) replacement of the native sugar transport system with a foreign CO_2 transport system, (2) deletion of part of the sugar metabolism pathway, (3) integration of systems for CO_2 fixation and central metabolism, (4) supply of reducing power, and (5) adaption of the strain to grow under this rewired metabolism. Fully considering these criteria, completely autotrophic microorganisms have been developed (Gleizer et al., 2019; Gassler et al., 2020) (**Figure 3**). For *E. coli*, carbonic anhydrase (CA, which catalyzes the reversible reaction between CO_2) was used to concentrate and transport CO_2 into cells. Key enzymes in the CBB cycle were heterologously expressed (Rubisco and PRK), whereas genes related to glycolysis and the oxidative pentose-phosphate pathway were knocked out. Importantly, NAD-dependent FDH was introduced into cell to generate NADH from formate. NADH provides the reducing power to drive carbon fixation and serves as the substrate for

ATP generation via oxidative phosphorylation. Although three necessary enzymes were introduced into *E. coli*, these efforts failed to generate a complete autotrophy due to the complexity of native metabolism and regulation networks in cells. Thus, long-time ALE was performed to redistribute the central metabolic flux. Finally, a complete autotrophic strain was obtained after 350 days of evolving. Genomic sequence analysis showed that CBB cycle-related genes, genetic selective pressure-related genes and nonfunctional genes were mutated (Erb et al., 2019; Gleizer et al., 2019). However, one molecule of CO_2 was inevitably lost during the process of oxidizing formate to supply NADH, resulting in a net CO_2 emission under autotrophic conditions.

As a model eukaryotic microbe, *Pichia pastoris* is also regarded as a proper chassis to construct autotrophs. The CBB cycle was introduced into cells though rewriting the xylulose monophosphate cycle and deleting methanol assimilation genes in peroxisomes. Energy and reducing power were provided by methanol oxidation. The maximum specific growth rate on CO_2 increased more than two-fold via adaptive evolution. Genomic sequence analysis showed that mutations were involved in CBB cycle related genes, NADH and ATP synthesis genes. These results indicated the importance of carbon fixation pathways, energy and reducing power supply on cell growth using CO_2 as a sole carbon source (Gassler et al., 2020). However, similar with employing formate as energy and reducing power source, the oxidation of methanol also resulted in the net emission of CO_2.

CONCLUSION AND PERSPECTIVES

Efforts to implement CO_2 fixation metabolism into heterotrophic microorganisms have not only focused on the well-known CBB cycle. Other naturally occurring pathways, as well as synthetic routes, have also been successfully introduced into heterotrophic hosts. Recent advances in the conversion of heterotrophic metabolism to fully autotrophic growth marked a new period of "artificial autotrophy." However, net CO_2 assimilation has not yet been demonstrated since fixed CO_2 is lost again during reducing power and energy generation. Sustainable production of biofuels and value-added compounds will become possible only if artificial autotrophy can efficiently fix CO_2 without carbon loss. Future efforts to develop artificial autotrophy are discussed in this section.

First of all, to achieve autotrophic growth, sustainable sources of energy and reducing equivalents are vital. Introducing light-cycle reactions into heterotrophic hosts remains challenging due to their extremely complex nature. Artificial photoautotrophy might be realized by introducing a fully functional proteorhodopsin photosystem into model hosts or hybridizing light-capturing nanoparticles with cells (Martinez et al., 2007; Guo et al., 2018). However, these photosynthetic biological hybridization systems are still in the early stages of development. Other challenges also require continuous research and exploration, such as biocompatibility of materials, selection of light collection devices, and seamless coupling of biological and nonbiological components (Cestellos-Blanco et al., 2020). In addition to light energy, electrical energy can also be used to produce energy carriers, such as formate, hydrogen, carbon monoxide, methanol, methane, and so on (Chen H. et al., 2020). In a pioneer study, a genetically engineered autotrophic microorganism, *Ralstonia eutropha* H16, produced higher alcohol levels in an electric bioreactor that used CO_2 as the sole carbon source and electricity as the sole energy input. The CO_2 on the cathode driven by electricity was reduced to formic acid, which was then converted into isobutanol and 3-methyl-1-butanol. This process integrated CO_2 fixation, electrochemical formic acid formation, and higher alcohol synthesis, opening up possibilities for electrically driving CO_2 to commercial chemicals (Li et al., 2012). Although this work proves the feasibility of electrochemical fixation of CO_2, the lack of a full understanding of the host and the production of hydrogen peroxide during the production process affected cell growth, limiting continuous improvement of the system. Enzymatic catalysis is a powerful platform to drive CO_2 fixation, such as NAD-dependent FDH and hydrogenase (Antonovsky et al., 2017). The former has been successfully applied in construction of artificial autotrophy via the CBB cycle as described above. However, carbon loss is inevitable during the generation of NADH. Therefore, hydrogenase is a promising option for providing energy and reducing equivalents without carbon loss (Yu, 2018). In this context, the (an)aerobic fermentation of synthesis gas (syngas) (H_2/CO/CO_2) and industrial off-gases has been proven to be an attractive platform for fixing CO_2 to produce a variety of chemicals in some natural autotrophic microorganisms, including acetogenic bacteria (*Clostridium autoethanogenum* and *Clostridium ljungdahlii*) (Mock et al., 2015; Emerson et al., 2019), *Cupriavidus necator* (Garcia-Gonzalez and De Wever, 2017) and *Oligotropha carboxidovorans* (Siebert et al., 2020), in which carbon can be fixed via CBB cycle or the Wood-Ljungdahl pathway with hydrogen as energy source. Similarly, Keller et al. (2013) expressed five genes of subpathway 1 in 3-HP/4-HB cycle from the thermophilic bacteria *Metallosphaera sedula* in *Pyrococcus furiosus*. The engineered strain used hydrogen as the electron donor to convert CO_2 and acetyl-CoA into the valuable chemical 3-hydroxypropionic acid (Keller et al., 2013).

Second, CO_2 fixation pathways are the key component of artificial autotrophy. As described above, although the CBB cycle is ubiquitous in the biosphere, carbon yield is lower and energy consumption is higher. Moreover, other natural aerobic CO_2 assimilation routes involve too many enzymes, for instance 3-HP bicycle. Hence, a synthetic pathway with higher carbon yield, reduced energy cost and relatively fewer enzymes is a more attractive candidate for reconstruction of artificial autotrophy. In this respect, strong advances in synthetic biology have enabled the rational design of a novel CO_2 fixation pathway based on a variety of established routes reported over the last decade. For example, the formate assimilation pathway has been engineered in model microorganisms, and an entire metabolic pathway can be developed by coupling upstream CO_2 capturing and downstream production of acetyl-CoA and other metabolites for cell growth and product biosynthesis. CO_2 can be reduced to formate by the action of NAD-independent FDH or electrodes, and the recruitment of SACA bypasses downstream

pathways and can efficiently produce acetyl-CoA without any carbon loss. Moreover, the influence of carbon flux regulation on CO_2 assimilation metabolism will be dramatically minimized due to few overlaps between exogenous metabolism and the endogenous cellular metabolic network. In addition to well-studied CO_2 capturing enzymes, such as Rubisco or NAD-independent FDH, more novel and efficient enzyme candidates in the CO_2 fixation pathway might be identified using advanced technologies for DNA sequencing, bioinformatics and structure-function predictions. Recently, a CO_2-reducing formate dehydrogenase complex (FdhAB) was identified from environmental samples by genome-resolved metagenomics (Figueroa et al., 2018). Moreover, the rate-limiting enzyme in CO_2 fixation pathways may have to be evolved or engineered with new features or improved kinetic properties.

Third, in most reactions, increased substrate concentrations can improve thermodynamics and enzyme conversion efficiency, as well as reducing enzyme side reaction activity. CO_2 capture mechanisms can be used to boost CO_2 concentration, including transmembrane bicarbonate pumps, transport proteins, carbonic anhydrase and microcompartments (Kerfeld and Erbilgin, 2015). Functional expression of foreign carboxysome in *E. coli* laid the groundwork for CO_2 condensation and fixation (Bonacci et al., 2012; Gong et al., 2015). Moreover, this spatial organization provides more stable enzyme structures, facilitates substrate channeling between active sites, and promotes carbon flux in a desirable direction (Siu et al., 2015).

Last but not least, the selection of a proper host plays a crucial role in the development of artificial autotrophy. A variety of criteria should be taken into account, including tolerance of feedstock, culture conditions, products of interest, cell growth rate, robustness, feasibility and stability of genetic manipulation. Compared to *E. coli*, *S. cerevisiae* has a higher tolerance for formate or other toxic substrates, as well as more endogenous carbon anabolic enzymes. From a biotechnology perspective, these features make *S. cerevisiae* a very promising chassis for the CO_2-fixing bio-industry.

Although all of abovementioned essential components for autotrophy are introduced into a suitable host, the constructed artificial autotrophic microorganism cannot grow solely on CO_2 since it is "accustomed" to heterotrophy. Therefore, this engineered strain should be adapted to be "fed" with CO_2. In recent studies, autotrophic growth was achieved by use of an ALE approach, and many essential mutation sites were identified, involving the CO_2 fixation pathway, central metabolism, reducing power and metabolic regulation (**Figure 3** and **Table 2**). These sites can be used for modified targets in future work.

In conclusion, the development of synthetic biology has provided the possibility of designing efficient biological carbon-fixing processes through understanding the diversity of carbon-fixing organisms and their metabolic pathways in nature, as well as the exploration of efficient carbon-fixing elements. We believe that CO_2 fixation by microbial organisms may make a significant contribution to building a sustainable society.

AUTHOR CONTRIBUTIONS

BL and JY designed the manuscript. BL and YZ prepared the manuscript. JY polished the manuscript. All authors contributed to the article and approved the submitted version.

FUNDING

This work was supported by grants from Key Laboratory of Biofuels, Qingdao Institute of Bioenergy and Bioprocess Technology, Chinese Academy of Sciences (CASKLB201805), the "First class grassland science discipline" program in Shandong Province, the National Natural Science Foundation of China (31860011), and the Talents of High Level Scientific Research Foundation (Grants 6651117005 and 6651119011) of Qingdao Agricultural University.

ACKNOWLEDGMENTS

We would like to thank Caroline S. Harwood for useful suggestions which helped to improve the quality of the manuscript.

REFERENCES

Alper, H., Moxley, J., Nevoigt, E., Fink, G. R., and Stephanopoulos, G. (2006). Engineering yeast transcription machinery for improved ethanol tolerance and production. *Science* 314, 1565–1568. doi: 10.1126/science.1131969

Altas, N., Aslan, A. S., Karatas, E., Chronopoulou, E., Labrou, N. E., and Binay, B. (2017). Heterologous production of extreme alkaline thermostable NAD(+)-dependent formate dehydrogenase with wide-range pH activity from *Myceliophthora thermophila*. *Process. Biochem.* 61, 110–118. doi: 10.1016/j.procbio.2017.06.017

Antonovsky, N., Gleizer, S., and Milo, R. (2017). Engineering carbon fixation in *E. coli*: from heterologous RuBisCO expression to the Calvin-Benson-Bassham cycle. *Curr. Opin. Biotechnol.* 47, 83–91. doi: 10.1016/j.copbio.2017.06.006

Antonovsky, N., Gleizer, S., Noor, E., Zohar, Y., Herz, E., Barenholz, U., et al. (2016). Sugar synthesis from CO2 in *Escherichia coli*. *Cell* 115–125. doi: 10.1016/j.cell.2016.05.064

Bang, J., and Lee, S. Y. (2018). Assimilation of formic acid and CO2 by engineered *Escherichia coli* equipped with reconstructed one-carbon assimilation pathways. *Proc. Natl. Acad. Sci. U.S.A.* E9271–E9279. doi: 10.1073/pnas.1810386115

Barenholz, U., Davidi, D., Reznik, E., Bar-On, Y., Antonovsky, N., Noor, E., et al. (2017). Design principles of autocatalytic cycles constrain enzyme kinetics and force low substrate saturation at flux branch points. *eLife* 6:e20667. doi: 10.7554/eLife.20667

Bar-Even, A. (2016). Formate assimilation: the metabolic architecture of natural and synthetic pathways. *Biochemistry* 55, 3851–3863. doi: 10.1021/acs.biochem.6b00495

Bar-Even, A., Noor, E., Lewis, N. E., and Milo, R. (2010). Design and analysis of synthetic carbon fixation pathways. *Proc. Natl. Acad. Sci. U.S.A.* 107, 8889–8894. doi: 10.1073/pnas.0907176107

Bar-Even, A., Noor, E., and Milo, R. (2012). A survey of carbon fixation pathways through a quantitative lens. *J. Exp. Bot.* 63, 2325–2342. doi: 10.1093/jxb/err417

Bassham, J. A., and Calvin, M. (1962). The way of CO2 in plant photosynthesis. *Comp. Biochem. Physiol.* 4, 187–204. doi: 10.1016/0010-406x(62)90004-x

Berg, I. A. (2011). Ecological aspects of the distribution of different autotrophic CO2 fixation pathways. *Appl. Environ. Microbiol.* 77, 1925–1936. doi: 10.1128/AEM.02473-10

Berg, I. A., Kockelkorn, D., Buckel, W., and Fuchs, G. (2007). A 3-hydroxypropionate/4-hydroxybutyrate autotrophic carbon dioxide assimilation pathway in Archaea. *Science* 318, 1782–1786. doi: 10.1126/science.1149976

Blankenship, R. E., Tiede, D. M., Barber, J., Brudvig, G. W., Fleming, G., Ghirardi, M., et al. (2011). Comparing photosynthetic and photovoltaic efficiencies and recognizing the potential for improvement. *Science* 332, 805–809. doi: 10.1126/science.1200165

Blatti, J. L., Michaud, J., and Burkart, M. D. (2013). Engineering fatty acid biosynthesis in microalgae for sustainable biodiesel. *Curr. Opin. Chem. Biol.* 17, 496–505. doi: 10.1016/j.cbpa.2013.04.007

Bogorad, I. W., Chen, C. T., Theisen, M. K., Wu, T. Y., Schlenz, A. R., Lam, A. T., et al. (2014). Building carbon-carbon bonds using a biocatalytic methanol condensation cycle. *Proc. Natl. Acad. Sci. U.S.A.* 111, 15928–15933. doi: 10.1073/pnas.1413470111

Bogorad, I. W., Lin, T. S., and Liao, J. C. (2013). Synthetic non-oxidative glycolysis enables complete carbon conservation. *Nature* 502, 693–697. doi: 10.1038/nature12575

Bonacci, W., Teng, P. K., Afonso, B., Niederholtmeyer, H., Grob, P., Silver, P. A., et al. (2012). Modularity of a carbon-fixing protein organelle. *Proc. Natl. Acad. Sci. U.S.A.* 109, 478–483. doi: 10.1073/pnas.1108557109

Buchanan, B. B., and Arnon, D. I. (1990). A reverse KREBS cycle in photosynthesis: consensus at last. *Photosynth. Res.* 24, 47–53. doi: 10.1007/BF00032643

Cai, Z., Liu, G. X., Zhang, J. L., and Li, Y. (2014). Development of an activity-directed selection system enabled significant improvement of the carboxylation efficiency of Rubisco. *Protein Cell* 5, 552–562. doi: 10.1007/s13238-014-0072-x

Caspeta, L., Buijs, N. A. A., and Nielsen, J. (2013). The role of biofuels in the future energy supply. *Energ. Environ. Sci.* 6, 1077–1082. doi: 10.1039/c3ee24403b

Cestellos-Blanco, S., Zhang, H., Kim, J. M., Shen, Y. X., and Yang, P. D. (2020). Photosynthetic semiconductor biohybrids for solar-driven biocatalysis. *Nat. Catal.* 3, 245–255. doi: 10.1038/s41929-020-0428-y

Chen, H., Dong, F. Y., and Minteer, S. D. (2020). The progress and outlook of bioelectrocatalysis for the production of chemicals, fuels and materials. *Nat. Catal.* 3, 225–244. doi: 10.1038/s41929-019-0408-2

Chen, Y., Banerjee, D., Mukhopadhyay, A., and Petzold, C. J. (2020). Systems and synthetic biology tools for advanced bioproduction hosts. *Curr. Opin. Biotechnol.* 64, 101–109. doi: 10.1016/j.copbio.2019.12.007

Choe, H., Joo, J. C., Cho, D. H., Kim, M. H., Lee, S. H., Jung, K. D., et al. (2014). Efficient CO2-reducing activity of NAD-dependent formate dehydrogenase from *Thiobacillus* sp KNK65MA for formate production from CO2 gas. *PLoS One* 9:e103111. doi: 10.1371/journal.pone.0103111

Claassens, N. J., Sousa, D. Z., dos Santos, V. A. P. M., de Vos, W. M., and van der Oost, J. (2016). Harnessing the power of microbial autotrophy. *Nat. Rev. Microbiol.* 14, 692–706. doi: 10.1038/nrmicro.2016.130

Clarke, L., and Kitney, R. (2020). Developing synthetic biology for industrial biotechnology applications. *Biochem. Soc. Trans.* 48, 113–122. doi: 10.1042/BST20190349

Cotton, C. A. R., Edlich-Muth, C., and Bar-Even, A. (2018). Reinforcing carbon fixation: CO2 reduction replacing and supporting carboxylation. *Curr. Opin. Biotech.* 49, 49–56. doi: 10.1016/j.copbio.2017.07.014

de la Cruz, J. G., Machens, F., Messerschmidt, K., and Bar-Even, A. (2019). Core catalysis of the reductive glycine pathway demonstrated in yeast. *Acs Synthet. Biol.* 8, 911–917. doi: 10.1021/acssynbio.8b00464

Ducat, D. C., and Silver, P. A. (2012). Improving carbon fixation pathways. *Curr. Opin. Chem. Biol.* 16, 337–344. doi: 10.1016/j.cbpa.2012.05.002

Durall, C., Lindberg, P., Yu, J. P., and Lindblad, P. (2020). Increased ethylene production by overexpressing phosphoenolpyruvate carboxylase in the cyanobacterium *Synechocystis* PCC 6803. *Biotechnol. Biofuels* 13:16. doi: 10.1186/s13068-020-1653-y

Emerson, D. F., Woolston, B. M., Liu, N., Donnelly, M., Currie, D. H., and Stephanopoulos, G. (2019). Enhancinghydrogen-dependent growth of and carbon dioxide fixation by *Clostridium ljungdahlii* through nitrate supplementation. *Biotechnol. Bioeng.* 116, 294–306. doi: 10.1002/bit.26847

Erb, T. J., Keller, P., and Vorholt, J. A. (2019). *Escherichia coli* in auto(trophic) mode. *Cell* 1244–1245. doi: 10.1016/j.cell.2019.10.040

Figueroa, I. A., Barnum, T. P., Somasekhar, P. Y., Carlstrom, C. I., Engelbrektson, A. L., and Coates, J. D. (2018). Metagenomics-guided analysis of microbial chemolithoautotrophic phosphite oxidation yields evidence of a seventh natural CO2 fixation pathway. *Proc. Natl. Acad. Sci. U.S.A.* 115, E92–E101. doi: 10.1073/pnas.1715549114

Garcia-Gonzalez, L., and De Wever, H. (2017). Valorisation of CO2 rich off gases to biopolymers through biotechnological process. *FEMS Microbiol. Lett.* 364, 1–8. doi: 10.1093/femsle/fnx196

Gassler, T., Sauer, M., Gasser, B., Egermeier, M., Troyer, C., Causon, T., et al. (2020). The industrial yeast *Pichia pastoris* is converted from a heterotroph into an autotroph capable of growth on CO2. *Nat. Biotechnol.* 38, 210–218. doi: 10.1038/s41587-019-0363-0

Gleizer, S., Ben-Nissan, R., Bar-On, Y. M., Antonovsky, N., Noor, E., Zohar, Y., et al. (2019). Conversion of *Escherichia coli* to generate all biomass carbon from CO2. *Cell* 179, 1255–1263. doi: 10.1016/j.cell.2019.11.009

Gong, F., Liu, G., Zhai, X., Zhou, J., Cai, Z., and Li, Y. (2015). Quantitative analysis of an engineered CO2-fixing *Escherichia coli* reveals great potential of heterotrophic CO2 fixation. *Biotechnol. Biofuels* 8:86. doi: 10.1186/s13068-015-0268-1

Guadalupe-Medina, V., Wisselink, H. W., Luttik, M. A. H., de Hulster, E., Daran, J. M., Pronk, J. T., et al. (2013). Carbon dioxide fixation by Calvin-Cycle enzymes improves ethanol yield in yeast. *Biotechnol. Biofuels* 6:125. doi: 10.1186/1754-6834-6-125

Guo, J., Suastegui, M., Sakimoto, K. K., Moody, V. M., Xiao, G., Nocera, D. G., et al. (2018). Light-driven fine chemical production in yeast biohybrids. *Science* 362, 813–816. doi: 10.1126/science.aat9777

Hagemann, M., and Bauwe, H. (2016). Photorespiration and the potential to improve photosynthesis. *Curr. Opin. Chem. Biol.* 35, 109–116. doi: 10.1016/j.cbpa.2016.09.014

Hagemann, M., and Hesse, W. R. (2018). Systems and synthetic biology for the biotechnological application of cyanobacteria. *Curr. Opin. Biotech.* 49, 94–99. doi: 10.1016/j.copbio.2017.07.008

Hartmann, T., and Leimkuhler, S. (2013). The oxygen-tolerant and NAD(+)-dependent formate dehydrogenase from *Rhodobacter capsulatus* is able to catalyze the reduction of CO2 to formate. *FEBS J.* 280, 6083–6096. doi: 10.1111/febs.12528

Hayer-Hartl, M., and Hartl, F. U. (2020). Chaperone machineries of Rubisco-The most abundant enzyme. *Trends Biochem. Sci.* 20:30119. doi: 10.1016/j.tibs.2020.05.001

Herter, S., Farfsing, J., Gad'On, N., Rieder, C., Eisenreich, W., Bacher, A., et al. (2001). Autotrophic CO2 fixation by *Chloroflexus aurantiacus*: study of glyoxylate formation and assimilation via the 3-hydroxypropionate cycle. *J. Bacteriol.* 183, 4305–4316. doi: 10.1128/JB.183.14.4305-4316.2001

Herz, E., Antonovsky, N., Bar-On, Y., Davidi, D., Gleizer, S., Prywes, N., et al. (2017). The genetic basis for the adaptation of *E-coli* to sugar synthesis from CO2. *Nat. Commun.* 8:1705. doi: 10.1038/S41467-017-01835-3

Hu, G. P., Li, Y., Ye, C., Liu, L. M., and Chen, X. L. (2018). Engineering microorganisms for enhanced CO2 sequestration. *Trends Biotechnol.* 37, 532–547. doi: 10.1016/j.tibtech.2018.10.008

Huber, H., Gallenberger, M., Jahn, U., Eylert, E., Berg, I. A., Kockelkorn, D., et al. (2008). A dicarboxylate/4-hydroxybutyrate autotrophic carbon assimilation cycle in the hyperthermophilic Archaeum Ignicoccus hospitalis. *Proc. Natl. Acad. Sci. U.S.A.* 105, 7851–7856. doi: 10.1073/pnas.0801043105

Iniguez, C., Capo-Bauca, S., Niinemets, U., Stoll, H., Aguilo-Nicolau, P., and Galmes, J. (2020). Evolutionary trends in RuBisCO kinetics and their co-evolution with CO2 concentrating mechanisms. *Plant J.* 101, 897–918. doi: 10.1111/tpj.14643

Irfan, M., Bai, Y., Zhou, L., Kazmi, M., Yuan, S., Mbadinga, S. M., et al. (2019). Direct microbial transformation of carbon dioxide to value-added chemicals: a comprehensive analysis and application potentials. *Bioresource Technol.* 288:121401. doi: 10.1016/j.biortech.2019.121401

Jormakka, M., Byrne, B., and Iwata, S. (2003). Formate dehydrogenase–a versatile enzyme in changing environments. *Curr. Opin. Struct. Biol.* 13, 418–423. doi: 10.1016/s0959-440x(03)00098-8

Keller, M. W., Schut, G. J., Lipscomb, G. L., Menon, A. L., Iwuchukwu, I. J., Leuko, T. T., et al. (2013). Exploiting microbial hyperthermophilicity to produce an industrial chemical, using hydrogen and carbon dioxide. *Proc. Natl. Acad. Sci. U.S.A.* 110, 5840–5845. doi: 10.1073/pnas.1222607110

Kerfeld, C. A., and Erbilgin, O. (2015). Bacterial microcompartments and the modular construction of microbial metabolism. *Trends Microbiol.* 23, 22–34. doi: 10.1016/j.tim.2014.10.003

Kim, B. W., Chang, H. N., Kim, I. K., and Lee, K. S. (1992). Growth kinetics of the photosynthetic bacterium *Chlorobium thiosulfatophilum* in a fed-batch reactor. *Biotechnol. Bioeng.* 40, 583–592. doi: 10.1002/bit.260400505

Kim, S., Lindner, S. N., Aslan, S., Yishai, O., Wenk, S., Schann, K., et al. (2020). Growth of *E. coli* on formate and methanol via the reductive glycine pathway. *Nat. Chem. Biol.* 16, 538–545. doi: 10.1038/s41589-020-0473-5

Kim, S. J., Yoon, J., Im, D. K., Kim, Y. H., and Oh, M. K. (2019). Adaptively evolved *Escherichia coli* for improved ability of formate utilization as a carbon source in sugar-free conditions. *Biotechnol. Biofuels* 12:207. doi: 10.1186/S13068-019-1547-Z

Koay, T. W., Wong, H. L., and Lim, B. H. (2016). Engineering of chimeric eukaryotic/bacterial Rubisco large subunits in *Escherichia coli*. *Genes Genet. Syst.* 139–150. doi: 10.1266/ggs.15-00054

Kubis, A., and Bar-Even, A. (2019). Synthetic biology approaches for improving photosynthesis. *J. Exp. Bot.* 70, 1425–1433. doi: 10.1093/jxb/erz029

Kushwaha, D., Upadhyay, S. N., and Mishra, P. K. (2018). Growth of Cyanobacteria: optimization for increased carbohydrate content. *Appl. Biochem. Biotechnol.* 184, 1247–1262. doi: 10.1007/s12010-017-2620-3

Lee, S., and Kim, P. (2020). Current status and applications of adaptive laboratory evolution in industrial microorganisms. *J. Microbiol. Biotechnol.* 30, 793–803. doi: 10.4014/jmb.2003.03072

Lemaire, O. N., Jespersen, M., and Wagner, T. (2020). CO2-fixation strategies in energy extremophiles: what can we learn from acetogens? *Front. Microbiol.* 11:486. doi: 10.3389/Fmicb.2020.00486

Li, D., Huang, L., Liu, T., Liu, J., Zhen, L., Wu, J., et al. (2019). Electrochemical reduction of carbon dioxide to formate via nano-prism assembled CuO microspheres. *Chemosphere* 237:124527. doi: 10.1016/j.chemosphere.2019.124527

Li, H., Opgenorth, P. H., Wernick, D. G., Rogers, S., Wu, T. Y., Higashide, W., et al. (2012). Integrated electromicrobial conversion of CO2 to higher alcohols. *Science* 335, 1596–1596. doi: 10.1126/science.1217643

Li, Y. J., Wang, M. M., Chen, Y. W., Wang, M., Fan, L. H., and Tan, T. W. (2017). Engineered yeast with a CO2-fixation pathway to improve the bio-ethanol production from xylose-mixed sugars. *Sci. Rep.* 7:43875. doi: 10.1038/srep43875

Liang, F. Y., Lindberg, P., and Lindblad, P. (2018). Engineering photoautotrophic carbon fixation for enhanced growth and productivity. *Sustain. Energ. Fuels* 2, 2583–2600. doi: 10.1039/c8se00281a

Lin, M. T., Occhialini, A., Andralojc, P. J., Parry, M. A. J., and Hanson, M. R. (2014). A faster Rubisco with potential to increase photosynthesis in crops. *Nature* 513, 547–550. doi: 10.1038/nature13776

Lin, P. P., Jaeger, A. J., Wu, T. Y., Xu, S. C., Lee, A. S., Gao, F. K., et al. (2018). Construction and evolution of an *Escherichia coli* strain relying on nonoxidative glycolysis for sugar catabolism. *Proc. Natl. Acad. Sci. U.S.A.* 115, 3538–3546. doi: 10.1073/pnas.1802191115

Liu, Z. H., Wang, K., Chen, Y., Tan, T. W., and Nielsen, J. (2020). Third-generation biorefineries as the means to produce fuels and chemicals from CO2. *Nat. Catal.* 3, 274–288. doi: 10.1038/s41929-019-0421-5

Ljungdahl, L. G. (1969). Total synthesis of acetate from CO2 by heterotrophic bacteria. *Annu. Rev. Microbiol.* 23, 515–538. doi: 10.1146/annurev.mi.23.100169.002503

Luan, G., Zhang, S., and Lu, X. (2020). Engineering cyanobacteria chassis cells toward more efficient photosynthesis. *Curr. Opin. Biotechnol.* 62, 1–6. doi: 10.1016/j.copbio.2019.07.004

Maia, L. B., Fonseca, L., Moura, I., and Moura, J. J. (2016). Reduction of carbon dioxide by a molybdenum-containing formate dehydrogenase: a kinetic and mechanistic study. *J. Am. Chem. Soc.* 138, 8834–8846. doi: 10.1021/jacs.6b03941

Maia, L. B., Moura, I., and Moura, J. J. G. (2017). Molybdenum and tungsten-containing formate dehydrogenases: aiming to inspire a catalyst for carbon dioxide utilization. *Inorg. Chim. Acta* 455, 350–363. doi: 10.1016/j.ica.2016.07.010

Mainguet, S. E., Gronenberg, L. S., Wong, S. S., and Liao, J. C. (2013). A reverse glyoxylate shunt to build a non-native route from C4 to C2 in *Escherichia coli*. *Metab. Eng.* 19, 116–127. doi: 10.1016/j.ymben.2013.06.004

Martinez, A., Bradley, A. S., Waldbauer, J. R., Summons, R. E., and DeLong, E. F. (2007). Proteorhodopsin photosystem gene expression enables photophosphorylation in a heterologous host. *Proc. Natl. Acad. Sci. U.S.A.* 104, 5590–5595. doi: 10.1073/pnas.0611470104

Mattozzi, M., Ziesack, M., Voges, M. J., Silver, P. A., and Way, J. C. (2013). Expression of the sub-pathways of the *Chloroflexus aurantiacus* 3-hydroxypropionate carbon fixation bicycle in *E. coli*: toward horizontal transfer of autotrophic growth. *Metab. Eng.* 16, 130–139. doi: 10.1016/j.ymben.2013.01.005

Mock, J., Zheng, Y. N., Mueller, A. P., Ly, S., Tran, L., Segovia, S., et al. (2015). Energy conservation associated with ethanol formation from H2 and CO2 in *Clostridium autoethanogenum* involving electron bifurcation. *J. Bacteriol.* 197, 2965–2980. doi: 10.1128/Jb.00399-15

Mueller-Cajar, O., Morell, M., and Whitney, S. M. (2007). Directed evolution of rubisco in *Escherichia coli* reveals a specificity-determining hydrogen bond in the form II enzyme. *Biochemistry* 16, 14067–14074. doi: 10.1021/bi700820a

Mueller-Cajar, O., and Whitney, S. M. (2008a). Directing the evolution of Rubisco and Rubisco activase: first impressions of a new tool for photosynthesis research. *Photosynth. Res.* 98, 667–675. doi: 10.1007/s11120-008-9324-z

Mueller-Cajar, O., and Whitney, S. M. (2008b). Evolving improved *Synechococcus* Rubisco functional expression in *Escherichia coli*. *Biochem. J.* 414, 205–214. doi: 10.1042/BJ20080668

Nielsen, J., and Keasling, J. D. (2016). Engineering cellular metabolism. *Cell* 164, 1185–1197. doi: 10.1016/j.cell.2016.02.004

Nielsen, J., Larsson, C., van Maris, A., and Pronk, J. (2013). Metabolic engineering of yeast for production of fuels and chemicals. *Curr. Opin. Biotech.* 24, 398–404. doi: 10.1016/j.copbio.2013.03.023

Niks, D., and Hille, R. (2019). Molybdenum- and tungsten-containing formate dehydrogenases and formylmethanofuran dehydrogenases: structure, mechanism, and cofactor insertion. *Protein Sci.* 28, 111–122. doi: 10.1002/pro.3498

Nogue, V. S., and Karhumaa, K. (2015). Xylose fermentation as a challenge for commercialization of lignocellulosic fuels and chemicals. *Biotechnol. Lett.* 37, 761–772. doi: 10.1007/s10529-014-1756-2

Pacala, S., and Socolow, R. (2004). Stabilization wedges: solving the climate problem for the next 50 years with current technologies. *Science* 305, 968–972. doi: 10.1126/science.1100103

Parikh, M. R., Greene, D. N., Woods, K. K., and Matsumura, I. (2006). Directed evolution of RuBisCO hypermorphs through genetic selection in engineered *E.coli*. *Protein Eng. Des. Sel.* 19, 113–119. doi: 10.1093/protein/gzj010

Ragsdale, S. W. (1997). The eastern and western branches of the Wood/Ljungdahl pathway: how the east and west were won. *Biofactors* 6, 3–11. doi: 10.1002/biof.5520060102

Satagopan, S., Huening, K. A., and Tabita, F. R. (2019). Selection of cyanobacterial (*Synechococcus* sp. Strain PCC 6301) RubisCO variants with improved functional properties that confer enhanced CO2-dependent growth of *Rhodobacter capsulatus*, a photosynthetic bacterium. *mBio* 10:e01537-19. doi: 10.1128/mBio.01537-19

Savakis, P., and Hellingwerf, K. J. (2015). Engineering cyanobacteria for direct biofuel production from CO2. *Curr. Opin. Biotech.* 33, 8–14. doi: 10.1016/j.copbio.2014.09.007

Schwander, T., von Borzyskowski, L. S., Burgener, S., Cortina, N. S., and Erb, T. J. (2016). A synthetic pathway for the fixation of carbon dioxide in vitro. *Science* 354, 900–904. doi: 10.1126/science.aah5237

Siebert, D., Busche, T., Metz, A. Y., Smaili, M., Queck, B. A. W., Kalinowski, J., et al. (2020). Genetic engineering of *Oligotropha carboxidovorans* strain OM5-A promising candidate for the aerobic utilization of synthesis gas. *Acs Synth. Biol.* 9, 1426–1440. doi: 10.1021/acssynbio.0c00098

Siegel, J. B., Smith, A. L., Poust, S., Wargacki, A. J., Bar-Even, A., Louw, C., et al. (2015). Computational protein design enables a novel one-carbon assimilation pathway. *Proc. Natl. Acad. Sci. U.S.A.* 112, 3704–3709. doi: 10.1073/pnas.1500545112

Siu, K. H., Chen, R. P., Sun, Q., Chen, L., Tsai, S. L., and Chen, W. (2015). Synthetic scaffolds for pathway enhancement. *Curr. Opin. Biotech.* 36, 98–106. doi: 10.1016/j.copbio.2015.08.009

Song, S., Timm, S., Lindner, S. N., Reimann, V., Hess, W. R., Hagemann, M., et al. (2020). Expression of formate-tetrahydrofolate ligase did not improve growth

but interferes with nitrogen and carbon metabolism of *Synechocystis* sp. *PCC* 6803. *Front. Microbiol.* 11:1650. doi: 10.3389/fmicb.2020.01650

Tilman, D., Socolow, R., Foley, J. A., Hill, J., Larson, E., Lynd, L., et al. (2009). Energy. Beneficial biofuels–the food, energy, and environment trilemma. *Science* 325, 270–271. doi: 10.1126/science.1177970

Veaudor, T., Blanc-Garin, V., Chenebault, C., Diaz-Santos, E., Sassi, J. F., Cassier-Chauvat, C., et al. (2020). Recent advances in the photoautotrophic metabolism of Cyanobacteria: biotechnological implications. *Life* 10:71. doi: 10.3390/life10050071

Wilson, R. H., Alonso, H., and Whitney, S. M. (2016). Evolving *Methanococcoides burtonii* archaeal Rubisco for improved photosynthesis and plant growth. *Sci. Rep.* 6:22284. doi: 10.1038/srep22284

Xia, P. F., Zhang, G. C., Walker, B., Seo, S. O., Kwak, S., Liu, J. J., et al. (2017). Recycling carbon dioxide during xylose fermentation by engineered *Saccharomyces cerevisiae*. *ACS Synth. Biol.* 6, 276–283. doi: 10.1021/acssynbio.6b00167

Xin, Y., Shi, Y., Niu, T., Wang, Q., Niu, W., Huang, X., et al. (2018). Cryo-EM structure of the RC-LH core complex from an early branching photosynthetic prokaryote. *Nat. Commun.* 9:1568. doi: 10.1038/s41467-018-03881-x

Yishai, O., Bouzon, M., Doring, V., and Bar-Even, A. (2018). *In vivo* assimilation of one-carbon via a synthetic reductive glycine pathway in *Escherichia coli*. *Acs Synth. Biol.* 2023–2028. doi: 10.1021/acssynbio.8b00131

Yu, H., Li, X., Duchoud, F., Chuang, D. S., and Liao, J. C. (2018). Augmenting the Calvin-Benson-Bassham cycle by a synthetic malyl-CoA-glycerate carbon fixation pathway. *Nat. Commun.* 9:2008. doi: 10.1038/s41467-018-04417-z

Yu, J. (2018). Fixation of carbon dioxide by a hydrogen-oxidizing bacterium for value-added products. *World J. Microb. Biot.* 34:89. doi: 10.1007/s11274-018-2473-0

Yu, X., Niks, D., Mulchandani, A., and Hille, R. (2017). Efficient reduction of CO2 by the molybdenum-containing formate dehydrogenase from *Cupriavidus necator* (*Ralstonia eutropha*). *J. Biol. Chem.* 292, 16872–16879. doi: 10.1074/jbc.M117.785576

Zelcbuch, L., Lindner, S. N., Zegman, Y., Slutskin, I. V., Antonovsky, N., Gleizer, S., et al. (2016). Pyruvate formate-lyase enables efficient growth of *Escherichia coli* on acetate and formate. *Biochemistry* 55, 2423–2426. doi: 10.1021/acs.biochem.6b00184

Zhou, Y., and Whitney, S. (2019). Directed evolution of an improved Rubisco; *In vitro* analyses to decipher fact from fiction. *Int. J. Mol. Sci.* 20:5019. doi: 10.3390/ijms20205019

Conflict of Interest: The authors declare that the research was conducted in the absence of any commercial or financial relationships that could be construed as a potential conflict of interest.

frontiers in Microbiology

CORRECTION
published: 14 December 2020
doi: 10.3389/fmicb.2020.632455

Corrigendum: Recent Advances in Developing Artificial Autotrophic Microorganism for Reinforcing CO_2 Fixation

Bo Liang[1,2]*, *Yukun Zhao*[3] *and Jianming Yang*[1,2]*

[1] Energy-rich Compounds Production by Photosynthetic Carbon Fixation Research Center, Qingdao Agricultural University, Qingdao, China, [2] Shandong Key Lab of Applied Mycology, College of Life Sciences, Qingdao Agricultural University, Qingdao, China, [3] Pony Testing International Group, Qingdao, China

Keywords: CO_2 fixation, autotrophy, heterotrophy, synthetic biology, reducing power, cell factory

Approved by:
Frontiers Editorial Office, Frontiers Media SA, Switzerland

***Correspondence:**
Bo Liang
liangboqdnd@163.com
Jianming Yang
yjming888@126.com

Specialty section:
This article was submitted to Microbiotechnology, a section of the journal Frontiers in Microbiology

Received: *23 November 2020*
Accepted: *25 November 2020*
Published: *14 December 2020*

Citation:
Liang B, Zhao Y and Yang J (2020) Corrigendum: Recent Advances in Developing Artificial Autotrophic Microorganism for Reinforcing CO_2 Fixation. Front. Microbiol. 11:632455. doi: 10.3389/fmicb.2020.632455

A Corrigendum on

Recent Advances in Developing Artificial Autotrophic Microorganism for Reinforcing CO_2 Fixation

by Liang, B., Zhao, Y., and Yang, J. (2020). Front. Microbiol. 11:592631. doi: 10.3389/fmicb.2020.592631

An author name was incorrectly spelled as Yunkun Zhao. The correct spelling is Yukun Zhao

The authors apologize for this error and state that this does not change the scientific conclusions of the article in any way. The original article has been updated.

frontiers in Microbiology

ORIGINAL RESEARCH
published: 11 February 2021
doi: 10.3389/fmicb.2021.638426

Improving the Methanol Tolerance of an *Escherichia coli* Methylotroph via Adaptive Laboratory Evolution Enhances Synthetic Methanol Utilization

*R. Kyle Bennett[1,2†], Gwendolyn J. Gregory[1,2†], Jacqueline E. Gonzalez[1], Jie Ren Gerald Har[1], Maciek R. Antoniewicz[1] and Eleftherios T. Papoutsakis[1,2]**

[1] Department of Chemical and Biomolecular Engineering, University of Delaware, Newark, DE, United States, [2] Molecular Biotechnology Laboratory, The Delaware Biotechnology Institute, University of Delaware, Newark, DE, United States

OPEN ACCESS

Edited by:
Guodong Luan,
Qingdao Institute of Bioenergy and Bioprocess Technology (CAS), China

Reviewed by:
Ludmila Chistoserdova,
University of Washington, United States
Yu Wang,
Chinese Academy of Sciences, China
Wenming Zhang,
Nanjing Tech University, China

***Correspondence:**
Eleftherios T. Papoutsakis
epaps@udel.edu

[†] These authors have contributed equally to this work

Specialty section:
This article was submitted to Microbiotechnology, a section of the journal Frontiers in Microbiology

Received: 06 December 2020
Accepted: 21 January 2021
Published: 11 February 2021

Citation:
Bennett RK, Gregory GJ, Gonzalez JE, Har JRG, Antoniewicz MR and Papoutsakis ET (2021) Improving the Methanol Tolerance of an Escherichia coli Methylotroph via Adaptive Laboratory Evolution Enhances Synthetic Methanol Utilization. Front. Microbiol. 12:638426. doi: 10.3389/fmicb.2021.638426

There is great interest in developing synthetic methylotrophs that harbor methane and methanol utilization pathways in heterologous hosts such as *Escherichia coli* for industrial bioconversion of one-carbon compounds. While there are recent reports that describe the successful engineering of synthetic methylotrophs, additional efforts are required to achieve the robust methylotrophic phenotypes required for industrial realization. Here, we address an important issue of synthetic methylotrophy in *E. coli*: methanol toxicity. Both methanol, and its oxidation product, formaldehyde, are cytotoxic to cells. Methanol alters the fluidity and biological properties of cellular membranes while formaldehyde reacts readily with proteins and nucleic acids. Thus, efforts to enhance the methanol tolerance of synthetic methylotrophs are important. Here, adaptive laboratory evolution was performed to improve the methanol tolerance of several *E. coli* strains, both methylotrophic and non-methylotrophic. Serial batch passaging in rich medium containing toxic methanol concentrations yielded clones exhibiting improved methanol tolerance. In several cases, these evolved clones exhibited a $>$ 50% improvement in growth rate and biomass yield in the presence of high methanol concentrations compared to the respective parental strains. Importantly, one evolved clone exhibited a two to threefold improvement in the methanol utilization phenotype, as determined via ^{13}C-labeling, at non-toxic, industrially relevant methanol concentrations compared to the respective parental strain. Whole genome sequencing was performed to identify causative mutations contributing to methanol tolerance. Common mutations were identified in 30S ribosomal subunit proteins, which increased translational accuracy and provided insight into a novel methanol tolerance mechanism. This study addresses an important issue of synthetic methylotrophy in *E. coli* and provides insight as to how methanol toxicity can be alleviated via enhancing methanol tolerance. Coupled improvement of methanol tolerance and synthetic methanol utilization is an important advancement for the field of synthetic methylotrophy.

Keywords: synthetic methylotrophy, methanol tolerance, *E. coli*, methanol, methanol toxicity

INTRODUCTION

There is great interest in utilizing methane and methanol from natural gas reserves as industrial feedstocks (Haynes and Gonzalez, 2014). Product yields from methane and methanol can be increased due to the fact that they more reduced than carbohydrates (Whitaker et al., 2015). Furthermore, biological conversion of methane and methanol is preferable to chemical catalysis, as it does not require extreme conditions and has higher specificity. Native methylotrophs are not as genetically tractable and have much slower growth kinetics than established platform hosts such as *E. coli* (Bennett et al., 2018b). Therefore, emphasis has been placed on the development and utilization of synthetic methylotrophic organisms that are engineered to utilize methane and methanol (Whitaker et al., 2015; Bennett et al., 2018b).

In the last several years, there have been multiple approaches to engineer synthetic methylotrophs, with most work done in *E. coli* (Price et al., 2016; Bennett et al., 2018a, 2020c; Chen et al., 2018; Gonzalez et al., 2018; Meyer et al., 2018; Woolston et al., 2018a; Zhang et al., 2018; Rohlhill et al., 2020), *Corynebacterium glutamicum* (Lessmeier et al., 2015; Witthoff et al., 2015; Tuyishime et al., 2018), and *Saccharomyces cerevisiae* (Dai et al., 2017). As illustrated in **Figure 1**, the ribulose monophosphate (RuMP) pathway is the most often employed pathway for synthetic methylotrophy. This pathway is made up of two enzymes, Hps (hexulose phosphate synthase) and Phi (phosphohexulose isomerase). Together with Mdh (methanol dehydrogenase), this pathway oxidizes methanol to formaldehyde (via Mdh), which is then fixed with ribulose 5-phosphate to produce hexulose 6-phosphate (via Hps), which is finally converted to fructose 6-phosphate (via Phi).

Autonomous synthetic methylotrophy, wherein growth on methane or methanol does not require additional carbon sources, has been difficult to realize. Only one study to date has reported the successful construction of a true *E. coli* methylotroph (Chen et al., 2020). In order to achieve this feat, the authors relied on a combination of rational engineering and adaptive laboratory evolution (ALE). The resulting evolved strain exhibited a doubling time of 8.5 h and was able to grow to an optical density (OD) of 2 in methanol minimal medium. Optimal growth was observed at methanol concentrations between 400 and 600 mM. Growth defects became obvious at 1 M methanol, and growth was completely abolished at 1.5 M methanol, highlighting the negative consequences of methanol toxicity and need for improved methanol tolerance in order to achieve a more robust phenotype.

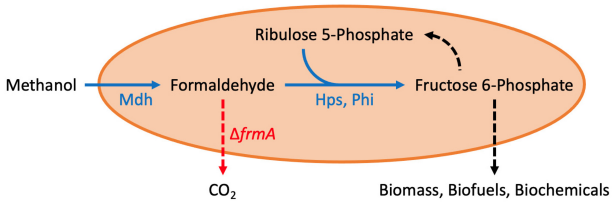

FIGURE 1 | Synthetic methanol metabolism in *E. coli*. Methanol dehydrogenase (mdh), hexulose phosphate synthase (hps), phosphohexulose isomerase (phi), and formaldehyde dissimilation pathway (*frmRAB*). See text for more details. This figure was adapted from Bennett et al. (2020a).

The difficulty in construction of true synthetic methylotrophs has been attributed to multiple causes, including poor enzyme kinetics (Wu et al., 2016; Roth et al., 2019), the inability to remove a native co-substrate due to growth dependence (Chen et al., 2018; Meyer et al., 2018; Antoniewicz, 2019), a lack of proper gene regulation in synthetic hosts (Rohlhill et al., 2017, 2020; Woolston et al., 2018b), poor synthesis of proteinogenic amino acids from methanol carbon (Gonzalez et al., 2018), and the cytotoxicity of methanol (Lessmeier and Wendisch, 2015; Wang et al., 2020). The cytotoxicity of methanol is twofold: methanol alters the fluidity and biological properties of cellular membranes (Gustafson and Tagesson, 1985; Sonmez et al., 2013) while formaldehyde, the oxidation product of methanol, reacts readily with proteins and DNA (Chang and Gershwin, 1992; Teng et al., 2001). Due to these cytotoxic effects, there is interest to improve the methanol and/or formaldehyde tolerance of native and synthetic methylotrophs. It has been demonstrated that *E. coli* tolerates methanol relatively well, growing in the presence of 4% (v/v), or ca. 1 M, methanol in Luria-Bertani (LB) media (Ganske and Bornscheuer, 2006). However, the same study reported complete growth inhibition at a methanol concentration of 10% (v/v), or ca. 2.5 M. Improved methanol tolerance is not only beneficial for methylotrophic *E. coli*, but also lends itself to fermentations where the substrates, media components or fermentation conditions contain methanol as an impurity. For example, crude glycerol may contain methanol as an impurity depending upon how it is processed (Yang et al., 2012).

Formaldehyde is a more potent cytotoxin to cells than methanol due to its high reactivity with nucleic acids and proteins, which results in cross-linking (Chang and Gershwin, 1992; Teng et al., 2001). Therefore, in addition to methanol's direct effect on cells, it also indirectly impacts cells via its oxidation product. Formaldehyde must therefore be assimilated or dissimilated readily. In *E. coli*, a linear dissimilation pathway, encoded by the *frmRAB* operon, exists to combat endogenous formaldehyde resulting from select metabolic pathways or oxidative demethylation of nucleic acids (Gonzalez et al., 2006). Specifically, formaldehyde induces expression of this operon via a formaldehyde-responsive promoter, which is transcriptionally regulated by the repressor *frmR* (Gonzalez et al., 2006; Rohlhill et al., 2017). In a two-step process, formaldehyde is readily oxidized to formate by *S*-hydroxymethylglutathione dehydrogenase (*frmA*) and *S*-formylglutathione hydrolase (*frmB*). Formate can then be further oxidized to CO_2. However, many studies geared toward engineering synthetic methylotrophs have relied on a Δ*frmA* genetic background in order to conserve formaldehyde carbon for assimilation to support methylotrophic growth (Muller et al., 2015; Whitaker et al., 2015). Thus, the need for improved methanol/formaldehyde tolerance becomes more apparent when this "safety valve" is removed from the cell. In order to utilize formaldehyde for cell growth, native and synthetic methylotrophs must contain a formaldehyde assimilation pathway to capture carbon and energy from formaldehyde while alleviating toxicity. As described above,

the RuMP pathway is of considerable interest for engineering synthetic methylotrophs since it is the most energy efficient pathway among the three candidates and requires only two core enzymes (Whitaker et al., 2015).

Efforts to improve the methanol tolerance of native and synthetic methylotrophs have been reported for *B. methanolicus* and *C. glutamicum*. For the *B. methanolicus* study, it was reported that upregulation of genes involved in methanol oxidation and the RuMP pathway contributed to improved methanol and formaldehyde tolerance (Jakobsen et al., 2006). For one *C. glutamicum* study, ALE was performed on a non-methylotrophic *C. glutamicum* wild-type strain, which resulted in an evolved clone that was more tolerant to all methanol concentrations up to 3 M (Lessmeier and Wendisch, 2015). A second *C. glutamicum* study improved the methanol tolerance of a methylotrophic *C. glutamicum* methanol auxotroph, which resulted in an evolved strain that could tolerate up to 20 g/L (ca. 600 mM) methanol without any growth defects (Tuyishime et al., 2018; Wang et al., 2020).

Collectively, these previous studies highlight the many direct and indirect effects of methanol toxicity and various ways that methanol tolerance can be achieved. In this study, we performed ALE to improve the methanol tolerance of several *E. coli* strains, both methylotrophic and non-methylotrophic, and used WGS analysis to identify the common mutations responsible for methanol tolerance. Our results provide insight into a novel mechanism for methanol tolerance, which occurs from mutations in 30S ribosomal subunit proteins, and emphasize the ability to couple improved methanol tolerance with enhanced synthetic methanol utilization.

MATERIALS AND METHODS

Chemicals

All chemicals were purchased from Sigma-Aldrich (St. Louis, MO) unless noted otherwise. ^{13}C-methanol (99% ^{13}C) was purchased from Cambridge Isotope Laboratories (Tewksbury, MA). *E. coli* NEB5α, Q5 DNA polymerase and NEBuilder HiFi DNA assembly master mix were purchased from NEB (Ipswich, MA). Restriction endonucleases were purchased from Thermo Fisher Scientific (Waltham, MA).

Strains and Plasmids

All strains, plasmids, and primers used in this study are listed in **Supplementary Tables S1–S3**, respectively. *E. coli* NEB5a was used for plasmid construction and propagation. *E. coli* BW25113 D*frmA* was obtained from the Keio collection and used for growth characterization (Baba et al., 2006). Deletion of *ihfA* was performed as previously described via the lambda red recombineering system (Datsenko and Wanner, 2000; Bennett et al., 2020a). Methanol assimilation genes were cloned into pETM6 (Xu et al., 2012) for episomal expression as previously described to produce the pUD9 plasmid (Bennett et al., 2018a). Overexpression of *crp* was achieved as previously described (Bennett et al., 2020a).

Media and Growth Conditions

E. coli strains were routinely cultured in LB medium supplemented with the appropriate antibiotics (100 μg/mL ampicillin, 25 μg/mL kanamycin) unless otherwise noted. Growth characterization of *E. coli* strains for methanol or formaldehyde tolerance was performed in 250 mL baffled flasks containing 30 mL LB medium supplemented with methanol or formaldehyde at the specified concentrations at 37°C and 250 RPM. Cell growth rate was determined every hour as follows: $\ln(C/C_0)/(t - t_0)$, where C and C_0 represent the biomass concentration at the current (t) and prior (t_0) times (e.g., 3 and 2 h). The highest value was selected as the maximum growth rate. For methylotrophic growth and ^{13}C-labeling assays, an overnight culture of the respective *E. coli* strain in LB medium was used to inoculate fresh M9 minimal medium containing 1 g/L yeast extract with or without 60 mM ^{13}C-methanol to an OD_{600} of approximately 0.05. Samples were collected at 48h for labeling analysis.

Chemical Mutagenesis and Adaptive Laboratory Evolution (ALE)

Chemical mutagenesis was performed as described previously (Sandoval et al., 2015). Briefly, 70 μL of an overnight culture of *E. coli* Δ*frmA* pUD9 was used to inoculate 7 mL of fresh LB medium. Cells were grown aerobically at 37°C until an OD_{600} of 1. Cells were then harvested via centrifugation (4,000 g, 10 min), washed once with 10 mL of PT buffer (0.1 g/L peptone, 8.5 g/L sodium chloride, 1 g/L sodium thioglycolate), harvested again via centrifugation (4,000 g, 10 min) and finally resuspended in 7 mL of fresh LB medium. 200 μL of 2.5 g/L *N*-methyl-*N*'-nitro-*N*-nitrosoguanidine (NTG) was then added, followed by a 20 min incubation at 37°C. Mutagenized cells were then harvested via centrifugation (4,000 g, 10 min) and washed thrice with 10 mL of PT buffer, followed by resuspension in 10 mL of fresh LB medium and outgrowth overnight at 37°C. The lethality of this chemical mutagenesis was determined to be ca. 99% as CFUs/mL directly prior to NTG treatment were ca. 7.2×10^8 and ca. 6.4×10^4 directly following NTG treatment.

After overnight recovery, mutagenized cells were subjected to directed evolution via passaging in fresh LB medium supplemented with methanol. After the initial recovery, cells were used to inoculate fresh LB medium supplemented with 1 M methanol. Upon growth of this culture, cells were used to inoculate fresh LB medium supplemented with 1.25 M methanol. This procedure was continued for 1.5, 1.75, and 2 M methanol. Upon growth in fresh LB medium supplemented 2 M methanol, a frozen stock in 20% glycerol was made. This frozen stock was streaked on a fresh LB agar plate to isolate individual clones. Six of these clones were analyzed for improved methanol tolerance over the non-evolved parent strain in fresh LB medium supplemented with 2 M methanol. The clone exhibiting the most improved methanol tolerance was used for further analysis.

Three other *E. coli* strains (Δ*frmA*, Δ*frmA*Δ*ihfA* + pUD9 and Δ*frmA* + pUD9 + pCrp) were also subjected to ALE without NTG mutagenesis. Serial batch passaging in LB medium supplemented with increasing methanol concentrations

was performed in a similar manner until methanol-tolerant clones could be isolated. Approximately 10 passages were required to achieve improved methanol tolerance when chemical mutagenesis was not used.

Resting Cell Assays

Mdh, Hps and Phi *in vivo* assays were performed as described (Whitaker et al., 2017). Briefly, *E. coli* Δ*frmA* strains expressing *B. stearothermophilus* Mdh and *B. methanolicus* Hps and Phi were grown from a colony in LB for 6 h at 37°C with shaking (225 rpm). Cells were then washed twice in M9 minimal medium and adjusted to an OD_{600} of 1.0 in M9 minimal medium. Methanol was added to a final concentration of 1 M while formaldehyde was added to a final concentration of 1 mM. At the indicated time points, samples were collected and 400 μL of culture supernatant was mixed with 800 μL of Nash reagent to assay for formaldehyde concentration (Nash, 1953).

Analytical Methods

Biomass concentration was determined as previously described (Whitaker et al., 2017; Bennett et al., 2018a). Briefly, OD_{600} was measured on a Beckman-Coulter DU730 spectrophotometer. Methanol boost was calculated as the percentage improvement of biomass yield of a culture in the presence of methanol as compared to the control without methanol (Whitaker et al., 2017; Bennett et al., 2020a,b). Methanol was measured via high performance liquid chromatography (HPLC) (Whitaker et al., 2017). Extraction of metabolites and proteinogenic amino acids was performed as previously described and analyzed for ^{13}C-labeling using gas chromatography-mass spectrometry (Whitaker et al., 2017; Bennett et al., 2018a, 2020a,b,c; Long and Antoniewicz, 2019). ^{13}C-labeling was determined from the measured mass isotopomer data (Whitaker et al., 2017; Long and Antoniewicz, 2019). Statistics were calculated using a two-tailed unpaired *t*-test with a 95% confidence interval.

Whole Genome Sequencing

Whole genome sequencing of Δ*frmA* parental and evolved strains, Δ*ihfA* parental and evolved strains, and KB201, a Δ*frmA* strain that was subjected to directed evolution without the pUD9 plasmid, was performed as previously described (Bennett et al., 2020c). Briefly, genomic DNA was extracted using a Qiagen DNeasy Blood and tissue kit per manufacturer's protocol (Germantown, MD). Genomic DNA was then sequenced on an RSII sequencer system (Pacific Biosciences, Menlo Park, CA) using single molecule, real time (SMRT) sequencing (University of Delaware DNA Sequencing and Genotyping Center), with average read length of 10 kb generated. Sequencing analysis was performed with the SMRT Link software via the resequencing application (Pacific Biosciences). *E. coli* BW25113 (GenBank CP009273.1) was used as the reference genome. Mutations unique to each sequenced strain in comparison to the respective parental strain were chosen.

RESULTS

Adaptive Laboratory Evolution, Combined With Chemical Mutagenesis, Enhances the Methanol Tolerance of a Synthetic *E. coli* Methylotroph

As discussed, methanol and formaldehyde are cytotoxic to cells. In LB medium, the growth rate of a synthetic *E. coli* methylotroph (*E. coli* BW25113 Δ*frmA* + pUD9) is severely inhibited above methanol concentrations of 1 M (**Figure 2** and **Supplementary Figure S1A**). Specifically, the growth rates in the presence of 0, 1, 2, and 3 M methanol are 1.2 ± 0.02, 1.0 ± 0.01, 0.47 ± 0.02, and 0.07 ± 0.00 h^{-1}, respectively. Since several studies have reported using high methanol concentrations, specifically ≥ 1 M, for natural and synthetic methylotrophs, specifically *B. methanolicus* (Bozdag et al., 2015) and *E. coli* (Muller et al., 2015), improved methanol tolerance at these high concentrations would be beneficial.

To improve the methanol tolerance of this synthetic *E. coli* methylotroph (*E. coli* BW25113 Δ*frmA* + pUD9), chemical mutagenesis and ALE were performed. Briefly, cells were first mutagenized with *N*-methyl-*N*'-nitro-*N*-nitrosoguanidine (NTG), which mutates DNA by alkylating guanine and thymine, resulting in transition mutations between GC and AT, recovered overnight in LB medium and then subjected to several rounds of passaging in LB medium supplemented with increasing methanol concentrations (**Supplementary Figure S1B**). After outgrowth in the presence of 2 M methanol, a frozen stock was prepared and subsequently streaked onto an LB agar plate to isolate individual clones. Six clones were examined for improved growth in LB medium supplemented with 2 M methanol (**Supplementary Figure S2**). One of these clones, "Evolved 3," simply referred to as "evolved," exhibited the largest improvement in growth and was selected for further analysis. Indeed, this evolved clone exhibited improved methanol tolerance at high methanol concentrations, i.e., 2–3 M (**Figures 2C,D** and **Supplementary Figure S1A**). Specifically, the growth rates in the presence of 0, 1, 2, and 3 M methanol were 1.2 ± 0.02, 1.1 ± 0.00, 0.65 ± 0.01, and 0.11 ± 0.01 h^{-1}, respectively (**Supplementary Table S4**). Thus, the evolved clone exhibited growth rate improvements of 10, 38, and 57% over the parental strain in 1, 2, and 3 M methanol, respectively. Additionally, the evolved clone achieved higher final biomass titers over the parent strain in LB medium supplemented with 2 and 3 M methanol (**Figures 2C,D**). Taken together, these results demonstrate the usefulness of chemical mutagenesis and ALE for improving tolerance to toxic substrates.

Methanol Tolerance of the Evolved Clone Is Specific to Methanol, Not Formaldehyde

To investigate whether the improved methanol tolerance of the evolved clone resulted from improved methanol and/or formaldehyde tolerance, the parental strain and evolved clone were cured of the pUD9 plasmid via serial passaging in the absence of the appropriate antibiotic so that formaldehyde

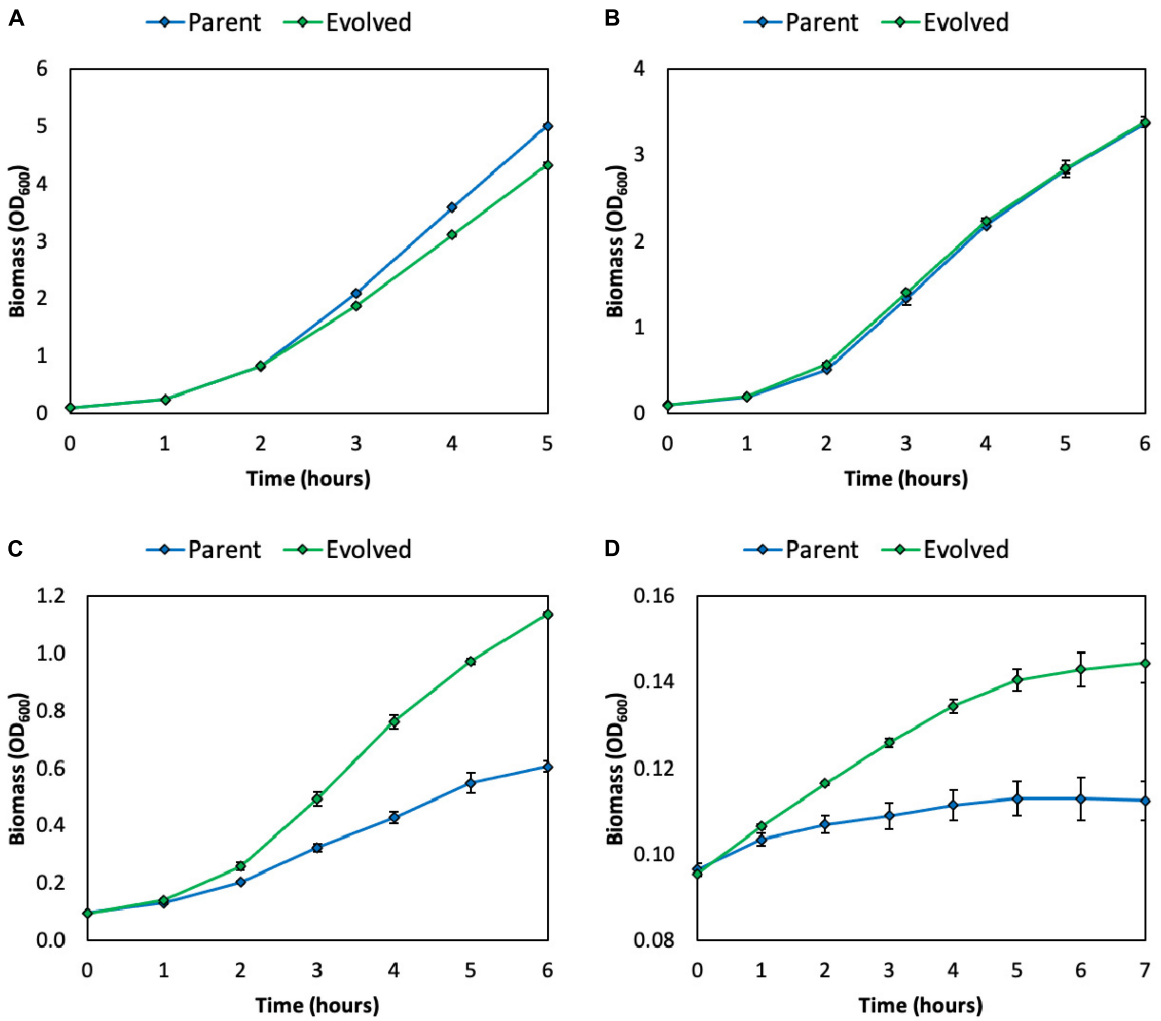

FIGURE 2 | Growth of parental and evolved methylotrophic *E. coli* strains in LB medium supplemented with 0 **(A)**, 1 **(B)**, 2 **(C)**, or 3 **(D)** M methanol. Error bars indicate standard error (n = 2).

tolerance of both strains could be determined. Plasmid curing was essential for this since both the Mdh and RuMP pathway enzymes readily consume formaldehyde, either via reducing it back to methanol or assimilating it into central carbon metabolism, respectively. Both pathways result in inaccurate growth rate measurements since the formaldehyde concentration is continually decreasing to non-toxic levels over time, thus yielding a dynamic growth rate (**Supplementary Figure S3**). Furthermore, the evolved, plasmid-containing clone was not observed to overcome formaldehyde toxicity more quickly than the plasmid-containing parental strain (**Supplementary Figure S3**), suggesting that the observed methanol tolerance of the evolved clone results from improved tolerance to methanol and not formaldehyde.

The resulting growth rates of both plasmid-cured strains in LB medium supplemented with varying levels of formaldehyde were similar (**Supplementary Figures S4, S5**), again suggesting that the observed methanol tolerance of the evolved clone results from improved tolerance to methanol and not formaldehyde, at least at the concentrations tested in this study. Furthermore, as discussed, formaldehyde exerts greater cytotoxicity on cells than does methanol, as indicated by the severe reduction in growth rate at low (i.e., mM) formaldehyde concentrations compared to high (i.e., M) methanol concentrations. Specifically, the growth rates of the plasmid-cured parental strain in the presence of 0, 0.25, 0.5, 1, and 1.5 mM formaldehyde were 1.4 ± 0.02, 1.0 ± 0.03, 0.75 ± 0.01, 0.33 ± 0.01, and 0.16 ± 0.01 h^{-1}, respectively (**Supplementary Table S4**). Comparatively, the growth rates of the plasmid-cured evolved clone in the presence of 0, 0.25, 0.5, 1, and 1.5 mM formaldehyde were 1.2 ± 0.00, 1.1 ± 0.01, 0.76 ± 0.00, 0.34 ± 0.00, and 0.18 ± 0.00 h^{-1}, respectively (**Supplementary Table S4**). The slight growth defect observed in the plasmid-cured evolved clone compared to the plasmid-cured parental strain likely results from genomic mutations developed during chemical mutagenesis and directed evolution. These mutations are discussed in the WGS section below.

Activities of the Methylotrophic Enzymes Are Retained Following Chemical Mutagenesis and Adaptive Laboratory Evolution

To investigate whether the improved methanol tolerance of the evolved clone results from improved rates of methanol and/or formaldehyde consumption via the Mdh and RuMP pathway enzymes, *in vivo* formaldehyde production and consumption assays were performed. Briefly, resting cells in minimal medium were used to monitor formaldehyde production following the addition of 1 M methanol (**Figure 3A**) or formaldehyde consumption following the addition of 1 mM formaldehyde (**Figure 3B**). The rates of formaldehyde production and consumption were similar between the parental strain and evolved clone, suggesting that the *in vivo* activities of the methylotrophic enzymes (Mdh, Hps, and Phi) are retained following chemical mutagenesis and ALE. Retention of *in vivo* activities of the methylotrophic enzymes, and thus a functional synthetic methanol utilization pathway, is further confirmed as methanol-derived carbon is still assimilated into intracellular metabolites following ALE, which is discussed in more detail in the methanol assimilation section below. These results are supported by WGS analysis (discussed in the WGS section below), which did not reveal any unique mutations in the pUD9 plasmid following chemical mutagenesis and ALE. Thus, it does not appear that the improved methanol tolerance of the evolved clone results from an increased rate of methanol and/or formaldehyde consumption through the synthetic methanol utilization pathway. Therefore, chromosomal mutations appear responsible for the improved methanol tolerance of the evolved clone, which agrees with the previous studies in *C. glutamicum* (Lessmeier and Wendisch, 2015; Wang et al., 2020).

Improved Methanol Tolerance Can Readily Be Achieved in Other *E. coli* Strains, Including Those That Are Non-methylotrophic

We previously examined mutants of several transcriptional regulators and found that deletion of integration host factor subunit α (*ihfA*), which is known to repress multiple amino acid metabolic pathways (Goosen and van de Putte, 1995; Karp et al., 2018), resulted in an improved methylotrophic phenotype, as indicated by increased ^{13}C-labeling of intracellular metabolites from ^{13}C-methanol (Bennett et al., 2020a). Overexpression of cAMP-receptor protein (*crp*), a known activator of multiple amino acid metabolic pathways (Karp et al., 2018), also resulted in an improved methylotrophic phenotype (Bennett et al., 2020a). Given the success of ALE in improving the methanol tolerance of the synthetic *E. coli* methylotroph described above (*E. coli* BW25113 Δ*frmA* + pUD9), we sought to also improve the methanol tolerance of these transcriptional regulator mutant strains. *E. coli* Δ*frmA*Δ*ihfA* + pUD9 (simply referred to as "Δ*ihfA*") and Δ*frmA* + pUD9 + pCrp (simply referred to as "pCrp") were serially passaged in LB medium supplemented with increasing methanol concentrations in a similar manner as before (**Supplementary Figure S6**). However, chemical mutagenesis was not used for this ALE. Once tolerance to 2 M methanol was achieved, which required ca. 10–15 passages, six clones of each strain were examined for improved growth in 2 M methanol as compared to the respective parental strains (**Supplementary Figure S7**). The "Evolved 2" clone from each strain, hereafter referred to as "evolved pCrp" and "evolved Δ*ihfA*," exhibited the most improved methanol tolerance and were selected for WGS analyses to identify common mutations responsible for methanol tolerance.

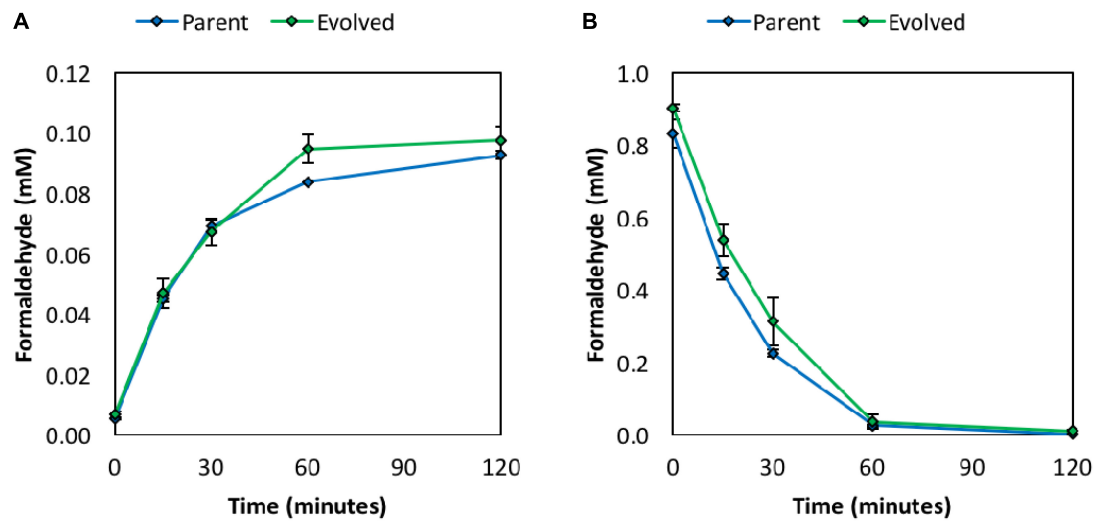

FIGURE 3 | Formaldehyde production from 1 M methanol *in vivo* **(A)** and formaldehyde consumption from 1 mM formaldehyde *in vivo* **(B)** in resting cells in M9 minimal medium. Error bars indicate standard error (n = 2).

To assess whether a non-methylotrophic *E. coli* strain could achieve improved methanol tolerance, we serially passaged *E. coli* Δ*frmA* (containing no plasmid) in LB medium supplemented with increasing methanol concentrations in a similar manner as before without chemical mutagenesis. After 11 passages, isolates were examined for improved methanol tolerance in 2 M methanol (**Supplementary Figure S8**). Interestingly, this non-methylotrophic *E. coli* strain did achieve improved methanol tolerance through ALE, suggesting that methanol tolerance is not specific to methylotrophic strains. The "KB201" clone (**Supplementary Figure S8B**), an evolved, non-methylotrophic *E. coli* BW25113 Δ*frmA* strain (containing no plasmid), was selected for WGS analyses to identify common mutations responsible for methanol tolerance.

Whole Genome Sequencing Revealed Common Mutations Responsible for Methanol Tolerance

We next sought to determine whether the evolved strains accumulated common genomic mutations that contributed to the methanol tolerance phenotype. We performed WGS analysis of the original evolved strain (Δ*frmA* + pUD9), KB201 and the evolved Δ*ihfA* clone. The evolved pCrp clone was excluded from WGS analysis for simplicity. Each evolved strain accumulated multiple unique mutations when compared to the respective parental strains (**Supplementary Table S5**). Of considerable interest were mutations found in 30S ribosomal subunit proteins, which were common among all of the evolved strains. Both the evolved Δ*ihfA* clone and KB201 had an identical mutation in *rpsQ*, a 30S ribosomal subunit protein S17, that resulted in a His31Pro change. The original evolved strain (Δ*frmA* + pUD9) had a point mutation in another 30S ribosomal subunit protein S12, *rpsL*, which resulted in a Gly92Ser amino acid change. The original evolved strain (Δ*frmA* + pUD9) was also observed to have a larger number of mutations, especially transition mutations, due to chemical mutagenesis prior to ALE. Since the only common mutation occurring in all three evolved strains was specific to a 30S ribosomal subunit protein, we hypothesize that methanol tolerance results from increased translational efficiency (Haft et al., 2014). To support this hypothesis, an identical mutation in *rpsQ* (H31P) was found in a previous study that examined ethanol tolerance of *E. coli* (Haft et al., 2014). This mutation was found to protect cells from ethanol toxicity by increasing the accuracy of protein synthesis. This suggests that the mechanisms of methanol and ethanol tolerance in *E. coli* are similar and not specific to methylotrophic metabolism, which is why methanol tolerance in the non-methylotrophic *E. coli* strain was readily achieved. Compared to previous methanol tolerance studies, these results provide a novel insight into alternative mechanisms of methanol tolerance.

Improved Methanol Tolerance Leads to Enhanced Synthetic Methanol Assimilation

Improving the methanol tolerance of a synthetic *E. coli* methylotroph is not beneficial unless the evolved clone retains the methylotrophic phenotype, i.e., growth on methanol, at low, non-toxic methanol concentrations, which are more practical for industrial bioprocesses to minimize substrate loss via evaporation and ensure complete substrate utilization. Previously, we demonstrated, for the first time, that a synthetic *E. coli* methylotroph is capable of growth on methanol with a small amount of yeast extract supplementation (Whitaker et al., 2017). To ensure that the original evolved strain (Δ*frmA* + pUD9) still exhibits the parental methylotrophic growth phenotype, methylotrophic growth assays in minimal medium supplemented with 1 g/L of yeast extract in the absence and presence of 60 mM ^{13}C-methanol were performed. Upon yeast extract exhaustion, we previously demonstrated that methylotrophic *E. coli* is able to grow on methanol for a brief period, resulting in improved biomass production and termed "methanol boost" (Whitaker et al., 2017). Here, we determined the methylotrophic characteristics of the original evolved strain (Δ*frmA* + pUD9) and compared them with the respective parental strain. Cultures were inoculated to an OD_{600} of approximately 0.05, and samples were collected at 48h for determination of biomass production, methanol consumption and ^{13}C-labeling. Both strains exhibited similar methylotrophic growth phenotypes in terms of biomass production as the total biomass production in the presence of methanol was approximately 25% higher than that in the absence of methanol, demonstrating that both strains exhibit growth on methanol and a methanol boost of ca. 25% (**Figure 4A**). Although biomass production profiles were similar between the two strains, total methanol consumption was improved in the original evolved strain (Δ*frmA* + pUD9), which consumed 11.1 ± 0.7 mM methanol over the course of 48 h, representing a 16% increase in total methanol consumption over the parental strain, which consumed 9.6 ± 0.2 mM methanol over the course of 48 h (**Figure 4B**).

Although total methanol consumption was improved in the original evolved strain (Δ*frmA* + pUD9), we aimed to determine whether more methanol was assimilated into metabolites and biomass components since methanol consumption includes both assimilation into central metabolism and dissimilation to formate and CO_2, even with Δ*frmA*. To quantify methanol assimilation, ^{13}C-labeling in intracellular metabolites and proteinogenic amino acids, derived from ^{13}C-methanol, was determined. Indeed, significantly higher ^{13}C-labeling was realized in the original evolved strain (Δ*frmA* + pUD9) as compared to the respective parental strain (**Figure 5**). For example, average carbon labeling in pyruvate (Pyr), a lower glycolytic intermediate, was increased from 26.7 ± 1.9% in the parental strain to 59.4 ± 0.7% in the evolved clone, representing an increase of 120%. Additionally, average carbon labeling in citrate (Cit), a TCA cycle intermediate, was increased from 19.8 ± 2.0% in the parental strain to 55.5 ± 1.7% in the evolved clone, representing an increase of 180%. Finally, average carbon labeling in alanine (Ala), a proteinogenic amino acid derived from Pyr, was increased from 26.2 ± 2.0% in the parental strain to 56.8 ± 0.9% in the evolved clone, representing an increase of 120%. Taken together, these results suggest that the original evolved strain (Δ*frmA* + pUD9) not only consumes more methanol, but also assimilates more methanol-derived carbon into intracellular

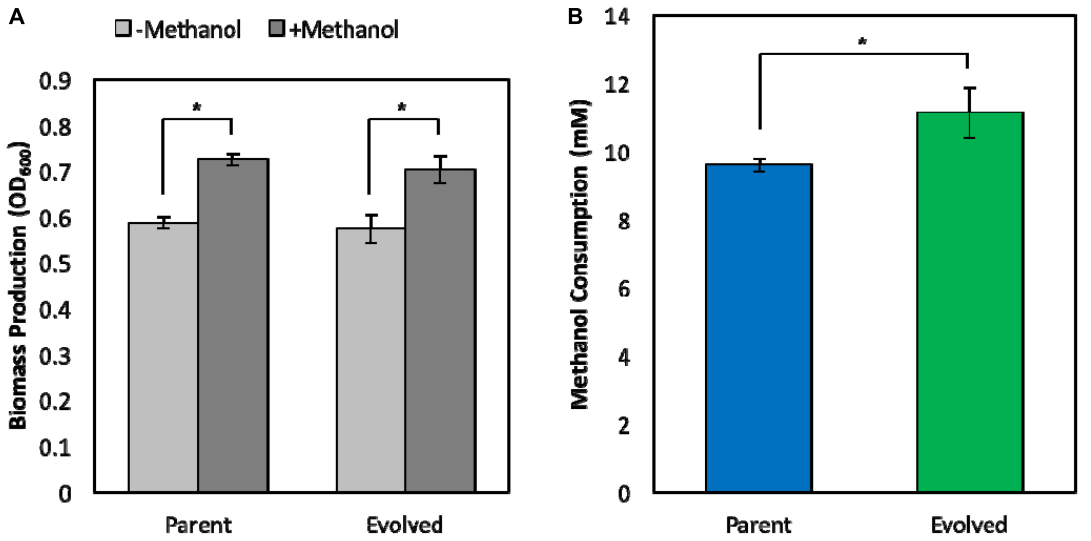

FIGURE 4 | Phenotypic characterization of parental and evolved methylotrophic *E. coli* strains. **(A)** Total biomass production during 48 h growth in M9 minimal medium supplemented with 1 g/L yeast extract in the absence (–Methanol) or presence (+Methanol) of 60 mM ^{13}C-methanol. **(B)** Total methanol consumption over the course of 48 h. Error bars indicate standard deviation ($n = 3$). *$p < 0.05$.

metabolites and proteinogenic amino acids, which is a crucial characteristic for industrial methanol bioprocesses. Though the evolved strain exhibited increased consumption and assimilation of ^{13}C-methanol, the absolute amount of improved consumption was low (ca. 2 mM) compared to the parental strain. This low amount is insufficient to generate a substantial improvement in biomass production, but it provides a step forward toward autonomous methylotrophy as indicated by the ^{13}C-labeling analysis. Furthermore, the ^{13}C metabolite data represent relative, not absolute, labeling, which further supports why consumption and assimilation of methanol, but not biomass production, are improved in the evolved strain.

DISCUSSION

Significant progress has been made toward developing synthetic methylotrophs for industrial methanol bioconversion. However there are still limitations that must be alleviated prior to industrial implementation. Here, we focused on improving the methanol tolerance of synthetic *E. coli* methylotrophs via ALE. Improved methanol tolerance was acquired by several distinct strains following ALE, and WGS analysis revealed that a common mutation in 30S ribosomal subunit proteins was responsible for methanol tolerance. Specifically, mutations found in the *rpsL* and *rpsQ* genes, which encode 30S ribosomal subunit proteins S12 and S17, respectively, are responsible for the improved methanol tolerance phenotype in all evolved strains.

Certain mutations in *rpsL* are known to cause hyperaccurate (restrictive) translational phenotypes, and were first discovered in connection with streptomycin resistant phenotypes (Gorini and Kataja, 1964; Ozaki et al., 1969). Hyperaccurate phenotypes typically result from mutations to residues in the decoding interface between S12 and 16S rRNA, where tRNA selection occurs (Ogle et al., 2002; Zaher and Green, 2010; Demirci et al., 2013). The mutation in *rpsL*, Gly92Ser, is close to the decoding interface of the ribosome (Wimberly et al., 2000; Ogle et al., 2002). A study on ethanol tolerance mechanisms in *E. coli* found that a His31Pro mutation in *rpsQ*, which resulted from ALE in the presence of increasing ethanol concentrations, conferred protection to the cells via increased ribosomal accuracy, suggesting that the mechanisms of methanol and ethanol tolerance in *E. coli* are similar and not specific to

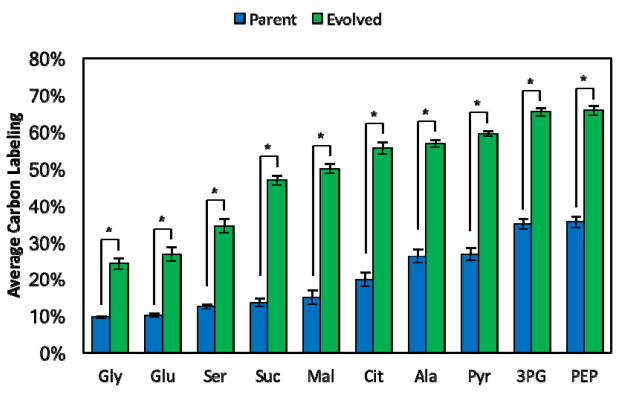

FIGURE 5 | Average carbon labeling of intracellular metabolites and amino acids at 48 h from parental and evolved methylotrophic *E. coli* strains grown in M9 minimal medium supplemented with 1 g/L yeast extract and 60 mM ^{13}C-methanol. Intracellular metabolites and amino acids: glycine (Gly), glutamate (Glu), serine (Ser), succinate (Suc), malate (Mal), citrate (Cit), alanine (Ala), pyruvate (Pyr), 3-phosphoglycerate (3PG), phosphoenolpyruvate (PEP). Error bars indicate standard deviation ($n = 3$). *$p < 0.05$.

methylotrophic metabolism. In the presence of 40 g/L ethanol, a strain harboring the *rpsQ* His31Pro mutation drastically reduced translational misreading to levels similar to that of the wild type strain grown without ethanol (Haft et al., 2014).

These findings provide a novel insight into methanol tolerance mechanisms in *E. coli* and other bacteria as earlier studies identified alternative mechanisms of methanol tolerance in *C. glutamicum*. In one study, it was determined that two point mutations, (A165T in O-acetylhomoserine sulfhydrolase (MetY) and Q342* in CoA transferase (Cat), were responsible for improving the methanol tolerance of a wild-type *C. glutamicum* strain. The enzymatic side reactions of MetY and Cat were found to contribute to methanol toxicity as MetY catalyzes the alkylation of O-acetylhomoserine with methanol to generate acetate and O-methylhomoserine, which inhibits bacterial growth (Lessmeier and Wendisch, 2015), and Cat acts as a potential acetyl-CoA hydrolase, alcohol acetyltransferase or for the generation of methyl-CoA, potentially generating intermediates that also inhibit growth (Lessmeier and Wendisch, 2015). A separate study found that two mutations were crucial for improving the methanol tolerance of a methylotrophic *C. glutamicum* methanol auxotroph (Tuyishime et al., 2018; Wang et al., 2020). One mutation was found in MetY, similar to the prior *C. glutamicum* study, and another mutation was found in a methanol-induced membrane-bound transporter. Taken together, these results highlight the many direct and indirect effects of methanol toxicity and various ways to achieve improved methanol tolerance.

Importantly, for the context of synthetic methylotrophy, the original evolved strain (Δ*frmA* + pUD9) exhibited improved methanol consumption and assimilation of methanol-derived carbon into intracellular metabolites and proteinogenic amino acids, highlighting the unique ability to couple improved methanol tolerance with enhanced synthetic methanol utilization. Overall, this study represents a step forward in the field of synthetic methylotrophy by providing novel insights into methanol tolerance mechanisms and strategies to improve methanol bioconversion without the need for rational engineering.

DATA AVAILABILITY STATEMENT

The datasets presented in this study can be found in online repositories. The names of the repository/repositories and accession number(s) can be found below: BioSample accessions SAMN17309453, SAMN17309454, and SAMN17309455.

AUTHOR CONTRIBUTIONS

RB, GG, and EP designed the research, analyzed the data, and wrote the manuscript. RB, GG, JG, and JH conducted the experiments. All authors read and approved the manuscript.

FUNDING

This work was supported by the Advanced Research Projects Agency-Energy (ARPA-E) Reducing Emissions using Methanotrophic Organisms for Transportation Energy (REMOTE) program (contract # DE-AR0000432). A portion of this work was adapted from RB's dissertation: Engineering a synthetic *Escherichia coli* methylotroph for conversion of methanol to fuels and chemicals.

SUPPLEMENTARY MATERIAL

The Supplementary Material for this article can be found online at: https://www.frontiersin.org/articles/10.3389/fmicb.2021.638426/full#supplementary-material

REFERENCES

Antoniewicz, M. R. (2019). Synthetic methylotrophy: strategies to assimilate methanol for growth and chemicals production. *Curr. Opin. Biotechnol.* 59, 165–174. doi: 10.1016/j.copbio.2019.07.001

Baba, T., Ara, T., Hasegawa, M., Takai, Y., Okumura, Y., Baba, M., et al. (2006). Construction of *Escherichia coli* K-12 in-frame, single-gene knockout mutants: the Keio collection. *Mol.Syst. Biol.* 2:20060008. doi: 10.1038/msb4100050

Bennett, R., Agee, A., Har, J., von Hagel, B., Antoniewicz, M., and Papoutsakis, E. (2020a). Regulatory interventions improve the biosynthesis of limiting amino acids from methanol carbon to improve synthetic methylotrophy in *Escherichia coli*. *Biotechnol. Bioeng.* 118, 43–47. doi: 10.1002/bit.27549

Bennett, R., Agee, A. H., Gerald Har, J. R., von Hage, l.B, Siu, K., Antoniewicz, M., et al. (2020b). Triggering the stringent response enhances synthetic methanol utilization in *Escherichia coli*. *Metab. Eng.* 61, 1–10. doi: 10.1016/j.ymben.2020.04.007

Bennett, R. K., Dillon, M., Gerald Har, J. R., Agee, A., von Hagel, B., Rohlhill, J., et al. (2020c). Engineering *Escherichia coli* for methanol-dependent growth on glucose for metabolite production. *Metab. Eng.* 60, 45–55. doi: 10.1016/j.ymben.2020.03.003

Bennett, R. K., Gonzalez, J. E., Whitaker, W. B., Antoniewicz, M. R., and Papoutsakis, E. T. (2018a). Expression of heterologous non-oxidative pentose phosphate pathway from *Bacillus methanolicus* and phosphoglucose isomerase deletion improves methanol assimilation and metabolite production by a synthetic *Escherichia coli* methylotroph. *Metab. Eng.* 45, 75–85. doi: 10.1016/j.ymben.2017.11.016

Bennett, R. K., Steinberg, L. M., Chen, W., and Papoutsakis, E. T. (2018b). Engineering the bioconversion of methane and methanol to fuels and chemicals in native and synthetic methylotrophs. *Curr. Opin. Biotechnol.* 50, 81–93. doi: 10.1016/j.copbio.2017.11.010

Bozdag, A., Komives, C., and Flickinger, M. C. (2015). Growth of *Bacillus methanolicus* in 2 M methanol at 50 degrees C: the effect of high methanol concentration on gene regulation of enzymes involved in formaldehyde detoxification by the ribulose monophosphate pathway. *J. Ind. Microbiol. Biotechnol.* 42, 1027–1038. doi: 10.1007/s10295-015-1623-8

Chang, C. C., and Gershwin, M. E. (1992). Perspectives on formaldehyde toxicity: separating fact from fantasy. *Regul. Toxicol. Pharmacol.* 16, 150–160. doi: 10.1016/0273-2300(92)90054-d

Chen, C. T., Chen, F. Y., Bogorad, I. W., Wu, T. Y., Zhang, R., Lee, A. S., et al. (2018). Synthetic methanol auxotrophy of *Escherichia coli* for methanol-dependent growth and production. *Metab. Eng.* 49, 257–266. doi: 10.1016/j.ymben.2018.08.010

Chen, F. Y., Jung, H. W., Tsuei, C. Y., and Liao, J. C. (2020). Converting *Escherichia coli* to a synthetic methylotroph growing solely on methanol. *Cell* 182, 933–946 e914. doi: 10.1016/j.cell.2020.07.010

Dai, Z., Gu, H., Zhang, S., Xin, F., Zhang, W., Dong, W., et al. (2017). Metabolic construction strategies for direct methanol utilization in *Saccharomyces cerevisiae*. *Bioresour. Technol.* 245(Pt B), 1407–1412. doi: 10.1016/j.biortech.2017.05.100

Datsenko, K. A., and Wanner, B. L. (2000). One-step inactivation of chromosomal genes in *Escherichia coli* K-12 using PCR products. *Proc. Natl. Acad. Sci. U.S.A.* 97, 6640–6645. doi: 10.1073/pnas.120163297

Demirci, H., Wang, L., Murphy, F., Murphy, E., Carr, J., Blanchard, S., et al. (2013). The central role of protein S12 in organizing the structure of the decoding site of the ribosome. *RNA* 19, 1791–1801. doi: 10.1261/rna.040030.113

Ganske, F., and Bornscheuer, U. T. (2006). Growth of *Escherichia coli*, Pichia pastoris and *Bacillus cereus* in the presence of the ionic liquids [BMIM][BF4] and [BMIM][PF6] and organic solvents. *Biotechnol. Lett.* 28, 465–469. doi: 10.1007/s10529-006-0006-7

Gonzalez, C. F., Proudfoot, M., Brown, G., Korniyenko, Y., Mori, H., Savchenko, A. V., et al. (2006). Molecular basis of formaldehyde detoxification characterization of two s-formylglutathione hydrolases from *Escherichia Coli*, FrmB and YeiG. *J. Biol. Chem.* 281, 14514–14522. doi: 10.1074/jbc.M600996200

Gonzalez, J. E., Bennett, R. K., Papoutsakis, E. T., and Antoniewicz, M. R. (2018). Methanol assimilation in *Escherichia coli* is improved by co-utilization of threonine and deletion of leucine-responsive regulatory protein. *Metab. Eng.* 45, 67–74. doi: 10.1016/j.ymben.2017.11.015

Goosen, N., and van de Putte, P. (1995). The regulation of transcription initiation by integration host factor. *Mol. Microbiol.* 16, 1–7. doi: 10.1111/j.1365-2958.1995.tb02386.x

Gorini, L., and Kataja, E. (1964). PHENOTYPIC REPAIR BY STREPTOMYCIN OF DEFECTIVE GENOTYPES IN *E. COLI*. *Proc. Natl. Acad. Sci. U.S.A.* 51, 487–493. doi: 10.1073/pnas.51.3.487

Gustafson, C., and Tagesson, C. (1985). Influence of organic solvent mixtures on biological membranes. *Br. J. Ind. Med.* 42, 591–595. doi: 10.1136/oem.42.9.591

Haft, R. J., Keating, D. H., Schwaegler, T., Schwalbach, M. S., Vinokur, J., Tremaine, M., et al. (2014). Correcting direct effects of ethanol on translation and transcription machinery confers ethanol tolerance in bacteria. *Proc. Natl. Acad. Sci. U.S.A.* 111, E2576–E2585. doi: 10.1073/pnas.1401853111

Haynes, C. A., and Gonzalez, R. (2014). Rethinking biological activation of methane and conversion to liquid fuels. *Nat. Chem. Biol.* 10, 331–339. doi: 10.1038/nchembio.1509

Jakobsen, O. M., Benichou, A., Flickinger, M. C., Valla, S., Ellingsen, T. E., and Brautaset, T. (2006). Upregulated transcription of plasmid and chromosomal ribulose monophosphate pathway genes is critical for methanol assimilation rate and methanol tolerance in the methylotrophic bacterium Bacillus methanolicus. *J. Bacteriol.* 188, 3063–3072. doi: 10.1128/Jb.188.8.3063-3072.2006

Karp, P. D., Ong, W. K., Paley, S., Billington, R., Caspi, R., Fulcher, C., et al. (2018). The ecocyc database. *EcoSal Plus* 8, 1–19. doi: 10.1128/ecosalplus.ESP-0006-2018

Lessmeier, L., Pfeifenschneider, J., Carnicer, M., Heux, S., Portais, J. C., and Wendisch, V. F. (2015). Production of carbon-13-labeled cadaverine by engineered *Corynebacterium glutamicum* using carbon-13-labeled methanol as co-substrate. *Appl. Microbiol. Biotechnol.* 99, 10163–10176. doi: 10.1007/s00253-015-6906-5

Lessmeier, L., and Wendisch, V. F. (2015). Identification of two mutations increasing the methanol tolerance of Corynebacterium glutamicum. *BMC Microbiol.* 15:216. doi: 10.1186/s12866-015-0558-6

Long, C. P., and Antoniewicz, M. R. (2019). High-resolution (13)C metabolic flux analysis. *Nat. Protoc.* 14, 2856–2877. doi: 10.1038/s41596-019-0204-0

Meyer, F., Keller, P., Hartl, J., Groninger, O. G., Kiefer, P., and Vorholt, J. A. (2018). Methanol-essential growth of *Escherichia coli*. *Nat. Commun.* 9:1508. doi: 10.1038/s41467-018-03937-y

Muller, J. E. N., Meyer, F., Litsanov, B., Kiefer, P., Potthoff, E., Heux, S., et al. (2015). Engineering *Escherichia coli* for methanol conversion. *Metab. Eng.* 28, 190–201. doi: 10.1016/j.ymben.2014.12.008

Nash, T. (1953). The colorimetric estimation of formaldehyde by means of the Hantzsch reaction. *Biochem. J.* 55, 416–421. doi: 10.1042/bj0550416

Ogle, J., Murphy, F., Tarry, M., and Ramakrishnan, V. (2002). Selection of tRNA by the ribosome requires a transition from an open to a closed form. *Cell* 111, 721–732. doi: 10.1016/s0092-8674(02)01086-3

Ozaki, M., Mizushima, S., and Nomura, M. (1969). Identification and functional characterization of the protein controlled by the streptomycin-resistant locus in *E. coli*. *Nature* 222, 333–339. doi: 10.1038/222333a0

Price, J. V., Chen, L., Whitaker, W. B., Papoutsakis, E., and Chen, W. (2016). Scaffoldless engineered enzyme assembly for enhanced methanol utilization. *Proc. Natl. Acad. Sci. U.S.A.* 113, 12691–12696. doi: 10.1073/pnas.1601797113

Rohlhill, J., Gerald Har, J. R., Antoniewicz, M. R., and Papoutsakis, E. T. (2020). Improving synthetic methylotrophy via dynamic formaldehyde regulation of pentose phosphate pathway genes and redox perturbation. *Metab. Eng.* 57, 247–255. doi: 10.1016/j.ymben.2019.12.006

Rohlhill, J., Sandoval, N. R., and Papoutsakis, E. T. (2017). Sort-seq approach to engineering a formaldehyde-inducible promoter for dynamically regulated *Escherichia coli* growth on methanol. *ACS Synth. Biol.* 6, 1584–1595. doi: 10.1021/acssynbio.7b00114

Roth, T. B., Woolston, B. M., Stephanopoulos, G., and Liu, D. R. (2019). Phage-assisted evolution of *Bacillus methanolicus* methanol dehydrogenase 2. *ACS Synth. Biol.* 8, 796–806. doi: 10.1021/acssynbio.8b00481

Sandoval, N. R., Venkataramanan, K. P., Groth, T. S., and Papoutsakis, E. T. (2015). Whole-genome sequence of an evolved *Clostridium pasteurianum* strain reveals Spo0A deficiency responsible for increased butanol production and superior growth. *Biotechnol. Biofuels* 8:227. doi: 10.1186/s13068-015-0408-7

Sonmez, M., Ince, H. Y., Yalcin, O., Ajdzanovic, V., Spasojevic, I., Meiselman, H. J., et al. (2013). The effect of alcohols on red blood cell mechanical properties and membrane fluidity depends on their molecular size. *PLoS One* 8:e76579. doi: 10.1371/journal.pone.0076579

Teng, S., Beard, K., Pourahmad, J., Moridani, M., Easson, E., Poon, R., et al. (2001). The formaldehyde metabolic detoxification enzyme systems and molecular cytotoxic mechanism in isolated rat hepatocytes. *Chem. Biol. Interact.* 130–132, 285–296. doi: 10.1016/s0009-2797(00)00272-6

Tuyishime, P., Wang, Y., Fan, L., Zhang, Q., Li, Q., Zheng, P., et al. (2018). Engineering *Corynebacterium glutamicum* for methanol-dependent growth and glutamate production. *Metab. Eng.* 49, 220–231. doi: 10.1016/j.ymben.2018.07.011

Wang, Y., Fan, L., Tuyishime, P., Liu, J., Zhang, K., Gao, N., et al. (2020). Adaptive laboratory evolution enhances methanol tolerance and conversion in engineered Corynebacterium glutamicum. *Commun. Biol.* 3:217. doi: 10.1038/s42003-020-0954-9

Whitaker, W. B., Jones, J. A., Bennett, R. K., Gonzalez, J. E., Vernacchio, V. R., Collins, S. M., et al. (2017). Engineering the biological conversion of methanol to specialty chemicals in *Escherichia coli*. *Metab. Eng.* 39, 49–59. doi: 10.1016/j.ymben.2016.10.015

Whitaker, W. B., Sandoval, N. R., Bennett, R. K., Fast, A. G., and Papoutsakis, E. T. (2015). Synthetic methylotrophy: engineering the production of biofuels and chemicals based on the biology of aerobic methanol utilization. *Curr. Opin. Biotechnol.* 33, 165–175. doi: 10.1016/j.copbio.2015.01.007

Wimberly, B., Brodersen, D., Clemons, W., Morgan-Warren, R., Carter, A., Vonrhein, C., et al. (2000). Structure of the 30S ribosomal subunit. *Nature* 407, 327–339. doi: 10.1038/35030006

Witthoff, S., Schmitz, K., Niedenfuhr, S., Noh, K., Noack, S., Bott, M., et al. (2015). Metabolic engineering of *Corynebacterium glutamicum* for methanol metabolism. *Appl. Environ. Microbiol.* 81, 2215–2225. doi: 10.1128/AEM.03110-14

Woolston, B. M., King, J. R., Reiter, M., Van Hove, B., and Stephanopoulos, G. (2018a). Improving formaldehyde consumption drives methanol assimilation in engineered E. coli. *Nat. Commun.* 9:2387. doi: 10.1038/s41467-018-04795-4

Woolston, B. M., Roth, T., Kohale, I., Liu, D. R., and Stephanopoulos, G. (2018b). Development of a formaldehyde biosensor with application to synthetic methylotrophy. *Biotechnol. Bioeng.* 115, 206–215. doi: 10.1002/bit.26455

Wu, T. Y., Chen, C. T., Liu, J. T., Bogorad, I. W., Damoiseaux, R., and Liao, J. C. (2016). Characterization and evolution of an activator-independent methanol dehydrogenase from *Cupriavidus necator* N-1. *Appl. Microbiol. Biotechnol.* 100, 4969–4983. doi: 10.1007/s00253-016-7320-3

Xu, P., Vansiri, A., Bhan, N., and Koffas, M. A. (2012). ePathBrick: a synthetic biology platform for engineering metabolic pathways in *E. coli*. *ACS Synth. Biol.* 1, 256–266. doi: 10.1021/sb300016b

Yang, F. X., Hanna, M. A., and Sun, R. C. (2012). Value-added uses for crude glycerol-a byproduct of biodiesel production. *Biotechnol. Biofuels* 5:13. doi: 10.1186/1754-6834-5-13

Zaher, H., and Green, R. (2010). Hyperaccurate and error-prone ribosomes exploit distinct mechanisms during tRNA selection. *Mol. Cell* 39, 110–120. doi: 10.1016/j.molcel.2010.06.009

Zhang, W., Zhang, T., Song, M., Dai, Z., Zhang, S., Xin, F., et al. (2018). Metabolic engineering of *Escherichia coli* for high yield production of succinic acid driven by methanol. *ACS Synth. Biol.* 7, 2803–2811. doi: 10.1021/acssynbio.8b00109

Conflict of Interest: The authors declare that the research was conducted in the absence of any commercial or financial relationships that could be construed as a potential conflict of interest.

frontiers in Microbiology

MINI REVIEW
published: 10 March 2021
doi: 10.3389/fmicb.2021.636486

Biotransformation of Methane and Carbon Dioxide Into High-Value Products by Methanotrophs: Current State of Art and Future Prospects

*Krishna Kalyani Sahoo[1], Gargi Goswami[2] and Debasish Das[1]**

[1] Department of Biosciences and Bioengineering, Indian Institute of Technology Guwahati, Guwahati, India, [2] Department of Biotechnology, Gandhi Institute of Technology and Management (GITAM) University, Visakhapatnam, India

Conventional chemical methods to transform methane and carbon dioxide into useful chemicals are plagued by the requirement for extreme operating conditions and expensive catalysts. Exploitation of microorganisms as biocatalysts is an attractive alternative to sequester these C1 compounds and convert them into value-added chemicals through their inherent metabolic pathways. Microbial biocatalysts are advantageous over chemical processes as they require mild-operating conditions and do not release any toxic by-products. Methanotrophs are potential cell-factories for synthesizing a wide range of high-value products via utilizing methane as the sole source of carbon and energy, and hence, serve as excellent candidate for methane sequestration. Besides, methanotrophs are capable of capturing carbon dioxide and enzymatically hydrogenating it into methanol, and hence qualify to be suitable candidates for carbon dioxide sequestration. However, large-scale production of value-added products from methanotrophs still presents an overwhelming challenge, due to gas-liquid mass transfer limitations, low solubility of gases in liquid medium and low titer of products. This requires design and engineering of efficient reactors for scale-up of the process. The present review offers an overview of the metabolic architecture of methanotrophs and the range of product portfolio they can offer. Special emphasis is given on methanol biosynthesis as a potential biofuel molecule, through utilization of methane and alternate pathway of carbon dioxide sequestration. In view of the gas-liquid mass transfer and low solubility of gases, the key rate-limiting step in gas fermentation, emphasis is given toward reactor design consideration essential to achieve better process performance.

Keywords: methanotrophs, carbon dioxide, methane, greenhouse gas sequestration, methanol, high-value products, reactor configuration

OPEN ACCESS

Edited by:
Pramod P. Wangikar, Indian Institute of Technology Bombay, India

Reviewed by:
Shireesh Srivastava, International Centre for Genetic Engineering and Biotechnology, India
Annesha Sengupta, Washington University in St. Louis, United States

****Correspondence:***
Debasish Das
debasishd@iitg.ac.in

Specialty section:
This article was submitted to Microbiotechnology, a section of the journal Frontiers in Microbiology

Received: *01 December 2020*
Accepted: *22 February 2021*
Published: *10 March 2021*

Citation:
Sahoo KK, Goswami G and Das D (2021) Biotransformation of Methane and Carbon Dioxide Into High-Value Products by Methanotrophs: Current State of Art and Future Prospects. Front. Microbiol. 12:636486. doi: 10.3389/fmicb.2021.636486

INTRODUCTION

Emission of greenhouse gases has been increasing globally at an alarming rate. Global anthropogenic emissions of CO_2 and CH_4 have almost hit 43.1 billion tons and 9390 mmtCO_2e, respectively (Global Carbon Project Budget-2019[1]; Global Methane Initiative Report-2018)[2]. The overall global atmospheric concentrations of CO_2 and CH_4 have increased by 12.07 and 5.9%,

[1]https://www.globalcarbonproject.org/carbonbudget/
[2]https://www.globalmethane.org/about/methane.aspx

respectively, in the last two decades (NOAA-ESRL, 2020)[3]. Moreover, the global warming potential of CH_4 is 28–36 times higher than CO_2 (US-EPA)[4]. There have been efforts to sequester CO_2 or CH_4 and catalytically convert them into various value-added products, through hydrogenation and oxidation, respectively. However, chemical processes for the conversion of these C1 compounds are plagued by requirement for expensive catalysts, high temperature (∼450°C), high pressure (∼30 MPa) and release of toxic by-products like carbon monoxide; making the overall technology expensive and non-sustainable.

The use of microorganisms as biocatalysts for the sequestration of CH_4 and CO_2 is an attractive alternative as they require milder operating conditions and do not release any toxic by-products. Naturally occurring methane-oxidizing microorganisms are known as methanotrophs. Owing to their ability to utilize methane as the source of carbon and energy, methanotrophs serve as excellent candidates for methane sequestration. Some methanotrophs possess an added advantage of sequestering CO_2 as substrate for enzymatic hydrogenation into methanol, and thereby qualify as suitable candidates for CO_2 sequestration. Besides their ability to harness noxious C1 compounds, methanotrophs can also serve as potential cell-factories for a wide-range of high-value products, e.g., methanol, ectoine/hydroxyectoine, poly-β-hydroxybutyrate (PHB), single cell protein, extracellular polysaccharide, lipids etc. (Xin et al., 2007; Rostkowski et al., 2013; Cantera et al., 2018; Rasouli et al., 2018; Tsapekos et al., 2020). Despite their enormous potential, large-scale production of these high-value products is constrained by various limitations in solubility of gases in liquid medium and gas-liquid mass transfer, eventually resulting in -insignificant product titer. The present review provides an overview of methanotrophs, metabolic pathways to utilize CH_4/CO_2 and the high-value products synthesized by them. This review also sheds light on the biological production of methanol, a key product targeted as solvent and biofuel, through oxidation of CH_4 and alternatively via reduction of CO_2. In view of overcoming the rate-limiting factors in gas fermentation, toward efficient capture and conversion of harmful C1 compounds into high-value products at industrial-scale, special emphasis has been given on reactor design and configuration.

METHANOTROPHS

Methanotrophs are Gram-negative proteobacteria, noted for their ability to utilize methane as the sole source of carbon and energy. Methanotrophic bacterium was discovered by Söhngen in 1906 (Hanson and Hanson, 1996). Whittenbury et al. (1970) carried out comprehensive isolation and characterization of methanotrophs and introduced the Type I, Type II, and Type X classification system. Methanotrophs utilize methane via a metabolic cascade comprising of four enzymes, namely, methane monooxygenase (MMO), methanol dehydrogenase (MDH), formaldehyde dehydrogenase (FADH), and formate dehydrogenase (FDH) (Xin et al., 2004a, 2007). Based on the type of MMO produced, the methanotrophs are divided into three categories namely, (a) Type I (produce particulate MMO), (b) Type II (produce both particulate as well as soluble MMO) and (c) Type X (comprises of specific features of both Type I and Type II methanotrophs).

Aerobic methanotrophs were later on classified broadly into two major groups of proteobacteria based on 16S rRNA gene sequencing, namely, gamma-proteobacteria (Group I) and alpha-proteobacteria (Group II), in place of the earlier 3-type classification (Ge et al., 2014). Gamma-proteobacteria (Group I) comprise of previously classified Type I and Type X methanotrophs and Alpha-proteobacteria (Group II) comprise of formerly known Type II methanotrophs (Fei et al., 2014). The sub-division alpha-proteobacteria consists of four genera namely, *Methylocella*, *Methylocapsa*, *Methylocystis,* and *Methylosinus*. The sub-division gamma-proteobacteria consists of 12 genera namely, *Methylothermus, Methylosoma, Methylosphaera, Methylosarcina, Methylomonas, Methylohalobius, Methylomicrobium, Methylococcus, Methylocaldum, Methylobacter, Clonothrix,* and *Crenothrix* (Ge et al., 2014). Gamma-proteobacteria (Type I and Type X) and alpha-proteobacteria (Type II) use ribulose monophosphate (RuMP) cycle and serine cycle, respectively, for utilization of C1-carbon sources, such as formaldehyde/formate. Although, Type X species (*Methylocaldum* and *Methylococcus*), also utilize formaldehyde through RuMP cycle, yet they differ from Type I species as they express small quantities of enzymes of the serine cycle, ribulose-bisphosphate carboxylase, present in the Calvin-Benson-Bassham (CBB) cycle (Hanson and Hanson, 1996; Park and Kim, 2019). Type X species reportedly possess genes encoding enzymes for CO_2-fixation through CBB cycle (Baxter et al., 2002). Novel methanotrophs have also been found in the phylum Verrumicrobia, which has been reported to fix CO_2 by utilizing CBB cycle (Rasigraf et al., 2014).

Gamma-proteobacterial and alpha-proteobacterial methanotrophs can also be distinguished based on few other characteristics. In terms of arrangement of their intracytoplasmic membranes (ICMs), gamma-proteobacterial species contain bundles of ICMs, whereas, ICMs in alpha-proteobacterial species are aligned around the cell's periphery (Kalyuzhnaya et al., 2019). As per cellular phospholipid fatty acid (PLFA) composition, Type I, Type II, and Type X methanotrophs, respectively, possess 14−16−, 18−, and 16-carbon long PLFA (Ge et al., 2014). On the basis of storage carbon, most species of gamma-proteobacteria are known for glycogen accumulation and a few species for PHB accumulation; while, alpha-proteobacterial species are predicted to mainly accumulate PHB, since they excrete acetone, succinate, acetate, etc. (which are probable derivatives of PHB) from methane fermentation (Kalyuzhnaya, 2016).

Typical growth rates for gamma-proteobacterial and alpha-proteobacterial methanotrophs ranges within 0.009–0.4 and 0.005–0.16 h^{-1}, respectively (Kalyuzhnaya, 2016). Methanotrophs are resistant to desiccation. They have been reported for bioremediation, bioleaching, and epoxidation. Conjugation (Nguyen et al., 2020) and electroporation-based (Yan et al., 2016) gene-transfer techniques have been developed for methanotrophs. However, the yield and productivity from

[3]https://www.esrl.noaa.gov/gmd/ccgg/trends/gl_data.html; www.esrl.noaa.gov/gmd/ccgg/trends_ch4/

[4]https://www.epa.gov/ghgemissions/understanding-global-warming-potentials

methanotrophic cell factories are relatively low as compared to other hosts such as *E. coli* (Lee et al., 2016). Moreover, their obligate methanotrophic characteristics and slow growth rates limits the application of genetic engineering techniques. On the contrary, their obligate methanotrophic nature makes them a cheap industrial platform which can sequester waste greenhouse gas (methane), relative to other platforms which consume expensive substrates like glucose, xylose etc.

Few studies have explored genome-scale metabolic models (GSMM) for methanotrophs for extensively modeling the entire array of genes, metabolites and biochemical reactions *in silico*. Gupta et al. (2019) built a GSMM for *Methylococcus capsulatus* (Bath) comprising of 865 metabolites, 899 reactions and 535 genes. The model could predict the pathways and amino acids necessary for growth, and identified essential metabolic genes and lethal genes in the bacterium. Lieven et al. (2018) using GSMM predicted that methane oxidation by pMMO can be stimulated either through uphill electron transfer or direct-coupling, at decreased efficiency. GSMM helps the authors to build a centralized knowledge-base for the model organism, understand its metabolic physiology and simulate its metabolic behavior under diverse conditions.

METABOLIC PATHWAY TOWARD UTILIZATION OF CH_4 AND CO_2

All aerobic methanotrophs oxidize CH_4 to CO_2 through a common enzymatic cascade. The oxidation process produces methanol, formaldehyde and formate as reaction intermediates (**Figure 1**). This is accomplished through sequential catalysis by the enzymes, MMO, MDH, FADH, and FDH. A fraction of the formate/formaldehyde, produced as an intermediate, gets incorporated into the biomass as a source of carbon through the serine cycle or RuMP cycle. RuMP cycle involves assimilation of formaldehyde and its further conversion into hexulose-6-phosphate. Successive conversions produce ribulose-5-phosphate, thus closing the cycle. Formaldehyde gets transformed into formate through H_4MPT pathway. Serine cycle involves assimilation of formate. Formate is transferred into serine cycle through H_4F pathway. Successive intermediate reactions convert serine into glycine, closing the cycle. Assimilation of CO_2 in Type X and Verrumicrobial methanotrophs via CBB cycle begins with the formation of 3-phospho-glycerate, which eventually gets converted into ribulose-1,5-bisphosphate, completing the cycle (Park and Kim, 2019).

Methane is oxidized to methanol by MMO, which requires two units of reducing equivalents (NADH) to break the double bond in oxygen. One of these oxygen atoms oxidizes methane into methanol, whereas the other gets hydrogenated to produce water. The oxidation of methanol to formaldehyde releases $PQQH_2$ and the oxidation of formaldehyde to CO_2 via formate releases NADH. NADH thus generated is reutilized by MMO for the oxidation of methane to methanol (Xin et al., 2007).

MMO is the key enzyme responsible toward growth of methanotrophs since these microbes utilize methane as the primary source of carbon and energy. MMO is of two types, soluble MMO (sMMO) and particulate MMO (pMMO). sMMO is synthesized in the cytoplasm and is made up of two monomeric units. Each sMMO monomer consists of two iron atoms (Rosenzweig et al., 1995). pMMO is impregnated on the membrane, and is composed of three monomeric units with each unit comprising of either a di-copper or a mono-copper center (Culpepper and Rosenzweig, 2012). Therefore, concentrations of iron and copper ions primarily affect the MMO activity in culture media. High concentration of iron ions is known to stimulate sMMO expression (Chidambarampadmavathy et al., 2015). Additionally, sMMO is actively expressed at lower ratios of copper to biomass, and its expression is repressed at higher concentrations of copper in the medium (Park et al., 1991). On the contrary, pMMO has increased levels of expression at higher ratios of copper to biomass, and hence corroborates improved activity with increase in copper concentration in the medium (Park et al., 1992). Since pMMO is integrated into the membrane, it is supposed to rapidly oxidize methane compared to sMMO. However, authors have outlined that sMMO causes rapid oxidation of methane as compared to pMMO (Sirajuddin and Rosenzweig, 2015). The concentrations of these metal ions significantly influence MMO activity. Higher cellular MMO activity is associated with higher NADH generation (Zhang et al., 2008), which is a necessary cofactor for formation of various methanotrophic products. Few studies have reported the effect of Cu^{2+} and Fe^{2+} ions on the production of PHB and methanol by methanotrophs (Zhang et al., 2008; Patel et al., 2016b).

Some methanotrophs can also utilize CO_2 as substrate and reduce it to methanol, in presence of excess CO_2 (Xin et al., 2007). This happens in a two-stage process, where methane is utilized as carbon substrate during the first-stage to produce biomass, and CO_2 is reduced by the generated biomass in the second-stage to produce methanol. CO_2-reduction to methanol is the reverse reaction of methane-oxidation to CO_2. It is a sequential catalysis carried out by FDH, FADH and MDH (**Figure 1**). Since MMO lacks the ability to catalyze this reverse reaction, the end-product of the CO_2 reduction pathway is methanol (Xin et al., 2004a). The reduction of CO_2 to methanol requires excess of reducing power to drive the reaction against the laws of energy. The reduction of CO_2 to formaldehyde via formate requires NADH while the reduction of formaldehyde to methanol requires $PQQH_2$. This exigency of reducing energy equivalent is compensated by the endogenous reductant source (PHB) of the cells, which is explained in "Biological Production of Methanol From Methane and Carbon Dioxide" section.

PRODUCTS SYNTHESIZED BY METHANOTROPHS

Wild type methanotrophs possess an inherent potential to synthesize a wide-range of products (**Table 1**). Molecules like ectoine (*Methylomicrobium alcaliphilum*, *Methylobacter marinus, Methylomicrobium kenyense, Methylobacter modestohalophilus*); hydroxyectoine (*Methylomicrobium alcaliphilum*); sucrose (*Methylomicrobium alcaliphilum,*

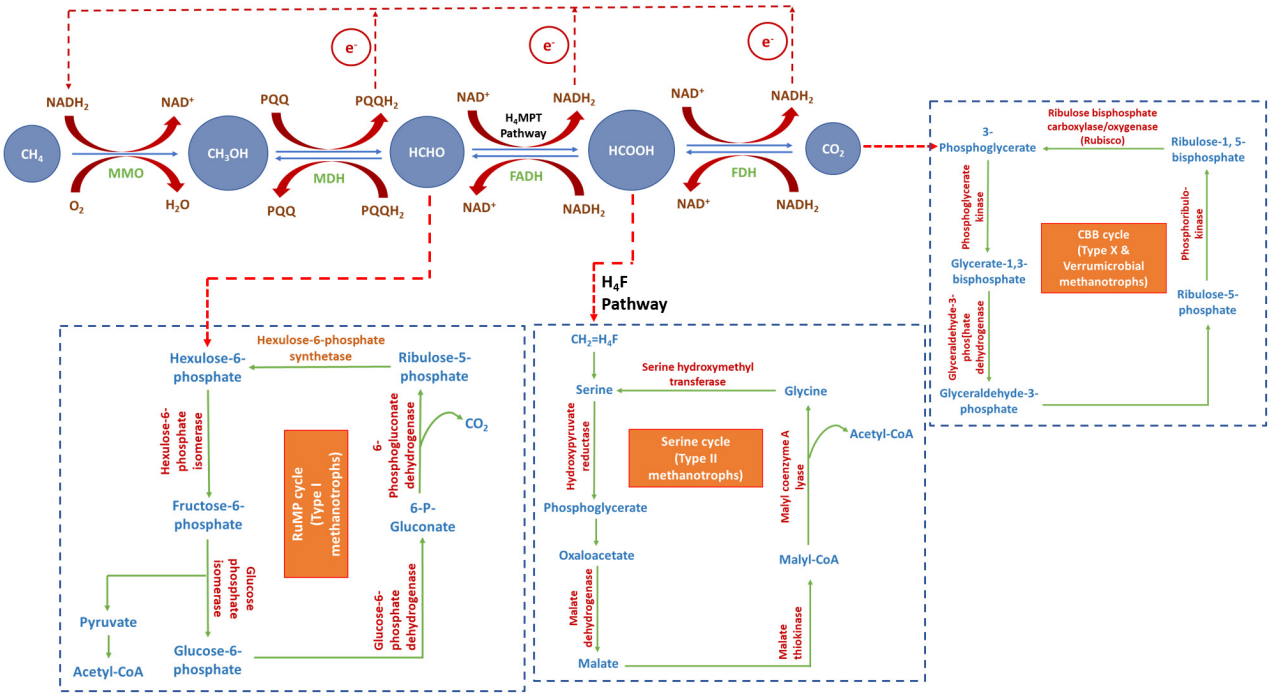

FIGURE 1 | Metabolism of CH_4 and CO_2 in methanotrophs (modified from Xin et al., 2007; Park and Kim, 2019). MMO, methane monooxygenase; MDH, methanol dehydrogenase; FADH, formaldehyde dehydrogenase; FDH, formate dehydrogenase.

Methylomicrobium buryatense, *Methylobacter marinus*); glutamate (*Methylobacter alcaliphilus, Methylomicrobium buryatense, Methylobacter modestohalophilus*); 5-oxoproline (*Methylobacter alcaliphilus*, *Methylobacter modestohalophilus*) are known as "compatible solutes." These are secreted by halotolerant and halophilic methanotrophs in response to high salinity in the environment in order to balance the turgor pressure and minimize water-loss across the cell membrane (Khmelenina et al., 1999). They have applications in pharmaceutical industries as stabilizers for nucleic acids, DNA-protein complexes and enzymes. Methanotrophs are also able to produce extracellular polysaccharide (EPS) (*Methylomicrobium alcaliphilum* and methanotrophs enriched from soil/compost) as a defense mechanism against heat, desiccation, predation and other adverse conditions (Cantera et al., 2018). EPS finds application in textile, pharmaceutical and food industries owing to their adhesive and colloid-like properties.

Methanotrophs also synthesize poly-β-hydroxybutyrate (PHB) (*Methylosinus trichosporium, Methylocystis parvus, Methylocystis hirsuta*), a potential replacement of conventional plastic owing to its biocompatible and biodegradable characteristics (Rodríguez et al., 2020). Single cell proteins, a major methanotrophic-product (*Methylococcus capsulatus, Methylomonas* sp., *Methylocystis* sp.), can be used as a prospective substitute for traditional protein sources viz., fishmeal and soymeal (Valverde-Pérez et al., 2020). Lipid molecules derived from methanotrophs (*Methylomicrobium buryatense, Methylococcus capsulatus*) can be explored as futuristic biofuel (Dong et al., 2017).

Studies have reported engineered (heterologous gene expression) methanotrophic strains to synthesize products beyond their innate metabolic potential. *Methylomicrobium buryatense* (Henard et al., 2016) and *Methylomicrobium alcaliphilum* (Henard et al., 2018) have been genetically engineered to produce lactate, which finds application in the production of bioplastics (from lactic acid polymers), cheese and yogurt, dermatological drugs etc. *Methylomonas* sp. 16a has been engineered to produce astaxanthin (Tao et al., 2007; Rick and Kelly, 2012), a carotenoid pigment with huge commercial significance.

Methanotrophs synthesize a wide-range of products (**Table 1**) using cheap and wasteful carbon-based substrates (CH_4 and/or CO_2) unlike microorganisms utilizing cost-intensive carbon sources like glucose, fructose, xylose etc. These features render methanotroph-based gas fermentation processes economical and sustainable.

BIOLOGICAL PRODUCTION OF METHANOL FROM METHANE AND CARBON DIOXIDE

Methanol is a clean-burning fuel with high specific-energy ratio, flame-speed and octane number; and low combustion temperature and volatility. As has been already discussed, methanotrophs utilize methane, which is subsequently oxidized to methanol, formaldehyde, formate, and finally CO_2 (**Figure 1**). To achieve direct production of methanol from methane, the

TABLE 1 | Products synthesized by methanotrophs.

Product	Strain	Substrate	Yield/Titer	References
Methanol	*Methylocella tundrae*	Methane-air mixture (50:50)	5.18 mM	Mardina et al., 2016
	Methylosinus sporium	Methane-air mixture (50:50)	5.80 mM	Patel et al., 2016c
	Methylocystis bryophila	Methane-air mixture (50:50)	4.63 mM	Patel et al., 2016b
	Methylocystis bryophila	Methane-air mixture (30:70)	52.9 mM	Patel et al., 2020c
	Methylosinus trichosporium IMV 3011	CO_2-air mixture (50:40)	0.004 μmol/mg dry cell weight	Xin et al., 2007
	Methylosinus sporium	CO_2-air mixture (30:70)	0.33 mM	Patel et al., 2016a
Ectoine	*Methylomicrobium alcaliphilum* ML1	Methane-air mixture (50:50)	230 mg g biomass^{-1}	Reshetnikov et al., 2011
	Methylobacter marinus 7C	Methane-air mixture (50:50)	60 mg g biomass^{-1}	Reshetnikov et al., 2011
	Methylomicrobium kenyense AMO1^T	Methane-air mixture (50:50)	70 mg g biomass^{-1}	Reshetnikov et al., 2011
	Methanotrophic bacterial consortium	Methane-air mixture (10:90)	0.42-1.33 mg g biomass^{-1}	Stępniewska et al., 2014
	Methylomicrobium alcaliphilum 20Z	Methane-air mixture (50:50)	79.7–94.2 mg g biomass^{-1}	Cantera et al., 2018
	Methylomicrobium alcaliphilum 20Z	Methane-air mixture (50:50)	12.3 mg g biomass^{-1}	Mustakhimov et al., 2019
Hydroxyectoine	*Methylomicrobium alcaliphilum* 20Z	Methane-air mixture (50:50)	13 mg g biomass^{-1}	Cantera et al., 2018
	Methylomicrobium alcaliphilum 20Z	Methane-air mixture (50:50)	19.7 mg g biomass^{-1}	Mustakhimov et al., 2019
Sucrose	*Methylomicrobium alcaliphilum, Methylomicrobium buryatense, Methylobacter marinus*	Methane-air mixture (50:50)	30–60 mg/g dry cells	Khmelenina et al., 2010
Glutamate	*Methylomicrobium alcaliphilum, Methylomicrobium buryatense, Methylobacter marinus*	Methane-air mixture (50:50)	25–55 mg/g dry cells	Khmelenina et al., 2010
Single cell protein	*Methylococcus capsulatus*	Methane: O_2: CO_2 mixture (60:30:10)	52.52% of dry cell weight	Rasouli et al., 2018
	Methylomonas spp. and *Methylophilus* spp.	Methane-O_2 mixture (40:60)	>50% of dry cell weight	Tsapekos et al., 2020
	Methylomonas sp. and *Methylocystis* sp.	Methane-O_2 mixture	51% of the dry weight	Valverde-Pérez et al., 2020
Poly-β-hydroxybutyrate (PHB)	*Methylocystis parvus* OBBP	Methane-O_2 mixture (50:50)	60% of dry weight	Rostkowski et al., 2013
	Methylosinus trichosporium OB3b	Methane-O_2 mixture (50:50)	29% of dry weight	Rostkowski et al., 2013
	Methylocystis hirsuta	Methane-air mixture (4:96)	34.6 % of dry weight	García-Pérez et al., 2018
	Methylocystis hirsuta	Methanol: ethanol mixture (1:1)	85% of dry weight	Ghoddosi et al., 2019
Lipids	*Methylosphaera hansonii*	Methane-air mixture (50:50)	57% of dry cell weight	Schouten et al., 2000
	Methylomicrobium buryatense	Methane-air mixture (20:80)	10% of dry cell weight	Dong et al., 2017
	Methylococcus capsulatus	Methane: O_2: CO_2 mixture (60:30:10)	21.82% of dry cell weight	Rasouli et al., 2018
Extracellular polysaccharides	*Methylomicrobium alcaliphilum* 20Z	Methane-air mixture (50:50)	2.6 g L culture broth^{-1}	Cantera et al., 2018
5-Oxoproline	*Methylobacter modestohalophilus* 10S	Methane-air mixture (50:50)	178 nmol (mg DCW)$^{-1}$	Khmelenina et al., 1999
	Methylobacter alcaliphilus 20Z	Methane-air mixture (50:50)	248 nmol (mg DCW)$^{-1}$	Khmelenina et al., 1999
Products obtained from genetically engineered methanotrophs				
Lactate	*Methylomicrobium buryatense*	Methane-air mixture (20:80)	0.8 g lactate/L	Henard et al., 2016
Astaxanthin	*Methylomonas* sp. 16a	Methane-air mixture (25:75)	80% of total carotenoids	Tao et al., 2007
	Methylomonas sp. 16a	Methane-air mixture (25:75)	95% of total carotenoids	Rick and Kelly, 2012

subsequent biochemical pathway leading to methanol oxidation needs to be blocked. This is often accomplished by adding MDH inhibitors in the medium. Several studies have reported various irreversible MDH inhibitors for directly producing methanol from methane, viz., cyclopropanol, phosphate, EDTA, $MgCl_2$, NaCl, and NH_4Cl (Takeguchi et al., 1997; Yoo et al., 2015; Patel et al., 2016c,b). However, the activity of MMO is dependent on NADH availability, and inhibition of methanol oxidation by MDH inhibitors results in the depletion of NADH. Hence, to accomplish uninterrupted oxidation of methane to methanol, it is essential to produce NADH by feeding formate to the culture medium (Xin et al., 2004b). Formate is added as a source of reducing power, which assists in the regeneration of NADH- the co-factor for methanol synthesis. However, the use of MDH inhibitors and formate is cost-intensive. Moreover, the supplementation of MDH inhibitors blocks the metabolic pathway in the methanotrophic strain. This affects the viability and biochemical and physiological functions of the culture. Consequently, it reduces the quantity and quality of the biomass produced. These factors lead to low methanol titer and also exclude the possibility of applying biomass-recycling strategy to this process.

Taking these drawbacks into consideration, it is imperative to look for alternative substrates or metabolic pathways which

can be exploited to produce methanol using methanotrophs. The limitations associated with biological production of methanol from methane can be overcome by utilizing CO_2 as the substrate for some methanotrophic species (Xin et al., 2007; Patel et al., 2016a). This is done in a two-stage process, where methane is utilized as carbon substrate during the first-stage to produce biomass, and CO_2 is reduced by the generated biomass in the second-stage to produce methanol (Xin et al., 2007). CO_2, an end-product of general methanotrophic metabolism (first-stage), tends to shift the reaction equilibrium in the backward direction if fed in excess to the cells (second-stage). Methanotrophic biomass act as biocatalyst for the reduction of CO_2 to methanol. The reduction of CO_2 to methanol is the reverse reaction of the oxidation of methane to CO_2 (**Figure 1**). However, MMO lacks the ability to catalyze the reverse reaction (reduction of methanol to methane). Therefore, the end-product of the CO_2 reduction pathway is methanol, which gets secreted extracellularly into the medium (Xin et al., 2004a, 2007). The reverse reaction requires excess of reducing equivalents, in the form of NADH, to drive the reaction against the laws of energy. Cells in general produce intracellular NADH. However, supply of endogenous NADH is limited and hence may be fed exogenously to the medium for uninterrupted progression of the batch; but this again adds to the cost of production. However, methanotrophs have an added advantage as they can produce PHB (Ghoddosi et al., 2019). PHB is also a source of intracellular reducing equivalents, in addition to NADH. β-hydroxybutyrate dehydrogenase, a NAD+-linked enzyme, catalyzes the decomposition of PHB to acetoacetic acid, and this subsequently generates reducing equivalents. Hence, the endogenously stored PHB in methanotrophs, plays a crucial role in accomplishing the reduction of CO_2 to methanol.

Xin et al. (2007) reported the production of 0.004 μmol methanol/mg (DCW) through reduction of CO_2 using *Methylosinus trichosporium* as a biocatalyst. The study also reports that cells having 38.6% PHB content showed highest methanol titers. Patel et al. (2016a) reported the production of 0.33 mM methanol using *Methylosinus sporium* from 30% CO_2 feed. These are few studies which demonstrate methanol production from CO_2. Although, there are reports suggesting CO_2 assimilation in Type X and Verrumicrobial methanotrophs toward biomass formation, however, there is no evidence in literature regarding these species converting CO_2 into methanol.

Authors have mainly demonstrated methanol production in batch and repeated-batch modes. Duan et al. (2011) has reported the production of 1.1 g/l methanol from 50% methane under optimum conditions in batch mode, using *M. trichosporium* OB3b. Patel et al. (2020c) reported the production of 30.9 mmol/l methanol from 30% methane using free-cells of *Methylocystis bryophila* under repeated-batch mode. Methanol production was reported to improve upto 52.9 mmol/l through covalent immobilization of cells on coconut coir (Patel et al., 2020c). Different studies have also reported improved methanol production through cell encapsulation in alginate and silica-gel (Patel et al., 2018), immobilization in polyvinyl alcohol (Patel et al., 2020b) and chemically modified chitosan (Patel et al., 2020a). Few key studies on methanol production using methanotrophs are listed in **Table 1**. Despite of the strategies involved, the processes are limited by low methanol titer and productivity. Yu et al. (2009) reported that methanol is toxic to *M. trichosporium* at concentrations above 3.0 g/l. This report illustrates that methanotrophs are able to tolerate a very low concentration of methanol and hence, suffer from end-product toxicity, leading to lower methanol titer and productivity.

MASS TRANSFER AND SOLUBILITY LIMITATIONS IN METHANOTROPH BASED GAS FERMENTATION

Common challenges associated with gas fermentation systems are gas-to-liquid mass transfer limitations and lower solubility of the gaseous substrates. Researchers have outlined the role of certain physico-chemical parameters like partial pressure, and extrinsic approaches like reactor configurations and mass transfer vectors to address these limitations.

Bioreactors help in achieving higher gas-to-liquid mass transfer rates as compared to other culture systems, facilitating easier and higher uptake of gases by the cells. Bubble column reactors have been predominantly used for cultivation systems where the objective is to replace mechanically driven stirring and to reduce the shear-stress on the cells. They are suitable for application when the requirement is to maintain directional flow and circulation, efficient mass transfer and heat transfer, especially while working with gas fermentation systems. Their application has mostly been reported for PHB production by methanotrophs (Ghoddosi et al., 2019; Rodríguez et al., 2020). Vertical tubular loop bioreactors have also been reported for gas fermentation. These reactors are characterized by defined direction of fluid circulation, often facilitated by a pump in gas-liquid based reactors and a propeller in fluidized bed reactors (Rahnama et al., 2012). Sheets et al. (2017) reported the production of methanol in a trickle-bed reactor (TBR) stuffed with ceramic beads. TBRs enhance air and methane mass transfer rates from the reactor headspace to the cells suspended in the medium. This study reported two-times greater oxygen mass transfer in the ceramic beads-stuffed reactor compared to the reactor without the bead-stuffing. The rate of methane oxidation was fourfold greater in the TBR as compared to shake-flask cultures. Volumetric mass-transfer coefficient (K_La) is a major metric for the performance evaluation of different reactor configurations. Airlift bioreactors have also been reported for high K_La values of upto 97.2 h^{-1} (Ghaz-Jahanian et al., 2018). Authors have reported the application of membrane biofilm reactors (MBR) for methanotroph-based bioremediation. MBRs overcome diffusional limitations by promoting high mass-transfer rates of sparingly soluble gaseous substrates to the biomass. MBRs have been reported for denitrification (Lee et al., 2019) and removal of perchlorate (Wu et al., 2019), chromate (Luo et al., 2019), vanadate (Wang et al., 2019), selenate (Shi et al., 2020), etc. from contaminated wastewater and groundwater using methanotrophs.

The problem of low solubility of gases in the liquid-phase in gas fermentation systems has been overcome by incorporating various modifications in the commonly used

reactor configurations. Studies have reported the addition of mass transfer vector, an organic phase, which has high affinity for the gaseous substrate and eventually improves the gas hold-up in the liquid media and consequent increased availability of the gaseous substrate to the microbial cells (Rocha-Rios et al., 2010; Zúñiga et al., 2011). Ten percent silicone oil has been prevalently added as a "methane-vector" to the aqueous medium to demonstrate "two-phase partition bioreactors (TPPB)." Rocha-Rios et al. (2010) and Zúñiga et al. (2011) have reported upto 33–45 and 700% increase in methane-degradation, respectively, using TPPBs. **Supplementary Table S1** summarizes different reactor configurations used for methanotrophic fermentations.

Partial pressure inside the reactor plays a crucial role in gas fermentation systems. The composition of the gas phase might vary depending upon the source, resulting in varying partial pressures. Timmers et al. (2015) reported that the growth of methanotrophs is faster at increased CH_4 partial pressures, as this is associated with highly negative Gibb's free energy change. While high partial pressures do result in increased solubility of the gases, they might interfere with the growth or product formation metabolism resulting from the interaction of the gaseous substrate with the key enzymes (Hurst and Lewis, 2010). In a study outlined by Soni et al. (1998), with pressure variation between 10 and 50 psi, *Methylomonas albus* showed a fourfold increase in methane uptake and 40% increase in biomass concentration at 20 psi, whereas higher pressure inhibited growth. Therefore, optimization of partial pressure is essential to maintain the balance between the solubility of gases and growth/product formation within the reactor.

CONCLUSION AND FUTURE PERSPECTIVES

Methanotrophs are excellent candidates for sequestration of harmful C1 compounds (CH_4 and CO_2). They are cellular factories for synthesis of a wide-range of value-added products. Amongst them, methanol has drawn significant attention owing to its potential applicability as a biofuel. Although, methanotrophs can synthesize methanol directly from methane, the associated limitations have driven the researchers to look for alternate pathways. Production of methanol from the methanotrophic reduction of CO_2 appears to be a promising alternative in this regard. The current state-of-the-art technology for the production of methanotrophic high-value products, is constrained by low product titer and productivity. As far as methanol production is concerned, limitations associated with product-toxicity are very challenging. Integration of the process with continuous/intermittent methanol recovery system may assist in overcoming product toxicity and improve its titer and productivity. Regardless of several reactor configurations outlined by researchers to deal with gas fermentation associated challenges, the technology stands at its "nascent stage of development." Hence, it becomes imperative to conduct detailed in-depth studies aiming at the development of process-engineering and design strategies for sustainable synthesis of methanotrophic high-value products on a commercial-scale. GSMM may be applied to evaluate different methanotrophic species *in silico* to predict their yields, rates of production and consumption, directed toward improved production of high-value products, without performing time- and labor-consuming experiments.

AUTHOR CONTRIBUTIONS

KS collected the data. KS and GG wrote the manuscript. DD did conceptualization, manuscript reviewing, and editing. All authors contributed to the article and approved the submitted version.

SUPPLEMENTARY MATERIAL

The Supplementary Material for this article can be found online at: https://www.frontiersin.org/articles/10.3389/fmicb.2021.636486/full#supplementary-material

REFERENCES

Baxter, N. J., Hirt, R. P., Bodrossy, L., Kovacs, K. L., Embley, M. T., Prosser, J. I., et al. (2002). The ribulose-1, 5-bisphosphate carboxylase/oxygenase gene cluster of *Methylococcus capsulatus* (Bath). *Archiv. Microbiol.* 177, 279–289. doi: 10.1007/s00203-001-0387-x

Cantera, S., Lebrero, R., Rodríguez, E., García-Encina, P. A., and Muñoz, R. (2017). Continuous abatement of methane coupled with ectoine production by *Methylomicrobium alcaliphilum* 20Z in stirred tank reactors: a step further towards greenhouse gas biorefineries. *J. Clean. Product.* 152, 134–141. doi: 10.1016/j.jclepro.2017.03.123

Cantera, S., Sánchez-Andrea, I., Lebrero, R., García-Encina, P. A., Stams, A. J., and Muñoz, R. (2018). Multi-production of high added market value metabolites from diluted methane emissions via methanotrophic extremophiles. *Bioresour. Technol.* 267, 401–407. doi: 10.1016/j.biortech.2018.07.057

Chidambarampadmavathy, K., Obulisamy, P. K., and Heimann, K. (2015). Role of copper and iron in methane oxidation and bacterial biopolymer accumulation. *Eng. Life Sci.* 15, 387–399. doi: 10.1002/elsc.201400127

Culpepper, M. A., and Rosenzweig, A. C. (2012). Architecture and active site of particulate methane monooxygenase. *Crit. Rev. Biochem. Mol. Biol.* 47, 483–492. doi: 10.3109/10409238.2012.697865

Dong, T., Fei, Q., Genelot, M., Smith, H., Laurens, L. M., Watson, M. J., et al. (2017). A novel integrated biorefinery process for diesel fuel blendstock production using lipids from the methanotroph, *Methylomicrobium buryatense*. *Energy Convers. Manag.* 140, 62–70. doi: 10.1016/j.enconman.2017.02.075

Duan, C., Luo, M., and Xing, X. (2011). High-rate conversion of methane to methanol by *Methylosinus trichosporium* OB3b. *Bioresour. Technol.* 102, 7349–7353. doi: 10.1016/j.biortech.2011.04.096

Fei, Q., Guarnieri, M. T., Tao, L., Laurens, L. M., Dowe, N., and Pienkos, P. T. (2014). Bioconversion of natural gas to liquid fuel: opportunities and challenges. *Biotechnol. Adv.* 32, 596–614. doi: 10.1016/j.biotechadv.2014.03.011

García-Pérez, T., López, J. C., Passos, F., Lebrero, R., Revah, S., and Muñoz, R. (2018). Simultaneous methane abatement and PHB production by *Methylocystis hirsuta* in a novel gas-recycling bubble column bioreactor. *Chemi. Eng. J.* 334, 691–697. doi: 10.1016/j.cej.2017.10.106

Ge, X., Yang, L., Sheets, J. P., Yu, Z., and Li, Y. (2014). Biological conversion of methane to liquid fuels: status and opportunities. *Biotechnol. Adv.* 32, 1460–1475. doi: 10.1016/j.biotechadv.2014.09.004

Ghaz-Jahanian, M. A., Khoshfetrat, A. B., Rostami, M. H., and Parapari, M. H. (2018). An innovative bioprocess for methane conversion to methanol using an efficient methane transfer chamber coupled with an airlift bioreactor. *Chem. Eng. Res. Design* 134, 80–89. doi: 10.1016/j.cherd.2018.03.039

Ghoddosi, F., Golzar, H., Yazdian, F., Khosravi-Darani, K., and Vasheghani-Farahani, E. (2019). Effect of carbon sources for PHB production in bubble column bioreactor: emphasis on improvement of methane uptake. *J. Environ. Chem. Eng.* 7:102978. doi: 10.1016/j.jece.2019.102978

Gupta, A., Ahmad, A., Chothwe, D., Madhu, M. K., Srivastava, S., and Sharma, V. K. (2019). Genome-scale metabolic reconstruction and metabolic versatility of an obligate methanotroph *Methylococcus capsulatus* str. Bath. *PeerJ* 7:e6685. doi: 10.7717/peerj.6685

Hanson, R. S., and Hanson, T. E. (1996). Methanotrophic bacteria. *Microbiol. Rev.* 60, 439–471.

Henard, C. A., Franklin, T. G., Youhenna, B., But, S., Alexander, D., Kalyuzhnaya, M. G., et al. (2018). Biogas biocatalysis: methanotrophic bacterial cultivation, metabolite profiling, and bioconversion to lactic acid. *Front. Microbiol.* 9:2610. doi: 10.3389/fmicb.2018.02610

Henard, C. A., Smith, H., Dowe, N., Kalyuzhnaya, M. G., Pienkos, P. T., and Guarnieri, M. T. (2016). Bioconversion of methane to lactate by an obligate methanotrophic bacterium. *Sci. Rep.* 6:21585. doi: 10.1038/srep21585

Hurst, K. M., and Lewis, R. S. (2010). Carbon monoxide partial pressure effects on the metabolic process of syngas fermentation. *Biochem. Eng. J.* 48, 159–165. doi: 10.1016/j.bej.2009.09.004

Kalyuzhnaya, M. G. (2016). "Methane biocatalysis: selecting the right microbe," in *Biotechnology for Biofuel Production and Optimization*, eds C. A. Eckert and C. T. Trinh (Amsterdam: Elsevier), 353–383. doi: 10.1016/B978-0-444-63475-7.00013-3

Kalyuzhnaya, M. G., Gomez, O. A., and Murrell, J. C. (2019). "The methane-oxidizing bacteria (methanotrophs)," in *Taxonomy, Genomics and Ecophysiology of Hydrocarbon-Degrading Microbes. Handbook of Hydrocarbon and Lipid Microbiology*, ed. T. McGenity (Cham: Springer), 245–278. doi: 10.1007/978-3-030-14796-9_10

Khmelenina, V. N., Kalyuzhnaya, M. G., Sakharovsky, V. G., Suzina, N. E., Trotsenko, Y. A., and Gottschalk, G. (1999). Osmoadaptation in halophilic and alkaliphilic methanotrophs. *Archiv. Microbiol.* 172, 321–329. doi: 10.1007/s002030050786

Khmelenina, V. N., Shchukin, V. N., Reshetnikov, A. S., Mustakhimov, I. I., Suzina, N. E., Eshinimaev, B. T., et al. (2010). Structural and functional features of methanotrophs from hypersaline and alkaline lakes. *Microbiology* 79, 472–482. doi: 10.1134/S0026261710040090

Lee, J., Alrashed, W., Engel, K., Yoo, K., Neufeld, J. D., and Lee, H. S. (2019). Methane-based denitrification kinetics and syntrophy in a membrane biofilm reactor at low methane pressure. *Sci. Total Environ.* 695:133818. doi: 10.1016/j.scitotenv.2019.133818

Lee, O. K., Hur, D. H., Nguyen, D. T. N., and Lee, E. Y. (2016). Metabolic engineering of methanotrophs and its application to production of chemicals and biofuels from methane. *Biofuels Bioprod. Biorefin.* 10, 848–863.

Lieven, C., Petersen, L. A., Jørgensen, S. B., Gernaey, K. V., Herrgard, M. J., and Sonnenschein, N. (2018). A genome-scale metabolic model for *Methylococcus capsulatus* (Bath) suggests reduced efficiency electron transfer to the particulate methane monooxygenase. *Front. Microbiol.* 9:2947. doi: 10.3389/fmicb.2018.02947

Luo, J. H., Wu, M., Liu, J., Qian, G., Yuan, Z., and Guo, J. (2019). Microbial chromate reduction coupled with anaerobic oxidation of methane in a membrane biofilm reactor. *Environ. Intern.* 130:104926. doi: 10.1016/j.envint.2019.104926

Mardina, P., Li, J., Patel, S. K., Kim, I. W., Lee, J. K., and Selvaraj, C. (2016). Potential of immobilized whole-cell *Methylocella tundrae* as a biocatalyst for methanol production from methane. *J. Microbiol. Biotechnol.* 26, 1234–1241. doi: 10.4014/jmb.1602.02074

Mustakhimov, I. I., Reshetnikov, A. S., But, S. Y., Rozova, O. N., Khmelenina, V. N., and Trotsenko, Y. A. (2019). Engineering of hydroxyectoine production based on the *Methylomicrobium alcaliphilum*. *Appl. Biochem. Microbiol.* 55, 626–630. doi: 10.1134/S0003683819130015

Nguyen, D. T. N., Lee, O. K., Lim, C., Lee, J., Na, J. G., and Lee, E. Y. (2020). Metabolic engineering of type II methanotroph, *Methylosinus trichosporium* OB3b, for production of 3-hydroxypropionic acid from methane via a malonyl-CoA reductase-dependent pathway. *Metab. Eng.* 59, 142–150. doi: 10.1016/j.ymben.2020.02.002

Park, S., Hanna, L., Taylor, R. T., and Droege, M. W. (1991). Batch cultivation of *Methylosinus trichosporium* OB3b. I: production of soluble methane monooxygenase. *Biotechnol. Bioeng.* 38, 423–433. doi: 10.1002/bit.260380412

Park, S., Shah, N. N., Taylor, R. T., and Droege, M. W. (1992). Batch cultivation of *Methylosinus trichosporium* OB3b: II. production of particulate methane monooxygenase. *Biotechnol. Bioeng.* 40, 151–157. doi: 10.1002/bit.260400121

Park, S. Y., and Kim, C. G. (2019). Application and development of methanotrophs in environmental engineering. *J. Mater. Cycles Waste Manag.* 21, 415–422. doi: 10.1007/s10163-018-00826-w

Patel, S. K., Gupta, R. K., Kondaveeti, S., Otari, S. V., Kumar, A., Kalia, V. C., et al. (2020a). Conversion of biogas to methanol by methanotrophs immobilized on chemically modified chitosan. *Bioresour. Technol.* 315:123791. doi: 10.1016/j.biortech.2020.123791

Patel, S. K., Gupta, R. K., Kumar, V., Kondaveeti, S., Kumar, A., Das, D., et al. (2020b). Biomethanol production from methane by immobilized co-cultures of methanotrophs. *Indian J. Microbiol.* 60, 318–324. doi: 10.1007/s12088-020-00883-6

Patel, S. K., Kalia, V. C., Joo, J. B., Kang, Y. C., and Lee, J. K. (2020c). Biotransformation of methane into methanol by methanotrophs immobilized on coconut coir. *Bioresour. Technol.* 297:122433. doi: 10.1016/j.biortech.2019.122433

Patel, S. K., Kumar, V., Mardina, P., Li, J., Lestari, R., Kalia, V. C., et al. (2018). Methanol production from simulated biogas mixtures by co-immobilized *Methylomonas methanica* and *Methylocella tundrae*. *Bioresour. Technol.* 263, 25–32. doi: 10.1016/j.biortech.2018.04.096

Patel, S. K., Mardina, P., Kim, D., Kim, S. Y., Kalia, V. C., Kim, I. W., et al. (2016a). Improvement in methanol production by regulating the composition of synthetic gas mixture and raw biogas. *Bioresour. Technol.* 218, 202–208. doi: 10.1016/j.biortech.2016.06.065

Patel, S. K., Mardina, P., Kim, S. Y., Lee, J. K., and Kim, I. W. (2016b). Biological methanol production by a type II methanotroph *Methylocystis bryophila*. *J. Microbiol. Biotechnol.* 26, 717–724. doi: 10.4014/jmb.1601.01013

Patel, S. K., Selvaraj, C., Mardina, P., Jeong, J. H., Kalia, V. C., Kang, Y. C., et al. (2016c). Enhancement of methanol production from synthetic gas mixture by *Methylosinus sporium* through covalent immobilization. *Appl. Energy* 171, 383–391. doi: 10.1016/j.apenergy.2016.03.022

Rahnama, F., Vasheghani-Farahani, E., Yazdian, F., and Shojaosadati, S. A. (2012). PHB production by *Methylocystis hirsuta* from natural gas in a bubble column and a vertical loop bioreactor. *Biochem. Eng. J.* 65, 51–56. doi: 10.1016/j.bej.2012.03.014

Rasigraf, O., Kool, D. M., Jetten, M. S., Damsté, J. S. S., and Ettwig, K. F. (2014). Autotrophic carbon dioxide fixation via the calvin-benson-bassham cycle by the denitrifying methanotroph "*Candidatus Methylomirabilis oxyfera*". *Appl. Environ. Microbiol.* 80, 2451–2460. doi: 10.1128/AEM.04199-13

Rasouli, Z., Valverde-Pérez, B., D'Este, M., De Francisci, D., and Angelidaki, I. (2018). Nutrient recovery from industrial wastewater as single cell protein by a co-culture of green microalgae and methanotrophs. *Biochem. Eng. J.* 134, 129–135. doi: 10.1016/j.bej.2018.03.010

Reshetnikov, A. S., Khmelenina, V. N., Mustakhimov, I. I., Kalyuzhnaya, M., Lidstrom, M., and Trotsenko, Y. A. (2011). Diversity and phylogeny of the ectoine biosynthesis genes in aerobic, moderately halophilic methylotrophic bacteria. *Extremophiles* 15:653. doi: 10.1007/s00792-011-0396-x

Rick, W. Y., and Kelly, K. (2012). "Construction of carotenoid biosynthetic pathways through chromosomal integration in methane-utilizing bacterium *Methylomonas* sp. strain 16a," in *Microbial Carotenoids from Bacteria and Microalgae*, ed. J.-L. Barredo (Totowa, NJ: Humana Press), 185–195. doi: 10.1007/978-1-61779-879-5_10

Rocha-Rios, J., Bordel, S., Hernández, S., and Revah, S. (2009). Methane degradation in two-phase partition bioreactors. *Chem. Eng. J.* 152, 289–292. doi: 10.1016/j.cej.2009.04.028

Rocha-Rios, J., Muñoz, R., and Revah, S. (2010). Effect of silicone oil fraction and stirring rate on methane degradation in a stirred tank reactor. *J. Chem. Technol. Biotechnol.* 85, 314–319. doi: 10.1002/jctb.2339

Rocha-Rios, J., Quijano, G., Thalasso, F., Revah, S., and Muñoz, R. (2011). Methane biodegradation in a two-phase partition internal loop airlift reactor with gas recirculation. *J. Chem. Technol. Biotechnol.* 86, 353–360. doi: 10.1002/jctb.2523

Rodríguez, Y., Firmino, P. I. M., Pérez, V., Lebrero, R., and Muñoz, R. (2020). Biogas valorization via continuous polyhydroxybutyrate production by *Methylocystis hirsuta* in a bubble column bioreactor. *Waste Manag.* 113, 395–403. doi: 10.1016/j.wasman.2020.06.009

Rosenzweig, A. C., Nordlund, P., Takahara, P. M., Frederick, C. A., and Lippard, S. J. (1995). Geometry of the soluble methane monooxygenase catalytic diiron center in two oxidation states. *Chem. Biol.* 2, 409–418.

Rostkowski, K. H., Pfluger, A. R., and Criddle, C. S. (2013). Stoichiometry and kinetics of the PHB-producing Type II methanotrophs *Methylosinus trichosporium* OB3b and *Methylocystis parvus* OBBP. *Bioresour. Technol.* 132, 71–77. doi: 10.1016/j.biortech.2012.12.129

Schouten, S., Bowman, J. P., Rijpstra, W. I. C., and Sinninghe Damsté, J. S. (2000). Sterols in a psychrophilic methanotroph, *Methylosphaera hansonii*. *FEMS Microbiol. Lett.* 186, 193–195. doi: 10.1111/j.1574-6968.2000.tb09103.x

Sheets, J. P., Lawson, K., Ge, X., Wang, L., Yu, Z., and Li, Y. (2017). Development and evaluation of a trickle bed bioreactor for enhanced mass transfer and methanol production from biogas. *Biochem. Eng. J.* 122, 103–114. doi: 10.1016/j.bej.2017.03.006

Shi, L. D., Lv, P. L., Wang, M., Lai, C. Y., and Zhao, H. P. (2020). A mixed consortium of *Methanotrophic archaea* and bacteria boosts methane-dependent selenate reduction. *Sci. Total Environ.* 732:139310. doi: 10.1016/j.scitotenv.2020.139310

Sirajuddin, S., and Rosenzweig, A. C. (2015). Enzymatic oxidation of methane. *Biochemistry* 54, 2283–2294. doi: 10.1021/acs.biochem.5b00198

Soni, B. K., Conrad, J., Kelley, R. L., and Srivastava, V. J. (1998). "Effect of temperature and pressure on growth and methane utilization by several methanotrophic cultures," in *Biotechnology for Fuels and Chemicals*, eds M. Finkelstein and B. H. Davison (Totowa, NJ: Humana Press), 729–738. doi: 10.1007/978-1-4612-1814-2_67

Stępniewska, Z., Goraj, W., Kuźniar, A., Pytlak, A., Ciepielski, J., and Frączek, P. (2014). Biosynthesis of ectoine by the methanotrophic bacterial consortium isolated from Bogdanka coalmine (Poland). *Appl. Biochem. Microbiol.* 50, 594–600. doi: 10.1134/S0003683814110039

Takeguchi, M., Furuto, T., Sugimori, D., and Okura, I. (1997). Optimization of methanol biosynthesis by *Methylosinus trichosporium* OB3b: an approach to improve methanol accumulation. *Appl. Biochem. Biotechnol.* 68, 143–152. doi: 10.1007/BF02785987

Tao, L., Sedkova, N., Yao, H., Rick, W. Y., Sharpe, P. L., and Cheng, Q. (2007). Expression of bacterial hemoglobin genes to improve astaxanthin production in a methanotrophic bacterium *Methylomonas* sp. *Appl. Microbiol. Biotechnol.* 74, 625–633. doi: 10.1007/s00253-006-0708-8

Timmers, P. H., Gieteling, J., Widjaja-Greefkes, H. A., Plugge, C. M., Stams, A. J., Lens, P. N., et al. (2015). Growth of anaerobic methane-oxidizing archaea and sulfate-reducing bacteria in a high-pressure membrane capsule bioreactor. *Appl. Environ. Microbiol.* 81, 1286–1296. doi: 10.1128/AEM.03255-14

Tsapekos, P., Zhu, X., Pallis, E., and Angelidaki, I. (2020). Proteinaceous methanotrophs for feed additive using biowaste as carbon and nutrients source. *Bioresour. Technol.* 313:123646. doi: 10.1016/j.biortech.2020.123646

Valverde-Pérez, B., Xing, W., Zachariae, A. A., Skadborg, M. M., Kjeldgaard, A. F., Palomo, A., et al. (2020). Cultivation of methanotrophic bacteria in a novel bubble-free membrane bioreactor for microbial protein production. *Bioresour. Technol.* 310:123388. doi: 10.1016/j.biortech.2020.123388

Wang, Z., Shi, L. D., Lai, C. Y., and Zhao, H. P. (2019). Methane oxidation coupled to vanadate reduction in a membrane biofilm batch reactor under hypoxic condition. *Biodegradation* 30, 457–466. doi: 10.1007/s10532-019-09887-6

Whittenbury, R., Phillips, K. C., and Wilkinson, J. F. (1970). Enrichment, isolation and some properties of methane-utilizing bacteria. *Microbiology* 61, 205–218. doi: 10.1099/00221287-61-2-205

Wu, M., Luo, J. H., Hu, S., Yuan, Z., and Guo, J. (2019). Perchlorate bio-reduction in a methane-based membrane biofilm reactor in the presence and absence of oxygen. *Water Res.* 157, 572–578. doi: 10.1016/j.watres.2019.04.008

Xin, J. Y., Cui, J., Niu, J. Z., Hua, S. F., Xia, C., Li, S., et al. (2004a). Biosynthesis of methanol from CO_2 and CH4 by methanotropic bacteria. *Biotechnology* 3, 67–71.

Xin, J. Y., Cui, J. R., Niu, J. Z., Hua, S. F., Xia, C. G., Li, S. B., et al. (2004b). Production of methanol from methane by methanotrophic bacteria. *Biocatalys. Biotransform.* 22, 225–229. doi: 10.1080/10242420412331283305

Xin, J. Y., Zhang, Y. X., Zhang, S., Xia, C. G., and Li, S. B. (2007). Methanol production from CO_2 by resting cells of the methanotrophic bacterium *Methylosinus trichosporium* IMV 3011. *J. Basic Microbiol.* 47, 426–435. doi: 10.1002/jobm.200710313

Yan, X., Chu, F., Puri, A. W., Fu, Y., and Lidstrom, M. E. (2016). Electroporation-based genetic manipulation in type I methanotrophs. *Appl. Environ. Microbiol.* 82, 2062–2069. doi: 10.1128/AEM.03724-15

Yoo, Y. S., Han, J. S., Ahn, C. M., and Kim, C. G. (2015). Comparative enzyme inhibitive methanol production by *Methylosinus sporium* from simulated biogas. *Environ. Technol.* 36, 983–991. doi: 10.1080/09593330.2014.971059

Yu, Y., Ramsay, J. A., and Ramsay, B. A. (2009). Production of soluble methane monooxygenase during growth of *Methylosinus trichosporium* on methanol. *J. Biotechnol.* 139, 78–83. doi: 10.1016/j.jbiotec.2008.09.005

Zhang, Y., Xin, J., Chen, L., Song, H., and Xia, C. (2008). Biosynthesis of poly-3-hydroxybutyrate with a high molecular weight by methanotroph from methane and methanol. *J. Nat. Gas Chem.* 17, 103–109. doi: 10.1016/S1003-9953(08)60034-1

Zúñiga, C., Morales, M., Le Borgne, S., and Revah, S. (2011). Production of poly-β-hydroxybutyrate (PHB) by *Methylobacterium organophilum* isolated from a methanotrophic consortium in a two-phase partition bioreactor. *J. Hazard. Mater.* 190, 876–882. doi: 10.1016/j.jhazmat.2011.04.011

Conflict of Interest: The authors declare that the research was conducted in the absence of any commercial or financial relationships that could be construed as a potential conflict of interest.

frontiers in Microbiology

ORIGINAL RESEARCH
published: 10 March 2021
doi: 10.3389/fmicb.2021.647370

Bioethanol Production From H_2/CO_2 by Solventogenesis Using Anaerobic Granular Sludge: Effect of Process Parameters

Yaxue He, Chiara Cassarini and Piet N. L. Lens*

National University of Ireland Galway, Galway, Ireland

OPEN ACCESS

Edited by:
Guodong Luan, Qingdao Institute of Bioenergy and Bioprocess Technology (CAS), China

Reviewed by:
Ioannis Vyrides, Cyprus University of Technology, Cyprus
Zhiyong Huang, Chinese Academy of Sciences, China

****Correspondence:***
Yaxue He
Y.HE2@nuigalway.ie

Specialty section:
This article was submitted to Microbiotechnology, a section of the journal Frontiers in Microbiology

Received: *29 December 2020*
Accepted: *15 February 2021*
Published: *10 March 2021*

Citation:
He Y, Cassarini C and Lens PNL (2021) Bioethanol Production From H_2/CO_2 by Solventogenesis Using Anaerobic Granular Sludge: Effect of Process Parameters. Front. Microbiol. 12:647370. doi: 10.3389/fmicb.2021.647370

CO_2 fermentation by biocatalysis is a promising route for the sustainable production of valuable chemicals and fuels, such as acetic acid and ethanol. Considering the important role of environmental parameters on fermentation processes, granular sludge from an industrial anaerobic wastewater treatment system was tested as inoculum for ethanol production from H_2/CO_2 at psychrophilic (18°C), submesophilic (25°C), and mesophilic (30°C) temperatures. The highest acetic acid and ethanol production was obtained at 25°C with a final concentration of 29.7 and 8.8 mM, respectively. The presence of bicarbonate enhanced acetic acid production 3.0 ∼ 4.1-fold, while inhibiting ethanol production. The addition of 0.3 g/L glucose induced butyric acid production (3.7 mM), while 5.7 mM ethanol was produced at the end of the incubation at pH 4 with glucose. The addition of 10 μM W enhanced ethanol production up to 3.8 and 7.0-fold compared to, respectively, 2 μM W addition and the control. The addition of 2 μM Mo enhanced ethanol production up to 8.1- and 5.4-fold compared to, respectively, 10 μM Mo and the control. This study showed that ethanol production from H_2/CO_2 conversion using granular sludge as the inoculum can be optimized by selecting the operational temperature and by trace metal addition.

Keywords: ethanol, H_2/CO_2, bioconversion, temperature, trace metals

HIGHLIGHTS

- Submesophilic temperatures (25°C) and an initial pH 6 enhanced ethanol production.
- Increased ratio of CO_2/H_2 by bicarbonate addition enhanced acetic acid production (3.0 ∼ 4.1-fold), but inhibited ethanol production.
- Glucose addition (0.3 g/L) enhanced butyric acid production (3.3 mM), while ethanol production occurred at pH 4.
- Addition of 10 μM W or 2 μM Mo enhanced ethanol production up to 7.0 or 5.4-fold, respectively.

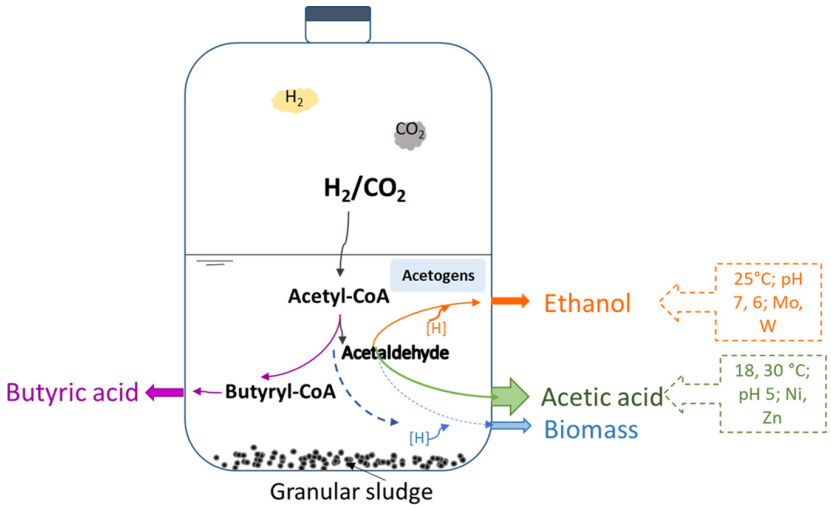

GRAPHICAL ABSTRACT | Bioethanol from H2/CO2 by solventogenesis using anaerobic granular sludges.

INTRODUCTION

The increasing demand for fuel energy and its gradual depletion renders the development of renewable energy necessary and emergent (Devarapalli and Atiyeh, 2015). An innovative solution is to use C_1 gasses (i.e., one carbon atom gasses) as the substrate to produce valuable chemicals, e.g., volatile fatty acids (VFAs) as well as ethanol and butanol by microbes (Sadhukhan et al., 2016; Fernández-Naveira et al., 2017a). These C_1 compounds include carbon monoxide (CO), carbon dioxide (CO_2), methane (CH_4), and synthesis gas (CO/CO_2 and H_2 mixtures) produced from biomass and domestic/agricultural wastes. Besides, H_2 becomes available from the conversion of excess power produced by renewable energy sources, such as wind and solar power, which face challenges of balancing power production and demand. The generation of valuable chemicals and fuels from H_2/CO_2 and syngas (mainly containing CO, H_2 and CO_2) fermentation is economic and has sustainable advantages (Burk et al., 2014) compared to traditional corn (Eisentraut, 2010; Mohammadi et al., 2011) or cellulosic material (Naik et al., 2010) fermentation. Moreover, ethanol has a higher energy density and easier storage and transportability than H_2 (Pereira, 2013; Sarkar et al., 2017). Homoacetogenesis and solventogenesis from H_2/CO_2 occur according to reactions 1 and 2:

$$2CO_2\,(g) + 4H_2\,(g) \rightarrow CH_3COOH\,(l) + 2H_2O\,(l)$$
$$\triangle G_r^{\theta} \; -75.4\,\text{kJ/moL} \qquad (1)$$

$$2CO_2(g) + 6H_2(g) \rightarrow CH_3CH_2OH(l) + 3H_2O\,(l)$$
$$\triangle G_r^{\theta} \; -96.5\text{kJ/moL} \qquad (2)$$

with $\triangle G_r^{\theta}$ is the standard reaction Gibbs energy, T = 298.15K and P = 100kPa.

Granular sludge from Upflow Anaerobic Sludge Bed (UASB) wastewater treatment plants can be used as inoculum for VFAs (Dogan et al., 2005) and ethanol (Steinbusch et al., 2008) production. UASB sludge consists of mixed microbial communities and its full-scale applications have less contamination problems compared to pure cultures. Temperature is an important factor influencing fermentation, for example, mesophilic conditions are optimum for homoacetogen *Clostridium* sp. in syngas fermentation (Singla et al., 2014; Shen et al., 2017). Limited studies focus on psychrophilic or submesophilic conditions for alcohol production from C_1 gas or syngas by mixed cultures (Liu et al., 2018). Instead, substantial studies focused on mesophilic conditions despite submesophilic conditions are with merits of low energy consumption for high temperature control (Ramió-Pujol et al., 2015). Also the pH can significantly affect both biomass growth and the product formation rate. As the external pH begins to drop due to acid accumulation, an organism may begin to produce alcohols to prevent a further drop in pH (Padan et al., 1981; Cotter et al., 2009). Glucose addition to the medium can enhance alcohol production via overexpressing the ferredoxin-dependent aldehyde oxidoreductase (AOR) gene in *Clostridium carboxidivorans* (Cheng et al., 2019). AOR is involved in conversion of carboxylic acids into their corresponding alcohols without ATP consumption in acetogens such as *C. ljungdahlii* and *C. autoethanogenum* (Liu et al., 2012; Cheng et al., 2019). Besides, glucose offers extra carbon source and releases CO_2 during the glycolysis pathway, which can be re-assimilated via the Wood Ljungdahl pathway (WLP) with H_2 as electron donor and thus enhance the carbon conversion efficiency.

Acetic acid and ethanol are produced from CO_2 by acetogens via the Wood-Ljungdahl pathway (WLP) catalyzed by different enzymes (Fast and Papoutsakis, 2012). Formate dehydrogenase (FDH) is one of the key enzymes in the WLP, converting CO_2 into acetyl-CoA and leading to the production of acetate. Acetate yields acetaldehyde catalyzed by ferredoxin aldehydeoxydoreductase (AOR). Then, ethanol is produced through the reduction of acetaldehyde by alcohol

dehydrogenase (ADH) catalyzing the reduction of acetyl CoA to ethanol (Andreesen and Makdessi, 2008; Jiann-Shin, 2010). Several studies compared the effect of trace metal addition on ethanol production from syngas in pure cultures of *Clostridium ragsdalei* (Saxena and Tanner, 2011). The presence of W enhances ethanol production compared to the absence of W from carbon monoxide by anaerobic granular sludge (Chakraborty et al., 2020). Molybdate (Mo) is an analog of tungsten (W) and binds in the active sites of some enzymes, such as AOR and ADH (Fernández-Naveira et al., 2017b). Other trace metals like zinc (Zn) and nickel (Ni) can stimulate alcohol production by enhancing the FDH and ADH synthesis and activity (Yamamoto et al., 1983).

Based on our previous study on the optimization of ethanol production from H_2/CO_2, the highest ethanol production was reached at 25°C compared to 37 and 55°C by anaerobic granular sludge (He et al., 2020). This study further investigated homoacetogenesis and solventogenesis under submesophilic conditions, i.e., 18, 25, and 30°C using CO_2 as carbon source and H_2 as sole electron donor by the same anaerobic granular sludge as used by He et al. (2020). Besides, the effects of pH, carbon source (HCO_3^- and glucose supplementation) and trace metals on ethanol production were also investigated.

MATERIALS AND METHODS

Biomass

The anaerobic granular sludge was obtained from a 200 m^3 UASB reactor producing methane from dairy industry effluent at 20°C and a hydraulic retention time (HRT) of 9–12 h. The total solid (TS) and volatile solid (VS) content was 42.7 (±1.0) g/L and 24.8 (±0.5) g/L, respectively. The granular sludge was first centrifuged at 5,500 rpm for 10 min to remove the supernatant and the pellet was heat- treated at 90°C for 15 min to select for spore forming acetogens as described by Dessì et al. (2017).

Medium Composition

Medium was prepared according to Stams et al. (1993) and modified as follows: 408 mg/L KH_2PO_4, 534 mg/L $Na_2HPO_4{\cdot}2H_2O$, 300 mg/L NH_4Cl, 300 mg/L NaCl, 100 mg/L $MgCl_2{\cdot}6H_2O$, 110 mg/L $CaCl_2{\cdot}2H_2O$; 1 mL trace metal and 1 mL vitamin stock solution (Stams et al., 1993). 1 L medium (except for $CaCl_2{\cdot}2H_2O$ and vitamins) was prepared and brought to boiling in order to remove O_2, cooled down to room temperature under an oxygen-free N_2 flow, then $CaCl_2{\cdot}2H_2O$ and the vitamins were added as well as Na_2S (0.24 g/L) as reducing agent.

Experimental Set-Up

Batch tests were conducted in 125 mL serum bottles with 50 mL medium (gas: liquid ratio of 3:2) and granular sludge with an initial VS. concentration of 1.0 g/L. The bottles were sealed with rubber inlets and capped with aluminum crimp caps. A H_2/CO_2 (v/v, 80/20) gas mixture was injected by a gas exchanger system (GW-6400-3111, Germany) to an initial pressure of 1.8 (±0.15) bar (P_{H2} = 1.44 bar, P_{CO2} = 0.36 bar), in which 124.4 mL of the gas mixture was compressed in the 75 mL headspace. Blank experiments were set up with a H_2/CO_2 (v/v, 80/20) headspace without the granular sludge as well as a N_2 (100%) headspace with the granular sludge (initial VS. concentration 1.0 g/L). At the start of the experiments, the gas pressure was measured every 24 h. H_2/CO_2 was injected when the gas pressure was detected below 1 bar. All experiments were performed in triplicates.

Experimental Design

In order to enhance the C/H ratio of the substrate and thus enhance the electron donor utilization efficiency considering the substrate C/H ratio is 1/4 lower than the theoretical utilization ratio (Eq. 1), 2.1 g/L $NaHCO_3$ (1.25 mmol carbon) was added in 50 mL medium to increase the CO_2/H_2 ratio to theoretically obtain a H_2/CO_2 ratio of 64/36 (v/v). 1 mL 1M HCl was also added to balance the pH increase by $NaHCO_3$ (He et al., 2020).

The first batch test was set up at different temperatures (18, 25, and 30°C) using H_2/CO_2 or H_2/CO_2 with HCO_3^-. The second batch test was performed at 25°C at different pH 7, 6, and 5 and 0.3 g/L glucose with initial pH of 6. 0.3 g/L glucose + H_2/CO_2, H_2/CO_2 with no glucose and 0.3 g/L glucose with no H_2/CO_2 were supplied again when they were totally consumed. The third batch test was set up with different trace metal concentrations, namely 2 μM W (20×), 2 μM Mo (20×), 10 μM W (100×), 10 μM Mo (100×), 10 μM Ni (100×), and 50 μM Zn (100×) compared with 0.1 μM W, 0.1 μM Mo, 0.1 μM Ni and 0.5 μM Zn in the control. Incubations with medium with no trace metals were set up as control experiments.

Headspace (1 mL) and liquid (1 mL) samples were withdrawn from each vial every 24 h to analyze the gas and liquid phase. Liquid samples were centrifuged at 8,000 × g for 5 min and the supernatant was filtered with a syringe using a 0.22 μm PTFE-filter prior to analyzing ethanol and acetic acid concentrations.

Analytical Methods

Gas-Phase Analysis

H_2, CO_2, and CH_4 concentrations were measured using a HP 6890 gas chromatograph (GC, Agilent Technologies, United States) equipped with a thermal conductivity detector (TCD). The GC was fitted with a 15 m HP-PLOT Molecular Sieve 5A column (ID 0.53 mm, film thickness 50 μm). The oven temperature was kept constant at 60°C. The temperature of the injection port and the detector were maintained constant at 250°C. Helium was used as the carrier gas. Standard gas mixtures of CH_4, H_2, and CO_2 were measured every time along with the sample measurements.

VFAs and Alcohols Analysis

VFA and alcohol concentrations were analyzed for each bottle from the liquid samples (1 mL) using high performance liquid chromatography (Agilent Co., United States) equipped with a refractive index detector (RID) and an Agilent Hi-Plex H column (Internal diameter × length, 7.7 × 300 mm, size 8 μm). A H_2SO_4 solution (5 mM) was used as mobile phase at a flow rate of 0.7 ml/min and with a sample injection volume of 50 μl. The column temperature was set at 60°C and the RID detector at 55°C. Total solid (TS) and volatile solid (VS) were measured according to standard methods (EPA, 2001). Calibration curves

from 0.5 to 100 mM acetic acid, ethanol and butyric acid were made. The carbon (C) and electron (e^-) recoveries were calculated according to our previous study (He et al., 2020).

RESULTS

Effect of Initial pH on H_2/CO_2 Bioconversion at 25°C

The highest ethanol production was 2.5, 3.6, and 1.7 mM at initial pH of 7, 6, and 5, respectively (**Table 1**). The highest ethanol concentration was reached at an initial pH of 6, while the highest acetic acid concentration at pH 7 (**Figures 1A,B** and **Table 1**). A neutral initial pH enhanced the acetic acid production, but this may not be the best condition for ethanol production (**Figure 1A**). The pH decreased along with time: after 168 h of fermentation all pH values had decreased below 5 (**Figure 1D**). Ethanol production was detected at 120 h for the batches with initial pH of 7 and 6, while for pH 5, ethanol was observed at 360 h (**Figure 1**). It was noted that at initial pH 5, the acetic acid concentration reached 7.4 mM at 120 h, similar for the batch experiment at pH 6 with an acetic acid concentration of 9.0 mM, but ethanol production was not observed (**Figures 1B,C**). The C and e- recovery were, respectively, 123.6 and 123.1% at pH 5, 151.8, and 137.1% at pH 6, 112.6, and 116.0% at pH 7 (**Table 1**). A small amount of acetic acid (data not shown) production was detected in the control bottles without H_2/CO_2 (with 100% N_2) (**Table 2**).

Effect of Temperature on H_2/CO_2 Fermentation by Granular Sludge

Acetic acid was the main fermentation product with the highest acetic acid concentration of 6.5 (±2.6), 29.7 (±3.3), and 27.0 (±2.4) mM at 18, 25, and 30°C, respectively (**Table 2**). The pH decreased along with the acetic acid accumulation from initially pH 6 to 5.0, 4.4, and 4.4 at 18, 25, and 30°C (**Figure 2B**), respectively. The highest ethanol concentration of 8.8 mM was obtained at 25°C with the highest average production rate of 0.03 mmol L^{-1} h^{-1} (**Table 2**). Ethanol started to be produced when acetic acid was more than 16.3 and 21.6 mM and the pH was lower than 4.9 at 25°C and 4.7 at 30°C, respectively (**Figure 2A**). The highest ethanol production rate was 0.11 mmoL·L^{-1}·h^{-1} after 140 h of incubation at 30°C, while the highest acetic acid production rate was 0.32 mmoL·L^{-1}·h^{-1} after 120 h of incubation at 25°C (**Supplementary Figure 1** and **Table 2**).

The mesophilic (30°C) or psychrophilic (18°C) temperatures with an initial incubation pH of 6.0 negatively affected the ethanol production. The highest C and e^- recovery obtained at 25°C were 120.4 (±36.9)% and 82.3 (±31.0)%, respectively (**Table 2**). The acetic acid concentration after 72 h of incubation varied at 0.8, 2.7, and 11.2 mM in the18, 25, and 30°C incubations, respectively (**Figure 2A**), which demonstrated that higher temperatures reduced the lag phase of the acetic acid production. The average acetic acid and ethanol production rate were much lower at 18°C than at 25 or 30°C (**Table 2**). At 30°C, the C and e^- recovery were 88.5 (±20.0)% and 75.5 (±20.0)%, respectively, which were both lower than at 25°C. The lowest C and e^- recovery of 25.5 (±10.2)% and 20.5 (±8.2)%, respectively, were observed at 18°C (**Table 2**).

Upon the addition of HCO_3^-, the acetic acid production was highly enhanced at 25 and 30°C, while the ethanol production was below 4 mM (**Figure 2C**). Up to 122.7 (±5.8) mM acetic acid was obtained, which was 4.1-fold more than the highest acetic acid concentration (29.7 ± 3.3 mM) without HCO_3^- addition at 25°C (**Table 2**). Similarly, the highest acetic acid concentration with HCO_3^- was 3.0-fold higher than without HCO_3^- at 30°C (**Table 2**). The highest acetic acid production rate amounted to 0.97, 0.79, and 1.58 mmoL·L^{-1}·h^{-1} at 18, 25, and 30°C, respectively, which are all higher than in the absence of HCO_3^- (**Supplementary Figure 1B** and **Table 2**). The pH increased initially from 6 to 6.2 at 120 h at 18, 25, and 30°C. At the end of the incubation, the pH varied between 6.2 and 6.5 at 18°C, decreased to 5.6 at 25°C and 5.3 at 30°C (**Figure 2D**). Overall, the pH kept stable between 5.2 and 6, although the acetic acid concentration was much higher than in the absence of HCO_3^- (**Figure 2D**).

Effect of Glucose on H_2/CO_2 Bioconversion at 25°C

The fermentation process using solely H_2/CO_2 could be separated in four stages (**Figure 3**): stage I (0–120 h) is the acetic acid accumulation phase, stage II (120–192 h), and III (192–264 h) represent, respectively, the quick acetic acid production and butyric acid accumulation, whereas ethanol was produced in stage IV (264–552 h). In stage I, when using glucose + H_2/CO_2 as the substrate, acetic acid was not detected after 48 h of incubation, then 16.5 mM acetic acid and 0.45 mM butyric acid were observed at 120 h. Thereafter, acetic acid production rate reached to its maximum (0.32 mmoL·L^{-1}·h^{-1}) at 168 h in stage II (**Figure 3A**). The acetic acid concentration kept relatively stable during stage III, during which the butyric acid concentration started to increase (from 0.5 to 3.3 mM) (**Figure 3A**). Ethanol started to increase during stage IV and reached to 5.7 (±2.4) mM when the pH decreased below 4 (**Figures 3A,D**).

When using glucose as the sole substrate, the acetic acid concentration reached 7.9 mM at 48 h. The highest acetic acid concentration reached 14.8 mM after 360 h of incubation. The highest butyric acid (3.3 mM) and ethanol (0.6 mM) concentrations were obtained at 360 h (**Figure 1C** and **Table 1**). The distinct change when adding glucose was the quick decrease in pH from initially 6 to 4.8 after 48 h of incubation (**Figure 3D**). During stage II and III, the pH decreased quickly to below 4 for the batches with both glucose and H_2/CO_2 and to 4.5 for the glucose only batches (**Figure 3D**). Compared to the H_2/CO_2 solely incubation (**Figure 3B**), the addition of glucose enhanced the butyric acid production. The C and e^- recovery were, respectively, 89.1 and 99.6% in the batches with glucose, compared to 89.0 and 80.4% for glucose + H_2/CO_2 (**Table 1**).

Effect of Trace Metals (W, Mo, Zn, Ni) on H_2/CO_2 Fermentation at 25°C

Upon the addition of 2 and 10 μM W, acetic acid production constantly increased to the highest concentration of 33.3 (±13.8)

TABLE 1 | Effect of pH, carbon supplements and trace metals on the maximum acetic acid and ethanol concentrations and H_2 and CO_2 consumption from H_2/CO_2 by heat-treated anaerobic granular sludge (at the end of incubation).

Conditions/Substrate	Products (mM)									
	Acetic acid	Butyric acid	Ethanol	CO_2	H_2	CH_4	H_2 consumption (%)	CO_2 consumption (%)	C recovery (%)	e^- recovery (%)
pH 7	65.3 ± 7.9	0.6	2.6 ± 3.1	−46.9[a]	−96.7[a]	0	35.5	69.0	123.6	123.1
pH 6	59.9 ± 6.3	0.7	8.5 ± 3.1	−38.0[a]	−86.1[a]	0	31.5	55.7	151.8	137.1
pH 5	58.1 ± 29.6	0.4	1.7 ± 2.7	−40.3[a]	−81.7[a]	0	29.4	58.0	112.6	116.0
Glucose	14.8 ± 0.3	3.3 ± 0.2	0.6 ± 0.5	–[b]	–[b]	0	–[b]	–[b]	89.1	99.6
Glucose+H_2/CO_2	44.9 ± 11.5	3.7 ± 0.5	5.7 ± 2.4	−39.3[a]	−104.9[a]	0	37.5	56.2	89.0	80.4
Control	38.4 ± 15.8	0	7.6 ± 4.3	−42.7[a]	−80.8[a]	0	26.8	56.5	141.2 ± 26.2	176.5 ± 20.2
2 μM W	33.3 ± 13.8	0	3.9 ± 2.6	−36.9[a]	−81.5[a]	0	26.6	48.2	130.0 ± 18.7	145.6 ± 52.8
10 μM W	53.0 ± 4.4	0	14.8 ± 10.2	−48.5[a]	−107.1[a]	0	34.9	63.3	153.0 ± 20.0	172.7 ± 22.8
2 μM Mo	40.2 ± 16.0	0	11.3 ± 2.1	−47.2[a]	−91.7[a]	0	31.5	64.6	141.9 ± 25.1	178.4 ± 32.8
10 μM Mo	66.9 ± 11.0	0	1.4 ± 1.1	−51.0[a]	−95.5[a]	0	31.2	66.7	174.9 ± 15.8	204.1 ± 9.8
10 μM Ni	42.7 ± 6.9	0	3.7 ± 2.2	−40.3[a]	−70.9[a]	0	23.2	52.8	150.5 ± 13.5	197.1 ± 20.9
50 μM Zn	28.5 ± 7.7	0	3.3 ± 2.3	−34.0[a]	−47.9[a]	0	16.6	47.4	122.6 ± 12.0	203.5 ± 30.0

[a]*Negative values indicate an overall consumption of component during the experiment.*
[b]*Data not known since carbon is excess.*

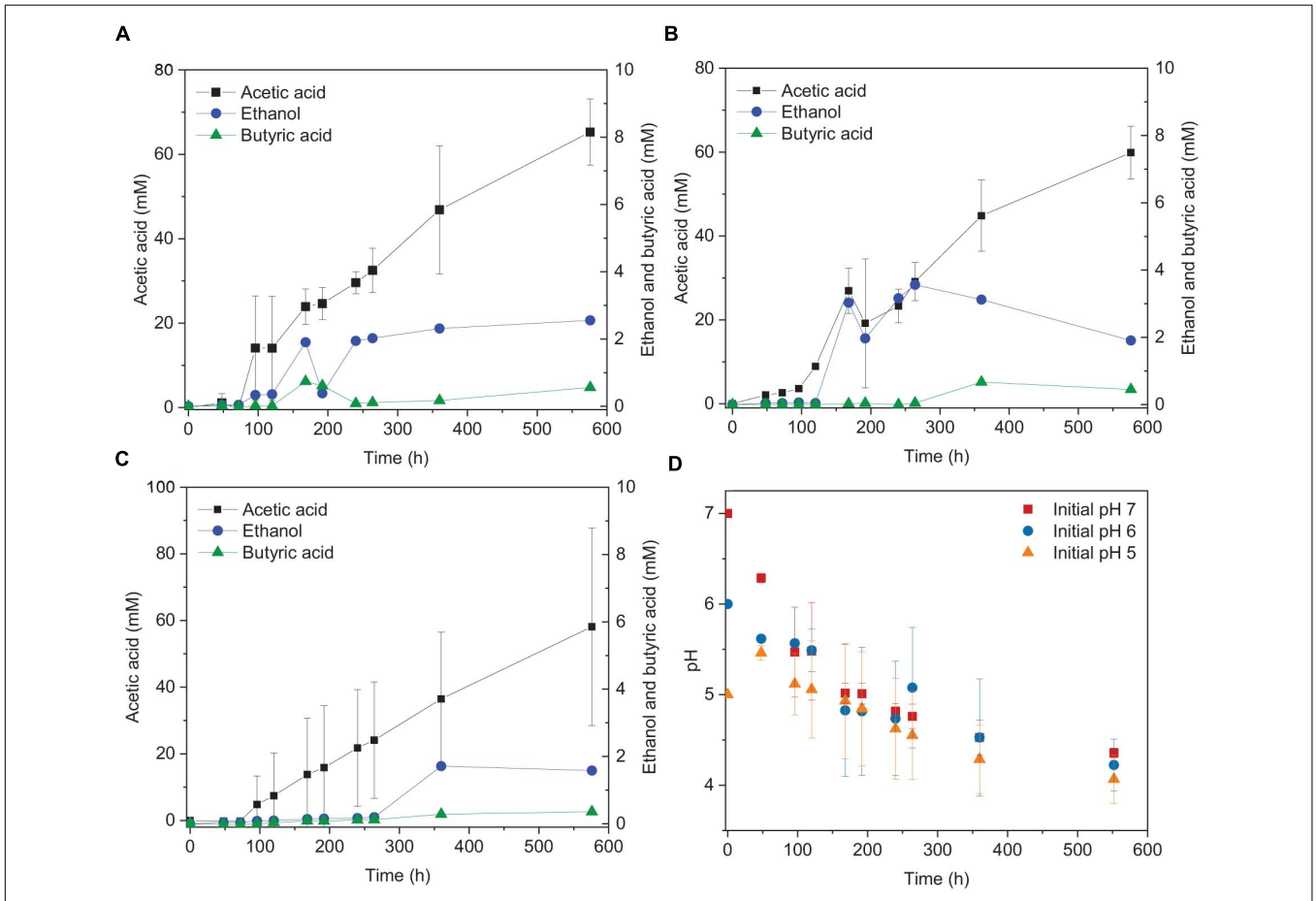

FIGURE 1 | Acetic acid and ethanol production from H_2/CO_2 by heat-treated granular sludge at 25°C at **(A)** pH 7, **(B)** pH 6, **(C)** pH 5, and **(D)** change of pH over time.

TABLE 2 | Effect of HCO_3^- on the maximum acetic acid and ethanol concentration from H_2/CO_2 by heat-treated anaerobic granular sludge at initial pH 6.

System conditions	Substrate					
	H_2/CO_2			$H_2/CO_2+HCO_3^-$		
	18°C	25°C	30°C	18°C	25°C	30°C
Products (mM)						
Acetic acid	6.5 ± 2.6	29.7 ± 3.3	27.0 ± 2.4	24.3 ± 31.2	122.7 ± 5.8	81.3 ± 23.3
Ethanol	0.1	8.7 ± 9.2	3.6 ± 3.7	0.1	6.3 ± 7.8	4.3 ± 7.0
CO_2	29.3	35.8	38.5	–	–	–
H_2	73.3	115.6	95.0	–	–	–
Undissociated acid	–	22 ± 0.1	19 ± 3.2	–	36 ± 7.5	16 ± 12.5
H_2 consumption (%)	26.4	41.7	34.0	–	–	–
CO_2 consumption (%)	42.3	51.6	55.3	–	–	–
C recovery (%) [a]	25.5 ± 10.2	120.4 ± 36.9	88.5 ± 20.0	–	–	–
e^- recovery (%) [b]	20.5 ± 8.2	82.3 ± 31.0	75.5 ± 20.0	–	–	–
Highest rate ($mmoL \cdot L^{-1} \cdot h^{-1}$)						
H_2 consumption	0.455	1.160	0.492	–	–	–
CO_2 consumption	0.188	0.411	0.229	–	–	–
CH_4	0	0	0	0	0	0
Acetic acid	0.145	0.32	0.289	0.97	0.79	1.58
Ethanol	0.00	0.11	0.05	0.00	0.09	0.10

[a] *Carbon recovery.* [b] *Electron recovery.*

and 53.0 (±4.4) mM, respectively (**Figure 4A**). Ethanol kept increasing after 120 h with the addition of 10 μM W and reached 14.8 (±10.2) mM (**Figure 4A**). The addition of 10 μM W also reached the highest mole ratio of ethanol to acetic acid of 0.48 at 263 h and 0.28 at the end of the incubation (**Figure 5**). With the addition of 2 μM W, ethanol increased to 3.2 mM then kept relatively stable till 3.9 (±2.6) mM at the end of the incubation (**Figure 4A**). The addition of 2 μM W reached the highest mole ratio of ethanol to acetic acid of 0.26 at 131 h and 0.12 at the end of the incubation (**Figure 5**). The addition of 10 μM W enhanced ethanol production up to 3.8 and 7.0-fold than with, respectively, 2 μM W and the control. Upon the addition of 2 and 10 μM W, H_2 consumption was, respectively, 81.5 (±32.5) and 107.1 (±50.5) mM (**Figure 6A**), which are both higher than in the absence of trace metals (80.8 ± 14.0 mM, **Figure 6A**). The addition of 10 μM W to the medium enhanced the ethanol production with the highest ethanol to acetic acid ratio of 0.48.

Upon addition of 2 and 10 μM Mo, the acetic acid concentration constantly increased to the highest value of 40.2 (±16.0) and 66.9 (±11.4) mM, respectively (**Figure 4B**). Ethanol kept increasing with the addition of 2 μM Mo and reached 11.3 (±2.1) mM at the end of the incubation (**Figure 4B**). However, ethanol was not significantly produced, with the maximum concentration of 1.4 (±1.1) mM with 10 μM Mo. The addition of 2 μM Mo enhanced ethanol production up to 8.1 and 5.4-fold, respectively, compared to 10 μM Mo and the control. The acetic acid production with the addition of 2 and 10 μM Mo was, respectively, 6.7 and 5.6 mM at 120 h, which was lower than the 11.7 mM produced by the control (**Figure 4B**). The acetic acid concentration increased quickly to a higher acetic acid concentration with 10 μM Mo compared to with 2 μM Mo and the control after 120 h. The pH decreased along with the accumulation of acetic acid (**Figure 4E**). The addition of 2 μM Mo reached the highest ethanol to acetic acid ratio of 0.28, while the ratio was 0.02 for 10 μM Mo addition at the end of the incubation (**Figure 5**).

With the addition of 10 μM Ni, the highest acetic acid and ethanol concentration amounted to, respectively, 42.7 (±6.9) and 3.7 (±2.2) mM (**Figure 4C**). The highest acetic acid and ethanol concentration with the addition of 50 μM Zn were 28.5 (±7.7) and 3.3 (±2.3) mM, respectively. Either 10 μM Ni or 50 μM Zn did not significantly enhance the ethanol production. The presence of 50 μM Zn inhibited the acetic acid production compared to the control (**Figure 4C**).

Surprisingly, the ethanol concentration in the incubation without trace metal supplementation is higher than with the control (**Figure 4D**). The highest acetic acid and ethanol concentration reached to 46.7 (±8.3) and 2.1 (± 1.9) mM, respectively, in the control. With no trace metals addition, ethanol started to be produced after 131 h and quickly increased to 6.7 mM, and then slightly increased to 7.6 mM at the end of the incubation. Ethanol production started at 131 h with a concentration of 1.7 mM, and then kept stable till the end of the incubation (2.1 mM) in the control (**Figure 4D**).

Overall, the acetic acid production was enhanced by the addition of 10 μM Mo, followed by 10 μM W and 2 μM Mo, whereas the presence of 50 μM Zn, 2 μM W, 10 μM Ni or the absence of trace metals inhibited acetic acid production compared to the control (**Figure 4**). The ethanol production was the highest in the presence of 10 μM W, followed by 2 μM Mo, while the absence of trace metals reached a higher ethanol production than the 10 μM Ni, 10 μM Mo, 2 μM W, 50 μM Zn, and control incubation (**Figure 4**).

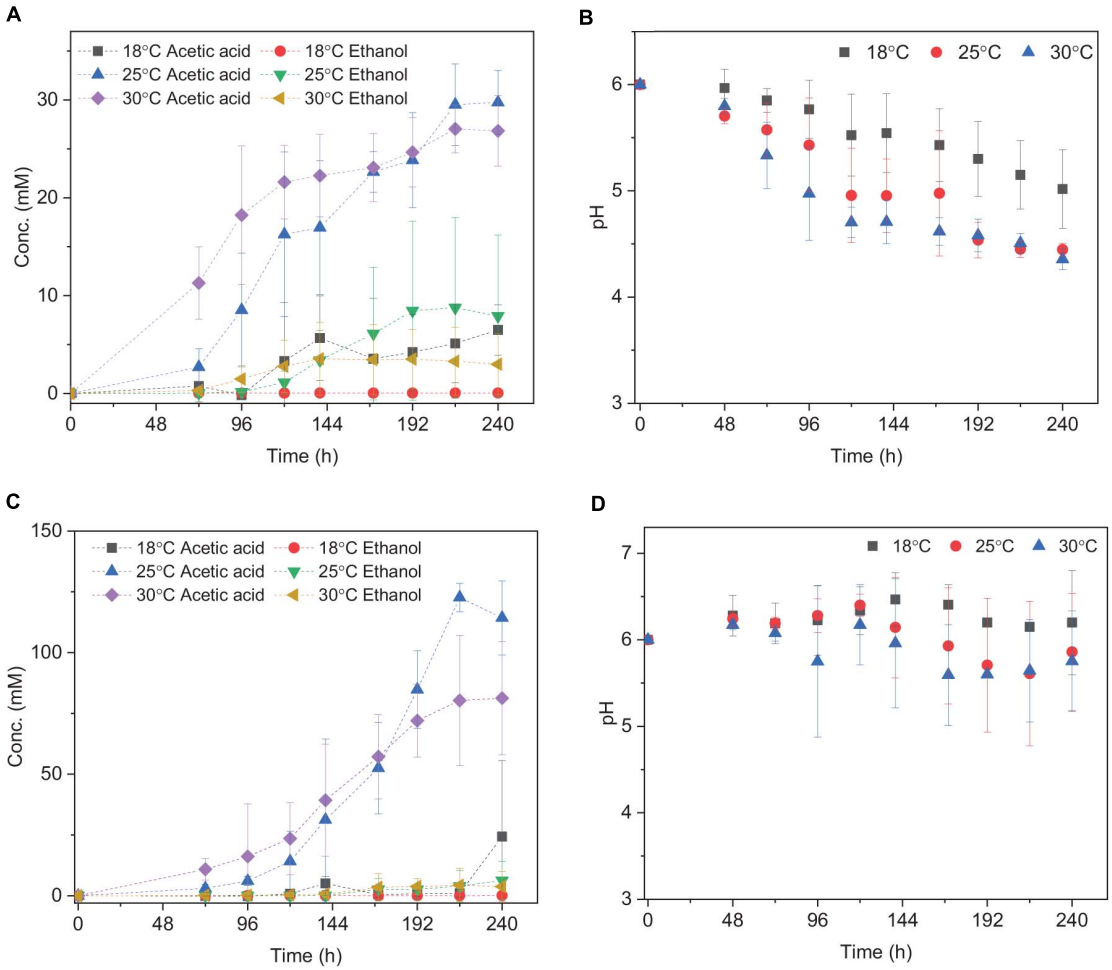

FIGURE 2 | Acetic acid and ethanol yield and pH change using **(A,B)** H_2/CO_2; **(C,D)** H_2/CO_2 + HCO_3^- by heat-treated granular sludge at 18, 25, and 30°C. Every point shown in the graphs is calculated as the average of three independent batch cultures, error bars indicate the standard deviation of the triplicates.

The decrease in pH corresponded to the accumulation of acetic acid. In the presence of 10 μM Mo, the pH reached the lowest value at the end of the incubation and the acetic acid concentration reached the highest compared to 2 μM and the control (**Figure 4E**). Ethanol production started after 120 h; the pH varied from 4.75 to 5.5 (**Figure 4E**). In the presence of 2 μM Mo and 10 μM W, ethanol production was enhanced even though the pH dropped to 4.2 (**Figure 4E**). The cumulative H_2 uptake in all media was between 211.7 and 245.3 mM. The cumulative CO_2 uptake with different trace metal concentrations was between 61.4 and 68.7 mM (**Figure 6**).

DISCUSSION

Effect of Temperature and pH on Solventogenesis

This study showed that the highest ethanol concentration was produced at an initial pH of 6 at 25°C in the H_2/CO_2 incubations. An initial pH of 6 favored the ethanol production compared to pH 7 and 5 from H_2/CO_2 by granular sludge (**Figure 1**). Ethanol production via solventogenesis is linked to the accumulation of undissociated acetic acid and pH (Richter et al., 2016). Solventogenesis occurs when the pH decreases to 4.5–5 and the undissociated acetic acid is able to cross the cytoplasmic membrane by diffusion: alcohol formation then avoids cell damage or death by the protons that would be released by dissociated acetic and butyric acids (Baronofsky et al., 1985; Jones and Woods, 1986; Richter et al., 2016). It should be noted that a low pH can stimulate ethanol production, however, incubations conducted with initial pH 5 did not reach higher ethanol concentrations than the incubation with initial pH 6. This could be because pH 6 facilitated cell growth and reached higher acetic acid concentrations than at pH 5 (**Figure 1**). Considering the acetic acid concentration of pH 5 and 6 were lower than the pH value that induces an "acid crash" (Mohammadi et al., 2011), the higher acetic acid concentration at pH 6 may obtain a higher ethanol production than at pH 5. Besides, fermentation at an initial pH 5 may have provided an unfavorable environment for cell growth, since the growth pH for the known autotrophic

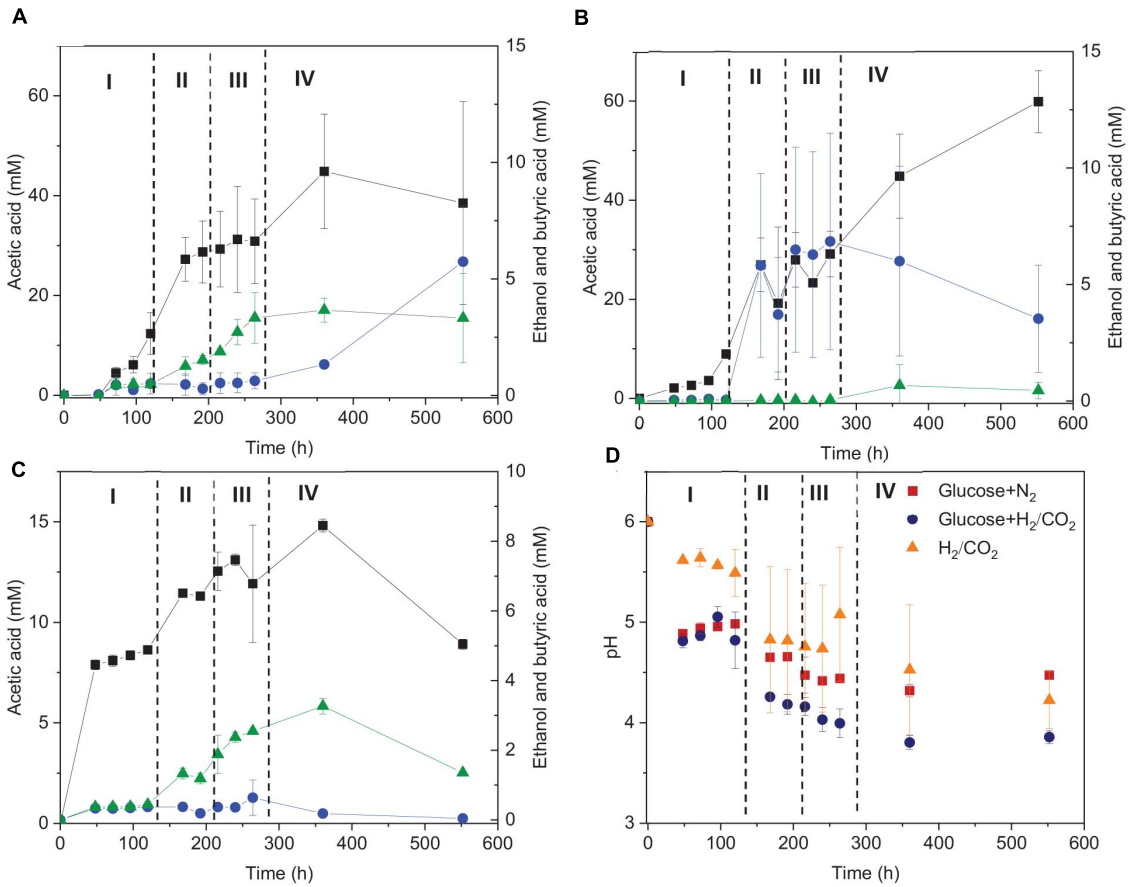

FIGURE 3 | Acetic acid, ethanol and butyric acid production by heated-treated granular sludge at 25°C using **(A)** glucose+H_2/CO_2, **(B)** H_2/CO_2, and **(C)** glucose as the substrate and **(D)** change of pH. The dashed vertical lines represent the different phases in the fermentation process; I: 0–120 h, II: 120–192 h, III: 192–264 h, IV: 264–552 h.

Clostridium sp. ranges from pH 5 to 7 (Fernández-Naveira et al., 2017a). Kundiyana et al. (2011) studied the ethanol production by *C. ragsdalei* from 10 g corn steep liquor purged daily with syngas (5% H_2, 15% CO_2, 20% CO) with initial incubation at pH 7, 6, and 5 at 32, 37, and 42°C. Without a buffer, their experiment at initial pH 5 produced less ethanol than at pH 7 and 6 at 32°C (Kundiyana et al., 2011).

With an initial pH of 6, submesophilic temperatures (25°C) enhanced ethanol production from H_2/CO_2 by granular sludge in this study (**Figure 2**). The growth temperature of most acetogens ranges from 20 to 42°C, with the optimum at 37°C (Naik et al., 2010; Munasinghe and Khanal, 2010). Fermentation at 25°C, which is below the optimum temperature, might slow down microbial metabolism and hence avoid the "acid crash" phenomenon. Solventogenesis is negatively affected or even terminated by a sharp increase of undissociated acids, a so called "acid crash" (Ramió-Pujol et al., 2015). Such an acid crash can be mitigated by slowing down the microbial metabolism, e.g., by lowing the temperature, thus reducing the acid accumulation rates. Similarly, 10 g corn steep liquor and syngas (5% H_2, 15% CO_2, 20% CO) were fermented by *C. ragsdalei* at 32, 37, and 42°C and 1.89 g/L of ethanol was obtained at 32°C, which is 2.7 fold higher than at 37°C (0.69 g/L) with an initial incubation pH of 6.0 (Kundiyana et al., 2011). The temperature of 18°C is lower than the reported growth temperatures for most of acetogens (Mohammadi et al., 2011), which likely caused the lower acetic acid production than at 25 and 37°C. Our previous tests demonstrated the *Clostridium* genus was successfully enriched under mesophilic and submesophilic conditions using the same inoculum (He et al., 2020). Chakraborty et al. (2020) demonstrated enhanced ethanol production from C_1 gas by granular sludge and *Clostridium autoethanogenum* was successfully enriched at 33°C. Similarly, Samanides et al. (2020) reported an increased relative abundance of *Clostridium* of 65.9% in anaerobic granular sludge for acetic acid production, when first exposed to heat (95°C for 30 min) and incubated with 100% CO_2 and 100 g/L zero valent iron at 33°C.

The higher C recovery in acetic acid and ethanol production from CO_2 (**Table 1**) can be attributed to the fact that granular sludge used as inoculum contains a certain amount of calcium carbonate precipitates. Calcium carbonate can precipitate both in the core and on the surface of granular sludge and the surface part of the calcium carbonate precipitates contributes to the aggregation of the granules (Yang et al., 2010). UASB sludge can

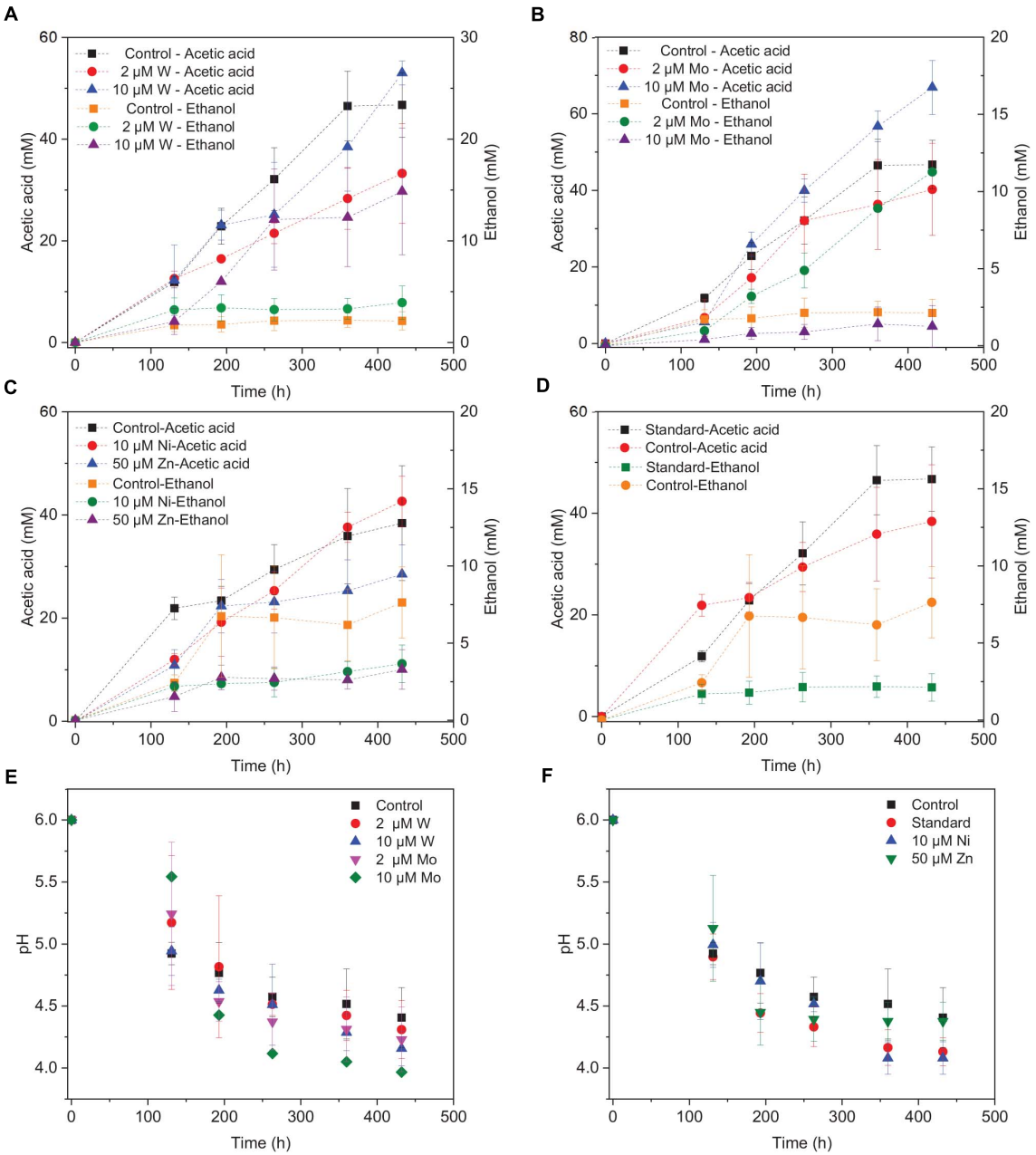

FIGURE 4 | Acetic acid and ethanol production by heat-treated granular sludge using H_2/CO_2 as the substrate at 25°C with the addition of **(A)** 2 μM, 10 μM W, **(B)** 2 μM, 10 μM Mo, **(C)** 10 μM Ni, 50 μM Zn, **(D)** No trace metals, and **(E,F)** change of pH.

reach a calcium carbonate content of up to 90% of the ash content in anaerobic wastewater treatment systems (Van Langerak et al., 1998). The high C recovery is in accordance with our previous results using the same UASB sludge (He et al., 2020). The carbon released from the calcium carbonate precipitates results in a positive carbon balance.

Methane was not observed during the whole incubation (**Supplementary Table 3**), which was attributed to the heat-pretreatment and initial pH of 6. Similarly, Modestra et al. (2020) reported that both heat and acid treatment of granular sludge inhibited methane production and enriched for homoacetogenic bacteria when using gaseous substrate H_2/CO_2.

Effect of Organic and Inorganic Carbon Source on Solventogenesis

Upon HCO_3^- addition to increase the C/H ratio, acetic acid production by granular sludge from H_2/CO_2 was enhanced at 18, 25, and 30°C, but not ethanol production. The failure of enhanced ethanol production could be due to the higher pH

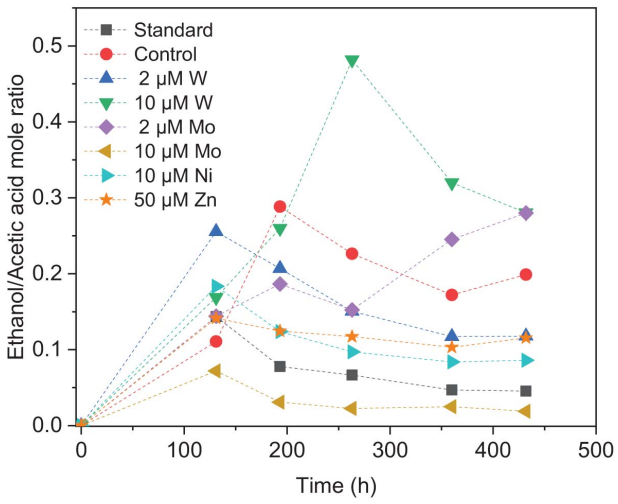

FIGURE 5 | Ethanol to acetic acid mole ratio by heat-treated granular sludge using H_2/CO_2 as the substrate at 25°C with the standard medium, control and addition of 2 μM, 10 μM W, 2 μM, 10 μM Mo, 10 μM Ni, and 50 μM Zn.

caused by the HCO_3^- buffering capacity. Ethanol production is triggered at low pH, for instance, 4.5–5 (Ganigué et al., 2016). However, the additional HCO_3^- acts as a buffer and prevents the pH decreasing sharply. The high acetic acid and lower ethanol production might thus be attributed to the higher pH: 5.2 and 6 for, respectively, without and with HCO_3^- addition than without HCO_3^- addition (**Figure 2D**). On the other hand, HCO_3^- offered extract carbon and increased the acetic acid production. Maddox et al. (2000) reported undissociated acid formation above 57–60 mM induced an "acid crash." However, the highest undissociated acetic acid concentrations obtained in this study were 36 and 16 mM at 25 and 30°C, respectively (**Table 2**), thus lower than the reported value at which an acid crash occurs. Upon the addition of HCO_3^-, the *Clostridium* genus had a similar relative abundance compared to without HCO_3^- addition at 25°C from the same inoculum (He et al., 2020).

Glucose enhances the growth of *C. autoethanogenum* and *C. carboxidivorans* (Fernández-Naveira et al., 2017a; Cheng et al., 2019). Addition of 0.3 g/L glucose enhanced the acetic and butyric acid production, but not the ethanol production by the granular sludge. 0.3 g/L glucose was added at the beginning of each of the four phases, from which 20 mM acetic acid or 13.3 mM butyric acid can be produced when the carbon from glucose is totally converted to acids. The inhibited ethanol production can be attributed to the different conversion pathway of the organic substrate glucose and the inorganic substrate H_2/CO_2. Indeed, the addition of glucose introduces another pathway: the glycolysis pathway. Marcellin et al. (2016) investigated the energy metabolism of a model acetogen *C. autoethanogenum* showing that during heterotrophic growth, cells relied mainly on the Embden–Meyerhof–Parnas (EMP) glycolysis pathway, whereas under autotrophic conditions exclusively the WLP pathway is used. The energy yield (ATP and redox state) is, however, unaffected between heterotrophic and autotrophic growth. Fernández et al. (2017) investigated the glucose (30 g/L) bioconversion profile at constant pH 6.2 and 5.2 by *Clostridium carboxidivorans*. Acetic acid was formed as the first metabolite and butyric acid appeared a few hours later and kept increasing, while ethanol was produced during the acidification stage at pH 6.2. Fernández et al. (2017) also found that the glucose consumption stopped after 72 h at pH 5.2. In this study, when the pH dropped to below 4 during stage IV (**Figure 3D**), increasing concentrations of acetic acid, butyric acid and ethanol were observed (**Figure 3A**). It should be noted that a small amount of ethanol was produced at a pH value as low as 4 by the granular sludge used in this study (**Figure 3A**), which is seldom reported before. Considering the mixed culture inoculum, one possible reason might be that heterotrophic acetogens consumed the glucose first and autotrophic acetogens adapted later and produced ethanol at the end of the incubation.

Enhanced Ethanol Production by Trace Metal Addition

Ethanol production from H_2/CO_2 by granular sludge was enhanced by the addition of 2 μM Mo or 10 μM W, while the addition of 10 μM Mo, 2 μM W, 10 μM Ni, and 50 μM Zn did not significantly affect the ethanol production. There are only few studies on the effect of trace metals on ethanol production by mixed cultures compared to studies using pure cultures. Saxena and Tanner (2011) increased the SeO_4^{2-} and WO_4^{2-} concentration to 5.3 and 6.8 μM, respectively, which resulted in an increased ethanol production from synthesis gas by *Clostridium ragsdalei* from 35.73 mM under standard metal concentrations to 54.4 and 72.3 mM, respectively, upon SeO_4^{2-} and WO_4^{2-} addition. They also observed that ethanol production decreased to 23.64 mM at higher concentrations of Mo (8.3 μM). The highest mole ratio of ethanol to acetic acid of 0.48 with 10 μM W is in accordance with the highest ethanol production in this study (**Figure 5**). Abubackar et al. (2015) investigated the carbon monoxide fermentation by *Clostridium autoethanogenum* and obtained the highest ethanol to acetic acid ratio of 0.19 in experiments with 0.75 μM W.

Saxena and Tanner (2011) found that ethanol production from synthesis gas by *C. ragsdalei* decreased to 22.02 and 1.55 mM when Fe, Co, Mo, and W were eliminated from the medium. This study, however, showed that without trace metals, the ethanol production was enhanced compared to the control. Nutrient-stress conditions such as lack of trace elements may also stimulate the shift from acetic acid to ethanol. Richter et al. (2016) performed proteomic and metabolomic analyses on a two-stage syngas fermentation (*Clostridium ljungdahlii)* system and did not find a difference in the abundance of enzymes of the central metabolic pathways, concluding that nutrient limitation and the resulting growth limitation redirect reducing equivalents toward ethanol production. The H_2 to CO_2 consumption ratio varies between 2.1 and 2.5 (**Figure 6D**) and thus conform the production of a mixture of acetic acid and ethanol (Eqs. 1, 2, **Table 1**). The trace metals affected the enzymes such as FDH,

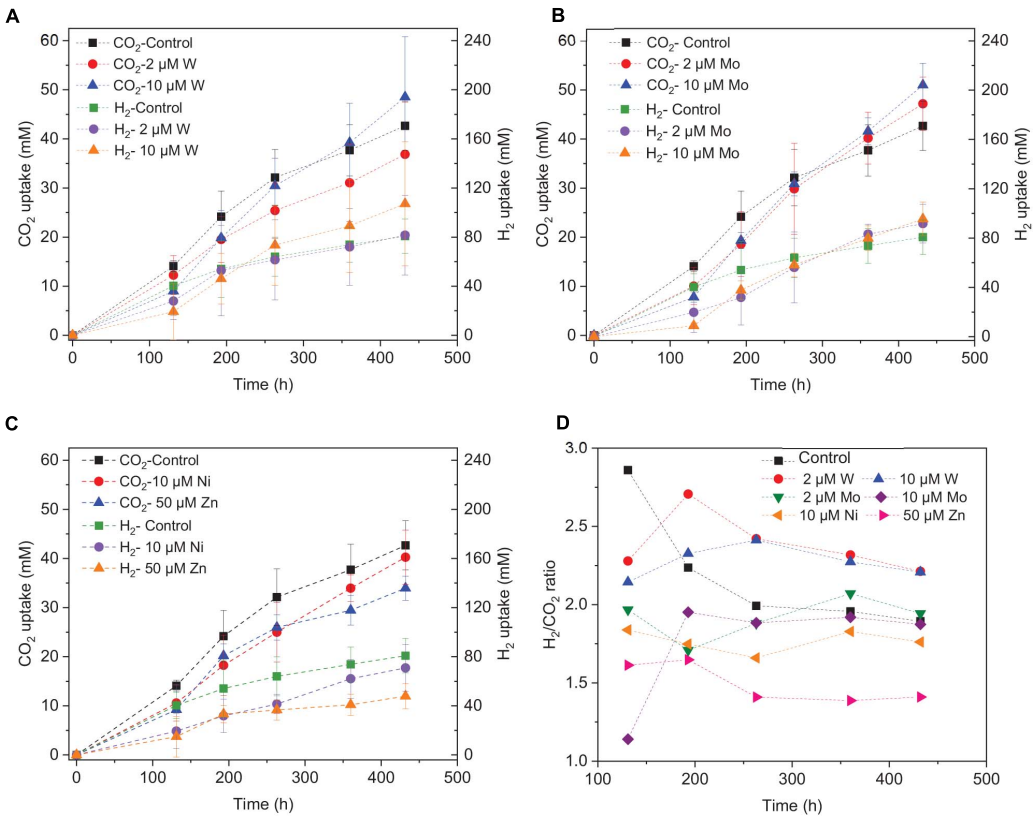

FIGURE 6 | H_2 and CO_2 uptake with the addition of **(A)** 2 μM, 10 μM Mo, **(B)** 2 μM, 10 μM W, **(C)** 10 μM Ni, 50 μM Zn, and **(D)** H_2/CO_2 uptake ratio by heat-treated granular sludge using H_2/CO_2 as the substrate at 25°C with initial pH 6.

AOR, and ADH to catalyze acetic acid and ethanol production and thus strengthen the homoacetogens, such as the *Clostridium* genus as reported by He et al. (2020). The W-containing AOR enzyme has been reported in *Clostridium thermoaceticum* (Strobl et al., 1992). Besides, W can serve as a potential acting element for CO_2 reduction FDHs, W even becomes an essential element for nearly all enzymes of the AOR family (Fernández-Naveira et al., 2019). This study reported lower ethanol production with Mo than W, despite the close chemical similarities between Mo and W. However, it has been demonstrated that W, different than Mo, can be selectively transported into some prokaryotic cells by two ABC-type transporters that contain the binding protein TupA or WtpA (Andreesen and Makdessi, 2008).

CONCLUSION

The optimum conditions for ethanol production by anaerobic granular sludge using H_2/CO_2 as the substrate were 25°C and an initial pH of 6. An initial pH of 7 enhanced acetic acid production, while an initial pH of 5 totally inhibited ethanol production. The use of glucose and CO_2 as co-substrate enhanced butyric acid production (3.3 mM), while ethanol production occurred at a pH as low as 4. The presence of 10 μM W and 2 μM Mo enhanced the ethanol production by 7.0 and 5.4-fold, respectively.

DATA AVAILABILITY STATEMENT

The original contributions presented in the study are included in the article/**Supplementary Material**, further inquiries can be directed to the corresponding author/s.

AUTHOR CONTRIBUTIONS

YH carried out all experimental incubations, data analysis, and drafted the manuscript. CC conceived the study, participated in its design and coordination, and reviewed the manuscript. PL conducted the project supervision and the manuscript revision. All authors contributed to the article and approved the submitted version.

FUNDING

This publication has emanated from research supported by the Science Foundation Ireland (SFI) through the SFI Research Professorship Programme entitled *Innovative Energy Technologies for Biofuels, Bioenergy and a Sustainable Irish Bioeconomy* (IETSBIO^3; grant no. 15/RP/2763) and the Research Infrastructure research grant *Platform for Biofuel Analysis* (Grant No. 16/RI/3401).

ACKNOWLEDGMENTS

We thank Flora Marciano (University of Cassino and Southern Lazio, Italy) for her help with the sampling and analysis.

SUPPLEMENTARY MATERIAL

The Supplementary Material for this article can be found online at: https://www.frontiersin.org/articles/10.3389/fmicb.2021.647370/full#supplementary-material

REFERENCES

Abubackar, H. N., Veiga, M. C., and Kennes, C. (2015). Carbon monoxide fermentation to ethanol by *Clostridium autoethanogenum* in a bioreactor with no accumulation of acetic acid. *Bioresour. Technol.* 186, 122–127. doi: 10.1016/j.biortech.2015.02.113

Andreesen, J. R., and Makdessi, K. (2008). Tungsten, the surprisingly positively acting heavy metal element for prokaryotes. *Ann. N. Y. Acad. Sci.* 1125, 215–229. doi: 10.1196/annals.1419.003

Baronofsky, J. J., Schreurs, W. J. A., and Kashket, E. R. (1985). Uncoupling by acetic acid limits growth of and acetogenesis by *Clostridium thermoaceticum*. *Appl. Environ. Microbiol.* 48, 1134–1139. doi: 10.1128/AEM.48.6.1134-1139.1984

Burk, M. J., Schilling, C. H., Burgard, A. P., and Trawick, J. D. (2014). *Methods and Organisms for Utilizing Synthesis gas or Other Gaseous Carbon Sources and Methanol*. California: Genomatica, Inc.

Chakraborty, S., Rene, E. R., Lens, P. N. L., Rintala, J., and Kennes, C. (2020). Effect of tungsten and selenium on C1 gas bioconversion by enriched anaerobic sludge and microbial community analysis. *Chemosphere* 250:126105. doi: 10.1016/j.chemosphere.2020.126105

Cheng, C., Li, W., Lin, M., and Yang, S. T. (2019). Metabolic engineering of *Clostridium carboxidivorans* for enhanced ethanol and butanol production from syngas and glucose. *Bioresour. Technol.* 284, 415–423. doi: 10.1016/j.biortech.2019.03.145

Cotter, J. L., Chinn, M. S., and Grunden, A. M. (2009). Ethanol and acetate production by *Clostridium ljungdahlii* and *Clostridium autoethanogenum* using resting cells. *Bioprocess Biosyst. Eng.* 32, 369–380. doi: 10.1007/s00449-008-0256-y

Dessì, P., Lakaniemi, A. M., and Lens, P. N. L. (2017). Biohydrogen production from xylose by fresh and digested activated sludge at 37, 55 and 70°C. *Water Res.* 115, 120–129. doi: 10.1016/j.watres.2017.02.063

Devarapalli, M., and Atiyeh, H. K. (2015). A review of conversion processes for bioethanol production with a focus on syngas fermentation. *Biofuel Res. J.* 2, 268–280. doi: 10.18331/BRJ2015.2.3.5

Dogan, T., Ince, O., Oz, N. A., and Ince, B. K. (2005). Inhibition of volatile fatty acid production in granular sludge from a UASB reactor. *J. Environ. Sci. Health* 40, 633–644. doi: 10.1081/ESE-200046616

Eisentraut, A. (2010*). *Sustainable Production of Second-Generation Biofuels*. Paris: OECD Publishing.

Fast, A. G., and Papoutsakis, E. T. (2012). Stoichiometric and energetic analyses of non-photosynthetic CO_2-fixation pathways to support synthetic biology strategies for production of fuels and chemicals. *Curr. Opin. Chem. Eng.* 1, 380–395. doi: 10.1016/j.coche.2012.07.005

Fernández, B. Y., Soares, A., Koch, K., Vale, P., and Cartmell, E. (2017). bioconversion of carbon dioxide in anaerobic digesters for on-site carbon capture and biogas enhancement–a review. *Crit. Rev. Environ. Sci. Technol.* 47, 1555–1580. doi: 10.1080/10643389.2017.1372001

Fernández-Naveira, Á, Veiga, M. C., and Kennes, C. (2017a). Glucose bioconversion profile in the syngas-metabolizing species *Clostridium carboxidivorans*. *Bioresour. Technol.* 244, 552–559. doi: 10.1016/j.biortech.2017.07.174

Fernández-Naveira, Á, Veiga, M. C., and Kennes, C. (2017b). H-B-E (hexanol-butanol-ethanol) fermentation for the production of higher alcohols from syngas/waste gas. *J. Chem. Technol. Biotechnol.* 92, 712–731. doi: 10.1002/jctb.5194

Fernández-Naveira, Á, Veiga, M. C., and Kennes, C. (2019). Selective anaerobic fermentation of syngas into either C2-C6 organic acids or ethanol and higher alcohols. *Bioresour. Technol.* 280, 387–395. doi: 10.1016/j.biortech.2019.02.018

Ganigué, R., Sanchez-Paredes, P., Baneras, L., and Colprim, J. (2016). Low fermentation pH is a trigger to alcohol production, but a killer to chain elongation. *Front. Microbiol.* 7:702. doi: 10.3389/fmicb.2016.00702

He, Y., Cassarini, C., Marciano, F., and Lens, P. N. L. (2020). Homoacetogenesis and solventogenesis from H_2/CO_2 by granular sludge at 25, 37 and 55° C. *Chemosphere* 265:128649. doi: 10.1016/j.chemosphere.2020.128649

Jiann-Shin, C. (2010). Alcohol dehydrogenase: multiplicity and relatedness in the solvent-producing clostridia. *FEMS Microbiolo. Rev.* 17, 263–273. doi: 10.1111/j.1574-6976.1995.tb00210.x

Jones, D. T., and Woods, D. R. (1986). Acetone-butanol fermentation revisited. *Microbiol. Rev.* 50, 484–524. doi: 10.1128/MR.50.4.484-524.1986

Kundiyana, D. K., Wilkins, M. R., Maddipati, P., and Huhnke, R. L. (2011). Effect of temperature, pH and buffer presence on ethanol production from synthesis gas by *Clostridium Ragsdalei*. *Bioresour. Technol.* 102, 5794–5799. doi: 10.1016/j.biortech.2011.02.032

Liu, C., Luo, G., Wang, W., He, Y., Zhang, R., and Liu, G. (2018). The effects of pH and temperature on the acetate production and microbial community compositions by syngas fermentation. *Fuel* 224, 537–544. doi: 10.1016/j.fuel.2018.03.125

Liu, K., Atiyeh, H. K., Tanner, R. S., Wilkins, M. R., and Huhnke, R. L. (2012). Fermentative production of ethanol from syngas using novel moderately alkaliphilic strains of *Alkalibaculum Bacchi*. *Bioresour. Technol.* 104, 336–341. doi: 10.1016/j.biortech.2011.10.054

Maddox, I. S., Steiner, E., Hirsch, S., Wessner, S., Gutierrez, N. A., Gapes, J. R., et al. (2000). The cause of" acid crash" and" acidogenic fermentations" during the batch acetone-butanol-ethanol (ABE) fermentation process. *J. Mol. Microbiol. Biotechnol.* 2, 95–100.

Marcellin, E., Behrendorff, J. B., Nagaraju, S., Detissera, S., and Nielsen, L. K. (2016). Low carbon fuels and commodity chemicals from waste gases–systematic approach to understand energy metabolism in a model acetogen. *Green Chem.* 18, 3020–3028. doi: 10.1039/C5GC02708J

Modestra, J. A., Katakojwala, R., and Mohan, S. V. (2020). CO_2 fermentation to short chain fatty acids using selectively enriched chemolithoautotrophic acetogenic bacteria. *Chem. Eng. J.* 394:124759. doi: 10.1016/j.cej.2020.124759

Mohammadi, M., Najafpour, G. D., Younesi, H., Lahijani, P., Uzir, M. H., and Mohamed, A. R. (2011). Bioconversion of synthesis gas to second generation biofuels: a review. *Renew. Sust. Energy Rev.* 15, 4255–4273. doi: 10.1016/j.rser.2011.07.124

Munasinghe, P. C., and Khanal, S. K. (2010). Biomass-derived syngas fermentation into biofuels: opportunities and challenges. *Bioresour. Technol.* 101, 5013–5022. doi: 10.1016/j.biortech.2009.12.098

Naik, S. N., Goud, V. V., Rout, P. K., and Dalai, A. K. (2010). Production of first and second generation biofuels: a comprehensive review. *Renew. Sust. Energy Rev.* 14, 578–597. doi: 10.1016/j.rser.2009.10.003

Padan, E., Zilberstein, D., and Schuldiner, S. (1981). pH homesstasis in bacteria. *Biochim. Biophys. Acta Rev. Biomembr.* 650, 151–166. doi: 10.1016/0304-4157(81)90004-6

Pereira, I. A. (2013). An enzymatic route to H_2 storage. *Science* 342, 1329–1330. doi: 10.1126/science.1247698

Ramió-Pujol, S., Ganigué, R., Bañeras, L., and Colprim, J. (2015). Incubation at 25°C prevents acid crash and enhances alcohol production in *Clostridium carboxidivorans* P7. *Bioresour. Technol.* 192, 296–303. doi: 10.1016/j.biortech.2015.05.077

Richter, H., Molitor, B., Wei, H., Chen, W., Aristilde, L., and Angenent, L. T. (2016). Ethanol production in syngas-fermenting *Clostridium ljungdahlii* is controlled by thermodynamics rather than by enzyme expression. *Energy Environ. Sci.* 9, 2392–2399. doi: 10.1039/C6EE01108J

Sadhukhan, J., Lloyd, J. R., Scott, K., Premier, G. C., Eileen, H. Y., Curtis, T., et al. (2016). A critical review of integration analysis of microbial electrosynthesis (MES) systems with waste biorefineries for the production of biofuel and chemical from reuse of CO2. *Renew. Sust. Energy Rev.* 56, 116–132. doi: 10.1016/j.rser.2015.11.015

Samanides, C. G., Koutsokeras, L., Constantinides, G., and Vyrides, I. (2020). Methanogenesis inhibition in anaerobic granular sludge for the generation of volatile fatty acids from CO_2 and zero valent iron. *Front. Energy Res.* 8:37. doi: 10.3389/fenrg.2020.00037

Sarkar, O., Butti, S. K., and Mohan, S. V. (2017). Acidogenesis driven by hydrogen partial pressure towards bioethanol production through fatty acids reduction. *Energy* 118, 425–434. doi: 10.1016/j.energy.2016.12.017

Saxena, J., and Tanner, R. S. (2011). Effect of trace metals on ethanol production from synthesis gas by the ethanologenic acetogen, *Clostridium ragsdalei*. *J. Ind. Microbiol. Biotechnol.* 38, 513–521. doi: 10.1007/s10295-010-0794-6

Shen, Y., Brown, R. C., and Wen, Z. (2017). Syngas fermentation by *Clostridium carboxidivorans* P7 in a horizontal rotating packed bed biofilm reactor with enhanced ethanol production. *Appl. Energy* 187, 585–594.

Singla, A., Verma, D., Lal, B., and Sarma, P. M. (2014). Enrichment and optimization of anaerobic bacterial mixed culture for conversion of syngas to ethanol. *Bioresour. Technol.* 172, 41–49.

Stams, A. J., Van Dijk, J. B., Dijkema, C., and Plugge, C. M. (1993). Growth of syntrophic propionate-oxidizing bacteria with fumarate in the absence of methanogenic bacteria. *Appl. Environ. Microbiol.* 59, 1114–1119.

Steinbusch, K. J. J., Hamelers, H. V. M., and Buisman, C. J. N. (2008). Alcohol production through volatile fatty acids reduction with hydrogen as electron donor by mixed cultures. *Water Res.* 42, 4059–4066.

Strobl, G., Feicht, R., White, H., Lottspeich, F., and Simon, H. (1992). The tungsten-containing aldehyde oxidoreductase from *Clostridium thermoaceticum* and its complex with a viologen-accepting nadph oxidoreductase. *Biol. Chem. Hoppe Seyler* 373, 123–132. doi: 10.1515/bchm3.1992.373.1.123

Van Langerak, E. P. A., Gonzalez-Gil, G., Van Aelst, A., Van Lier, J. B., Hamelers, H. V. M., and Lettinga, G. (1998). Effects of high calcium concentrations on the development of methanogenic sludge in upflow anaerobic sludge bed (UASB) reactors. *Water Res.* 32, 1255–1263. doi: 10.1016/S0043-1354(97)00335-7

Yamamoto, I., Saiki, T., Liu, S. M., and Ljungdahl, L. G. (1983). Purification and properties of NADP-dependent formate dehydrogenase from *Clostridium Thermoaceticum*, a tungsten-selenium-iron protein. *J. Biol. Chem.* 258, 1826–1832. doi: 10.1016/S0021-9258(18)33062-X

Yang, S., He, Y., Liu, Y., Chou, C., Zhang, P., and Wang, D. (2010). Effect of wastewater composition on the calcium carbonate precipitation in upflow anaerobic sludge blanket reactors. *Front. Environ. Sci. Eng. China* 4:142–149. doi: 10.1007/s11783-010-0026-3

Conflict of Interest: The authors declare that the research was conducted in the absence of any commercial or financial relationships that could be construed as a potential conflict of interest.

frontiers in Microbiology

ORIGINAL RESEARCH
published: 22 March 2021
doi: 10.3389/fmicb.2021.639266

Switching Between Methanol Accumulation and Cell Growth by Expression Control of Methanol Dehydrogenase in *Methylosinus trichosporium* OB3b Mutant

*Hidehiro Ito[1,2], Kosei Yoshimori[1], Masahito Ishikawa[2], Katsutoshi Hori[2] and Toshiaki Kamachi[1]**

[1]*Department of Life Science and Technology, Tokyo Institute of Technology, Tokyo, Japan,* [2]*Department of Biomolecular Engineering, Nagoya University, Nagoya, Japan*

OPEN ACCESS

Edited by:
Yu Wang,
Chinese Academy of Sciences, China

Reviewed by:
Qiang Fei,
Xi'an Jiaotong University, China
Marina G. Kalyuzhanaya,
San Diego State University, United States
Muhammad Farhan Ul Haque,
University of the Punjab, Pakistan

***Correspondence:**
Toshiaki Kamachi
tkamachi@bio.titech.ac.jp

Specialty section:
This article was submitted to Microbiotechnology, a section of the journal Frontiers in Microbiology

Received: *08 December 2020*
Accepted: *28 February 2021*
Published: *22 March 2021*

Citation:
Ito H, Yoshimori K, Ishikawa M, Hori K and Kamachi T (2021) Switching Between Methanol Accumulation and Cell Growth by Expression Control of Methanol Dehydrogenase in Methylosinus trichosporium OB3b Mutant. Front. Microbiol. 12:639266. doi: 10.3389/fmicb.2021.639266

Methanotrophs have been used to convert methane to methanol at ambient temperature and pressure. In order to accumulate methanol using methanotrophs, methanol dehydrogenase (MDH) must be downregulated as it consumes methanol. Here, we describe a methanol production system wherein MDH expression is controlled by using methanotroph mutants. We used the MxaF knockout mutant of *Methylosinus trichosporium* OB3b. It could only grow with MDH (XoxF) which has a cerium ion in its active site and is only expressed by bacteria in media containing cerium ions. In the presence of 0 μM copper ion and 25 μM cerium ion, the mutant grew normally. Under conditions conducive to methanol production (10 μM copper ion and 0 μM cerium ion), cell growth was inhibited and methanol accumulated (2.6 μmol·mg^{-1} dry cell weight·h^{-1}). The conversion efficiency of the accumulated methanol to the total amount of methane added to the reaction system was ~0.3%. The aforementioned conditions were repeatedly alternated by modulating the metal ion composition of the bacterial growth medium.

Keywords: methanotroph, methane, methanol, methane monooxygenase, methanol dehydrogenase

INTRODUCTION

Methane is a principal component of natural and shale gases. As its global reserves are vast, it is regarded as a next-generation carbon feedstock. Biogas produced by microbial biomass digestion under anaerobic conditions is composed mainly of methane. Microbial methane fermentation can use carbon dioxide as a carbon source. Therefore, methane is expected to be a valuable industrial fuel source as it is renewable and the technologies associated with its collection, production, and consumption are sustainable. Nevertheless, its global warming potential is 25× higher than that of carbon dioxide [U.S. Environmental Protection Agency (EPA), 2019]. Hence, it is a prime mitigation target in greenhouse gas reduction (Shindell et al., 2012). A major source of atmospheric methane is the anaerobic decomposition of biomass from anthropogenic industrial waste production and agricultural activity (Conrad, 2009). However, the methane produced by archaea is low concentration and the collectable gas contains

impurities such as carbon dioxide. Thus, it can only be used as fuel without any purification. In contrast, methanol is readily available as a carbon feedstock for further chemical conversion and is easy to store and transport because it is a liquid. Therefore, the efficient conversion of methane to methanol may help increase the availability of heretofore underutilized methane resources.

As methanotrophs are powerful oxidizers, their exploitation in the industrial oxidation of methane to methanol has been investigated. Aerobic methanotrophs oxidize methane to methanol *via* methane monooxygenase (MMO) and NADH at ambient temperature and pressure. Thence, the methanol is oxidized to formaldehyde by methanol dehydrogenase (MDH). The formaldehyde may either be assimilated into biomass or oxidized to formate by formaldehyde dehydrogenase (FADH). The formate is then converted to carbon dioxide *via* formate dehydrogenase (FDH), the NADH is regenerated for MMO, and the cycle is completed. The simplest and most cost-effective approach to the foregoing process is the use of whole-cell methanotroph cultures (Bjorck et al., 2018). Whole cells undergo autopoiesis by biosynthesizing enzymes and replicating themselves. Moreover, the methanol biosynthesized by whole cells can be easily separated. In methanol biosynthesis *via* MMO and methane oxidation, reducing equivalents are required. Whole-cell methanotrophs can supply the reducing equivalent in the form of NADH. A major problem with the application of whole-cell methanotrophs for methanol production is that the microorganisms continue to oxidize the methanol to formaldehyde and thence to formate. Therefore, methanol oxidation must be interrupted so that the methanol can accumulate. The irreversible MDH inhibitor cyclopropanol binds pyrroloquinoline quinone (PQQ) and deactivates MDH (Frank et al., 1989; Shimoda and Okura, 1990; Takeguchi et al., 1997; Furuto et al., 1999). High phosphate or sodium chloride concentrations in the medium also promote methanol accumulation (Mehta et al., 1987; Cox et al., 1992; Dales and Anthony, 1995; Lee et al., 2004; Duan et al., 2011; Han et al., 2013). However, complete MDH inhibition arrests cell growth and the loss of reducing power it causes impedes the natural biochemical pathways of the cell. For efficient methanol production by MDH inhibition, external electron donors such as formate must be added to regenerate NADH (Mehta et al., 1991; Furuto et al., 1999; Lee et al., 2004; Kim et al., 2010; Duan et al., 2011; Pen et al., 2014, 2016). Even when these are supplied, however, the methanotrophs cannot be reused as their MMO activity is destabilized. Hence, the strategic design of methanol production and cell growth with enzyme recovery and reducing equivalents is necessary for continuous methanol production with whole-cell methanotrophs. In this process, it is important to control MDH activity in the bacteria. Lowering MDH activity causes methanol to accumulate, restores MDH activity, and provides intracellular reducing power. However, it is difficult to modulate intracellular MDH activity *via* conventional inhibitor-based methods.

To solve this problem, we examined gene regulation systems in methanotrophs in response to certain metal ions. The canonical "copper switch" controls the expression of two types of MMO (Yoon et al., 2010). Particulate MMO (pMMO) is localized to the intracytoplasmic membranes and its expression and activity increase with copper ion availability. In contrast, soluble MMO (sMMO) occurs in the cytoplasm and is only expressed in the absence of copper ions. MxaF and XoxF are forms of the main component of PQQ-dependent MDH and are found in certain methanotrophs such as *Methylosinus trichosporium* OB3b. MxaF has a calcium ion in its active site (Williams et al., 2005) whereas the active site of XoxF has a rare earth element such as a cerium, lanthanum, or praseodymium ion (Hibi et al., 2011; Nakagawa et al., 2012; Keltjens et al., 2014; Pol et al., 2014). Rare earth elements are gene-regulating factors and control MxaF and XoxF expression. Farhan Ul Haque et al. (2015) first reported that *mxaF* and *xoxF* expression in *M. trichosporium* OB3b substantially decreased and increased, respectively, with increasing cerium ion concentration. This mechanism is known as the "lanthanide switch" (Vu et al., 2016; Groom et al., 2019). Therefore, this lanthanide switch could effectively control MDH activity in whole-cell methanotrophs.

Here, we used the MxaF knockout mutant of *M. trichosporium* OB3b to test the aforementioned strategic methanol production and cell growth design (**Figure 1**). This mutant was constructed by referring to the methods of previous studies (Semrau et al., 2013; Farhan Ul Haque et al., 2016). This mutant can only use XoxF MDH for methanol oxidation. Hence, XoxF MDH downregulation is expected to result in methanol generation in the absence of cerium. This mutant can again resume growth back by re-expression of XoxF MDH in the presence of cerium. In addition, NADH recycling and/or MMO refreshing through the methanol metabolic pathway restoration may be achieved. Using the lanthanide switch over a long methanol production period without the addition of an external electron source. In this study, we reported switching of methanol production and cell growth in this mutant by modulating the copper and cerium ion content in the growth medium.

MATERIALS AND METHODS

Microbial Growth Conditions

Nitrate mineral salt (NMS) medium (Whittenbury et al., 1970) was used to grow wild type *M. trichosporium* OB3b and the *mxaF* knockout mutant (*ΔmxaF*, **Table 1**). Methane was the sole carbon and energy source in the growth substrate. Cultures were supplemented with copper ion (as $CuSO_4$) and/or cerium ion (as $CeCl_3$) from stock solutions prepared in ultrapure water. Copper or cerium ion stock solutions were sterilized by filtration through polyvinylidene fluoride (PDVF) membranes with 0.22-μm pore size. *Methylosinus trichosporium* OB3b wild type and *ΔmxaF* cultures were grown at 30°C with constant shaking at 130 rpm and under a 1:4 (v/v) methane/air mixture in 30 ml NMS in 200-ml Erlenmeyer flasks fitted with baffles. All reagents were obtained from commercial suppliers and were of the highest available purity.

A starter culture grown in NMS with 25 μM cerium ion was used as an inoculum to examine the growth of the OB3b *ΔmxaF* mutant in the presence of copper and cerium ions.

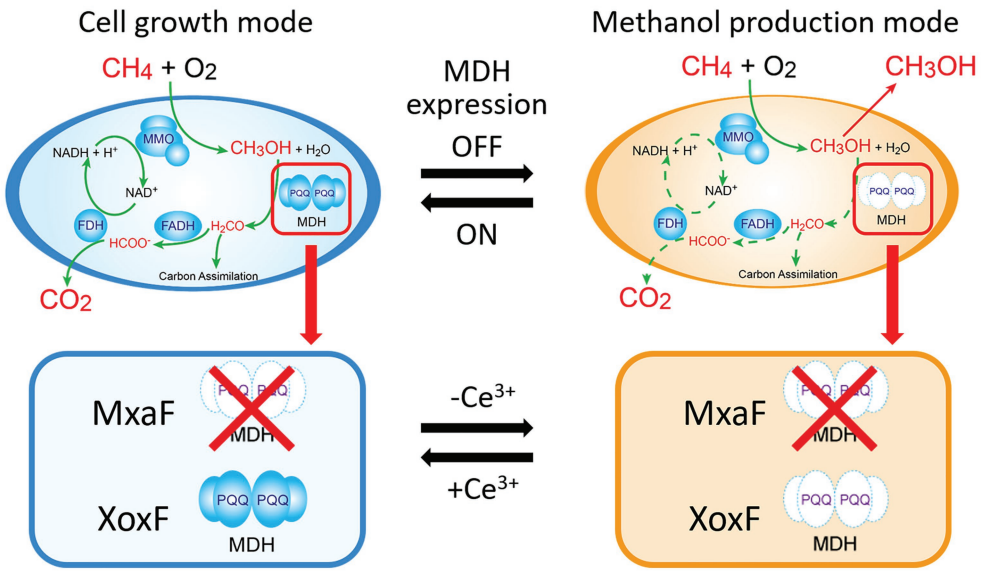

FIGURE 1 | Cell growth and methanol production induced in methanotrophs by switching methanol dehydrogenase gene expression. Solid green line in the cell growth mode means the metabolic pathway of methane in the presence of cerium ions. Dotted green line in the methanol production mode means that the pathway is blocked in the absence of cerium ions. MMO: methane monooxygenase; MDH: methanol dehydrogenase; FADH: formaldehyde dehydrogenase; FDH: formate dehydrogenase; PQQ: pyrroloquinoline quinone.

At the late exponential phase, the cultures were harvested by centrifugation at 3,000 × g and 4°C for 10 min. The cell pellets were washed twice in NMS free of copper and cerium. After each washing, the pellets were resuspended in an equal volume of NMS free of copper and cerium and centrifuged at 3,000 × g and 4°C for 10 min. After the second washing, the cell pellets were resuspended in NMS and inoculated into new cultures in 50-ml serum bottles each containing 10 ml NMS. The initial target OD_{540} was 0.1. Four different culture conditions were considered and cell growth and methanol production were measured under various metal ions concentrations. The bottles were sealed with rubber stoppers and aluminum caps and the headspaces were filled with a 1:4 (v/v) methane/air mixture. The serum bottles were incubated at 30°C and 130 rpm in a shaking incubator (BR-43FL·MR; TAITEC, Saitama, Japan). At the stationary phase, the cultures were harvested by centrifugation at 3,000 × g and 4°C for 10 min and washed twice under the aforementioned conditions. In one experiment, cell pellets were transferred to 50-ml serum bottles each containing 10 ml identical fresh medium and the initial target OD_{540} was 0.1 (transfer A). In another experiment, cell pellets were transferred to 50-ml serum bottles each containing 10 ml identical fresh medium (transfer B). To toggle between cell growth and methanol production, the initial medium OD_{540} was adjusted to 0.1 after inoculation.

Escherichia coli were grown in Luria-Bertani (LB) medium. Gentamicin (10 μg ml^{-1}) or kanamycin (20 μg ml^{-1}) was used to conserve *E. coli* containing mutant construct plasmids and *M. trichosporium* OB3b mutant cultures after the first homologous recombination.

Construction of the *Methylosinus trichosporium* OB3b *ΔmxaF* Mutant

The double homologous recombination method was used to construct the OB3b *ΔmxaF* mutant by referring to the methods of previous studies (**Supplementary Figure S1**; Semrau et al., 2013; Farhan Ul Haque et al., 2016). Briefly, pJQ200SK and pk18mobsacB plasmids were amplified in *E. coli* Turbo by the Inoue method (Sambrook and Russell, 2006). Two DNA fragments ~1 kb distant from the 5' to 3' ends (arms A and B, respectively) of *mxaF* in *M. trichosporium* OB3b were amplified by PCR. Specific primers (**Table 2**) were designed to amplify arms A and B, introduce the *Bam*HI restriction site sequences, and facilitate directional cloning into the pJQ200SK and pk18mobsacB suicide vectors. The PCR products of arms A and B were gel-purified with a QIAquick gel extraction kit (Qiagen, Valencia, CA, United States) following the manufacturer's instructions. The pJQ200SK plasmid was digested with *Bam*HI and gel-purified with a QIAquick gel extraction kit. The PCR product and linearized pJQ200SK were ligated with an In-Fusion cloning kit (TaKaRa Bio Inc., Kusatsu, Shiga, Japan) following the manufacturer's instructions. Then *mxaF* in the pJQ200SK_UpMxaDw plasmid was removed with PrimeStar Max DNA polymerase (TaKaRa Bio Inc., Kusatsu, Shiga, Japan) following the deletion protocol. The resulting plasmid was named pJQ200SK_UpDw and digested with *Bam*HI. The connected regions upstream and downstream from *mxaF* (UpDw arm) were gel-purified with a QIAquick gel extraction kit. The pk18mobsacB plasmid was digested with *Bam*HI and gel-purified with a QIAquick gel extraction kit. The UpDw arm and linearized pk18mobsacB were ligated with a ligation-convenience kit (NIPPON GENE, Toyama, Japan). The resulting plasmid was the final construct.

TABLE 1 | Bacterial strains and plasmids used in this study.

Strain or plasmid	Description	Reference or source
***Methylosinus trichosporium* OB3b**		
Wild type	Wild type strain	ATCC35070
SC-SacB	Single-crossover mutant constructed by integration of pK18mobsacB_UpDw in flanking region of *mxaF* of *M. trichosporium* OB3b	In this work
OB3b *ΔmxaF*	Unmarked mutant of *mxaF* (METTRDRAFT_RS0210410)	In this work
Escherichia coli		
Turbo	*F' proA+B+lacIq ΔlacZM15/ fhuA2 Δ(lac-proAB) glnV galK16 galE15 R(zgb-210::Tn10) Tets endA1 thi-1 Δ(hsdS-mcrB)5*	NEB product info.
S17-1	*recA1 thi pro hsd*R-RP4-2Tc::Mu Km:Tn7	Simon, 1984
Plasmids		
pJQ200SK	Suicide vector, *P15A*, *traJ*, *oriT*, *sacB*, Gm^r	Quandt and Hynes, 1993
pJQ200SK_UpMxaDw	DNA fragment containing from upstream to downstream regions of *mxaF* ligated into *Bam*HI site of pJQ200SK	In this work
pJQ200SK_UpDw	DNA fragment containing upstream and downstream regions of *mxaF* ligated into *Bam*HI site of pJQ200sk	In this work
pK18mobsacB	Suicide vector, *oriT*, Km^r, *lacZ*, *sacB*	Schäfer et al., 1994
pK18mobsacB_UpDw	DNA fragment containing upstream and downstream regions of *mxaF* ligated into *Bam*HI site of pK18mobsacB	In this work

Km^r, kanamycin resistance; Gm^r, gentamicin resistance.

TABLE 2 | Primers used in this study.

Name	Sequence 5'>3'
Nup-F (armA)	CAGCCCGGGGGATCCAATGTGGGTTTCGGTC
Ndown-R (armB)	AGAACTAGTGGATCCTCAATGAGCGAGCG
DLmxaF-F	TCGTCGATAACTGACCCTTCGCCGC
DLmxaF-R	GGTCAGTTATCGACGAGTCCTCCTGC
mxaF_upst-F1 (P1)	CACCATTTCGCCTATCGTCTCAATC
mxaF_dwst-R1 (P2)	CCGGTGACCGTGTTGTGAAAG
mxaF-F2 (P3)	TACCGAGCTCGAATTCAGGAGGACTCGTCGATGAG GAAG
mxaF_R2 (P4)	ACGGCCAGTGAATTCTCAGTTCGCCTTGTACTCGCC
mxaF_mid-F	AAGGGCGTCGAATATGTCGCGATCCTGTAC
mxaF_mid-R	TTCGTCAGAGCCTCGAGCTTGTCCTC
mxaF_upst-F2	GGCGAGAATATTGGCGTAGGCCGGATAG
mxaF_dwst-R2	TGGGGTCATGCTTGGGATCGTATTTCGAG
pK18mobsacB_seq-F	AAGCCCACTGCAAGCTACCTG
pK18mobsacB_seq-R	ACCTACACCGAACTGAGATACCTAC

Underlined sequences represent different restriction sites.

It was named pK18mobsacB_UpDw, transferred to chemically competent *E. coli* S17.1 λpir (Simon, 1984) by the heat shock method, and transferred to *M. trichosporium* OB3b *via* conjugation between the donor (*E. coli* S17.1 λpir containing the pK18mobsacB_UpDw construct) and the recipient (*M. trichosporium* OB3b) strains according to previously described methods (Martin and Murrell, 1995; Farhan Ul Haque et al., 2016). The mixture (1:5 donor:recipient ratio at OD_{540}) was passed through a 0.2-μm nitrocellulose filter (ADVANTEC Co. Ltd., Tokyo, Japan). The obtained filter was then incubated at 30°C on NMS agar containing 0.02% (w/v) proteose peptone under a 50:50 (v/v) methane/air atmosphere for 24 h. The cells were removed by vortexing the filter in 1 ml NMS medium. The suspension was spread onto NMS agar plates containing 10 μg ml^{-1} kanamycin to select for *M. trichosporium* OB3b harboring the kanamycin resistance cassette and other pK18mobsacB_UpDw regions and 10 μg ml^{-1} nalidixic acid to prevent *E. coli* growth. The NMS agar plates were incubated at 30°C under a 50:50 (v/v) methane/air atmosphere for 2–3 weeks. The *M. trichosporium* OB3b colonies (first homologous recombinants; *M. trichosporium* OB3b SC-SacB) were suspended in NMS and inoculated onto NMS agar plates containing 0.5% (w/v) sucrose to select for *M. trichosporium* OB3b without the *sacB* regions and 25 μM cerium to express XoxF instead of MxaF. The NMS agar plates were incubated at 30°C under a 50:50 (v/v) methane/air atmosphere for 10 days. The *M. trichosporium* OB3b colonies (second homologous recombinants; *M. trichosporium* OB3b *ΔmxaF* mutant) obtained were suspended in NMS containing 25 μM cerium. PCR and sequencing analysis confirmed success of the double homologous recombinants and crossover mutant genotypes.

Methanol Concentration

Methanol concentrations were measured by a gas chromatograph (GC-2014; Shimadzu Corp., Kyoto, Japan) fitted with a flame ionization detector (FID) and a packed glass column (2 m × 3 mm i.d.; GL Science, Tokyo, Japan) containing sorbitol 25%-gasport B (60/80 mesh; GL Science, Tokyo, Japan). Nitrogen was the carrier gas and the flow rate was 40 ml/min. The operating temperatures were injection, 150°C; column, 100°C; and detector, 150°C. Five microliters sample solution was injected for each measurement.

Immunodetection

Anti-XoxF and anti-MxaF antisera were generated against synthesized peptides corresponding to residues 339–351 of MxaF and residues 374–387 of XoxF1, respectively. Whole-cell lysates of *M. trichosporium* OB3b and OB3b *ΔmxaF* mutant were separated on 10% (w/v) acrylamide gel and transferred to a PVDF membrane following general protocols. The Precision Plus Protein™ Dual Color Standards (Bio-Rad Laboratories, Hercules, CA, United States) were used for the molecular weight marker. The blotted membrane was blocked with 5% (w/v) skim milk at room temperature for 1 h and treated at room temperature for 1 h with anti-MxaF or anti-XoxF1 antisera at 1:2,000 dilution in Tris-buffered saline (TBS) containing 0.05% (v/v) Tween 20 (TBS-T; Calbiochem, San Diego, CA, United States). Membrane-bound MxaF and XoxF1 were detected with horseradish peroxidase-conjugated anti-rabbit IgG antibody (GE Healthcare, Little Chalfont, United Kingdom) at 1:10,000 dilution in TBS-T and visualized using EzWestLumi Plus (ATTO Corp., Tokyo, Japan) according to the manufacturer's instructions.

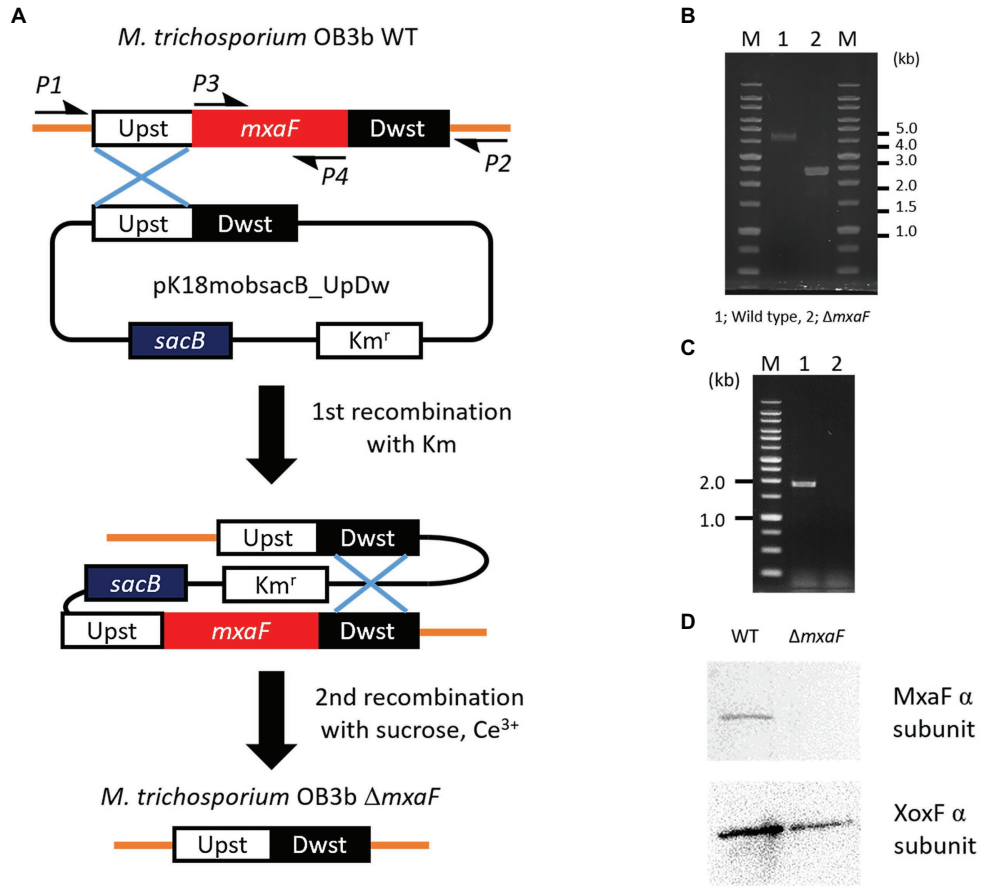

FIGURE 2 | Plasmid-based counterselection. **(A)**. Suicide plasmids used *Kmr* (kanamicine resistance gene) and *sacB* as counterselectable markers. Half arrows indicate primers (P1, mxaF_upst-F1; P2, mxaF_dwst-R1; P3, mxaF-F; P4, mxaF-R). Primer nucleotide sequences are shown in **Table 2**. WT, wild type; *ΔmxaF*, MxaF knockout mutant. PCR confirmation of *mxaF* disruption using primers P1 and P2 **(B)**, P3 and P4 **(C)**. From genome sequence information for *M. trichosporium* OB3b, lengths of PCR amplicons using primers P1 and P2 from wild type and *ΔmxaF* mutant are expected to be 4.3 and 2.4 kbp, respectively **(B)**. PCR amplicons using primers P3 and P4 are expected to be 1.9 kbp from wild type only **(C)**. MxaF and XoxF immunodetection using specific antisera **(D)**.

RESULTS

Construction of *Methylosinus trichosporium* OB3b *ΔmxaF* Mutant

We constructed a mutant of *ΔmxaF* in *M. trichosporium* OB3b using counterselection and double homologous recombination methods with *sacB* as a counterselectable marker (**Figure 2A**). We prepared the plasmids pJQ200SK_UpDw and pK18mobsacB_UpDw (**Supplementary Figure S1**). However, construction of the mutant succeeded only when pK18mobsacB_UpDw was used. Plasmid integration into the target site was confirmed by PCR with the primer sets A (mxaF_upst-F2 and mxaF_mid-R) and B (mxaF_dwst-R2 and mxaF_mid-F) on a single-crossover mutant grown on NMS with kanamycin (**Supplementary Figure S2**). The single-crossover mutant was plated on NMS containing sucrose and cerium for counterselection. We applied PCR to the surviving colonies and selected double-crossover mutants using primers P1 and P2. The PCR amplicons from the *ΔmxaF* mutants were shorter (2.4 kbp) than those from the wild type (4.3 kbp; **Figure 2B**). The PCR product was confirmed by sequencing. No PCR product from the *ΔmxaF* mutants was detected using primers P3 and P4 (**Figure 2C**). Hence, *mxaF* and the region derived from the integrated plasmid were successfully deleted. It was established that the mutant was resistant to sucrose but sensitive to kanamycin. Immunodetection with anti-MxaF and anti-XoxF antisera demonstrated the absence of MxaF expression and the presence of XoxF expression in the *ΔmxaF* mutant (**Figure 2D**). Thus, the targeted mutant without *mxaF* or the region from the integrated plasmid was successfully created.

Cell Growth and Methanol Accumulation in the OB3b *ΔmxaF* Mutant

To evaluate our strategic design for methanol production and cell growth, we examined the OB3b *ΔmxaF* mutant construct in media with and without copper and cerium ions. We isolated the OB3b *ΔmxaF* mutant using selective growth media and

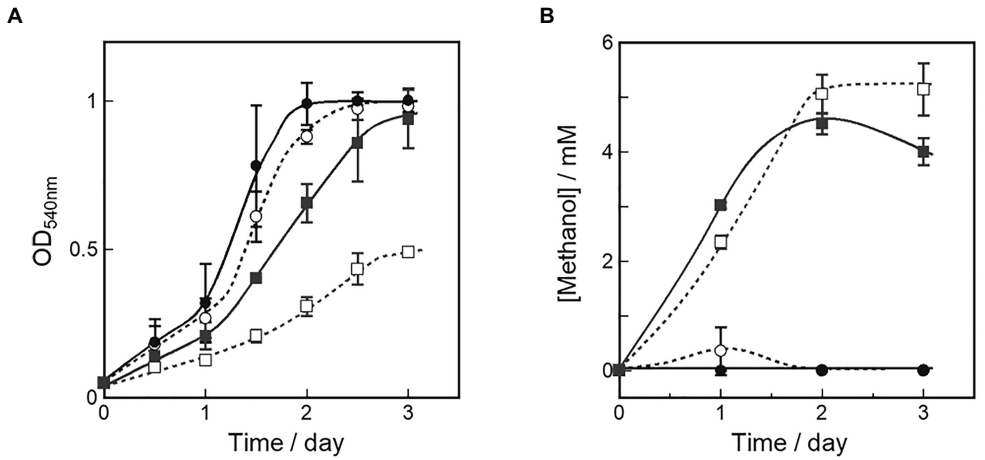

FIGURE 3 | Cell growth **(A)** and methanol production **(B)** in OB3b *ΔmxaF* mutant in presence of various copper and cerium concentrations. A starter culture grown in NMS with 25 μM cerium ion was used as an inoculum to examine the growth and methanol production of the OB3b *ΔmxaF* mutant in the fresh medium of four different culture conditions. ○, 0 μM copper ion plus 0 μM cerium ion; ●, 0 μM copper ion plus 25 μM cerium ion; □, 10 μM copper ion plus 0 μM cerium ion; ■, 10 μM copper ion plus 25 μM cerium ion. Errors bars: duplicate sample ranges.

incubated it in 20 ml NMS medium containing 25 μM cerium ion plus 0 μM copper ion. After OD_{540} = 0.8 was attained, the culture was washed twice with 8 ml fresh cerium- and copper-free NMS and transferred at a 1:9 ratio to NMS containing various copper and/or cerium ion concentrations. **Figure 3A** shows that the OB3b *ΔmxaF* mutant grew under all conditions but most slowly in the presence of 10 μM copper ion and the absence of cerium ion. According to the previous report, this growth of the OB3b *ΔmxaF* mutant can be caused by any remaining XoxF and cerium ion in the initial seed cells (Farhan Ul Haque et al., 2016). To evaluate whether the OB3b *ΔmxaF* mutants could be propagated, the cultures were inoculated into identical fresh media under the same conditions. When the mutants were transferred to identical fresh media at initial OD_{540} = 0.1 (transfer A), they grew in the presence of cerium ion (**Supplementary Figure S3**). However, the growth of the mutants was almost stopped in the absence of cerium ion. Therefore, this mutant required cerium ions to grow normally.

Methanol concentrations in the medium were measured simultaneously to evaluate methanol accumulation by the OB3b *ΔmxaF* mutant under each condition. **Figure 3B** shows that methanol accumulation was detected in all OB3b *ΔmxaF* mutants except those in the medium containing only 25 μM cerium ion plus 0 μM copper ion. Thus, methanol production with the OB3b *ΔmxaF* mutant can be realized by modulating the copper and cerium ion concentrations. Methanol production was also observed in the absence of an external electron donor. The methanol concentration was higher in the presence of 10 μM copper ion than it was in its absence. When the OB3b *ΔmxaF* mutant was cultured in medium containing 10 μM copper ion plus 0 μM cerium ion, the maximum methanol content was 2.6 $\mu mol \cdot mg^{-1}$ dry cell $weight \cdot h^{-1}$. One OD_{540} unit of *M. trichosporium* OB3b corresponds to 0.15 $mg \cdot ml^{-1}$ dry cell weight. Within 2 days, the methanol was saturated in the medium containing 10 μM copper ion plus 0 μM cerium ion. The conversion efficiency of the accumulated methanol to the total amount of methane added to the reaction system was ~0.3%. The methanol accumulation in the OB3b *ΔmxaF* mutant decreased with increasing incubation time except in the presence of 10 μM copper ion plus 0 μM cerium ion. The recovery of methanol accumulation was assessed in the OB3b *ΔmxaF* mutant *via* inoculation experiments under two conditions. After the cultures were transferred to identical fresh medium at the initial OD_{540} = 0.1 (transfer A), no methanol production was observed under any conditions (**Supplementary Figure S3B**). When the cultures were transferred to the same volume of identical fresh medium (transfer B; constant cell density), the methanol accumulation was maintained in the presence of 10 μM copper ion but stopped within 1 day after the medium was exchanged (**Supplementary Figure S4**). The methanol accumulation decreased on day 2 after the medium exchange in the presence of 10 μM copper ion plus 25 μM cerium ion. The cells were then replenished with identical fresh medium on day 5. Only slight methanol accumulation was detected in the medium containing 10 μM copper ion plus 0 μM cerium ion. Methanol accumulation was recovered by exchanging the medium but its activity nonetheless gradually declined thereafter. Though methanol accumulated in the presence of 25 μM cerium, there was an evident reduction in methanol concentration in the presence of 10 μM copper. Thus, XoxF consumed the methanol in the latter case.

We compared intracellular MDH expression by using *M. trichosporium* OB3b cultured in the medium under four different conditions. Western blotting of MDH showed that MxaF was absent in the OB3b *ΔmxaF* mutant under all conditions (**Figure 4A**). XoxF was expressed in the OB3b *ΔmxaF* mutant in the presence of cerium ion (**Figure 4B**). XoxF expression was higher in the absence than the presence of copper ion and the same held true for the OB3b wild type.

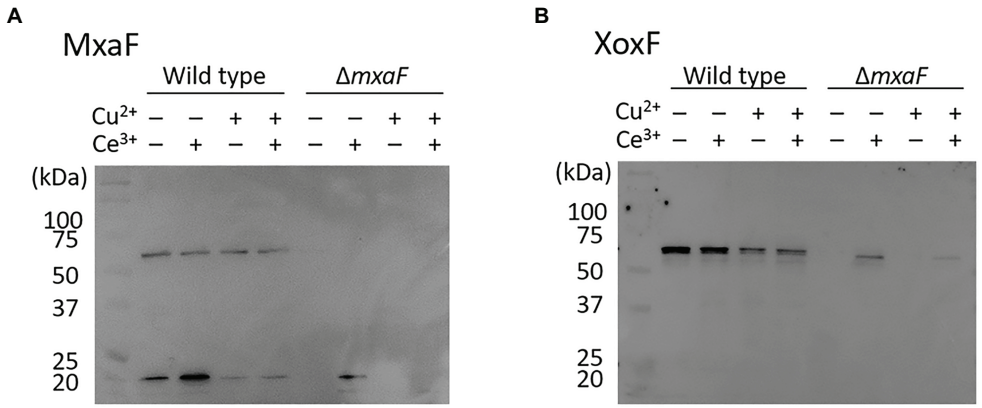

FIGURE 4 | Western blot of wild type and *ΔmxaF* mutant of *M. trichosporium* OB3b. Immunodetection of MxaF **(A)** and XoxF **(B)** using specific antisera. Molecular weight marker (in kDa) of protein standards are shown on left.

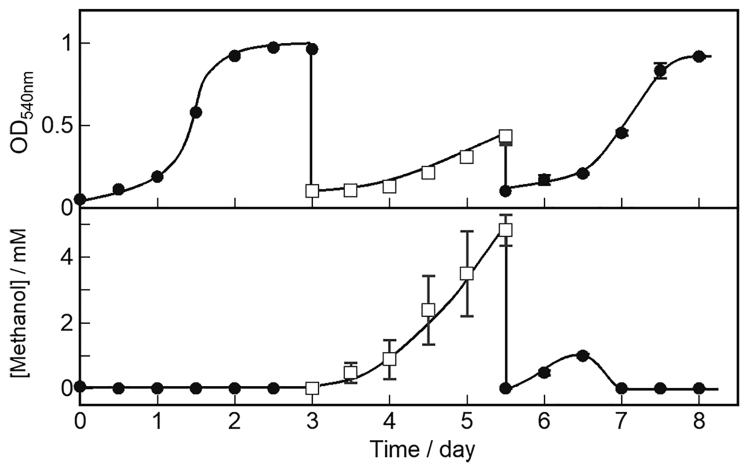

FIGURE 5 | OB3b *ΔmxaF* mutant switching between cell growth and methanol production conditions by modulating copper and cerium concentrations. ●, cell growth condition (0 μM copper ion plus 25 μM cerium ion); □, methanol production condition (10 μM copper ion plus 0 μM cerium ion). Errors bars: duplicate sample ranges.

Switching Between Cell Growth and Methanol Production in OB3b *ΔmxaF* Mutant

We characterized cell growth and methanol accumulation in the OB3b *ΔmxaF* mutant and demonstrated that its phenotype switched in response to changes in the metal ions in the medium. The cell growth curve and methanol concentration in the medium are shown in **Figure 5**. The OB3b *ΔmxaF* mutant was cultured with 0 μM copper ion plus 25 μM cerium ion. After 3 days, the cultures were collected, washed twice, and resuspended in NMS under conditions conducive to methanol production (10 μM copper ion plus 0 μM cerium ion) to obtain OD_{540} = 0.1 after inoculation (first switch). After 2.5 days, the cultures were collected, washed twice, and resuspended in NMS under cell growth conditions to obtain the initial OD_{540} = 0.1 (second switch). In the first switch, the growth rate of the OB3b *ΔmxaF* mutant decreased and methanol accumulation increased without the addition of any external electron source. The amount of methanol per unit cell (mg dry cell weight) increased until 1.5 days and then remained constant until 2.5 days (**Supplementary Figure S5**). In the second switch, the growth rate was restored to the same level as that of the first step. Methanol accumulation increased until day 1 but the methanol disappeared by day 1.5 when the cells entered the log phase. Therefore, cell growth was recovered because XoxF expression consumed methanol. The foregoing results disclosed that the OB3b *ΔmxaF* mutant alter its phenotype and XoxF MDH expression can be controlled by altering the medium such that it favors cell growth or methanol production.

DISCUSSION

The culture of whole-cell methanotrophs requires a strategic design to optimize both methanol production and cell growth.

In the present study, we characterized the continuous cell growth and methanol production in the OB3b *ΔmxaF* mutant in nutrient media containing four different copper and cerium ion configurations (**Table 3**). We modulated the medium conditions to promote cell growth (0 μM copper ion plus 25 μM cerium ion) and methanol production (10 μM copper ion plus 0 μM cerium ion) and switch the OB3b *ΔmxaF* mutant phenotype. The mutant presented with nearly the same growth as the wild type under conditions conducive to cell growth and it expressed XoxF in the presence of cerium ion. **Figure 3A** shows that mutant grew under all conditions but had a longer lag phase in the presence than the absence of copper ion. Furthermore, its overall growth was slowest under conditions conducive to methanol production. For transfer A (**Supplementary Figure S3**), the OB3b *ΔmxaF* mutant grew best under cell growth conditions. Though it also grew in the presence of 10 μM copper and 25 μM cerium, its lag phase there was longer than it was under cell growth conditions. Cell growth was strongly inhibited when XoxF was not expressed and cerium ion was absent (**Figure 4B**). Mutant growth under each condition of the present study resembled that of another *M. trichosporium* OB3b *mxaF* knockout mutant reported by Muhammad Farhan Ul Haque et al. (2016). These authors also indicated a reduction in cell growth in the presence of copper ions and total cell growth arrest in the absence of cerium ions. Thus, the OB3b *ΔmxaF* mutant can grow using any remaining XoxF and cerium ion in the initial seed cells. It was shown that >98% of the added cerium is associated with microbial biomass (Farhan Ul Haque et al., 2015).

Methanol accumulation by the OB3b *ΔmxaF* mutant occurred in the medium containing copper ion. This condition is a requirement for pMMO expression (**Figure 3B**). Methane consumption was higher in whole-cell *M. trichosporium* OB3b expressing sMMO than it was in whole-cell *M. trichosporium* OB3b expressing pMMO (Sirajuddin and Rosenzweig, 2015). However, methanol did not accumulate in this mutant in the absence of copper and cerium ions which causes sMMO expression to predominate and represses XoxF (**Figure 3B**). Hence, methanol from sMMO was consumed more efficiently than methanol from pMMO by the remaining XoxF. The foregoing results and a previous study showed that pMMO forms a supercomplex with MxaF MDH (Culpepper and Rosenzweig, 2014). Coupling between pMMO and XoxF MDH is weaker than coupling between pMMO and MxaF MDH. Methanol may accumulate in cells expressing XoxF and pMMO because of weak coupling between XoxF and pMMO. XoxF does not oxidize methanol from pMMO as effectively as MxaF. This hypothesis explains the results shown in **Figure 3B** and **Supplementary Figure S4**. In the presence of 10 μM copper ion plus 25 μM cerium ion, the aforementioned mutant could accumulate methanol as it does under methanol production conditions. In the former scenario, however, it consumes any methanol generated thereafter. Despite pMMO and XoxF expression in the presence of 10 μM copper ion plus 25 μM cerium ion (Farhan Ul Haque et al., 2015, 2016), there was no methanol accumulation in the case of transfer A (**Supplementary Figure S3**). Methane oxidation by pMMO is evident in the presence of 10 μM copper ion plus 25 μM cerium ion. Hence, the mutant may regulate the balance between pMMO and XoxF and changes to the state appropriate for methane utilization. The methanol concentration reached saturation (~6 mM) in the OB3b *ΔmxaF* mutant grown in medium containing 10 μM copper ion plus 0 μM cerium ion (**Figure 3B**). Methanol accumulation was arrested as methanol inhibited pMMO activity reversibly (Furuto et al., 1999). The observed recovery of methanol accumulation in the OB3b *ΔmxaF* mutant after the fresh medium was exchanged corroborated this hypothesis (**Supplementary Figure S4**). One way to overcome this limitation is to use a continuous culture system wherein the medium is exchanged constantly and the methanol is removed.

To the best of our knowledge, this study is the first to report methanol production using a genetically modified methanotroph lacking MDH activity. Changing the phenotype of this mutant by altering the metal ion concentrations in its growth medium facilitates the recovery of bacterial enzymes, reducing equivalents, and methanol production. Therefore, this mutant can function as a methanol production biocatalyst for longer periods of time than conventional methods. A previous study on methanol production by methanotrophs revealed that several MDH inhibitors have been implemented to stop methanol metabolism. Furuto et al. (1999) reported semicontinuous methanol synthesis with *M. trichosporium* OB3b in the presence of the MDH inhibitor cyclopropanol. The methanol production rate was 3.2 $\mu mol \cdot mg^{-1}$ $cell \cdot h^{-1}$ after the addition of 14.3 mM sodium formate. Methanol production rates of 6.0 $\mu mol \cdot mg^{-1}$ $cell \cdot h^{-1}$ (Mehta et al., 1987) and 2.6 $\mu mol \cdot mg^{-1}$ $cell \cdot h^{-1}$ (In Yeub et al., 2015) were reported for *M. trichosporium* OB3b. The methanol production rate for *M. trichosporium* OB3b mutant in this study (2.6 $\mu mol \cdot mg^{-1}$ $cell \cdot h^{-1}$) was similar to those of previous reports. The mutant had the same methanol production capacity as the wild type subjected to MDH inhibitors. However, the OB3b *ΔmxaF* mutant requires time to switch between cell growth and methanol production. After its phenotype was switched by changing the growth medium, the former characteristics of the mutant were restored for ~1 day before the phenotype transitions occurred (**Figure 5**). This lag time may be explained by the persistence of XoxF MDH and/or pMMO from the previous state in the medium. One day after modulating the metal ion composition of the medium, the

TABLE 3 | Characterization of the continuous cell growth and methanol production in the OB3b *ΔmxaF* mutant under four conditions containing copper and cerium ions.

Metal ions in medium	MMO type	MDH type	Continuous cell growth	Methanol production
0 μM Cu^{2+} plus 0 μM Ce^{3+}	sMMO	–	–	–
0 μM Cu^{2+} plus 25 μM Ce^{3+}	sMMO	XoxF	++	–
10 μM Cu^{2+} plus 0 μM Ce^{3+}	pMMO	–	–	++
10 μM Cu^{2+} plus 25 μM Ce^{3+}	pMMO	XoxF	+	+

characteristics of the alternate phenotype may be observed in most cells under the new condition. Therefore, strategies are required to improve the efficacy of the switching system to reduce the lag time in the phenotypic change. In addition, the low methanol conversion efficiency for *M. trichosporium* OB3b mutant in this study (~0.3% of the total amount of methane added to the reaction system) is an issue that needs to be improved. In recent years, new bioreactors that are effective for methanotrophs have been reported (Chen et al., 2020; Valverde-Pérez et al., 2020). It is expected that more efficient carbon conversion can be achieved by using these bioreactors.

Here, the *M. trichosporium* OB3b mutant of mxaF knockout (OB3b *ΔmxaF* mutant) was constructed by a double homologous recombination method and *sacB* was used as a counterselectable marker. The OB3b *ΔmxaF* mutant normally grows by expressing XoxF MDH in media containing cerium ion. It accumulates methanol by expressing pMMO in media containing copper ion and no external metabolic electron donors. The phenotype of the OB3b *ΔmxaF* mutant can be altered between that which is found under cell growth conditions and that which occurs under methanol production conditions by changing the cerium and copper ion content in the growth media. Phenotype switching in the OB3b *ΔmxaF* mutant achieves continuous methanol production by restoring reducing power. The present study proposes an innovative strategy for methanol production using genetically engineered, metabolically modified methanotrophs. Although it is not yet cost-effective for industrial methanol production, this study shows a new possibility for methanol production using methanotrophs. Subsequent research should focus on optimizing the medium conditions and culture system under which the mutant could serve as an industrial biocatalyst converting methane to methanol.

DATA AVAILABILITY STATEMENT

The raw data supporting the conclusions of this article will be made available by the authors, without undue reservation.

AUTHOR CONTRIBUTIONS

HI and KY conducted the experiments. MI and KH assisted in the experiment design and gave a hand in performing the experiments. HI and TK analyzed the data and wrote the manuscript. All authors contributed to the article and approved the submitted version.

FUNDING

This study was conducted under the JPMJAL1402 Project of the Advanced Low Carbon Technology Research and Development Program (ALCA) funded by the Japan Science and Technology Agency (JST).

ACKNOWLEDGMENTS

We would like to thank Editage (www.editage.com) for English language editing.

SUPPLEMENTARY MATERIAL

The Supplementary Material for this article can be found online at: https://www.frontiersin.org/articles/10.3389/fmicb.2021.639266/full#supplementary-material

Supplementary Figure S1 | Plasmid construction protocol. **(A)** pJQ200SK_UpDw, **(B)** pK18mobsacB_UpDw. Suicide plasmids used *Gm*^{r} (gentamicin resistance gene), *Km*^{r} (kanamycin resistance gene), and *sacB* as counterselectable markers.

Supplementary Figure S2 | PCR analysis of single crossover strains in genomic DNA of *M. trichosporium* OB3b::pK18mobsacB_UpDw using primer sets A (mxaF_upst-F2 and mxaF_mid-R) and B (mxaF_dwst-R2 and mxaF_mid-F). **(A)** Outline of experiment. **(B)** Electrophoresis of colony PCR amplicon using primer sets A and B. M, marker; WT, wild type. Red square: PCR product of recombination between downstream regions. Blue square: PCR product of recombination between upstream regions.

Supplementary Figure S3 | Cell growth and methanol accumulation in OB3b Δ*mxaF* mutant after subculture with identical media at initial OD_{540} = 0.1. ○, 0 μM copper ion plus 0 μM cerium ion; ●, 0 μM copper ion plus 25 μM cerium ion; □, 10 μM copper ion plus 0 μM cerium ion; ■, 10 μM copper ion plus 25 μM cerium ion.

Supplementary Figure S4 | Continuous methanol production using OB3b Δ*mxaF* mutant in presence of various copper and cerium concentrations. ○, 0 μM copper ion plus 0 μM cerium ion; ●, 0 μM copper ion plus 25 μM cerium ion; □, 10 μM copper ion plus 0 μM cerium ion; ■, 10 μM copper ion plus 25 μM cerium ion. Exchange of identical fresh media containing all cultures on days 3 and 5.

Supplementary Figure S5 | OB3b *ΔmxaF* mutant switching between cell growth and methanol production conditions by modulating copper and cerium concentrations. One OD_{540} unit of *M. trichosporium* OB3b corresponds to 0.15 mg·ml^{-1} dry cell weight. ●, cell growth condition (0 μM copper ion plus 25 μM cerium ion); □, methanol production condition (10 μM copper ion plus 0 μM cerium ion). Errors bars: duplicate sample ranges.

REFERENCES

Bjorck, C. E., Dobson, P. D., and Pandhal, J. (2018). Biotechnological conversion of methaneto methanol: evaluation of progress and potential. *AIMS Bioeng.* 5, 1–38. doi: 10.3934/bioeng.2018.1.1

Chen, Y. -Y., Ishikawa, M., Suzuki, R., Ito, H., Kamachi, T., and Hori, K. (2020). Evaluation of methane degradation performance in microbial gas-phase reactions using effectively immobilized methanotrophs. *Biochem. Eng. J.* 154:107441. doi: 10.1016/j.bej.2019.107441

Conrad, R. (2009). The global methane cycle: recent advances in understanding the microbial processes involved. *Environ. Microbiol. Rep.* 1, 285–292. doi: 10.1111/j.1758-2229.2009.00038.x

Cox, J. M., Day, D. J., and Anthony, C. (1992). The interaction of methanol dehydrogenase and its electron acceptor, cytochrome cL in methylotrophic bacteria. *Biochim. Biophys. Act* 1119, 97–106. doi: 10.1016/0167-4838(92)90240-E

Culpepper, M. A., and Rosenzweig, A. C. (2014). Structure and protein–protein interactions of methanol dehydrogenase from *Methylococcus capsulatus* (Bath). *Biochemistry* 53, 6211–6219. doi: 10.1021/bi500850j

Dales, S. L., and Anthony, C. (1995). The interaction of methanol dehydrogenase and its cytochrome electron acceptor. *Biochem. J.* 312, 261–265. doi: 10.1042/bj3120261

Duan, C., Luo, M., and Xing, X. (2011). High-rate conversion of methane to methanol by *Methylosinus trichosporium* OB3b. *Bioresour. Technol.* 102, 7349–7353. doi: 10.1016/j.biortech.2011.04.096

Farhan Ul Haque, M., Gu, W., DiSpirito, A. A., and Semrau, J. D. (2016). Marker exchange mutagenesis of mxaF, encoding the large subunit of the Mxa methanol dehydrogenase, in *Methylosinus trichosporium* OB3b. *Appl. Environ. Microbiol.* 82, 1549–1555. doi: 10.1128/aem.03615-15

Farhan Ul Haque, M., Kalidass, B., Bandow, N., Turpin, E. A., DiSpirito, A. A., and Semrau, J. D. (2015). Cerium regulates expression of alternative methanol dehydrogenases in *Methylosinus trichosporium* OB3b. *Appl. Environ. Microbiol.* 81, 7546–7552. doi: 10.1128/aem.02542-15

Frank, J. Jr., van Krimpen, S. H., Verwiel, P. E. J., Jongejan, J. A., Mulder, A. C., and Duine, J. A. (1989). On the mechanism of inhibition of methanol dehydrogenase by cyclopropane-derived inhibitors. *Eur. J. Biochem.* 184, 187–195. doi: 10.1111/j.1432-1033.1989.tb15006.x

Furuto, T., Takeguchi, M., and Okura, I. (1999). Semicontinuous methanol biosynthesis by *Methylosinus trichosporium* OB3b. *J. Mol. Catal. A Chem.* 144, 257–261. doi: 10.1016/S1381-1169(99)00007-2

Groom, J. D., Ford, S. M., Pesesky, M. W., and Lidstrom, M. E. (2019). A mutagenic screen identifies a tonb-dependent receptor required for the lanthanide metal switch in the type i methanotroph "*Methylotuvimicrobium buryatense*" 5GB1C. *J. Bacteriol.* 201:e00120-19. doi: 10.1128/JB.00120-19

Han, J. -S., Ahn, C. -M., Mahanty, B., and Kim, C. -G. (2013). Partial oxidative conversion of methane to methanol through selective inhibition of methanol dehydrogenase in methanotrophic consortium from landfill cover soil. *Appl. Biochem. Biotechnol.* 171, 1487–1499. doi: 10.1007/s12010-013-0410-0

Hibi, Y., Asai, K., Arafuka, H., Hamajima, M., Iwama, T., and Kawai, K. (2011). Molecular structure of La^{3+}-induced methanol dehydrogenase-like protein in *Methylobacterium radiotolerans*. *J. Biosci. Bioeng.* 111, 547–549. doi: 10.1016/j.jbiosc.2010.12.017

Hwang, I. Y., Hur, D. H., Lee, J. H., Park, C. -H.., Chang, I. S., and Lee, J. W., et al. (2015). Batch conversion of methane to methanol using *Methylosinus trichosporium* OB3b as biocatalyst. *J. Microbiol. Biotechnol.* 25, 375–380. doi: 10.4014/jmb.1412.12007

Keltjens, J. T., Pol, A., Reimann, J., and Op den Camp, H. J. M. (2014). PQQ-dependent methanol dehydrogenases: rare-earth elements make a difference. *Appl. Microbiol. Biotechnol.* 98, 6163–6183. doi: 10.1007/s00253-014-5766-8

Kim, H. G., Han, G. H., and Kim, S. W. (2010). Optimization of lab scale methanol production by *Methylosinus trichosporium* OB3b. *Biotechnol. Bioprocess Eng.* 15, 476–480. doi: 10.1007/s12257-010-0039-6

Lee, S. G., Goo, J. H., Kim, H. G., Oh, J. -I., Kim, Y. M., and Kim, S. W. (2004). Optimization of methanol biosynthesis from methane using *Methylosinus trichosporium* OB3b. *Biotechnol. Lett.* 26, 947–950. doi: 10.1023/B:bile.0000025908.19252.63

Martin, H., and Murrell, J. C. (1995). Methane monooxygenase mutants of *Methylosinus trichosporium* constructed by marker-exchange mutagenesis. FEMS Microbiol. *FEMS Microbiol. Lett.* 127, 243–248. doi: 10.1111/j.1574-6968.1995.tb07480.x

Mehta, P. K., Ghose, T. K., and Mishra, S. (1991). Methanol biosynthesis by covalently immobilized cells of *Methylosinus trichosporium*: batch and continuous studies. *Biotechnol. Bioeng.* 37, 551–556. doi: 10.1002/bit.260370609

Mehta, P. K., Mishra, S., and Ghose, T. K. (1987). Methanol accumulation by resting cells of *Methylosinus trichosporium* (I). *J. Gen. Appl. Microbiol.* 33, 221–229. doi: 10.2323/jgam.33.221

Nakagawa, T., Mitsui, R., Tani, A., Sasa, K., Tashiro, S., Iwama, T., et al. (2012). A catalytic role of XoxF1 as La^{3+}-dependent methanol dehydrogenase in *Methylobacterium extorquens* strain AM1. *PLoS One* 7:e50480. doi: 10.1371/journal.pone.0050480

Pen, N., Soussan, L., Belleville, M. P., Sanchez, J., Charmette, C., and Paolucci-Jeanjean, D. (2014). An innovative membrane bioreactor for methane biohydroxylation. *Bioresour. Technol.* 174, 42–52. doi: 10.1016/j.biortech.2014.10.001

Pen, N., Soussan, L., Belleville, M. P., Sanchez, J., and Paolucci-Jeanjean, D. (2016). Methane hydroxylation by *Methylosinus trichosporium* OB3b: monitoring the biocatalyst activity for methanol production optimization in an innovative membrane bioreactor. *Biotechnol. Bioprocess Eng.* 21, 283–293. doi: 10.1007/s12257-015-0762-0

Pol, A., Barends, T. R. M., Dietl, A., Khadem, A. F., Eygensteyn, J., Jetten, M. S. M., et al. (2014). Rare earth metals are essential for methanotrophic life in volcanic mudpots. *Environ. Microbiol.* 16, 255–264. doi: 10.1111/1462-2920.12249

Quandt, J., and Hynes, M. F. (1993). Versatile suicide vectors which allow direct selection for gene replacement in gram-negative bacteria. *Gene* 127, 15–21. doi: 10.1016/0378-1119(93)90611-6

Sambrook, J., and Russell, D. W. (2006). The inoue method for preparation and transformation of competent *E. coli*: "ultra-competent" cells. *CSH Protoc.* 2006:pdb.prot3944. doi: 10.1101/pdb.prot3944

Schäfer, A., Tauch, A., Jäger, W., Kalinowski, J., Thierbach, G., and Pühler, A. (1994). Small mobilizable multi-purpose cloning vectors derived from the *Escherichia coli* plasmids pK18 and pK19: selection of defined deletions in the chromosome of *Corynebacterium glutamicum*. *Gene* 145, 69–73. doi: 10.1016/0378-1119(94)90324-7

Semrau, J. D., Jagadevan, S., DiSpirito, A. A., Khalifa, A., Scanlan, J., Bergman, B. H., et al. (2013). Methanobactin and MmoD work in concert to act as the 'copper-switch' in methanotrophs. *Environ. Microbiol.* 15, 3077–3086. doi: 10.1111/1462-2920.12150

Shimoda, M., and Okura, I. (1990). Effect of cyclopropane treatment of *Methylosinus trichosporium* (OB3b) for methane hydroxylation. *J. Chem. Soc. Chem. Comm.* 7, 533–534. doi: 10.1039/C39900000533

Shindell, D., Kuylenstierna, J. C. I., Vignati, E., van Dingenen, R., Amann, M., Klimont, Z., et al. (2012). Simultaneously mitigating near-term climate change and improving human health and food security. *Science* 335, 183–189. doi: 10.1126/science.1210026

Simon, R. (1984). High-frequency mobilization of gram-negative bacterial replicons by the *in vitro* constructed Tn5-Mob transposon. *Mol. Gen. Genet.* 196, 413–420. doi: 10.1007/BF00436188

Sirajuddin, S., and Rosenzweig, A. C. (2015). Enzymatic oxidation of methane. *Biochemistry* 54, 2283–2294. doi: 10.1021/acs.biochem.5b00198

Takeguchi, M., Furuto, T., Sugimori, D., and Okura, I. (1997). Optimization of methanol biosynthesis by *Methylosinus trichosporium* OB3b: an approach to improve methanol accumulation. *Appl. Biochem. Biotechnol.* 68, 143–152.

U.S. Environmental Protection Agency (EPA) (2019). Global non-CO_2 greenhouse gas emission projections & mitigation: 2015-2050. Report No.: EPA 430-R-19-010. Available at: https://www.epa.gov/sites/production/files/2019-09/documents/epa_non-co2_greenhouse_gases_rpt-epa430r19010.pdf (Accessed Novenber 10, 2019).

Valverde-Pérez, B., Xing, W., Zachariae, A. A., Skadborg, M. M., Kjeldgaard, A. F., Palomo, A., et al. (2020). Cultivation of methanotrophic bacteria in a novel bubble-free membrane bioreactor for microbial protein production. *Bioresour. Technol.* 310:123388. doi: 10.1016/j.biortech.2020.123388

Vu, H. N., Subuyuj, G. A., Vijayakumar, S., Good, N. M., Martinez-Gomez, N. C., and Skovran, E. (2016). Lanthanide-dependent regulation of methanol oxidation systems in *Methylobacterium extorquens* AM1 and their contribution to methanol growth. *J. Bacteriol.* 198, 1250–1259. doi: 10.1128/jb.00937-15

Whittenbury, R., Phillips, K., and Wilkinson, J. (1970). Enrichment, isolation and some properties of methane-utilizing bacteria. *Microbiology* 61, 205–218. doi: 10.1099/00221287-61-2-205

Williams, P. A., Coates, L., Mohammed, F., Gill, R., Erskine, P. T., Coker, A., et al. (2005). The atomic resolution structure of methanol dehydrogenase from *Methylobacterium extorquens*. *Acta Crystallogr. D Biol. Crystallogr.* 61, 75–79. doi: 10.1107/S0907444904026964

Yoon, S., Semrau, J. D., and DiSpirito, A. A. (2010). Methanotrophs and copper. *FEMS Microbiol. Rev.* 34, 496–531. doi: 10.1111/j.1574-6976.2010.00212.x

Conflict of Interest: The authors declare that the research was conducted in the absence of any commercial or financial relationships that could be construed as a potential conflict of interest.

frontiers in Microbiology

ORIGINAL RESEARCH
published: 01 April 2021
doi: 10.3389/fmicb.2021.639482

Computational Analysis of Dynamic Light Exposure of Unicellular Algal Cells in a Flat-Panel Photobioreactor to Support Light-Induced CO_2 Bioprocess Development

Nicolò S. Vasile[1], Alessandro Cordara[1], Giulia Usai[1,2] and Angela Re[1]**

[1] Centre for Sustainable Future Technologies, Fondazione Istituto Italiano di Tecnologia, Genova, Italy, [2] Department of Applied Science and Technology, Politecnico di Torino, Torino, Italy

OPEN ACCESS

Edited by:
Pramod P. Wangikar, Indian Institute of Technology Bombay, India

Reviewed by:
Hesham Ali El Enshasy, University of Technology Malaysia, Malaysia
Jinjin Diao, Washington University in St. Louis, United States

***Correspondence:**
Alessandro Cordara
Alessandro.Cordara@iit.it
Angela Re
Angela.Re@iit.it;
angeladotre@gmail.com

Specialty section:
This article was submitted to Microbiotechnology, a section of the journal Frontiers in Microbiology

Received: *09 December 2020*
Accepted: *25 February 2021*
Published: *01 April 2021*

Citation:
Vasile NS, Cordara A, Usai G and Re A (2021) Computational Analysis of Dynamic Light Exposure of Unicellular Algal Cells in a Flat-Panel Photobioreactor to Support Light-Induced CO_2 Bioprocess Development. Front. Microbiol. 12:639482. doi: 10.3389/fmicb.2021.639482

Cyanobacterial cell factories trace a vibrant pathway to climate change neutrality and sustainable development owing to their ability to turn carbon dioxide-rich waste into a broad portfolio of renewable compounds, which are deemed valuable in green chemistry cross-sectorial applications. Cell factory design requires to define the optimal operational and cultivation conditions. The paramount parameter in biomass cultivation in photobioreactors is the light intensity since it impacts cellular physiology and productivity. Our modeling framework provides a basis for the predictive control of light-limited, light-saturated, and light-inhibited growth of the *Synechocystis* sp. PCC 6803 model organism in a flat-panel photobioreactor. The model here presented couples computational fluid dynamics, light transmission, kinetic modeling, and the reconstruction of single cell trajectories in differently irradiated areas of the photobioreactor to relate key physiological parameters to the multi-faceted processes occurring in the cultivation environment. Furthermore, our analysis highlights the need for properly constraining the model with decisive qualitative and quantitative data related to light calibration and light measurements both at the inlet and outlet of the photobioreactor in order to boost the accuracy and extrapolation capabilities of the model.

Keywords: computational fluid dynamics, particle tracing, carbon dioxide bioconversion, algal bioprocess, simulation modeling, photobioreactor, light distribution analysis, *Synechocystis* sp. PCC 6803

INTRODUCTION

One of the most compelling long-term global sustainability goals is not just to abate the emissions of greenhouse gasses, but also to substitute environmentally expensive processes based on fossil fuels with biobased sustainable alternatives (Sustainabledevelopment Organization, 2015). Carbon dioxide (CO_2) sequestration and transformation using microorganisms as catalysts could lead to breakthroughs in CO_2 capture and utilization (Lorenzo et al., 2018; McCarty and Ledesma-Amaro, 2019). Photosynthetic microorganisms have garnered an enormous interest since they can be repurposed to convert atmospheric carbon dioxide and renewable electricity-based light, acting,

respectively, as carbon and energy sources, into biobased value-added compounds (Luan and Lu, 2018; van den Berg et al., 2019). Indeed, the biosynthesized compounds can be functionalized in the transport (Lan and Liao, 2012; Gao et al., 2017b; Vidal, 2017; Shabestary et al., 2018; Liu et al., 2019; Wang L. et al., 2020) and energy (Saper et al., 2018) sectors as well as in the packaging (Ni et al., 2016; Nozzi et al., 2017; Yao et al., 2020), health (Lin et al., 2019; Dienst et al., 2020), cosmetic and personal care sectors (Choi et al., 2016; Derikvand et al., 2017), and in the food industry (Caporgno and Mathys, 2018; Bernaerts et al., 2019; Grossmann et al., 2020) among others. The synthetic biology toolkit to unlock the potential of cyanobacterial cell factories has substantially increased in recent years (Taton et al., 2014; Wendt et al., 2016; Vogel et al., 2017; Janasch et al., 2018; Santos-Merino et al., 2019; Vasudevan et al., 2019; Vavitsas et al., 2019). Nonetheless, a great deal of improvement is still needed to simplify and accelerate the transfer of bench-scale bioproduction processes into commercial plants (Jones, 2014; Johnson et al., 2018; Gifuni et al., 2019; Xia et al., 2019). In addition to the availability of metabolic engineering tools, the advantageous factors are cyanobacterial genetic malleability (Xiong et al., 2017), competitive carbon conversion efficiency (Pérez et al., 2019), and native ability to grow in a very poor culture medium (Jahn et al., 2018). These biocatalysts could integrate into climate-mitigating industrial pipelines and sustainably fuel the circular bioeconomy. The potential of photoautotrophic microorganisms such as cyanobacteria to pursue the biobased production of marketable products is being exploited by several companies developing renewable fuels (Farrokh et al., 2019; Yen et al., 2019) and developing innovative solutions to supply bio-based chemical intermediates in green chemistry formulations (Corbion, 2020; Cyano Biotech GmbH, 2020; Photanol, 2020; Pond Tech, 2020).

Efforts are being intensified to enhance the operating reliability of the newly developed biotechnologies (Gifuni et al., 2019). In this perspective, also, a large number of computational approaches are now used to achieve an enhanced understanding (Asplund-Samuelsson et al., 2018; Broddrick et al., 2019), analytical quantification (Zavřel et al., 2019), and control of bioprocesses (Narayanan et al., 2020). In addition to approaches accounting for the multi-factorial design of experiments (Kommareddy and Anderson, 2013), there exists a plethora of computational simulation approaches in process design such as multi-scale physical models (Pruvost and Cornet, 2012; Solimeno et al., 2017; Weise et al., 2019), coupling computational fluid dynamics and kinetic modeling (Perner-Nochta and Posten, 2007; Seo et al., 2014; Loomba et al., 2018; Scheufele et al., 2019), and artificial intelligence-based models (Rio-Chanona et al., 2016, Rio-Chanona et al., 2019).

In the drive to identify the conditions maximizing the productivity of a photobioreactor as a whole, it is necessary to understand the coupling among hydrodynamics and mass transport, radiation, and cellular growth kinetics. Modeling approaches, which invoke excessively restrictive assumptions, such as mono-dimensionality in light transmission (Beer-Lamber law and its variants) or perfect mixing (Carvalho and Malcata, 2003; Krujatz et al., 2015), oversimplify the problem and are bound to provide scarce predictive accuracy (Csgör et al., 2001; Straub, 2011). The variation over time of the environmental physical features to which cells are exposed has to be accounted for. Indeed, flow hydrodynamics influences the availability of substrates for the cells and the history of cells exposure to light. Therefore, several approaches, such as the Lagrangian and Eulerian simulation approaches, have been developed to couple fluid dynamics and radiation transport with cell growth (Gao et al., 2018). In some articles, simulations are performed with simplifying assumptions with respect to the geometry, thus, simulating the phenomena internal to the reactor in 1D (Koller et al., 2017) or 2D (Wheaton and Krishnamoorthy, 2012) configurations, while in the most complete articles, the models are developed in a 3D configuration (Solimeno et al., 2015; Loomba et al., 2018). As for the analysis of the phenomena principally analyzed in our article, i.e., those related to light transmission, many different simulation scenarios are reported in literature. In some cases, the transmission of light radiation is supposed to be monodirectional (Zhang et al., 2015; Naderi et al., 2017), while in other cases, like ours, all possible directions of propagation are considered (Zhang et al., 2015). Furthermore, it is worthwhile to note that the culture medium is multiphasic as it includes a liquid (nutrients, dissolved reagents, and reaction products), gaseous (bubbles), and solid phase. Hence, in a faithful reproduction of light transmission, it is appropriate to consider the specific effects of the different components with the help of different parameters related to the absorption and scattering of the light. However, the medium is usually assumed to exhibit a single liquid phase. As a consequence of this unrealistic assumption, the effect of light scattering/absorption due to bubbles (Csgör et al., 2001; Zhang et al., 2015) is not accounted for. Similarly neglected is the effect of light absorption by particles (Seo et al., 2014; Solimeno et al., 2017), which induces the classical shadow effect, decreasing the amount of light available to the bacterial cells as one moves away from the light source. Our modeling approach, instead, explicitly accounts for the multiphysical nature of the environment within the reactor. When these phenomena are considered, the related coefficients are usually set according to the literature (Fernández et al., 2012; Naderi et al., 2017), whereas in our study, they are fitted from experimental data. The correct modeling reproduction of the light pattern makes it possible to improve the accuracy in simulating the biochemical phenomena taking place inside the reactor (Fernández et al., 2012), and to correlate bacterial growth and its possible limitation and inhibition with light transmission (Huang et al., 2012; Koller et al., 2017; Zhang et al., 2017).

This study proposes a 3D multi-physics mathematical model of a flat-panel photobioreactor, developed on the Comsol® platform, which enables the comprehensive simulation of different phenomena such as thermo-fluid dynamics, cyanobacterial growth kinetics, mass transfer, and light transmission by formulating the corresponding equations. The discrete ordinates method was used to calculate the light radiation in all the photobioreactor domains for each time step. Computing particle trajectories was instrumental to characterize the exposure of individual cells to light, which primarily influences the growth rate, biomass concentration, and ultimately, biomass productivity. Local light radiation

profiles were simulated in order to assess the amount of light that is actually perceived and absorbed by bacterial cells in relation to different illumination conditions. The validity of the model was examined by comparing model predictions with direct measurements of key process parameters. Here, with our approach, we could appraise the remarkable difference between the externally supplied light and the light received by the cells and we could deepen the plurality of the underlying reasons. We linked the study of light transmission inside the PBR vessel and the exploration of the residence time of bacterial cells in different PBR domains to the experimental observation of cyanobacterial physiological parameters. Our modeling framework is able to couple the reconstruction of single cell trajectories across differently irradiated PBR zones with cellular growth kinetics. Therefore, our simulation framework is exploitable to screen and identify the operating conditions of the photobioreactor which optimize the accumulation of productive algal biomass.

The understanding generated by our model, which unveils otherwise inaccessible characteristics of an artificially lit photoautotrophic cultivation environment, allows guiding the PBR optimization toward an enhanced biomass photosynthetic growth efficiency and productivity. Nonetheless, the complete realization of the extrapolation capabilities of a modeling approach requires the model to be a representative of the system of interest. In this regard, we argue that, as a prerequisite of the implementation of effective modeling, it is crucial for the model to be backed by consistent process data acquisition and management. We show, with a tailored experimental design, how the predictions of relevant process characteristics resulting from the model depend on the existence of accurate information concerning both the light entering and the light leaving the photobioreactor.

To unveil the interrelationships between model predictions and the nature of light at the entrance of the photobioreactor, our experimental plan varied the intensity of the light supplied to the photobioreactor from 50 to 1,200 μE every 24 h under three different types of calibration of the LED light source. According to our results, the initialization of the source of light at the entrance of the photobioreactor should not be limited to the prearranged light intensity but should also account for the effects related to the specific calibration procedure. Indeed, our results demonstrated that setting the model with the light resulting from different calibrating configurations impacts differently on the local light distribution inside the photobioreactor and thus on the light that is actually perceived by the bacteria, obviously influencing microorganism growth kinetics.

Alongside a careful definition of the light entering the photobioreactor, we demonstrated the benefits of accompanying the modeling with measurements of light intensity at the exit of the photobioreactor under both abiotic and biotic culture conditions. Indeed, informing the model with experimental data acquired in the absence/presence of photosynthetic cells facilitates the estimation of the interconnections between local environmental traits and *Synechocystis* physiological and growth attributes.

This work proposes an innovative modeling framework which allows gaining insights in the complex relationships between several light characteristics and cell physiology. Furthermore, our analysis highlights the opportunities and challenges in properly constraining the model with decisive qualitative and quantitative data related to the light at the entrance and at the exit of the photobioreactor.

MATERIALS AND METHODS

Pre-cultures Conditions

For all the experiments, the pre-cultures of glucose-tolerant wild-type *Synechocystis* sp. PCC6803, kindly provided by Devaki Bhaya (Department of Plant Biology, Carnegie Institution for Science, Stanford, CA, United States), were prepared by growing cells in flasks in 25 ml of BG 11 medium with a modified recipe as described in van Alphen and Hellingwerf (2015).

Pre-cultures were grown for 1 week at 30°C in a shaking incubator at 120 rmp (Innova 44, New Brunswick Scientific, Edison, United States) under constant white light illumination at approximately 50 μmolphotons $m^{-2}s^{-1}$ (μE), measured with the photometer (2102.2, Delta Ohm s.r.l, Padua, Italy).

PBR Growth Conditions

Synechocystis pre-culture was used to seed a temperature-controlled flat panel photobioreactor (PBR)—model FMT150.2/400 (Photon Systems Instruments, Drasov, Czech Republic) (Nedbal et al., 2008)—with 20 ml of culture. This study was performed in a customized 380 ml vessel for FMT150 (**Supplementary Figure 1**). Cells were grown in the BG11 medium modified as described above and supplemented by 10 mM of NaCHO3.

The lid of the PBR held a combined pH/temperature probe and a Clark-type dissolved O_2 (dO_2) probe (Photon Systems Instruments, Drasov, Czech Republic). The optical density (OD) was measured by an integrated densitometer at 720 and 680 nm. The temperature was settled at 30 ± 1°C and pH ~ 8.

A constant supply of CO_2 was provided by sparging the medium with 1% CO_2 (v/v) in N_2. A gas mixer (GMS150 micro, Photon Systems Instruments, Drásov, Czech Republic) coupled to a mass flow controller (EL-FLOW prestige FG-201CV, Bronkhorst High-Tech BV, AK Ruurlo, Netherland) were employed to supply 150 ml/min of gas mixture to the PBR.

The cellular suspension was illuminated from one side of the PBR by orange–red light (636 nm) emitting diodes (LEDs). The light calibration was performed with the assistance of the PBR software and the use of a light photometer (2102.2 photometer, Delta Ohm s.r.l, Padua, Italy), as shown in **Supplementary Figure 2**. For each VDC value (0–100%) set by the PBR software, we adopted three different types of calibration of the LED panel, which differed in the relative distances between the light meter and the LED panel and in the position(s) selected for acquiring the light intensity measurement(s). We refer to the three calibration setups under consideration in our study as case 1, case 2, and case 3 (**Figure 1**). More in detail, in case 1, the light sensor was positioned on the LED light panel and a single

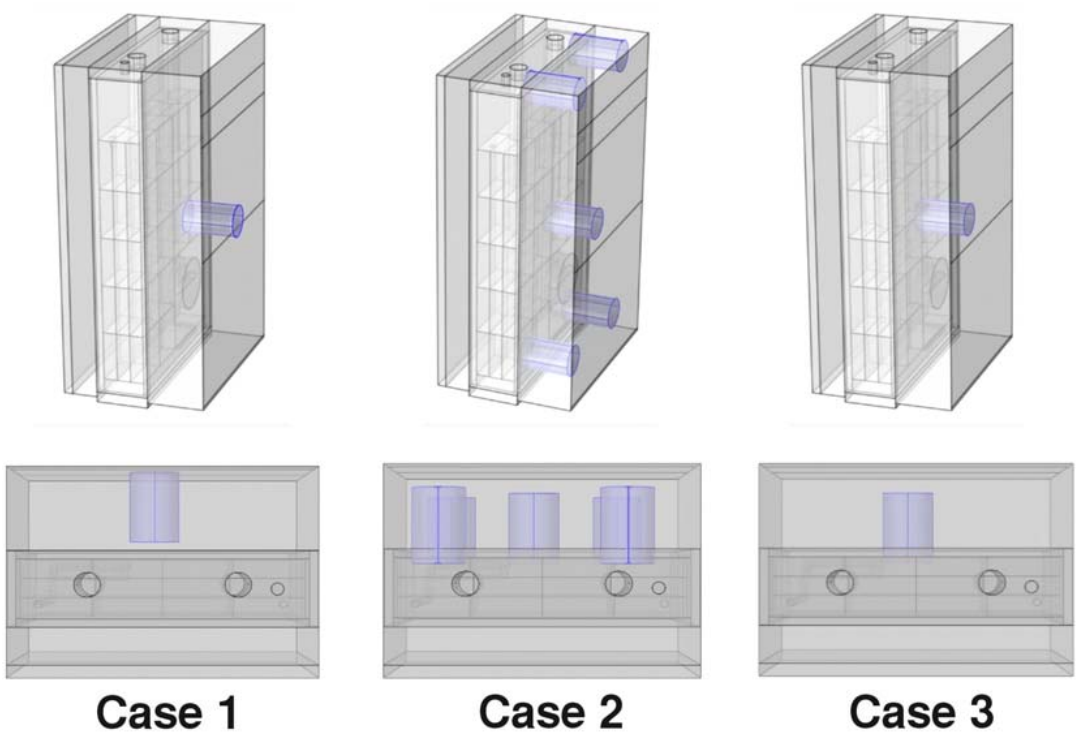

FIGURE 1 | Positioning of the PAR probe for the three calibration procedures. Calibration cases 1, 2, and 3 are shown from left to right. In case 1, the light sensor was positioned on the LED light panel and a single measure was acquired in the middle position of the panel. In case 2, the light sensor was positioned at 1 cm from the LED panel and the measurements acquired in the central position and in four angular positions. In case 3, the light sensor was positioned at 1 cm from the LED panel and a single measure was acquired in the middle position.

measure was acquired in the middle position of the panel. In case 2, the light sensor was positioned at 1 cm from the LED panel and the measurements acquired in the central position and in four angular positions (**Figure 1**) were averaged, Finally, in case 3, the light sensor was positioned at 1 cm from the LED panel and a single measure was acquired in the middle position.

For each configuration tested in the calibration stage, cells were grown at 50, 100, 200, 300, 500, 950, and 1,200 μmolphotons $m^{-2}s^{-1}$. Cyanobacterial cultures were subject to increasing light intensities every 24 h and each light regime was kept for at least 24 h as this time frame was found to be long enough for reaching a stable growth rate and dissolved oxygen in the culture medium (**Supplementary Figure 3**). For each light regime settled, the light in output from the PBR was measured at the central and angular positions, both in the presence and absence of the *Synechocystis* culture. Experiments were performed in three replicates for calibration case 1 and in two replicates for calibration cases 2 and 3.

The PBR was run in a semicontinuous mode by controlled dilution (turbidostat) of the growing cell suspension. Dilution was based on the changes at OD720, measured by the integrated densitometer and calibrated to the benchtop spectrometer OD730 to maintain the OD730 approximately at 0.4 ± 2.5%. Dilution was performed by a peristaltic pump automatically controlled by the software of the photobioreactor. The range of 2.5% was intentionally chosen to be large enough to allow the software to calculate the cells growth rate from the curve of the OD slope between the dilutions.

Dry Weight

For the determination of the dry cell weight, at the end of each 24 h step light increment, an aliquot of 20 ml of culture was harvested in a sterile 50 ml falcon tube. The suspension was pelleted at 1,500× g at room temperature for 15 min. The supernatant was gently removed, and the pellet was delicately washed with 2 ml of sterilized MilliQ water to remove medium salts. The sample was again pelleted at 1,500× g for 15 min, the supernatant was carefully removed and other 2 ml of MilliQ distilled water were used to resuspend the pellet in a preweighted 2 ml eppendorf. After centrifugation (1,500× g for 15 min), the supernatant was discarded. The tubes were subsequently dried overnight in a stove at 90°C and finally weighted again. In parallel, the OD730 of the sampled cells was measured with a Bench spectrophotometer (7315, Jenway, Staffordshire, England) and used to normalize the dry cell weight per OD730 (Andreas Angermayr et al., 2016; Du et al., 2016; Cordara et al., 2018).

Determination of Photosynthetic Efficiency

The photosynthetic efficiency was calculated as grams of biomass formed per mole of photons (van Alphen and Hellingwerf, 2015;

Luimstra et al., 2019). We calculated the amount of light available to the culture as the difference between the light in input to the PBR, which we called $I_{s,in}$, and the light remaining after the passage through the PBR, which we called I_{out}. I_{out} was both experimentally measured and calculated through model simulations in order to calculate the amount of light absorbed in the reactor volume. We used the growth rate and cell dry weight values to calculate the amount of biomass produced in the actual volume during 24 h for each $I_{s,in}$ used.

Mathematical Model Description

The 3D multi-physics, multi-component, multi-phase, and not isothermal model of the photobioreactor was developed on the COMSOL 5.5® platform and allowed us to simulate different phenomena such as fluid dynamic, heat transfer and radiation in different media, bacterial growth kinetics, gas-liquid mass transfer, transport of species, and particle tracing by formulating the corresponding equations. **Supplementary Table 1** reports the equations sets described in detail in Cordara et al. (2018). Particle tracing related equations are described separately in the following.

Supplementary Figure 4A shows the general design of the 3D model based on the PBR geometry. It is worth noting that our model accounts also for the presence of the glass and probes for O_2 and pH inside the liquid mixture (**Supplementary Figure 1D**) and their effect on light transmission. **Table 1** contains the geometrical parameters of the vessel.

Free tetrahedral meshing was applied to the created model prior to analysis (**Supplementary Figure 4B**). Meshing size (1,253,654) was selected in order to prevent model inaccuracy and imprecision resulting from model meshing. In fact, with this huge number of tetrahedral elements we are able to perform the calculations with an adequate degree of convergence of the results.

Particle Tracing

In addition to the previously considered equations, in this work, we also take into account the presence of solid particles. The assumptions underlying this type of modeling are described as follows:

(i) the particles have a spherical geometric shape;
(ii) particle initial mass and density has been derived from the experimental results;
(iii) particle motion inside the reactor is straightly linked to the fluid-dynamic calculations;
(iv) the reactions take place at the bacterium/liquid mixture interface;
(v) particle growth during the cultivation period is calculated through Eq. (33) in **Supplementary Table 1** and is homogeneous for all the particles.

TABLE 1 | Geometrical parameters of the PBR and its components.

Domain	Element size	[m]
Reator	Height	0.1983
	Width	0.11
	Thickness	0.024
Sparger	Diameter of inlet	0.002
	Diameter of holes	0.0004
	Number of holes	7
	Lenght	0.03
Anchor	Diameter	0.006
	Lenght	0.035
Vessel	Glass Thickness	0.0033

The particle trajectory and physical properties in the photobioreactor is determined by the particle tracing module for the fluid flow interface in Comsol®. In this module, the motion, v_p, of a particle with mass m_p in the vessel is described by Eq. (34) in **Supplementary Table 1** (Seo et al., 2014).

$$\frac{d}{dt}\left(m_p v_p\right) = F_D + F_g + F_{ext} \tag{1}$$

where F_D and F_g are, respectively, the drag and gravity force the particles are subjected to. F_{ext} stands for some additional (e.g., electric, magnetic) force acting on a particle. The particle momentum is defined by Newton's second law, which states that the net force on a particle is equal to the time rate of change of its linear momentum in an inertial reference frame (Loomba et al., 2018).

The drag force is defined by Eq. (35) in **Supplementary Table 1**.

$$F_D = m_p F_d (v - v_p) \tag{2}$$

where $F_d = 18\eta/(\rho_p {d_p}^2)$ is the drag force per unit mass, ρ_p the particle density, and d_p the particle diameter. The gravity force is defined by Eq. (36) in **Supplementary Table 1**.

$$F_g = m_p g \frac{\rho_p - \rho}{\rho_p} \tag{3}$$

From the particle velocity, its trajectory, x_p, is determined by solving the differential equation

$$\frac{dx_p}{dt} = v_p \tag{4}$$

When the particle mass is being computed, such that accretion or evaporation can take place, the mass is moved outside the time derivative to prevent non-physical acceleration of the particles. This assumption is that any mass lost by the particles continues to move with the particle velocity and does not cause the particle to decelerate.

We also consider particle-particle interactions to make particles exert forces on each other (linear elastic forces) as described by Eq. (38) in **Supplementary Table 1**.

$$F = -k_{EL} \sum_{j=1}^{N} \left(|r - r_j| - r_0\right) \frac{r - r_j}{|r - r_j|} \tag{5}$$

Where k_{EL} is the spring constant (N/m), r_0 (m) is the equilibrium distance between particles, and r (m) is the relative distance between particles.

RESULTS

Cyanobacteria are remarkably promising oxygenic phototrophic cell factories for manifold applications through the integration within innovative business models (Venkata Mohan et al., 2016).

Since the livelihood of cyanobacteria is directly dependent upon light, the technological exploitation of photosynthetic chassis strains is obligatorily reliant on a comprehensive investigation and understanding of the interrelationships between the irradiated light and the physiological traits of the cyanobacterial cells in the artificially lit cultivation environment (Andersson et al., 2019; Luimstra et al., 2019; Ho et al., 2020). To this aim, we designed an experimental campaign to explore the effects of illumination characteristics, including variation of orange-red light intensities and calibration procedures, on cyanobacterial physiology in a flat-panel photobioreactor. The experimental dataset on cyanobacterial physiology at varied illumination conditions was complemented with model simulations comprehensive of heat transfer with light transmission, fluid dynamics, and cellular growth kinetics. It was of utmost importance to acquire experimental data both in the absence and in the presence of cyanobacterial cells in order to facilitate the estimation of the radiation parameters employed in our modeling framework.

The exploration of the calibration effects on our simulation-aided analysis of the artificially lit flat-panel bioreactor envisaged three possible configurations thereafter referred to as calibration case 1, case 2, and case 3 and illustrated in **Figure 1**. Different from case 1, where the light sensor is placed on the LED panel, cases 2–3 envisage the light sensor at 1 cm from the LED panel. Cases 2 and 3 differ from each other by the number of measurement points used for light calibration, one central position and four angular positions for case 2 and one central position for case 3. To unveil the interrelationships between the illumination of the photobioreactor and the exposure of cyanobacterial cells to light, our experimental plan varied, for each type of calibration of the LED panel, the intensity of the light preset for the photobioreactor from 50 to 1,200 μE. The increase in the incident light intensity occurred every 24 h and the cell cultures were maintained at each light regime for at least 24 h. The duration of the exposition time at a certain lightening was indeed sufficient to achieve stable measurements of growth rate and dissolved oxygen in the culture medium (**Supplementary Figure 3**). For each light regime settled, the light in the output from the PBR was measured at the central and angular positions, both in the presence and in the absence of the *Synechocystis* culture.

Model Accurately Predicts the Phototrophic Properties of the Cell Culture

The experimental values of the transmitted light and of the light detected at the vessel output, in biotic and abiotic conditions, have been used to fit the parameters related to light transmission in the various PBR domains taken into consideration, namely: air, vessel glass, stainless steel (wall, probes, and sparger), water with medium, bacteria, and gas bubbles (**Supplementary Figure 1**). The estimated parameters set was used to obtain the modeled trends for cyanobacterial growth rate (**Figure 2A**) and oxygen released in the medium (**Figure 2B**). The agreement between the experimental and simulated values with regard to both of these physiological traits demonstrates the solidity of the model built. The effect of different calibration approaches on growth rate μ and dissolved oxygen is neatly evident at the extreme light intensities which were set in our experiments. Specifically, **Figure 2** shows the existence of opposite trends in the extreme regions corresponding to low incident light ($I_{s,in} < 400$ μE) and high incident light ($I_{s,in} > 600$ μE). In the intermediate region ($400 < I_{s,in} < 600$ μE), the values of μ and dissolved oxygen are almost uniform. In the low incident light region, we noticed a higher growth rate in the calibration cases 2–3 than in the case 1, with a more pronounced oxygen production for case 2 with respect to case 3. In the high incident light region, the trend is reversed with growth being faster in case 1 than in cases 2–3. This observation is due to the fact that in the calibration case 1, where the sensor is placed on the panel, the value of light intensity preset via software can be achieved by supplying less electrical power to the panel compared to cases 2–3, and that, as a consequence of it, LEDs emit at lower light intensity. When we place the sensor at 1 cm from the panel, according to the calibration cases 2–3, calibration is necessarily influenced by the absorption and scattering of light, which occurs in the space separating the sensor from the panel, and by the absorption of light by the

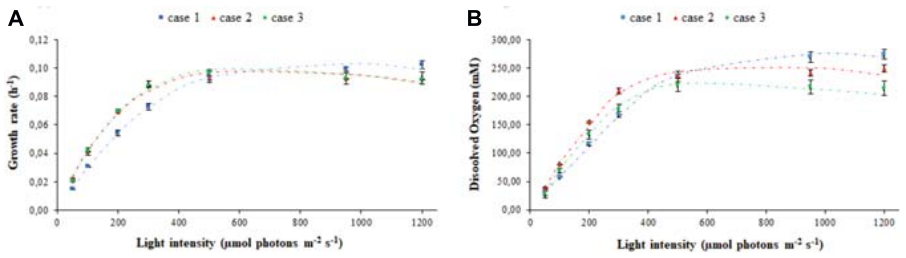

FIGURE 2 | Calibration affects the assessment of photo-limited, photo-saturated, and photo-inhibited growth of cyanobacterial cells. Shown are the experimental (symbols) and simulated (dashed line) values of **(A)** growth rate and **(B)** oxygen released in the medium by *Synechocystis* at increasing light intensity $I_{s,in}$, in relation to each calibration case. Symbols show the mean values over the biological replicates for each calibration case and are accompanied by their respective standard deviation bars.

surrounding black surfaces (Huang et al., 2011). Therefore, in the calibration cases 2–3, the LED panel has to be supplied with more electrical power and the LEDs have to emit light at a higher intensity to measure the prescribed light intensity in the sensor. Consequently, the light at which bacteria are exposed in the calibration case 1 is attenuated, when compared to the calibration cases 2–3. Since cyanobacterial photoinhibition is known to be induced by extreme high light intensity (Ogawa et al., 2018), it follows that, when the prescribed light intensity is low, bacteria grow faster (**Figure 2A**) and release more oxygen in the medium of the PBR (**Figure 2B**) in the calibration cases 2–3 than in the case 1. When the prescribed intensity is high, the physiological response of the bacterial culture is opposite: bacteria grow faster, and the dissolved oxygen registered in the medium is higher in the case 1 than in cases 2–3. Therefore, our experiments quantitatively show that calibration affects the physiological traits of the cyanobacterial culture in a non-negligeable manner.

The values inferred for the light at the outlet of the photobioreactor were contrasted with those experimentally determined, in the abiotic (**Figure 3A**) and biotic (**Figure 3B**) cases in each calibration setup. In the abiotic condition, modeling effectiveness is largely insensitive to the calibration choice and the prescribed light intensity at the photobioreactor entrance. In the biotic condition, predictability was found to generally improve with increasing light intensity and to be influenced by the calibration choice. In this regard, our model is particularly effective in inferring the transmitted light in calibration case 2 whereby the light sensor is placed at 1 cm from the panel of LEDs and the light intensities measurements at the central and angular positions are averaged.

Moreover, the outlet light intensities derived from our model simulations were employed to estimate the light-dependent photosynthetic efficiency of the photobioreactor in terms of grams of biomass produced per mole of photons available in the photobioreactor. The full agreement with photosynthetic efficiency values derived from experimentally acquired outlet light intensities confirmed the plausibility of our modeling framework (**Figure 4**), As expected at low OD batch cultures, the photosynthetic efficiency of *Synechocystis* obtained by our model simulations showed that efficiency starts to drop the fastest in the initial increase in intensity. Furthermore, owing to the aforementioned dependency of incident light on calibration, this trend appeared accentuated in the calibration cases 2–3 where efficiency turned out to decrease from the highest value, observed at 50 μE where 0.47 g (case 2) and 0.45 g (case 3) of biomass were produced per mole of photons available to the PBR domains, to the lowest value observed at 1,200 μE where 0.12 g (cases 2–3) of biomass were produced per mole of photons. In summary, we provided a quantitative study of light-limited, light-saturated, and light-inhibited growth of the cyanobacterium

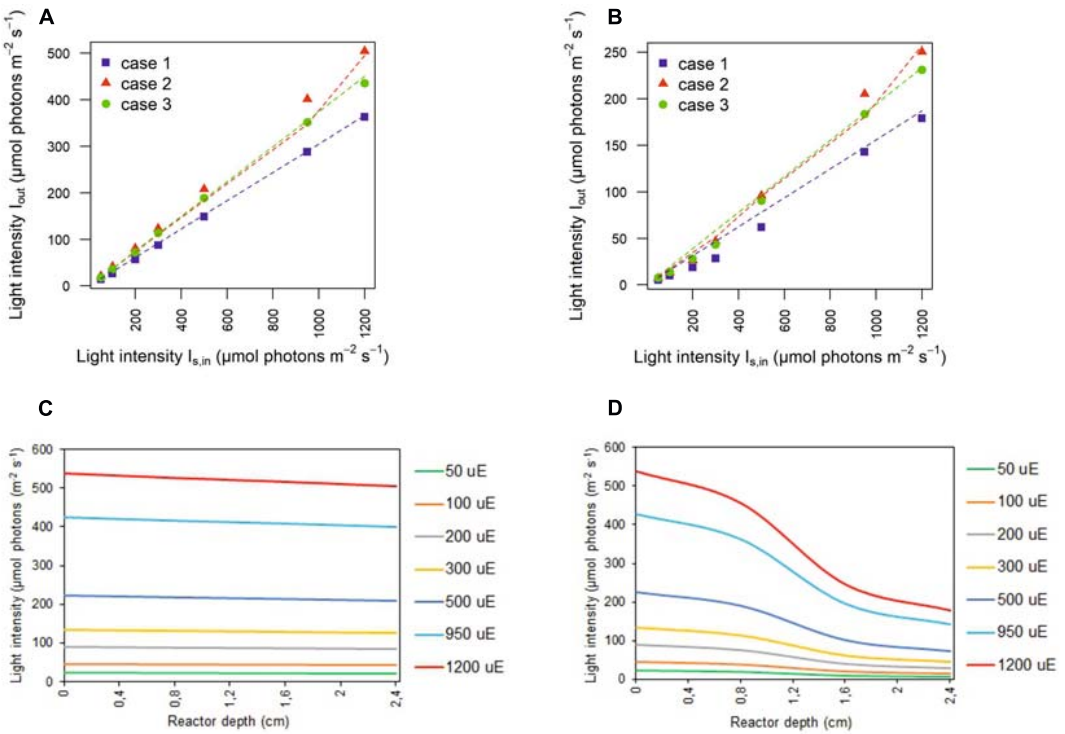

FIGURE 3 | Simulated light intensities recapitulate experimental light intensities at the outlet of the photobioreactor. Comparison between experimental (symbols) and simulated (dashed line) light intensities at the outlet of the photobioreactor in correspondence to each calibration case at increasing light intensity $I_{s,in}$ in abiotic **(A)** and biotic **(B)** conditions. Symbols show the mean values over the biological replicates for each calibration case. The light transmitted along the PBR depth is attenuated as a result of cyanobacterial cells. 1D trend of simulated light intensity along the reactor depth for the calibration case 1, in abiotic **(C)** and biotic **(D)** configurations.

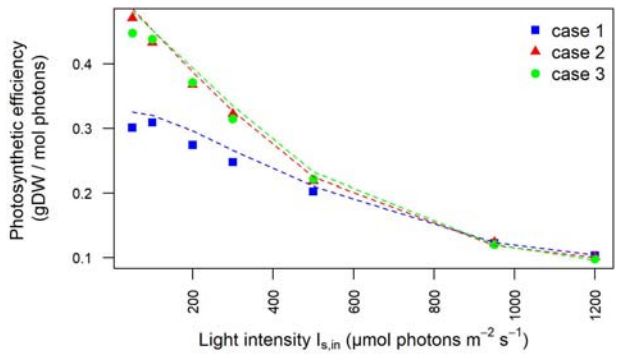

FIGURE 4 | Photosynthetic efficiency dependency on light intensity is influenced by calibration. Photosynthetic efficiency is displayed at increasing light intensity under each calibration case. The values derived from experimentally determined light intensities at the inlet and outlet of the photobioreactor are shown by symbols. The photosynthetic efficiency values derived from simulated light intensities at the inlet/outlet of the photobioreactor are shown by dotted lines.

Synechocystis sp. PCC 6803 by monitoring key physiological properties, such as changes in dry weight, gas exchange (O_2), and photosynthetic efficiency under different lightening and calibration setups in a controlled cultivation environment. The results obtained in this study showed that a quantitative experimental assessment of phototrophic parameters is subject to a number of technical difficulties, which are often reported in insufficient detail. In particular, our analysis illustrated the influence of calibration choices on the characterization of phototrophic growth and activity, which, when superficially treated, can make direct comparison of the literature data difficult and drawn conclusions faulty.

Light Intensity Profiling Within the Flat-Panel Photobioreactor

The outlined observations and the plausibility shown by our model elicited our interest to exploit our simulation framework to explore the properties of the light that is actually perceived and absorbed by bacterial cells while migrating within the artificially lit vessel of the photobioreactor. The local light intensity profiles were simulated at increasing red-orange light intensities ($I_{s,in}$), ranging between 50 and 1,200 µE, for each type of calibration of the LED panel. By way of example, **Figure 5** and **Supplementary Figure 5** show the local light intensity profiles corresponding to $I_{s,in}$ = 300 µE and $I_{s,in}$ = 1,200 µE for the three calibration settings in both biotic and abiotic conditions. Close inspection of our simulation results allowed us to discern fine-grained features of light intensity distribution owing to distinct factors. Sources of variation of the light spatial distribution were identified in the boundary regions, at the interface between the gaseous and liquid phase and at the interface between the liquid phase and the bottom steel base, as well as in the rotating domain created by the stirring bar, as previously detailed in Cordara et al. (2018). Additionally, it is worthwhile noting that these patterns were more accentuated at decreasing values of the incident illumination intensity (Huang et al., 2011). Contrasting the local radiation profiles in various calibration cases allowed us to confirm that the calibration cases 2–3 favor light transmission inside the vessel more than the calibration case 1, at both low and high $I_{s,in}$, as highlighted in **Figure 5** and **Supplementary Figure 5**.

Biotic Effects on Light Transmission in the Photobioreactor Vessel

Contrasting the abiotic and biotic cases allowed us to notice the effects which could be ascribed to the presence of the bacterial culture on light transmission inside the PBR vessel. For each irradiated light and calibration choice analyzed in the biotic cases, light absorption and scattering by bacterial cells accentuated the attenuation of the incident light intensity, when compared to the abiotic cases (Olivieri et al., 2015). In particular, we noticed approximately 6% of light lost in the liquid phase in the abiotic cases against 66% of light lost in the biotic cases, regardless of the calibration setup and of the incident light intensity (**Supplementary Table 2**). In this regard, the 1D trends of simulated light intensity show a more accentuated light attenuation along the reactor depth, in the biotic case (**Figure 3D**) compared to the abiotic one (**Figure 3C**), by way of example, in calibration case 1. Therein, we could notice the highest loss of irradiated light in the inlet and middle area of the vessel (Csögör et al., 1999; Gao et al., 2017a; Naderi et al., 2017). The results of our simulations are in line with the experimentally determined values of light leaving the cultivation system which were previously described in the abiotic (**Figure 3A**) and biotic (**Figure 3B**) cases.

As shown in **Figure 5** and **Supplementary Figure 5**, light absorption and scattering by bacterial cells accentuated also the heterogeneity in the light intensity distribution within the liquid phase, when compared to the abiotic case (Soman and Shastri, 2015). These effects get more pronounced as the incident light intensity gets lower. Light reduction is obviously accentuated in the light inlet area of the vessel where, by virtue of reactor design in this study (**Supplementary Figure 1**), bacterial cells tend to move by effect of the local liquid movement propelled by the stirring bar rotation.

Characterization of Light Perception and Absorption by Single Particles

We then employed our modeling framework to relate the trajectories of bacterial cells in the PBR domains featuring different light intensities to cyanobacterial growth. Particle tracing simulations, shown by way of example in **Supplementary Figure 6**, provide time-dependent trajectories of the light intensity perceived by individual cells and afford the visualization of kinetic and radiation characteristics on particles' skin (Olivieri et al., 2015; Loomba et al., 2018). We thus computed the one-dimensional trends of the radiation perceived by individual cells along the simulated time (Olivieri et al., 2015; Soman and Shastri, 2015; Iluz and Abu-Ghosh, 2016). The average value of the perceived light intensities over all the cells at each discrete time in the 1 h window of simulated process is displayed in **Figure 6** in the three calibration cases at two extreme light intensities,

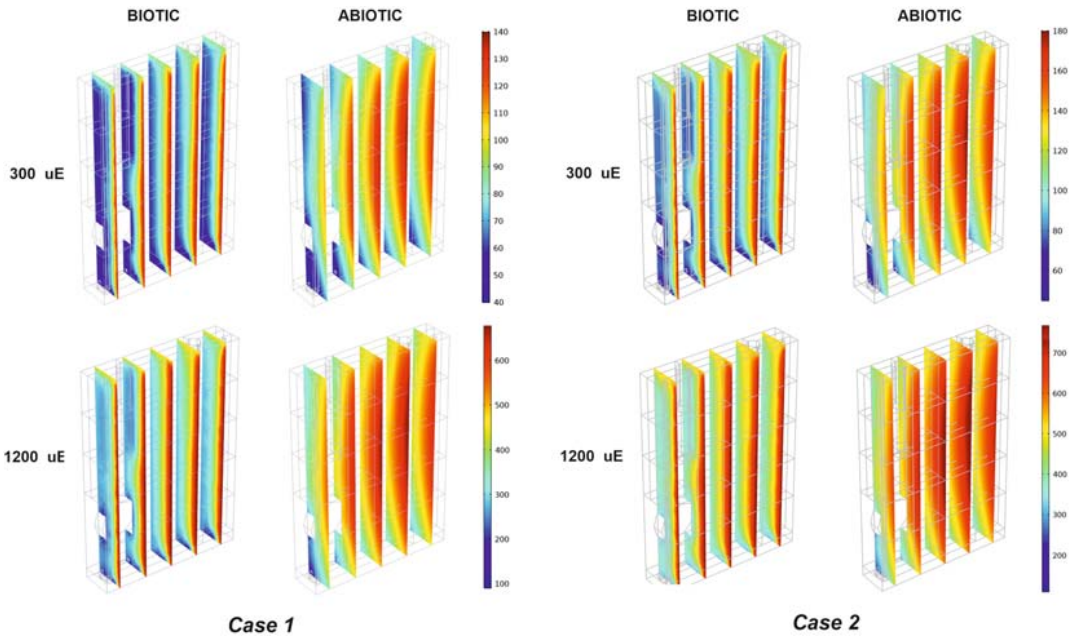

FIGURE 5 | Biotic effects on light transmission through the photobioreactor depend on the incident light and calibration. 3D trend of perceived light intensity along YZ slices of the model PBR acquired at 24 h of simulated time for calibration cases 1–2, in biotic and abiotic conditions, at 300 and 1,200 μE.

300 and 1,200 μE. The shown trends, net of fluctuations ranging between 3 and 6% of the average over the whole cells, and 1 h simulated time, confirmed that, at a certain settled $I_{s,in}$ value, the calibration setup influences the light actually perceived by cyanobacterial cells, with the latter being higher in cases 2–3 than in case 1. Moreover, the influence ascribed to calibration became accentuated when lowering the settled light intensity.

Figure 7, which reports the averaged values over the whole cells at a discrete simulated time, confirms that the light intensity that is actually perceived and absorbed by bacterial cells is substantially lower than the light prescribed. The perceived light (I_p) is reduced by approximately 64% in calibration case 1, 53% in calibration case 2, and 52% in calibration case 3. When considering the amount of light absorbed by the culture (I_{ab}), our simulation results show that in case 1, the culture absorbs about 27% of the light sent; in case 2, about 32%; and in case 3, about 34% (**Supplementary Table 3**). As previously noted, the main difference in the light perceived and absorbed is registered between case 1 and cases 2–3, where the trends are similar to each other, for each simulated incident light intensity.

Estimation of the Photosynthetic Regime of the Algal Culture by the Simulation Framework

The parameters of the modified Monod kinetics were fitted using a self-implemented Matlab code according to Eq. (33) (del Rio-Chanona et al., 2018). The relevant parameters are μ_{max}, $k_{I,s}$, and $k_{I,i}$ which account for the maximum growth rate, light saturation, and photo-inhibition, respectively. These parameters are only dependent on cyanobacterial properties and were fitted from the experimental data on the growth rate previously displayed in **Figure 2** and employed to obtain the modeled trends also shown in the same figure. The estimated values for the parameters in the Monod kinetics model are reported in **Table 2**. The estimated parameters values enabled us to gauge how the different calibration setups of the radiant LED panel influence the photo-limitation regime under low light intensity, the photo-saturation regime under optimal light intensity, and the photo-inhibition regime under intense light intensities (Pilon et al., 2011; Kommareddy and Anderson, 2013). More specifically we could conclude that: (i) case 1 is associated with a higher photo-limitation compared to cases 2–3; (ii) case 1 is associated with a higher photo-saturation compared to cases 2–3; (iii) cases 2–3 are associated with accentuated photo-inhibition compared to case 1.

These results are reflected also in the trends of the photosynthetic efficiency displayed in **Figure 8**. Here, differently from **Figure 4**, the photosynthetic efficiency has been calculated from the simulated values of the light in input and output of the liquid phase (**Supplementary Figure 1**), hence referring only to the culture domain, and not to the whole reactor system, as it occurred in relation to **Figure 4**. As a consequence of it, the photosynthetic efficiency values displayed in **Figure 8** are clearly higher than those shown in **Figure 4**, since the estimates here do not take into account the losses of transmitted radiation due to the other domains of the photobioreactor (Huang et al., 2011). The lower values of the light perceived and absorbed by bacterial cells in case 1 compared to cases 2–3 reflected in the photosynthetic efficiency values: at lower incident light intensity, efficiency is 20% lower for case 1 than for cases 2–3, at high intensities the photosynthetic efficiency is 37% higher in case 1 compared to cases 2–3 (**Supplementary Table 4**). These findings justify the trends of growth rate and dissolved

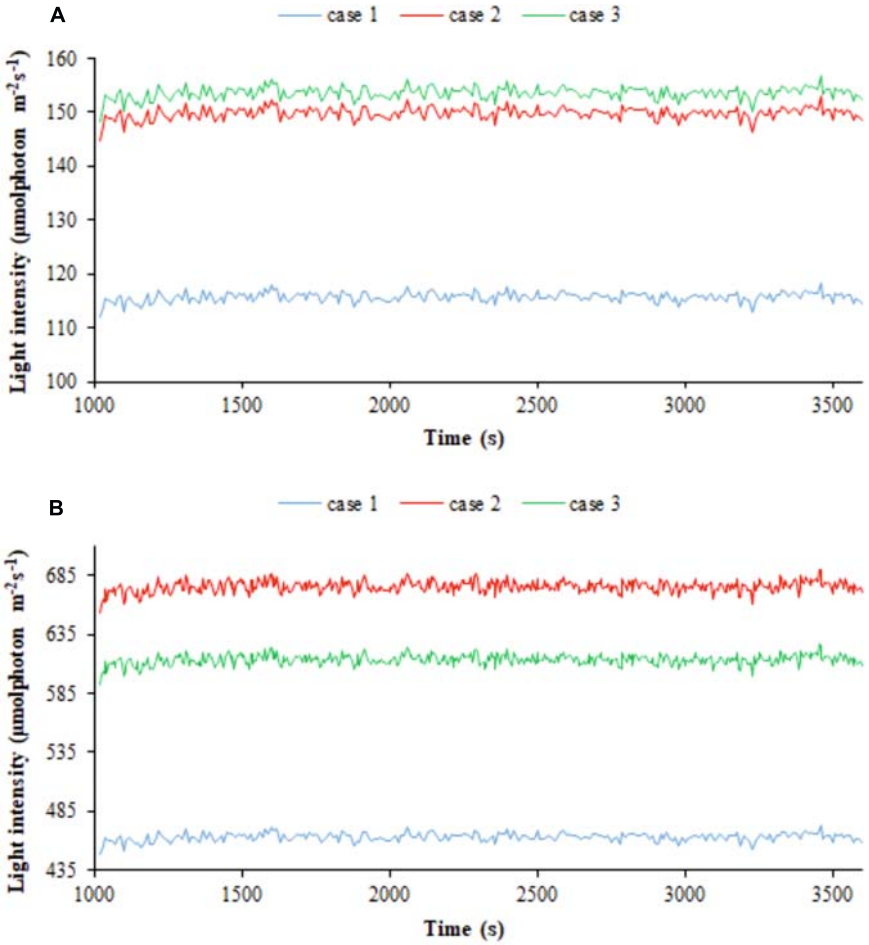

FIGURE 6 | Calibration influences the light perceived by individual cells. 1D simulated trends of radiation perceived by bacterial cells for the three calibration cases at **(A)** 300 μE incident light intensity and **(B)** 1,200 μE incident light intensity. The average of the simulated light intensity values perceived by all the particles is plotted along 1 h of simulated time. Calibration cases are color-coded.

oxygen shown in **Figure 2**, further validating the considerations previously proposed on the influence of calibration setups on the characterization of relevant physiological parameters.

Light Absorption Coefficient Depends on Bacterial Biomass Concentration

The estimation of the parameters related to the transmission of light in the modeled domain hosting the cell culture was enhanced by explicitly taking into account the experimentally detected light values and the simulation results pertaining cell density at different $I_{s,in}$ and growth kinetics (**Supplementary Table 5**). The relationship between the bacterial absorption parameter and the bacterial biomass concentration resulting from the fitting procedure is shown in **Figure 9**. The values and the trend obtained from our simulations and shown in **Figure 9** are in line with previously published reports according to which the absorption coefficient increases with increasing cell concentration (Agusti and Phlips, 1992; Molina Grima et al., 1994), varying from around 1.34 m^{-1} for 0.1 gDCW/L to around 4 m^{-1} for 2 gDCW/L (Zhang et al., 2015).

DISCUSSION

Optimal exploitation of the production capabilities of cyanobacterial growth potential is reliant on how the inherent properties of photobioreactors can be adjusted to create an environment able to accommodate the culture growth and physiology optimally. The photophysiological performances, which are usually detected experimentally, result from the superposition of several highly variable aspects related to gas exchange, mixing regime, reactor geometry, and light intensity distribution (Béchet et al., 2013; Huang et al., 2017). Direct access to the processes within the reactor environment is burdensome; therefore, simulation modeling is invaluable to shed insights into the reasons underlying the photosynthetic performances (Wang B. et al., 2020). The engineering and/or operational solutions consequently devised can improve biomass photosynthetic growth efficiency and productivity. For these reasons, we coupled the acquisition of experimental data from a carefully designed campaign to a mechanistic simulation modeling of a wide range of processes intervening in a conventional flat-panel

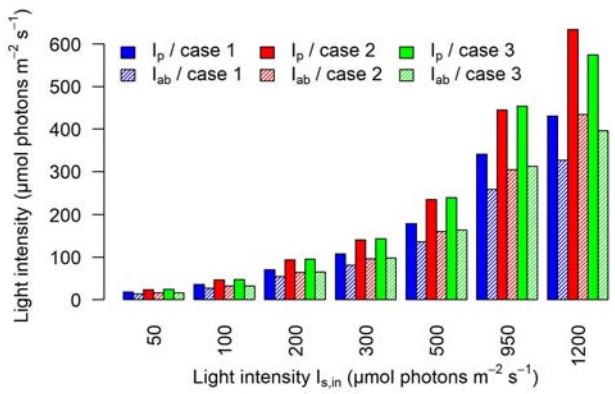

FIGURE 7 | Calibration affects the light perceived and absorbed by individual cells. The barplot shows the light perceived I_p and the light absorbed I_{ab} on average by cyanobacterial cells at each discrete simulated time, for each calibration case and each incident light intensity $I_{s,in}$.

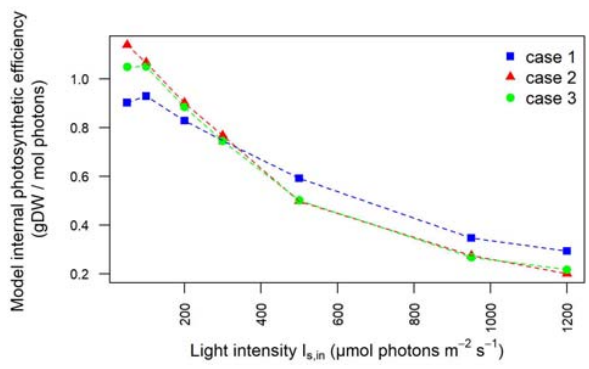

FIGURE 8 | Photosynthetic efficiency based on light intensities at the inlet/outlet of the liquid phase decreases at increasing light intensity. Photosynthetic efficiency is displayed at increasing light intensity under each calibration case. Calibration cases are color-coded. The values shown are derived from simulated light intensities at the inlet and outlet of the liquid phase.

TABLE 2 | Comparison of saturation/inhibition/limitation parameters corresponding to each calibration case.

Calibration	$K_{I,S}$ [W m^{-2}]	$K_{I,i}$ [W m^{-2}]	μ_{max} [h^{-1}]
Case 1	114.5	72.46	0.364
Case 2	43.32	114.9	0.221
Case 3	55.39	82.64	0.265

μ_{max}, $k_{I,s}$, and $k_{I,i}$ account, respectively, for the maximum growth rate, light saturation, and photo-inhibition.

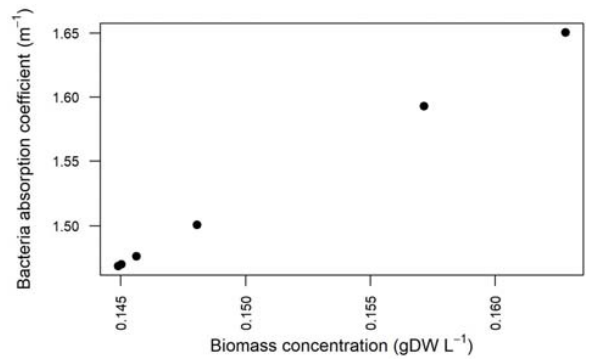

FIGURE 9 | Absorption coefficients for *Synechocystis* at different biomass concentration values for the three calibration cases.

photobioreactor in order to provide a quantitative study of light-limited, light-saturated, and light-inhibited growth of *Synechocystis* sp. PCC 6803 turbidostat cultures.

Robust quantification of light intensity dependence of cyanobacterial activity (Sarkar et al., 2019; Zavřel et al., 2019; Toyoshima et al., 2020) is instrumental for predicting a bioprocess performance and designing an efficient photobioreactor (Zhang et al., 2015; Papacek et al., 2018). Cyanobacterial physiology at different light regimes was thus characterized by gauging the oxygen evolution (Jeon et al., 2005; Cordara et al., 2018) and by expressing the photosynthetic efficiency as moles of photons absorbed per gram of biomass formed (Schuurmans et al., 2015). Our characterization of cyanobacterial response to increasing incident light intensities allowed us to identify a range of low incident light intensities, which afford fast cellular growth and pronounced release of oxygen in the medium, and a range of high light intensities inducing photoinhibition (Ogawa et al., 2018). Photosynthetic efficiency estimates were found in agreement with the observed oxygen evolution. The fast decrease of photosynthetic activity at moderately increased light intensity is in line with experimental data acquired also in previous studies, if we account for the difference existing in growth rate and light transmission (Schuurmans et al., 2015). Notably, we could observe that the highlighted trends were sensibly affected by the calibration choice.

The experimentally observed relation between the physiological properties and the supply of external light was effectively recapitulated, corroborating the validity of our modeling framework. Combining the simulation of the evolution of cells with the reconstruction of differently lit domains of the photobioreactor allowed us to relate the observed photophysiological properties to the transmission of light in the medium and to the patterns of light actually perceived and absorbed by bacterial cells. The acquisition of a deeper understanding of the relation between physiological traits and local patterns in light transfer can inform the photobioreactor design and the operational choices (Gao et al., 2018). Leveraging experimental data on light intensity and simulated data on cell density and growth kinetics, our modeling approach also allowed us to explore the dependence of light absorption on cell concentration (Huang et al., 2012). The latter reparameterization is useful to enhance our understanding of light distribution and, hence, to guide the optimization of the photobioreactor operating conditions (Huang et al., 2017).

Of particular interest were the trends of physiological parameters (growth rate, dissolved oxygen, and photosynthetic efficiency) at increasing light intensity with respect to different calibration cases. Indeed, we showed how the assessment of the physiological response to illumination depends on the initialization of the externally supplied light with regard not only to prearranged light wavelength and intensity but also to the specific light calibration procedure. Our simulation results demonstrated that setting the model with the light resulting from different calibrating configurations impacts differently on the local light distribution inside the photobioreactor and thus on the light actually perceived by the bacteria, obviously influencing microorganism growth kinetics.

In summary, our modeling framework can be integrated into procedures for effective and stable control based on the monitoring of process data that cannot be directly measured and for dynamic bioprocess modeling. The combination of experimental data acquisition and simulation modeling allows understanding how experimental data, often partially overlooked, have to be included to enhance the accuracy and extrapolation capabilities of the model to shorten the bioprocess development. Finally, our study suggests that full transparency in reporting experimental design and methodological details is paramount to reproduce and understand scientific outcomes and build upon valuable findings to foster the collective achievement of innovation goals in bioprocess engineering.

DATA AVAILABILITY STATEMENT

The original contributions presented in the study are included in the article/**Supplementary Material**, further inquiries can be directed to the corresponding author/s.

AUTHOR CONTRIBUTIONS

NV, AC, and AR: conceptualization. NV: modeling methodology. NV and AR: formal analysis and writing—original draft. AC and GU: experiments. AC: experimental data treatment. NV, AC, GU, and AR: writing—review and editing. All authors contributed to the article and approved the submitted version.

FUNDING

The research leading to this publication has received funding from the European Union's Horizon 2020 Research and Innovation Programme under grant agreement No. 760994 (ENGICOIN project). The funders had no role in study design, data collection and analysis, decision to publish, or preparation of the manuscript.

SUPPLEMENTARY MATERIAL

The Supplementary Material for this article can be found online at: https://www.frontiersin.org/articles/10.3389/fmicb.2021.639482/full#supplementary-material

Supplementary Figure 1 | (A) Body of the flat panel PBR FMT150.2/400 composed of a 390 ml transparent removable flat vessel. On top of the vessel, a stainless lid accommodates different tubes, connectors, and sensors. The base of the instrument contains a control unit with analogic and digital electronic circuits. Enlarged the details of the red and blue LEDs installed in the light panel of the reactor, the densitometer, and the fluorometer. **(B)** Red and blue LED spectra of PBR FMT150.2/400. **(C)** Transmission spectrum of cyanobacterial culture affected by light absorptions, light scattering. The lines and arrows indicate wavelength of the light sources present in the flat panel reactor and the detection range of the detector filter. **(D)** 3D modeled geometry of PBR with modeled domains selection: 1-closing, 2-inoculum, 3-sparger, 4-liquid immission, 5-sampling/liquid extraction, 6-culture, 7-stirring bar domain, 8-stainless steel walls of vessel, 9-base of vessel, 10-gas outlet, 11,O2 probe, 12-pH probe, 13-air, 14-glass walls of vessel, 15-LED panel.

Supplementary Figure 2 | LED panel calibration trendlines in the three calibration cases.

Supplementary Figure 3 | Stability of growth rate during 24 h at each step-wise increase in the intensity value $I_{s,in}$ supplied to the PBR. By way of example, the figure refers to the calibration case 1.

Supplementary Figure 4 | PBR design. **(A)** 3D CAD geometries and **(B)** system mesh.

Supplementary Figure 5 | 3D trend of perceived light intensity along YZ slices of the model PBR for calibration case 3, in biotic and abiotic conditions, at 300 and 1,200 μE.

Supplementary Figure 6 | 3D, lateral (XZ), and top (XY) view particles spatial distribution in function of skin velocity **(A)** and radiation perceived **(B)**.

Supplementary Table 1 | Model Equations. The table displays the equation sets employed to simulate each phenomenon included in the model. The table reports also the domains in the 3D geometry of the photobioreactor to which each listed equation applies.

Supplementary Table 2 | Experimental and simulated light intensities at the outlet of the PBR in abiotic and biotic configurations at increasing incident light intensity.

Supplementary Table 3 | Simulated values for the average light perceived and absorbed by bacteria at all the simulated $I_{s,n}$.

Supplementary Table 4 | Comparisons of efficiency of photosynthesis between the three calibration cases at increasing incident light intensity.

Supplementary Table 5 | Model parameters for heat transfer with radiation.

REFERENCES

Aden, M., Roesner, A., and Olowinsky, A. (2010). Optical characterization of polycarbonate: influence of additives on optical properties. *J. Polym. Sci. Part B Polym. Phys.* 48, 451–455. doi: 10.1002/polb.21906

Agusti, S., and Phlips, E. J. (1992). Light absorption by cyanobacteria: implications of the colonial growth form. *Limnol. Oceanogr.* 37, 434–441. doi: 10.4319/lo.1992.37.2.0434

Andersson, B., Shen, C., Cantrell, M., Dandy, D. S., and Peers, G. (2019). The fluctuating cell-specific light environment and its effects on cyanobacterial physiology. *Plant Physiol.* 181, 547–564. doi: 10.1104/pp.19.00480

Andreas Angermayr, S., van Alphen, P., Hasdemir, D., Kramer, G., Iqbal, M., van Grondelle, W., et al. (2016). Culturing *synechocystis* sp. Strain pcc 6803 with N2 and CO2 in a diel regime reveals multiphase glycogen dynamics with low maintenance costs. *Appl. Environ. Microbiol.* 82, 4180–4189. doi: 10.1128/AEM.00256-16

Asplund-Samuelsson, J., Janasch, M., and Hudson, E. P. (2018). Thermodynamic analysis of computed pathways integrated into the metabolic networks of E. coli and *Synechocystis* reveals contrasting expansion potential. *Metab. Eng.* 45, 223–236. doi: 10.1016/j.ymben.2017.12.011

Béchet, Q., Shilton, A., and Guieysse, B. (2013). Modeling the effects of light and temperature on algae growth: state of the art and critical assessment for productivity prediction during outdoor cultivation. *Biotechnol. Adv.* 31, 1648–1663. doi: 10.1016/j.biotechadv.2013.08.014

Bernaerts, T. M. M., Gheysen, L., Foubert, I., Hendrickx, M. E., and Van Loey, A. M. (2019). The potential of microalgae and their biopolymers as structuring ingredients in food: a review. *Biotechnol. Adv.* 37, 107419. doi: 10.1016/j.biotechadv.2019.107419

Broddrick, J. T., Welkie, D. G., Jallet, D., Golden, S. S., Peers, G., and Palsson, B. O. (2019). Predicting the metabolic capabilities of *Synechococcus* elongatus PCC 7942 adapted to different light regimes. *Metab. Eng.* 52, 42–56. doi: 10.1016/j.ymben.2018.11.001

Bucholtz, A. (1995). Rayleigh-scattering calculations for the terrestrial atmosphere. *Appl. Opt.* 34, 2765. doi: 10.1364/ao.34.002765

Caporgno, M. P., and Mathys, A. (2018). Trends in Microalgae Incorporation Into Innovative Food Products With Potential Health Benefits. *Front. Nutr.* 5:58. doi: 10.3389/fnut.2018.00058

Carvalho, A. P., and Malcata, F. X. (2003). Kinetic modeling of the autotrophic growth of Pavlova lutheri: study of the combined influence of light and temperature. *Biotechnol. Prog* 19, 1128–1135. doi: 10.1021/bp034083

Choi, S. Y., Lee, H. J., Choi, J., Kim, J., Sim, S. J., Um, Y., et al. (2016). Photosynthetic conversion of CO2 to farnesyl diphosphate-derived phytochemicals (amorpha-4,11-diene and squalene) by engineered cyanobacteria. *Biotechnol. Biofuels* 9, 202. doi: 10.1186/s13068-016-0617-8

Corbion (2020). Available online at: http://www.corbion.com/ (accessed December 6, 2020)

Cordara, A., Re, A., Pagliano, C., Van Alphen, P., Pirone, R., Saracco, G., et al. (2018). Analysis of the light intensity dependence of the growth of Synechocystis and of the light distribution in a photobioreactor energized by 635 nm light. *PeerJ* 2018, 1–28. doi: 10.7717/peerj.5256

Csgör, Z., Herrenbauer, M., Schmidt, K., and Posten, C. (2001). Light distribution in a novel photobioreactor – modelling for optimization. *J. Appl. Phycol.* 13, 325–333. doi: 10.1023/A:1017974232510

Csögör, Z., Herrenbauer, M., Perner, I., Schmidt, K., and Posten, C. (1999). Design of a photo-bioreactor for modelling purposes. *Chem. Eng. Process. Process Intensif.* 38, 517–523. doi: 10.1016/S0255-2701(99)00048-3

Cyano Biotech GmbH (2020). *Cyano Biotech GmbH*. Available online at: http://www.cyano-biotech.com/content/home/index.php (accessed December 6, 2020).

del Rio-Chanona, E. A., Liu, J., Wagner, J. L., Zhang, D., Meng, Y., Xue, S., et al. (2018). Dynamic modeling of green algae cultivation in a photobioreactor for sustainable biodiesel production. *Biotechnol. Bioeng.* 115, 359–370. doi: 10.1002/bit.26483

Derikvand, P., Llewellyn, C. A., and Purton, S. (2017). Cyanobacterial metabolites as a source of sunscreens and moisturizers: a comparison with current synthetic compounds. *Eur. J. Phycol.* 52, 43–56. doi: 10.1080/09670262.2016.1214882

Dienst, D., Wichmann, J., Mantovani, O., Rodrigues, J. S., and Lindberg, P. (2020). High density cultivation for efficient sesquiterpenoid biosynthesis in Synechocystis sp. PCC 6803. *Sci. Rep.* 10, 1–16. doi: 10.1038/s41598-020-62681-w

Downing, J. (2008). *Effects of Light Absorption and Scattering in Water Samples on OBS Measurements*. Logan, UT: Campbell Scientific, Inc.

Du, W., Jongbloets, J. A., Pineda Hernández, H., Bruggeman, F. J., Hellingwerf, K. J., and Branco dos Santos, F. (2016). Photonfluxostat: a method for light-limited batch cultivation of cyanobacteria at different, yet constant, growth rates. *Algal Res.* 20, 118–125. doi: 10.1016/j.algal.2016.10.004

Erukhimovich, I., and de la Cruz, M. O. (2004). Phase equilibria and charge fractionation in polydisperse polyelectrolyte solutions. *J. Polym. Sci. Part B Polym. Phys.* 48, 451–455. doi: 10.1002/polb

Farrokh, P., Sheikhpour, M., Kasaeian, A., Asadi, H., and Bavandi, R. (2019). Cyanobacteria as an eco-friendly resource for biofuel production: a critical review. *Biotechnol. Prog* 35, e2835. doi: 10.1002/btpr.2835

Fenn, R. W., Clough, S. A., Gallery, W. O., Good, R. E., Kneizys, F. X., Mill, J. D., et al. (1985). "Optical and infrared properties of the atmosphere," in *Handbook of Geophysics and the Space Environment*, ed. A. S. Jursa (Hanscom AFB, MA: Air Force Geophysics Laboratory).

Fernández, I., Acién, F. G., Fernández, J. M., Guzmán, J. L., Magán, J. J., and Berenguel, M. (2012). Dynamic model of microalgal production in tubular photobioreactors. *Bioresour. Technol.* 126, 172–181. doi: 10.1016/j.biortech.2012.08.087

Gao, X., Kong, B., and Dennis Vigil, R. (2017a). Comprehensive computational model for combining fluid hydrodynamics, light transport and biomass growth in a Taylor vortex algal photobioreactor: eulerian approach. *Algal Res.* 24, 1–8. doi: 10.1016/j.algal.2017.03.009

Gao, X., Kong, B., and Vigil, R. D. (2018). Multiphysics simulation of algal growth in an airlift photobioreactor: effects of fluid mixing and shear stress. *Bioresour. Technol.* 251, 75–83. doi: 10.1016/j.biortech.2017.12.014

Gao, X., Sun, T., Wu, L., Chen, L., and Zhang, W. (2017b). Co-overexpression of response regulator genes slr1037 and sll0039 improves tolerance of Synechocystis sp. PCC 6803 to 1-butanol. *Bioresour. Technol.* 245, 1476–1483. doi: 10.1016/j.biortech.2017.04.112

Gifuni, I., Pollio, A., Safi, C., Marzocchella, A., and Olivieri, G. (2019). Current bottlenecks and challenges of the microalgal biorefinery. *Trends Biotechnol.* 37, 242–252. doi: 10.1016/j.tibtech.2018.09.006

Grossmann, L., Hinrichs, J., and Weiss, J. (2020). Cultivation and downstream processing of microalgae and cyanobacteria to generate protein-based technofunctional food ingredients. *Crit. Rev. Food Sci. Nutr.* 60, 2961–2989. doi: 10.1080/10408398.2019.1672137

Ho, M. Y., Niedzwiedzki, D. M., MacGregor-Chatwin, C., Gerstenecker, G., Hunter, C. N., Blankenship, R. E., et al. (2020). Extensive remodeling of the photosynthetic apparatus alters energy transfer among photosynthetic complexes when cyanobacteria acclimate to far-red light. *Biochim. Biophys. Acta Bioenerg.* 1861:148064. doi: 10.1016/j.bbabio.2019.148064

Huang, Q., Jiang, F., Wang, L., and Yang, C. (2017). Design of photobioreactors for mass cultivation of photosynthetic organisms. *Engineering* 3, 318–329. doi: 10.1016/J.ENG.2017.03.020

Huang, Q., Liu, T., Yang, J., Yao, L., and Gao, L. (2011). Evaluation of radiative transfer using the finite volume method in cylindrical photoreactors. *Chem. Eng. Sci.* 66, 3930–3940. doi: 10.1016/j.ces.2011.05.032

Huang, Q., Yao, L., Liu, T., and Yang, J. (2012). Simulation of the light evolution in an annular photobioreactor for the cultivation of *Porphyridium cruentum*. *Chem. Eng. Sci.* 84, 718–726. doi: 10.1016/j.ces.2012.09.017

Iluz, D., and Abu-Ghosh, S. (2016). A novel photobioreactor creating fluctuating light from solar energy for a higher light-to-biomass conversion efficiency. *Energy Convers. Manag.* 126, 767–773. doi: 10.1016/j.enconman.2016.08.045

Jacobsen, A., Neuroth, N., and Reitmayer, F. (1971). Absorption and scattering losses in glasses and fibers for light guidance. *J. Am. Ceram. Soc.* 54, 186–187. doi: 10.1111/j.1151-2916.1971.tb12260.x

Jahn, M., Vialas, V., Karlsen, J., Maddalo, G., Edfors, F., Forsström, B., et al. (2018). Growth of cyanobacteria is constrained by the abundance of light and carbon assimilation proteins. *Cell Rep.* 25, 478.e–486.e. doi: 10.1016/j.celrep.2018.09.040

Janasch, M., Asplund-Samuelsson, J., Steuer, R., and Hudson, E. P. (2018). Kinetic modeling of the calvin cycle identifies flux control and stable metabolomes in *Synechocystis* carbon fixation. *J. Exp. Bot.* 70, 1017–1031. doi: 10.1093/jxb/ery382

Jeon, Y. C., Cho, C. W., and Yun, Y. S. (2005). Measurement of microalgal photosynthetic activity depending on light intensity and quality. *Biochem. Eng. J.* 27, 127–131. doi: 10.1016/j.bej.2005.08.017

Johnson, T. J., Katuwal, S., Anderson, G. A., Gu, L., Zhou, R., and Gibbons, W. R. (2018). Photobioreactor cultivation strategies for microalgae and cyanobacteria. *Biotechnol. Prog.* 34, 811–827. doi: 10.1002/btpr.2628

Jones, P. R. (2014). Genetic instability in cyanobacteria – an elephant in the room? *Front. Bioeng. Biotechnol.* 2:12. doi: 10.3389/fbioe.2014.00012

Koller, A. P., Löwe, H., Schmid, V., Mundt, S., and Weuster-Botz, D. (2017). Model-supported phototrophic growth studies with *Scenedesmus obtusiusculus* in a flat-plate photobioreactor. *Biotechnol. Bioeng.* 114, 308–320. doi: 10.1002/bit.26072

Kommareddy, A. R., and Anderson, G. A. (2013). "Mechanistic modeling of a Photobioreactor system," in *Proceeding of the Paper Number 054167, 2005*

ASAE Annual Meeting, (St. Joseph, MI: American Society of Agricultural and Biological Engineers), doi: 10.13031/2013.20123

Krujatz, F., Illing, R., Krautwer, T., Liao, J., Helbig, K., Goy, K., et al. (2015). Light-field-characterization in a continuous hydrogen-producing photobioreactor by optical simulation and computational fluid dynamics. *Biotechnol. Bioeng.* 112, 2439–2449. doi: 10.1002/bit.25667

Lan, E. I., and Liao, J. C. (2012). ATP drives direct photosynthetic production of 1-butanol in cyanobacteria. *Proc. Natl. Acad. Sci. U. S. A.* 109, 6018–6023. doi: 10.1073/pnas.1200074109

Lin, W. R., Tan, S. I., Hsiang, C. C., Sung, P. K., and Ng, I. S. (2019). Challenges and opportunity of recent genome editing and multi-omics in cyanobacteria and microalgae for biorefinery. *Bioresour. Technol.* 291:121932. doi: 10.1016/j.biortech.2019.121932

Liu, X., Miao, R., Lindberg, P., and Lindblad, P. (2019). Modular engineering for efficient photosynthetic biosynthesis of 1-butanol from CO2 in cyanobacteria. *Energy Environ. Sci.* 12, 2765–2777. doi: 10.1039/c9ee01214a

Loomba, V., Huber, G., and Von Lieres, E. (2018). Single-cell computational analysis of light harvesting in a flat-panel photo-bioreactor. *Biotechnol. Biofuels* 11:149. doi: 10.1186/s13068-018-1147-3

Lorenzo, V., Prather, K. L., Chen, G., O'Day, E., Kameke, C., Oyarzún, D. A., et al. (2018). The power of synthetic biology for bioproduction, remediation and pollution control. *EMBO Rep.* 19:e45658. doi: 10.15252/embr.201745658

Luan, G., and Lu, X. (2018). Tailoring cyanobacterial cell factory for improved industrial properties. *Biotechnol. Adv.* 36, 430–442. doi: 10.1016/j.biotechadv.2018.01.005

Luimstra, V. M., Schuurmans, J. M., de Carvalho, C. F. M., Matthijs, H. C. P., Hellingwerf, K. J., and Huisman, J. (2019). Exploring the low photosynthetic efficiency of cyanobacteria in blue light using a mutant lacking phycobilisomes. *Photosynth. Res.* 141, 291–301. doi: 10.1007/s11120-019-00630-z

McCarty, N. S., and Ledesma-Amaro, R. (2019). Synthetic biology tools to engineer microbial communities for biotechnology. *Trends Biotechnol.* 37, 181–197. doi: 10.1016/j.tibtech.2018.11.002

Mikron Instrument Company (2014). *Table of Emissivity of Various Surfaces. 1–13*. Available online at: http://www.czlazio.com/tecnica/TabelladelleEmissività.pdf (accessed July 18, 2020).

Mogo, S., Cachorro, V. E., Sorribas, M., de Frutos, A., and Fernández, R. (2005). Measurements of continuous spectra of atmospheric absorption coefficients from UV to NIR via optical method. *Geophys. Res. Lett.* 32, 1–5. doi: 10.1029/2005GL022938

Molina Grima, E., Garcia Carnacho, F., Sanchez Perez, J. A., Fernandez Sevilla, J. M., Acien Fernandez, F. G., and Contreras Gomez, A. (1994). A mathematical model of microalgal growth in light-limited chemostat culture. *J. Chem. Technol. Biotechnol.* 61, 167–173. doi: 10.1002/jctb.280610212

Naderi, G., Znad, H., and Tade, M. O. (2017). Investigating and modelling of light intensity distribution inside algal photobioreactor. *Chem. Eng. Process. Process Intensif.* 122, 530–537. doi: 10.1016/j.cep.2017.04.014

Narayanan, H., Luna, M. F., Stosch, M., Cruz Bournazou, M. N., Polotti, G., Morbidelli, M., et al. (2020). Bioprocessing in the digital age: the role of process models. *Biotechnol. J.* 15:1900172. doi: 10.1002/biot.201900172

Nedbal, L., Trtílek, M., Červený, J., Komárek, O., and Pakrasi, H. B. (2008). A photobioreactor system for precision cultivation of photoautotrophic microorganisms and for high-content analysis of suspension dynamics. *Biotechnol. Bioeng.* 100, 902–910. doi: 10.1002/bit.21833

Ni, J., Tao, F., Wang, Y., Yao, F., and Xu, P. (2016). A photoautotrophic platform for the sustainable production of valuable plant natural products from CO2. *Green Chem.* 18, 3537–3548. doi: 10.1039/c6gc00317f

Nozzi, N. E., Case, A. E., Carroll, A. L., and Atsumi, S. (2017). Systematic approaches to efficiently produce 2,3-butanediol in a marine cyanobacterium. *ACS Synth. Biol.* 6, 2136–2144. doi: 10.1021/acssynbio.7b00157

Ogawa, K., Yoshikawa, K., Matsuda, F., Toya, Y., and Shimizu, H. (2018). Transcriptome analysis of the cyanobacterium Synechocystis sp. PCC 6803 and mechanisms of photoinhibition tolerance under extreme high light conditions. *J. Biosci. Bioeng.* 126, 596–602. doi: 10.1016/j.jbiosc.2018.05.015

Olivieri, G., Gargiulo, L., Lettieri, P., Mazzei, L., Salatino, P., and Marzocchella, A. (2015). Photobioreactors for microalgal cultures: a lagrangian model coupling hydrodynamics and kinetics. *Biotechnol. Prog.* 31, 1259–1272. doi: 10.1002/btpr.2138

Papacek, S., Jablonsky, J., and Petera, K. (2018). Advanced integration of fluid dynamics and photosynthetic reaction kinetics for microalgae culture systems. *BMC Syst. Biol.* 12:93. doi: 10.1186/s12918-018-0611-9

Pérez, A. A., Chen, Q., Hernández, H. P., Branco dos Santos, F., and Hellingwerf, K. J. (2019). On the use of oxygenic photosynthesis for the sustainable production of commodity chemicals. *Physiol. Plant.* 166, 413–427. doi: 10.1111/ppl.12946

Perner-Nochta, I., and Posten, C. (2007). Simulations of light intensity variation in photobioreactors. *J. Biotechnol.* 131, 276–285. doi: 10.1016/j.jbiotec.2007.05.024

Photanol (2020). Available online at: https://photanol.com/ (accessed December 6, 2020).

Pilon, L., Berberoğlu, H., and Kandilian, R. (2011). Radiation transfer in photobiological carbon dioxide fixation and fuel production by microalgae. *J. Quant. Spectrosc. Radiat. Transf.* 112, 2639–2660. doi: 10.1016/j.jqsrt.2011.07.004

Pond Tech (2020). *Pond Tech | We Derive Value From Emissions – Pond Tech*. Available online at: https://www.pondtech.com/ (accessed December 6, 2020).

Pope, R. M., and Fry, E. S. (1997). ST-Absorption spectrum (380-700 nm) pure water {II} Integrating cavity measurements. *Appl. Opt.* 36, 8710–8723.

Pruvost, J., and Cornet, J.-F. (2012). "10 Knowledge models for the engineering and optimization of photobioreactors," in *Microalgal Biotechnology: Potential and Production*, eds C. Posten and C. Walter (Berlin: De Gruyter), 181–224. doi: 10.1515/9783110225020.181

Refractive Index Calculator (2020).Available online at: https://refractiveindex.info/?shelf=3d&book=glass&page=BAF10 (accessed July 18, 2020).

Rio-Chanona, E. A., Manirafasha, E., Zhang, D., Yue, Q., and Jing, K. (2016). Dynamic modeling and optimization of cyanobacterial C-phycocyanin production process by artificial neural network. *Algal Res.* 13, 7–15. doi: 10.1016/j.algal.2015.11.004

Rio-Chanona, E. A., Wagner, J. L., Ali, H., Fiorelli, F., Zhang, D., and Hellgardt, K. (2019). Deep learning-based surrogate modeling and optimization for microalgal biofuel production and photobioreactor design. *AIChE J.* 65, 915–923. doi: 10.1002/aic.16473

Röttgers, R., Doerffer, R., Mckee, D., and Schönfeld, W. (2010). *Pure Water Spectral Absorption, Scattering, and Real Part of Refractive Index Model Algorithm Technical Basis Document – Draft*. Glasgow: University of Strathclyde, 1–18.

Santos-Merino, M., Singh, A. K., and Ducat, D. C. (2019). New applications of synthetic biology tools for cyanobacterial metabolic engineering. *Front. Bioeng. Biotechnol* 7:33. doi: 10.3389/fbioe.2019.00033

Saper, G., Kallmann, D., Conzuelo, F., Zhao, F., Tóth, T. N., Liveanu, V., et al. (2018). Live cyanobacteria produce photocurrent and hydrogen using both the respiratory and photosynthetic systems. *Nat. Commun.* 9, 1–9. doi: 10.1038/s41467-018-04613-x

Sarkar, D., Mueller, T. J., Liu, D., Pakrasi, H. B., and Maranas, C. D. (2019). A diurnal flux balance model of Synechocystis sp. PCC 6803 metabolism. *PLoS Comput. Biol.* 15:1–29. doi: 10.1371/journal.pcbi.1006692

Scheufele, F. B., Hinterholz, C. L., Zaharieva, M. M., Najdenski, H. M., Módenes, A. N., Trigueros, D. E. G., et al. (2019). Complex mathematical analysis of photobioreactor system. *Eng. Life Sci.* 19, 844–859. doi: 10.1002/elsc.201800044

Schuurmans, R. M., van Alphen, P., Schuurmans, J. M., Matthijs, H. C. P., and Hellingwerf, K. J. (2015). Comparison of the photosynthetic yield of cyanobacteria and green algae: different methods give different answers. *PLoS One* 10:e0139061. doi: 10.1371/journal.pone.0139061

Seo, I. H., Lee, I. B., Hong, S. W., Bitog, J. P., Kwon, K. S., Lee, C. G., et al. (2014). Evaluation of a photobioreactor performance grafting microalgal growth model and particle tracking technique using CFD. *Trans. ASABE* 57, 121–139. doi: 10.13031/trans.57.10339

Shabestary, K., Anfelt, J., Ljungqvist, E., Jahn, M., Yao, L., and Hudson, E. P. (2018). Targeted repression of essential genes to arrest growth and increase carbon partitioning and biofuel titers in cyanobacteria. *ACS Synth. Biol.* 7, 1669–1675. doi: 10.1021/acssynbio.8b00056

Solimeno, A., Gabriel, F., and García, J. (2017). Mechanistic model for design, analysis, operation and control of microalgae cultures: calibration and application to tubular photobioreactors. *Algal Res.* 21, 236–246. doi: 10.1016/j.algal.2016.11.023

Solimeno, A., Samsó, R., Uggetti, E., Sialve, B., Steyer, J. P., Gabarró, A., et al. (2015). New mechanistic model to simulate microalgae growth. *Algal Res.* 12, 350–358. doi: 10.1016/j.algal.2015.09.008

Soman, A., and Shastri, Y. (2015). Optimization of novel photobioreactor design using computational fluid dynamics. *Appl. Energy* 140, 246–255. doi: 10.1016/j.apenergy.2014.11.072

Straub, Q. (2011). *Es2011-54 a Methodology for the Determination of the Light Distribution*. Washington: ASME, 1–9.

Sustainabledevelopment Organization. (2015). *Transforming Our World: The 2030 Agenda For Sustainable Development United Nations United Nations Transforming Our World: The 2030 Agenda For Sustainable Development*. New York, NY: Sustainabledevelopment Organization.

Table, I., and Gases, M. (1974). ING Data Obtained by Different Workers. The Opportunity was Also Taken to Study the Effect of Assuming that the Molecular gas is not an Ideal Gas. The Scattering Coefficient for a Pure Molecular gas that is Assumed to have the Properties of an Ideal Gas, Vol. 13. Washington, USA: OSA, 468–469.

Taton, A., Unglaub, F., Wright, N. E., Zeng, W. Y., Paz-Yepes, J., Brahamsha, B., et al. (2014). Broad-host-range vector system for synthetic biology and biotechnology in cyanobacteria. *Nucleic Acids Res.* 42, 136. doi: 10.1093/nar/gku673

Thermoworks (2020). *Emissivity Table*. Available online at: https://www.thermoworks.com/emissivity-table (accessed July 18, 2020).

Toyoshima, M., Toya, Y., and Shimizu, H. (2020). Flux balance analysis of cyanobacteria reveals selective use of photosynthetic electron transport components under different spectral light conditions. *Photosynth. Res.* 143, 31–43. doi: 10.1007/s11120-019-00678-x

van Alphen, P., and Hellingwerf, K. J. (2015). Sustained circadian rhythms in continuous light in *Synechocystis* sp. PCC6803 growing in a well-controlled photobioreactor. *PLoS One* 10:e0127715. doi: 10.1371/journal.pone.0127715

van den Berg, C., Eppink, M. H. M., and Wijffels, R. H. (2019). Integrated product recovery will boost industrial cyanobacterial processes. *Trends Biotechnol.* 37, 454–463. doi: 10.1016/j.tibtech.2018.11.006

Vasudevan, R., Gale, G. A. R., Schiavon, A. A., Puzorjov, A., Malin, J., Gillespie, M. D., et al. (2019). Cyanogate: a modular cloning suite for engineering cyanobacteria based on the plant moclo syntax. *Plant Physiol.* 180, 39–55. doi: 10.1104/pp.18.01401

Vavitsas, K., Crozet, P., Vinde, M. H., Davies, F., Lemaire, S. D., and Vickers, C. E. (2019). The synthetic biology toolkit for photosynthetic microorganisms[OPEN]. *Plant Physiol.* 181, 14–27. doi: 10.1104/pp.19.00345

Venkata Mohan, S., Modestra, J. A., Amulya, K., Butti, S. K., and Velvizhi, G. (2016). A circular bioeconomy with biobased products from CO2 sequestration. *Trends Biotechnol.* 34, 506–519. doi: 10.1016/j.tibtech.2016.02.012

Vidal, R. (2017). Alcohol dehydrogenase AdhA plays a role in ethanol tolerance in model cyanobacterium *Synechocystis* sp. PCC 6803. *Appl. Microbiol. Biotechnol.* 101, 3473–3482. doi: 10.1007/s00253-017-8138-3

Vogel, A. I. M., Lale, R., and Hohmann-Marriott, M. F. (2017). Streamlining recombination-mediated genetic engineering by validating three neutral integration sites in Synechococcus sp. PCC 7002. *J. Biol. Eng.* 11:19. doi: 10.1186/s13036-017-0061-8

Wang, B., Wang, Z., Chen, T., and Zhao, X. (2020). Development of novel bioreactor control systems based on smart sensors and actuators. *Front. Bioeng. Biotechnol.* 8:7. doi: 10.3389/fbioe.2020.00007

Wang, L., Chen, L., Yang, S., and Tan, X. (2020). Photosynthetic conversion of carbon dioxide to oleochemicals by cyanobacteria: recent advances and future perspectives. *Front. Microbiol.* 11:634. doi: 10.3389/fmicb.2020.00634

Weise, T., Reinecke, J. M., Schuster, S., and Pfaff, M. (2019). Optimizing turbidostatic microalgal biomass productivity: a combined experimental and coarse-grained modelling approach. *Algal Res.* 39:101439. doi: 10.1016/j.algal.2019.101439

Wendt, K. E., Ungerer, J., Cobb, R. E., Zhao, H., and Pakrasi, H. B. (2016). CRISPR/Cas9 mediated targeted mutagenesis of the fast growing cyanobacterium *Synechococcus elongatus* UTEX 2973. *Microb. Cell Fact.* 15:115. doi: 10.1186/s12934-016-0514-7

Wheaton, Z. C., and Krishnamoorthy, G. (2012). Modeling radiative transfer in photobioreactors for algal growth. *Comput. Electron. Agric.* 87, 64–73. doi: 10.1016/j.compag.2012.05.002

Xia, P., Ling, H., Foo, J. L., and Chang, M. W. (2019). Synthetic biology toolkits for metabolic engineering of cyanobacteria. *Biotechnol. J.* 14:1800496. doi: 10.1002/biot.201800496

Xiong, W., Cano, M., Wang, B., Douchi, D., and Yu, J. (2017). The plasticity of cyanobacterial carbon metabolism. *Curr. Opin. Chem. Biol.* 41, 12–19. doi: 10.1016/j.cbpa.2017.09.004

Yao, L., Shabestary, K., Björk, S. M., Asplund-Samuelsson, J., Joensson, H. N., Jahn, M., et al. (2020). Pooled CRISPRi screening of the cyanobacterium *Synechocystis* sp PCC 6803 for enhanced industrial phenotypes. *Nat. Commun.* 11:1666. doi: 10.1038/s41467-020-15491-7

Yen, H.-W., Hu, I.-C., Chen, C.-Y., Nagarajan, D., and Chang, J.-S. (2019). "Design of photobioreactors for algal cultivation," in *Biofuels from Algae*, eds A. Pandey, J.-S. Chang, C. R. Soccol, D.-J. Lee, and Y. Chisti (Amsterdam: Elsevier), 225–256. doi: 10.1016/b978-0-444-64192-2.00010-x

Zavřel, T., Faizi, M., Loureiro, C., Poschmann, G., Stühler, K., Sinetova, M., et al. (2019). Quantitative insights into the cyanobacterial cell economy. *Elife* 8, e42508. doi: 10.7554/eLife.42508

Zhang, D., Dechatiwongse, P., and Hellgardt, K. (2015). Modelling light transmission, cyanobacterial growth kinetics and fluid dynamics in a laboratory scale multiphase photo-bioreactor for biological hydrogen production. *Algal Res.* 8, 99–107. doi: 10.1016/j.algal.2015.01.006

Zhang, Z., Zhou, X., Hu, J., Zhang, T., Zhu, S., and Zhang, Q. (2017). Photo-bioreactor structure and light-heat-mass transfer properties in photo-fermentative bio-hydrogen production system: a mini review. *Int. J. Hydrogen Energy* 42, 12143–12152. doi: 10.1016/j.ijhydene.2017.03.111

Conflict of Interest: The authors declare that the research was conducted in the absence of any commercial or financial relationships that could be construed as a potential conflict of interest.

NOMENCLATURE

Symbol	Description	Symbol	Description
A	area, m^2	v_F	the convective velocity, m s^{-1}
c_d	mass fraction of dispersed phase, kg kg^{-1}	w	volume fraction
C	concentration, mol m^{-3}	X	mass fraction
C_p	specific heat at constant pressure, J m^{-3} K^{-1}	$I_{s,in}$	Incident light intensity set via software, W m^{-2}
D	diffusion coefficients, m^2 s^{-1}	I_p	Light intensity perceived by bacterial cell, W m^{-2}
D_{md}	turbulent dispersion coefficient, m^2 s^{-1}	I_{ab}	Light intensity absorbed by bacterial cell, W m^{-2}
e	enthalpy flux density, J m^{-2} s^{-1}	FD	Drag force
E_A	activation energy, J mol^{-1}	Fg	Gravity force
F	force term, kg m^{-2} s^{-2}	$Fext$	Additional force
G	incident light radiation, W m^{-2}	mp	Particle mass
$h_j(T)$	enthalpies heat flux densities, J m^{-2} s^{-1}	$rhop$	Particle density
I	incident light intensity, W m^{-2}	dp	Particle diameter
I_b	black body radiation, Wm^{-2}	xp	Particle trajectory
J	diffusion vector	vp	Particle velocity
k	turbulent kinetic energy, m^2s^{-3}	**Greek symbols**	
K_r	reaction rate constant, m^2 s^{-1}	β	extinction coefficient, m^{-1}
m	mass of species, kg	ε	turbulent energy dissipation, m^2s^{-3}
m_{dc}	mass transfer from dispersed to continuous phase, kg $m^{-3}s^{-1}$	k_c	effective thermal conductivity coefficient, W m^{-1} K^{-1}
M	molar mass, kg mol^{-1}	κ	absorbance coefficient, m^{-1}
n	flux density, mol m^{-2} s^{-1}	μ	dynamic viscosity, kg_f s m^{-2}
n_d	relative mass flux, mol m^{-2} s^{-1}	μ_{gr}	growth rate, h^{-1}
p	pressure, Pa	μ_T	turbulent viscosity,
q	heat flux densities, W m^{-2}	ν	stoichiometric coefficients
Q	volumetric charge density, C m^{-3}	ρ	density, Kg m^{-3}
Q_r	radiative flux, W m^{-2}	σ_S	scattering coefficient, m^{-1}
R	universal gas constant, J K^{-1} mol^{-1}	τ	turbulent stress,
T	temperature, K	φ_χ	continuous phase fraction, –
u	velocity vector, m s^{-1}	φ_δ	dispersed phase fraction, –
u_c	continuous phase velocity vector, m s^{-1}	ω	rotational velocity, rad s^{-1}
u_d	dispersed phase velocity vector, m s^{-1}	η	dynamic viscosity, Pa s^{-1}
u_{slip}	slip velocity vector, m s^{-1}		

frontiers in Microbiology

ORIGINAL RESEARCH
published: 08 April 2021
doi: 10.3389/fmicb.2021.647164

Rapidly Improving High Light and High Temperature Tolerances of Cyanobacterial Cell Factories Through the Convenient Introduction of an AtpA-C252F Mutation

Shanshan Zhang[1,2,3], Sini Zheng[1,2,4], Jiahui Sun[1,2,3], Xuexia Zeng[1,2,4], Yangkai Duan[1,2], Guodong Luan[1,2] and Xuefeng Lu[1,2,3,5,6]**

[1] Key Laboratory of Biofuels, Qingdao Institute of Bioenergy and Bioprocess Technology, Chinese Academy of Sciences, Qingdao, China, [2] Shandong Provincial Key Laboratory of Synthetic Biology, Qingdao Institute of Bioenergy and Bioprocess Technology, Chinese Academy of Sciences, Qingdao, China, [3] College of Life Science, University of Chinese Academy of Sciences, Beijing, China, [4] College of Life Science and Technology, Central South University of Forestry and Technology, Changsha, China, [5] Dalian National Laboratory for Clean Energy, Dalian, China, [6] Laboratory for Marine Biology and Biotechnology, Qingdao National Laboratory for Marine Science and Technology, Qingdao, China

OPEN ACCESS

Edited by:
Tian Zhang,
Wuhan University of Technology, China

Reviewed by:
Lei Chen,
Tianjin University, China
Jinjin Diao,
Washington University in St. Louis, United States

***Correspondence:**
Guodong Luan
luangd@qibebt.ac.cn
Xuefeng Lu
lvxf@qibebt.ac.cn

Specialty section:
This article was submitted to Microbiotechnology, a section of the journal Frontiers in Microbiology

Received: *29 December 2020*
Accepted: *22 February 2021*
Published: *08 April 2021*

Citation:
Zhang S, Zheng S, Sun J, Zeng X, Duan Y, Luan G and Lu X (2021) Rapidly Improving High Light and High Temperature Tolerances of Cyanobacterial Cell Factories Through the Convenient Introduction of an AtpA-C252F Mutation. Front. Microbiol. 12:647164. doi: 10.3389/fmicb.2021.647164

Photosynthetic biomanufacturing is a promising route for green production of biofuels and biochemicals utilizing carbon dioxide and solar energy. Cyanobacteria are important microbial platforms for constructing photosynthetic cell factories. Toward scaled outdoor cultivations in the future, high light and high temperature tolerances of cyanobacterial chassis strains and cell factories would be determinant properties to be optimized. We proposed a convenient strategy for rapidly improving high light and high temperature tolerances of an important cyanobacterial chassis *Synechococcus elongatus* PCC 7942 and the derived cell factories. Through introduction and isolation of an AtpA-C252F mutation, PCC 7942 mutants with improved high light and high temperature tolerances could be obtained in only 4 days with an antibiotics-free mode. Adopting this strategy, cellular robustness and sucrose synthesizing capacities of a PCC 7942 cell factory were successfully improved.

Keywords: cyanobacteria, *Synechococcus elongatus* PCC 7942, ATP synthase, sucrose, high temperature and high light tolerances

INTRODUCTION

With resource shortages and environmental pollution issues becoming increasingly prominent, photosynthetic biomanufacturing provides important options for the green and sustainable production of biofuels and biochemicals (Melis, 2009; Lu, 2010). Cyanobacteria are potential photosynthetic platforms and have been successfully engineered for production of multiple natural and non-natural products (Oliver and Atsumi, 2014). To put cyanobacterial photosynthetic biomanufacturing technology into practice, high light and high temperature tolerances would be important properties of the cyanobacterial cell factories, aiming to facilitate stable growth and production under stressful conditions during scaled outdoor cultivations (Luan and Lu, 2018). To improve high light and high temperature tolerances of cyanobacterial cells, complex genetic

engineering strategies have been explored and adopted to modify or to update the native stress-response protective systems or the photosystems. For example, overexpression of specific heat shock proteins improved high temperature tolerance of cyanobacterial cells (Chaurasia and Apte, 2009; Su et al., 2017), and reduction of light harvesting antenna led to improved tolerances to high light stress (Kirst et al., 2014). However, implementations of these strategies rely on antibiotic resistance selection based on genetic manipulations and require long-term cultivations and passages for isolation of the homozygous mutant, and the entire cycle would usually take several weeks.

Synechococcus elongatus PCC 7942 (PCC 7942 for short) is a widely used cyanobacterial chassis strain and has been engineered to be cell factories for producing dozens of chemicals, including ethanol (Deng and Coleman, 1999), 2,3-butanediol (Oliver et al., 2013), isobutyraldehyde (Atsumi et al., 2009), ethylene (Sakai et al., 1997), acetone (Chwa et al., 2016), 1-butanol (Lan and Liao, 2011), isopropanol (Kusakabe et al., 2013), 2-methyl-1-butanol (Shen and Liao, 2012), 1,2-propanediol (Li and Liao, 2013), sucrose (Ducat et al., 2012), hexose sugars (Niederholtmeyer et al., 2010), free fatty acid (Ruffing and Jones, 2012), and 3-hydroxypropionic acid (Lan et al., 2015). Moreover, PCC 7942 is a critical platform to explore mechanisms and strategies for optimizing stabilities and efficiency of photosynthetic carbon fixation (Su et al., 2017; Ungerer et al., 2018; Yu et al., 2018). Thus, the improvement of the efficiency and effects on engineering PCC 7942 high light and high temperature tolerances will be of broad and important biotechnological significance.

Previously, we have demonstrated that specific point mutations in F_OF_1 ATP synthase α subunit (AtpA), converting the 252^{nd} amino acid from cysteine to any of the four conjugated amino acids (tyrosine/phenylalanine/tryptophan/histidine), could endow PCC 7942 cells with high temperature and high light resistances (Lou et al., 2018). Inspired by this, we proposed a convenient strategy for rapidly improving high light and high temperature tolerances of PCC 7942 derived cell factories by targeted mutagenesis of AtpA-C252. Compared with previously reported approaches, this new strategy has two potential advantages. First, the direct stress selection (with high light and high temperature) process would eliminate the dependence on introducing and screening antibiotics markers in the recombinant strains. Second, the growth advantages of the desired transformants would reduce the time required for cultivation and segregation. For proof-of-concept, we successfully isolated the PCC 7942 mutant strains with improved high light and high temperature tolerances that could be obtained in only 4 days in an antibiotics-free mode. In addition, cellular robustness and sucrose synthesizing capacities of a previously constructed PCC 7942 cell factory were significantly optimized, increasing the sucrose productivities by nearly onefold.

RESULTS AND DISCUSSION

Overview

To facilitate rapid mutagenesis of AtpA-C252 and effective isolation of the mutants, we designed a three-step procedure, consisting of transformation, initial screening, and rescreening. As shown in **Figure 1**, plasmids carrying tailored AtpA fragments would be transformed into PCC 7942 to induce homologous recombination. During the initial screening step, mutant cells obtaining the AtpA-C252 mutagenesis would survive under the selective conditions and form colonies on the agar plates. To exclude false positive results and to confirm the tolerant phenotypes of the mutants, the colonies obtained from the initial screening step would be streaked and cultivated on fresh agar plates under the same selective conditions. The final colonies would be collected for further assays and evaluations.

Rapid Isolation of PCC 7942 Mutants Carrying the AtpA-C252F Mutation

Among the four AtpA-C252 mutations endowing PCC 7942 with improved tolerances to high light and high temperature (Lou et al., 2018), we selected AtpA-C252F for proof-of-concept of the proposed strategy in this work. A plasmid carrying an AtpA-C252F gene fragment (termed as pSS18 in **Figure 1**) was constructed and transformed into PCC 7942 cells, and another plasmid carrying wild-type (WT) AtpA was used as a control. PCC 7942 tolerant transformants appeared on BG11 agar plates after only 48 h of cultivation in the selective conditions with high light and high temperature. More than 1,000 transformants were obtained on the screening plate of PCC 7942 (transformed with pSS18, AtpA-C252F), whereas no transformants appeared on PCC 7942 transformed with pSS3 (AtpA WT). Phenotypes of the transformants were further checked by re-screening under the same conditions, and 23 randomly selected transformants (from the initial screening step) all survived in the rescreening step. We further collected the 23 transformants (after the two-round selection) for AtpA sequence analysis, and the Sanger sequencing results revealed all of the strains carrying the AtpA-C252F mutation, indicating that the tolerances to high light and high temperature were endowed by the targeted mutagenesis. In addition, the sequencing results showed that all the mutants carrying the AtpA-C252F mutation existed as homozygous (as shown in **Supplementary Figure 1**), indicating that the significant growth advantages caused by the AtpA-C252F facilitated effective segregation of the mutated chromosomes.

High light and high temperature tolerances of the isolated mutants were further evaluated by liquid cultivation in column photobioreactors. As shown in **Figure 2A**, the growth of the PCC 7942 mutants carrying the AtpA-C252F mutation was similar to that of the control under normal conditions (30°C and 50 μmol photons/m^2/s). While in a stressful environment (44°C and 400 μmol photons/m^2/s), the mutant strain exhibited significantly improved adaptabilities compared with the WT control and maintained rapid growth (**Figure 2B**). WT cells of PCC 7942 could not survive or grow facing the environmental stress, whereas OD_{730} of the AtpA-C252F mutant cells reached up to 7 with a significantly improved growth rate compared with when cultivated in normal conditions (30°C and 50 μmol photons/m^2/s). The results indicated that

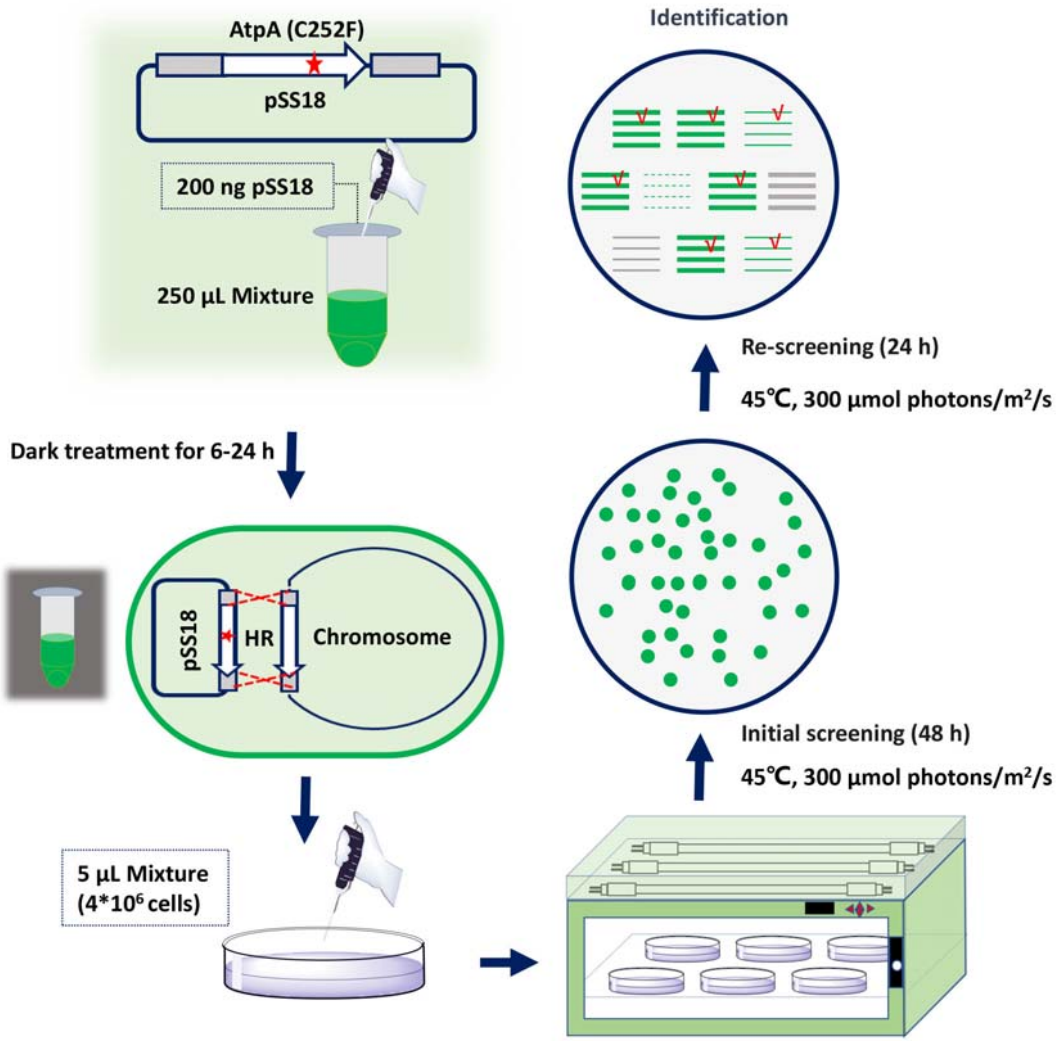

FIGURE 1 | Procedures for rapid isolation of high light and high temperature tolerant PCC 7942 mutants by introduction of the AtpA-C252F mutation.

the mutant strain of PCC 7942 obtained through the rapid isolation process displayed significantly improved capacities to tolerate and utilize strong illuminations even when cultivated at high temperatures.

AtpA-C252F Mutagenesis Rapidly Improves High Light and High Temperature Tolerances and Sucrose Production Rates of a PCC 7942 Cell Factory

We further adopted this strategy to engineer a sucrose synthesizing cyanobacterial cell factory. Previously, we have introduced an *Escherichia coli* sourced sucrose permease CscB into PCC 7942 to facilitate the secretory production of sucrose under salts stress and overexpressed the native sucrose-phosphate synthase Sps to enhance sucrose synthesis (Duan et al., 2016; Qiao et al., 2018). The final strain FL130 was transformed with the pSS18 plasmid (AtpA-C252F) to confirm the feasibility and effectiveness of our strategy when adopted on cell factories. Following the described procedures, we successfully isolated high light and high temperature tolerant transformants of FL130 (**Figure 3A**). The final isolated and verified FL130 mutant (AtpA-C252F) was termed as SZ41, which was able to grow under the conditions of 45°C with 300 µmol photons/m^2/s illumination (**Figure 3B**).

When cultivated under normal conditions of 30°C and 100 µmol photons/m^2/s, growths FL130 and SZ41 show minor differences (**Figure 3C**, FL130-NTL and SZ41-NTL), and the sucrose production reached up to 1,835 and 2,025 mg/L in 8 days, respectively (**Figure 3D**, FL130-NTL and SZ41-NTL). The slight increase of total carbon fixation (the sum of biomass and sucrose) in SZ41 might result from an increased oxygen evolution rate (**Figure 4A**), indicating that the introduction of AtpA-C252F brought in benefits on the overall efficiency or

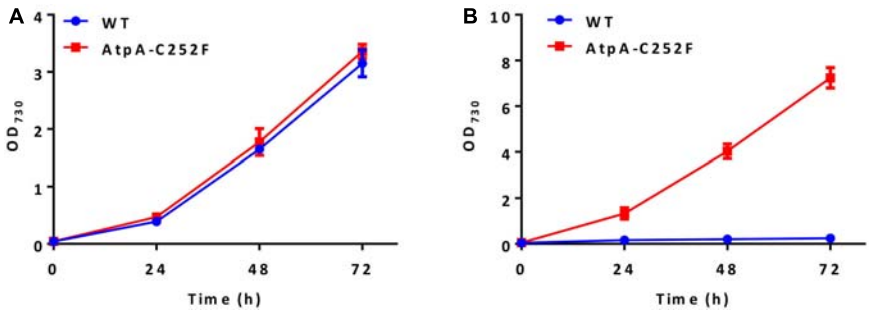

FIGURE 2 | Effect of the AtpA-C252F mutation on cellular growth and tolerances of PCC 7942. Growth of the PCC 7942 strain with or without the AtpA-C252F mutation in liquid BG11 medium at 30°C with 50 μmol photons/m^2/s illumination **(A)** and at 44°C with 400 μmol photons/m^2/s illumination **(B)**. Error bars indicate standard deviations (n = 3).

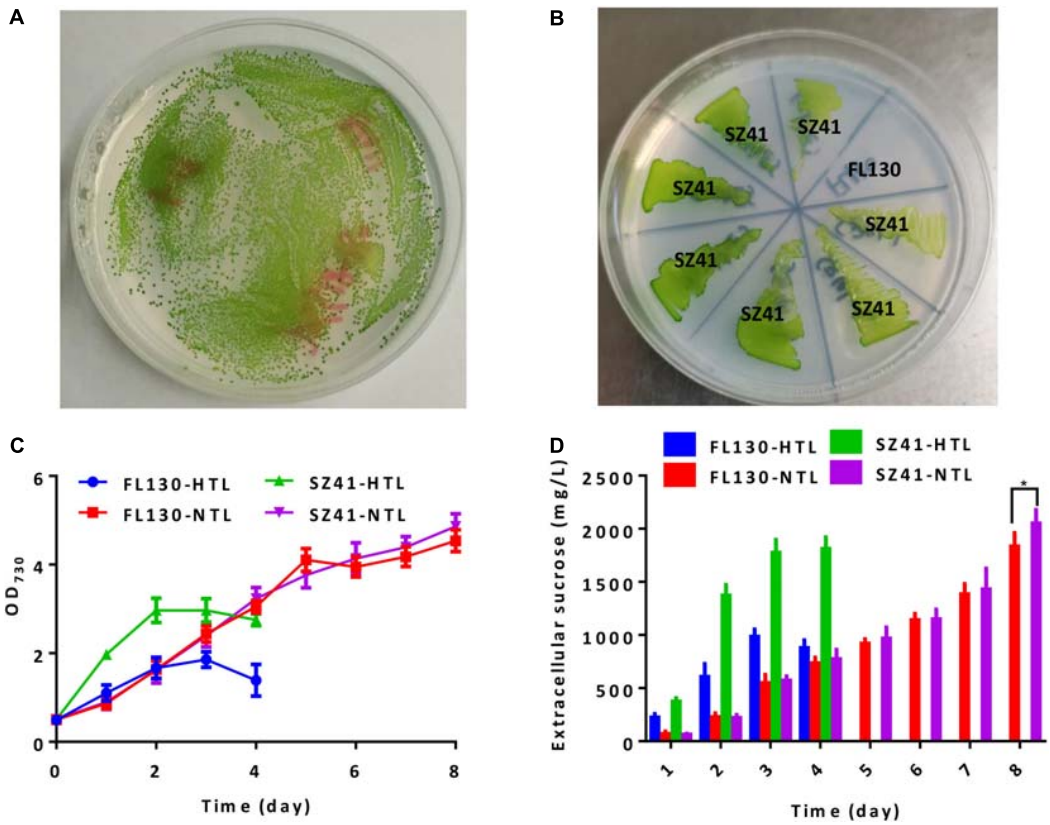

FIGURE 3 | Effects of the AtpA-C252F mutation on growth, tolerance, and sucrose synthesis of a PCC 7942 derived cell factory. **(A)** Tolerant transformants (with the AtpA-C252F mutation) of FL130 on BG11 agar plates after 2 days of cultivation under high light and high temperature conditions (45°C with 300 μmol photons/m^2/s illumination). **(B)** FL130 and the derived SZ41 strain (FL130-AtpA-C252F) grown on BG11 plates at 45°C with 300 μmol photons/m^2/s illumination. **(C)** Cell growth of FL130 and SZ41 under normal (NTL, 30°C with 100 μmol photons/m^2/s illumination) and stressful (HTL, 40°C with 400 μmol photons/m^2/s illumination) conditions as measured by OD_{730}. **(D)** Extracellular sucrose production of FL130 and SZ41. NaCl (150 mM) and IPTG (0.1 mM) were added to the BG11 medium **(C,D)**. Error bars indicate standard deviations ($n \geq 3$). Statistical analysis was performed by using Student's t-test (*$p < 0.05$).

stability of cellular photosynthesis in PCC 7942 under these conditions (30°C, 100 μmol photons/m^2/s, 150 mM NaCl). When stressful high light and high temperature conditions (40°C and 400 μmol photons/m^2/s) were adopted, SZ41 exhibited significantly improved growth advantages over FL130. After 4 days of cultivation supplemented with 150 mM NaCl, the cell density of the SZ41 culture broth reached about 3, whereas that of the FL130 was lower than 2.0 (**Figure 3C**). The bleaching phenotypes might be caused by the synergy effects of high light and high temperature stress and salts stress on the *Synechococcus* cells, and during this process, 1.8 and 0.98 g/L of extracellular sucrose were synthesized by

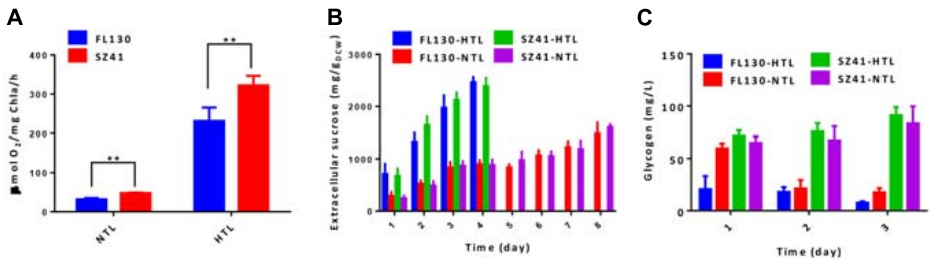

FIGURE 4 | Effects of the AtpA-C252F mutation on carbohydrate production of a PCC 7,942 derived cell factory. **(A)** Oxygen evolution rate of the FL130 and SZ41 strains under normal (NTL, 30°C with 100 μmol photons/m^2/s illumination) and stressful (HTL, 40°C with 400 μmol photons/m^2/s illumination) conditions. **(B)** Specific sucrose productivities of the FL130 and SZ41 strains under normal (NTL, 30°C with 100 μmol photons/m^2/s illumination) and stressful (HTL, 40°C with 400 μmol photons/m^2/s illumination) conditions. **(C)** Glycogen accumulation of the FL130 and SZ41 strains under normal (NTL, 30°C with 100 μmol photons/m^2/s illumination) and stressful (HTL, 40°C with 400 μmol photons/m^2/s illumination) conditions during the initial 3 days of cultivation. Error bars indicate standard deviations ($n \geq 3$). Statistical analysis was performed by using Student's *t*-test (**$p < 0.01$).

SZ41 and FL130, respectively, under the high light and high temperature conditions (**Figure 3D**). The different performances on cell growths and sucrose production between the two strains under the stressful conditions are in accordance with the photosynthesis activities differences revealed from the oxygen evolution rates. With enhanced illumination strengths (and increased temperatures), photosynthesis activities of FL130 and SZ41 were both significantly elevated compared with these under normal conditions, and the oxygen evolution rate of SZ41 would be 40% higher than that of FL130 (**Figure 4A**).

It is noteworthy that the specific sucrose production on per cell levels was on similar levels between the two strains (**Figure 4B**) whether in normal or stressful conditions, indicating that the improved accumulation of sucrose in the SZ41 strain resulted from the optimized cell growth and enhanced carbon fixation caused by the AtpA-C252F mutation, rather than a distribution of a larger portion of biomass to sucrose synthesis. After 4 days of high light and high temperature cultivation, bleaching phenotypes would be observed for both the SZ41 and FL130 cells, and the sucrose production would be terminated. However, it is noteworthy that the AtpA-C252F mutation carrying the SZ41 strain under the stressful conditions could synthesize similar concentrations of sucrose utilizing half of the cultivation term as that obtained under normal conditions (1.8 g/L in 4 days versus 2.0 g/L in 8 days). In addition to sucrose, the SZ41 strain also accumulated higher intracellular glycogen contents than the FL130 under high light and high temperature conditions, confirming the improved capacities for carbohydrates synthesis caused by the AtpA-C252F mutations (**Figure 4C**). Both sucrose and glycogen biosyntheses depend on the precursor glucose-1-phosphate, and it has been reported that the metabolic flux through glucose-1-phosphate significantly determines the flexibility of the intracellular carbon distribution of cyanobacteria *via* a dynamic balance between different metabolic branches (Luan et al., 2019). Furthermore, it has been reported that *S. elongatus* UTEX 2973, the fast-growing strain carrying AtpA-C252Y single nucleotide polymorphism (SNP) compared with PCC 7942, would overaccumulate glycogen to buffer the enhanced carbon flux from the CBB cycle (Song et al., 2016; Tan et al., 2018). Glycogen storage serves as the main carbon sink mechanism of cyanobacterial cells and could play the role of carbon pool for synthesis of desired metabolites; thus, the enhanced glycogen synthesis activities and glycogen contents could be an additional advantage of the strategy developed in this work.

We also evaluated the effects of this strategy on engineering an ethanologenic cell factory derived from PCC 7942. A previously optimized ethanologenic pathway consisting of the pyruvate decarboxylase from *Zymomonas mobilis* and a type II alcohol dehydrogenase from *Synechocystis* sp. PCC 6803 was introduced into PCC 7942 to generate the ZN44 strain, producing about 0.22 g/L ethanol in 2 days (**Supplementary Figure 2**). Introduction of the AtpA-C252F mutation into ZN44 significantly improved the growth of the ethanologenic cell factory (ZN45) under high light conditions (OD_{730} of 7.2 in ZN45 compared with OD_{730} of 5.1 in ZN44 after 2 days of cultivation). However, the ethanol production was just slightly improved from 0.22 to 0.25 g/L, indicating that as for the PCC 7942 derived ethanologenic cell factory, the activities of the ethanol synthesis pathways rather than the total were holding control over the ethanol production capacities, and the increase of carbon fixation could not be effectively rewired into ethanol synthesis, which could be solved through further metabolic engineering.

Compared with the recently reported fast-growing and robust cyanobacteria *S. elongatus* UTEX 2973, PCC 7942 still possesses the advantages of clear genetic background and more convenient genetic manipulation, and dozens of photosynthetic cell factories have been engineered based on this typical model strain. The strategy developed in this work provided a convenient approach to update the related PCC 7942 derived cell factories, which would avoid repeated implementations of the complex metabolic engineering with a new chassis. In addition, the success in this work provided a novel targeted mutagenesis and selective isolation manipulation paradigm for cyanobacterial phenotypes improvements. In recent years, many SNPs have been identified to be related with cellular growth or survival benefits, e.g., acid tolerances (Uchiyama et al., 2015), alcohol tolerances (Hirokawa et al., 2018), high light and high temperature tolerances (Lou et al., 2018), and growth rates (Ungerer et al., 2018). Regarding such mutations endowing cells with specific growth advantages, rapid and convenient

TABLE 1 | Cyanobacterial strains and plasmids used in this study.

Strain	Genotypes[a]	References
PCC 7942	*Synechococcus elongatus* PCC 7942 wild-type	Gifted by Prof. Xudong Xu, Institute of Hydrobiology, Chinese Academy of Sciences
PCC 7942-C252F	Mutant strain of PCC 7942 harboring a AtpA with C252F point mutation	Lou et al., 2018
FL130	Mutant strain of PCC 7942 harboring NS1::P_{trc}-*sps* and NS3::P_{trc}-*cscB*, Sp^r Cm^r	Duan et al., 2016
SZ41	Mutant strain derived from FL130, carrying atpA with the C252F point mutation	This study
ZN44	Mutant strain of PCC 7942 harboring NS1::P_{rbcL}-pdc_{ZM}-*slr1192*, Sp^r	This study
ZN45	Mutant strain derived from ZN44, carrying AtpA with the C252F point mutation	This study
Plasmids		
pSS3	Carrying the wild-type PCC 7942 *atpA* gene	This study
pSS18	Carrying the PCC 7942 *atpA* mutant gene with the C252F mutation	This study
pZN45	Carrying the NS1UP-Sp^r-P_{rbcL}-pdc_{ZM}-*slr1192*-NS1DOWN cassette	This study

[a] *P_{trc}, trc promoter; cscB, proton/sucrose exporter gene from Escherichia coli; sps, encoding a natively fused protein of sucrose-phosphate synthase SPS; NS1 and NS3, different neutral sites in the genome of PCC 7942; Ap^r, ampicillin resistance; Cm^r, chloramphenicol resistance; Sp^r, spectinomycin resistance.*

TABLE 2 | Primers used in this study.

Primer	Sequence (5′ → 3′)	Purpose
AtpA-UP500-F-*Nde*I	AAATTCATATGGGATGCAGCCCTATTCCGAA	Amplifying the *atpA* gene
AtpA-Down500-R-*Eco*RI	AACCTGAATTCCGGGATTTGCTCCAAACCAC	Amplifying the *atpA* gene
AtpA-before-F	GATTTCGATCAGTTTGGCCGCC	Checking AtpA genotypes of *Synechococcus elongatus* PCC 7942 mutants
AtpA-after-R	TCGCGAATCGCCTTGAGGTTTG	Checking AtpA genotypes of *Synechococcus elongatus* PCC 7942 mutants
pSN44-NS1-r	TTTGTTCGCCCAGCTTCTGTATGGCTCGAGCTTCT GGAGCAGGAAGATGT	Amplifying the backbone of pSN44
pSN44-NS1-f	TGCTCAGCCATAGTAAAAATTAGTCCCTGCTCGTC ACGCTTTCAGGCACC	Amplifying the backbone of pSN44
pSN44-slr1192-r	CTAATTTTTACTATGGCTGA	Amplifying the Sp^r-P_{rbcL}-pdc_{ZM}-*slr1192* DNA fragment
pSN44-sp-f	GCATGCCCGTTCCATACAGA	Amplifying the Sp^r-P_{rbcl}-pdc_{ZM}-*slr1192* DNA fragment

transplantation to photosynthetic cell factories could be expected through similar procedures developed in this manuscript, aiming to optimize the growth or tolerance properties. In addition, to some gene deficiency-related growth advantages (meaning benefits caused by loss of specific gene functions) (Joseph et al., 2014; Kirst et al., 2014), this strategy could be expected to work and facilitate the rapid isolation of the gene-deficient mutants. However, it is still noteworthy that the application of this strategy to other targets might be limited by the significant degrees of the growth advantages endowed by specific mutations, which might not be as effective as that from AtpA-C252 (stress tolerances coupled with growth advantages). To this end, systematic optimization of selective pressure strengths and methods would be required in order to achieve the ideal effects of strain improvements.

CONCLUSION

High light and high temperature tolerances are important properties for cyanobacterial cell factories, aiming to put the photosynthetic biomanufacturing technology into practice. We developed a rapid and convenient strategy for improving cellular tolerances to high light and high temperature in an important cyanobacterial chassis PCC 7942 derived cell factory by antibiotics-free introduction of an AtpA-C252F mutation. Adopting this strategy, cellular robustness and sucrose synthesizing capacities of the PCC 7942 derived cell factory were significantly improved.

MATERIALS AND METHODS

Chemicals and Reagents

All reagents were purchased from Sigma-Aldrich (United States). *Taq* and *pfu* DNA polymerases for PCR were purchased from Transgene Biotech (Beijing, China). T4 DNA ligase and restriction enzymes were purchased from Fermentas (Canada) or New England Biolabs (Japan). The kits for molecular cloning were from Omega Bio-tek (Norcross, GA, United States). Oligonucleotides were synthesized, and DNA sequencing was performed by Tsingke (Qingdao, China).

Construction of Plasmids and Strains

Escherichia coli DH5α (TaKaRa, Dalian, China) was used as a host for cloning. The strains constructed and used in the present study are listed in **Table 1**. All the constructed plasmids employed pUC19 as backbone. To construct pSS3 and pSS18, AtpA-encoding gene containing 252C/252F was cloned from the chromosome of PCC 7942 and PCC 7942-C252F *via* PCR using the primers AtpA-UP500-F-*Nde*I and AtpA-Down500-R-*Eco*RI listed in **Table 2**. PCR products were purified using the E.Z.N.A

Cycle Pure Kit (Omega Bio-Tek, Norcross, GA, United States), and then the AtpA/AtpA-C252F fragments were digested with *Nde*I and *Eco*RI and inserted into pUC19 for constructing the target plasmids pSS3 and pSS18. To construct the ZN44 strain, a cassette containing the spectinomycin resistance gene, the *PrbcL* promoter sequence, the Pdc_{ZM} gene, and the *slr1192* gene was amplified from a previously constructed pZG25 plasmid (Gao et al., 2012) and ligated with the backbone of another previously constructed plasmid pFL20n (Duan et al., 2016) containing the upstream and downstream sequences of neutral site I (NS1). The final obtained plasmid was termed as pZN44. All the resulting plasmids were then verified by Sanger gene sequencing and are listed in **Table 1**.

Transformation of the PCC 7942 Strains

Transformation of PCC 7942 derived cell factory FL130 was performed according to a previously reported method with optimization and quantitation (Lou et al., 2018). Briefly, 2 ml WT or FL130 broth with an OD_{730} of 1.0 was centrifuged at 6,000 × *g* for 5 min and then re-suspended in 250 μl of fresh BG11 medium. Next, 200 ng plasmid was added and incubated in the dark at 150 rpm and 30°C for 6–24 h. Then, 5 μl of the mixtures (about 4×10^6 cells) was plated on solid BG11 plates with 1.5% agar after transformation and incubated at 45°C and 300 μmol photons/m^2/s for 2 days. The obtained colonies would be picked, streaked on fresh BG11 plates, and incubated for another 24 h under the same conditions. Genotypes of the final survived transformants would be checked, and the *atpA* gene would be amplified for Sanger sequencing.

Cultivations of Cyanobacterial Strains

For phenotypes evaluations, PCC 7942 WT and the derived strains would be cultivated in BG11 medium with column photobioreactors (3 cm diameter), and the temperature and illumination strengths would be set as required. The light would be provided by incandescent lamps (NVC, NDL433SI-28W). Then, 3% (volume to volume) CO_2 air would be bubbled for carbon source supplementations. For liquid cultivation of the WT PCC 7942 and the derived mutant carrying the AtpA-C252F mutation, the normal conditions were set as 30°C and 50 μmol photons/m^2/s, and the respective stressful conditions were set as 44°C and 400 μmol photons/m^2/s. For sucrose production, 150 mM NaCl and 0.1 mM isopropyl-D-1-thiogalactopyranoside (IPTG) would be added to the culture medium. During this process, normal conditions were set as 30°C and 100 μmol photons/m^2/s, whereas stressful conditions were set as 40°C and 400 μmol photons/m^2/s. The growth of each cyanobacterial strain was monitored by measuring the optical density at 730 nm (OD_{730}). Dry cell weights (DCWs) were determined following the methods previously described (Wang et al., 2019). As for the cultivation of ethanologenic strains, the conditions were also set as 30°C and 400 μmol photons/m^2/s, and the ethanol production would be evaluated as previously described (Wang et al., 2019).

Oxygen Evolution Rates Determination

Oxygen concentration was measured using fiber-based and contactless oxygen microsensors (PyroScience, Aachen, Germany). The sensor was calibrated with air-saturated water and de-oxygenated water as 100% and 0% O_2 levels. The culture broths of FL130 or SZ41 were transferred to the respiration vials and placed in the corresponding culture conditions. The oxygen concentration in the respiration vials was continuously monitored by the oxygen microsensor connected to the oxygen logger software. The final photosynthetic oxygen evolution rate was calculated according to the *Chl*a content, which was determined spectrophotometrically at OD_{665} and OD_{720} in methanol extracts and calculated with the formula: *Chl*a (mg/L) = 12.9447 × (A665 − A720).

Determination of Sucrose and Glycogen Contents in PCC 7942

To determine the amount of extracellular sucrose in PCC 7942 culture broth, 1 ml of cyanobacterial culture was centrifuged, and sucrose in the supernatant was measured using the sucrose/D-glucose assay kit (Megazyme). The glycogen contents in PCC 7942 cells were measured as previously introduced with modifications (Chi et al., 2019). After the glycogen precipitants were hydrolyzed to glucose by treatment with amyloglucosidase at 60°C for 2 h, glucose in 100 mM sodium acetate (pH 4.5) solution was measured using the sucrose/D-glucose assay kit (Megazyme).

DATA AVAILABILITY STATEMENT

The raw data supporting the conclusions of this article will be made available by the authors, without undue reservation.

AUTHOR CONTRIBUTIONS

SZha, SZhe, XZ, and YD performed the research project. GL and XL supervised the research project and guided the design of experiments. SZha, GL, and XL drafted and revised the manuscript. All authors contributed to the article and approved the submitted version.

FUNDING

This work was supported by the National Natural Science Foundation of China (grant numbers 31525002, 31872624, 31770092, 32070084, and 31700048), Strategic Priority Research Program of the Chinese Academy of Sciences (Transformational Technologies for Clean Energy and Demonstration, XDA21010211), and Shandong Taishan Scholarship (to XL).

SUPPLEMENTARY MATERIAL

The Supplementary Material for this article can be found online at: https://www.frontiersin.org/articles/10.3389/fmicb.2021.647164/full#supplementary-material

REFERENCES

Atsumi, S., Higashide, W., and Liao, J. C. (2009). Direct photosynthetic recycling of carbon dioxide to isobutyraldehyde. *Nat. Biotechnol.* 27, 1177–1142. doi: 10.1038/nbt.1586

Chaurasia, A. K., and Apte, S. K. (2009). Overexpression of the groESL operon enhances the heat and salinity stress tolerance of the nitrogen-fixing *Cyanobacterium* anabaena sp strain PCC7120. *Appl. Environ. Microbiol.* 75, 6008–6012. doi: 10.1128/Aem.00838-09

Chi, X., Zhang, S., Sun, H., Duan, Y., Qiao, C., Luan, G., et al. (2019). Adopting a theophylline-responsive riboswitch for flexible regulation and understanding of glycogen metabolism in *Synechococcus elongatus* PCC7942. *Front. Microbiol.* 10:551. doi: 10.3389/fmicb.2019.00551

Chwa, J. W., Kim, W. J., Sim, S. J., Um, Y., and Woo, H. M. (2016). Engineering of a modular and synthetic phosphoketolase pathway for photosynthetic production of acetone from CO in *Synechococcus elongatus* PCC 7942 under light and aerobic condition. *Plant Biotechnol. J.* 14, 1768–1776. doi: 10.1111/pbi.12536

Deng, M. D., and Coleman, J. R. (1999). Ethanol synthesis by genetic engineering in cyanobacteria. *Appl. Environ. Microbiol.* 65, 523–528.

Duan, Y., Luo, Q., Liang, F., and Lu, X. (2016). Sucrose secreted by the engineered cyanobacterium and its fermentability. *J. Ocean Univ. China* 15, 890–896. doi: 10.1007/s11802-016-3007-8

Ducat, D. C., Avelar-Rivas, J. A., Way, J. C., and Silver, P. A. (2012). Rerouting carbon flux to enhance photosynthetic productivity. *Appl. Environ. Microbiol.* 78, 2660–2668. doi: 10.1128/Aem.07901-11

Gao, Z. X., Zhao, H., Li, Z. M., Tan, X. M., and Lu, X. F. (2012). Photosynthetic production of ethanol from carbon dioxide in genetically engineered cyanobacteria. *Energy. Environ. Sci.* 5, 9857–9865. doi: 10.1039/C2ee22675h

Hirokawa, Y., Kanesaki, Y., Arai, S., Saruta, F., Hayashihara, K., Murakami, A., et al. (2018). Mutations responsible for alcohol tolerance in the mutant of *Synechococcus elongatus* PCC 7942 (SY1043) obtained by single-cell screening system. *J. Biosci. Bioengin.* 125, 572–577. doi: 10.1016/j.jbiosc.2017.11.012

Joseph, A., Aikawa, S., Sasaki, K., Matsuda, F., Hasunuma, T., and Kondo, A. (2014). Increased biomass production and glycogen accumulation in apcE gene deleted Synechocystis sp PCC 6803. *Amb. Express* 4:17. doi: 10.1186/s13568-014-0017-z

Kirst, H., Formighieri, C., and Melis, A. (2014). Maximizing photosynthetic efficiency and culture productivity in cyanobacteria upon minimizing the phycobilisome light-harvesting antenna size. *Biochim. Et Biophys. Acta-Bioenerg.* 1837, 1653–1664. doi: 10.1016/j.bbabio.2014.07.009

Kusakabe, T., Tatsuke, T., Tsuruno, K., Hirokawa, Y., Atsumi, S., Liao, J. C., et al. (2013). Engineering a synthetic pathway in cyanobacteria for isopropanol production directly from carbon dioxide and light. *Metab. Eng.* 20, 101–108. doi: 10.1016/j.ymben.2013.09.007

Lan, E. I., Chuang, D. S., Shen, C. R., Lee, A. M., Ro, S. Y., and Liao, J. C. (2015). Metabolic engineering of cyanobacteria for photosynthetic 3-hydroxypropionic acid production from CO2 using *Synechococcus elongatus* PCC 7942. *Metab. Eng.* 31, 163–170. doi: 10.1016/j.ymben.2015.08.002

Lan, E. I., and Liao, J. C. (2011). Metabolic engineering of cyanobacteria for 1-butanol production from carbon dioxide. *Metab. Eng.* 13, 353–363. doi: 10.1016/j.ymben.2011.04.004

Li, H., and Liao, J. C. (2013). Engineering a cyanobacterium as the catalyst for the photosynthetic conversion of CO2 to 1,2-propanediol. *Microb. Cell. Fact.* 12:4. doi: 10.1186/1475-2859-12-4

Lou, W. J., Tan, X. M., Song, K., Zhang, S. S., Luan, G. D., Li, C., et al. (2018). A specific single nucleotide polymorphism in the ATP synthase gene significantly improves environmental stress tolerance of *Synechococcus elongatus* PCC 7942. *Appl. Environ. Microbiol.* 84, e1218–e1222. doi: 10.1128/AEM.01222-18

Lu, X. (2010). A perspective: photosynthetic production of fatty acid-based biofuels in genetically engineered cyanobacteria. *Biotechnol. Adv.* 28, 742–746. doi: 10.1016/j.biotechadv.2010.05.021

Luan, G., and Lu, X. (2018). Tailoring cyanobacterial cell factory for improved industrial properties. *Biotechnol. Adv.* 36, 430–442. doi: 10.1016/j.biotechadv.2018.01.005

Luan, G., Zhang, S., Wang, M., and Lu, X. (2019). Progress and perspective on cyanobacterial glycogen metabolism engineering. *Biotechnol. Adv.* 37, 771–786. doi: 10.1016/j.biotechadv.2019.04.005

Melis, A. (2009). Solar energy conversion efficiencies in photosynthesis: minimizing the chlorophyll antennae to maximize efficiency. *Plant Sci.* 177, 272–280. doi: 10.1016/j.plantsci.2009.06.005

Niederholtmeyer, H., Wolfstadter, B. T., Savage, D. F., Silver, P. A., and Way, J. C. (2010). Engineering cyanobacteria to synthesize and export hydrophilic products. *Appl. Environ. Microbiol.* 76, 3462–3466. doi: 10.1128/AEM.00202-10

Oliver, J. W., and Atsumi, S. (2014). Metabolic design for cyanobacterial chemical synthesis. *Photosynth. Res.* 120, 249–261. doi: 10.1007/s11120-014-9997-4

Oliver, J. W. K., Machado, I. M. P., Yoneda, H., and Atsumi, S. (2013). Cyanobacterial conversion of carbon dioxide to 2,3-butanediol. *Proc. Natl. Acad. Sci. U S A* 110, 1249–1254.

Qiao, C., Duan, Y., Zhang, M., Hagemann, M., Luo, Q., and Lu, X. (2018). Effects of reduced and enhanced glycogen pools on salt-induced sucrose production in a sucrose-secreting strain of *Synechococcus elongatus* PCC 7942. *Appl. Environ. Microbiol.* 84, e02017–e02023. doi: 10.1128/AEM.02023-17

Ruffing, A. M., and Jones, H. D. T. (2012). Physiological effects of free fatty acid production in genetically engineered *Synechococcus elongatus* PCC 7942. *Biotechnol. Bioengin.* 109, 2190–2199. doi: 10.1002/bit.24509

Sakai, M., Ogawa, T., Matsuoka, M., and Fukuda, H. (1997). Photosynthetic conversion of carbon dioxide to ethylene by the recombinant cyanobacterium, Synechococcus sp. PCC 7942, which harbors a gene for the ethylene-forming enzyme of *Pseudomonas* syringae. *J. Ferment. Bioeng.* 84, 434–443. doi: 10.1016/S0922-338x(97)82004-1

Shen, C. R., and Liao, J. C. (2012). Photosynthetic production of 2-methyl-1-butanol from CO2 in cyanobacterium *Synechococcus elongatus* PCC7942 and characterization of the native acetohydroxyacid synthase. *Energy Environ. Sci.* 5, 9574–9583. doi: 10.1039/c2ee23148d

Song, K., Tan, X., Liang, Y., and Lu, X. (2016). The potential of *Synechococcus elongatus* UTEX 2973 for sugar feedstock production. *Appl. Microbiol. Biotechnol.* 100, 7865–7875. doi: 10.1007/s00253-016-7510-z

Su, H. Y., Chou, H. H., Chow, T. J., Lee, T. M., Chang, J. S., Huang, W. L., et al. (2017). Improvement of outdoor culture efficiency of cyanobacteria by over-expression of stress tolerance genes and its implication as bio-refinery feedstock. *Biores. Technol.* 244, 1294–1303. doi: 10.1016/j.biortech.2017.04.074

Tan, X., Hou, S., Song, K., Georg, J., Klahn, S., Lu, X., et al. (2018). The primary transcriptome of the fast-growing cyanobacterium *Synechococcus elongatus* UTEX 2973. *Biotechnol. Biofuels* 11:218. doi: 10.1186/s13068-018-1215-8

Uchiyama, J., Kanesaki, Y., Iwata, N., Asakura, R., Funamizu, K., Tasaki, R., et al. (2015). Genomic analysis of parallel-evolved cyanobacterium *Synechocystis* sp. PCC 6803 under acid stress. *Photosynth Res.* 125, 243–254. doi: 10.1007/s11120-015-0111-3

Ungerer, J., Wendt, K. E., Hendry, J. I., Maranas, C. D., and Pakrasi, H. B. (2018). Comparative genomics reveals the molecular determinants of rapid growth of the cyanobacterium *Synechococcus elongatus* UTEX 2973. *Proc. Natl. Acad. Sci. U S A* 115, E11761–E11770. doi: 10.1073/pnas.1814912115

Wang, M., Luan, G., and Lu, X. (2019). Systematic identification of a neutral site on chromosome of *Synechococcus sp*. PCC7002, a promising photosynthetic chassis strain. *J. Biotechnol.* 295, 37–40. doi: 10.1016/j.jbiotec.2019.02.007

Yu, H., Li, X., Duchoud, F., Chuang, D. S., and Liao, J. C. (2018). Augmenting the calvin-benson-bassham cycle by a synthetic malyl-CoA-glycerate carbon fixation pathway. *Nat. Commun.* 9:2008. doi: 10.1038/s41467-018-04417-z

Conflict of Interest: The authors declare that the research was conducted in the absence of any commercial or financial relationships that could be construed as a potential conflict of interest.

frontiers in Microbiology

ORIGINAL RESEARCH
published: 13 April 2021
doi: 10.3389/fmicb.2021.607411

The Effect of Promoter and RBS Combination on the Growth and Glycogen Productivity of Sodium-Dependent Bicarbonate Transporter (SbtA) Overexpressing *Synechococcus* sp. PCC 7002 Cells

Jai Kumar Gupta[1] *and Shireesh Srivastava*[1,2]*

[1] *Systems Biology for Biofuels Group, International Centre for Genetic Engineering and Biotechnology (ICGEB), New Delhi, India,* [2] *Department of Biotechnology-International Centre for Genetic Engineering and Biotechnology (DBT-ICGEB), Centre for Advanced Bioenergy Research, New Delhi, India*

OPEN ACCESS

Edited by:
Pramod P. Wangikar, Indian Institute of Technology Bombay, India

Reviewed by:
Reena Ajit Pandit, Institute of Chemical Technology, India
Annesha Sengupta, Washington University in St. Louis, United States
Debasish Das, Indian Institute of Technology Guwahati, India

***Correspondence:**
Shireesh Srivastava
shireesh@icgeb.res.in

Specialty section:
This article was submitted to Microbiotechnology, a section of the journal Frontiers in Microbiology

Received: *17 September 2020*
Accepted: *22 March 2021*
Published: *13 April 2021*

Citation:
Gupta JK and Srivastava S (2021) The Effect of Promoter and RBS Combination on the Growth and Glycogen Productivity of Sodium-Dependent Bicarbonate Transporter (SbtA) Overexpressing Synechococcus sp. PCC 7002 Cells. Front. Microbiol. 12:607411. doi: 10.3389/fmicb.2021.607411

Sodium dependent bicarbonate transporter, SbtA is a high-affinity, inducible bicarbonate transporter in cyanobacterial cells. Our previous work has shown that overexpression of this transporter can significantly increase growth and glycogen accumulation in *Synechococcus* sp. PCC 7002 cells. In this work, we have tested the effect of two different RBS sequences (RBS1: GGAGGA and RBS2: AGGAGA) and three different promoters (P_{cpcB}, $P_{cpcB560}$, and P_{rbcL2}) on the growth and glycogen production in SbtA-overexpressing *Synechococcus* sp. PCC 7002 cells. Our results show that P_{cpcB} or $P_{cpcB560}$ were more effective than P_{rbcL2} in increasing the growth and glycogen content. The choice of RBS sequence had relatively minor effect, though RBS2 was more effective than RBS1. The transformant E, with $P_{cpcB560}$ and RBS2, showed the highest growth. The biomass after 5 days of growth on air or 1% CO_2 was increased by about 90% in the strain E compared to PCC 7002 cells. All transformants overexpressing SbtA had higher glycogen content. However, growing the cells with bubbling of 1% CO_2 did not increase cellular glycogen content any further. The strain E had about 80% higher glycogen content compared to WT PCC 7002 cells. Therefore, the glycogen productivity of the strain E grown with air-bubbling was about 2.5-fold that of the WT PCC 7002 cells grown similarly. Additionally, some of the transformants had higher chlorophyll content while all the transformants had higher carotenoid content compared to the PCC 7002 cells, suggesting interaction between carbon transport and pigment levels. Thus, this work shows that the choice of photosynthetic promoters and RBSs sequences can impact growth and glycogen accumulation in SbtA-overexpressing cells.

Keywords: promoter, cyanobacteria, biomass, feedstock, glycogen stores, bicarbonate transport, RBS

INTRODUCTION

Cyanobacteria are fast-growing prokaryotic microorganisms capable of oxygenic photosynthesis. They offer advantages of small genome size and genetic amenability (Gantt, 2011; Nozzi et al., 2013; Singh et al., 2016; Jaiswal et al., 2018; Ahmad et al., 2020) and serve as attractive hosts for synthetic biology applications, ranging from metabolic engineering for the production of industrial

biochemicals to microbial energy storage (Englund et al., 2016; Vavitsas et al., 2019; Sengupta et al., 2020b). Genetic engineering approaches and tools have been developed for some species (Huang and Lindblad, 2013). Many cyanobacteria, including all the model species, are naturally transformable and can integrate transgenes into their chromosomes by homologous recombination (Ludwig and Bryant, 2012; Vavitsas et al., 2019; Sengupta S. et al., 2020). Cultivation of marine cyanobacteria would help in large scale sustainable conversion of greenhouse CO_2 to useful products while reducing freshwater usage (Markley et al., 2015; Englund et al., 2016).

Synechococcus sp. PCC 7002 (hereafter PCC 7002) is a fast-growing marine cyanobacterium with an optimal growth temperature of 38°C (Ludwig and Bryant, 2012), and is tolerant to variations in nutrient availability, salinity, pH, irradiance and temperature (Ludwig and Bryant, 2012). PCC 7002 has been engineered earlier for the synthesis of a number of bioproducts viz. ethanol (Kopka et al., 2017), succinic acid, bioplastics, terpenoids (Davies et al., 2014). However, the growth rate and cell titers are still low to be commercially viable (Markley et al., 2015). We have previously engineered PCC 7002 with the bicarbonate transporters SbtA and BicA and shown improvement in their growth and intracellular product (glycogen) content (Gupta et al., 2020). While BicA is a relatively well-studied bicarbonate transporter, there are only a few studies on SbtA. SbtA is a high-affinity, low flux, inducible sodium (Na +) dependent HCO_3^- transporter, functioning as an Na^+/HCO_3^- symporter, that has been shown to be upregulated in carbon limiting conditions in earlier studies (Shibata et al., 2002; Price, 2011). Our work had shown that overexpression of SbtA can promote the growth of PCC 7002 cells to the same levels as that observed with the overexpression of BicA (Gupta et al., 2020).

Protein levels are commonly controlled through regulation of transcription and translation initiation rates (Markley et al., 2015). In previous studies it has been shown that promoter and ribosome binding sites (RBS) sequences greatly affect expression of a target gene (Shi et al., 2018). Promoters are one of the key synthetic biology components in cyanobacteria. Transcription rates can be regulated by choosing a suitable promoter for a target gene (Markley et al., 2015). Many promoters—constitutive, inducible and repressible are available (Vavitsas et al., 2019). Strength of a promoter shows a direct relationship with the gene expression (Bienick et al., 2014). Activity of promoters can vary based on culture conditions and presence of metal ions (Englund et al., 2016). The promoters P_{rbcL2A} and P_{cpcB} are responsible for the transcription of genes coding for large subunit 2A of RuBisCO and c-phycocyanin beta subunit, respectively (Huang et al., 2010; Markley et al., 2015). These are among the most common promoters used in cyanobacteria (Till et al., 2020). Presence of multiple transcription factor binding sites (TFBSs) is crucial for the promoter strength. $P_{cpcB560}$, a modified version of *Synechocystis* sp. PCC 6803 *cpcB* promoter, was reported in an earlier study and contains the P_{cpcB} promoter with 14 TFBSs (Zhou et al., 2014). The promoter size of $P_{cpcB560}$ was smaller than the native promoter P_{cpcB} by 29 bps. The expression of heterologous genes using the $P_{cpcB560}$ promoter in *Synechocystis* sp. PCC 6803 cells resulted in expression level comparable to that obtained in *Escherichia coli* (*E. coli*) (Zhou et al., 2014).

Another element that can significantly impact the translation rate and hence the protein levels is the strength or accessibility of ribosome-binding sites (RBS) (Reeve et al., 2014; Markley et al., 2015).

In the present study we have investigated the combinatorial effect of three strong promoters (viz. P_{rbcL2A}, P_{cpcB}, and $P_{cpcB560}$, all from *Synechocystis* sp. PCC 6803) and two RBSs, of different strengths, viz. RBS1 (GGAGGA) and RBS2 (AGGAGA), on the expression of a membrane protein, SbtA, and the associated physiological responses (cellular growth and glycogen content) in the PCC 7002 cells. Our results indicate that the appropriate combination of strong promoter and RBS can indeed impact SbtA expression, growth and glycogen levels.

MATERIALS AND METHODS

Materials

Ampicillin disodium salt, KCl, bacteriological agar and kanamycin monosulfate were purchased from Amresco (Solon, OH, United States). Tris base and NaCl were from Thermo Fisher Scientific (Mumbai, India) while $CuSO_4{\cdot}5H_2O$, H_3BO_3, KH_2PO_4, $Na_2EDTA.2H_2O$, $CaCl_2{\cdot}2H_2O$, $MgSO_4{\cdot}7H_2O$, $NaNO_3$, $FeCl_3{\cdot}6H_2O$, $CoCl_2{\cdot}6H_2O$ $MnCl_2{\cdot}4H_2O$, $ZnCl_2$, vitamin B_{12}, and RNaseZAP were from Sigma-Aldrich (St. Louis, MO, United States). Primers were purchased from Sigma Aldrich. Details of kits used in various molecular biological methods such as genomic DNA and plasmid isolation, PCR purification etc. are mentioned further. All the restriction enzymes used in the study were from Thermo-Scientific (Mumbai, India).

Cyanobacterial Strains and Growth Conditions

Synechococcus sp. PCC 7002 cells, originally obtained from the Pasteur Culture Collection (PCC), Paris, France, were cultured in A^+ medium in 250 mL shake flasks (Ludwig and Bryant, 2012) in an incubator shaker (Innova 44R, New Brunswick Scientific, Edison, NJ, US) at 150 rpm and 30°C with a light:dark cycle of 16:8 h under a light intensity of 150 μmol m^{-2} s^{-1}, illuminated by LED lamps. The composition of medium A^+ is 18 g L^{-1} NaCl, 5.0 g L^{-1} $MgSO_4{\cdot}7H_2O$, 30 mg L^{-1} Na_2 $EDTA{\cdot}2H_2O$, 0.6 g L^{-1} KCl, 0.37 g L^{-1} $CaCl_2$, 1.0 g L^{-1} $NaNO_3$, 50 mg L^{-1} KH_2PO_4, 10 mL L^{-1} Tris/HCl (Stock solution 100 g L^{-1}, pH 8.2), 1 mL L^{-1} A + trace components. 1 mL L^{-1} vitamin B_{12} (stock solution 4 mg L^{-1}) was added. A+ trace components (1000X) composition includes: 34.3 g L^{-1} H_3BO_3, 0.315 g L^{-1} $ZnCl_2$, 30 mg L^{-1} MoO_3 (85%), 0.389 g L^{-1} $FeCl_3{\cdot}6H_2O$, 0.43 g L^{-1} $MnCl_2{\cdot}4H_2O$, 0.3 mg L^{-1} $CuSO_4{\cdot}5H_2O$, 1.2 mg L^{-1} $CoCl_2{\cdot}6H_2O$ (Utex Culture Collection of Algae, 2021). Experiments were conducted in 250 mL Dreschel (gas-washing) bottles (Borosil, India) containing 150 mL culture. The cultures were bubbled with air or 1% CO_2 in air through a gas dispersion tube with porous fritted glass tip (Sigma Aldrich Chemical Co.) at the rate of 0.5 L/min. The culture bottles were kept in a water bath shaker maintained at an optimal temperature of

38°C (Ludwig and Bryant, 2012) and continuously illuminated from the top with LED lights having a light intensity of 350 μmol m^{-2} s^{-1}. Biomass density was monitored every 24 h by measuring the optical density at 730 nm (OD_{730}). Cultures were stopped at the end of 5 days for quantification of various parameters.

Plasmids Construction and Cloning

The promoters used in this study- P_{cpcB}, $P_{cpcB560}$ and P_{rbcL2A}, were amplified from the genomic DNA of *Synechocystis* sp. PCC 6803 while the kanR2 gene was amplified from the commercial vector pET-28a(+). The genes *sbtA* (SYNPCC7002_A0470) encoding the HCO_3^- transporter (Price et al., 2011), neutral sites NS1 (SYNPCC7002_A0935) and NS2 (SYNPCC7002_A0936) (Davies et al., 2014) encoding hypothetical proteins and GroEL terminator were amplified from the genomic DNA of PCC 7002 cells. The DNA fragments cloned are shown in **Figure 1**. These DNA sequences were PCR amplified using Phusion polymerase (Thermo Scientific, Mumbai, India). GeneJET PCR purification kit (Thermo Fisher Scientific, Lithuania) was used for purification of the PCR-amplified products. The RBS sequences and an extra 7 bp sequence for ribosome binding were included in the forward primers designed for the *sbtA* gene (see **Supplementary Table 2** for the list of primers used in this study). The promoters stretch used in this work did not include the native RBS sequence. pBluescript II SK(+) was used as a cloning vector for the ligation of DNA fragments by sticky-end cloning, performed using the specific restriction enzymes and T4 DNA ligase. pBluescript II SK(+) was selected as a cloning vector because of its small backbone size (2961 base pairs) and presence of a large number of common restriction enzyme recognition sites in its MCS (multiple cloning site) region (Alting-Mees and Short, 1989; Abe et al., 1996; Hong et al., 2009). The cloning was performed in *E. coli* DH-5α as follows. Competent cells were prepared using a previously-published protocol (Im, 2011). Transformation of the competent *E. coli* cells was done as per an earlier published protocol (Froger and Hall, 2007) with some modifications. A vial containing 50 μL stock of competent cells, kept at −80°C was thawed on ice. Three to five microliter of the ligation mixture was added to the competent cells. The tube was flicked 3–4 times to mix the cells and DNA. Cells were further kept on ice for 30 min. Heat shock was given at 42°C for 90 s, following which the tube was quickly kept on ice for 2 min. Eight hundred microliter of sterile LB broth (Himedia, India) was added and the tube was kept in a 37°C incubator shaker at 150 rpm for 1 h. Cells were then centrifuged at 4,000 × *g* for 5 min at room temperature. Eight hundred microliter of the supernatant was discarded and the pellet was resuspended and spread on a LB agar plate containing 100 μg/mL ampicillin, and incubated overnight (~16 h) at 37°C. Single colonies obtained were used for further analyses. After transformation with the respective plasmids, the *E. coli* cells were cultured overnight at 37°C in glass tubes containing 5 mL LB medium supplemented with the appropriate antibiotic concentration at 150 rpm in an incubator shaker (Innova 44R, New Brunswick Scientific, NJ). For the extraction of plasmids, the GeneJET Plasmid Miniprep Kit (Thermo Fisher Scientific, Vilnius, Lithuania) was used.

Two microgram g of the cloned plasmids, viz. pA, pB, pC, pD, pE, and pF (**Supplementary Figure 4**) were digested with the restriction enzymes *Xho*I and *Sac*I for 30 min in a 1.5 mL tube with 30 μL reaction mixture at 37°C in a water bath to separate the cassette of interest from the host vector. The digested vector was separated on a 1% agarose gel and the DNA of interest was eluted in MilliQ water using a gel extraction kit (Thermo Scientific, Vilnius, Lithuania). PCC 7002 cells were transformed with the resulting DNA solution as per the following protocol.

Transformation of *Synechococcus* sp. PCC 7002 Cells

The work was approved by the institutional biosafety committee (IBSC). Transformation was based on the earlier protocols (Ruffing, 2014). Linearized DNA fragments obtained from DNA extracted from respective transformed *E. coli* host cells were used for the transformation of PCC 7002. PCC 7002 cells were grown in A^+ medium under 150 μmol m^{-2} s^{-1} in incubator shaker (Innova 44R, New Brunswick Scientific) at 30°C with 150 rpm until an $OD_{730} \sim 1$. Eight hundred microliter culture was taken in a microcentrifuge tube and the DNA (∼ 1 μg) was added. The tube was kept for 24 h in the incubator shaker and then centrifuged at room temperature for 5 min at 2,500 × *g*. The pellet obtained was spread on A^+ agar plates containing 50 μg/mL kanamycin monosulfate. The single isolated colonies were re-streaked four more times on antibiotic plates for complete segregation of transformants. Genomic DNA of the colonies was extracted and PCR was done to confirm integration of the constructs in the genome. Positive clones were used for further analyses.

Analysis of Gene Expression by Real-Time PCR and Western Blotting

RNA and proteins were extracted as in our earlier study (Gupta et al., 2020). For RNA isolation, 50 mL culture in exponential phase was centrifuged for 5 min at 4000 × *g*. The pellet was crushed in presence of liquid nitrogen using a pestle wiped with RNaseZAP and washed with RNase-free water. RNeasy Plant Mini Kit (Qiagen, Hilden, Germany) was used as per the kit's protocol to isolate RNA. The resulting RNA was treated with DNase-I to remove any traces of DNA. cDNA was synthesized from 1 μg of the DNase-treated RNA using a cDNA synthesis kit (Thermo Fisher Scientific, Lithuania). Quantitative real time PCR (qRT-PCR) was conducted using KAPA SYBR Fast Kit (Kapa Biosystems, Sigma-Aldrich, South Africa). An earlier study, that had compared suitability of six candidate genes to be used as internal reference gene in PCC 7002 cells, reported phosphoenolpyruvate carboxylase (SYNPCC7002_A1414, *ppC*), as a suitable reference gene on the basis of its M-value (gene stability measure) (Szekeres et al., 2014). Therefore, in this study, *ppc* was used as the internal reference gene. Primers used in qRT-PCR are listed in **Supplementary Table 4**). $2^{(-\Delta\Delta Ct)}$ values were calculated for the relative change in expression.

An earlier published protocol was used (Gupta et al., 2020) for western blotting. 20 mL culture was centrifuged and the

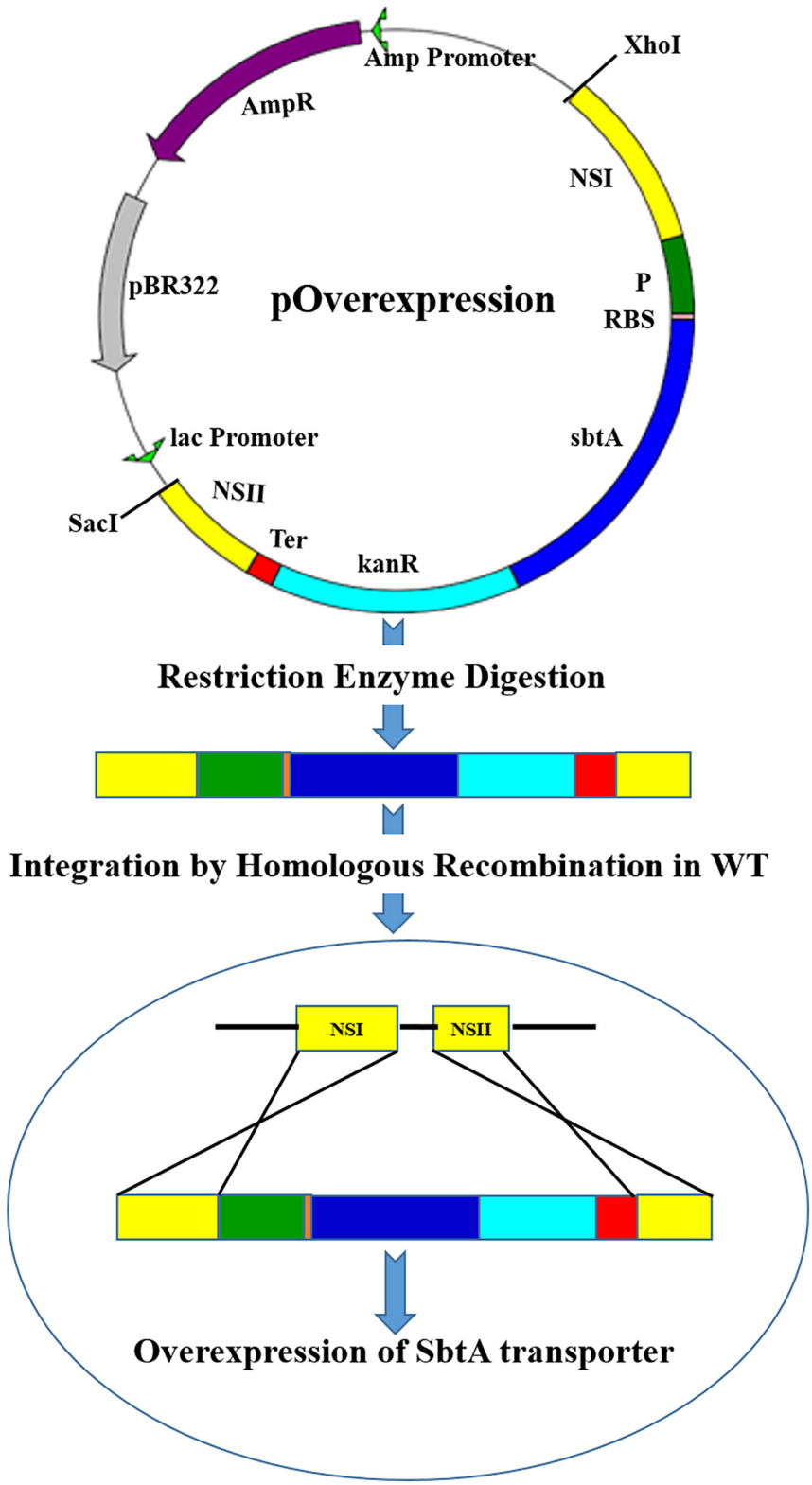

FIGURE 1 | A diagram showing integration of the gene cassettes into the genomic DNA of PCC 7002 through homologous recombination. The vector pOverexpression shows a generalized plasmid for the overexpression of SbtA with different promoters and RBSs sequences. NSI (neutral site I), P (Promoter), RBS (ribosome binding site), *sbtA* (gene coding for sodium dependent bicarbonate transporter SbtA), kanR (kanamycin resistance gene), Ter (terminator), and NSII (neutral site II).

pellet collected. 1mL lysis buffer (Du et al., 2014) and 100 μL of 0.1 mm glass beads were added and the cells were lysed using a beadbeater (FastPrep-24, MP Biomedicals, India) for 10 cycles of 30 s each with alternate chilling in between. The resulting cell lysate was centrifuged at 4°C for 15 s at 21,000 × *g*; the supernatant was transferred to another tube and centrifuged for 10 min. The pellet obtained was supplemented with sodium dodecyl sulfate (SDS) sample buffer containing 4% (w/v) SDS, 10% glycerol, 1 mM dithiothreitol (DTT) and 62.5 mM Tris–HCl, pH 6.8. Samples were incubated for 20 min at 70°C, and centrifuged for 15 min at 21,000 × *g*. Supernatant fraction was collected and protein concentration measured with a Pierce BCA Protein Assay Kit (Thermo Fisher Scientific, Rockford, United States). 100 μg protein sample was loaded and separated on a 12% SDS-polyacrylamide gel. Proteins were transferred onto a 0.22 μm PVDF membrane (Bio-Rad, United States) using a semi-dry transfer apparatus (Bio-Rad, United States) as per the company's protocol. The expression of His6-tagged SbtA was detected with a monoclonal anti-His antibody (Sigma-Aldrich) and a horseradish peroxidase-conjugated secondary antibody. Proteins were stained using a DAB substrate kit (Thermo Fisher Scientific, Rockford, United States) and visualized using chemiluminescence.

Dry Cell Weight Determination

The dry cell weights were measured as per our previously published protocol (Gupta et al., 2020). After centrifuging the cell culture (50 mL) at 2,500 × *g* for 10 min, the pellet obtained was washed twice in 8.25 mM Tris–HCl buffer (pH 8.2). Then, the pellet was dried for approximately 36 h at 65°C until the weight of the tube became constant. The weight of the tube was subtracted from the total weight to calculate the dry cell weights.

Measurement of Glycogen Content

Glycogen content was determined as per the earlier published literature (Dutt and Srivastava, 2018; Gupta et al., 2020). Cells were resuspended to reach OD_{730} of ∼2. 1 mL of the culture was pelleted down at room temperature for 5 min at 4,000 × *g*, and 7.5% H_2SO_4 was added to the pellet, and kept for 2 h at 100°C. The mixture was filtered through a 0.22 μm filter (Nylon-66, MDI Membrane Technologies, India) and separated in an HPLC (Agilent Technologies, United States) for the measurement of released glucose. Aminex HPX 87H column was used and 5 mM sulfuric acid was employed as the mobile phase at a flow rate of 0.3 mL min^{-1}.

Measurement of Photosynthetic Pigments

The photosynthetic pigments chlorophyll *a* and the carotenoids were measured as described in Gupta et al. (2020). One milliliter culture of cells resuspended at OD730 of ∼2 was centrifuged in a 1.5 mL microcentrifuge tube at 4,000 × *g* for 5 min. One milliliter ice-cold methanol (from Sigma-Aldrich, United States) was added to the pellet and mixed well. The tubes were then kept on ice in dark for 1 h to complete extraction of photosynthetic pigments. The tubes were then centrifuged at 4°C for 7 min at 21,000 × *g*. The resulting supernatant was analyzed spectrophotometrically at specific wavelengths (Lichtenthaler, 1987; Wellburn, 1994).

Statistical Analysis

Experiments were conducted in biological triplicates. Two-way ANOVA along with Tukey test for pairwise comparison was used for statistical analysis (SigmaPlot version 12.5, Systat Software Inc.).

RESULTS

Screening and Confirmation of Transformants by Genomic DNA PCR, qRT-PCR and Western Blotting

Table 1 shows the list of the transformants generated.

NSI to NSII sequence was PCR amplified from the genomic DNA of the WT and transformed PCC 7002 cells. The PCR product size was larger for the transformed cells than for the PCC 7002 cells, indicating integration of the gene cassette in genomic DNA within the neutral sites (**Figure 2A**). The size of PCR product from the transformants C and F is smaller because the P_{rbcL2A} promoter is about 300 bases smaller than the other 2 promoters. Transformant F has also been reported our earlier study (Gupta et al., 2020). The expression levels of SbtA were also determined through qRT-PCR. While all the transformants had 60–90-fold higher SbtA levels than WT, transformants

TABLE 1 | Showing the strains and plasmids used in our study.

Strain	Description
PCC 7002	Wild type *Synechococcus* sp. PCC 7002
A	7002 cells overexpressing SbtA under promoter P_{cpcB} and RBS1
B	7002 cells overexpressing SbtA under promoter $P_{cpcB560}$ and RBS1
C	7002 cells overexpressing SbtA under promoter P_{rbcL2A} and RBS1
D	7002 cells overexpressing SbtA under promoter P_{cpcB} and RBS2
E	7002 cells overexpressing SbtA under promoter $P_{cpcB560}$ and RBS2
F	7002 cells overexpressing SbtA under promoter P_{rbcL2A} and RBS2
Plasmid	**Description**
pSK +	pBlueScript II SK(+) as backbone vector
pA	Plasmid containing *sbtA* gene cassette, with promoter P_{cpcB} and RBS1
pB	Plasmid containing *sbtA* gene cassette, with promoter $P_{cpcB560}$ and RBS1
pC	Plasmid containing *sbtA* gene cassette, with promoter P_{rbcL2A} and RBS1
pD	Plasmid containing *sbtA* gene cassette, with promoter P_{cpcB} and RBS2
pE	Plasmid containing *sbtA* gene cassette, with promoter $P_{cpcB560}$ and RBS2
pF	Plasmid containing *sbtA* gene cassette, with promoter P_{rbcL2A} and RBS2

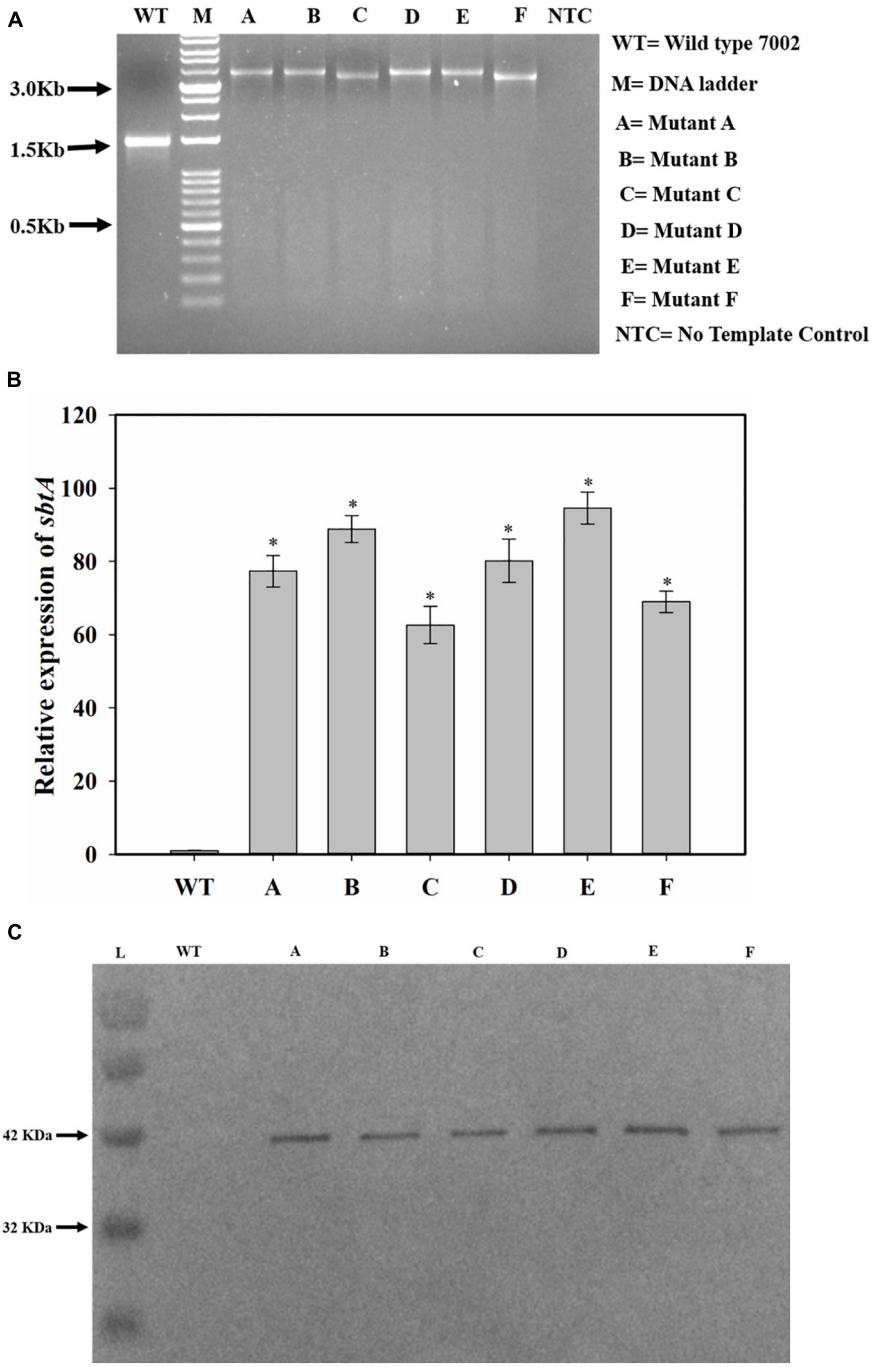

FIGURE 2 | Screening and confirmation of transformants. **(A)** Screening for integration of gene cassette by genomic DNA PCR. *sbtA* gene constructs with different promoters and RBS, containing kanamycin resistance gene as the selection marker were cloned between NSI and NSII in PCC 7002 cells by homologous recombination. The whole insert was PCR amplified using forward primer for NSI and reverse primer for NSII. M is DNA molecular weight marker. Lanes WT, A, B, C, D, E, and F represent the PCR product upon using the genomic DNA from PCC 7002, A, B, C, D, E, and F cells, respectively, as the template. NTC is the no template control in which no DNA template was added. **(B)** Measurement of relative levels of *sbtA* mRNA in the strains A to F by qRT-PCR, n = 3. $^*p < 0.05$ compared to WT PCC 7002 cells. **(C)** Expression of His-tagged SbtA protein in different strains was measured by Western blotting. L = Protein molecular weight marker. Lanes WT, A, B, C, D, E, and F represent proteins extracted from WT PCC 7002, A, B, C, D, E, and F cells, respectively.

C and F had lower levels compared to other transformants (**Figure 2B**). Relative expression levels of genetically engineered strains A, B, C, D, E, and F were found to be 77.4 ± 4.3, 88.9 ± 3.7, 62.6 ± 5.1, 80.2 ± 5.9, 94.6 ± 4.4, and 68.9 ± 2.9, respectively. All the transformants expressed the His-tagged SbtA protein (**Figure 2C**).

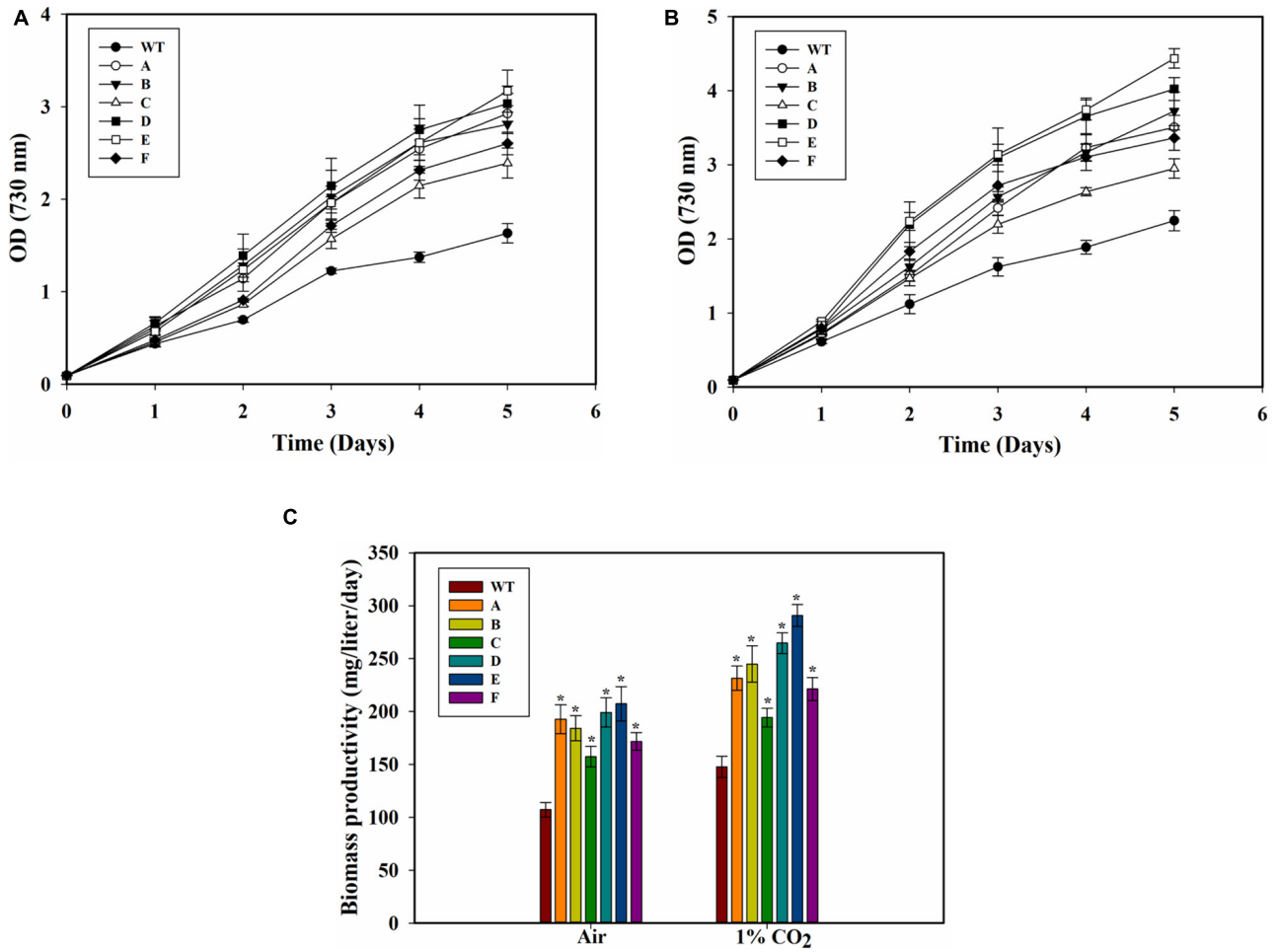

FIGURE 3 | Growth of WT PCC 7002 and transformants. **(A)** Growth with air bubbling. *$p < 0.05$ for all strains A to F compared to WT PCC 7002 cells for the same day. **(B)** Growth with 1% CO_2 bubbling. *$p < 0.05$ compared to WT PCC 7002 cells for the same day. **(C)** Biomass productivity with bubbling of air and 1% CO_2 after 5 days of growth. *$p < 0.05$ compared to WT PCC 7002 cells for the same CO_2 level. $n = 3$ for all the experiments.

Growth of Wild Type and Transformed Cells at Different CO_2 Concentrations

The SbtA-overexpressing transformed cells with different promoters and RBSs exhibited significant improvement in growth as compared to the WT PCC 7002 cells when the cultures were bubbled either with air or 1% CO_2 (**Figures 3A,B**). Importantly, the cell density (OD730) of all the transformants with air bubbling was higher than that of the WT PCC 7002 cells with 1% CO_2 bubbling. There was also a significant difference in growth among some of the transformants with either 1% CO_2 or air bubbling. When cultured either with air bubbling or 1% CO_2 bubbling, the transformant E (promoter $P_{cpcB560}$ and RBS2) showed highest difference in growth compared to the WT PCC 7002 cells, with about 90% higher OD with air or 1% CO_2 bubbling (**Figures 3A,B**). Transformant C (promoter P_{rbcL2A} with RBS1) showed the least, nonetheless significant, difference in growth compared to the WT cells.

Biomass productivity of the WT PCC 7002 cells increased with 1% CO_2 bubbling, with values of 107.6 ± 5.7 and 148.2 ± 7.1 $mg{\cdot}L^{-1}d^{-1}$ on air and 1% CO_2, respectively (**Figure 3C**). The transformants showed greater biomass productivity compared to the WT PCC 7002 in both air and 1% CO_2 bubbled cultures. Strain E (the SbtA transformant with $P_{cpcB560}$ and RBS2) had the highest biomass productivity of 207 ± 16 $mg^{TN}L^{-1}{\cdot}day^{-1}$ and 290 ± 10 $mg{\cdot}L^{-1}{\cdot}day^{-1}$ with bubbling of air and 1% CO_2, respectively. Among the transformants, strain C had the lowest biomass productivity of about 157 ± 9.6 $mg{\cdot}L^{-1}{\cdot}d^{-1}$ with air and 194 ± 8.8 $mg{\cdot}L^{-1}{\cdot}d^{-1}$ with 1% CO_2, although these values are still significantly higher than the WT PCC 7002 cells grown under similar conditions.

Glycogen Content and Productivity

Because glycogen is a major storage polysaccharide of the cyanobacterial cells, the glycogen content of the cells was also measured. Higher glycogen content was found in all the SbtA-overexpressing strains compared to WT PCC 7002 cells. The highest glycogen levels in strain E, was observed when the cells were cultured either with air or 1% CO_2 bubbling (**Figure 4A**).

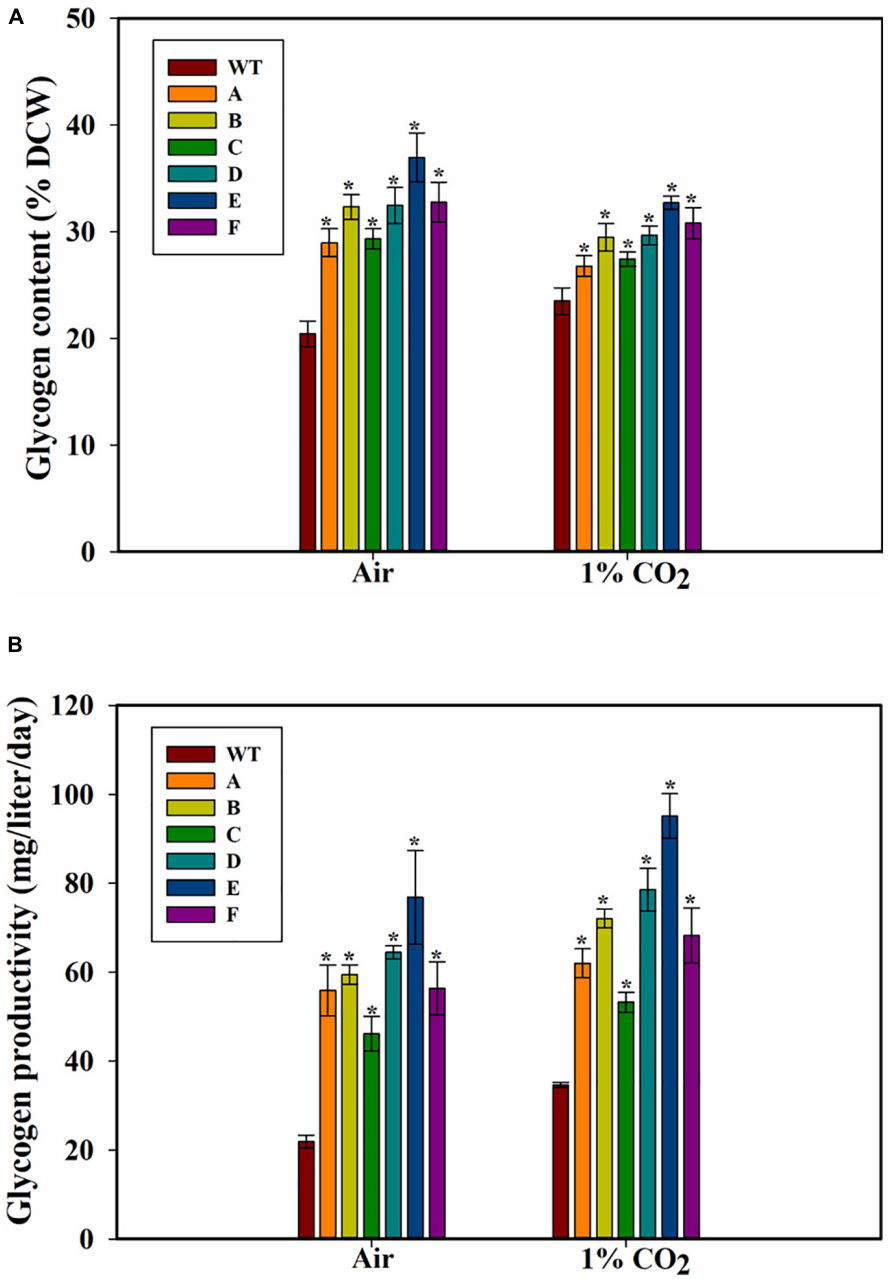

FIGURE 4 | Glycogen content and productivity of the cells. **(A)** Intracellular glycogen content, **(B)** glycogen productivity of WT PCC 7002 and transformants with bubbling of air or 1% CO_2, measured after 5 days of growth. *$p < 0.05$ compared to WT PCC 7002 cells grown at the same CO_2 concentrations. $n = 3$.

After 5 days of growth on air bubbling, the glycogen content was up to 36.9 ± 2.3% (of DCW) in the strain E while it was only 20 ± 1% (of DCW) in WT PCC 7002 cells (**Figure 4A**). However, unlike the significant increase in growth observed when the cells were bubbled with 1% CO_2 compared to air bubbling, there was not a significant change in glycogen content of the cells when bubbled with 1% CO_2 compared to when bubbled with air.

The glycogen productivities of the transformants were significantly higher than that of WT PCC 7002 cells whether with air bubbling or with 1% CO_2 bubbling (**Figure 4B**). Strain E grown on air showed the greatest increase in glycogen productivity of about 2.5-fold compared to WT PCC 7002 (**Figure 4B**) while the transformant C showed the least increase in productivity (∼60% increase when grown on 1% CO_2). Interestingly, while the WT PCC 7002 cells showed 1.5-fold glycogen productivity when grown on 1% CO_2 compared to air, the transformants showed only a slight increase in productivity at 1% CO_2 compared to air. Thus, the increase in glycogen productivity in 1% CO_2 is primarily due to the faster growth of cells.

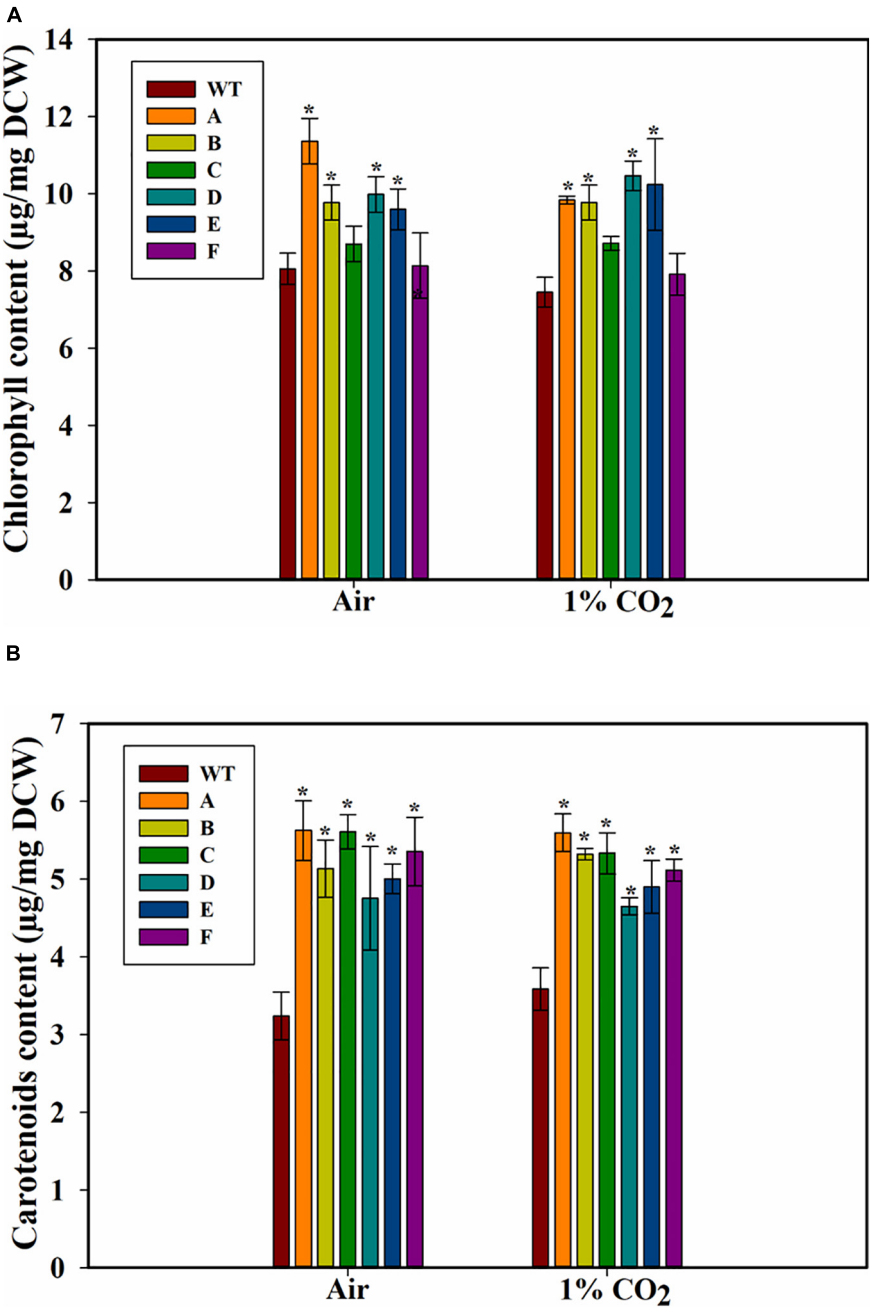

FIGURE 5 | Pigment content of wild type (PCC 7002) and transformants overexpressing SbtA with different promoters and RBSs (strains A to F) after 5 days of growth. **(A)** Chlorophyll content, and **(B)** carotenoids content, with the bubbling of air or 1% CO_2. *$p < 0.05$ compared to WT PCC 7002 cells grown under similar CO_2 level, $n = 3$.

Pigment Content of the Transformed Cells

Because growth can also be affected by chlorophyll levels, we measured the cellular chlorophyll contents of the WT PCC 7002 and transformants. The strain A showed the highest amount of chl *a* among all the strains when cultured on air (**Figure 5A**). Strains C and F, when grown on air or 1% CO_2, did not have higher chlorophyll levels compared to WT PCC 7002 cells. Transformants A, B, D, and E had similar levels of chlorophyll, which was higher than that in the PCC 7002 cells. Also, no effect of higher CO_2 concentration on chlorophyll levels was observed.

A significant increase in the amount of carotenoids was observed in the transformants both either with air and 1% CO_2, and an increase of up to ~70% in the content of carotenoids (accessory light harvesting pigments) was observed in the transformed cells when grown in presence of air (**Figure 5B**).

Interestingly, unlike the response of chlorophyll content, all the transformants had higher carotenoid content.

DISCUSSION

Glycogen is a potential fermentation feedstock (Möllers et al., 2014). Also, glycogen is more water soluble and can be more easily hydrolyzed to simple sugars compared to other storage polysaccharides like starch because it is more branched (Ball et al., 2011). Our study shows that improving Carbon transport through overexpression of SbtA can increase cyanobacterial biomass and glycogen productivity. The combinatorial effects of choice of RBS and promoters on the expression of a membrane protein, and its physiological effects, are presented for the first time. A correlation between SbtA expression and growth rate was observed among the transformants. The transformant E with $P_{cpcB560}$ and RBS2 showed the highest growth and the glycogen content. An interesting outcome was that all the transformants grown on air had higher glycogen productivity than WT PCC 7002 cells grown on 1% CO_2 with the transformant E showing up to 2.5-fold increase. The increased glycogen productivity in 1% CO_2 grown cells due to increased biomass accumulation and not due to increased cellular glycogen levels.

Among the promoters tested, $P_{cpcB560}$ had the strongest effect, in agreement with its super-strong activity due to the presence of multiple TFBS in its sequence (Zhou et al., 2014). This is in spite of previous reports that P_{cpcB} is inhibited under strong light conditions (Sengupta et al., 2020a). The strong and continuous illumination was chosen in our study because previous studies, including our own preliminary studies, have shown that it leads to higher biomass accumulation for the WT PCC 7002 cells. P_{rbcL2A} had a slightly lesser effect on SbtA expression, growth and glycogen accumulation compared to the P_{cpcB} promoters. Our study shows that even under air bubbling and high illumination, very similar to the "optimal" conditions for high P_{rbcL} activity (Sengupta et al., 2020a) $P_{cpcB560}$ has higher activity compared to PrbcL2A. Promoter activity may also be affected by the length of the promoter chosen. We chose lengths of 272 bp for P_{rbcL2A}, 589 for P_{cpcB} and 560 bp of $P_{cpcB560}$, respectively based the high activity in PCC 7002 reported in a previous study (Huang et al., 2010; Zhou et al., 2014).

Another factor we tested was the choice of RBSs. AGGAGG has been suggested as the common RBS for PCC 7002 (Gordon and Pfleger, 2018). A previous study (Markley et al., 2015) had studied 11 different RBS sequences in PCC 7002 cells and reported highest eYFP levels when RBS2 (AGGAGA) was used. The levels for AGGAGA were about twice than that for AGGAGG. As such, the choice of RBS had only a minor effect on SbtA expression, growth and glycogen productivity. Therefore, we do not expect any significant improvement when using the common RBS (AGGAGG) of PCC 7002 cells.

Our study shows that overexpression of SbtA can change the cellular chlorophyll and carotenoids content. One common response was that chlorophyll levels are not affected by the concentration of the CO_2 bubbled, i.e., either with air and 1% CO_2 bubbling, even though biomass productivity of cells grown on 1% CO_2 was 30–45% higher than those grown on air. This indicates that the basal chlorophyll level is enough to support elevated growth. One possible reason for increased carotenoids in the transformants could be that due to their faster growth, the transformants experience nutrient stress before the WT PCC 7002 cells. Nutrient stress is associated with higher carotenoid levels (Wang and Peng, 2008; Lemoine and Schoefs, 2010; Minhas et al., 2016). Carotenoids also play an important role in protecting the cells from photo-oxidative damage (Demmig-Adams and Adams, 2002). However, our cultures were exposed to similar light intensity and this cannot explain the variation observed. The underlying mechanisms of regulation of the pigments are not clear and will require further investigation which is out of the scope of current study. Of interest will be to identify the metabolomic changes in the transformants (Hasunuma et al., 2013; Schwarz et al., 2013; Behrendt et al., 2018; Jaiswal and Wangikar, 2020) and how the variation in SbtA levels alter the bicarbonate uptake rates and intracellular labeling rates through 13C-metabolic labeling studies (Alagesan et al., 2013; Prasannan et al., 2019) as well as the proteomic changes in the transformants.

Overall, our results show that choice of a strong RBS and promoter while overexpressing the bicarbonate transporter SbtA can have significant impact on cellular physiology. Our results suggests that engineering high activity, regulatable promoters will help improving protein expression and hence product formation. Our results also show a complex regulation of cellular pigments which warrant further studies.

CONCLUSION

Our results show significant improvements in growth and glycogen content of the cells overexpressing the bicarbonate transporter SbtA. Additionally, the promoter as well as the RBS chosen to overexpress SbtA was shown to impact glycogen productivity. A combination of a strong promoter and a strong RBS led to a transformant with glycogen productivity that was about 2.7–3.5-fold that of the WT PCC 7002 cells depending on whether 1% CO_2 or air was used for growth. This increase was due to higher biomass as well as increased glycogen content in the transformants.

DATA AVAILABILITY STATEMENT

The original contributions presented in the study are included in the article/**Supplementary Material**, further inquiries can be directed to the corresponding author/s.

AUTHOR CONTRIBUTIONS

SS and JG designed the study and wrote the manuscript together. JG conducted all the experimental work which was supervised by SS. Both authors contributed to the article and approved the submitted version.

FUNDING

This work was supported by the Department of Biotechnology (DBT), Ministry of Science and Technology, India, through the grant no. BT/PB/Center/03/ICGEB/2011-Phase II.

ACKNOWLEDGMENTS

We are thankful to Dr. Prachi Nawkarkar, Metabolic Engineering Group, ICGEB, New Delhi for her help with the RT-PCR and Western Blot analyses. JG acknowledges the support of Department of Biotechnology, Ministry of Science and Technology, Government of India for his Ph.D. fellowship, and ICGEB for providing the research opportunity.

SUPPLEMENTARY MATERIAL

The Supplementary Material for this article can be found online at: https://www.frontiersin.org/articles/10.3389/fmicb.2021.607411/full#supplementary-material

Supplementary Table 1 | The raw data used to construct various figures.

Supplementary Data Sheet 1 | The sequence of sbtA gene from PCC 7002, promoters sequences, the RBS sequences used in the study, genes and their sources, primers used for cloning, and RT-PCR primers used to check expression. It also includes maps of various vectors.

REFERENCES

Abe, K., Ruan, Z.-S., and Maloney, P. C. (1996). Cloning, sequencing, and expression in *Escherichia coli* of OxlT, the oxalate:formate exchange protein of Oxalobacter formigenes. *J. Biol. Chem.* 271, 6789–6793. doi: 10.1074/jbc.271.12.6789

Ahmad, A., Pathania, R., and Srivastava, S. (2020). Biochemical characteristics and a genome-scale metabolic model of an indian euryhaline cyanobacterium with high polyglucan content. *Metabolites* 10:177. doi: 10.3390/metabo10050177

Alagesan, S., Gaudana, S. B., Sinha, A., and Wangikar, P. P. (2013). Metabolic flux analysis of *Cyanothece sp.* ATCC 51142 under mixotrophic conditions. *Photosynth. Res.* 118, 191–198. doi: 10.1007/s11120-013-9911-5

Alting-Mees, M. A., and Short, J. M. (1989). pBluescript II: gene mapping vectors. *Nucleic Acids Res.* 17:9494. doi: 10.1093/nar/17.22.9494

Ball, S., Colleoni, C., Cenci, U., Raj, J. N., and Tirtiaux, C. (2011). The evolution of glycogen and starch metabolism in eukaryotes gives molecular clues to understand the establishment of plastid endosymbiosis. *J. Exp. Bot.* 62, 1775–1801. doi: 10.1093/jxb/erq411

Behrendt, L., Raina, J.-B., Lutz, A., Kot, W., Albertsen, M., Halkjær-Nielsen, P., et al. (2018). In situ metabolomic- and transcriptomic-profiling of the host-associated cyanobacteria *Prochloron* and *Acaryochloris* marina. *ISME J.* 12, 556–567. doi: 10.1038/ismej.2017.192

Bienick, M. S., Young, K. W., Klesmith, J. R., Detwiler, E. E., Tomek, K. J., and Whitehead, T. A. (2014). The interrelationship between promoter strength, gene expression, and growth rate. *PLoS One* 9:e109105. doi: 10.1371/journal.pone.0109105

Davies, F. K., Work, V. H., Beliaev, A. S., and Posewitz, M. C. (2014). Engineering limonene and bisabolene production in wild type and a glycogen-deficient mutant of *Synechococcus sp.* PCC 7002. *Front. Bioeng. Biotechnol.* 2:21. doi: 10.3389/fbioe.2014.00021

Demmig-Adams, B., and Adams, W. W. (2002). Antioxidants in photosynthesis and human nutrition. *Science* 298, 2149–2153. doi: 10.1126/science.1078002

Du, J., Förster, B., Rourke, L., Howitt, S. M., and Price, G. D. (2014). Characterisation of cyanobacterial bicarbonate transporters in *E. coli* Shows that SbtA homologs are functional in this heterologous expression system. *PLoS One* 9:e115905. doi: 10.1371/journal.pone.0115905

Dutt, V., and Srivastava, S. (2018). Novel quantitative insights into carbon sources for synthesis of poly hydroxybutyrate in *Synechocystis* PCC 6803. *Photosynth. Res.* 136, 303–314. doi: 10.1007/s11120-017-0464-x

Englund, E., Liang, F., and Lindberg, P. (2016). Evaluation of promoters and ribosome binding sites for biotechnological applications in the unicellular cyanobacterium *Synechocystis sp.* PCC 6803. *Sci. Rep.* 6:36640. doi: 10.1038/srep36640

Froger, A., and Hall, J. E. (2007). Transformation of plasmid DNA into *E. coli* using the heat shock method. *J. Vis. Exp. JoVE* 6:253. doi: 10.3791/253

Gantt, E. (2011). Oxygenic photosynthesis and the distribution of chloroplasts. *Photosynth. Res.* 107, 1–6. doi: 10.1007/s11120-010-9605-1

Gordon, G., and Pfleger, B. (2018). Regulatory tools for controlling gene expression in cyanobacteria. *Adv. Exp. Med. Biol.* 1080:281. doi: 10.1007/978-981-13-0854-3_12

Gupta, J. K., Rai, P., Jain, K. K., and Srivastava, S. (2020). Overexpression of bicarbonate transporters in the marine cyanobacterium *Synechococcus sp.* PCC 7002 increases growth rate and glycogen accumulation. *Biotechnol. Biofuels* 13:17. doi: 10.1186/s13068-020-1656-8

Hasunuma, T., Kikuyama, F., Matsuda, M., Aikawa, S., Izumi, Y., and Kondo, A. (2013). Dynamic metabolic profiling of cyanobacterial glycogen biosynthesis under conditions of nitrate depletion. *J. Exp. Bot.* 64, 2943–2954. doi: 10.1093/jxb/ert134

Hong, S. G., Choi, J. Y., Pryor, B. M., and Lee, H. K. (2009). An efficient method to prepare PCR cloning vectors. *Mycobiology* 37, 240–242. doi: 10.4489/MYCO.2009.37.3.240

Huang, H.-H., Camsund, D., Lindblad, P., and Heidorn, T. (2010). Design and characterization of molecular tools for a synthetic biology approach towards developing cyanobacterial biotechnology. *Nucleic Acids Res.* 38, 2577–2593. doi: 10.1093/nar/gkq164

Huang, H.-H., and Lindblad, P. (2013). Wide-dynamic-range promoters engineered for cyanobacteria. *J. Biol. Eng.* 7:10. doi: 10.1186/1754-1611-7-10

Im, H. (2011). The inoue method for preparation and transformation of competent *E. coli*: "ultra competent" cells. *CSH Protoc.* 101:e143. doi: 10.21769/BioProtoc.143

Jaiswal, D., Sengupta, A., Sohoni, S., Sengupta, S., Phadnavis, A. G., Pakrasi, H. B., et al. (2018). Genome features and biochemical characteristics of a robust, fast growing and naturally transformable Cyanobacterium *Synechococcus elongatus* PCC 11801 isolated from India. *Sci. Rep.* 8:16632. doi: 10.1038/s41598-018-34872-z

Jaiswal, D., and Wangikar, P. P. (2020). Dynamic inventory of intermediate metabolites of cyanobacteria in a diurnal cycle. *iScience* 23:101704. doi: 10.1016/j.isci.2020.101704

Kopka, J., Schmidt, S., Dethloff, F., Pade, N., Berendt, S., Schottkowski, M., et al. (2017). Systems analysis of ethanol production in the genetically engineered cyanobacterium *Synechococcus sp.* PCC 7002. *Biotechnol. Biofuels* 10:56. doi: 10.1186/s13068-017-0741-0

Lemoine, Y., and Schoefs, B. (2010). Secondary ketocarotenoid astaxanthin biosynthesis in algae: a multifunctional response to stress. *Photosynth. Res.* 106, 155–177. doi: 10.1007/s11120-010-9583-3

Lichtenthaler, H. K. (1987). "[34] Chlorophylls and carotenoids: Pigments of photosynthetic biomembranes," in *Methods in Enzymology Plant Cell Membranes*, eds R. Douce and L. Packer (New York, NY: Academic Press), 350–382. doi: 10.1016/0076-6879(87)48036-1

Ludwig, M., and Bryant, D. A. (2012). *Synechococcus sp.* Strain PCC 7002 transcriptome: acclimation to temperature, salinity, oxidative stress, and mixotrophic growth conditions. *Front. Microbiol.* 3:354. doi: 10.3389/fmicb.2012.00354

Markley, A. L., Begemann, M. B., Clarke, R. E., Gordon, G. C., and Pfleger, B. F. (2015). Synthetic biology toolbox for controlling gene expression in

the Cyanobacterium *Synechococcus sp.* strain PCC 7002. *ACS Synth. Biol.* 4, 595–603. doi: 10.1021/sb500260k

Minhas, A. K., Hodgson, P., Barrow, C. J., and Adholeya, A. (2016). A review on the assessment of stress conditions for simultaneous production of microalgal lipids and carotenoids. *Front. Microbiol.* 7:546. doi: 10.3389/fmicb.2016.00546

Möllers, K., Cannella, D., Jørgensen, H., and Frigaard, N.-U. (2014). Cyanobacterial biomass as carbohydrate and nutrient feedstock for bioethanol production by yeast fermentation. *Biotechnol. Biofuels* 7:64. doi: 10.1186/1754-6834-7-64

Nozzi, N. E., Oliver, J. W. K., and Atsumi, S. (2013). Cyanobacteria as a platform for biofuel production. *Front. Bioeng. Biotechnol.* 1:7. doi: 10.3389/fbioe.2013.00007

Prasannan, C. B., Mishra, V., Jaiswal, D., and Wangikar, P. P. (2019). Mass isotopologue distribution of dimer ion adducts of intracellular metabolites for potential applications in 13C metabolic flux analysis. *PLoS One* 14:e0220412. doi: 10.1371/journal.pone.0220412

Price, G. D. (2011). Inorganic carbon transporters of the cyanobacterial CO_2 concentrating mechanism. *Photosynth. Res.* 109, 47–57. doi: 10.1007/s11120-010-9608-y

Price, G. D., Shelden, M. C., and Howitt, S. M. (2011). Membrane topology of the cyanobacterial bicarbonate transporter, SbtA, and identification of potential regulatory loops. *Mol. Membr. Biol.* 28, 265–275. doi: 10.3109/09687688.2011.593049

Reeve, B., Hargest, T., Gilbert, C., and Ellis, T. (2014). Predicting translation initiation rates for designing synthetic biology. *Front. Bioeng. Biotechnol.* 2:1. doi: 10.3389/fbioe.2014.00001

Ruffing, A. M. (2014). Improved free fatty acid production in cyanobacteria with *Synechococcus sp.* PCC 7002 as host. *Front. Bioeng. Biotechnol.* 2:17. doi: 10.3389/fbioe.2014.00017

Schwarz, D., Orf, I., Kopka, J., and Hagemann, M. (2013). Recent applications of metabolomics toward cyanobacteria. *Metabolites* 3, 72–100. doi: 10.3390/metabo3010072

Sengupta, A., Madhu, S., and Wangikar, P. P. (2020a). A library of tunable, portable, and inducer-free promoters derived from cyanobacteria. *ACS Synth. Biol.* 9, 1790–1801. doi: 10.1021/acssynbio.0c00152

Sengupta, A., Pritam, P., Jaiswal, D., Bandyopadhyay, A., Pakrasi, H. B., and Wangikar, P. P. (2020b). Photosynthetic co-production of succinate and ethylene in a fast-growing cyanobacterium, *Synechococcus elongatus* PCC 11801. *Metabolites* 10:250. doi: 10.3390/metabo10060250

Sengupta, S., Jaiswal, D., Sengupta, A., Shah, S., Gadagkar, S., and Wangikar, P. P. (2020). Metabolic engineering of a fast-growing cyanobacterium *Synechococcus elongatus* PCC 11801 for photoautotrophic production of succinic acid. *Biotechnol. Biofuels* 13:89. doi: 10.1186/s13068-020-01727-7

Shibata, M., Katoh, H., Sonoda, M., Ohkawa, H., Shimoyama, M., Fukuzawa, H., et al. (2002). Genes essential to sodium-dependent bicarbonate transport in cyanobacteria: function and phylogenetic analysis. *J. Biol. Chem.* 277, 18658–18664. doi: 10.1074/jbc.M112468200

Shi, F., Luan, M., and Li, Y. (2018). Ribosomal binding site sequences and promoters for expressing glutamate decarboxylase and producing γ-aminobutyrate in *Corynebacterium glutamicum*. *AMB Express* 8:61. doi: 10.1186/s13568-018-0595-2

Singh, J. S., Kumar, A., Rai, A. N., and Singh, D. P. (2016). Cyanobacteria: a precious bio-resource in agriculture, ecosystem, and environmental sustainability. *Front. Microbiol.* 7:529. doi: 10.3389/fmicb.2016.00529

Szekeres, E., Sicora, C., Dragoș, N., and Drugă, B. (2014). Selection of proper reference genes for the cyanobacterium *Synechococcus PCC 7002* using real-time quantitative PCR. *FEMS Microbiol. Lett.* 359, 102–109. doi: 10.1111/1574-6968.12574

Till, P., Toepel, J., Bühler, B., Mach, R. L., and Mach-Aigner, A. R. (2020). Regulatory systems for gene expression control in cyanobacteria. *Appl. Microbiol. Biotechnol.* 104, 1977–1991. doi: 10.1007/s00253-019-10344-w

Utex Culture Collection of Algae (2021). *UTEX Cult. Collect. Algae*. Available online at: https://utex.org/products/a-plus-medium (accessed February 21, 2021).

Vavitsas, K., Crozet, P., Vinde, M. H., Davies, F., Lemaire, S. D., and Vickers, C. E. (2019). The synthetic biology toolkit for photosynthetic microorganisms. *Plant Physiol.* 181, 14–27. doi: 10.1104/pp.19.00345

Wang, Y., and Peng, J. (2008). Growth-associated biosynthesis of astaxanthin in heterotrophic *Chlorella zofingiensis* (Chlorophyta). *World J. Microbiol. Biotechnol.* 24, 1915–1922. doi: 10.1007/s11274-008-9692-8

Wellburn, A. R. (1994). The spectral determination of chlorophylls a and b, as well as total carotenoids, using various solvents with spectrophotometers of different resolution. *J. Plant Physiol.* 144, 307–313. doi: 10.1016/S0176-1617(11)81192-2

Zhou, J., Zhang, H., Meng, H., Zhu, Y., Bao, G., Zhang, Y., et al. (2014). Discovery of a super-strong promoter enables efficient production of heterologous proteins in cyanobacteria. *Sci. Rep.* 4:4500. doi: 10.1038/srep04500

Conflict of Interest: The authors declare that the research was conducted in the absence of any commercial or financial relationships that could be construed as a potential conflict of interest.

frontiers in Microbiology

ORIGINAL RESEARCH
published: 18 May 2021
doi: 10.3389/fmicb.2021.650217

Salt-Tolerant *Synechococcus elongatus* UTEX 2973 Obtained *via* Engineering of Heterologous Synthesis of Compatible Solute Glucosylglycerol

Jinyu Cui[1,2,3†], *Tao Sun*[1,2,4†], *Lei Chen*[1,2,3*] *and Weiwen Zhang*[1,2,3,4*]

[1] *Laboratory of Synthetic Microbiology, School of Chemical Engineering & Technology, Tianjin University, Tianjin, China,* [2] *Frontier Science Center for Synthetic Biology and Key Laboratory of Systems Bioengineering, Tianjin University, Tianjin, China,* [3] *SynBio Research Platform, Collaborative Innovation Center of Chemical Science and Engineering, Tianjin, China,* [4] *Center for Biosafety Research and Strategy, Tianjin University, Tianjin, China*

The recently isolated cyanobacterium *Synechococcus elongatus* UTEX 2973 (Syn2973) is characterized by a faster growth rate and greater tolerance to high temperature and high light, making it a good candidate chassis for autotrophic photosynthetic microbial cell factories. However, Syn2973 is sensitive to salt stress, making it urgently important to improve the salt tolerance of Syn2973 for future biotechnological applications. Glucosylglycerol, a compatible solute, plays an important role in resisting salt stress in moderate and marine halotolerant cyanobacteria. In this study, the salt tolerance of Syn2973 was successfully improved by introducing the glucosylglycerol (GG) biosynthetic pathway (OD_{750} improved by 24% at 60 h). In addition, the salt tolerance of Syn2973 was further enhanced by overexpressing the rate-limiting step of glycerol-3-phosphate dehydrogenase and downregulating the gene *rfbA*, which encodes UDP glucose pyrophosphorylase. Taken together, these results indicate that the growth of the end-point strain M-2522-GgpPS-drfbA was improved by 62% compared with the control strain M-pSI-pSII at 60 h under treatment with 0.5 M NaCl. Finally, a comparative metabolomic analysis between strains M-pSI-pSII and M-2522-GgpPS-drfbA was performed to characterize the carbon flux in the engineered M-2522-GgpPS-drfbA strain, and the results showed that more carbon flux was redirected from ADP-GLC to GG synthesis. This study provides important engineering strategies to improve salt tolerance and GG production in Syn2973 in the future.

Keywords: cyanobacteria, GG, metabolomic analysis, salt tolerance, small RNA regulation

OPEN ACCESS

Edited by:
Guodong Luan, Qingdao Institute of Bioenergy and Bioprocess Technology (CAS), China

Reviewed by:
Stephan Klähn, Helmholtz Centre for Environmental Research (UFZ), Germany
Xiaoming Tan, Hubei University, China
Jie Zhou, Institute of Microbiology, Chinese Academy of Sciences, China
Kuo Song, University of Freiburg, Germany

***Correspondence:**
Lei Chen
lchen@tju.edu.cn
Weiwen Zhang
wwzhang8@tju.edu.cn

[†] *These authors have contributed equally to this work*

Specialty section:
This article was submitted to Microbiotechnology, a section of the journal Frontiers in Microbiology

Received: *06 January 2021*
Accepted: *25 March 2021*
Published: *18 May 2021*

Citation:
Cui J, Sun T, Chen L and Zhang W (2021) Salt-Tolerant Synechococcus elongatus UTEX 2973 Obtained via Engineering of Heterologous Synthesis of Compatible Solute Glucosylglycerol. Front. Microbiol. 12:650217. doi: 10.3389/fmicb.2021.650217

INTRODUCTION

Cyanobacteria have attracted significant attention recently for the production of green fuels and chemicals due to their ability to absorb sunlight and CO_2 as sole energy and carbon sources, respectively (Gao et al., 2012, 2016a,b; Luan and Lu, 2018; Matson and Atsumi, 2018). A recently isolated cyanobacterium, *Synechococcus elongatus* UTEX 2973 (hereafter Syn2973), is characterized

by a faster growth rate and more tolerance to high temperature and high light (Mueller et al., 2017; Ungerer et al., 2018b). The doubling time of Syn2973 can reach 1.9 h in BG11 medium at 41°C under continuous 500 μmol photons m^{-2} s^{-1} white light with 3% CO_2 (Yu et al., 2015), which is very similar to that of the heterotrophic yeast *Saccharomyces cerevisiae* (1.67 h) (Herskowitz, 1988). However, as a freshwater cyanobacterium, Syn2973 is very sensitive to salt stress, and its growth was significantly inhibited by high concentrations of salt (Song et al., 2016; Cui et al., 2020b). Meanwhile, large-scale cultivation of cyanobacteria with seawater is necessary for industrial biotechnological applications (Silkina et al., 2019; Cui et al., 2020a). It is therefore urgent to improve the salt tolerance of Syn2973 for the future application of this promising chassis for green fuels and chemical production.

Acclimation to high external salinities involves the accumulation of compatible solutes and the active export of ions (Hagemann, 2011). Compatible solutes are a diverse class of low-molecular-weight compounds that accumulate at high intracellular concentrations in response to hyperosmotic or salt stress (Da Costa et al., 1998). Glucosylglycerol (GG) is a potent compatible solute consisting of glucose and glycerol linked by a glycosidic bond (Tan et al., 2016) and has a wide range of beneficial functions as a health food material, therapeutic agent, cosmetic ingredient, and enzyme stabilizer (Sawangwan et al., 2010; Luley-Goedl and Nidetzky, 2011). The marine cyanobacterium *Synechococcus* sp. PCC 7002 (hereafter Syn7002) and moderate halotolerant cyanobacterium *Synechocystis* sp. PCC 6803 (hereafter Syn6803) could accumulate GG to resist salt stress (Hagemann, 2011). The synthesis of GG has been elucidated in Syn6803, which depends strictly on ADP-glucose and consists of two steps involved in two enzymes [GG-phosphate-synthase (GGPS) and GG-phosphate-phosphatase (GGPP)] (Hagemann and Erdmann, 1994). In addition, the regulatory mechanisms involved in the synthesis of GG have mainly been investigated in *Synechocystis* (Kirsch et al., 2019). However, GG was not synthesized natively in Syn2973; instead, sucrose was synthesized as the only compatible solute under salt stress (Song et al., 2016). Heterologous synthesis of compatible solutes in salt-sensitive strains has been considered a key strategy for improving the salt tolerance of hosts (Waditee-Sirisattha et al., 2012; Singh et al., 2013). For example, the introduction of glycine methylation genes (*ApGSMT-DMT*) associated with glycine betaine synthesis successfully improved the salt tolerance of *Anabaena* sp. PCC 7120, and the growth of *Anabaena* sp. The PCC 7120-expressing *ApGSMT-DMT* gene cluster was improved by ∼70% under conditions with 0.12 M NaCl (Waditee-Sirisattha et al., 2012). It is thus interesting to explore the effect of heterologous GG synthesis on the salt tolerance of Syn2973. Notably, Syn2973 is known to undergo higher carbon flux into the sugar phosphate pathway and accumulates greater amounts of glycogen and sucrose (Abernathy et al., 2017; Ungerer et al., 2018a), which might also be beneficial for the heterologous synthesis of GG to improve salt tolerance.

In this study, multiple efforts were made to improve the salt tolerance of Syn2973 by achieving highly efficient biosynthesis of GG (**Figure 1**). Specifically, GG biosynthesis was first established in Syn2973 upon introducing genes encoding GgpS and GgpP. Second, the rate-limiting step in the process of converting DHAP to G3P was identified and strengthened by overexpressing genes from different sources. Third, redirection of carbon flux toward GG production by a small RNA (sRNA) regulatory tool was performed. Finally, the salt tolerance of different mutants was tested under different culture conditions. Together, these integrated efforts improved the salt tolerance of Syn2973 by 62% and represent the first attempt to increase salt stress tolerance by *de novo* biosynthesis of GG in Syn2973.

Abbreviations: AcCoA, acetyl-CoA; AKG, a-ketoglutarate; ADP-GLC, adenosine diphosphoglucose; ATP, adenosine triphosphate; CIT, citrate; D, day; DHAP, dihydroxyacetone phosphate; E4P, erythrose-4-phosphate; F6P, fructose-6-phosphate; FBP, fructose 1,6-diphosphate; G6P, glucose-6-phosphate; G1P, glucose 1-phosphate; G3P, glycerol-3-phosphate; GAP, glyceraldehyde 3-phosphate; 3-PG, glycerate 3-phosphate; 2-PG, glycerate-2-phosphate; GC-MS, gas chromatography mass spectrometry; h, hour; ICT, isocitrate; LC-MS, liquid chromatography mass spectrometry; MAL, malate; NADH, nitcotinamide adenine dinucleotide (reduced); OAA, oxaloacetate; 6PG, 6-phospho-gluconate; PYR, pyruvate; PEP, phosphoenolpyruvate; Ru5P, ribulose 5-phosphate; RUBP, ribulose 1,5-diphosphate; R5P, ribose 5-phosphate; S7P, seduheptulose-7-phosphate; SUC, succinate; Suc-6-P, sucrose 6-phosphate; UDP-GLC, uridine diphosphate glucose; UTP, uridine-5′(1-thiotriphosphate); X5P, xylulose 5-phosphate.

MATERIALS AND METHODS

Bacterial Growth Conditions

The wild-type Syn2973 and engineered strains were grown on BG11 medium (pH 7.5) under a light intensity of approximately 200 μmol photons m^{-2} s^{-1} or 500 μmol photons m^{-2} s^{-1} in a shaking incubator at 130 rpm at 37°C (HNYC-202T, Honour, Tianjin, China) (Li et al., 2018). CO_2 from the air was used as the only carbon source. Appropriate antibiotics, 20 μg/ml spectinomycin or chloromycetin (Solarbio, Beijing, China), were added to maintain the stability of the Syn2973 engineered strains. Inoculum and 0 M NaCl BG11 medium were mixed with 1 M NaCl BG11 medium and adjusted to a certain NaCl concentration. Cell optical density was measured by a spectrophotometer (UV-1750, Shimadzu, Kyoto, Japan) at 750 nm. *Escherichia coli* DH5α was grown on LB agar plates or in LB liquid medium in an incubator at 37°C or shaking incubator at 200 rpm supplemented with 50 μg/ml spectinomycin or 200 μg/ml ampicillin (Solarbio, Beijing, China).

For GG production, prior to production experiments, mutants were inoculated in BG11 medium containing appropriate antibiotics and grown photoautotrophically. For the production experiments, mutant cultures were incubated in fresh BG11 medium without antibiotics under different NaCl concretions at the initial OD_{750} of 0.1 and cultivated photoautotrophically.

Construction of Strains and Plasmids

The strains and plasmids used in this study are listed in **Table 1**. Among them, *E. coli* DH5α was used for vector construction and amplification. For gene overexpression, the integrative vector pSI with a spectinomycin-resistant cassette and pSII with a chloromycetin-resistant cassette were used (Li et al., 2018). Primers for gene amplification are listed

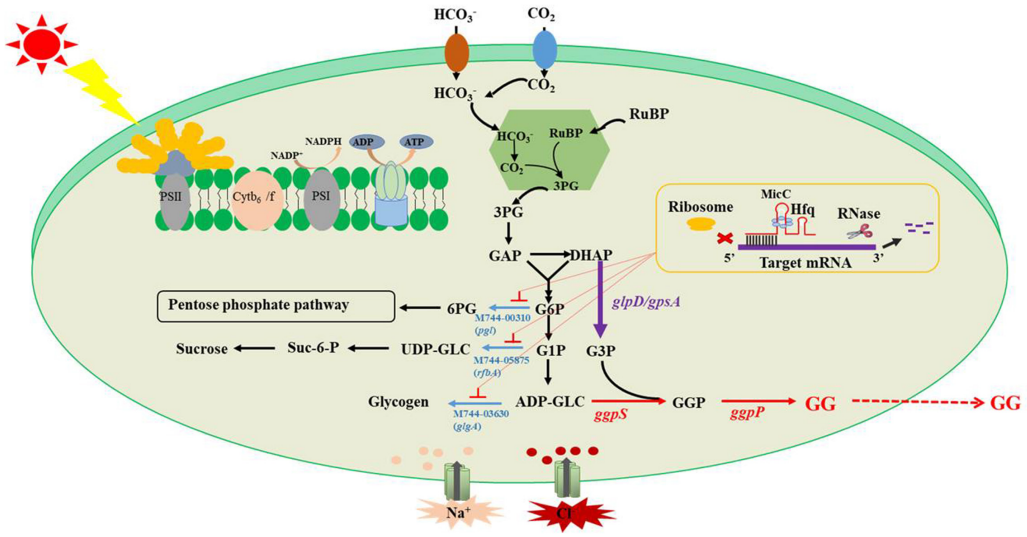

FIGURE 1 | Schematic diagram of GG synthesis optimization.

TABLE 1 | Strains and plasmids used in this study.

Strains/plasmids	Genotype or relevant features	References
Plasmids		
pSI	NSI:P_{trc}-*mcs*-T_{rbcL}; spe^R	Li et al., 2018
pSII	NSII:P_{cpc560}-*mcs*-T_{rbcL}; cm^R	Li et al., 2018
pBA3031 M	pBA3031 M:P*psbA2 M-aslacZ2-micC*-T*rbcL*-Pcpc560-*hfq*-T*rbcL*; spe^R	Sun et al., 2018
Strains		
M-pSI	NSI:P_{trc}-*mcs*-T_{rbcL}; spe^R	
M-GgpPS	NSI:P_{trc}-*sll0746*-P_{trc}-*sll1566*-T_{rbcL}; spe^R	In this study
M-1085-GgpPS	NSI:P_{cpc560}-*sll1085*-P_{trc}-*sll0746*-P_{trc}-*sll1566*-T_{rbcL}; spe^R	In this study
M-1175-GgpPS	NSI:P_{cpc560}-*sll1755*-P_{trc}-*sll0746*-P_{trc}-*sll1566*-T_{rbcL}; spe^R	In this study
M-2522-GgpPS	NSI:P_{cpc560}-*Syn2522*-P_{trc}-*sll0746*-P_{trc}-*sll1566*-T_{rbcL}; spe^R	In this study
M-Glpd1-GgpPS	NSI:P_{cpc560}-*glpd1*-P_{trc}-*sll0746*-P_{trc}-*sll1566*-T_{rbcL}; spe^R	In this study
M-pSI-pSII	NSI:P_{trc}-*mcs*-T_{rbcL}; spe^R; NSII:P_{cpc560}-*mcs*-T_{rbcL}; cm^R	In this study
M-2522-GgpPS-pSII	NSI:P_{cpc560}-*Syn2522*-P_{trc}-*sll0746*-P_{trc}-*sll1566*-T_{rbcL}; spe^R; NSII:P_{cpc560}-*mcs*-T_{rbcL}; cm^R	In this study
M-2522-GgpPS-dpgl	NSI:P_{cpc560}-*Syn2522*-P_{trc}-*sll0746*-P_{trc}-*sll1566*-T_{rbcL}; spe^R; NSII:P*psbA2 M-aspgl-micC*-T*rbcL*-P_{cpc560}-*hfq*-T*rbcL*; cm^R	In this study
M-2522-GgpPS-drfbA	NSI:P_{cpc560}-*Syn2522*-P_{trc}-*sll0746*-P_{trc}-*sll1566*-T_{rbcL}; spe^R; NSII:P*psbA2 M-asrfbA-micC*-T*rbcL*-P_{cpc560}-*hfq*-T*rbcL*; cm^R	In this study
M-2522-GgpPS-dglgA	NSI:P_{cpc560}-*Syn2522*-P_{trc}-*sll0746*-P_{trc}-*sll1566*-T_{rbcL}; spe^R; NSII:P*psbA2 M-asglgA-micC*-T*rbcL*-P_{cpc560}-*hfq*-T*rbcL*; cm^R	In this study

in **Supplementary Table 1**. All primers were synthesized by GENEWIZ Inc. (Suzhou, China). The target genes were amplified by Phanta Super-Fidelity DNA Polymerase (Vazyme Biotech, Nanjing, China), purified by a Cycle Pure Kit (Omega Bio-Tek, Norcross, GA, United States), and then phosphorylated by T4 Polynucleotide Kinase (Thermo Fisher Scientific Inc., CA, United States). Then, the gene products were ligated into pSI/pSII (linearized by PCR) by blunt end connection. All constructs were validated by colony PCR and confirmed by Sanger sequencing. The constructed plasmid was finally transferred into Syn2973 according to a method reported previously (Li et al., 2018). Briefly, *E. coli* HB101 harboring pRL443 and pRL623 and *E. coli* DH5α harboring the target plasmid were cultured overnight and then transferred into fresh LB medium with 50 μg/ml spectinomycin or 200 μg/ml ampicillin (Solarbio, Beijing, China) at a 1:50 ratio. When cells grew to exponential phase (OD_{600} ≈ 0.5), 2 ml of each *E. coli* strain was washed twice with fresh (LB) medium to remove all antibiotics, resuspended in 0.1 ml of LB medium, mixed together, and incubated for 30 min. One milliliter of the exponentially growing Syn2973 (OD_{750} ≈ 1) culture was centrifuged and resuspended in 0.2 ml of BG11 medium for each conjugation. The sample was then mixed with the *E. coli* suspension mentioned above and incubated for 30 min. The mixtures were spread on sterile filters (0.45 μm pore size) coated on BG11 agar plates. After incubation for 24 h at an intensity of approximately 100 μmol photons m^{-2} s^{-1}, the filter was transferred onto new BG11 agar plates with 80 μg/ml spectinomycin or chloromycetin. Clones were observed after incubation at an intensity of approximately 200 μmol photons m^{-2} s^{-1} for approximately 5 days. All strains obtained

were validated by colony PCR (**Supplementary Figure 1**) and Sanger sequencing.

GG and Sucrose Extraction and Measurement

Based on the methods of a previous study (with minor modifications) (Tan et al., 2015), samples (1 OD) of mid-exponential cultures under salt stress were centrifuged at 12,000 rpm for 5 min. Harvested cells were suspended in the same volume (0.8 ml) of 80% ethanol, incubated at 65°C for 4 h, and centrifuged at 12,000 rpm for 5 min; 0.2 ml of supernatant solution was taken for analysis, and internal standard 13C-sorbitol with a final certain concentration of 62.5 mg/L was added. The solvents were removed using a vacuum concentration system (ZLS-1, Her-exi, Hunan, China). For GC-MS analysis, each sample was further derivatized in a two-step process as previously published (Cui et al., 2016). The derivatized samples were analyzed by GCMS using an Agilent 5975 MSD/7890 instrument (Agilent Corp., Santa Clara, CA, United States). The column was a HP-5MS (Restek, Bellefonte, PA, United States). The oven temperature was initially held at 80°C for 2 min and reached 280°C at 10°C per min, then held at 280°C for 5 min. The GG production per OD was calculated by internal standard method. The dry cell weight corresponded to $OD_{750\ nm}$ by the regression equation $y = 0.9x + 4E{-}5$ ($r^2 = 0.9998$, $p < 0.05$), where y is the dry cell weight (mg) and x is the absorbance of the cell suspension at 750 nm.

LC-MS-Based Targeted Metabolomics Analysis

Samples (8 ml) of mid-exponential cultures (48 h) at an OD_{750} of 1 ± 0.1 were rapidly harvested by centrifugation at 8000 × *g* for 8 min at 25°C (Eppendorf 5430R, Hamburg, Germany). The extraction of metabolites was carried out as previously published with slight modifications (Bennette et al., 2011; Wang et al., 2014). $^{13}C3,^{15}N$-alanine (Cambridge Isotope Laboratories, Inc., Andover, MA, United States) was added as the internal standard to correct for variation due to sample extraction and injection. Briefly, approximately eight OD_{750} cells were added to 900 μl of the solution containing methanol/H_2O (8:2, *v*/*v*) and then frozen-thawed three times. Samples were centrifuged at 15,000 × *g* for 5 min at 4°C. The supernatant was extracted, and the sediment was subjected to the above extraction process. The supernatants were mixed, and the solvents were removed using a vacuum concentration system (ZLS-1, Her-exi, Hunan, China). For LC-MS analysis, each dried sample was dissolved in 100 μl of purified water.

LC-MS analysis was conducted on an Agilent 1260 series binary HPLC system (Agilent Technologies, Santa Clara, CA, United States) using an XBridge Amide column (150 × 2.1 mm, 3.5 μm; Waters, Milford, MA, United States) coupled to an Agilent 6410 550 triple quadrupole mass analyzer equipped with an electrospray ionization source (ESI). Multiple reaction monitoring (MRM) mode was used for scanning according to Cui et al. (2020b). All of the peaks were integrated by Qualitative Analysis B.06.00 software and Xcalibur (version 2.1) (Niu et al., 2015). Sucrose was derivatized and analyzed on an Agilent 5975B/6890N GC-MS instrument (Agilent Technologies, Santa Clara, CA, United States) as previously described (Cui et al., 2016). The metabolite data were normalized to internal standards and cell numbers. Glycogen extraction and determination were performed according to the method described by Song et al. (2016).

Quantitative RT-PCR Analysis

Total RNA extraction of samples was achieved through a miRNeasy Mini Kit (Qiagen, Valencia, CA, United States) following the protocols described by Sun et al. (2017). In addition, DNase treatment after RNA preparation to ensure degradation of copurified gDNA and 500 ng of total RNA were subjected to cDNA synthesis using a RevertAid First Strand cDNA Synthesis Kit following the manufacturer's protocol (Thermo Fisher Scientific Inc., CA, United States). Then, 1 μl of each dilution was used as a template for the qRT-PCR described previously (Sun et al., 2018). Three technical replicates were performed for each condition. Data analysis was carried out using StepOnePlus analytical software (Applied Biosystems, CA, United States) and the $2^{-\Delta\Delta\ CT}$ method (Livak and Schmittgen, 2001).

Statistical Analysis

In this study, each experiment was performed with three biological replicates. All data were reported as the means ± standard deviations. A statistical *t*-test model was applied for the comparative analysis, and a *p*-value of less than 0.05 was considered statistically significant.

RESULTS

Improved Salt Tolerance of Syn2973 by Heterologous Expression of the GG Biosynthetic Pathway

To improve the salt tolerance of Syn2973, the synthetic pathway of the compatible solute GG was introduced into Syn2973. First, the *ggps* and *ggpp* genes were cloned from Syn6803 onto plasmid pSI with a strong P*trc* promoter. Then, the resulting plasmid was introduced into Syn2973, generating strain M-GgpPS. Compared with the control strain M-pSI, which only harbored the empty plasmid, the growth of strain M-GgpPS showed no difference under 0 M NaCl addition but was improved by approximately 24% under 0.4 M NaCl at a cultivation time point of 60 h (**Figure 2A**). In addition, a time course of GG production of strain M-GgpPS was determined under 0.4 M NaCl (**Supplementary Figure 2**), and the chromatogram analysis of GG is shown in **Supplementary Figure 3**. The results showed that GG production reached 51 mg/g under 0.4 M NaCl at a cultivation time point of 60 h. Meanwhile, no GG production was detected under normal conditions without salt stress (**Figure 2B**). Early studies showed that the GgpS protein is activated and catalyzes the synthesis of α-glucosylglycerol-phosphate in Syn6803 once under certain salt concentrations (Novak et al., 2011). Moreover, a recent study showed that NaCl

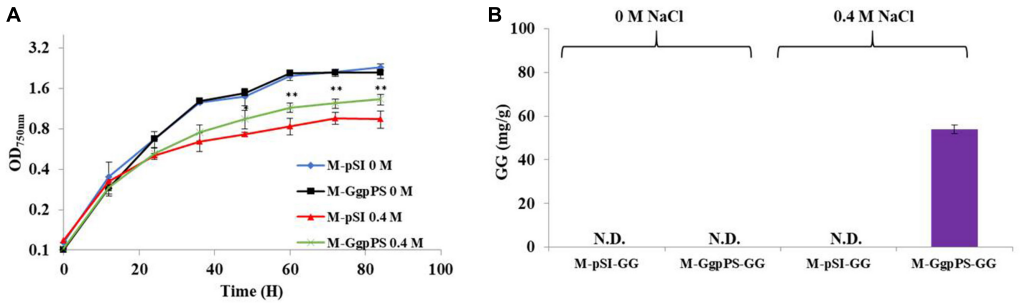

FIGURE 2 | Growth curves and GG synthesis of strains M-pSI and M-GgpPS. **(A)** Growth curves of strains M-pSI and M-GgpPS under 0 M and 0.4 M NaCl; **(B)** GG synthesis of strain M-pSI and M-GgpPS under 0 M and 0.4 M NaCl. N.D., not detected.

stress was required to initiate αGG synthesis in *Corynebacterium glutamicum* cells, suggesting that the mechanism of osmosensing of GGPS by salt-dependent protein–nucleic acid interactions might be conserved even when the coding gene of the enzyme is transferred into a heterologous host (Roenneke et al., 2018). Consistently, our results showed that upon NaCl-induced stress, GgpS was activated in Syn2973, similar to Syn6803 (Tan et al., 2015), leading to the synthesis of GG. Furthermore, the synthesis of GG slightly enhanced the salt tolerance of Syn2973 (**Figure 2A**) under the tested condition. Next, it is necessary to improve GG synthesis to further enhance the salt tolerance of Syn2973.

Screening the Rate-Limiting Steps of Precursor Supply for GG Synthesis

Metabolomics, which involves the measurement of various cellular metabolites, is indispensable for understanding the cellular status, rate-limiting steps of metabolic flow, and productivity of metabolites. Metabolomics based on gas chromatography (GC), liquid chromatography (LC), and capillary chromatography with mass spectrometry (MS) have been performed to analyze cyanobacterial cells for the production of ethanol (Yoshikawa et al., 2017), succinic acid (Osanai et al., 2015), PHB (Arisaka et al., 2019), and others. To determine the possible regulatory mechanism relevant to GG biosynthesis in Syn2973, a better understanding of the intracellular metabolism in the GG-producing strain is required. Thus, the metabolites of strains M-pSI and M-GgpPS cultivated under 0.4 M NaCl conditions were extracted and subjected to LC-MS-based targeted metabolomics analysis. The constructed central metabolic pathways in Syn2973 are shown in **Figure 3**. Notably, the metabolomic results showed that the precursor metabolite of GG synthesis, G3P, was decreased by 26.02% in strain M-GgpPS compared with strain M-pSI, indicating that the synthesis of G3P might be a limiting step and could be further strengthened to improve GG biosynthesis. Interestingly, the metabolites that were involved in sucrose and glycogen metabolism, such as ADP-GLC and UDP-GLC, in strain M-GgpPS were increased by 2.31- and 1.44-fold compared with those of the control strain M-pSI, respectively. To further evaluate the effect of GG production on sucrose and glycogen metabolism, the contents of sucrose and glycogen were also measured, and the results showed that the content of sucrose was significantly decreased by approximately 50%, while no significant change in the glycogen content was observed in strain M-GgpPS. The glycogen synthase (encoded by gene *glgA*) incorporates glucose monomers into the growing 1,4-α-linked glucose polymer. UDP glucose pyrophosphorylase (encoded by gene *rfbA*) catalyzes the production of UDP-GLC from G1P and UTP. In addition, the sucrose phosphate synthase (SPS) and sucrose phosphophosphatase (SPP) encoded by gene *Syn0808* catalyzes the synthesis of sucrose from UDP-GLC and F6P. Previous studies have shown that this enzyme reaction is the limiting step of sucrose synthesis in cyanobacteria (Du et al., 2013; Lin et al., 2020). To further explore the effects of GG synthesis on sucrose and glycogen metabolism, qRT-PCR was performed to determine the mRNA abundance of three target genes (*glgA*, *rfbA*, and *Syn0808*) of strains M-pSI and M-GgpPS under salt stress. As illustrated in **Supplementary Figure 4**, the transcriptional levels of *glgA* and *rfbA* were increased by 39 and 62%, respectively, while the transcriptional level of *Syn0808* was decreased by 42% compared with that of strain M-pSI. In addition, the metabolites R5P and E4P associated with the pentose phosphate pathway were decreased by 13.8 and 20.2%, respectively. These results suggested that more carbon flux might be redirected though sucrose and GG metabolism in the GG-producing strain M-GgpPS, while decreased carbon flux was directed to the pentose phosphate pathway. We next sought to enhance GG synthesis in Syn2973 by improving G3P contents and regulating ADP-GLC flux toward GG biosynthesis and away from glycogen and sucrose biosynthesis.

Enhancing GG Synthesis by Overexpressing the Glycerol-3-Phosphate Dehydrogenase Gene

To further improve GG synthesis, heterologous genes that encoded glycerol-3-phosphate dehydrogenase (GlpD) were overexpressed in Syn2973 to enhance G3P supply and GG synthesis. In detail, four genes, *sll1085* encoding GlpD (glycerol-3-phosphate dehydrogenase) from Syn6803, *slr1755* encoding GpsA (NAD^+-dependent glycerol-3-phosphate dehydrogenase) from Syn6803, Synpcc7942-2522 from Syn7942, and YDL022 W (*glpd1*) from *S. cerevisiae*, were cloned into the plasmid

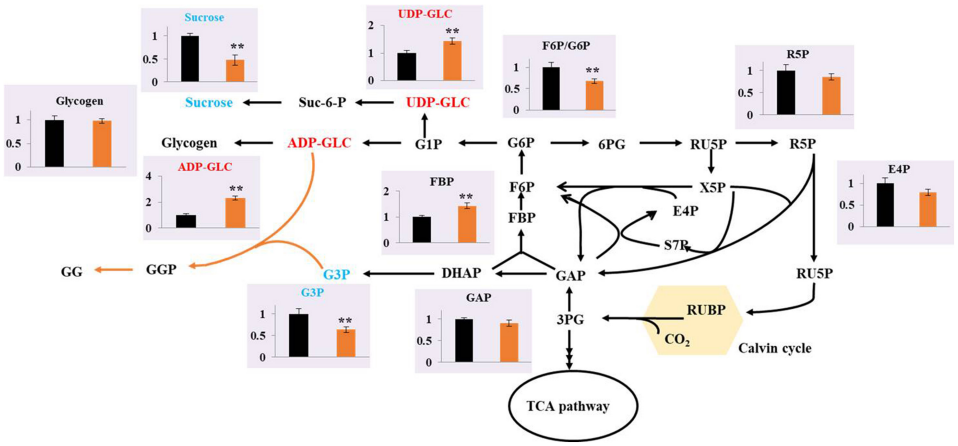

FIGURE 3 | Comparison of the metabolites between the strains M-pSI (black) and M-GgpPS (orange) under 0.4 M NaCl. The *y*-axis is the ratio of the abundance of strain M-GgpPS to strain M-pSI under 0.4 M NaCl. The average value for strain M-pSI was set to 1. Data show the mean with error bars indicating the standard deviation calculated from three independent biological replicates.

pSI-*ggpPS* with a strong P*cpc560* promoter and introduced into the wild-type Syn2973 strain. The strain M-Glpd1-GgpPS overexpressing *glpd1* could not survive under salt stress (data not shown), indicating that *glpd1* from *S. cerevisiae* might be toxic to Syn2973 under salt stress, although it had a positive effect on the G3P supply for lipid accumulation in Syn6803 (Wang et al., 2016). Then, the total GG production of strains M-1085-GgpPS, M-1175-GgpPS, and M-2522-GgpPS reached 65, 62, and 70 mg/g at a cultivation time point of 60 h, respectively, improving 32, 26, and 42% compared with strain M-GgpPS, respectively (**Figure 4A**).

Knockdown of the Competing Pathway Using Hfq-MicC to Improve GG Production

The glycogen, sucrose, and pentose phosphate pathways are the major carbon competition pathways for GG synthesis (**Figure 1**). However, knockout of genes in essential pathways might cause severe growth inhibition. An sRNA regulatory tool that introduces an exogenous Hfq chaperone and MicC scaffold with a binding sequence (Hfq-MicC) was developed in Syn6803, achieving the accurate regulation of endogenous and exogenous genes (Sun et al., 2018). Recently, the utilization of the Hfq-MicC tool was also established and tested in Syn2973, suggesting that this tool was effective in Syn2973 and demonstrated the essential role of Hfq (Li et al., 2018). To drive more carbon flux from the competing pathways to GG biosynthesis, the sRNA regulatory tool above was employed, and the M744-00310-encoding gene *pgl* related to the pentose phosphate pathway, the M744-05875-encoding gene *rfbA* related to sucrose synthesis, and the M744-03630-encoding gene *glgA* related to glycogen synthesis were selected as target genes. The strains M-2522-GgpPS-dpgl, M-2522-GgpPS-dglgA, and M-2522-GgpPS-drfbA were constructed, targeting the *pgl*, *rfbA*, and *glgA* genes, respectively (**Table 1**). qRT-PCR assays were carried out to determine the mRNA abundances of three target genes in the mutant strains. As illustrated in **Supplementary Figure 5**, the transcriptional levels of *pgl*, *rfbA*, and *glgA* were decreased by 52, 45, and 38%, respectively, compared to those in the control strain M-2522-GgpPS-pSII. In addition, the GG production of strains M-2522-GgpPS-pSII, M-2522-GgpPS-dpgl, M-2522-GgpPS-dglgA, and M-2522-GgpPS-drfbA achieved 68, 66, 64, and 80 mg/g, respectively, at a cultivation time point of 60 h (**Figure 4B**). Compared with the control strain M-2522-GgpPS-pSII, GG synthesis in strains M-2522-GgpPS-dpgl and M-2522-GgpPS-dglgA was slightly decreased, while GG production in strain M-2522-GgpPS-drfbA was increased by 17%. The GG productivity was up to 1.3 mg/g/h, which represented an increase of 56.8% compared with the initial strain M-GgpPS. Together, these results demonstrated that among these three tested genes, downregulating the gene *rfbA* produced the best enhancement of GG production.

Comparative Targeted Metabolomics Analysis of Strains M-2522-GgpPS-drfbA and M-pSI-pSII

To further explore the mechanisms relevant to high GG biosynthesis, the metabolites of strain M-2522-GgpPS-drfbA and the control strain M-pSI-pSII under 0.4 M NaCl and 200 μmol photons m^{-2} s^{-1} conditions were extracted and subjected to LCMS-based targeted metabolomics analysis. As shown in **Figure 5**, the G3P content in strain M-2522-GgpPS-drfbA was increased by threefold compared to the control strain M-pSI-pSII, suggesting that it was effective for G3P and GG accumulation by overexpressing the gene *glpD*. The UDP-GLC in strain M-2522-GgpPS-drfbA was decreased by 24%, while sucrose was further decreased by 60% compared with the control strain M-pSI-pSII, suggesting that more carbon flux might be redirected from sucrose metabolism to GG synthesis. The key metabolites of the gluconeogenic pathway in strain M-2522-GgpPS-drfbA, such as FBP and F6P, were decreased by 11 and

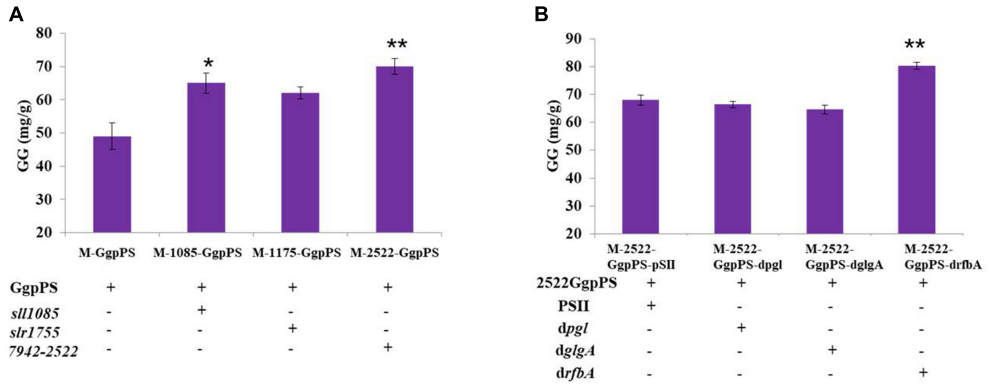

FIGURE 4 | (A) GG synthesis of strains M-GgpPS, M-1085-GgpPS, M-1175-GgpPS, and M-2522-GgpPS; **(B)** GG synthesis of strains M-2522-GgpPS-pSII, M-2522-GgpPS-dpgl, M-2522-GgpPS-drfbA, and M-2522-GgpPS-dglgA. Statistical analysis was conducted as described in the text, as statistical significance indicated by $^{**}p < 0.01$; $^{*}p < 0.05$.

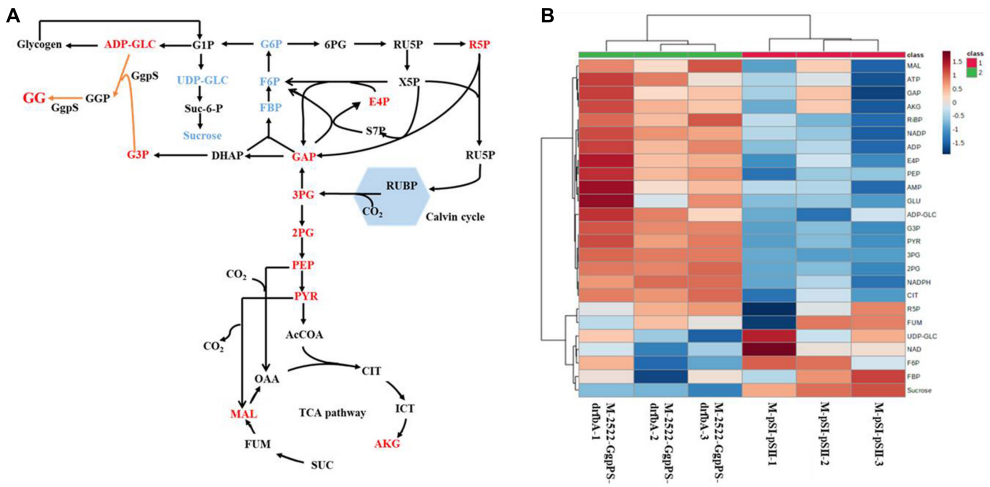

FIGURE 5 | Targeted metabolomics analysis of strain M-2522-GgpPS-drfbA and M-pSI-pSII. **(A)** Comparison of the metabolites in central metabolic pathway between strain M-2522-GgpPS-drfbA and the control strain M-pSI-pSII, red: increased, blue: decreased; **(B)** heatmaps of metabolomics profiles in strains M-2522-GgpPS-drfbA and M-pSI-pSII. Each colored cell on the heatmap corresponds to a concentration value. The higher the concentration, the darker the color (red represents the increase, and blue represents the decrease).

12%, respectively. However, GAP as the precursor to G3P was increased by 25% compared with the control strain M-pSI-pSII. In addition, the metabolites 3PG, PEP and PYR in the glycolytic pathway were increased by 6-, 1. 9-, and 2.4-fold compared with the control strain M-pSI-pSII, respectively, suggesting that more carbon might be redirected to the TCA cycle, which is necessary for biomass accumulation.

GG Synthesis for the Salt Tolerance of Syn2973

Glucosylglycerol, a compatible solute, plays an important role in moderate and halotolerant cyanobacterial strains with salt tolerance (Klahn and Hagemann, 2011). To test the salt tolerance of different GG-producing strains, growth curves of strains were measured under added 0.5 M NaCl. The results showed that the OD_{750} values of strains M-GgpPS and M-2522-GgpPS were increased by 27 and 52% compared with the control strain M-pSI at a cultivation time point of 60 h, respectively. The OD_{750} value of strain M-2522-GgpPS-drfbA was improved by 62% compared with that of the control strain M-pSI-pSII (**Figure 6**). These results indicated that the salt tolerance of Syn2973 was enhanced in association with the increase in GG synthesis in Syn2973.

In addition, the growth of strain M-2522-GgpPS-drfbA and control strain M-pSI-pSII was also measured under high light (500 μmol photons m^{-2} s^{-1}) and salt stress conditions, and the growth of strain M-2522-GgpPS-drfbA was improved by threefold compared with the control strain M-pSI-pSII under high light and 0.4 M NaCl (**Supplementary Figure 6**). However, neither of the strains survived under high light and 0.5 M NaCl, suggesting that further improvement is still necessary for growth under high-light and high-salt conditions.

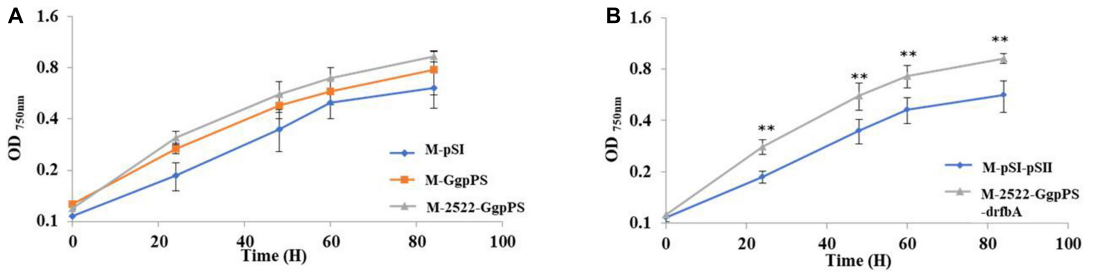

FIGURE 6 | Growth curves of strains under 0.5 M NaCl and 200 μmol photons m^{-2} s^{-1} conditions. **(A)** Growth curves of strains M-pSI, M-GgpPS, and M-2522-GgpPS; **(B)** growth curves of strains M-2522-GgpPS-pSII and M-2522-GgpPS-drfbA. Statistical analysis was conducted as described in the text, as statistical significance indicated by $^{**}p < 0.01$.

DISCUSSION

Syn2973 has a faster growth rate and is more tolerant to high temperature and high light, making it a good candidate chassis for autotrophic photosynthetic microbial cell factories. However, Syn2973 is sensitive to salt stress. In this study, the salt tolerance of Syn2973 was preliminarily improved by heterologously expressing *ggpP* and *ggpS*. Overexpressing the *glpD* gene and downregulating the *rfbA* gene further improved GG production and enhanced the salt tolerance of Syn2973. Under 0.5 M NaCl, the OD_{750} value of strain M-2522-GgpPS-drfbA was improved by 62% compared with that of the control strain M-pSI-pSII. A comparative metabolomic analysis between strains M-pSI-pSII and M-2522-GgpPS-drfbA showed that more carbon flux was redirected from ADP-GLC to GG synthesis. In addition, more carbon was directed to the TCA cycle for cell growth compared with the control strain M-pSI-pSII.

Glucosylglycerol synthesis was achieved in Syn2973 under salt stress conditions, and GG production reached 51 mg/g under salt stress in strain M-GgpPS. The GG production in wild-type *Synechocystis* was up to 100 mg/L (Tan et al., 2015), suggesting that the accumulation level of GG was relatively lower than that in *Synechocystis*. Reasons for the limited accumulation of GG in Syn2973 cells are not entirely clear but could be speculated, such as insufficient precursor supply. To confirm this hypothesis, targeted metabolomics analysis was conducted, and the results showed that the G3P content was decreased in strain M-GgpPS, suggesting that it was a limiting step for GG synthesis. G3P is a key precursor for triacylglycerol synthesis (Dulermo and Nicaud, 2011; Wang et al., 2016). A previous study showed that lipid production was enhanced by overexpressing the *glpD* gene (Wang et al., 2016). In addition, the production of 1,3-propanediol was increased by heterologous overexpression of the *glpD* gene (Liu et al., 2018). It is interesting to explore the relationship between GG synthesis and G3P supply. Moreover, ADP-GLC and UDP-GLC in strain M-GgpPS were increased, and pentose phosphate pathways, such as E4P and R5P, were decreased, suggesting that there might be more flux through the sucrose phosphate pathway due to the introduction of GG synthesis. The sucrose content decreased, which might be due to GG synthesis driving part of the flux. The qRT-PCR assay showed that expression of the *sps* gene was downregulated and that of *rfbA* was upregulated. The *sps* gene in Syn2973 was the limiting step for sucrose synthesis (Lin et al., 2020), suggesting that some carbon might accumulate in UDP-GLC. Cyanobacterial glycogen can be utilized as a sugar feedstock by microbes for ethanol fermentation (Aikawa et al., 2013) and has significant roles in tolerance to nitrogen, salt, or oxidative stress. Previous studies showed that sucrose and GG could be enhanced by blocking glycogen synthesis (Miao et al., 2003; Xu et al., 2013). The glycogen content did not show a significant change in strain M-GgpPS. It is necessary to enhance GG synthesis by improving G3P contents and directing ADP-GLC flux toward GG and away from glycogen and sucrose biosynthesis in future research.

By performing overexpression of *glpD* genes from different sources, we found that *glpD* from Syn7942 demonstrated the best effect in terms of improved GG synthesis, suggesting that it was effective for improving GG production by increasing the G3P supply. Surprisingly, GG production by strain M-2522-GgpPS-dglgA with *glgA* downregulation was decreased. A recent study showed that downregulation of glycogen has little effect on sucrose production (Lin et al., 2020). Another study suggested that reducing glycogen content could not increase sucrose content in Syn7942 (Ducat et al., 2012). Meanwhile, a previous study indicated a close link between the glycogen pool and compatible solute synthesis in Syn7942 and strongly suggested that intracellular glycogen serves, at least partially, as a carbon pool supporting sucrose synthesis rather than competing with sucrose synthesis (Qiao et al., 2018). A previous study also showed that overexpression of genes associated with glycogen synthesis, such as ADP-glucose pyrophosphorylase (GlgC), could enhance sucrose production (Lin et al., 2020). More recently, a study showed that trehalose production was increased by overexpressing *glgC* and isoamylase-type debranching enzyme (*glgX*) (associated with glycogen degradation) (Choi and Woo, 2020). It is thus worth further exploring how to increase glycogen metabolism for GG synthesis in the future. In addition, GG synthesis in strain M-2522-GgpPS-dpgl with downregulation of *pgl* was slightly decreased. The reason might be associated with the roles of the *pgl* gene in the pentose phosphate pathway, which was associated with CO_2 fixation. The GG synthesis of strain M-2522-GgpPS-drfbA was increased by downregulating the *rfbA* gene, suggesting that more carbon flux was redirected from sucrose to GG synthesis.

To further decipher the possible mechanisms involved in GG synthesis and its regulation, targeted metabolomics analysis was also performed for strain M-2522-GgpPS-drfbA and the control strain M-pSI-pSII. The G3P in strain M-2522-GgpPS-drfbA was increased, suggesting that overexpressing *glpD* was effective for G3P accumulation. In addition, sucrose as a compatible solute in strain M-2522-GgpPS-drfbA was further decreased, which was closely related to the limited improvement of salt tolerance. The key metabolites of the gluconeogenic pathway in strain M-2522-GgpPS-drfbA, such as FBP, F6P, and GAP, were decreased. A previous study showed that fructose 1,6-bisphosphate aldolase (FBA) was associated with glycolysis, gluconeogenesis, and the Calvin cycle (Zgiby et al., 2000), which is known to be associated with salt stress (Patipong et al., 2019). It is interesting to check whether improving FBA activity could further redirect more carbon flux to the sugar synthesis pathway to further improve GG production. The metabolites 3PG, PEP, and PYR in the glycolytic pathway were increased compared with the control strain M-pSI-pSII, which was consistent with the better growth phenotype of strain M-2522-GgpPS-drfbA. It is expected that more carbon flow can be driven into the TCA cycle to maintain cell growth in the early stage, and more carbon flow can be redirected to the gluconeogenic pathway to promote GG synthesis by induced sRNA interference in the later stage.

Glucosylglycerol represents the primary compatible solute for salt resistance in many marine cyanobacteria (Kirsch et al., 2019). To validate whether the GG accumulation level was associated with the salt tolerance of Syn2973, different mutant strains were chosen to evaluate their growth under salt stress. The results suggested that the salt tolerance of mutants increased with increasing GG production ability, indicating that GG production was beneficial for Syn2973 under salt stress. Together, these results indicated that the heterologous synthetic compatible solutes could function as compatible solutes for resisting salt stress. In addition, the strain M-2522-GgpPS-drfbA and control strain M-pSI-pSII were tested under high-light culture conditions. The growth of strain M-2522-GgpPS-drfbA was far better than that of control strain M-pSI-pSII under high light and 0.4 M NaCl; however, neither of the strains survived under conditions of high light and 0.5 M NaCl, suggesting that high light could inhibit the growth of Syn2973 under salt stress. It is speculated that several mechanisms might be involved: (*i*) excess light energy could break the balance between energy supply and consumption of cyanobacteria, leading to the intracellular accumulation of reactive oxygen species (ROS) (Muramatsu and Hihara, 2012); meanwhile, high salt stress could also induce ROS accumulation (Swapnil et al., 2017). The accumulated ROS further disrupted key cellular components, seriously restricting cell viability; (*ii*) salt stress inhibited photosystems II and I in cyanobacteria (Allakhverdiev and Murata, 2008), which could interfere with photosynthesis under high light; and (*?*) a previous study showed that energy metabolites such as ATP and NADPH might be necessary contributors to the rapid growth of Syn2973 under high-light conditions (Ungerer et al., 2018b). However, energy metabolites are also directly associated with Na^+ excretion from the cytoplasm, such as Na^+/H^+ antiporters that utilize the energy of the transmembrane proton gradient for Na^+ exclusion (Cui et al., 2020a). Therefore, energy metabolites might be urgent for cell growth under high-light and high-salt-stress conditions. In this study, we preliminarily tested the heterologous synthesis of GG and its effect on salt tolerance of Syn2973 under low CO_2 concentration from the air, the same condition for both engineered strain and wild-type, which could tell the preliminary difference. It also worth evaluating the detailed performance of the engineered strains and wild-type employing other conditions or methods, such as under carbon-sufficient cultivation condition, or a spot assay on agar plates for salt tolerance monitoring in future research. Together, the study provides important engineering strategies to further improve salt tolerance and GG production of Syn2973 in the near future, and further work is still necessary to engineer Syn2973 to reach high salt and high light tolerance for future cultivation applications.

DATA AVAILABILITY STATEMENT

The datasets presented in this study can be found in online repositories. The names of the repository/repositories and accession number(s) can be found in the article/**Supplementary Material**.

AUTHOR CONTRIBUTIONS

LC and WZ designed the research. JC and TS performed the major experiments and wrote the draft manuscript. JC, TS, LC, and WZ analyzed the data and drafted and revised the manuscript. All authors contributed to the article and approved the submitted version.

FUNDING

This research was supported by grants from the National Key Research and Development Program of China (Grant nos. 2020YFA0906800, 2019YFA0904600, 2018YFA0903600, and 2018YFA0903000), the National Natural Science Foundation of China (Grant nos. 31770035, 31901016, 91751102, 31770100, 31972931, 21621004, 31370115, and 3140217), and the Tianjin Synthetic Biotechnology Innovation Capacity Improvement Project (no. TSBICIP-KJGG-007).

SUPPLEMENTARY MATERIAL

The Supplementary Material for this article can be found online at: https://www.frontiersin.org/articles/10.3389/fmicb.2021.650217/full#supplementary-material

Supplementary Figure 1 | Identification of correct strains by colony PCR. **(A)** Amplification of the fragment *Ptrc-sll0746-Ptrc-sll1566-TrbcL* from strains M-pSI (control strain) and M-GgpPS; **(B)** amplification of the fragment P_{cpc560}-*Syn2522*-P_{trc}-*sll0746*-P_{trc}-*sll1566*-T_{rbcL} from strains M-pSI and M-2522-GgpPS; **(C)** amplification of the fragment *asrfbA-micC-TrbcL-Pcpc560-hfq-TrbcL* from strains M-pSI-pSII (control strain) and M-2522-GgpPS-drfbA. M, marker.

Supplementary Figure 2 | GG production at different cultivation points of strain M-GgpPS.

Supplementary Figure 3 | Chromatograms of GG, sucrose and internal standard 13C-sorbitol. **(A)** Chromatogram of the derivatized 13C-sorbitol and GG standard; **(B)** chromatogram of control strain M-pSI; **(C)** chromatogram of strain M-GgpPS; **(D)** mass spectrometry of GG.

Supplementary Figure 4 | Transcript level measurements of *glgA*, *rfbA*, and *Syn0808* in strains M-GgpPS (orange) and M-pSI (black) using qRT-PCR.

Supplementary Figure 5 | Transcript level measurements of *pgl*, *glgA*, and *rfbA* in strains M-2522-GgpPS-dpgl, M-2522-GgpPS-dglgA, and M-2522-GgpPS-drfbA (orange) and the control strain M-2522-GgpPS-pSII (blue) using qRT-PCR.

Supplementary Figure 6 | Growth curves of strains under salt and high light (500 μmol photons m^{-2} s^{-1}) stress conditions.

Supplementary Table 1 | Primers used in this study.

Supplementary Table 2 | The raw metabolomics data of the heatmap.

REFERENCES

Abernathy, M. H., Yu, J., Ma, F., Liberton, M., Ungerer, J., Hollinshead, W. D., et al. (2017). Deciphering cyanobacterial phenotypes for fast photoautotrophic growth via isotopically nonstationary metabolic flux analysis. *Biotechnol. Biofuels* 10:273.

Aikawa, S., Joseph, A., Yamada, R., Izumi, Y., Yamagishi, T., Matsuda, F., et al. (2013). Direct conversion of *Spirulina* to ethanol without pretreatment or enzymatic hydrolysis processes. *Energy Environ. Sci.* 6, 1844–1849. doi: 10.1039/C3EE40305J

Allakhverdiev, S. I., and Murata, N. (2008). Salt stress inhibits photosystems II and I in cyanobacteria. *Photosynth. Res.* 98, 529–539. doi: 10.1007/s11120-008-9334-x

Arisaka, S., Terahara, N., Oikawa, A., and Osanai, T. (2019). Increased polyhydroxybutyrate levels by *ntcA* overexpression in *Synechocystis* sp. PCC 6803. *Algal Res.* 41:101565. doi: 10.1016/j.algal.2019.101565

Bennette, N. B., Eng, J. F., and Dismukes, G. C. (2011). An LC-MS-based chemical and analytical method for targeted metabolite quantification in the model cyanobacterium *Synechococcus* sp. PCC 7002. *Anal. Chem.* 83, 3808–3816. doi: 10.1021/ac200108a

Choi, S. Y., and Woo, H. M. (2020). CRISPRi-dCas12a: a dCas12a-mediated CRISPR interference for repression of multiple genes and metabolic engineering in cyanobacteria. *ACS Synthet. Biol.* 9, 2351–2361. doi: 10.1021/acssynbio.0c00091

Cui, J., Sun, T., Chen, L., and Zhang, W. (2020a). Engineering salt tolerance of photosynthetic cyanobacteria for seawater utilization. *Biotechnol. Adv.* 43:107578. doi: 10.1016/j.biotechadv.2020.107578

Cui, J., Sun, T., Li, S., Xie, Y., Song, X., Wang, F., et al. (2020b). Improved salt tolerance and metabolomics analysis of *Synechococcus elongatus* UTEX 2973 by Overexpressing Mrp Antiporters. *Front. Bioeng. Biotechnol.* 8:500. doi: 10.3389/fbioe.2020.00500

Cui, J. Y., Good, N. M., Hu, B., Yang, J., Wang, Q. W., Sadilek, M., et al. (2016). Metabolomics revealed an association of metabolite changes and defective growth in *Methylobacterium extorquens* AM1 overexpressing *ecm* during growth on methanol. *PLoS One* 11:e0154043. doi: 10.1371/journal.pone.0154043

Da Costa, M. S., Santos, H., and Galinski, E. A. (1998). "An overview of the role and diversity of compatible solutes in *Bacteria* and *Archaea*," in *Biotechnology of Extremophiles*, ed. G. Antranikian (Berlin: Springer), 117–153.

Du, W., Liang, F., Duan, Y., Tan, X., and Lu, X. (2013). Exploring the photosynthetic production capacity of sucrose by cyanobacteria. *Metab. Eng.* 19, 17–25. doi: 10.1016/j.ymben.2013.05.001

Ducat, D. C., Avelar-Rivas, J. A., Way, J. C., and Silver, P. A. (2012). Rerouting carbon flux to enhance photosynthetic productivity. *Appl. Environ. Microbiol.* 78, 2660–2668. doi: 10.1128/aem.07901-11

Dulermo, T., and Nicaud, J. M. (2011). Involvement of the G3P shuttle and beta-oxidation pathway in the control of TAG synthesis and lipid accumulation in *Yarrowia lipolytica*. *Metab. Eng.* 13, 482–491. doi: 10.1016/j.ymben.2011.05.002

Gao, X., Gao, F., Liu, D., Zhang, H., Nie, X., and Yang, C. (2016a). Engineering the methylerythritol phosphate pathway in cyanobacteria for photosynthetic isoprene production from CO_2. *Energy Environ. Sci.* 9, 1400–1411. doi: 10.1039/c5ee03102h

Gao, X., Sun, T., Pei, G., Chen, L., and Zhang, W. (2016b). Cyanobacterial chassis engineering for enhancing production of biofuels and chemicals. *Appl. Microbiol. Biotechnol.* 100, 3401–3413. doi: 10.1007/s00253-016-7374-2

Gao, Z., Zhao, H., Li, Z., Tan, X., and Lu, X. (2012). Photosynthetic production of ethanol from carbon dioxide in genetically engineered cyanobacteria. *Energy Environ. Sci.* 5, 9857–9865. doi: 10.1039/c2ee22675h

Hagemann, M. (2011). Molecular biology of cyanobacterial salt acclimation. *FEMS Microbiol. Rev.* 35, 87–123. doi: 10.1111/j.1574-6976.2010.00234.x

Hagemann, M., and Erdmann, N. (1994). Activation and pathway of glucosylglycerol synthesis in the cyanobacterium *Synechocystis* sp. PCC 6803. *Microbiology* 140, 1427–1431. doi: 10.1099/00221287-140-6-1427

Herskowitz, I. (1988). Life cycle of the budding yeast *Saccharomyces cerevisiae*. *Microbiol. Rev.* 52, 536–553. doi: 10.1128/mr.52.4.536-553.1988

Kirsch, F., Klahn, S., and Hagemann, M. (2019). Salt-regulated accumulation of the compatible solutes sucrose and glucosylglycerol in cyanobacteria and its biotechnological potential. *Front. Microbiol.* 10:2139. doi: 10.3389/fmicb.2019.02139

Klahn, S., and Hagemann, M. (2011). Compatible solute biosynthesis in cyanobacteria. *Environ. Microbiol.* 13, 551–562. doi: 10.1111/j.1462-2920.2010.02366.x

Li, S., Sun, T., Xu, C., Chen, L., and Zhang, W. (2018). Development and optimization of genetic toolboxes for a fast-growing cyanobacterium *Synechococcus elongatus* UTEX 2973. *Metab. Eng.* 48, 163–174. doi: 10.1016/j.ymben.2018.06.002

Lin, P. C., Zhang, F., and Pakrasi, H. B. (2020). Enhanced production of sucrose in the fast-growing cyanobacterium *Synechococcus elongatus* UTEX 2973. *Sci. Rep.* 10:390.

Liu, H., Ni, J., Xu, P., and Tao, F. (2018). Enhancing light-driven 1,3-propanediol production by using natural compartmentalization of differentiated cells. *ACS Synth. Biol.* 7, 2436–2446. doi: 10.1021/acssynbio.8b00239

Livak, K. J., and Schmittgen, T. D. (2001). Analysis of relative gene expression data using real-time quantitative PCR and the $2^{-\Delta\Delta CT}$ method. *Methods* 25, 402–408. doi: 10.1006/meth.2001.1262

Luan, G., and Lu, X. (2018). Tailoring cyanobacterial cell factory for improved industrial properties. *Biotechnol. Adv.* 36, 430–442. doi: 10.1016/j.biotechadv.2018.01.005

Luley-Goedl, C., and Nidetzky, B. (2011). Glycosides as compatible solutes: biosynthesis and applications. *Nat. Prod. Rep.* 28, 875–896. doi: 10.1039/c0np00067a

Matson, M. M., and Atsumi, S. (2018). Photomixotrophic chemical production in cyanobacteria. *Curr. Opin. Biotechnol.* 50, 65–71. doi: 10.1016/j.copbio.2017.11.008

Miao, X., Wu, Q., Wu, G., and Zhao, N. (2003). Sucrose accumulation in salt-stressed cells of *agp* gene deletion-mutant in cyanobacterium *Synechocystis* sp. PCC 6803. *FEMS Microbiol. Lett.* 218, 71–77. doi: 10.1111/j.1574-6968.2003.tb11500.x

Mueller, T. J., Ungerer, J. L., Pakrasi, H. B., and Maranas, C. D. (2017). Identifying the metabolic differences of a fast-growth phenotype in *Synechococcus* UTEX 2973. *Sci. Rep.* 7:41569.

Muramatsu, M., and Hihara, Y. (2012). Acclimation to high-light conditions in cyanobacteria: from gene expression to physiological responses. *J. Plant Res.* 125, 11–39. doi: 10.1007/s10265-011-0454-6

Niu, X., Zhang, X., Yu, X., Su, Y., Chen, L., and Zhang, W. (2015). Optimization and application of targeted LC-MS metabolomic analyses in photosynthetic cyanobacteria. *Chin. J. Biotechnol.* 31, 577–590.

Novak, J. F., Stirnberg, M., Roenneke, B., and Marin, K. (2011). A novel mechanism of osmosensing, a salt-dependent protein-nucleic acid interaction in the cyanobacterium *Synechocystis* Species PCC 6803. *J. Biol. Chem.* 286, 3235–3241. doi: 10.1074/jbc.m110.157032

Osanai, T., Shirai, T., Iijima, H., Nakaya, Y., Okamoto, M., Kondo, A., et al. (2015). Genetic manipulation of a metabolic enzyme and a transcriptional regulator increasing succinate excretion from unicellular cyanobacterium. *Front. Microbiol.* 6:1064. doi: 10.3389/fmicb.2015.01064

Patipong, T., Ngoennet, S., Honda, M., Hibino, T., Waditee-Sirisattha, R., and Kageyama, H. (2019). A class I fructose-1,6-bisphosphate aldolase is associated with salt stress tolerance in a halotolerant cyanobacterium *Halothece* sp. PCC 7418. *Arch. Biochem. Biophys.* 672:108059. doi: 10.1016/j.abb.2019.07.024

Qiao, C., Duan, Y., Zhang, M., Hagemann, M., Luo, Q., and Lu, X. (2018). Effects of reduced and enhanced glycogen pools on salt-induced sucrose production in a sucrose-secreting strain of *Synechococcus elongatus* PCC 7942. *Appl. Environ. Microbiol.* 84:e002023-17.

Roenneke, B., Rosenfeldt, N., Derya, S. M., Novak, J. F., Marin, K., Kramer, R., et al. (2018). Production of the compatible solute alpha-D-glucosylglycerol by metabolically engineered *Corynebacterium glutamicum*. *Microb. Cell Fact* 17:94.

Sawangwan, T., Goedl, C., and Nidetzky, B. (2010). Glucosylglycerol and glucosylglycerate as enzyme stabilizers. *Biotechnol. J.* 5, 187–191. doi: 10.1002/biot.200900197

Silkina, A., Kultschar, B., and Llewellyn, C. A. (2019). Far-red light acclimation for improved mass cultivation of cyanobacteria. *Metabolites* 9:170. doi: 10.3390/metabo9080170

Singh, M., Sharma, N. K., Prasad, S. B., Yadav, S. S., Narayan, G., and Rai, A. K. (2013). The freshwater cyanobacterium *Anabaena doliolum* transformed with *ApGSMT-DMT* exhibited enhanced salt tolerance and protection to nitrogenase activity, but became halophilic. *Microbiology* 159, 641–648. doi: 10.1099/mic.0.065078-0

Song, K., Tan, X., Liang, Y., and Lu, X. (2016). The potential of *Synechococcus elongatus* UTEX 2973 for sugar feedstock production. *Appl. Microbiol. Biotechnol.* 100, 7865–7875. doi: 10.1007/s00253-016-7510-z

Sun, T., Li, S., Song, X., Pei, G., Diao, J., Cui, J., et al. (2018). Re-direction of carbon flux to key precursor malonyl-CoA via artificial small RNAs in photosynthetic *Synechocystis* sp. PCC 6803. *Biotechnol. Biofuels* 11:26.

Sun, T., Pei, G., Wang, J., Chen, L., and Zhang, W. (2017). A novel small RNA CoaR regulates coenzyme A biosynthesis and tolerance of *Synechocystis* sp. PCC6803 to 1-butanol possibly via promoter-directed transcriptional silencing. *Biotechnol. Biofuels* 10:42.

Swapnil, P., Yadav, A. K., Srivastav, S., Sharma, N. K., Srikrishna, S., and Rai, A. K. (2017). Biphasic ROS accumulation and programmed cell death in a cyanobacterium exposed to salinity (NaCl and Na_2SO_4). *Algal Res.* 23, 88–95. doi: 10.1016/j.algal.2017.01.014

Tan, X., Du, W., and Lu, X. (2015). Photosynthetic and extracellular production of glucosylglycerol by genetically engineered and gel-encapsulated cyanobacteria. *Appl. Microbiol. Biotechnol.* 99, 2147–2154. doi: 10.1007/s00253-014-6273-7

Tan, X., Luo, Q., and Lu, X. (2016). Biosynthesis, biotechnological production, and applications of glucosylglycerols. *Appl. Microbiol. Biotechnol.* 100, 6131–6139. doi: 10.1007/s00253-016-7608-3

Ungerer, J., Lin, P.-C., Chen, H.-Y., and Pakrasi, H. B. (2018a). Adjustments to photosystem stoichiometry and electron transfer proteins are key to the remarkably fast growth of the cyanobacterium *Synechococcus elongatus* UTEX 2973. *mBio* 9:e02327-17.

Ungerer, J., Wendt, K. E., Hendry, J. I., Maranas, C. D., and Pakrasi, H. B. (2018b). Comparative genomics reveals the molecular determinants of rapid growth of the cyanobacterium *Synechococcus elongatus* UTEX 2973. *Proc. Natl. Acad. Sci. U.S.A.* 115, E11761–E11770.

Waditee-Sirisattha, R., Singh, M., Kageyama, H., Sittipol, D., Rai, A., and Takabe, T. (2012). *Anabaena* sp. PCC7120 transformed with glycine methylation genes from *Aphanothece halophytica* synthesized glycine betaine showing increased tolerance to salt. *Arch. Microbiol.* 194, 909–914. doi: 10.1007/s00203-012-0824-z

Wang, X., Xiong, X., Sa, N., Roje, S., and Chen, S. (2016). Metabolic engineering of enhanced glycerol-3-phosphate synthesis to increase lipid production in *Synechocystis* sp. PCC 6803. *Appl. Microbiol. Biotechnol.* 100, 6091–6101. doi: 10.1007/s00253-016-7521-9

Wang, J., Zhang, X., Shi, M., Gao, L., Niu, X., Te, R., et al. (2014). Metabolomic analysis of the salt-sensitive mutants reveals changes in amino acid and fatty acid composition important to long-term salt stress in *Synechocystis* sp. PCC 6803. *Funct. Integr. Genomics* 14, 431–440. doi: 10.1007/s10142-014-0370-7

Xu, Y., Guerra, L. T., Li, Z., Ludwig, M., Dismukes, G. C., and Bryant, D. A. (2013). Altered carbohydrate metabolism in glycogen synthase mutants of *Synechococcus* sp. strain PCC 7002: Cell factories for soluble sugars. *Metab. Eng.* 16, 56–67. doi: 10.1016/j.ymben.2012.12.002

Yoshikawa, K., Toya, Y., and Shimizu, H. (2017). Metabolic engineering of *Synechocystis* sp. PCC 6803 for enhanced ethanol production based on flux balance analysis. *Bioprocess. Biosyst. Eng.* 40, 791–796. doi: 10.1007/s00449-017-1744-8

Yu, J., Liberton, M., Cliften, P. F., Head, R. D., Jacobs, J. M., Smith, R. D., et al. (2015). *Synechococcus elongatus* UTEX 2973, a fast growing cyanobacterial chassis for biosynthesis using light and CO_2. *Sci. Rep.* 5:8132.

Zgiby, S. M., Thomson, G. J., Qamar, S., and Berry, A. (2000). Exploring substrate binding and discrimination in fructose1,6-bisphosphate and tagatose 1,6-bisphosphate aldolases. *Eur. J. Biochem.* 267, 1858–1868. doi: 10.1046/j.1432-1327.2000.01191.x

Conflict of Interest: The authors declare that the research was conducted in the absence of any commercial or financial relationships that could be construed as a potential conflict of interest.

frontiers in Microbiology

ORIGINAL RESEARCH
published: 02 June 2021
doi: 10.3389/fmicb.2021.677596

Non-natural Aldol Reactions Enable the Design and Construction of Novel One-Carbon Assimilation Pathways *in vitro*

Yufeng Mao[1,2†], Qianqian Yuan[1,2†], Xue Yang[1,2], Pi Liu[1,2], Ying Cheng[3], Jiahao Luo[4], Huanhuan Liu[3], Yonghong Yao[2], Hongbing Sun[2], Tao Cai[2] and Hongwu Ma[1,2]*

[1]Biodesign Center, Key Laboratory of Systems Microbial Biotechnology, Tianjin Institute of Industrial Biotechnology, Chinese Academy of Sciences, Tianjin, China, [2]Tianjin Institute of Industrial Biotechnology, Chinese Academy of Sciences, Tianjin, China, [3]State Key Laboratory of Food Nutrition and Safety, Tianjin University of Science and Technology, Tianjin, China, [4]Key Laboratory of Systems Bioengineering (Ministry of Education), SynBio Research Platform, Collaborative Innovation Center of Chemical Science and Engineering (Tianjin), School of Chemical Engineering and Technology, Tianjin University, Tianjin, China

OPEN ACCESS

Edited by:
Guodong Luan,
Qingdao Institute of Bioenergy and Bioprocess Technology, Chinese Academy of Sciences (CAS), China

Reviewed by:
Steffen N. Lindner,
Max Planck Institute of Molecular Plant Physiology, Germany
Xavier Garrabou Pi,
ETH Zürich, Switzerland
Fei Tao,
Shanghai Jiao Tong University, China

***Correspondence:**
Hongwu Ma
ma_hw@tib.cas.cn

[†]These authors have contributed equally to this work

Specialty section:
This article was submitted to Microbiotechnology, a section of the journal Frontiers in Microbiology

Received: 08 March 2021
Accepted: 04 May 2021
Published: 02 June 2021

Citation:
Mao Y, Yuan Q, Yang X, Liu P, Cheng Y, Luo J, Liu H, Yao Y, Sun H, Cai T and Ma H (2021) Non-natural Aldol Reactions Enable the Design and Construction of Novel One-Carbon Assimilation Pathways in vitro. Front. Microbiol. 12:677596. doi: 10.3389/fmicb.2021.677596

Methylotrophs utilizes cheap, abundant one-carbon compounds, offering a promising green, sustainable and economical alternative to current sugar-based biomanufacturing. However, natural one-carbon assimilation pathways come with many disadvantages, such as complicated reaction steps, the need for additional energy and/or reducing power, or loss of CO_2, resulting in unsatisfactory biomanufacturing performance. Here, we predicted eight simple, novel and carbon-conserving formaldehyde (FALD) assimilation pathways based on the extended metabolic network with non-natural aldol reactions using the comb-flux balance analysis (FBA) algorithm. Three of these pathways were found to be independent of energy/reducing equivalents, and thus chosen for further experimental verification. Then, two novel aldol reactions, condensing D-erythrose 4-phosphate and glycolaldehyde (GALD) into 2*R*,3*R*-stereo allose 6-phosphate by DeoC or 2*S*,3*R*-stereo altrose 6-phosphate by TalB^{F178Y}/Fsa, were identified for the first time. Finally, a novel FALD assimilation pathway proceeding *via* allose 6-phosphate, named as the glycolaldehyde-allose 6-phosphate assimilation (GAPA) pathway, was constructed *in vitro* with a high carbon yield of 94%. This work provides an elegant paradigm for systematic design of one-carbon assimilation pathways based on artificial aldolase (ALS) reactions, which could also be feasibly adapted for the mining of other metabolic pathways.

Keywords: synthetic methylotrophy, computational pathway design, allose 6-phosphate, *In vitro* pathway construction, aldolase reaction, glycolaldehyde-allose 6-phosphate assimilation pathway

INTRODUCTION

Growing concerns over global fossil-resources and food shortages have motivated the development of sustainable commodity biomanufacturing from alternative resources (Clomburg et al., 2017). Over the past decade, advances in the bioconversion of non-food, low-cost, and abundant one-carbon compounds such as methanol, formate, and CO_2 using native or synthetic methylotrophs highlighted a potentially green and economical alternative to current sugar-based biomanufacturing

(Liang et al., 2020; Mao et al., 2020; Nguyen and Lee, 2020). Notably, electron-enriched methanol (CH_4O) is expected to support more economical biosynthesis of chemicals with higher theoretical carbon-molar yields than sugars. However, the development of efficient methylotrophs, especially ones with carbon-conserving metabolism, is still hindered by the inherent drawbacks of natural methanol assimilation pathways (**Figure 1A**). These include complicated pathway, high energy, and reducing force requirements, as well as carbon loss during the conversion of methanol into the key metabolite acetyl-coenzyme A (AcCoA; Yang et al., 2019b; He et al., 2020).

Substantial efforts have been devoted to designing artificial methanol assimilation pathways that can outperform their natural counterparts (**Figure 1B**). Yu and Liao (2018) simplified the natural serine cycle by assimilating formaldehyde (FALD) instead of formate and halving the number of steps from serine to phosphoenolpyruvate. He et al. (2020) proposed the homoserine cycle, which halves the number of required enzymes and quarters the ATP demand for AcCoA synthesis compared with the serine cycle. However, both these pathways are still ATP- and NADH-dependent, which not only necessitates efficient cofactor regeneration but also lowers the yields of AcCoA derivatives (**Figure 1B**). By combining the ribulose monophosphate (RuMP) pathway and non-oxidative glycolysis (NOG), Bogorad et al. (2014) designed a carbon-conserving ATP-independent methanol condensation cycle (MCC), which achieved a final carbon yield of 80% for the synthesis of AcCoA derivatives *in vitro*. Although its yield surpassed the 67% theoretical yield of native RuMP and XuMP pathways coupled with the EMP, the construction of MCC pathway is still complicated, because it requires nine enzymes (Yang et al., 2019b).

Most methanol assimilation pathways must form FALD for further metabolism, making FALD assimilation a key step in methanol metabolism (Müller et al., 2015; Whitaker et al., 2017; Meyer et al., 2018). The introduction of computationally designed formolase (Fls; Siegel et al., 2015) or evolved glycolaldehyde

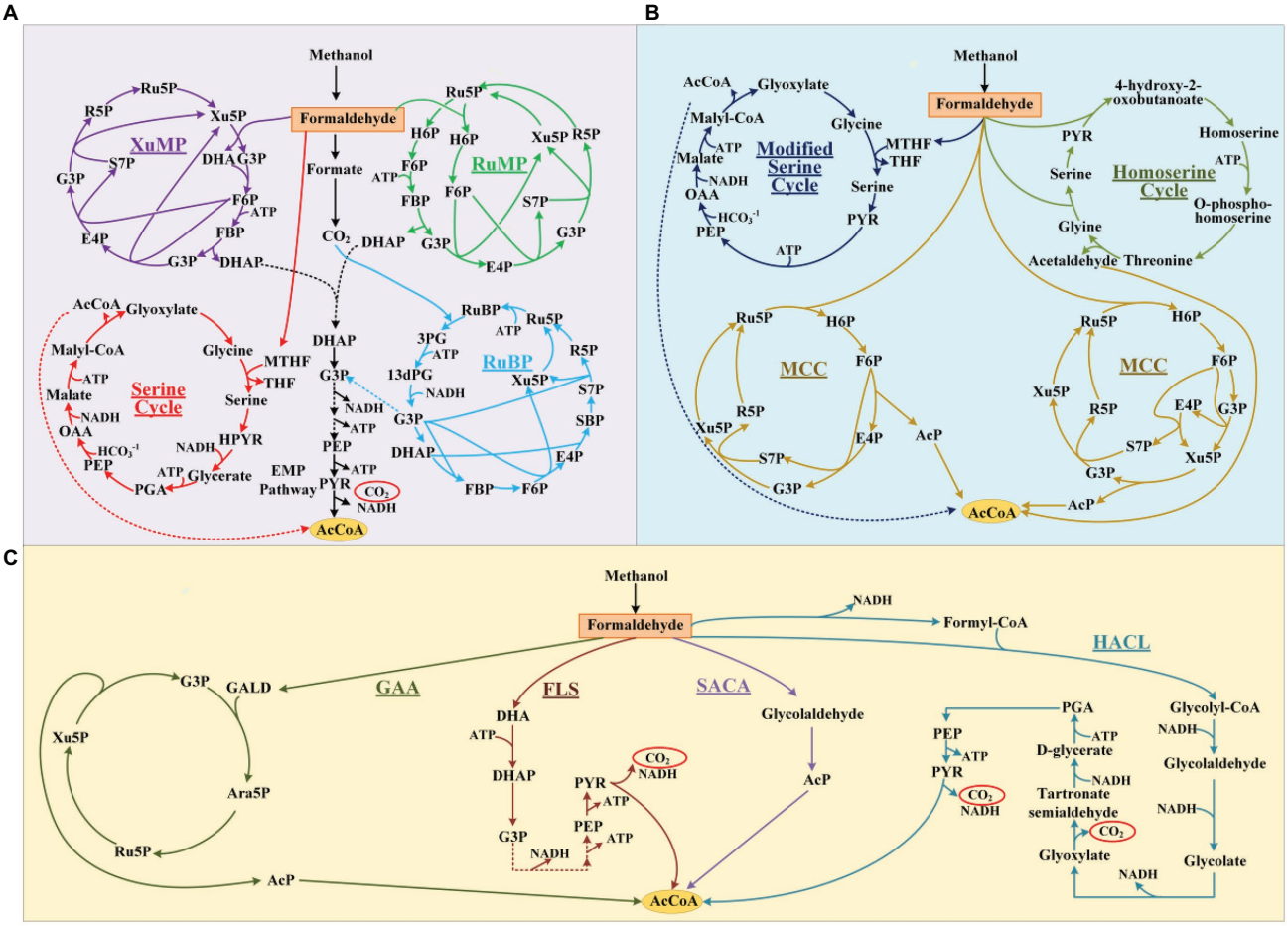

FIGURE 1 | Methanol assimilation pathways. The natural pathways **(A)** and artificial pathways without non-natural reactions **(B)** or artificial pathways based on non-natural reactions **(C)**. R5P, D-ribose 5-phosphate; Ru5P, D-ribulose 5-phosphate; Xu5P, D-xylulose 5-phosphate; DHA, dihydroxyacetone; G3P, D-glyceraldehyde 3-phosphate; F6P, D-fructose 6-phosphate; FBP, fructose 1,6-bisphosphate; E4P, D-erythrose 4-phosphate; H6P, D-hexulose 6-phosphate; S7P, D-sedoheptulose 7-phosphate; SBP, D-sedoheptulose 1,7-bisphosphate; DHAP, dihydroxyacetone phosphate; PEP, phosphoenolpyruvate; PYR, pyruvate; RuBP, D-ribulose 1,5-bisphosphate; 3PG, D-glycerate 3-phosphophosphate; 13dPG, 3-phospho-D-glyceroyl phosphate; OAA, oxaloacetate; GALD, glycolaldehyde; Ara5P, D-arabinose 5-phosphate; PGA, D-glycerate 2-phosphate; AcP, acetyl-phosphate; and AcCoA, acetyl-coenzyme A.

synthase (Gals; Lu et al., 2019), which can condense three or two FALD molecules into dihydroxyacetone (DHA) or glycolaldehyde (GALD), enabled the construction of novel FALD assimilation pathways. However, the Fls-based pathways still exhibit one-third carbon loss during AcCoA synthesis. Our colleagues proposed a Gals-based pathway named synthetic acetyl-CoA (SACA), in which GALD is converted into acetyl-phosphate (AcP) by a repurposed PK (Lu et al., 2019). However, the *in vitro* performance of this pathway was not satisfactory, with a final carbon yield of ~50%, probably due to the unfavorable substrate affinity and low catalytic efficiency of Gals. Chou et al. (2019) constructed a kinetically favorable pathway for the bioconversion of FALD into GALD by coupling an evolved 2-hydroxyacyl-CoA lyase (Hacl) with acyl-CoA reductase (Acr; **Figure 1C**), which finally achieved an 84% carbon yield for glycolate production *in vivo*. Although the current route from glycolate to AcCoA is still long and subject to carbon loss (**Figure 1C**), this kinetically favorable GALD pathway laid the foundation for prospectively more efficient bioconversion of GALD into AcCoA by coupling it with other artificial routes.

Although pathway design based on artificial/non-natural reactions has enabled the construction of brand-new methanol assimilation pathways that avoid the inherent drawbacks of their natural counterparts, rich experience is indispensable for assembling artificial reactions into pathways. Model-based pathway design using mathematical algorithms is increasingly favored for novel one-carbon assimilation pathway mining due to their systematic and innovative advantages (Trudeau et al., 2018; Yang et al., 2019b). Previously, our group constructed a large metabolic network model (Yang et al., 2019b) by integrating 6,578 known reactions from MetaCyc (Caspi et al., 2018) and 73 hypothetical aldolase (ALS) reactions from ATLAS (Hadadi et al., 2016; Hafner et al., 2020). By conducting comb-FBA, we predicted 59 ATP/NAD(P)H independent FALD assimilation pathways with 100% theoretical carbon yield for AcCoA-derived acetate production. Finally, the glycolaldehyde assimilation (GAA) pathway (**Figure 1C**) was constructed and verified with a high acetate yield of 88% *in vitro*. Inspired by this result, here, we further artificially proposed 28 non-natural aldolase reactions based on the aldol reaction mechanism, which were not present in the ATLAS database. These 28 possible aldolase reactions were added into an extended known reaction set for pathway calculation using our previously developed comb-FBA algorithm. Eight novel carbon conserving FALD assimilation cycles were calculated. Two novel aldol reactions were identified with feasible aldolases. Finally, a novel FALD assimilation pathway, proceeding *via* the condensation of GALD and E4P into allose 6-phosphate, was named as the glycolaldehyde-allose 6-phosphate assimilation (GAPA) pathway and constructed *in vitro*.

MATERIALS AND METHODS

Metabolic Reaction Set for Pathways Design

The reactions set[6578] constructed in our previous work (Yang et al., 2019b), containing 6,566 unblocked MetaCyc reactions, 11 exchange reactions and one objective reaction (**Supplementary Material; Supplementary Table A**) was used as the base reaction set. Then, a total of 28 newly proposed aldol reactions using FALD/GALD as acceptor or donor, and theoretically feasible based on the aldolase reaction mechanism (**Supplementary Table 1**), were added to this base set for pathway calculation.

Calculation Method

The parsimonious flux balance analysis (pFBA) algorithm, which minimizes the sum of flux distribution, was used to obtain the solution (Lewis et al., 2010). The comb-FBA (combination of combinatorial algorithm and pFBA algorithm) algorithm developed in our previous work (Yang et al., 2019b) was used for pathway design. Simulations were performed in Python using the COBRApy (Ebrahim et al., 2013). The exchange reaction for acetate was defined as the objective reaction and the input rate of FALD was set to 10 mmol·(g DCW)$^{-1}$·h^{-1}.

Reagents, Strains and Media

D-Erythrose 4-phosphate (E4P), glycolaldehyde, D-glucose 6-phosphate, D-mannose 6-phosphate, methoxyamine hydrochloride, pyridine and N-methyl-N-(trimethylsilyl) trifluoroacetamide (MSTFA) were purchased from Sigma-Aldrich (St. Louis, MO, United States). D-Allose and D-altrose were purchased from Macklin Biochemical (Shanghai, China). Other regents such as D-glucose, D-mannose, ATP, ADP, thiamine pyrophosphate (TPP), and $MgCl_2$ were all purchased from Sangon Biotech (Shanghai, China), unless noted otherwise. *Escherichia coli* DH5α was used for plasmid construction and preservation. *Escherichia coli* BL21 (DE3) was used for protein expression. Luria-Bertani (LB) medium (10 g/L tryptone, 5 g/L yeast extract and 10 g/L NaCl) was used for *E. coli* cell culture and recombinant protein expression, supplemented with 50 μg/ml kanamycin or 100 μg/ml ampicillin when necessary.

Construction of Plasmids

The plasmids used in this work are listed in **Table 1**. The *manA* gene was amplified by PCR from the genome of *E. coli* MG1655 using the primer pair manA-F/R (**Table 2**), and cloned between the *Nhe*I/*Xho*I restriction sites of pET28a(+), generating plasmid pET28a-*manA*. The plasmid pET28a-*alsE* was constructed analogously, using *Nhe*I and *Xho*I.

Protein Expression and Purification

Escherichia coli BL21 (DE3) strains carrying pET28a/pET32a-derived plasmids were used for protein expression. Cells were cultured in 5 ml of LB medium at 37°C and 220 rpm overnight. Then, 2 ml of the culture was used to inoculate 200 ml of LB medium in a 1 L shake flask, and grown at 37°C and 220 rpm. For induction of protein expression, isopropyl β-D-1-thiogalactopyranoside (IPTG) was added to a final concentration of 0.5 mM when the optical density at 600 nm (OD_{600}) reached 0.6–0.8, and the cultivation temperature was set and maintained at 16°C for 16–18 h. Recombinant cells were harvested by centrifugation at 6,000 × *g* and 4°C for 40 min, and then

TABLE 1 | Plasmids used in this study.

Plasmids	Relevant characteristics	NCBI-Protein ID	Ref.
pET32a-*talBF178Y*	Amp^R, N-terminally His-tagged *talBF178Y*, inserted between the *BamH*I and *Xho*I sites	NP_414549	Yang et al., 2019b
pET28a-*fsa*	Kan^R, N-terminally His-tagged *fsa*, inserted between the *Nhe*I and *Xho*I sites	NP_415346	Yang et al., 2019b
pET28a-*deoC*	Kan^R, N-terminally His-tagged *deoC*, inserted between the *Nhe*I and *Xho*I sites	NP_418798	Yang et al., 2019b
pET28a-*rpiB*	Kan^R, N-terminally His-tagged *rpiB*, inserted between the *Nhe*I and *Xho*I sites	NP_418514	Yang et al., 2019b
pET28a-*pgi*	Kan^R, N-terminally His-tagged *pgi*, inserted between the *Nde*I and *EcoR*I sites	NP_418449	Chunling et al., 2017
pET28a-*manA*	Kan^R, N-terminally His-tagged *manA*, inserted between the *Nhe*I and *Xho*I sites	NP_416130	This study
pET28a-*kdsD*	Kan^R, N-terminally His-tagged *kdsD*, inserted between the *Nhe*I and *Xho*I sites	NP_417664	Yang et al., 2019b
pET28a-*alsE*	Kan^R, N-terminally His-tagged *alsE*, inserted between *Nhe*I and *Xho*I sites	NP_418509	This study
pET28a-*fpk*	Kan^R, N-terminally His-tagged *fpk*, inserted between the *Nhe*I and *Hind*III sites	BAF39468	Yang et al., 2019b

TABLE 2 | Primers used in this study.

Primers	Sequence (5'-3')
manA-F	GTACGGCTAGCATGCAAAAACTCATTAACTC
manA-R	CATTGCTCGAGTTACAGCTTGTTGTAAACAC
alsE-F	TATCGGCTAGCATGAAAATCTCCCCCTCGTT
alsE-R	TGGTGCTCGAGTTATGCTGTTTTTGCATGAGG

re-suspended in 20 ml of phosphate buffer (PB, 50 mM, pH 7.5) containing 150 mM NaCl. The cell pellets were lysed using a high-pressure homogenizer at 4°C, and subsequently centrifuged at 6,000 × *g* and 4°C for 40 min to remove cell debris. The clear lysate was onto a Ni-NTA His-binding column and concentrated as described previously (Cui et al., 2018, 2019). The purity of the enzymes was analyzed by 12% SDS-PAGE (**Supplementary Figure 1**) and quantified using a bicinchoninic acid (BCA) Kit (CWBiotech, Beijing, China).

Enzymatic Reaction Condition

For aldol reaction, the reaction systems containing 100 mM PB (pH = 7.0), 10 mM GALD, 2.5 mM E4P, 1 mM TPP, 5 mM $MgCl_2$, and 5 mg/ml different aldolases were incubated at 37°C and 220 rpm for 2 h. For preparation of aldohexose 6-phosphate samples, the reaction systems containing 100 mM PB (pH = 7.0), 10 mM GALD, 2.5 mM E4P, 1 mM TPP, 5 mM $MgCl_2$, and 5 mg/ml glucokinase (Glk) with 10 mM different aldohexoses (D-glucose, D-mannose, D-allose, or D-altrose) were incubated at 37°C and 220 rpm for 2 h. For isomerization of aldohexose 6-phosphate, the reaction systems containing 100 mM PB (pH = 7.0), 1 mM TPP, 5 mM $MgCl_2$, 10 mM G6P, or M6P (or 10 mM ATP, 5 mg/ml Glk, and 10 mM allose/altrose) and 5 mg/ml different isomerases were incubated at 37°C and 220 rpm for 2 h. These reaction products were used for subsequently qualitative analysis.

GC-TOFMS Analysis

Samples were dried using a CentriVap vacuum concentrator at 4°C. Then, the dried samples were dissolved in 50 μl of pyridine containing 40 mg/ml methoxyamine hydrochloride, and incubated for 90 min at 30°C. Finally, 50 μl of the MSTFA regent (containing 1% TMCS, v/v) was added to the sample aliquots, mixed well, incubated for 30 min at 37°C, and then sealed in amber gas chromatography-time of flight mass spectrometry (GC-TOFMS) sample vials containing glass inserts. The GC-TOFMS analysis was carried out on an Agilent 7890A gas chromatography system coupled with a quadrupole time-of-flight (Q-TOF) mass spectrometer and an inert electron ionization (EI) ion source (Agilent, United States). A DB-5MS capillary column coated with 5% diphenyl cross-linked with 95% dimethylpolysiloxane (30 m × 250 μm inner diameter, 0.25 μm film thickness; J&W Scientific, United States) was used. The oven temperature program was as follows: 60°C (initial), ramp to 180°C (2 min) at 10°C min^{-1}, followed by a ramp to 230°C at 10°C min^{-1}, then 5°C min^{-1} to 260°C, and finally 10°C min^{-1} to 320°C (4 min). The injection, transfer line, and ion source temperatures were 250, 290, and 230°C, respectively. The instrument was operated in electron impact mode at 70 eV. The sample injection volume was 1 μl with a split ratio of 10:1. Helium was used as the carrier gas, the front inlet purge flow was 3 ml min^{-1}, and the gas flow rate through the column was 1.2 L min^{-1}. The mass spectrometry data were acquired in full-scan mode in the m/z range of 35–650 at a rate of 5 spectra per second after a solvent delay of 7.5 min. Agilent MassHunter 10.0 software with NIST2020 libraries was used for data analysis.

Measurement of Metabolite Concentrations

Acetyl-phosphate was converted into brown ferric acetyl-hydroxamate, and its concentration was analyzed by measuring the absorption at 505 nm (A_{505}) using a multifunctional microplate reader (BioTek, Winooski, VT, United States) as previously reported (Bogorad et al., 2013). GALD was converted into a blue-violet diphenylamine derivative, and was analyzed by measuring the A_{620} as previously reported (Yang et al., 2019b). The reported values are the averages and SDs of three measurements.

RESULTS

Proposal of Potential Aldolase Reactions With Different Product Stereoselectivity

Aldolases are proven tools for effective C-C bond formation with unrivaled efficiency in the synthesis of carbohydrates and complex polyhydroxylated molecules (Clapés et al., 2010; Windle et al., 2014; Roldán et al., 2017). Aldolases can generally use a broad range of aldehydes as acceptors, while some also

showed an unprecedented donor spectrum, such as the transaldolase B mutant (TalB^{F178Y}; Rale et al., 2011) and the D-fructose 6-phosphate aldolase (Fsa; Castillo et al., 2006). Based on the mechanism of known aldol reactions, four stereo configurations can be obtained by different specific aldolases (**Figure 2A**; Samland and Sprenger, 2006). For example, when GALD serves as donor and D-glyceraldehyde 3-phosphate (G3P) serves as acceptor, four isomeric products can be generated (**Figure 2B**), namely D-lyxose 5-phosphate (L5P), D-arabinose-5P (Ara5P), D-xylose 5-phosphate (X5P), and D-ribose 5-phosphate (R5P). However, only Ara5P (ID: rat131949) and R5P (ID: rat132073) are included in the ATLAS database. In order to design as many novel methanol assimilation pathways as possible, we proposed 28 potential new aldolase reactions whose aldol products contain no more than six carbons to include all possible stereo configurations (**Supplementary Table 1**).

Prediction of FALD Assimilation Pathways

In order to ensure the lowest possible number of non-natural reactions in the predicted pathways, the comb-FBA algorithm (Yang et al., 2019b) was used as shown in **Figure 3**. The simulated metabolic network contained the known reaction set^{6578} (6,578 MetaCyc reactions) and the aldolase reaction set^{33} (five experimentally verified reactions from ATLAS and 28 artificially proposed reactions; **Supplementary Material**; **Supplementary Table A**). Then, 12 known FALD utilization reactions from set^{6578} were extracted together with the aldolase reaction set^{33} to compose the combinatorial reaction set. The remaining set^{6566} (set^{6578} minus set^{12}) was taken as the main reaction set. In view of the difficulties in establishing non-natural reactions *in vitro*, we chose no more than three reactions from set^{45}, namely 15,225 combinations ($C_{45}^{1} + C_{45}^{2} + C_{45}^{3}$), to enter the main reaction set^{6566} for subsequent pathway calculation using the pFBA algorithm (Lewis et al., 2010). FALD was set

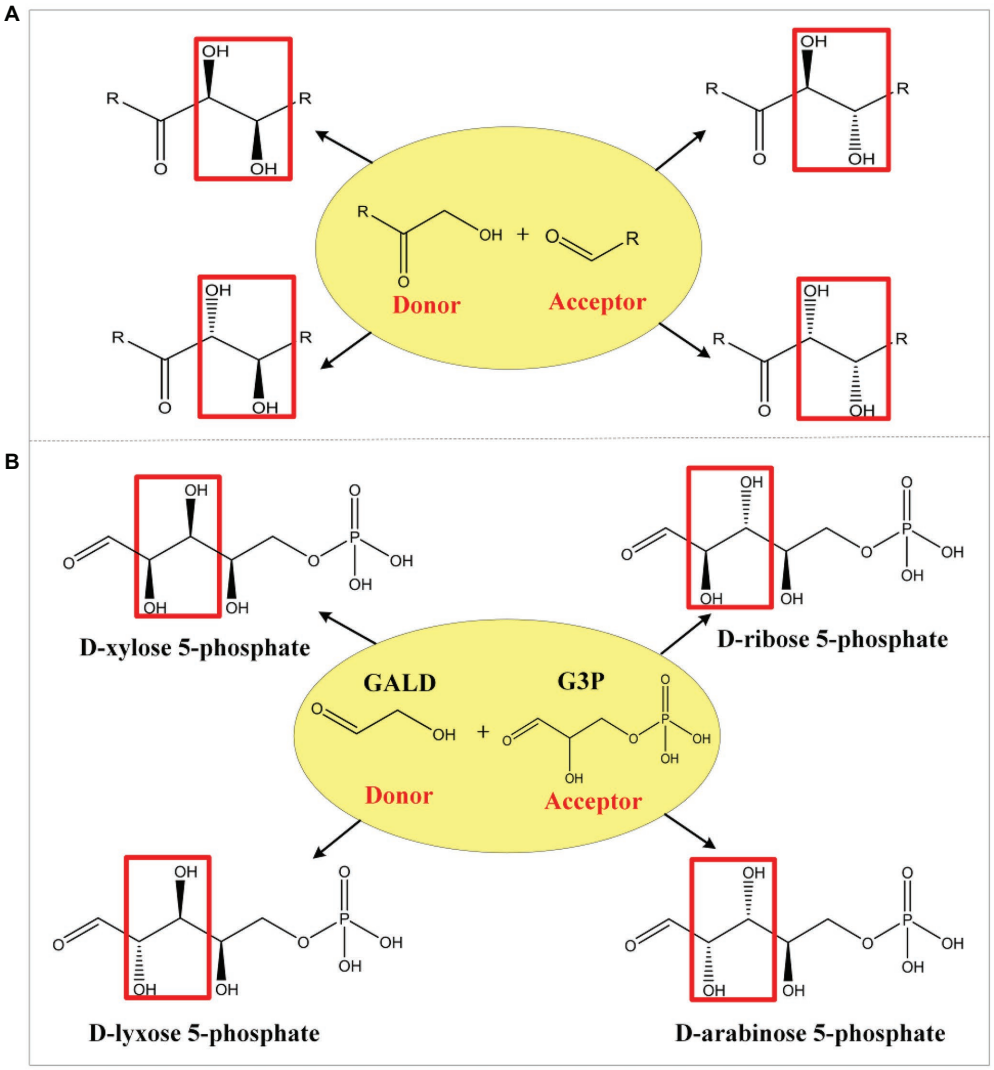

FIGURE 2 | Schematic diagram of aldol reaction mechanism. Complementary stereochemistry of aldolases **(A)** and the four stereo configurations **(B)** when GALD serves as donor and G3P serves as acceptor.

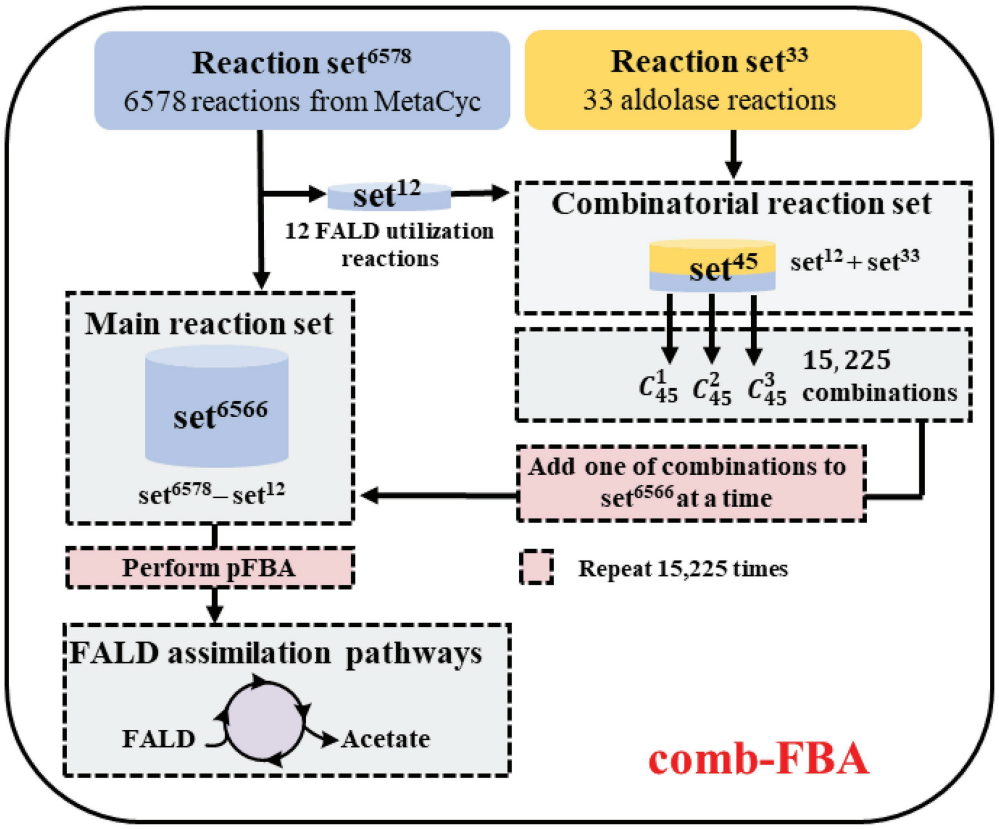

FIGURE 3 | Workflow for the calculation of formaldehyde (FALD) assimilation pathways. Comb-flux balance analysis (FBA) is performed based on two reaction sets: the main reaction set^{6566} and the combinatorial reaction set^{45}. In each iteration of comb-FBA calculation, a combination with one reaction (C_{45}^{1}), two reactions (C_{45}^{2}), or three reactions (C_{45}^{3}) from set^{45} was added to the reaction set^{6566} to predict FALD assimilation pathways.

as the substrate, and acetate, the simplest AcCoA derivative, was defined as the objective product.

Novel FALD assimilation pathways were selected based on the following criteria: (i) no more than 10 reactions from FALD to acetate; (ii) no carbon loss; and (iii) independent of ATP and reducing equivalents. Eight novel FALD assimilation pathways (P1–P8) meeting criteria (i) and (ii) were predicted (**Figure 4A**). Among them, the pathways P1, P2, and P3, meeting all these criteria, were chosen for further *in vitro* validation.

Identification of Novel Aldol Reactions for the Condensation of GALD With E4P

Formaldehyde assimilation proceeded through common/similar steps in pathways P1–P3 (**Figure 4A**). These included the conversion of FALD into GALD by Gals, the condensation of GALD with E4P by unknown ALS enzymes, the isomerization of generated aldohexose 6-phosphates (M6P, A6P, or G6P) to ketohexose 6-phosphates (Au6P and/or F6P) by isomerases and/or epimerases, and the hydrolysis of F6P into E4P and AcP by Fpk. Since the conversion of FALD into GALD has been proven in our previous work (Lu et al., 2019; Yang et al., 2019b), the first cornerstone of constructing pathways P1–P3 was realizing the artificially proposed condensation of GALD with E4P.

Previously, three aldolases with broad donor spectra (TalB^{F178Y}, Fsa, and DeoC) were tested for the similar condensation of GALD with G3P, and transaldolase TalB^{F178Y} exhibited the highest activity (Yang et al., 2019b). Therefore, TalB^{F178Y}, Fsa, and DeoC (**Supplementary Figure 1**) were firstly chosen to test if any can catalyze the proposed condensation reaction. The aldol products from the GALD and E4P catalyzed by different aldolases (TalB^{F178Y}, Fsa, or DeoC) were derivatized using methoxymation and trimethylsilylation methods (Mairinger et al., 2020), by which the ketone or aldehyde carbonyl groups were converted into methoxyamine groups and the active hydrogen atoms of the hydroxyl groups were replaced by trimethylsilyl groups (**Supplementary Figure 2**). It is worth mentioning that the methoxymation method produces two different stereoisomers, with either the *syn*- or the *anti*-form of the methoxyamine group (Gullberg et al., 2004; Engel et al., 2020). As shown in **Figure 5A**, the aldol products of aldolase-catalyzed condensation of GALD with E4P formed two main peaks at 26.307 and 26.511 min (by TalB^{F178Y} or Fsa) or 26.274 and 26.650 min (by DeoC). All the peaks showed similar fragment distributions (**Figure 5B**), which were consistent with aldohexose 6-phosphates according to the Agilent NIST2020 GC-TOFMS libraries. However, standards or

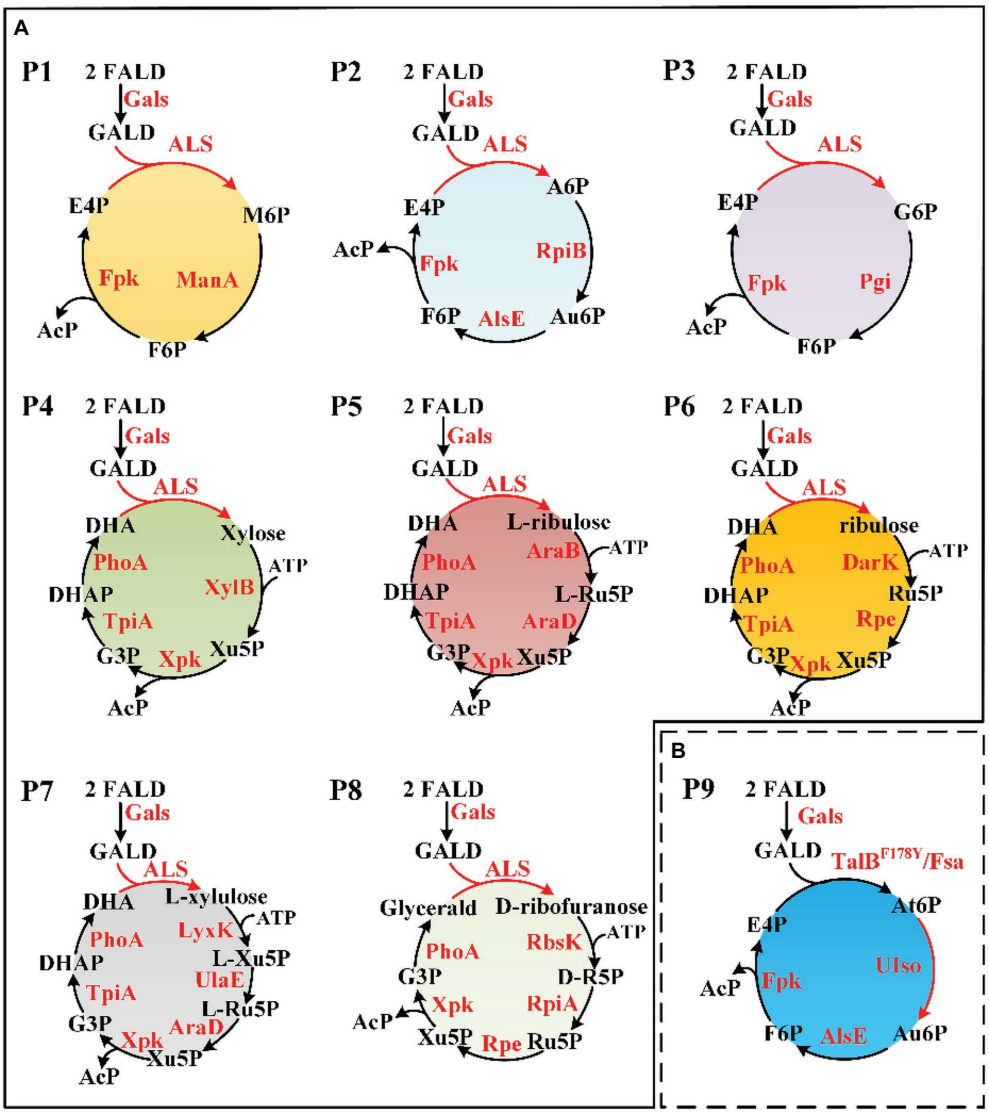

FIGURE 4 | Novel FALD assimilation pathways. **(A)** Predicted pathways (P1–P8). **(B)** Proposed novel pathway P9 based on TalB^{Y178F}/Fsa. For simplicity, AcP to Ac (AcP => Acetate) was not shown. M6P, D-mannose 6-phosphate; A6P, D-allose 6-phosphate; Au6P, D-allulose 6-phosphate; G6P, D-glucose 6-phosphate; At6P, D-altrose 6-phosphate; AcP, acetyl-phosphate. Gals, evolved glycolaldehyde synthase; Fpk, fructose 6-phosphate phosphoketolase; ManA, mannose-6-phosphate isomerase; RpiB, allose-6-phosphate isomerase/ribose-5-phosphate isomerase B; AlsE, D-allulose-6-phosphate 3-epimerase; Pgi, glucose-6-phosphate isomerase; XylB, xylulokinase; Xpk, xylulose 5-phosphate phosphoketolase; TpiA, triose phosphate isomerase; PhoA, alkaline phosphatase; AraB, ribulokinase; AraD, L-ribulose-5-phosphate 4-epimerase; DarK, D-ribulokinase; Rpe, ribulose-phosphate 3-epimerase; LyxK, L-xylulose kinase; UlaE, L-ribulose-5-phosphate 3-epimerase; RbsK, ribokinase; RpiA, ribose-5-phosphate isomerase A; TalB, transaldolase; Fsa, fructose 6-phosphate aldolase; and Uiso, unknown altrose 6-phosphate isomerase.

equivalents were required to distinguish the number and type of stereoisomers among the aldol reaction products.

As we failed to obtain an A6P standard, an alternative method, using Glk to produce aldohexose 6-phosphates from corresponding aldohexoses, was tried. The reaction products from different aldohexoses (D-glucose, D-mannose, or D-allose) catalyzed by Glk were qualitatively analyzed using the same GC-TOFMS method. As shown in **Supplementary Figure 3**, three aldohexose 6-phosphates (G6P, M6P, and A6P) were successfully produced by Glk from D-glucose, D-mannose, and D-allose, respectively. The aldolase product of DeoC was identified as A6P, since its GC-TOFMS retention time was identical with that of Glk-based A6P (**Figure 5C**). However, the aldohexose 6-phosphate generated by TalB^{F178Y}/Fsa remained unknown, as its retention time was not consistent with any of G6P, M6P, and A6P.

After checking the possible aldol reaction products (**Figure 2**; **Supplementary Table 1**), altrose 6-phosphate (At6P), which was previously omitted as it was not included in the MetaCyc database, was identified as a likely candidate for the missing stereoisomer. Indeed, the retention time of the unknown aldohexose 6-phosphate was consistent with that of Glk-based altrose 6-phosphate

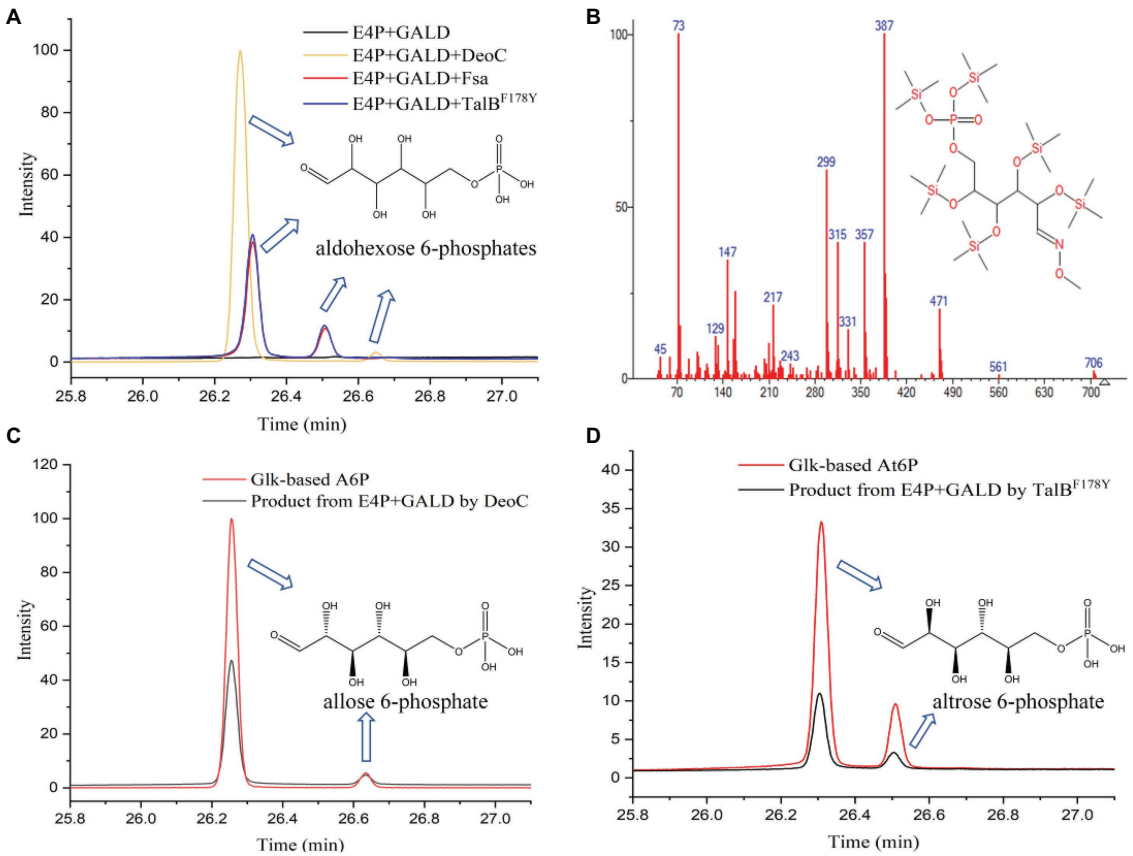

FIGURE 5 | Identification of aldol reaction products by GC-TOFMS. **(A)** The products of the condensation of GALD with E4P by TalB^{F178Y}, Fsa, and DeoC. **(B)** Fragment distributions of peaks with retention times of 26.307, 26.274, 26.511, and 26.650 min. **(C)** Glk-based A6P and the product from E4P and GALD catalyzed by DeoC. **(D)** Glk-based At6P and product from E4P and GALD catalyzed by TalB^{F178Y}.

(**Figure 5D**). Therefore, the aldol product of TalB^{F178Y}/Fsa was identified as At6P, and the pathway P9 with non-natural isomerization of At6P into Au6P was newly proposed (**Figure 4B**). Thus, we finally identified two novel aldol reactions for the condensation of GALD with E4P into 2*S*,3*R*-configurated At6P by TalB^{F178Y}/Fsa or 2*R*,3*R*-configurated A6P by DeoC.

Isomerization of A6P Into F6P by RpiB and AlsE

The next step following the condensation of GALD with E4P was predicted to be the isomerization of the obtained aldohexose 6-phosphate into F6P. The reaction products from different aldohexose 6-phosphates catalyzed by different isomerases (Pgi, ManA, RpiB, KdsD, and/or AlsE) were qualitatively analyzed using GC-TOFMS. According to the generated peaks and their retention time, Glk-based G6P and M6P were successfully isomerized into F6P by Pgi and ManA, respectively (**Figures 6A–D**). A6P was isomerized into another ketohexose 6-phosphate by RpiB, followed by epimerized to F6P by AlsE (**Figure 6E**). Although, we failed to obtain an Au6P standard or equivalent, this ketohexose 6-phosphate was probably Au6P because (1), the 3*R*-configurated A6P/At6P was supposed to be isomerized into 3*R*-configurated Au6P rather than 3*S*-configurated F6P (**Supplementary Figure 4**), and (2), RpiB was reported to be able to isomerize A6P into Au6P (Roos et al., 2008), while Au6P could be epimerized into F6P by AlsE as described by Chan et al. (2008). Thus, enzymes catalyzing all the reactions in pathway P2 were identified.

Because At6P is an unnatural metabolite and was not included in the MetaCyc database, no known isomerization reaction for At6P was available. Therefore, we examined three aldohexose 6-phosphate isomerases (RpiB, ManA, and Pgi) as well as the arabinose-5-phosphate isomerase (KdsD) to see if any could isomerize At6P into Au6P. Unfortunately, no ketohexose 6-phosphate was observed in the systems containing Glk-based At6P with all the aldose phosphate isomerases (**Figure 6F**), resulting in a temporary failure to realize pathway P9 (**Figure 4B**). Nevertheless, these isomerases did not show strict stereo selectivity for G6P, M6P, or A6P (**Supplementary Figures 3H–J**). This result suggested that 2*S*,3*R*-At6P prefers specific aldohexose 6-phosphate isomerases.

In vitro Construction of the GAPA Pathway

In order to test the feasibility of the GAPA pathway, we assembled the purified enzymes *in vitro* (DeoC, RpiB, AlsE, and/or Fpk) with GALD and E4P as reaction substrates. As shown in **Figure 7A**, when DeoC, RpiB, and AlsE were successively

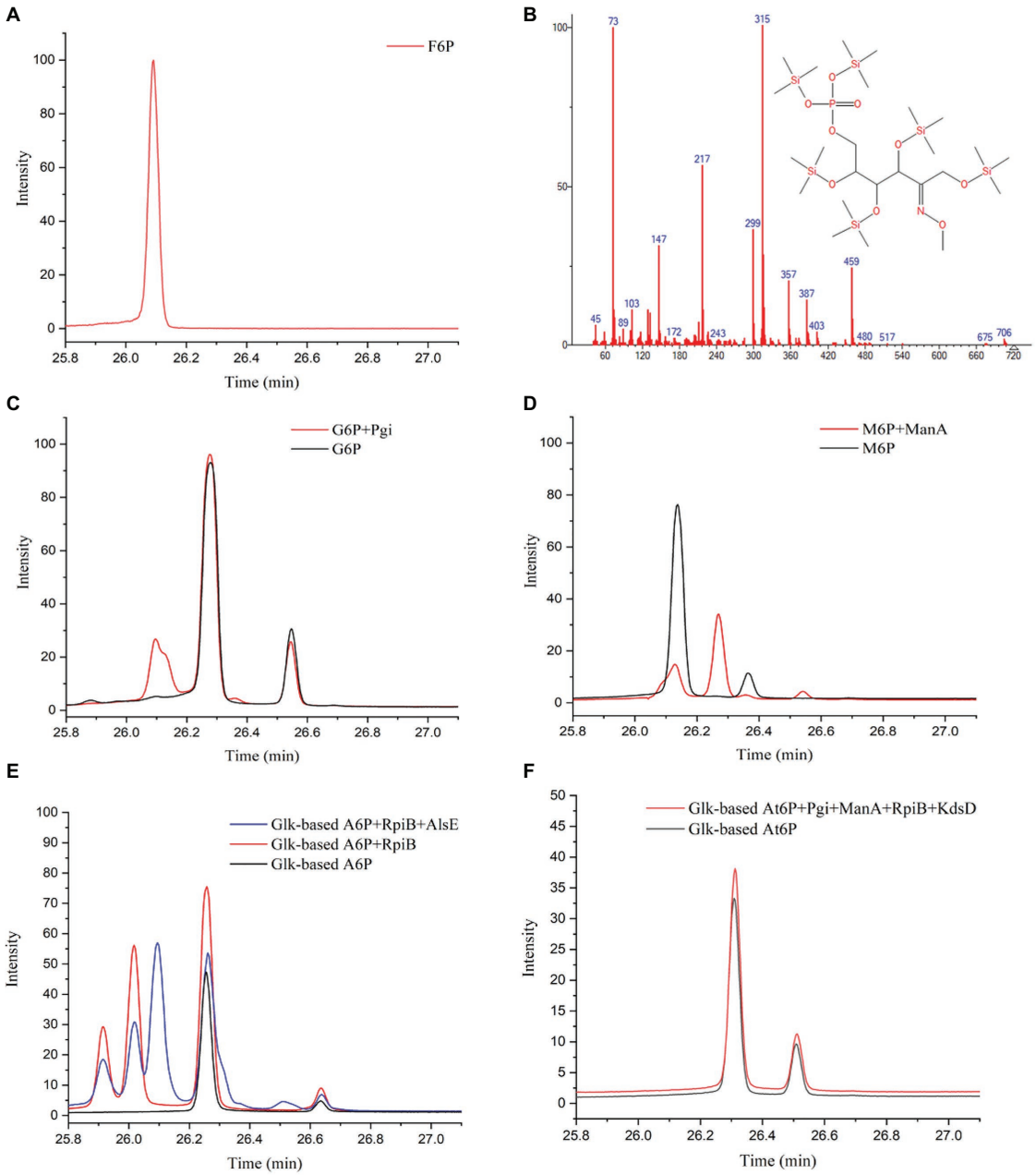

FIGURE 6 | Identification of isomerized products from aldohexose 6-phosphates by GC-TOFMS method. **(A)** F6P standard. **(B)** Fragment distributions of ketohexose 6-phosphates produced *via* the isomerization of G6P, M6P, or A6P with retention times of 25.915, 26.018, and 26.094 min. **(C)** G6P standard and product from G6P catalyzed by Pgi. **(D)** M6P standard and product from M6P catalyzed by ManA. **(E)** Glk-based A6P and product from A6P catalyzed by RpiB (and AlsE). **(F)** Glk-based At6P and product from At6P catalyzed by Pgi, ManA, RpiB, and KdsD.

added into the reaction system, GALD and E4P were condensed into A6P, then isomerized to Au6P, and finally epimerized into F6P. After further addition of Fpk, all the peaks for ketohexose 6-phosphate or aldohexose 6-phosphate significantly decreased, which indicated that the GAPA pathway (**Figure 7B**) was successfully constructed. Subsequently, the concentrations of AcP generated by the different reaction systems were determined to evaluate the efficiency of the GAPA pathway. As shown in **Figure 8A**, very little AcP could be obtained without the addition of Fpk, which might be caused by unclearly spontaneous reaction. When only Fpk was added, 2.61 mM AcP was obtained after 2 h, likely representing the reported direct conversion of GALD into AcP by phosphoketolase (Lu et al., 2019). However, when all the enzymes were added into reaction system (DeoC 2 mg/ml, RpiB 2 mg/ml, AlsE 2 mg/ml, and Fpk 1 mg/ml), the AcP concentration was significantly

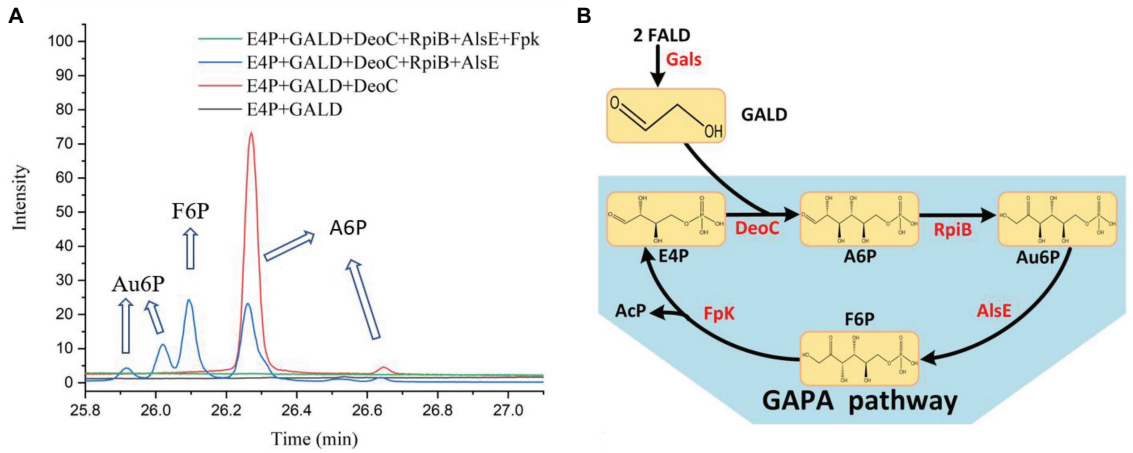

FIGURE 7 | Identification of the GAPA pathway. **(A)** The reaction products of the condensation of GALD with E4P by DeoC, RpiB, AlsE, and/or Fpk as determined by GC-TOFMS. **(B)** The proved GAPA pathway.

increased by 97% to 5.15 mM after 2 h (**Figure 8A**), indicating that the GAPA pathway did play a major role in AcP synthesis. After 3 h, the maximal AcP concentration of 5.60 mM was obtained, while 5.95 mM GALD was consumed (**Figure 8B**), corresponding to a carbon yield of 94% for GALD.

DISCUSSION

Artificial construction of non-natural reactions has facilitated the *de novo* design of metabolic pathways (Kumar et al., 2018; Saa et al., 2019; Hafner et al., 2020), among which the screening of new aldolase reactions plays an important role in mining novel one-carbon assimilation pathways (Siegel et al., 2015; Lu et al., 2019; Yang et al., 2019b; He et al., 2020). In this study, we identified 28 novel theoretically feasible, non-natural aldolase reactions, and based on these, calculated eight simple, novel, and carbon-conserving FALD assimilation pathways (P1–P8, **Figure 4A**) using the comb-FBA algorithm (**Figure 2**). Notably, three of the predicted FALD assimilation pathways (P1–P3), proceeding *via* GALD and different aldohexose 6-phosphates, were independent from energy/reducing equivalents seen from FALD to AcP, and were therefore given with priority for experimental verification. Since the feasibility for their common conversion of FALD into GALD by Gals has been proven (Lu et al., 2019; Yang et al., 2019b), this work focused on the identification of unknown aldolase reactions and the *in vitro* construction of pathways P1–P3 starting from GALD.

During the condensation of GALD with E4P, two new asymmetric centers are formed, resulting in four theoretical stereo configurations (2*R*,3*S*-G6P, 2*S*,3*S*-M6P, 2*R*,3*R*-A6P, and 2*S*,3*R*-At6P). Although specific dihydroxyacetone phosphate (DHAP) aldolases are able to generate corresponding stereo configurations (Samland and Sprenger, 2006; Clapés et al., 2010), DHAP aldolases are usually strictly specific for DHAP as the donor (Gefflaut et al., 1995). Therefore, two well-known DHA aldolases with tolerances for different aldol donors, TalB^{F178Y} and Fsa (Garrabou et al., 2009; Rale et al., 2011; Lachaux et al., 2019), were tried and successfully condensed GALD with E4P into the 2*S*,3*R*-stereo configuration At6P (**Figure 5D**). This 2*S*,3*R*-configuration was consistent with the strict stereoselectivity of DHA aldolases for the *S*,*R*-stereo configuration during aldol reactions (Clapés et al., 2010). However, aldolase candidates for the other three configurations were rarely reported.

Interestingly, the 2-deoxy-D-ribose-5-phosphate aldolase (DERA, encoded by *deoC* in *E. coli*) exhibited a different stereoselectivity for the 2*R*,3*R*-stereo configuration (**Figure 5C**). In our previous work, the product of GALD and G3P catalyzed by DeoC exhibited similar retention times with those by TalB^{F178Y}/Fsa during GC-TOFMS analysis (Yang et al., 2019b). These were supposed to be the 2*S*,3*R*-stereo arabinose 5-phosphate (Ara5P) according to their acceptance as substrates by known isomerases. In this study, a simple but more rigorous method was adopted to qualitatively analyze the aldol products. The equivalents of G6P, M6P, A6P, and At6P were produced by Glk from corresponding aldohexoses (**Supplementary Figure 3**). Subsequently, GC-TOFMS analysis coupled with isomerization by known aldose phosphate isomerases was used to judge the stereo configuration of the aldol products. Thus, the aldol product of GALD and E4P by DeoC was determined as the 2*R*,3*R*-form A6P. Chambre et al. (2019) recently discovered that the DERA from *Arthrobacter chlorophenolicus*, sharing a 34% amino acid sequence identity with DeoC from *E. coli*, also exhibited selectivity for the *R*,*R*-stereo configuration when using GALD or DHA as donors and L-glyceraldehyde 3-phosphate as acceptor. It is worth mentioning that the identification of both the non-natural production of At6P production from GALD and E4P by TalB^{F178Y}/Fsa and the rare *R*,*R*-stereo configuration aldolase reaction catalyzed by DeoC may facilitate future biosynthesis of high-valued rare saccharides in various stereoisomers (Roca et al., 2015; Yang et al., 2019a; Li et al., 2021).

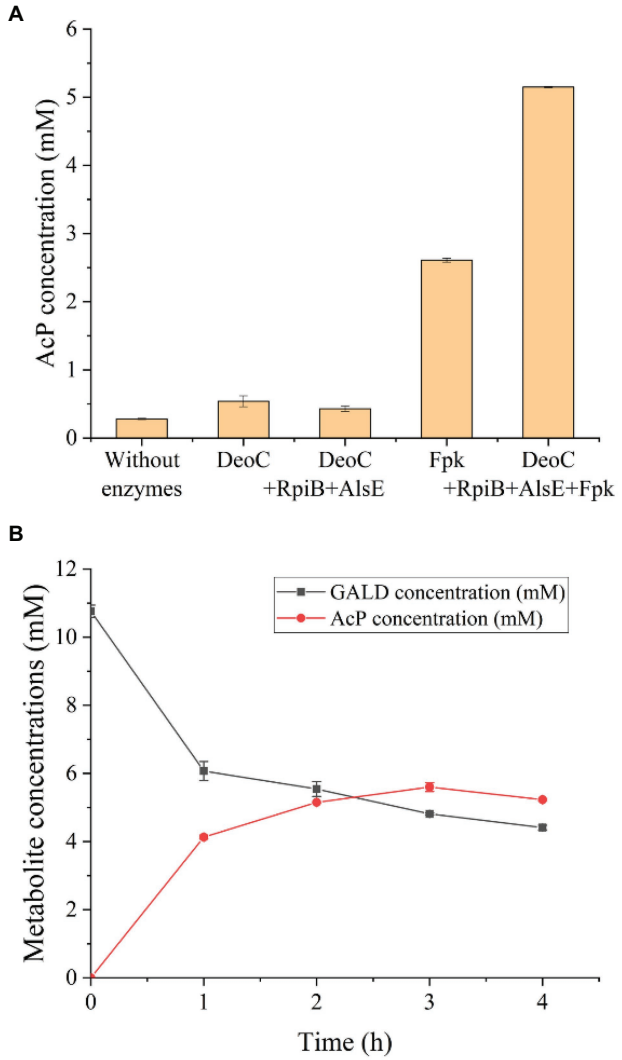

FIGURE 8 | Efficiency evaluation of the GAPA pathway. **(A)** AcP concentrations produced from 2.5 mM E4P and 10 mM GALD after 2 h using different enzymes (DeoC 2 mg/ml, RpiB 2 mg/ml, AlsE 2 mg/ml, and/or Fpk 1 mg/ml). **(B)** Time profile of GALD and AcP concentration in reaction system containing 10 mM GALD, 2.5 mM E4P, 2 mg/ml DeoC, 2 mg/ml RpiB, 2 mg/ml AlsE, and 1 mg/ml Fpk.

However, the underlying mechanism of the different stereoselectivity between DHA aldolase and DERA need further investigation.

After the aldol products were clearly distinguished as 2*S*,3*R*-form At6P or 2*R*,3*R*-form A6P, efforts were paid to isomerize them into F6P. After A6P was successfully converted into F6P by RpiB and AlsE, the DeoC-based GAPA pathway was finally constructed *in vitro*, exhibiting a high carbon yield of 94% from GALD (**Figure 8B**), which confirmed the feasibility of mining novel pathways using model-based pathway design combined with artificially proposed reactions. Moreover, it is worth noting that more novel one-carbon assimilation pathways could be identified with future efforts to realize aldol condensation for 2*S*,3*S*-stereo M6P or 2*R*,3*S*-stereo G6P (pathways P1 and P3, **Figure 4A**), as well as the isomerization of At6P into Au6P (pathway P9, **Figure 4B**). We believe that the GAPA pathway is a promising candidate for a GALD-based one-carbon assimilation pathway if it is coupled with a kinetically favorable bioconversion of FALD into GALD using either HacI and Acr (Chou et al., 2019) or an improved variant of Gals (Lu et al., 2019). The GAPA pathway still faced many other problems such as kinetic trap caused by broad substrate activities of Fpk (Yang et al., 2019b). However, promiscuous enzymes with side reactions in addition to the main reactions are universal *in vivo* and there are many metabolic engineering studies using promiscuous enzymes such as aldolases and PKTs without any problem (Yang et al., 2019a; Hellgren et al., 2020). Moreover, since the pathway discovery and enzyme engineering are mutually reinforcing each other, we believe that the promiscuities and kinetics problems of used enzymes can be eventually overcame by further development of enzyme engineering. Therefore, the GAPA will be feasible *in vivo* with future efforts. Besides one-carbon compound assimilation, these GALD-based pathways also provide promising alternative routes for assimilation of GALD generated from the poly(ethylene glycol) plastics, which is one of the most widely used biopolymers in the pharmaceutical industry (Knop et al., 2010). Taken together, this work not only provides an elegant paradigm for systematic pathway mining, but also uncovers non-natural aldolase reactions with rarely reported product stereoselectivity, which offers novel elements for valuable biosynthesis/biodegradation processes more than one-carbon assimilation.

DATA AVAILABILITY STATEMENT

The original contributions presented in the study are included in the article/**Supplementary Material**, further inquiries can be directed to the corresponding author.

AUTHOR CONTRIBUTIONS

QY and YM designed pathway. YM, XY, YC, and JL performed the experiments. YY and HS prepared the samples. YM, XY, JL, HL, TC, PL, and HM performed the data analysis. YM, QY, XY, and HM wrote and revised the manuscript. HM, YM, and QY conceived the concept. HM supervised the work. All authors contributed to the article and approved the submitted version.

FUNDING

This work was funded by the National Key Research and Development Program of China (2018YFA0901400 and 2018YFA0900300), the International Partnership Program of Chinese Academy of Sciences (153D31KYSB20170121), the National Natural Science Foundation of China (21908239), the Tianjin Synthetic Biotechnology Innovation Capacity

Improvement Project (TSBICIP-PTJS-001 and TSBICIP-KJGG-005), and the China Postdoctoral Science Foundation (2018M641658).

ACKNOWLEDGMENTS

We thank Jiangang Yang and Ting Shi (Tianjin Institute of Industrial Biotechnology, Chinese Academy of Sciences) for discussion on aldolase product stereoselectivity and assistance in protein purification.

SUPPLEMENTARY MATERIAL

The Supplementary Material for this article can be found online at: https://www.frontiersin.org/articles/10.3389/fmicb.2021.677596/full#supplementary-material

REFERENCES

Bogorad, I. W., Chen, C.-T., Theisen, M. K., Wu, T.-Y., Schlenz, A. R., Lam, A. T., et al. (2014). Building carbon–carbon bonds using a biocatalytic methanol condensation cycle. *Proc. Natl. Acad. Sci.* 111:15928. doi: 10.1073/pnas.1413470111

Bogorad, I. W., Lin, T. S., and Liao, J. C. (2013). Synthetic non-oxidative glycolysis enables complete carbon conservation. *Nature* 502, 693–697. doi: 10.1038/nature12575

Caspi, R., Billington, R., Fulcher, C. A., Keseler, I. M., Kothari, A., Krummenacker, M., et al. (2018). The MetaCyc database of metabolic pathways and enzymes. *Nucleic Acids Res.* 46, D633–D639. doi: 10.1093/nar/gkx935

Castillo, J. A., Calveras, J., Casas, J., Mitjans, M., Vinardell, M. P., Parella, T., et al. (2006). Fructose-6-phosphate aldolase in organic synthesis: preparation of D-fagomine, N-alkylated derivatives, and preliminary biological assays. *Org. Lett.* 8, 6067–6070. doi: 10.1021/ol0625482

Chambre, D., Guérard-Hélaine, C., Darii, E., Mariage, A., Petit, J.-L., Salanoubat, M., et al. (2019). 2-Deoxyribose-5-phosphate aldolase, a remarkably tolerant aldolase towards nucleophile substrates. *Chem. Commun.* 55, 7498–7501. doi: 10.1039/C9CC03361K

Chan, K. K., Fedorov, A. A., Fedorov, E. V., Almo, S. C., and Gerlt, J. A. (2008). Structural basis for substrate specificity in phosphate binding $(\beta/\alpha)_8$-barrels: D-allulose 6-phosphate 3-epimerase from *Escherichia coli* K-12. *Biochemistry* 47, 9608–9617. doi: 10.1021/bi800821v

Chou, A., Clomburg, J. M., Qian, S., and Gonzalez, R. (2019). 2-Hydroxyacyl-CoA lyase catalyzes acyloin condensation for one-carbon bioconversion. *Nat. Chem. Biol.* 15, 900–906. doi: 10.1038/s41589-019-0328-0

Chunling, M., Yanfei, Z., Xue, Y., Xiaozhi, J., Aipo, D., and Hongwu, M. (2017). Determination of key enzymes for lactate synthesis through *in vitro* metabolic pathway construction. *China Brewing* 35, 144–148.

Clapés, P., Fessner, W. D., Sprenger, G. A., and Samland, A. K. (2010). Recent progress in stereoselective synthesis with aldolases. *Curr. Opin. Chem. Biol.* 14, 154–167. doi: 10.1016/j.cbpa.2009.11.029

Clomburg, J. M., Crumbley, A. M., and Gonzalez, R. (2017). Industrial biomanufacturing: The future of chemical production. *Science* 355:aag0804. doi: 10.1126/science.aag0804

Cui, Z., Mao, Y., Zhao, Y., Chen, C., Tang, Y.-J., Chen, T., et al. (2018). Concomitant cell-free biosynthesis of optically pure D-(−)-acetoin and xylitol via a novel NAD^+ regeneration in two-enzyme cascade. *J. Chem. Technol. Biotechnol.* 93, 3444–3451. doi: 10.1002/jctb.5702

Cui, Z., Zhao, Y., Mao, Y., Shi, T., Lu, L., Ma, H., et al. (2019). *In vitro* biosynthesis of optically pure D-(−)-acetoin from *meso*-2,3-butanediol using 2,3-butanediol dehydrogenase and NADH oxidase. *J. Chem. Technol. Biotechnol.* 94, 2547–2554. doi: 10.1002/jctb.6050

Ebrahim, A., Lerman, J. A., Palsson, B. O., and Hyduke, D. R. (2013). COBRApy: COnstraints-based reconstruction and analysis for Python. *BMC Syst. Biol.* 7:74. doi: 10.1186/1752-0509-7-74

Engel, B., Suralik, P., and Marchetti-Deschmann, M. (2020). Critical considerations for trimethylsilyl derivatives of 24 primary metabolites measured by gas chromatography–tandem mass spectrometry. *Sep. Sci. Plus* 3, 407–418. doi: 10.1002/sscp.202000025

Garrabou, X., Castillo, J. A., Guérard-Hélaine, C., Parella, T., Joglar, J., Lemaire, M., et al. (2009). Asymmetric self- and cross-aldol reactions of glycolaldehyde catalyzed by d-fructose-6-phosphate aldolase. *Angew. Chem. Int. Ed.* 48, 5521–5525. doi: 10.1002/anie.200902065

Gefflaut, T., Blonski, C., Perie, J., and Willson, M. (1995). Class I aldolases: substrate specificity, mechanism, inhibitors and structural aspects. *Prog. Biophys. Mol. Biol.* 63, 301–340. doi: 10.1016/0079-6107(95)00008-9

Gullberg, J., Jonsson, P., Nordström, A., Sjöström, M., and Moritz, T. (2004). Design of experiments: an efficient strategy to identify factors influencing extraction and derivatization of *Arabidopsis thaliana* samples in metabolomic studies with gas chromatography/mass spectrometry. *Anal. Biochem.* 331, 283–295. doi: 10.1016/j.ab.2004.04.037

Hadadi, N., Hafner, J., Shajkofci, A., Zisaki, A., and Hatzimanikatis, V. (2016). ATLAS of biochemistry: A repository of all possible biochemical reactions for synthetic biology and metabolic engineering studies. *ACS Synth. Biol.* 5, 1155–1166. doi: 10.1021/acssynbio.6b00054

Hafner, J., Mohammadipeyhani, H., Sveshnikova, A., Scheidegger, A., and Hatzimanikatis, V. (2020). Updated ATLAS of biochemistry with new metabolites and improved enzyme prediction power. *ACS Synth. Biol.* 9, 1479–1482. doi: 10.1021/acssynbio.0c00052

He, H., Höper, R., Dodenhöft, M., Marlière, P., and Bar-Even, A. (2020). An optimized methanol assimilation pathway relying on promiscuous formaldehyde-condensing aldolases in *E. coli*. *Metab. Eng.* 60, 1–13. doi: 10.1016/j.ymben.2020.03.002

Hellgren, J., Godina, A., Nielsen, J., and Siewers, V. (2020). Promiscuous phosphoketolase and metabolic rewiring enables novel non-oxidative glycolysis in yeast for high-yield production of acetyl-CoA derived products. *Metab. Eng.* 62, 150–160. doi: 10.1016/j.ymben.2020.09.003

Knop, K., Hoogenboom, R., Fischer, D., and Schubert, U. S. (2010). Poly(ethylene glycol) in drug delivery: pros and cons as well as potential alternatives. *Angew. Chem. Int. Ed.* 49, 6288–6308. doi: 10.1002/anie.200902672

Kumar, A., Wang, L., Ng, C. Y., and Maranas, C. D. (2018). Pathway design using de novo steps through uncharted biochemical spaces. *Nat. Commun.* 9:184. doi: 10.1038/s41467-017-02362-x

Lachaux, C., Frazao, C. J. R., Krauβer, F., Morin, N., Walther, T., and François, J. M. (2019). A new synthetic pathway for the bioproduction of glycolic acid from lignocellulosic sugars aimed at maximal carbon conservation. *Front. Bioeng. Biotechnol.* 7:359. doi: 10.3389/fbioe.2019.00359

Lewis, N. E., Hixson, K. K., Conrad, T. M., Lerman, J. A., Charusanti, P., Polpitiya, A. D., et al. (2010). Omic data from evolved *E. coli* are consistent with computed optimal growth from genome-scale models. *Mol. Syst. Biol.* 6:390. doi: 10.1038/msb.2010.47

Li, Y., Shi, T., Han, P., and You, C. (2021). Thermodynamics-driven production of value-added D-allulose from inexpensive starch by an *in vitro* enzymatic synthetic biosystem. *ACS Catal.* 11, 5088–5099. doi: 10.1021/acscatal.0c05718

Liang, B., Zhao, Y., and Yang, J. (2020). Recent advances in developing artificial autotrophic microorganism for reinforcing CO_2 fixation. *Front. Microbiol.* 11:592631. doi: 10.3389/fmicb.2020.632455

Lu, X., Liu, Y., Yang, Y., Wang, S., Wang, Q., Wang, X., et al. (2019). Constructing a synthetic pathway for acetyl-coenzyme A from one-carbon through enzyme design. *Nat. Commun.* 10:1378. doi: 10.1038/s41467-019-09095-z

Mairinger, T., Weiner, M., Hann, S., and Troyer, C. (2020). Selective and accurate quantification of N-acetylglucosamine in biotechnological cell samples via GC-MS/MS and GC-TOFMS. *Anal. Chem.* 92, 4875–4883. doi: 10.1021/acs.analchem.9b04582

Mao, W., Yuan, Q., Qi, H., Wang, Z., Ma, H., and Chen, T. (2020). Recent progress in metabolic engineering of microbial formate assimilation. *Appl. Microbiol. Biotechnol.* 104, 6905–6917. doi: 10.1007/s00253-020-10725-6

Meyer, F., Keller, P., Hartl, J., Gröninger, O. G., Kiefer, P., and Vorholt, J. A. (2018). Methanol-essential growth of *Escherichia coli*. *Nat. Commun.* 9:1508. doi: 10.1038/s41467-018-03937-y

Müller, J. E. N., Meyer, F., Litsanov, B., Kiefer, P., Potthoff, E., Heux, S., et al. (2015). Engineering *Escherichia coli* for methanol conversion. *Metab. Eng.* 28, 190–201. doi: 10.1016/j.ymben.2014.12.008

Nguyen, A. D., and Lee, E. Y. (2020). Engineered methanotrophy: a sustainable solution for methane-based industrial biomanufacturing. *Trends Biotechnol.* 39, 381–396. doi: 10.1016/j.tibtech.2020.07.007

Rale, M., Schneider, S., Sprenger, G. A., Samland, A. K., and Fessner, W. D. (2011). Broadening deoxysugar glycodiversity: natural and engineered transaldolases unlock a complementary substrate space. *Chem. Eur. J.* 17, 2623–2632. doi: 10.1002/chem.201002942

Roca, C., Alves, V. D., Freitas, F., and Reis, M. A. M. (2015). Exopolysaccharides enriched in rare sugars: bacterial sources, production, and applications. *Front. Microbiol.* 6:288. doi: 10.3389/fmicb.2015.00288

Roldán, R., Sanchez-Moreno, I., Scheidt, T., Hélaine, V., Lemaire, M., Parella, T., et al. (2017). Breaking the dogma of aldolase specificity: simple aliphatic ketones and aldehydes are nucleophiles for fructose-6-phosphate aldolase. *Chem. Eur. J.* 23, 5005–5009. doi: 10.1002/chem.201701020

Roos, A. K., Mariano, S., Kowalinski, E., Salmon, L., and Mowbray, S. L. (2008). D-Ribose-5-phosphate isomerase B from *Escherichia coli* is also a functional D-allose-6-phosphate isomerase, while the *Mycobacterium tuberculosis* enzyme is not. *J. Mol. Biol.* 382, 667–679. doi: 10.1016/j.jmb.2008.06.090

Saa, P. A., Cortés, M. P., López, J., Bustos, D., Maass, A., and Agosin, E. (2019). Expanding metabolic capabilities using novel pathway designs: computational tools and case studies. *Biotechnol. J.* 14:e1800734. doi: 10.1002/biot.201800734

Samland, A. K., and Sprenger, G. A. (2006). Microbial aldolases as C-C bonding enzymes - unknown treasures and new developments. *Appl. Microbiol. Biotechnol.* 71, 253–264. doi: 10.1007/s00253-006-0422-6

Siegel, J. B., Smith, A. L., Poust, S., Wargacki, A. J., Bar-Even, A., Louw, C., et al. (2015). Computational protein design enables a novel one-carbon assimilation pathway. *Proc. Natl. Acad. Sci. U. S. A.* 112, 3704–3709. doi: 10.1073/pnas.1500545112

Trudeau, D. L., Edlich-Muth, C., Zarzycki, J., Scheffen, M., Goldsmith, M., Khersonsky, O., et al. (2018). Design and *in vitro* realization of carbon-conserving photorespiration. *Proc. Natl. Acad. Sci.* 115, E11455–E11464. doi: 10.1073/pnas.1812605115

Whitaker, W. B., Jones, J. A., Bennett, R. K., Gonzalez, J. E., Vernacchio, V. R., Collins, S. M., et al. (2017). Engineering the biological conversion of methanol to specialty chemicals in *Escherichia coli*. *Metab. Eng.* 39, 49–59. doi: 10.1016/j.ymben.2016.10.015

Windle, C. L., Müller, M., Nelson, A., and Berry, A. (2014). Engineering aldolases as biocatalysts. *Curr. Opin. Chem. Biol.* 19, 25–33. doi: 10.1016/j.cbpa.2013.12.010

Yang, X., Yuan, Q., Luo, H., Li, F., Mao, Y., Zhao, X., et al. (2019b). Systematic design and *in vitro* validation of novel one-carbon assimilation pathways. *Metab. Eng.* 56, 142–153. doi: 10.1016/j.ymben.2019.09.001

Yang, J., Zhang, T., Tian, C., Zhu, Y., Zeng, Y., Men, Y., et al. (2019a). Multi-enzyme systems and recombinant cells for synthesis of valuable saccharides: advances and perspectives. *Biotechnol. Adv.* 37:107406. doi: 10.1016/j.biotechadv.2019.06.005

Yu, H., and Liao, J. C. (2018). A modified serine cycle in *Escherichia coli* coverts methanol and CO_2 to two-carbon compounds. *Nat. Commun.* 9:3992. doi: 10.1038/s41467-018-06496-4

Conflict of Interest: The authors declare that the research was conducted in the absence of any commercial or financial relationships that could be construed as a potential conflict of interest.

frontiers in Microbiology

ORIGINAL RESEARCH
published: 29 July 2021
doi: 10.3389/fmicb.2021.693106

Channeling of Carbon Flux Towards Carotenogenesis in *Botryococcus braunii*: A Media Engineering Perspective

*Iqra Mariam, Mukul Suresh Kareya, Mohammed Rehmanji, Asha Arumugam Nesamma and Pannaga Pavan Jutur**

Omics of Algae Group and DBT-ICGEB Centre for Advanced Bioenergy Research, Industrial Biotechnology, International Centre for Genetic Engineering and Biotechnology, New Delhi, India

OPEN ACCESS

Edited by:
Pramod P. Wangikar, Indian Institute of Technology Bombay, India

Reviewed by:
Zhenlin Han, University of Hawaii at Manoa, United States
Vijai Singh, Indrashil University, India
John Beardall, Monash University, Australia
Rajib Saha, University of Nebraska-Lincoln, United States

***Correspondence:**
Pannaga Pavan Jutur
jppavan@icgeb.res.in

Specialty section:
This article was submitted to Microbiotechnology, a section of the journal Frontiers in Microbiology

Received: *09 April 2021*
Accepted: *30 June 2021*
Published: *29 July 2021*

Citation:
Mariam I, Kareya MS, Rehmanji M, Nesamma AA and Jutur PP (2021) Channeling of Carbon Flux Towards Carotenogenesis in Botryococcus braunii: A Media Engineering Perspective. Front. Microbiol. 12:693106. doi: 10.3389/fmicb.2021.693106

Microalgae, due to their unique properties, gained attention for producing promising feedstocks having high contents of proteins, antioxidants, carotenoids, and terpenoids for applications in nutraceutical and pharmaceutical industries. Optimizing production of the high-value renewables (HVRs) in microalgae requires an in-depth understanding of their functional relationship of the genes involved in these metabolic pathways. In the present study, bioinformatic tools were employed for characterization of the protein-encoding genes of methyl erythritol phosphate (MEP) pathway involved in carotenoid and squalene biosynthesis based upon their conserved motif/domain organization. Our analysis demonstrates nearly 200 putative genes showing a conservation pattern within divergent microalgal lineages. Furthermore, phylogenomic studies confirm the close evolutionary proximity among these microalgal strains in the carotenoid and squalene biosynthetic pathways. Further analysis employing STRING predicts interactions among two rate-limiting genes, i.e., phytoene synthase (PSY) and farnesyl diphosphate farnesyl synthase (FPPS), which are specifically involved in the synthesis of carotenoids and squalene. Experimentally, to understand the carbon flux of these rate-limiting genes involved in carotenogenesis, an industrial potential strain, namely, *Botryococcus braunii*, was selected in this study for improved biomass productivity (i.e., 100 mg L^{-1} D^{-1}) along with enhanced carotenoid content [0.18% dry cell weight (DCW)] when subjected to carbon supplementation. In conclusion, our approach of media engineering demonstrates that the channeling of carbon flux favors carotenogenesis rather than squalene synthesis. Henceforth, employing omics perspectives will further provide us with new insights for engineering regulatory networks for enhanced production of high-value carbon biorenewables without compromising growth.

Keywords: *Botryococcus braunii*, carotenoids, isoprenoids, methyl erythritol phosphate, phylogenomics, squalene

INTRODUCTION

The rapid increase in energy consumption globally along with greenhouse gas emissions and depletion of fossil fuels has raised the requirement for the development of sustainable renewable energy sources (Davis et al., 2011; Lim et al., 2015). This leads to the increased production of biodiesel in recent times with annual production reaching over billions of liters (Ogunkunle and Ahmed, 2019). The conventional source of biodiesel production from *Pongamia pinnata*, *Jatropha curcas*, etc., may not be sustainable due to competition of land in terms of fuel vs. food (Chisti, 2007; Ogunkunle and Ahmed, 2019). Nonetheless, microalgae in due course of time emerged as a feasible alternative for biodiesel production because of their higher yields, their efficient light channeling leading to better photosynthetic efficiencies, their rapid reproduction cycles, and their ability to grow in variety of water resources (brackish, saline, and even wastewaters) (Guedes et al., 2011; Ratha and Prasanna, 2012; Abdelaziz et al., 2013; Leite et al., 2015). Other advantages include their ability to synthesize certain high-value renewables (HVRs) such as long-chain polyunsaturated fatty acids (LC-PUFAs), carotenoids such as β-carotene, astaxanthin, lutein, and isoprenoids like squalene, which are compounds of nutraceutical and pharmaceutical relevance (Spolaore et al., 2006; Raja et al., 2008).

Microalgae tend to accumulate lipids in the form of triacylglycerols (TAGs) and starch as carbon storage compounds in nutrient deprivation and other abiotic factors such as light, temperature, and carbon supplementation in the form of CO_2 and bicarbonate (Gardner et al., 2012; Menon et al., 2013; Abdelaziz et al., 2014; Tsai et al., 2014; Srinivasan et al., 2018). However, enhanced lipid accumulation in nutrient-deprived condition is concomitant with retarded growth leading to lower biodiesel productivity, which is a major bottleneck (Tsai et al., 2014; Srinivasan et al., 2018). Microalgae are also known for the production of various other HVRs such as eicosapentaenoic acid (Szklarczyk et al., 2019), docosahexaenoic acid (DHA), vitamin E (α-tocopherol), carotenoids, and squalene (Singh et al., 2020; Mariam et al., 2021; Paliwal and Jutur, 2021). The co-production of such HVRs will further be a cost-effective addition in terms of commercial value of biodiesel production from microalgae (Dewapriya and Kim, 2014; Jutur et al., 2015).

Despite the structural difference existing between carotenoids and squalene, both compounds share a common intermediate, i.e., geranyl geranyl diphosphate (GGPP), formed by condensation of two isoprene units: isopentenyl diphosphate (IPP) and dimethylallyl phosphate (DMAPP) (Matsushima et al., 2012; Zeng and Dehesh, 2021). This condensation reaction of IPP and DMAPP occurs within the chloroplast through the methyl erythritol phosphate (MEP) pathway (Scodelaro Bilbao et al., 2020). Moreover, the MEP pathway and lipid biosynthesis participate in a complex crosstalk between each other and appear to be upregulated upon carbon supplementation (Kareya et al., 2020; Scodelaro Bilbao et al., 2020). Overall, the MEP pathway encompasses an extensive list of compounds, owing to its comprehensiveness and because its regulatory hubs in microalgae have largely remained elusive. Henceforth, it is important to understand the mechanisms in microalgae that alter the regulation of the specific pathways upon carbon supplementation.

In this context, in the present study, we have selected an industrial potential strain, i.e., *Botryococcus braunii*, a colonial microalga belonging to the Trebouxiophyceae family, known for production of squalene and carotenoids (Uchida et al., 2018). As a result, this microalga has gained tremendous commercialization due to its high isoprenoid and lipid contents. However, its high doubling time and difficult handling present a major bottleneck for mass cultivation in open ponds (Hirano et al., 2019). Moreover, the cellular machineries are inadequately understood in this microalga, and there is a need to reveal the regulation of MEP pathway. In the present work, our aim was to predict the changes within the molecular profiles occurring when supplemented with carbon, thus filling the gaps and providing insights in understanding the intricate networks of the MEP pathway for the production of squalene and carotenoids. Carbon supplementation enhances the photosynthetic carbon fixation in microalgae generating glyceraldehyde 3-phosphate (G3P) pool through the Calvin–Benson cycle. This G3P pool along with pyruvate is the precursor molecule for MEP pathway. Furthermore, in several microalgal species such as *Microchloropsis gaditana*, *Chlorella pyrenoidosa*, and *Dunaliella salina*, carbon supplementation in the form of CO_2 or sodium bicarbonate has been reported to enhance carotenoid production (Sampathkumar and Gothandam, 2019; Kareya et al., 2020; Xi et al., 2020). Studies on phylogenomics demonstrate the evolutionary relationship at the genetic level of these protein-encoding genes involved in carotenogenesis among divergent microalgal lineage. Additionally, quantification of the HVRs in *B. braunii* reveals the channeling of carbon flux toward squalene and carotenoid biosynthesis when supplemented with additional carbon without compromising growth. Overall, this study reveals that a new approach of media engineering; i.e., carbon supplementation enhances the photosynthetic performance in microalga *B. braunii*, which further helps us to understand the crosstalk between different metabolic pathways involved in enhanced production of biomass, biofuels, and biorenewables (B^3).

MATERIALS AND METHODS

In silico Analysis

Identification of Putative Genes Involved in Methyl Erythritol Phosphate Biosynthetic Pathway

The protein-encoding genes involved in carotenoid biosynthesis was retrieved from the Kyoto Encyclopedia of Genes and Genomes[1] (Kanehisa et al., 2010). The reference dataset for the above-mentioned genes was obtained from *Chlamydomonas reinhardtii*, which was subjected to BLASTp[2] (Altschul et al., 1990) with a set threshold

[1]https://www.genome.jp/kegg/KEGG

[2]https://blast.ncbi.nlm.nih.gov/Blast.cgi

e-value of $1e^{-10}$. Homologs were identified in different microalgal species, as these species have well-annotated genomes available, which include *Volvox carteri*, *Coccomyxa subellipsoidea*, *Micromonas pusilla*, *Micromonas commoda*, *Ostreococcus tauri*, *Ostreococcus lucimarinus*, *Aurantiochytrium limacinum*, *B. braunii*, *D. salina*, *Nannochloropsis gaditana*, *Phaeodactylum tricornutum*, and *Chlorella variabilis*. The gene set was chosen based on query coverage (>60%), percentage identity (>30–40%), and *e*-value scores (**Supplementary Table 1**). A schematic representation of MEP biosynthetic pathway existing among microalgal lineages was illustrated (**Figure 1**; Kanehisa et al., 2010), depicting the presence of various functional genes involved in the carotenogenesis, facilitating better understanding of the individual components involved in the production of these high-value carbon molecules.

Prediction of Subcellular Localization/Motif and Domain Organization

In silico predictions for protein localization was performed using four online prediction software, namely, TargetP (Emanuelsson et al., 2000), Cello (Yu et al., 2004), ngLOC (King and Guda, 2007), and WoLF PSORT (Horton et al., 2007). Each protein sequence was examined using all four prediction algorithms, and the protein with the highest consensus predicted location was assigned to it. Motif prediction for the protein sequences was performed using the MEME suite[3] (Bailey et al., 2015). Parameters used for the motif prediction consisted of number of sites, 2–600; number of repetitions, 0–1 per sequence; width limit, 6–50; and maximum number of motifs, up to 3. The domain was predicted using HMMER v3.3.2 (Potter et al., 2018)[4] web server and constructed using an online ExPASy tool MyDomains-Image Creator.

[3]https://meme-suite.org/meme/tools/meme

[4]http://hmmer.org

Physico-Chemical Properties/Guanine–Cytosine Content Characterization of Protein-Encoding Genes

Computational analysis of physico-chemical parameters was performed using ExPASy's ProtParam server that computes molecular weight, aliphatic index, instability index, grand average of hydropathy (GRAVY), and isoelectric point (pI) (Gasteiger et al., 2005). The guanine–cytosine (GC) content was determined using the GENSCAN web server (Burge and Karlin, 1997).

Evolutionary Phylogenomics and Subcellular Network Prediction

To comprehend the evolutionary relationships among the protein-encoding genes in the studied microalgal species, a phylogenetic tree was constructed using MEGA X software (Kumar et al., 2018). After alignment of the sequences by ClustalW, the phylogenetic tree was constructed using neighbor-joining (N-J) method, and the evolutionary distances was computed using the Jones–Taylor–Thornton (JTT) matrix-based method (Shaikh et al., 2020). The parameters were as follows: phylogeny test, bootstrap method; no. of bootstrap replications, 1,000; and gaps/missing data treatment, pairwise deletion. Interacting networks of carotenoid biosynthesis proteins were constructed using the STRING database[5] (version 11.0; Szklarczyk et al., 2019).

Functional Analysis of Isopentenyl Diphosphate Pathway in Microalgal Species

Culture Conditions

For functional validation of these protein-encoding genes involved in carotenoid biosynthetic pathway in microalgae, a freshwater industrial strain *B. braunii* (Race B, NIES-836) procured from the Microbial Culture Collection at the National Institute for Environmental Studies (NIES Collection, Tsukuba,

[5]https://string-db.org/

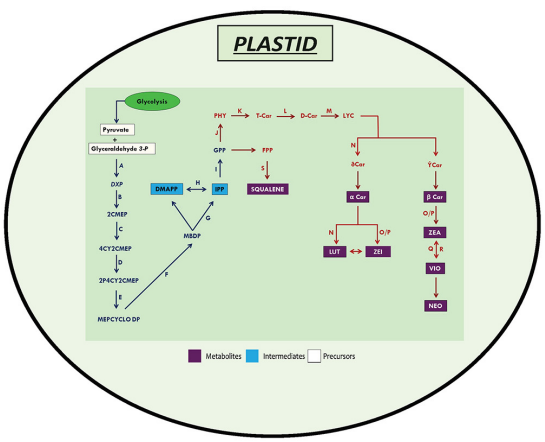

Sr. No.	Enzyme Name	Label
1	1-deoxy-D-xylulose-5-phosphate synthase (DXS1)	A
2	1-deoxy-D-xylulose-5-phosphate reductoisomerase (DXR1)	B
3	2-C-methyl-D-erythritol 4-phosphate cytidylyltransferase (CMS)	C
4	4-diphosphocytidyl-2-C-methyl-D-erythritol kinase (CMK1)	D
5	2-C-methyl-D-erythritol 2,4-cyclodiphosphate synthase (CMPS)	E
6	(E)-4-hydroxy-3-methylbut-2-enyl-diphosphate synthase (HDS1)	F
7	4-hydroxy-3-methylbut-2-en-1-yl diphosphate reductase (IDS1)	G
8	Isopentyl – diphosphate delta isomerase (IDI1)	H
9	geranyl diphosphate synthase (GDPS)	I
10	15-cis-phytoene/all-trans-phytoene synthase (PSY1)	J
11	15-cis-phytoene desaturase (PDS1)	K
12	zeta-carotene isomerase (ZCI)	L
13	zeta-carotene desaturase (ZDS1)	M
14	lycopene epsilon-cyclase (LCYE)	N
15	beta-ring hydroxylase/Cytochrome P451 (CYP97A5)	O
16	beta-carotene 3-hydroxylase (CHYB)	P
17	zeaxanthin epoxidase (ZEP1)	Q
18	violaxanthin de epoxidase (VDE)	R
19	farnesyl diphosphate farnesyl transferase (FPPS)	S

Sr. No.	Labels	Product Name	Sr. No.	Labels	Product Name
1	DXP	1-Deoxy-D-Xylulose 5-phosphate	13	LYC	Lycopene
2	2CMEP	2-C Methyl-D-erythrito 4-phosphate	14	δCar	δ Carotene
3	4CY2CMEP	4-(Cytidine 5'-PP)-2-C-Methyl-D-erythritol	15	α Car	α Carotene
4	2P4CY2CMEP	2-Phospho-4-(Cytidine 5'-PP)-2-C-Methyl-D-erythritol	16	LUT	Lutein
5	MEPCYCLO DP	2-C-Methyl-D-erythritol 2,4-cyclodiphosphate	17	ZEI	Zelnoxanthin
6	MBDP	1-Hydroxy-2-methyl-2-butenyl-4-diphosphate	18	γCar	γ Carotene
7	DMAPP	Dimethyl-PP	19	β Car	β Carotene
8	IPP	Isopentenyl-PP	20	ZEA	Zeaxanthin
9	GPP	Geranyl-PP	21	VIO	Violaxanthin
10	PHY	Phytoene	22	NEO	Neoxanthin
11	T-Car	Tri- cis ζ Carotene	23	FPP	Farnesyl-PP
12	D-Car	Di- cis ζ Carotene			

FIGURE 1 | An overview of methyl erythritol phosphate (MEP) pathway in microalgal cells depicting carotenoid and squalene biosynthesis. Genes marked in blue are initial steps of MEP pathway, and those in red are involved in high-value renewables (HVR) (squalene and carotenoids) synthesis.

Japan) was cultured in BG-11 media at 24°C with 150 μE of light intensity and a photoperiod of 16:8 (L:D) at a constant shaking of 150 rpm (Singh et al., 2020). Growth was monitored by measuring optical density at 750 nm and by dry cell weight (DCW) analysis. Growth rates were obtained using the following equation:

$$K = \frac{\frac{lnN2}{N1}}{t2 - t1} \quad (1)$$

where N1 and N2 represent optical density at initial time (t1 = day 2) and final time (t2 = day 6) during the exponential phase, respectively. Doubling time was calculated depending on the specific growth rate.

$$\text{Doubling } time = \frac{\ln 2}{K} \quad (2)$$

Experiments demonstrating the channeling of carbon flux toward these energy rich molecules were screened as follows: BG-11 supplemented with bicarbonate (BG-11 + 0.08% $NaHCO_3$), CO_2 (BG-11 + 3% v/v CO_2), and both (BG-11 + 0.08% $NaHCO_3$ + 3% v/v CO_2) against a control (BG-11) for 10 days for all further analyses and profiling. In the present study, CO_2 was continuously bubbled in the culture medium, whereas bicarbonate was added as a single dose in the culture medium at the start of the experiment.

Quantification of Carotenoids Employing High-Performance Liquid Chromatography Analysis

Total pigments were estimated employing high-performance liquid chromatography (HPLC) analysis, and the extraction procedure was performed as described in Paliwal and Jutur (2021). Briefly, 10^6 cells were centrifuged and resuspended in 1 ml of absolute methanol. For extraction of pigments, cell suspension was vortexed briefly with glass beads for 20 min. Supernatant was collected and used for HPLC-UV analysis carried out through Agilent Infinity series 1,260 HPLC system (Agilent Technologies, Santa Clara, CA, United States). The samples were run through a C30 Acclaim column (4.6 × 250 mm, 5 μm) maintained at 35°C with the binary solvent system as the mobile phase consisting methanol as primary solvent A and methyl *tert*-butyl ether (MTBE) as solvent B. The run conditions were as follows: 2–20% B for an initial 10 min, followed by 20% B (10–12 min), 20–80% B (12–30 min), 80% B (30–32 min), and 80–2% B (32–35 min) (Gleize et al., 2012). Pigments were detected at 437 nm and identified by comparing the retention time of the standards obtained from DHI, Hørsholm, Denmark.

Chlorophyll *a* Fluorescence Measurement

Chlorophyll fluorescence was estimated using Dual-PAM-100 fluorometer (Heinz Walz GmbH, Pfullingen, Germany). Samples were kept in the dark and incubated for a period of 30 min to ensure complete oxidation of all the reaction centers. The photosynthetic parameters were estimated as described previously (Kareya et al., 2020). For PSI: Y(I) = (Pm′–P)/Pm, Y(NA) = (Pm–Pm′)/Pm, Y(ND) = P/Pm as described by Klughammer and Schreiber (1994); Baker (2008), and Fang et al. (2020). The $P700^+$ signals (P) could range from a minimum (P700 entirely reduced) to a maximum level (P700 fully oxidized), where P denotes $P700^+$ signals, Pm is P700 fully oxidized, and Pm′ is P700 fully reduced.

Extraction and Quantification of Squalene

Squalene content was quantified as described by Kajikawa et al. (2015). Microalgal cells (10^9 cells) were saponified in 2 ml of 10% KOH prepared in 50% methanol for 30 min by sonication. Squalene was extracted with the same volume of hexane, the solvent was evaporated, and the leftover dried residue was dissolved in 20 μl of chloroform. Derivatization was done by adding 20 μl of *N*,*O*-bis(trimethylsilyl)trifluoroacetamide (Sigma-Aldrich, St. Louis, MO, United States) to the samples and incubated at 80°C for 30 min. Chloroform was added to the derivatized samples to increase the reaction volume to 40 μl. A 2 μl aliquot of the solution was analyzed using gas chromatography–mass spectrometry (GC-MS) (Agilent Technologies, Santa Clara, CA, United States) equipped with an DB-5 MS capillary column (30 m × 0.25 mm × 0.25 mm). The carrier gas used in the experiment was helium with a flow rate of 1 ml min^{-1}, and the initial oven temperature was 150°C, which was increased to 300°C (ramp rate 20°C min^{-1}). The ionization voltage was 70 eV, and scan range was 40–500 Da. The squalene content was calculated from the ratio of the peak areas of the standard procured from Sigma-Aldrich, United States.

Statistical Analysis

All the experiments were performed as biological triplicates and are represented as average ± SE. Statistical analyses such as ANOVA and *t*-test were performed using Microsoft excel for determination of significance.

RESULTS

In silico Analysis of Methyl Erythritol Phosphate Pathway

The schematic representation of MEP pathway for the biosynthesis of squalene and carotenoids is illustrated in **Figure 1**. The first committed step of MEP pathway is catalyzation by DXS1, which results in the production of deoxy-xylulose phosphate. Isopentenyl pyrophosphate, the five-carbon isoprenoid precursor, condenses to form geranyl diphosphate, which has two fates: either it can be converted to phytoene through phytoene synthase (PSY), or it can be converted to squalene through two-step reaction catalyzed by farnesyl diphosphate farnesyl synthase (FPPS).

Prediction of the Subcellular Localization for Protein-Encoding Genes

In the present study, the compartmentalization of all the proteins was predicted using four different tools: Cello, TargetP, WoLF PSORT, and ngLOC. These tools use different algorithms to predict subcellular localization for a particular protein, in order to obtain more reliable results based on the average data plotted. It

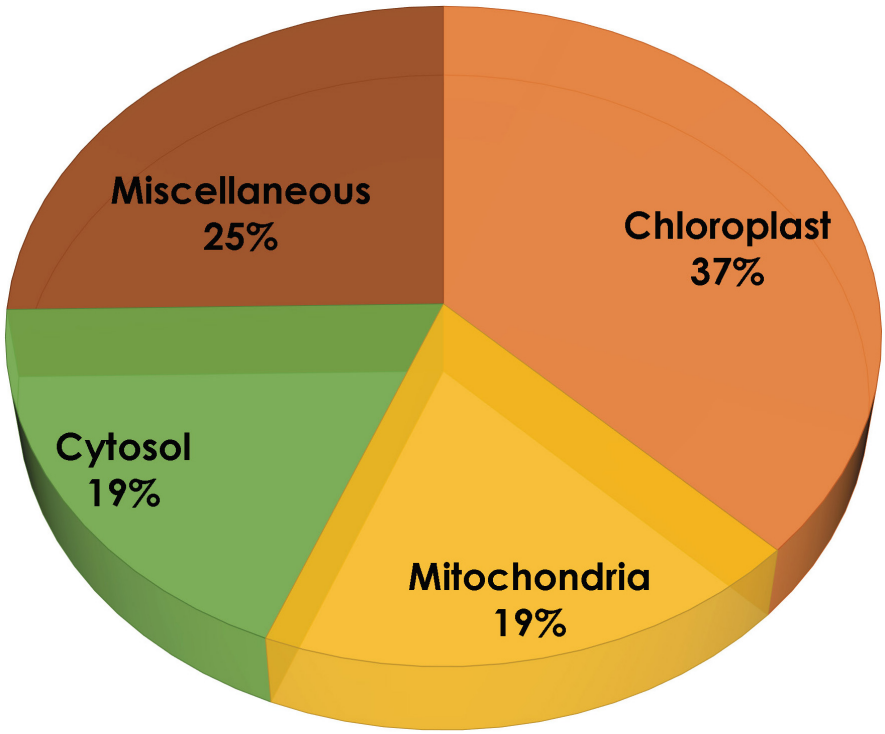

FIGURE 2 | Subcellular localization of methyl erythritol phosphate (MEP) pathway genes using TargetP, WoLF PSORT, ngLOC, and Cello.

is evident from **Figure 2** that 59% of proteins are predominantly present in the chloroplast, 12% remain systematically organized in the cytoplasm, 13% of proteins are in mitochondria, and the remaining 16% are predicted to be localized in other compartments (like the nucleus, endoplasmic reticulum, and plasma membrane). As reported earlier, our study also predicts the localization of proteins involved in MEP pathway majorly within the plastids.

Characterization of the Physico-Chemical Properties

The physico-chemical properties characterized using Expasy's ProtParam tool compute various parameters of proteins like instability index, molecular weight, pI, aliphatic index, and GRAVY index. The graph plotted from the average values of all parameters corresponding to all the proteins is shown in **Figure 3**. Molecular weight is observed between the range of 18,916.14 and 80,004.235 Da. The pI of the orthologous proteins lies in the range of 5–8, and majority of the proteins have their pI below 7, which indicates that they are acidic in nature. These values of the pI prove to be valuable and beneficial for developing a buffer system for purification of enzymes. Instability index defines the stability of proteins in their *in vitro* conditions. The existence of particular dipeptides occurring at significantly different frequencies between stable and unstable proteins is revealed by the instability index. Majority of the protein-encoding genes are stable, which are ideal prospects for genetic engineering involved in enhancement of biorenewables. The aliphatic index refers to the percentage of a protein's volume filled by aliphatic side chains (alanine, leucine, isoleucine, and valine) and contributes to the globular proteins' high thermal stability (Ikai, 1980). The average aliphatic index of all the proteins ranged from 76.49 to 98.47, with proteins with a high aliphatic index indicating structural stability over a wide temperature range. The GRAVY value for a protein is the sum of hydropathy value 10 of all the amino acids divided by the number of residues in the sequence. The GRAVY index can be used to measure the hydrophobicity of a protein. It is clearly evident from the plot in **Figure 3** that all the proteins are hydrophilic, as their GRAVY index lies below zero. The GC content plot in **Figure 3** shows the average GC content of all the genes ranging between 56 and 63%, which demonstrates the presence of a very high GC content.

Identification of Motif and Domain Organization

A motif is a pattern of sequence that is found conserved among a group of related protein or sequence. MEME algorithm is used widely for the discovery of DNA and protein sequence motifs. This computational tool predicts the conserved pattern amid the proteins, and result is depicted in a form of logo plot. In a sequence logo plot, the height of each stack indicates the relative occurrence of the corresponding amino acid, while the color indicates the nature of the amino acid. In addition to motif analyses, a detailed comparison of the domain architectures of the proteins was performed using HMMER. In this study, we

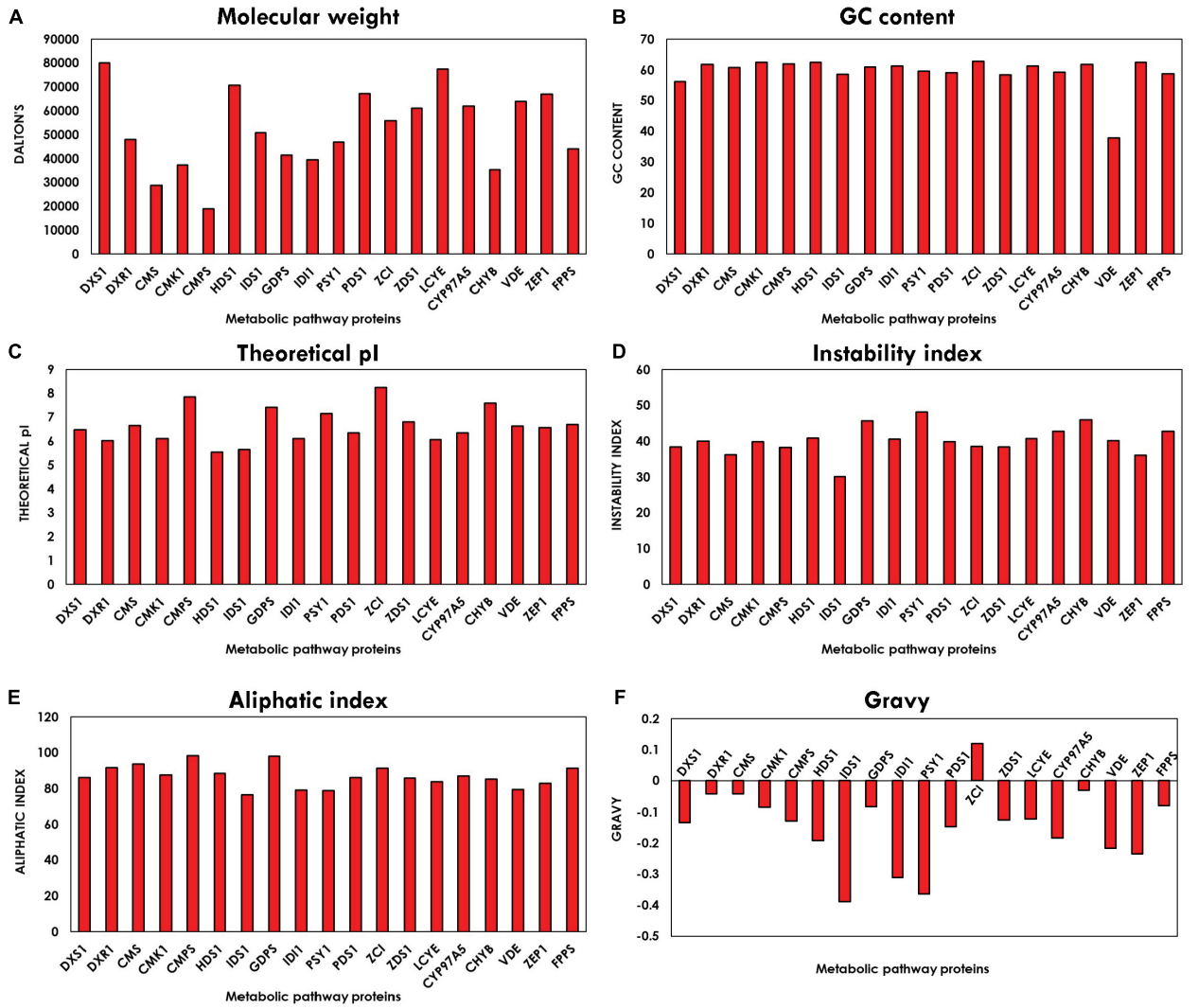

FIGURE 3 | Bar plot depicting physico-chemical characteristics: **(A)** molecular weight **(B)**, guanine–cytosine (GC) content, **(C)** isoelectric point (pI), **(D)** instability index, **(E)** aliphatic index, and **(F)** grand average of hydropathy (GRAVY) index of methyl erythritol phosphate (MEP) pathway genes using ExPASy-ProtParam tool.

were successful in identifying motifs of all the proteins involved in the carotenoid biosynthesis (**Figure 4**). Our analysis of domains revealed that phytoene desaturase (PDS1) and carotene desaturase (ZDS1) showed amino oxidase domain. Deoxy-D-xylulose-5-phosphate synthase (DXS), deoxy-D-xylulose 5-phosphate reductoisomerase (DXR), and 4-hydroxy-3-methyl-butenyl 1-diphosphate reductase displayed highly conserved motifs. HDS1 and IDS1 both were predicted to have GcpE domain, indicating that the proteins still retained the domain during the course of evolution. The domains in all these proteins show a pattern of high conservation among the microalgal species.

Phylogenomic Analysis

To understand the evolutionary relationship among the proteins involved in carotenoid and squalene synthesis among 13 species, a phylogenetic tree was constructed in the MEGA X software based on their protein sequences. The phylogenetic tree was constructed with 1,000 rounds of bootstrapping test in order to obtain exhaustive and detailed information. Homologs of proteins distributed among different species with similar functions were found to be clustered together in the tree as shown in **Figure 5**. Rate-limiting gene *DXS1* was found to be conserved among all the selected species, while three variants for this gene were retrieved in *B. braunii*. Proteins with the same domains were present in the neighboring clads as observed in phytoene desaturase and carotene desaturase, further proving the assumption that the domains and the sequence might be conserved in this protein during the course of evolution. The FPPS, a potential target gene for enhancement of squalene production, was found to be most conserved among chlorophytes as well as heterokont *Aurantiochytrium* sp. (which is a leading producer of squalene).

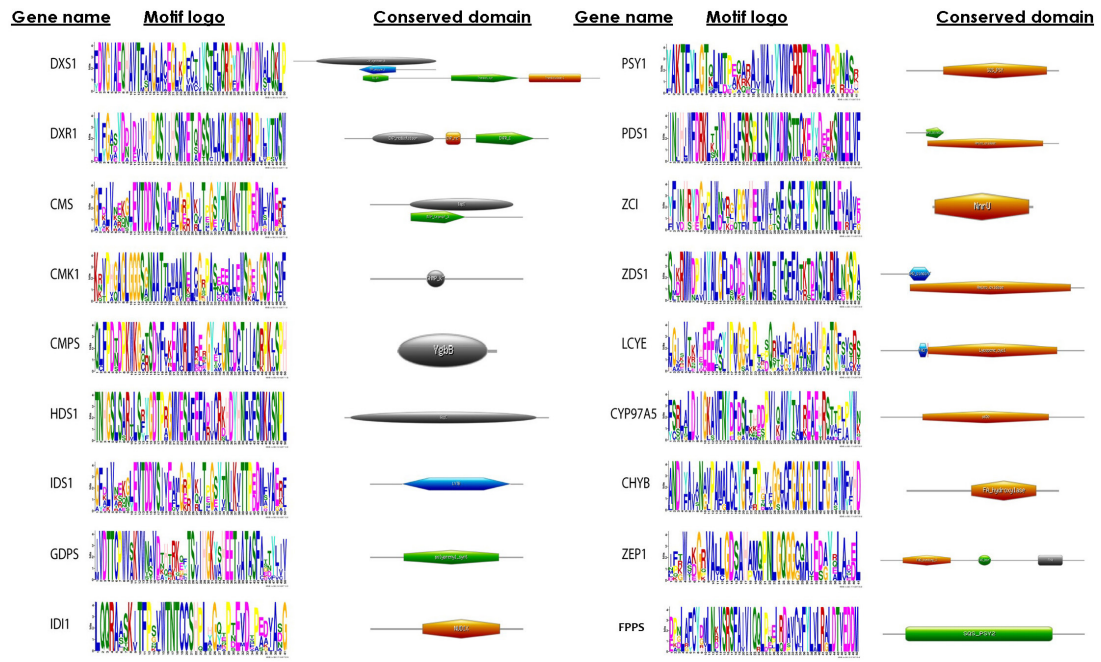

FIGURE 4 | Conserved sequence logo plots representing motifs and domain architecture of methyl erythritol phosphate (MEP) pathway genes constructed using MEME suite and HMMER tool, respectively. In the sequence logo plot, the height of symbol represents the relative frequency of amino acid conserved at that position, whereas the color corresponds to nature of amino acid (such as DE, magenta; KR, red).

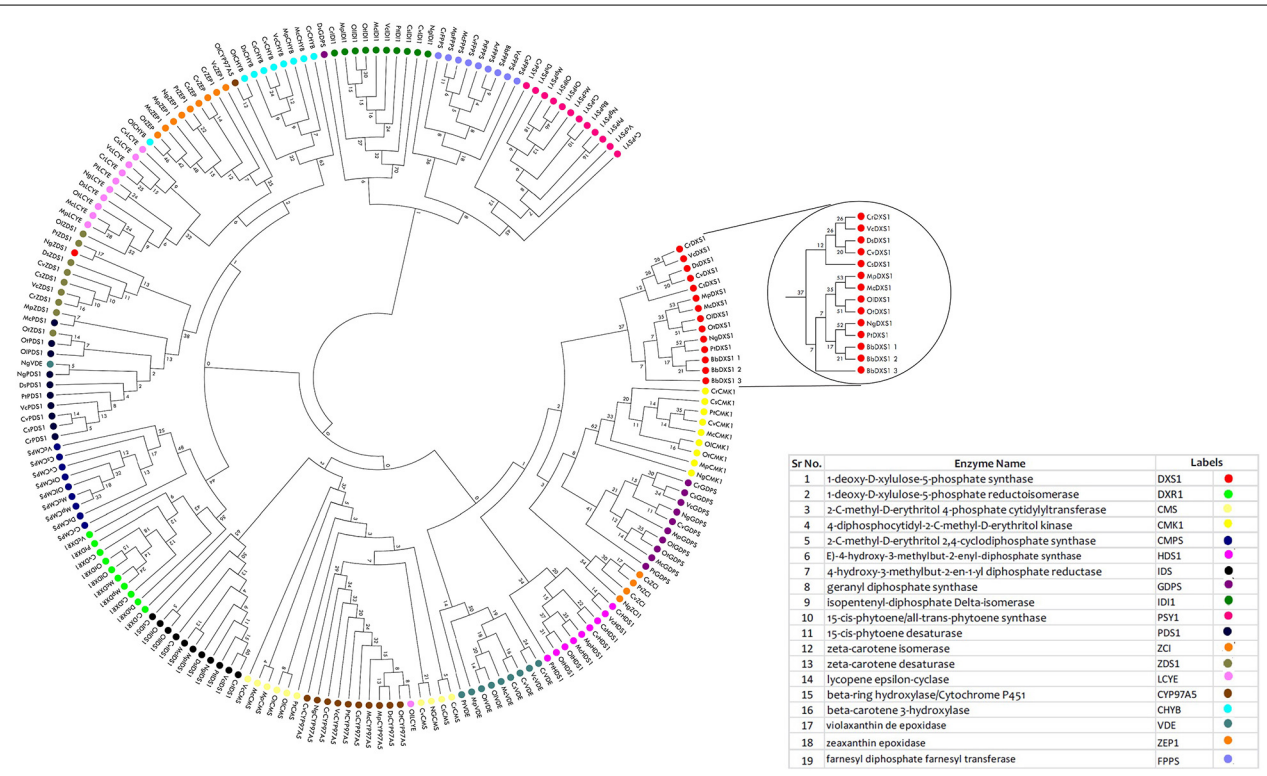

Sr No.	Enzyme Name	Labels
1	1-deoxy-D-xylulose-5-phosphate synthase	DXS1
2	1-deoxy-D-xylulose-5-phosphate reductoisomerase	DXR1
3	2-C-methyl-D-erythritol 4-phosphate cytidylyltransferase	CMS
4	4-diphosphocytidyl-2-C-methyl-D-erythritol kinase	CMK1
5	2-C-methyl-D-erythritol 2,4-cyclodiphosphate synthase	CMPS
6	E)-4-hydroxy-3-methylbut-2-enyl-diphosphate synthase	HDS1
7	4-hydroxy-3-methylbut-2-en-1-yl diphosphate reductase	IDS
8	geranyl diphosphate synthase	GDPS
9	isopentenyl-diphosphate Delta-isomerase	IDI1
10	15-cis-phytoene/all-trans-phytoene synthase	PSY1
11	15-cis-phytoene desaturase	PDS1
12	zeta-carotene isomerase	ZCI
13	zeta-carotene desaturase	ZDS1
14	lycopene epsilon-cyclase	LCYE
15	beta-ring hydroxylase/Cytochrome P451	CYP97A5
16	beta-carotene 3-hydroxylase	CHYB
17	violaxanthin de epoxidase	VDE
18	zeaxanthin epoxidase	ZEP1
19	farnesyl diphosphate farnesyl transferase	FPPS

FIGURE 5 | Phylogenomic tree constructed for methyl erythritol phosphate (MEP) pathway proteins employing neighbor-joining (N-J) method with evaluation of 1,000 rounds of bootstrapping test using MEGA 10.0. Each colored symbol denotes a specific protein, and the highlighted circle represents the rate-limiting enzyme deoxy xylulose phosphate synthase (DXS1) found to be conserved among microalgal species.

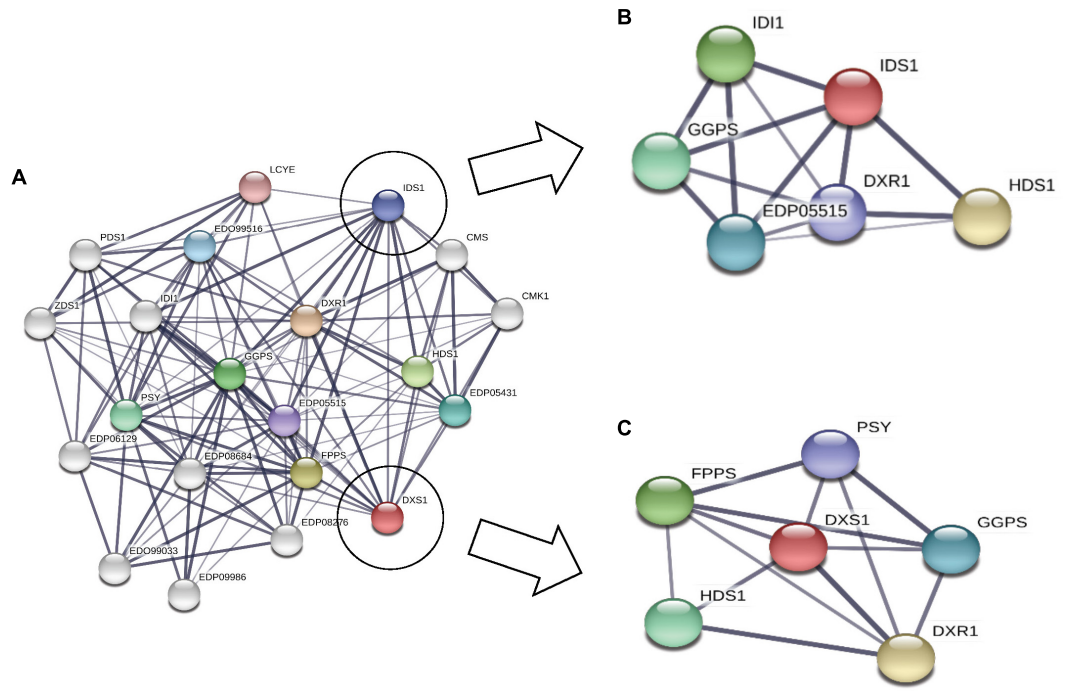

FIGURE 6 | Subcellular network prediction using STRING database: **(A)** complete network where each node represents a particular protein of methyl erythritol phosphate (MEP) pathway protein; **(B)** subnetwork of IDS1 protein representing interaction with GGPS and DXR1; **(C)** subnetwork of DXS1 protein interacting with farnesyl diphosphate farnesyl synthase (FPPS) (squalene biosynthesis) and phytoene synthase (PSY) (carotenoid biosynthesis).

Analysis of Subcellular Networking

The regulatory network for MEP pathway proteins, which is predicted using STRING database (**Figure 6**), clearly shows the interaction between DXS1 and IDS1 proteins (gene involved in IPP synthesis pathway). Similarly, the rate-limiting enzymes for both carotenoid and squalene biosynthesis, i.e., PSY and FPPS, were found to be interacting, thus suggesting strong interaction and crosstalk among carotenoid and squalene synthesis pathway.

Functional Characterization of Methyl Erythritol Phosphate Pathway in Green Alga *Botryococcus braunii*

The green microalga *B. braunii* was cultivated in the above-mentioned four conditions, i.e., in the presence of bicarbonate and CO_2 supplementation. **Table 1** represents the growth profile of *B. braunii* and shows that it is a slow-growing strain with a specific growth rate of 0.21 (day^{-1}), doubling time of 3.37 days, and biomass productivity of 70 mg L^{-1} D^{-1}. The growth rate has increased in the presence of $NaHCO_3$, i.e., 0.23 (day^{-1}), and a doubling time of 3.04 days and 77 mg L^{-1} D^{-1}, but the change was not significant. In the presence of 3% CO_2 alone, the biomass productivity increased 1.2-fold, i.e., 90 mg L^{-1} D^{-1} with the specific growth rate of 0.26 (day^{-1}) and doubling time of 2.65 days. However, the addition of both bicarbonate and CO_2 sparging has shown to be more promising than either of the factors alone and showed a 1.4-fold increase in the biomass productivity (100 mg L^{-1} D^{-1}), although the specific growth rate and doubling time remains to be similar in the CO_2 supplementation.

Dynamics of Chlorophyll *a* Fluorescence

We estimated the transient regulation of chlorophyll fluorescence using Dual-PAM, and different parameters for the photosynthetic efficiency of PSII and PSI were calculated and listed in **Table 2**. The maximum quantum efficiency of PSII photochemistry (F_v/F_m) of the cultures supplemented with CO_2 and bicarbonate were found to be higher. The data predict the photosynthetic machinery in control conditions to be less responsive than cultures with additional carbon supplementation. The PSII

TABLE 1 | Growth parameters of *Botryococcus braunii* subjected to carbon supplementation.

Conditions	Specific growth rate (μ) (day^{-1})	Doubling time (days)	Biomass productivity (mg L^{-1} D^{-1})
BG-11 (control)	0.21 ± 0.02	3.37 ± 0.08	70.99 ± 2.14
BG-11 (+$NaHCO_3$)	0.23 ± 0.01	3.04 ± 0.03	76.86 ± 2.29
BG-11 (+3% CO_2)	0.26 ± 0.06	2.65 ± 0.02	89.51 ± 2.84
BG-11 (+$NaHCO_3$ + 3% CO_2)	0.26 ± 0.04	2.70 ± 0.05	100.03 ± 2.44*

**Statistical significance by one-way ANOVA, $p < 0.05$.*

TABLE 2 | Photosynthetic efficiency of *Botryococcus braunii* cultivated in different carbon supplementations.

Parameters	BG-11 (Control)	BG-11 (+$NaHCO_3$)	BG-11 (+3% CO_2)	BG-11 (+$NaHCO_3$ + 3% CO_2)
F_v/F_m	0.62 ± 0.02	0.74 ± 0.02	0.77 ± 0.01*	0.74 ± 0.02
Y(II)	0.15 ± 0.09	0.44 ± 0.003	0.42 ± 0.02	0.45 ± 0.01
Y(NPQ)	0.66 ± 0.09*	0.38 ± 0.02	0.31 ± 0.00	0.31 ± 0.00
Y(NO)	0.19 ± 0.01	0.18 ± 0.02	0.27 ± 0.02	0.24 ± 0.01
F_q'/F_m'	0.18 ± 0.01	0.44 ± 0.06	0.42 ± 0.02	0.45 ± 0.01
Y(I)	0.37 ± 0.01	0.49 ± 0.01	0.71 ± 0.01*	0.694 ± 0.01
Y(ND)	0.15 ± 0.01	0.11 ± 0.02	0.17 ± 0.01	0.22 ± 0.00*
Y(NA)	0.48 ± 0.01*	0.40 ± 0.02	0.12 ± 0.00	0.09 ± 0.01
ETR(I)	29.8 ± 0.80	39.4 ± 0.80	61.9 ± 1.40*	55.4 ± 1.60

*Abbreviations for the labels included in the table are as follows: F_v/F_m, maximum photochemical efficiency of PSII; F_q'/F_m', PSII operating efficiency; Y(II), quantum yield of photochemical quenching; Y(NPQ), quantum yield of non-photochemical quenching; Y(NO), energy dissipated as heat or fluorescence; Y(I), quantum yield of photochemical energy conversion; Y(ND), quantum yield of non-photochemical energy dissipation due to donor side limitation; Y(NA), quantum yield of non-photochemical energy dissipation due to acceptor side limitation; ETR(I), electron transport rate through PSI. * Statistical significance by one-way ANOVA, $p < 0.05$.*

operating efficiency, which can also be used as a proxy for the approximation of linear electron flux through the PSII, also seems to be enhanced in carbon-supplemented cultures. It is evident from **Table 2** that the energy allocation is higher for NPQ in control conditions as compared with cultures with carbon supplementation. Furthermore, there is a distinct increase in the quantum yield of PSII photochemistry in cultures with additional carbon source. These results further indicate that the cells supplemented with carbon have an enhanced linear electron flow that supports the lowering of doubling time and enhanced growth rates for *B. braunii*. The quantum yield of PSI, denoted as Y(I), was distinctly more limited due to acceptor side limitation. Carbon supplementation increased the Y(I), while there was a decline in the control condition.

Quantification of Squalene and Carotenoids

The carotenoid profile of *B. braunii* was found to be affected in the presence of both bicarbonate and CO_2 supplementation (**Figure 7**). It has been found that carbon supplementation enhances chlorophyll content, which further enhances the photosynthetic efficiency and reduces the doubling time. In the presence of bicarbonate alone, echinenone was found to be 57.3% of total carotenoids, which was 1.5 times higher ($p < 0.05$) as compared with control. As compared with CO_2 supplementation, there was significant difference in the carotenoid profile for cultures supplemented with both CO_2 and bicarbonate. The antheraxanthin content has increased from 6.6% of total carotenoids in CO_2 supplementation to 9.9% in the presence of both bicarbonate and CO_2. Also, the β-carotene content was found to be the lowest in the presence of bicarbonate and CO_2, which was significantly higher in the presence of bicarbonate alone (20% of total carotenoid content).

Table 3 represents the content of different HVRs obtained for *B. braunii* in the presence of $NaHCO_3$ (0.8% w/v) and CO_2 (3% v/v) on the 10th day. The squalene content significantly decreased in the carbon supplementation from 0.32% of DCW in control, 0.16% in $NaHCO_3$, 0.06% in CO_2, and 0.08% ($p < 0.05$) in the presence of both. However, the content of

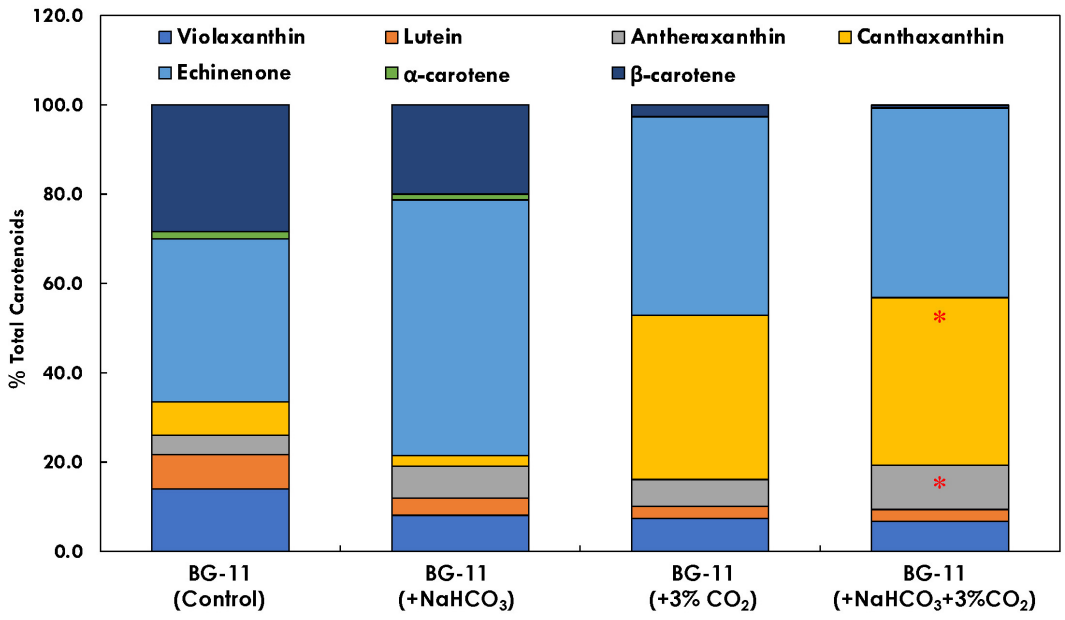

FIGURE 7 | Bar plot depicting the distribution of individual carotenoids (% total carotenoid content) in *Botryococcus braunii* subjected to different carbon supplementations. * Statistical significance by one-way ANOVA, $p < 0.05$.

TABLE 3 | The high value-added renewable profile of *Botryococcus braunii* on the 10th day supplemented with different carbon sources.

HVRs (% DCW)	BG-11 (control)	BG-11 (+$NaHCO_3$)	BG-11 (+3% CO_2)	BG-11 (+$NaHCO_3$ + 3% CO_2)
Squalene	0.326 ± 0.02*	0.014 ± 0.06	0.006 ± 0.01	0.008 ± 0.05
Carotenoids	0.059 ± 0.01	0.036 ± 0.08	0.068 ± 0.03	0.180 ± 0.02*
Botryococcane	0.023 ± 0.05	0.021 ± 0.05	0.014 ± 0.03	0.055 ± 0.07

*HVRs, high-value renewables; DCW, dry cell weight. *Statistical significance by one-way ANOVA, $p < 0.05$.*

another HVR botryococcene was found to increase from 0.023% DCW in control to 0.055% DCW with bicarbonate and CO_2 supplementation.

DISCUSSION

Recently, microalgae attracted considerable interest worldwide as a promising feedstock for biofuels and various high-value biorenewables. Microalgae are preferred over higher plants due to their high photosynthetic efficiency, greater ability to fix carbon dioxide (CO_2) and convert CO_2 into biomass, and shorter life cycle. The potential of several microalgae species in the renewable energy, biopharmaceutical, and nutraceutical sectors has been evaluated (Khan et al., 2018; Sun et al., 2018). Microalgae are an excellent source of HVRs such as polysaccharides, carotenoids, sterols, terpenoids, OMEGAs, and proteins, which are beneficial to human health (Chew et al., 2017; Shaikh et al., 2019). Simultaneous production of specific high-value compounds along with biofuels in a biorefinery concept could make the process economically feasible (Carriquiry et al., 2011; Campenni et al., 2013; Nobre et al., 2013). The major strategy applied for the enhancement of biofuel is stress biology aspects, which retard the biomass production. Another factor that can be applied for enhancing biomass along with certain other high-value products is carbon supplementation, which paved new way for increased production of HVRs (Markou and Nerantzis, 2013). Therefore, the biotechnological application in microalgae is limited under industrial conditions for the lack of comprehensive understanding of metabolic pathways and their regulation.

In the present study, phylogenomic analysis carried out for the MEP pathway is responsible for the production of carotenoids and squalene along with providing isoprenoid backbone to variety of other HVRs such as tocopherols (vitamins) and sterol. The MEP pathway genes of *C. reinhardtii* were retrieved and aligned with 13 other microalgal strains belonging to different classes of Chlorophyceae and Heterokonts. The nucleotide sequence for the hits obtained is used for understanding the sequence similarity and evolutionary gene–function relationship among various microalgal species.

IPP is a common precursor for the production of majority of HVRs. These compounds, apart from having commercial relevance, also impart certain benefits to organisms themselves, and hence, a detailed investigation of isoprenoid pathway will be crucial for further tuning the HVR production. In plants, IPP is synthesized *via* two different pathways: firstly, the cytoplasmic mevalonate (MVA) pathway that initiates with the condensation of three units of acetyl-CoA to 3-hydroxy-3-methylglutaryl-CoA (HMG-CoA) and subsequently reduction to MVA, followed by successive phosphorylation of MVA, and a decarboxylation/elimination step leading to IPP (Lange et al., 2000). Secondly, IPP, which is derived from 2-*C*-methyl-D-erythritol 4-phosphate (MEP) pathway, occurs in chloroplast. The first step of this pathway is the condensation of pyruvate with the aldehyde group of D-G3P leading to the production of 1-deoxy-D-xylulose 5-phosphate (DXP), which is catalyzed by a thiamine-dependent synthase, i.e., 1-deoxy-D-xylulose 5-phosphate synthase (DXS). An intramolecular rearrangement and reduction of DXP by the enzyme DXP reducto-isomerase (DXR) yields 2-*C*-methyl-D-erythritol 4-phosphate (MEP) in the second step. This follows the conversion of MEP into 2-*C*-methyl-D-erythritol 2,4-cyclodiphosphate (ME-2,4cPP) in three enzymatic steps, and the subsequent reduction produces 1-hydroxy-2-methyl-2-butenyl 4-diphosphate (HMBPP), catalyzed by HMBPP synthase (HDS). This HMBPP is finally converted into a mixture of IPP and dimethylallyl diphosphate (DMAPP) by the enzyme HMBPP reductase (Carretero-Paulet et al., 2010), and the interconversion of IPP and DMAPP is controlled by IPP isomerase.

Majority of the microalgae were reported to have only MEP pathway for the production of IPP molecules that were further confirmed by labeling experiments (Rosa Putra et al., 1998). However, there are reports that rhodophyte possesses both the pathways, whereas chlorophyte has only MEP pathway (Lichtenthaler et al., 1997). Hence, there is load on plastid for generation of abundant pool of IPP, which is efficiently transported to the cytoplasm for sterols and other high-value products.

The two pathways for carotenoid and squalene bifurcate from GPP, one of which is a multistep pathway for the synthesis of the former, while the latter one is a two-step pathway. **Figure 1** shows a complete picture of the carotenoid and squalene biosynthetic pathway along with the proteins present (DellaPenna and Pogson, 2006). It was revealed (**Supplementary Table 1**) that algal species maintain the basic genomic repertoire required for the production of isoprenoids. Furthermore, subcellular localization of proteins was performed, which gives an idea of its spatial organization and improves our knowledge of cellular metabolism. It also helps us to determine subcellular network topology. Our analysis revealed that 59% of the total proteins were localized in chloroplast, which as well supported by previous literature (Gong and Bassi, 2016). The IPP pathway enzymes are nucleus encoded and transported into plastids post-translationally, as evidenced by the presence of characteristic N-terminal transit peptides (Lohr et al., 2012).

The physico-chemical properties of proteins provide insight into the stability and functionality of proteins, further increasing the information regarding protein, helping in maintaining the structure, function, and the stability of the proteins in molecular work. For example, proteins having an instability index of less than 40 are considered stable, whereas those with a value of

more than 40 are considered unstable (Misra et al., 2012). Our analysis revealed that the majority of the proteins are highly stable with high GC content, which makes it difficult for genetic manipulation. Furthermore, the motif and domain architecture revealed the evolutionary conservation of the proteins among the microalgae. The gene having similar domain were found to cluster together in the phylogenomic tree (**Figure 5**), which was constructed to understand the evolutionary relationship. Some of the interesting observations of this study were occurrences of three variants of DXS1; the rate-limiting gene of MEP pathway in *B. braunii* and only FPPS gene was found to align for *Aurantiochytrium* sp.

Botryococcus are green photosynthetic microalgae with the ability to constitutively synthesize, accumulate, and secrete substantial amounts of hydrocarbons such as alkadienes (A-race) or tri-terpenoids (B-race) and have the ability to synthesize odd-numbered hydrocarbons (C-23–C-33) (Jin et al., 2016). The green microalga can produce hydrocarbons in the range of 2–86% (% DCW) depending among strains/races and changes in cultural and physiological conditions (Rao et al., 2012). Despite the high hydrocarbon content, this microalga cannot be utilized on a larger-scale due to its slow growth. Therefore, in order to improve biomass production, the alga requires supplementation of carbon source (CO_2, glucose sodium acetate, etc.) (Yoshimura et al., 2013; Barajas-Solano et al., 2016). In the present study, we have used two carbon sources, i.e., 0.08% (w/w) $NaHCO_3$ and 3% CO_2 (v/v), and a combination of both to enhance their biomass productivity.

Our preliminary analysis revealed that the green microalga is a slow-growing strain that has a doubling time of 3.2 days (**Table 1**). However, the supplementation of CO_2 reduces doubling time significantly, i.e., 2.6 days. Previous studies have suggested that adding carbon to microalgae culture is a major determinant, as excessive concentrations can inhibit growth or accumulation of particular metabolites, while low quantities might restrict it (Tapie and Bernard, 1988; Olaizola et al., 1991). As a result, carbon source optimization is required, which varies by species. Concentrations must not only be lower than a particular value that meets the algae's carbon needs but also not exceed this value in order to avoid a significant loss that can ultimately lead to waste and significantly rise of production cost (Cheng et al., 2006). Yoshimura et al. (Yoshimura et al., 2013) screened different concentrations of CO_2 from 0.02 to 5% for cultivation of *B. braunii* Showa and found that the specific growth rate remained similar for the aforementioned CO_2 concentrations; however, growth has declined above 5%, which may be due to the drop in pH. This further supports the enhanced biomass productivity of 100 mg L^{-1} D^{-1} with a combination of both bicarbonate and CO_2 supplementation.

It has been reported that biomass concentration increases in cultures supplemented with additional source of carbon (Sforza et al., 2012; Adamczyk et al., 2016). Moreover, the chlorophyll content along with the photosynthetic efficiencies appears to be enhanced upon CO_2 supplementation in *M. gaditana*, further lowering the doubling time (Kareya et al., 2020). We demonstrate that the additional supplementation of carbon in *B. braunii* significantly reduces the doubling time, which is accompanied by higher chlorophyll content F_v/F_m ratio. The maximum quantum efficiency of PSII remains similar in cultures supplemented with carbon source and is ∼1.2-fold higher than control conditions. Similarly, the PSII operating efficiencies of cells supplemented with carbon are clearly higher (∼4.0-fold) than those of control. The increase in quantum efficiency of PSII along with PSII operating efficiency, which provides an estimate of the quantum yield of linear electron flux through PSII, is also reported to be due to the synergistic effect of certain pigments on the photosystems (Kareya et al., 2020). The low photochemical efficiencies in control cultures further influence the lack of effective electron flux through the photosystems, and this manifestation is also noticeable in the growth of all the cultures.

The quantum yield of non-photochemical quenching Y(NPQ) is prominently higher in the control condition compared with cells supplemented with carbon source. Conversely, the quantum yield of PSII photochemistry Y(II) is higher in cultures supplemented with carbon than in the control condition. As a result, we demonstrate that the carbon flux helps the cells to undergo regulated changes efficiently as compared with the control condition; moreover, due to the lack of carbon, control cells might undergo photoinhibition, suggesting that a greater number of PSII reaction centers are closed in the control condition (Fang et al., 2020; Lu et al., 2020). Carbon supplementation further helped in the increase in the Y(I), suggesting that the photosynthetic efficiency was stable and balanced as compared with that in the control condition. Furthermore, there was an increase in Y(NA) in the control condition, suggesting the limitation due to the acceptor side in the photosystems and high Y(ND) in carbon-supplemented cells displaying the necessity of carbon to inhibit the over-reduction of PSI electron carriers (Sun et al., 2020).

The xanthophyll and carotene compositions are crucial for photoprotection and PSI stability, as it helps in reactive oxygen species (ROS) scavenging and quenching of Chl* (Grung et al., 1994). The xanthophyll violaxanthin is rapidly de-epoxidized to intermediate antheraxanthin and zeaxanthin in order to convert conversion of PSII to a state of high thermal energy dissipation and low Chl fluorescence emission, hence lowering the photoinhibition (Havaux and Niyogi, 1999). In the presence of carbon supplementation, antheraxanthin accumulation was found (**Figure 7**), which relates with the lower NPQ and higher biomass accumulation. Additionally, the primary carotenoids α- and β-carotenes were found to be lower in the presence of additional carbon; however, canthaxanthin was higher. This may be attributed to the upregulation of lycopene epsilon cyclase in the presence of carbon supplementation.

Two of the HVRs, carotenoid and squalene, were found to have an entirely opposite effect in the presence of carbon supplementation. The carotenoid content increased in the presence of carbon source: maximum for the 3% CO_2 and $NaHCO_3$, i.e., 0.18% of DCW (**Table 3**) with $p < 0.05$, whereas the squalene content has declined threefold from 0.32% in control to 0.08% in CO_2 supplementation. Carotenoid content can be enhanced by employing various media engineering approach

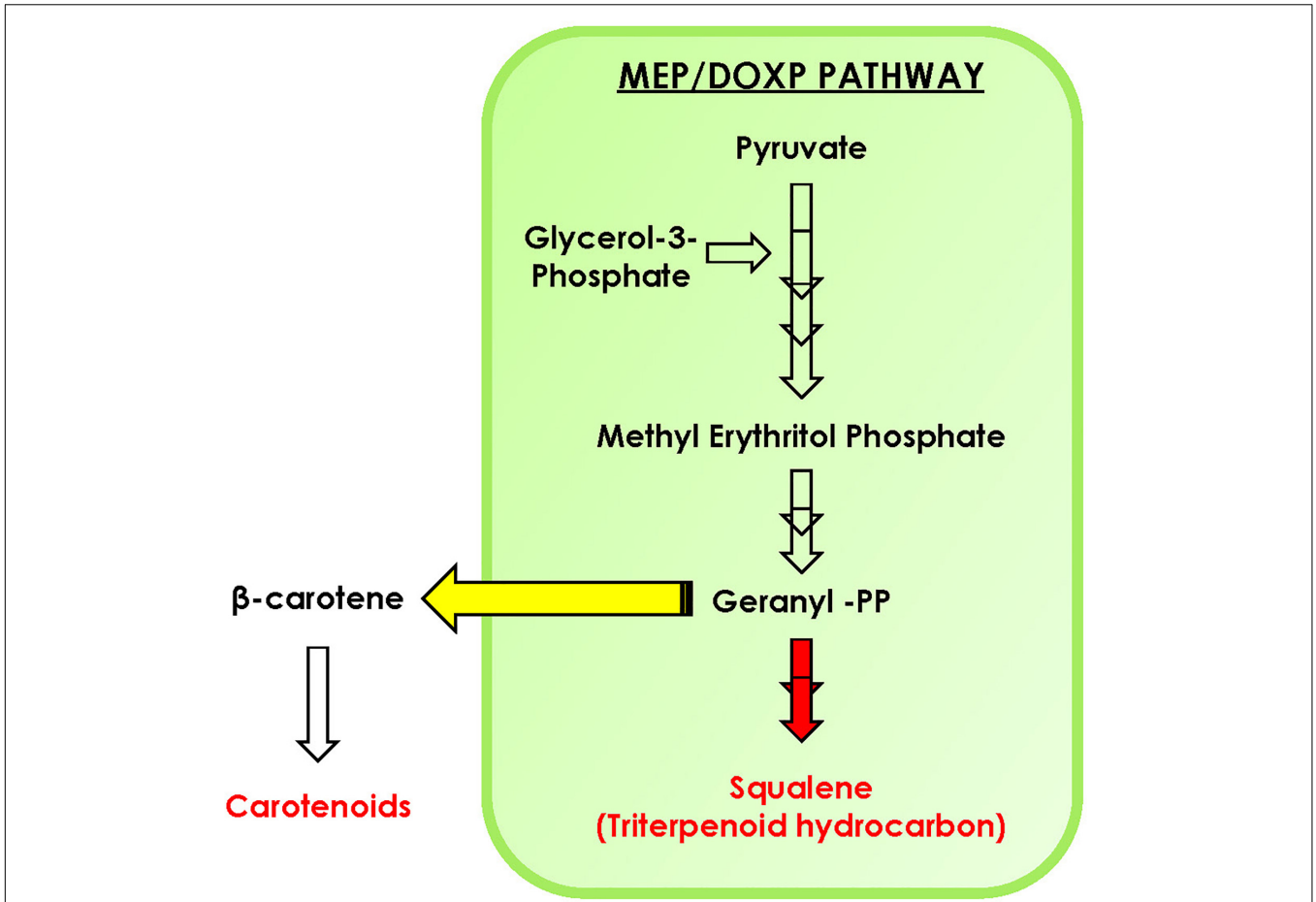

FIGURE 8 | Schematic representation of carotenoid and squalene biosynthesis in *Botryococcus braunii*. Yellow arrow indicates the diversion toward carotenoids, while red indicates downregulation of squalene production upon carbon supplementation.

such as nutrient starvation, salinity, high light irradiance, and carbon supplementation (Paliwal et al., 2017). Also, there are certain regulatory proteins such as PSY and phytoene desaturase, which were overexpressed for enhanced carotenoid production in various plants and microalgal species. Wang et al. (2021) identified three variants of PSY in tobacco plant, i.e., PSY1, PSY2, and PSY3, and found that silencing of PSY1 and PSY2 remarkedly decreased chlorophyll and carotenoid content in leaves. In *Arabidopsis thaliana*, an ORANGE (OR) protein that regulates chromoplast differentiation was found to interact with PSY, and overexpression of OR significantly enhanced the enzymatically active PSY, which leads to enhanced carotenoid production (Zhou et al., 2015).

CONCLUSION

In conclusion, with the help of phylogenomic analysis, we demonstrate that isoprenoid pathway in the microalgal lineage is highly conserved and is highly regulated with complex crosstalk within the pathway. Furthermore, upon carbon supplementation in selected microalga *B. braunii*, doubling time declines significantly along with diverting the carbon flux toward accumulation of carotenoids, specifically lutein. The STRING analysis predicts the interaction between various proteins of MEP pathway such as DXS1, IDS1, GGPS, PSY, and FPPS. Overall, we hypothesize that the enhancement in carotenoid biosynthesis might be attributed toward the upregulation of PSY, whereas the FPPS was downregulated in the presence of external carbon source (**Figure 8**). Thus, engineering of such regulatory proteins may further enhance the carotenoid content of *B. braunii*. Our present study highlights for the first time the crosstalk between carotenoid and squalene biosynthesis pathway in the presence of carbon supplementation, a new perspective of media engineering a cost-effective approach to enhance production of biorenewables without compromising growth.

DATA AVAILABILITY STATEMENT

The original contributions presented in the study are included in the article/**Supplementary Material**, further inquiries can be directed to the corresponding author/s.

AUTHOR CONTRIBUTIONS

IM, AN, and PJ designed the experiments. IM, MR, and MK executed the experiments. AN and PJ supervised the project. IM, MR, MK, and AN wrote the manuscript with all the input from the authors. All authors contributed to the article and approved the submitted version.

FUNDING

The work was supported by the grants from the Department of Biotechnology, Government of India, to PJ (Sanction No. BT/PB/Center/03/2011-Phase II). The Senior Research Fellowship to MK and IM from the Department of Biotechnology and University Grants Commission (UGC), Government of India, is duly acknowledged.

ACKNOWLEDGMENTS

We would like to thank Mr. Girish H. Rajacharya (technical manager, ICGEB) for providing support with analytical instrumentation.

SUPPLEMENTARY MATERIAL

The Supplementary Material for this article can be found online at: https://www.frontiersin.org/articles/10.3389/fmicb.2021.693106/full#supplementary-material

REFERENCES

Abdelaziz, A. E. M., Leite, G. B., and Hallenbeck, P. C. (2013). Addressing the challenges for sustainable production of algal biofuels: II. Harvesting and conversion to biofuels. *Environ. Technol.* 34, 1807–1836. doi: 10.1080/09593330.2013.831487

Abdelaziz, A. E., Leite, G. B., Belhaj, M. A., and Hallenbeck, P. C. (2014). Screening microalgae native to Quebec for wastewater treatment and biodiesel production. *Bioresour. Technol.* 157, 140–148. doi: 10.1016/j.biortech.2014.01.114

Adamczyk, M., Lasek, J., and Skawinska, A. (2016). CO2 biofixation and growth kinetics of *Chlorella vulgaris* and *Nannochloropsis gaditana*. *Appl. Biochem. Biotechnol.* 179, 1248–1261. doi: 10.1007/s12010-016-2062-3

Altschul, S. F., Gish, W., Miller, W., Myers, E. W., and Lipman, D. J. (1990). Basic local alignment search tool. *J. Mol. Biol.* 215, 403–410. doi: 10.1016/s0022-2836(05)80360-2

Bailey, T. L., Johnson, J., Grant, C. E., and Noble, W. S. (2015). The MEME suite. *Nucleic Acids Res.* 43, W39–W49. doi: 10.1093/nar/gkv416

Baker, N. R. (2008). Chlorophyll fluorescence: a probe of photosynthesis in vivo. *Annu. Rev. Plant Biol.* 59, 89–113. doi: 10.1146/annurev.arplant.59.032607.092759

Barajas-Solano, A., Guzmán-Monsalve, A., and Kafarov, V. (2016). Effect of carbon–nitrogen ratio for the biomass production, hydrocarbons and lipids on *Botryoccus braunii* UIS 003. *Chem. Eng. Trans.* 49, 247–252.

Burge, C., and Karlin, S. (1997). Prediction of complete gene structures in human genomic DNA. *J. Mol. Biol.* 268, 78–94. doi: 10.1006/jmbi.1997.0951

Campenni, L., Nobre, B. P., Santos, C. A., Oliveira, A., Aires-Barros, M., Palavra, A., et al. (2013). Carotenoid and lipid production by the autotrophic microalga Chlorella protothecoides under nutritional, salinity, and luminosity stress conditions. *Appl. Microbiol. Biotechnol.* 97, 1383–1393. doi: 10.1007/s00253-012-4570-6

Carretero-Paulet, L., Galstyan, A., Roig-Villanova, I., Martínez-García, J. F., Bilbao-Castro, J. R., and Robertson, D. L. (2010). Genome-wide classification and evolutionary analysis of the bhlh family of transcription factors in arabidopsis, poplar, rice, moss, and algae. *Plant Physiol.* 153:1398. doi: 10.1104/pp.110.153593

Carriquiry, M. A., Du, X., and Timilsina, G. R. (2011). Second generation biofuels: economics and policies. *Energy policy* 39, 4222–4234. doi: 10.1016/j.enpol.2011.04.036

Cheng, L., Zhang, L., Chen, H., and Gao, C. (2006). Carbon dioxide removal from air by microalgae cultured in a membrane-photobioreactor. *Sep. Purif. Technol.* 50, 324–329. doi: 10.1016/j.seppur.2005.12.006

Chew, K. W., Yap, J. Y., Show, P. L., Suan, N. H., Juan, J. C., Ling, T. C., et al. (2017). Microalgae biorefinery: high value products perspectives. *Bioresour. Technol.* 229, 53–62. doi: 10.1016/j.biortech.2017.01.006

Chisti, Y. (2007). Biodiesel from microalgae. *Biotechnol. Adv.* 25, 294–306. doi: 10.1016/j.biotechadv.2007.02.001

Davis, R., Aden, A., and Pienkos, P. T. (2011). Techno-economic analysis of autotrophic microalgae for fuel production. *Appl. Energy* 88, 3524–3531. doi: 10.1016/j.apenergy.2011.04.018

DellaPenna, D., and Pogson, B. J. (2006). Vitamin synthesis in plants: tocopherols and carotenoids. *Annu. Rev. Plant Biol.* 57, 711–738. doi: 10.1146/annurev.arplant.56.032604.144301

Dewapriya, P., and Kim, S.-K. (2014). Marine microorganisms: an emerging avenue in modern nutraceuticals and functional foods. *Food Res. Int.* 56, 115–125. doi: 10.1016/j.foodres.2013.12.022

Emanuelsson, O., Nielsen, H., Brunak, S., and von Heijne, G. (2000). Predicting subcellular localization of proteins based on their N-terminal amino acid sequence. *J. Mol. Biol.* 300, 1005–1016. doi: 10.1006/jmbi.2000.3903

Fang, Y., Jiang, Z., Zhao, C., Li, L., Ranvilage, C. I. P. M., Liu, S., et al. (2020). Efficient heat dissipation and cyclic electron flow confer daily air exposure tolerance in the intertidal seagrass halophila beccarii asch. *Front. Plant Sci.* 11:571627. doi: 10.3389/fpls.2020.571627

Gardner, R. D., Cooksey, K. E., Mus, F., Macur, R., Moll, K., Eustance, E., et al. (2012). Use of sodium bicarbonate to stimulate triacylglycerol accumulation in the chlorophyte Scenedesmus sp. and the diatom Phaeodactylum tricornutum. *J. Appl. Phycol.* 24, 1311–1320. doi: 10.1007/s10811-011-9782-0

Gasteiger, E., Hoogland, C., Gattiker, A., Duvaud, S. E., Wilkins, M. R., Appel, R. D., et al. (2005). "Protein identification and analysis tools on the ExPASy server," in *The Proteomics Protocols Handbook*, ed. J. M. Walker (Totowa, NJ: Humana Press), 571–607. doi: 10.1385/1-59259-890-0:571

Gleize, B., Steib, M., André, M., and Reboul, E. (2012). Simple and fast HPLC method for simultaneous determination of retinol, tocopherols, coenzyme Q10 and carotenoids in complex samples. *Food Chem.* 134, 2560–2564. doi: 10.1016/j.foodchem.2012.04.043

Gong, M., and Bassi, A. (2016). Carotenoids from microalgae: a review of recent developments. *Biotechnol. Adv.* 34, 1396–1412. doi: 10.1016/j.biotechadv.2016.10.005

Grung, M., Metzger, P., and Liaaen-Jensen, S. V. (1994). Algal carotenoids 53; secondary carotenoids of algae 4; secondary carotenoids in the green alga *Botryococcus braunii*, race L, new strain. *Biochem. Syst. Ecol.* 22, 25–29. doi: 10.1016/0305-1978(94)90111-2

Guedes, A. C., Amaro, H. M., and Malcata, F. X. (2011). Microalgae as sources of high added-value compounds–a brief review of recent work. *Biotechnol. Prog.* 27, 597–613. doi: 10.1002/btpr.575

Havaux, M., and Niyogi, K. K. (1999). The violaxanthin cycle protects plants from photooxidative damage by more than one mechanism. *Proc. Natl. Acad. Sci. U.S.A.* 96, 8762–8767. doi: 10.1073/pnas.96.15.8762

Hirano, K., Hara, T., Ardianor, A., Nugroho, R. A., Segah, H., Takayama, N., et al. (2019). Detection of the oil-producing microalga *Botryococcus braunii* in natural freshwater environments by targeting the hydrocarbon biosynthesis gene SSL-3. *Sci. Rep.* 9:16974. doi: 10.1038/s41598-019-53619-y

Horton, P., Park, K. J., Obayashi, T., Fujita, N., Harada, H., Adams-Collier, C. J., et al. (2007). WoLF PSORT: protein localization predictor. *Nucleic Acids Res.* 35, W585–W587. doi: 10.1093/nar/gkm259

Ikai, A. (1980). Thermostability and aliphatic index of globular proteins. *J. Biochem.* 88, 1895–1898.

Jin, J., Dupré, C., Yoneda, K., Watanabe, M. M., Legrand, J., and Grizeau, D. (2016). Characteristics of extracellular hydrocarbon-rich microalga *Botryococcus braunii* for biofuels production: recent advances and opportunities. *Process Biochem.* 51, 1866–1875. doi: 10.1016/j.procbio.2015.11.026

Jutur, P. P., Asha, A., and Se Kwon, K. (2015). "Marine microalgae: exploring the systems through an omics approach for biofuel production," in *Marine Bioenergy-Trends And Developments*, eds S. K. Kim and C. G. Lee (Abingdon: Taylor and Francis Group), 149–162.

Kajikawa, M., Kinohira, S., Ando, A., Shimoyama, M., Kato, M., and Fukuzawa, H. (2015). Accumulation of squalene in a microalga chlamydomonas reinhardtii by genetic modification of squalene synthase and squalene epoxidase genes. *PLoS One* 10:e0120446. doi: 10.1371/journal.pone.0120446

Kanehisa, M., Goto, S., Furumichi, M., Tanabe, M., and Hirakawa, M. (2010). KEGG for representation and analysis of molecular networks involving diseases and drugs. *Nucleic Acids Res.* 38(suppl_1), D355–D360.

Kareya, M. S., Mariam, I., Shaikh, K. M., Nesamma, A. A., and Jutur, P. P. (2020). Photosynthetic carbon partitioning and metabolic regulation in response to very-low and high CO2 in microchloropsis gaditana NIES 2587. *Front. Plant Sci.* 11:981. doi: 10.3389/fpls.2020.00981

Khan, M. I., Shin, J. H., and Kim, J. D. (2018). The promising future of microalgae: current status, challenges, and optimization of a sustainable and renewable industry for biofuels, feed, and other products. *Microb. Cell Fact.* 17:36. doi: 10.1186/s12934-018-0879-x

King, B. R., and Guda, C. (2007). ngLOC: an n-gram-based Bayesian method for estimating the subcellular proteomes of eukaryotes. *Genome Biol.* 8:R68. doi: 10.1186/gb-2007-8-5-r68

Klughammer, C., and Schreiber, U. (1994). Saturation pulse method for assessment of energy conversion in PS I. *Planta* 192, 261–268.

Kumar, S., Stecher, G., Li, M., Knyaz, C., and Tamura, K. (2018). MEGA X: molecular evolutionary genetics analysis across computing platforms. *Mol. Biol. Evol.* 35, 1547–1549. doi: 10.1093/molbev/msy096

Lange, B. M., Rujan, T., Martin, W., and Croteau, R. (2000). Isoprenoid biosynthesis: the evolution of two ancient and distinct pathways across genomes. *Proc. Natl. Acad. Sci. U.S.A.* 97, 13172–13177. doi: 10.1073/pnas.240454797

Leite, G. B., Paranjape, K., Abdelaziz, A. E., and Hallenbeck, P. C. (2015). Utilization of biodiesel-derived glycerol or xylose for increased growth and lipid production by indigenous microalgae. *Bioresour. Technol.* 184, 123–130. doi: 10.1016/j.biortech.2014.10.117

Lichtenthaler, H. K., Rohmer, M., Schwender, J., Disch, A., and Seemann, M. (1997). "A novel mevalonate-independent pathway for the biosynthesis of carotenoids, phytol and prenyl chain of plastoquinone-9 in green algae and higher plants," in *Physiology, Biochemistry and Molecular Biology of Plant Lipids*, eds J. P. Williams, M. U. Khan, and N. W. Lem (Dordrecht: Springer Netherlands), 177–179. doi: 10.1007/978-94-017-2662-7_56

Lim, D. K. Y., Schuhmann, H., Sharma, K., and Schenk, P. M. (2015). Isolation of high-lipid tetraselmis suecica strains following repeated UV-C mutagenesis, FACS, and high-throughput growth selection. *BioEnergy Res.* 8, 750–759. doi: 10.1007/s12155-014-9553-2

Lohr, M., Schwender, J., and Polle, J. E. (2012). Isoprenoid biosynthesis in eukaryotic phototrophs: a spotlight on algae. *Plant Sci.* 185-186, 9–22. doi: 10.1016/j.plantsci.2011.07.018

Lu, J., Yin, Z., Lu, T., Yang, X., Wang, F., Qi, M., et al. (2020). Cyclic electron flow modulate the linear electron flow and reactive oxygen species in tomato leaves under high temperature. *Plant Sci.* 292:110387. doi: 10.1016/j.plantsci.2019.110387

Mariam, I., Kareya, M. S., Nesamma, A. A., and Jutur, P. P. (2021). Delineating metabolomic changes in native isolate Aurantiochytrium for production of docosahexaenoic acid in presence of varying carbon substrates. *Algal Res.* 55:102285. doi: 10.1016/j.algal.2021.102285

Markou, G., and Nerantzis, E. (2013). Microalgae for high-value compounds and biofuels production: a review with focus on cultivation under stress conditions. *Biotechnol. Adv.* 31, 1532–1542. doi: 10.1016/j.biotechadv.2013.07.011

Matsushima, D., Jenke-Kodama, H., Sato, Y., Fukunaga, Y., Sumimoto, K., Kuzuyama, T., et al. (2012). The single cellular green microalga *Botryococcus braunii*, race B possesses three distinct 1-deoxy-D-xylulose 5-phosphate synthases. *Plant Sci.* 18, 309–320. doi: 10.1016/j.plantsci.2012.01.002

Menon, K. R., Balan, R., and Suraishkumar, G. (2013). Stress induced lipid production in *Chlorella vulgaris*: relationship with specific intracellular reactive species levels. *Biotechnol. Bioeng.* 110, 1627–1636. doi: 10.1002/bit.24835

Misra, N., Panda, P. K., Parida, B. K., and Mishra, B. K. (2012). Phylogenomic study of lipid genes involved in microalgal biofuel production-candidate gene mining and metabolic pathway analyses. *Evol. Bioinform. Online* 8, 545–564. doi: 10.4137/ebo.s10159

Nobre, B. P., Villalobos, F., Barragán, B. E., Oliveira, A. C., Batista, A. P., Marques, P. A., et al. (2013). A biorefinery from *Nannochloropsis* sp. microalga–extraction of oils and pigments. Production of biohydrogen from the leftover biomass. *Bioresour. Technol.* 135, 128–136. doi: 10.1016/j.biortech.2012.11.084

Ogunkunle, O., and Ahmed, N. A. (2019). A review of global current scenario of biodiesel adoption and combustion in vehicular diesel engines. *Energy Rep.* 5, 1560–1579. doi: 10.1016/j.egyr.2019.10.028

Olaizola, M., Duerr, E., and Freeman, D. (1991). Effect of CO2 enhancement in an outdoor algal production system using *Tetraselmis*. *J. Appl. Phycol.* 3, 363–366. doi: 10.1007/BF00026099

Paliwal, C., and Jutur, P. P. (2021). Dynamic allocation of carbon flux triggered by task-specific chemicals is an effective non-gene disruptive strategy for sustainable and cost-effective algal biorefineries. *Chem. Eng. J.* 418:129413. doi: 10.1016/j.cej.2021.129413

Paliwal, C., Mitra, M., Bhayani, K., Bharadwaj, S. V. V., Ghosh, T., Dubey, S., et al. (2017). Abiotic stresses as tools for metabolites in microalgae. *Bioresour. Technol.* 244, 1216–1226. doi: 10.1016/j.biortech.2017.05.058

Potter, S. C., Luciani, A., Eddy, S. R., Park, Y., Lopez, R., and Finn, R. D. (2018). HMMER web server: 2018 update. *Nucleic Acids Res.* 46, W200–W204. doi: 10.1093/nar/gky448

Raja, R., Hemaiswarya, S., Kumar, N. A., Sridhar, S., and Rengasamy, R. (2008). A perspective on the biotechnological potential of microalgae. *Crit. Rev. Microbiol.* 34, 77–88. doi: 10.1080/10408410802086783

Rao, A. R., Ravishankar, G., and Sarada, R. (2012). Cultivation of green alga Botryococcus braunii in raceway, circular ponds under outdoor conditions and its growth, hydrocarbon production. *Bioresour. Technol.* 123, 528–533. doi: 10.1016/j.biortech.2012.07.009

Ratha, S. K., and Prasanna, R. (2012). Bioprospecting microalgae as potential sources of "Green Energy"—challenges and perspectives (Review). *Appl. Biochem. Microbiol.* 48, 109–125. doi: 10.1134/S000368381202010X

Rosa Putra, S., Disch, A., Bravo, J.-M., and Rohmer, M. (1998). Distribution of mevalonate and glyceraldehyde 3-phosphate/pyruvate routes for isoprenoid biosynthesis in some Gram-negative bacteria and mycobacteria. *FEMS Microbiol. Lett.* 164, 169–175. doi: 10.1111/j.1574-6968.1998.tb13082.x

Sampathkumar, S. J., and Gothandam, K. M. (2019). Sodium bicarbonate augmentation enhances lutein biosynthesis in green microalgae *Chlorella pyrenoidosa*. *Biocatal. Agric. Biotechnol.* 22:101406. doi: 10.1016/j.bcab.2019.101406

Scodelaro Bilbao, P. G., Garelli, A., Díaz, M., Salvador, G. A., and Leonardi, P. I. (2020). Crosstalk between sterol and neutral lipid metabolism in the alga *Haematococcus pluvialis* exposed to light stress. *Biochim. Biophys. Acta (BBA) Mol. Cell Biol. Lipids* 1865:158767. doi: 10.1016/j.bbalip.2020.158767

Sforza, E., Simionato, D., Giacometti, G. M., Bertucco, A., and Morosinotto, T. (2012). Adjusted light and dark cycles can optimize photosynthetic efficiency in algae growing in photobioreactors. *PLoS One* 7:e38975. doi: 10.1371/journal.pone.0038975

Shaikh, K. M., Kumar, P., Nesamma, A. A., Abdin, M. Z., and Jutur, P. P. (2020). Hybrid genome assembly and functional annotation reveals insights on lipid biosynthesis of oleaginous native isolate Parachlorella kessleri, a potential industrial strain for production of biofuel precursors. *Algal Res.* 52:102118. doi: 10.1016/j.algal.2020.102118

Shaikh, K. M., Nesamma, A. A., Abdin, M. Z., and Jutur, P. P. (2019). Molecular profiling of an oleaginous trebouxiophycean alga Parachlorella kessleri subjected to nutrient deprivation for enhanced biofuel production. *Biotechnol. Biofuels* 12:182. doi: 10.1186/s13068-019-1521-9

Singh, R., Paliwal, C., Nesamma, A. A., Narula, A., and Jutur, P. P. (2020). Nutrient deprivation mobilizes the production of unique tocopherols as a

stress-promoting response in a new indigenous isolate *Monoraphidium* sp. *Front. Mar. Sci.* 7:575817. doi: 10.3389/fmars.2020.575817

Spolaore, P., Joannis-Cassan, C., Duran, E., and Isambert, A. (2006). Commercial applications of microalgae. *J. Biosci. Bioeng.* 101, 87–96. doi: 10.1263/jbb.101.87

Srinivasan, R., Mageswari, A., Subramanian, P., Suganthi, C., Chaitanyakumar, A., Aswini, V., et al. (2018). Bicarbonate supplementation enhances growth and biochemical composition of *Dunaliella salina* V-101 by reducing oxidative stress induced during macronutrient deficit conditions. *Sci. Rep.* 8, 1–14.

Sun, H., Zhang, S.-B., Liu, T., and Huang, W. (2020). Decreased photosystem II activity facilitates acclimation to fluctuating light in the understory plant *Paris polyphylla*. *Biochim.Biophys. Acta (BBA) Bioenerg.* 1861:148135. doi: 10.1016/j.bbabio.2019.148135

Sun, X.-M., Ren, L.-J., Zhao, Q.-Y., Ji, X.-J., and Huang, H. (2018). Microalgae for the production of lipid and carotenoids: a review with focus on stress regulation and adaptation. *Biotechnol. Biofuels* 11:272. doi: 10.1186/s13068-018-1275-9

Szklarczyk, D., Gable, A. L., Lyon, D., Junge, A., Wyder, S., Huerta-Cepas, J., et al. (2019). STRING v11: protein–protein association networks with increased coverage, supporting functional discovery in genome-wide experimental datasets. *Nucleic Acids Res.* 47, D607–D613. doi: 10.1093/nar/gky1131

Tapie, P., and Bernard, A. (1988). Microalgae production: technical and economic evaluations. *Biotechnol. Bioeng.* 32, 873–885. doi: 10.1002/bit.260320705

Tsai, C.-H., Warakanont, J., Takeuchi, T., Sears, B. B., Moellering, E. R., and Benning, C. (2014). The protein Compromised Hydrolysis of Triacylglycerols 7 (CHT7) acts as a repressor of cellular quiescence in *Chlamydomonas*. *Proc. Natl. Acad. Sci. U.S.A.* 111, 15833–15838. doi: 10.1073/pnas.1414567111

Uchida, H., Mizohata, E., and Okada, S. (2018). Docking analysis of models for 4-hydroxy-3-methylbut-2-enyl diphosphate reductase and a ferredoxin from *Botryococcus braunii*, race B. *Plant Biotechnol. (Tokyo, Japan)* 35, 297–301. doi: 10.5511/plantbiotechnology.18.0601a

Wang, Z., Zhang, L., Dong, C., Guo, J., Jin, L., Wei, P., et al. (2021). Characterization and functional analysis of phytoene synthase gene family in tobacco. *BMC Plant Biol.* 21:32. doi: 10.1186/s12870-020-02816-3

Xi, Y., Wang, J., Xue, S., and Chi, Z. (2020). β-Carotene production from *Dunaliella salina* cultivated with bicarbonate as carbon source. *J. Microbiol. Biotechnol.* 30, 868–877. doi: 10.4014/jmb.1910.10035

Yoshimura, T., Okada, S., and Honda, M. (2013). Culture of the hydrocarbon producing microalga *Botryococcus braunii* strain showa: optimal CO2, salinity, temperature, and irradiance conditions. *Bioresour. Technol.* 133, 232–239. doi: 10.1016/j.biortech.2013.01.095

Yu, C.-S., Lin, C.-J., and Hwang, J.-K. (2004). Predicting subcellular localization of proteins for Gram-negative bacteria by support vector machines based on n-peptide compositions. *Protein Sci.* 13, 1402–1406. doi: 10.1110/ps.03479604

Zeng, L., and Dehesh, K. (2021). The eukaryotic MEP-pathway genes are evolutionarily conserved and originated from Chlaymidia and cyanobacteria. *BMC Genomics* 22:137. doi: 10.1186/s12864-021-07448-x

Zhou, X., Welsch, R., Yang, Y., Álvarez, D., Riediger, M., Yuan, H., et al. (2015). Arabidopsis OR proteins are the major posttranscriptional regulators of phytoene synthase in controlling carotenoid biosynthesis. *Proc. Natl. Acad. Sci.U.S.A.* 112:3558. doi: 10.1073/pnas.1420831112

Conflict of Interest: The authors declare that the research was conducted in the absence of any commercial or financial relationships that could be construed as a potential conflict of interest.

Publisher's Note: All claims expressed in this article are solely those of the authors and do not necessarily represent those of their affiliated organizations, or those of the publisher, the editors and the reviewers. Any product that may be evaluated in this article, or claim that may be made by its manufacturer, is not guaranteed or endorsed by the publisher.

frontiers in Microbiology

METHODS
published: 04 August 2021
doi: 10.3389/fmicb.2021.717033

Exploration of an Efficient Electroporation System for Heterologous Gene Expression in the Genome of Methanotroph

Lizhen Hu[1†], Shuqi Guo[1†], Xin Yan[2], Tianqing Zhang[1], Jing Xiang[1] and Qiang Fei[1,3]*

[1] School of Chemical Engineering and Technology, Xi'an Jiaotong University, Xi'an, China, [2] Key Laboratory of Agricultural Environmental Microbiology, Ministry of Agriculture, College of Life Sciences, Nanjing Agricultural University, Nanjing, China, [3] Shaanxi Key Laboratory of Energy Chemical Process Intensification, Xi'an Jiaotong University, Xi'an, China

OPEN ACCESS

Edited by:
Yu Wang,
Tianjin Institute of Industrial Biotechnology, Chinese Academy of Sciences, China

Reviewed by:
Yongjin Zhou,
Dalian Institute of Chemical Physics Chinese Academy of Sciences (CAS), China
Toshiaki Kamachi,
Tokyo Institute of Technology, Japan

***Correspondence:**
Qiang Fei
feiqiang@xjtu.edu.cn

[†] These authors have contributed equally to this work

Specialty section:
This article was submitted to Microbiotechnology, a section of the journal Frontiers in Microbiology

Received: 30 May 2021
Accepted: 07 July 2021
Published: 04 August 2021

Citation:
Hu L, Guo S, Yan X, Zhang T, Xiang J and Fei Q (2021) Exploration of an Efficient Electroporation System for Heterologous Gene Expression in the Genome of Methanotroph. Front. Microbiol. 12:717033. doi: 10.3389/fmicb.2021.717033

One-carbon (C1) substrates such as methane and methanol have been considered as the next-generation carbon source in industrial biotechnology with the characteristics of low cost, availability, and bioconvertibility. Recently, methanotrophic bacteria naturally capable of converting C1 substrates have drawn attractive attention for their promising applications in C1-based biomanufacturing for the production of chemicals or fuels. Although genetic tools have been explored for metabolically engineered methanotroph construction, there is still a lack of efficient methods for heterologous gene expression in methanotrophs. Here, a rapid and efficient electroporation method with a high transformation efficiency was developed for a robust methanotroph of *Methylomicrobium buryatense* 5GB1. Based on the homologous recombination and high transformation efficiency, gene deletion and heterologous gene expression can be simultaneously achieved by direct electroporation of PCR-generated linear DNA fragments. In this study, the influence of several key parameters (competent cell preparation, electroporation condition, recovery time, and antibiotic concentration) on the transformation efficiency was investigated for optimum conditions. The maximum electroporation efficiency of 719 ± 22.5 CFU/μg DNA was reached, which presents a 10-fold improvement. By employing this method, an engineered *M. buryatense* 5GB1 was constructed to biosynthesize isobutyraldehyde by replacing an endogenous *fadE* gene in the genome with a heterologous *kivd* gene. This study provides a potential and efficient strategy and method to facilitate the cell factory construction of methanotrophs.

Keywords: one-carbon substrate, site-specific chromosome expression, transformation efficiency, gene deletion, heterologous gene expression, methanotroph

INTRODUCTION

Methane, derived from natural gas and biogas, is the second most abundant greenhouse gas whose global warming potential is 25 times more than that of carbon dioxide (Fei et al., 2014; Pariatamby et al., 2015). Excessive methane emissions can not only cause a waste of carbon sources but also endanger the environment by causing the global warming effect (Bjorck et al., 2018;

Hu et al., 2020). Thus, it is urgent to seek a potential, green, and sustainable strategy for the efficient utilization of methane.

With the development of molecular biology, the bioconversion of methane into chemicals or biofuels by special industrial microbial catalysts has become a promising trend for its mitigation (Nguyen and Lee, 2020). Compared with chemical methods, the biological routes of methane utilization are relatively simple with the potential to directly activate methane at ambient temperature and atmospheric pressure (Conrado and Gonzalez, 2014). Methanotrophs are capable of utilizing methane as the sole energy and carbon source, which also constituted the main biocatalysts for the production of C1-based chemicals or biofuels (Hur et al., 2017; Su et al., 2017; Nguyen et al., 2018). Notably, the methanotroph *Methylomicrobium buryatense* 5GBl, which can utilize one-carbon (C1) substrates (methane and methanol) for growth, has been studied extensively and in depth due to its promising characteristics for industrial application, including a fast growth rate, strong anti-contamination ability, a robust endogenous methane assimilation pathway, and the availability of genetic manipulation tools and bioreactor (Alexey et al., 2015; Yan et al., 2016; Fei et al., 2018). Currently, conjugation-based transformation plays an important role in achieving gene transfer and expression in *M. buryatense* 5GBl (Puri et al., 2015), which usually requires a helper strain such as *Escherichia coli* S17-1 λpir to transfer DNA into a host due to the restriction–modification (R-M) system (Yan et al., 2016). Nevertheless, the time-consuming elimination of *E. coli* after conjugation limited the use of this method. Hence, to broaden the industrial application of *M. buryatense* 5GBl in C1 substrate conversion, many gaps still need to be further solved, especially the development of efficient genetic manipulation methods for the metabolic engineering of methanotrophs.

Electroporation, as a direct gene transfer system, is widely used in various bacteria for DNA transfer (Itoh et al., 1994). It is reported that the key steps such as the preparation of competent cells, electroporation process, recovery process, and plating screening mainly affect the number of transformants and the transformation efficiency during the electroporation process (Fu et al., 2017; Morales-Ruiz et al., 2019). Moreover, compared with conjugation-based transformation methods, the electroporation method is relatively easy to perform for directly and efficiently inserting DNA fragments into specific sites of the genome to complete the heterologous gene expression. Because the R-M system of *M. buryatense* 5GBl can be interfered by the plasmid transfer during electroporation, it could be an ideal choice to introduce linear DNA fragments by electroporation for efficiently achieving gene deletion and plasmid-free gene expression. In addition, the marker system Flp/FRT and a markerless system using the counterselectable marker *sacB* or *pheS* have been used for chromosomal modification in methanotrophs (Liu et al., 2021), but an available and efficient method to establishing a common site for completing heterologous gene expression in the genome of *M. buryatense* 5GBl is still required.

This study aimed to develop a site-specific chromosome expression (SSCE) method with an efficient electroporation system for methanotrophs using an antibiotic-selected marker due to its stability (Yan et al., 2016). Since the deletion of beta-oxidation did not show a negative influence on the growth of *M. buryatense* 5GB1 (Demidenko et al., 2016), the position of the *fadE* gene on the chromosome was selected as a specific site. The key parameters of the gene manipulation method, such as the DNA concentration, cell density, methanol concentration, recovery time, field strength, and the antibiotic concentration, that affect the transformation efficiency of *M. buryatense* 5GBl were investigated and optimized in this study. To demonstrate the feasibility of this novel electroporation-based method, the gene deletion and heterologous gene expression strategies in *M. buryatense* 5GBl were established by artificially replacing the endogenous *fadE* gene with the heterologous *kivd* gene for isobutyraldehyde biosynthesis. Finally, the performances of the plasmid-based method and the SSCE method were analyzed and compared in order to evaluate the specific site of *fadE* for exogenous gene expression.

MATERIALS AND METHODS

Strains, Plasmid, Culture, and Antibiotic Screening

The strains and plasmids used in the study are listed in **Table 1**. Competent cells (*E. coli* DH5α) were cultured on Luria broth (LB) agar plates and *M. buryatense* 5GBlS were stocked on nitrate mineral salt (NMS) agar medium with 1% methanol. Liquid cultures of 50 ml were used for culturing *M. buryatense* 5GBlS in 250-ml flasks in a shaker at 30°C and 200 rpm. The mating plate (NMS2) consisted of 85% NMS and 15% LB agar culture media. The concentrations of the carbonate buffer and the phosphate buffer were individually adjusted to 5 and 5.8 mM, respectively, for the conjugation process, according to a previous report (Puri et al., 2015). Methanol, which could fulfill the requirements of genetic manipulation for the growth of *M. buryatense* 5GBlS, was utilized as the carbon source in all methanotrophic cultures instead of methane to simplify the procedure of cultivation (Hu and Lidstrom, 2014; Wang et al., 2020). The antibiotic concentrations used for screening colonies were as follows: kanamycin (Km^r), 50–100 μg/ml; gentamicin (Gm^r), 10–40 μg/ml. All experiments were carried out in duplicate or triplicate. Data were processed and analyzed with SPSS 18.0 software, and *P*-values with statistical significance at $P < 0.05$ were obtained.

DNA Manipulation

The plasmid pAWP89 was separated from *E. coli* DH5α with an AxyPrep Plasmid Miniprep Kit (Axygen, Suzhou, China) and linearized by NSPl (NEB, Beijing, China). The concentration of DNA was measured by the DS-11 spectrophotometer (DeNovix, Wilmington, DE, United States). The oligonucleotides used to amplify the DNA fragments are listed in **Supplementary Table 1**. The complex (DNA fragment) was obtained by overlap PCR. The fragments were retrieved using MonPure Gel and PCR Clean Kit (Monad Biotech, Wuhan, China). The transformants were identified by two oligonucleotides of the target gene, and a 2 × Rapid Taq Master Mix (Vazyme, Nanjing,

TABLE 1 | List of the strains and plasmids used in the study.

Strains and plasmids	Description	References
E. coli DH5α	*E. coli*, F^-, φ80, *lac*ZΔM15, Δ(*lac*ZYA-*arg*F) U169 *end*A1, *rec*A1, *hsd*R17 (r_k^-, m_k^+) supE44, λ^-, *thi*-1, *gyr*A96, *rel*A1, *pho*A	Sangon Biotech Co. (Shanghai, China)
E. coli DH5α-*kivd*	Variant of *E. coli* DH5α, Km^r, pAWP89 vector containing *kivd*	This study
E. coli DH5α (pRK600)	Variant of *E. coli* DH5α, Cm^r, triparental conjugation helper	This study
M. buryatense 5GBlS	Variant of *M. buryatense* 5GB1, capable of being conjugated with small IncP-based plasmid	Puri et al., 2015
M. buryatense 5GBlSΔ*fadE*	*M. buryatense* 5GBlSΔ*fadE*:Km^r (MBURv2_190114)	This study
M. buryatense 5GBlSΔ*fadE*:Km^r:*kivd*	Variant of *M. buryatense* 5GB1SΔ*fadE*; Km^r and *kivd* were attached to the *fadE* site in the genome.	This study
M. buryatense 5GBlSΔ*fadE*:Gm^r:*pos*5	Variant of *M. buryatense* 5GB1SΔ*fadE*; Gm^r and *pos*5 were attached to the *fadE* site in the genome.	This study
M. buryatense 5GBlS-pAWP89:*kivd*	Variant of *M. buryatense* 5GB1S, containing pHLZ66	This study
pAWP89	IncP-based broad host range plasmid containing dTomato, Km^r	Puri et al., 2015
pHLZ66	Variant of pAWP89 containing *kivd*, Km^r	This study

China) was used. The Ezup Column Bacteria Genomic DNA Purification Kit (Sangon Biotech Co., Shanghai, China) was used to extract genomic DNA.

Electroporation Protocol

Methylomicrobium buryatense 5GBlS was firstly cultured at 30°C with shaking until the optical density at 600-nm wavelength (OD_{600}) reaches 2.0, checked with UV spectrophotometry (TU-1810, PERSEE, Beijing, China). Then, the cells in the logarithmic phase were collected and 50 ml of the bacterial solution was centrifuged to remove supernatants (5,000 × *g*, 10 min at 4°C), then cleaned three times with ice-cold water (autoclave sterilization, 121°C for 20 min). Finally, methanotroph competent cells were completely dissolved with 500 μl deionized water, and 50 μl of competent cells was mixed with 100, 200, 400, 600, 800, or 1,000 ng of DNA fragment. For the electroporation process, 1-mm-gap cuvettes were placed into the Gemini SC2 instrument (BTX, Holliston, MA, United States) to finish the electroporation process. After electroporation, 1 ml of fresh NMS was added to the cuvette, which was transferred into the 10 ml NMS medium in 250-ml serum bottles. Different concentrations of methanol (0.02–0.5%) were added to the resuscitation medium to culture the cells. The cells were collected and transferred into plates containing different concentrations of kanamycin after 3, 6, 9, 12, and 24 h of resuscitation. The plates were incubated for 4 days at 30°C for screening of transformants. The cell density (1.0, 2.9, 4.9, 9.7, and 19.4 × 10^{11} CFU/ml), field strength (12, 15, 18, and 25 kV/cm), and recovery time (3, 6, 9, 12, and 24 h) were also explored individually in the study for higher transformation efficiency by electroporation.

The basic conditions used in this method were as follows: cell density, OD_{600} = 0.4–0.6; DNA concentration, 500–1,000 ng; field strength, 12–20 kV/cm; methanol concentration, 0.02–0.5% in NMS medium; and resistance concentration, 50–100 μg/ml (Yan et al., 2016; Nguyen et al., 2018; Liu et al., 2021). According to the conditions mentioned above, the basic transformation parameters set as the standard conditions in this experiment were as follows: cell density, 4.9 × 10^{11} CFU/ml; DNA concentration, 600 ng; electric field strength, 15 kV/cm; methanol concentration, 0.1%; and resistance concentration, 50 μg/ml. Among them, a cell density of 4.9 × 10^{11} CFU/ml was obtained according to the initial cell density given in the reference (OD_{600} = 0.4; 50 ml culture solution was concentrated to 200 μl) (Nguyen et al., 2018).

Method for Recombinant Plasmid Transfer

Escherichia coli DH5α, *M. buryatense* 5GBlS, and *E. coli* DH5α (PRK600) were involved in the conjugation process. NMS2 mating plates were prepared according to a previous literature (Puri et al., 2015). Firstly, we transferred the recombinant plasmid pHLZ66 into *E. coli* DH5α (donor bacteria). Secondly, one loop of *M. buryatense* 5GBlS was evenly coated in NMS2 mating plates (15% LB + 85% NMS) and cultured overnight at 30°C. Then, *E. coli* DH5α and PRK600 were cultured on LB medium overnight at 37°C. Equal volumes of *E. coli* DH5α and *E. coli* DH5α (PRK600) were evenly spread on NMS2 mating plates and cultured at 30°C for 2 days. One loop of mixed cells was transferred to a selective NMS plate with kanamycin (100 μg/ml) for the selection of transconjugants, which were then transferred into a new selective NMS plate.

Isobutyraldehyde Detection

The concentration of isobutyraldehyde was determined using Agilent Technologies 7890A GC System (Agilent Technologies, Santa Clara, CA, United States) with a DB-Wax column (30 m × 0.32 mm × 0.5 μm; Agilent Technologies) and a flame ionization detector. The flow rates of hydrogen, air, and nitrogen were 30, 400, and 25 ml/min, respectively. The oven temperature was held at 35°C for 5 min, then heated to 230°C at a rate of 12°C/min, and ending at 230°C. The retention time of isobutyraldehyde was 1.667 min. A standard curve was obtained

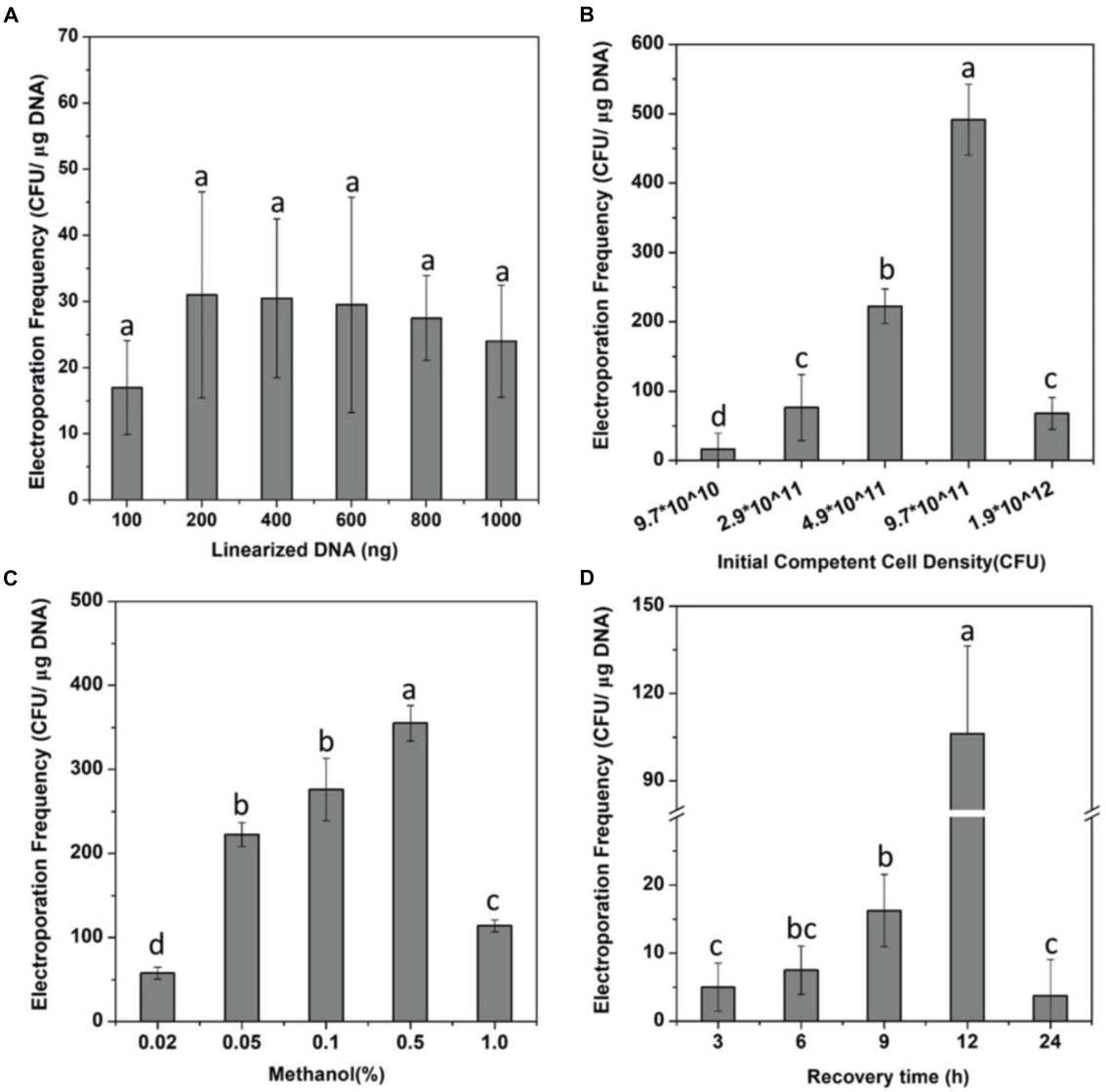

FIGURE 1 | Optimization of the electroporation system. **(A)** Effect of the number of linearized DNA fragments on the electroporation efficiency of strain *Methylomicrobium buryatense* 5GBlSΔ*fadE*. **(B–D)** Effects of the cell density **(B)**, methanol concentration **(C)**, and the recovery time **(D)** on the electroporation efficiency of strain *Methylomicrobium buryatense* 5GB1S. *Lowercase letters above bars* indicate significant differences ($P < 0.05$).

after commercial isobutyraldehyde was treated with the sample with the above method.

RESULTS

Establishment of a Fast Electroporation Method for Endogenous Gene Deletion

Although it has been shown that DNA transfer can be achieved through electroporation into methanotrophs (Yan et al., 2016; Nguyen et al., 2018; Liu et al., 2021), optimum conditions of the electroporation system for *M. buryatense* 5GBlS are still needed to ensure a higher transformation efficiency of gene deletion before developing the SSCE method. After obtaining the *fadE* gene deletion complex (PCR product) for the construction of *M. buryatense* 5GBlSΔ*fadE* by electroporation (**Supplementary Figure 1**), the influence of six different DNA concentrations on the number of transformants was firstly investigated. As can be seen in **Figure 1A**, the number of transformants was less than 20 at a DNA concentration of 100 ng, which increased to up to 30 at 200 ng, which is in good agreement with a previous report (Yekta et al., 2013). However, the number of transformants showed a plateau effect after using 400 ng DNA, which was finally selected for subsequent experiments.

The cell density can also affect the transformation efficiency, showing a positive relation in **Figure 1B**. At a cell density of 3.9×10^{11} CFU/ml, the transformation efficiency increased to 14 times higher than that of 1.0×10^{11} CFU/ml; the

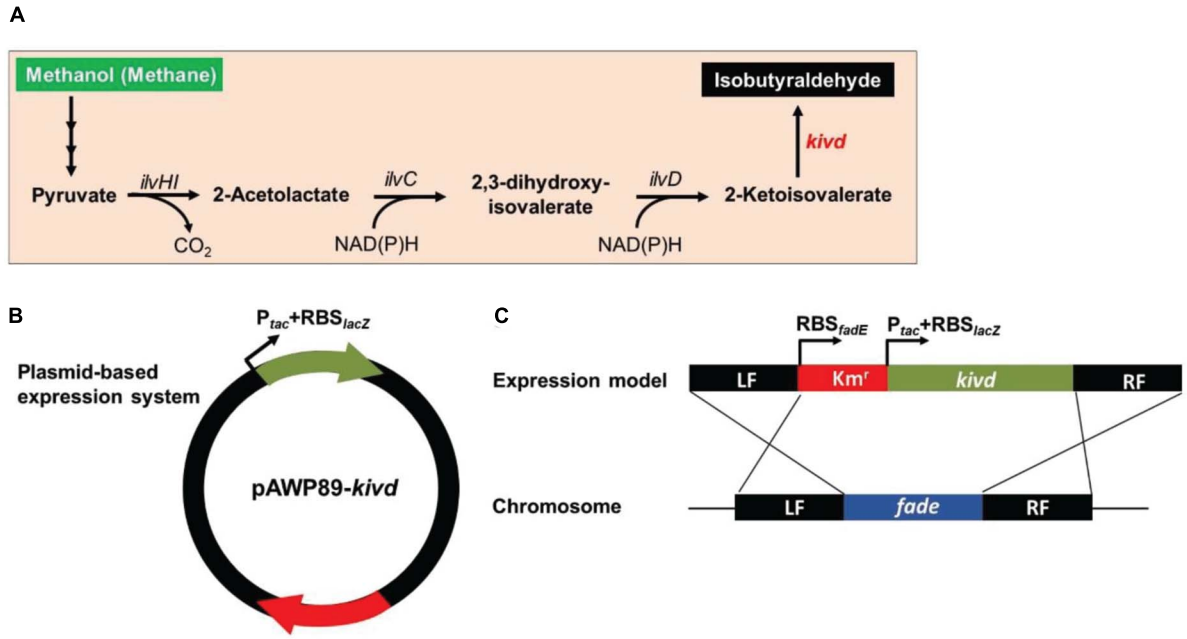

FIGURE 2 | Framework of the heterologous expression of 2-ketoisovalerate decarboxylase (KivD) in strain *Methylomicrobium buryatense* 5GB1S. **(A)** Artificial pathway for isobutyraldehyde production from methanol or methane in strain *M. buryatense* 5GB1S. **(B)** Scheme of the plasmid-based expression of the foreign gene *kivd* in strain *M. buryatense* 5GB1S. **(C)** Scheme of the integration of the foreign gene *kivd* into the chromosome of strain *M. buryatense* 5GB1S. *Word in red* represents an exogenous gene. *Words in black* represent endogenous genes. These genes coded for acetohydroxyacid synthase (*ilvHI*), acetohydroxyacid isomeroreductase (*ilvC*), and dihydroxyacid dehydratase (*ilvD*). *Intersecting lines* indicate homologous recombination. *LF*, left flanking region; *RF*, right flanking region.

highest transformation efficiency in *M. buryatense* 5GBlSΔ*fadE* of 491 CFU/μg DNA was achieved at a cell density of 9.7×10^{11} CFU/ml, which can be considered as a statistically significant effect. These findings can be explained by the higher cell concentration indirectly promoting the efficiency of transformation by increasing the probability of binding with DNA. Nevertheless, when the cell density was 1.9×10^{12} CFU/ml, the transformation efficiency was less than 100 CFU/μg DNA. Methanol, as an essential carbon source, was explored for cell recovery and growth after electroporation. As shown in **Figure 1C**, when the concentration of methanol added into NMS increased from 0.02 to 0.5%, the transformation efficiency was enhanced from less than 60 to up to 400 CFU/μg DNA. These results revealed that a higher methanol concentration is needed to improve the transformation efficiency by promoting the growth and reproduction of transformants. But it is worth noting that only a few transformants were observed with the concentration of 1%, which may be due to the inhibition effect of methanol.

In addition, studies have shown that the field strength and antibiotic concentration also affected the efficiency of transformation because a high field strength during electroporation is likely to destabilize the cell walls of Gram-positive bacteria and different antibiotic concentrations can affect the growth and reproduction of transformants (Dower et al., 1988; Mcintyre and Harlander, 1989; Steele et al., 1994; Shimogawara et al., 1998; Min et al., 2018). However, our data showed that field strength of 12–25 kV/cm and antibiotic concentrations of 50–100 μg/ml did not provide significant improvements in the transformation efficiency of *M. buryatense* 5GBlS (data not shown). The process of recovery is a stage of cell growth, reproduction, damage repair, and resistance gene expression (Li et al., 2014). Therefore, a relatively long recovery benefits the rapid growth of cells and the successful recombination of exogenous DNA fragments into the genome. However, a satisfactory transformation efficiency can only be achieved with a recovery time of 12 h (**Figure 1D**). In the end, the electroporation conditions used for the SSCE method were as follows: cell density, $OD_{600} = 9.7 \times 10^{11}$ CFU/ml; field strength, 18 kV/cm; recovery time, 12 h; carbon source concentration, 0.5%; and kanamycin concentration, 100 μg/ml. Finally, the highest transformation efficiency for *fadE* gene deletion was 719 ± 22.5 CFU/μg DNA, which was 10 times more than that of the initial condition (66.25 CFU/μg DNA).

Development of the SSCE Method for Heterologous Gene Expression

To evaluate the SSCE method, *M. buryatense* 5GBlS was engineered for the biosynthesis of isobutyraldehyde, which is the key precursor of isobutanol applied as an attractive fuel substitute (Atsumi et al., 2010). The gene encoding alpha-ketoisovalerate decarboxylase (KivD) from *Lactococcus lactis*, which can catalyze 3-methyl-2-oxybutyric acid to isobutyraldehyde, was used as the heterologous gene, as shown in **Figure 2A**. Two strategies can be employed for the expression of the heterologous gene *kivd* in methanotrophs: a plasmid-based expression (**Figure 2B**) and

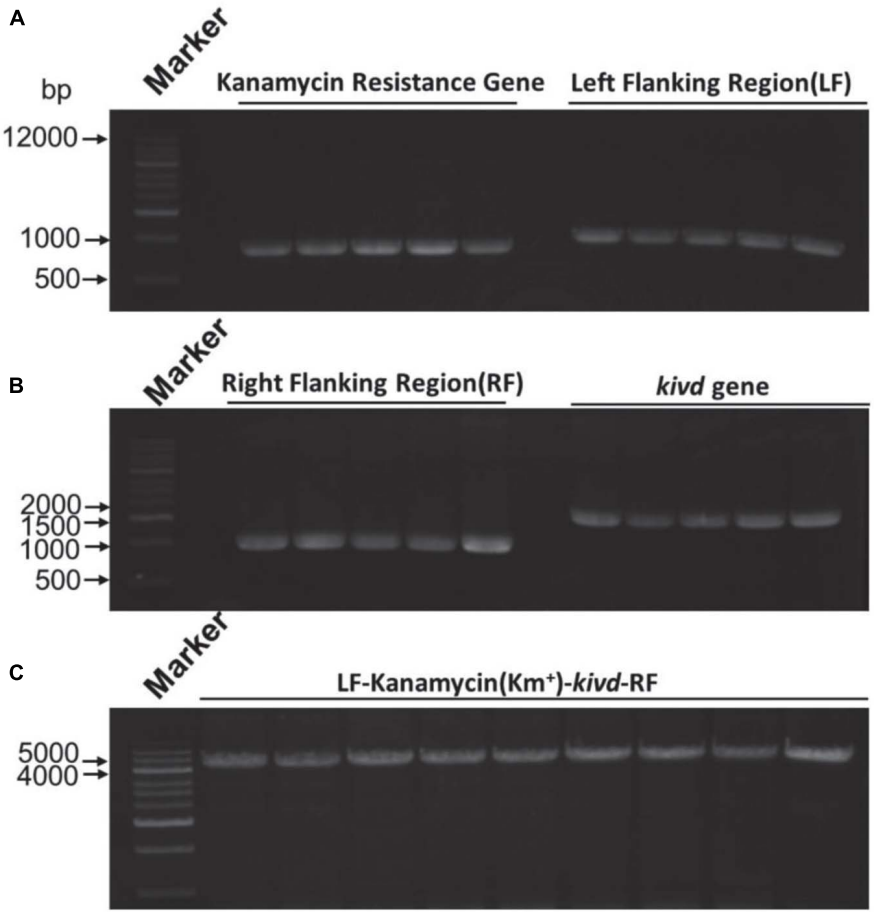

FIGURE 3 | Expression of the *kivd* gene in the *fadE* site of strain *Methylomicrobium buryatense* 5GB1S. **(A)** Agarose gel electrophoresis results of the kanamycin gene (816 bp) and the left flanking region (1,000 bp) for *kivd* expression. **(B)** Agarose gel electrophoresis results of the right flanking region (1,000 bp) for *kivd* expression of the kanamycin gene (1,000 bp) and the *kivd* gene (1,719 bp). **(C)** PCR confirmation of the expression complex of the *kivd* gene (LF + Km^r + *kivd* + RF). A 1-kb marker was used. *LF*, left flanking region; *RF*, right flanking region; Km^r, kanamycin.

a chromosome-based homologous recombination (**Figure 2C**). Although the former has been applied in many model strains with better outcomes, the R-M system in methanotrophs results in a lower efficiency. Therefore, a modified chromosome-based method was developed to provide a fast and efficient system. As shown in **Figure 3** and **Supplementary Figure 2**, the recombinant strain (*M. buryatense* 5GBlSΔ*fadE*:Km^r:*kivd*) was constructed by replacing the specific site of the *fadE* gene in the genome with the exogenous DNA fragment of *kivd* and Km^r. Furthermore, to verify the validity of the *fadE* gene site as an effective and specific site for heterologous gene expression, the *pos*5 gene, for regulating the reducing power level and promoting product accumulation from *Saccharomyces cerevisiae* coding for NADH kinase along with the Gm^r fragment, was also introduced into the *fadE* site, giving the recombinant strain of *M. buryatense* 5GBlSΔ*fadE*:Gm^r:*pos*5 successfully (**Supplementary Figures 3–5**).

To investigate the expression efficiency of the exogenous gene insertion at the *fadE* site, a plasmid-based recombinant (*M. buryatense* 5GBlS-pAWP89:*kivd*) was constructed for comparison. As shown in **Figure 4**, *M. buryatense* 5GBlSΔ*fadE*:Km^r:*kivd*, with the best situation for growth, displayed the highest OD_{600} of 7.0, followed by OD_{600} = 6.0 for *M. buryatense* 5GBlS (wild type) and OD_{600} = 5.0 for *M. buryatense* 5GBlS-pAWP89:*kivd*. The biosynthesis of isobutyraldehyde was also validated in the recombinants and wild type. As shown in **Table 2**, it is clear that the wild-type strain could not accumulate isobutyraldehyde due to the lack of the *kivd* gene. Because of the successful overexpression of the heterologous *kivd* gene, the accumulation of isobutyraldehyde was obtained in both recombinants with a similar titer around 3.3 mg/L. Overall, the SSCE method with the *fadE* site was developed as a promising and plasmid-free strategy for heterologous gene expression with chromosome integration.

DISCUSSION

To obtain powerful cell factories, faster and more convenient genetic tools are essential. Electroporation-based transformation

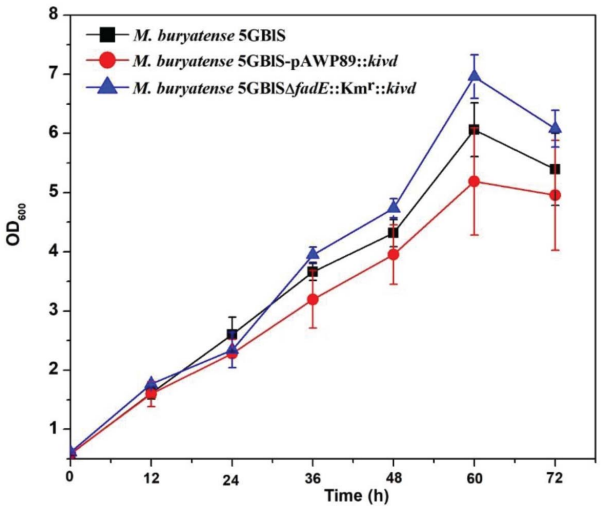

FIGURE 4 | Growth performance of the wild-type (*Methylomicrobium buryatense* 5GB1S) and mutant strains for isobutyraldehyde biosynthesis.

is a simple and efficient method for the genetic engineering modification of microorganisms, so improving the DNA transfer efficiency of electroporation is conducive to the rapid and efficient construction of engineered bacteria, which can be applied in industrial applications of methanotrophs. In *M. buryatense* 5GB1S, C1 substrates are taken up and bioconverted into ketoisovalerate, which is the main precursor for the synthesis of isobutyraldehyde (Matsuda et al., 2013; Miao et al., 2018).

To complete the heterologous gene expression, an efficient electroporation system based on *M. buryatense* 5GB1S was firstly optimized. Key factors including the cell density, methanol concentration, and recovery time were investigated based on previous reports (Puri et al., 2015; Yan et al., 2016; Nguyen et al., 2018; Liu et al., 2021). Therein, the cell density also showed a positive relation with the electroporation efficiency of *M. buryatense* 5GB1S, and this is consistent with previous reports (Holo and Nes, 1989; Shimogawara et al., 1998; Wu and Letchworth, 2004). For example, researchers have explored the influence of the DNA concentration on the transformation efficiency of fibroblasts and found that the transformation efficiency was increased by 17 times with the DNA concentration increasing fourfold (Yekta et al., 2013). Moreover, it was reported that the ability of electroporation to transfer DNA into cells was limited under a fixed cell concentration, and excess DNA remained inefficient (Hattermann and Stacey, 1990; Rittich and Španová, 1996). It is believed that a high substrate concentration will facilitate cell growth and improve efficiency. It has been reported that a high methanol concentration in the electroporation system could easily trigger cell lysis, resulting in low conversion efficiency (Yan et al., 2016). Consequently, similar findings were observed when the methanol concentration was 1.0%, providing a dramatically low efficiency. Furthermore, an appropriate recovery time is beneficial to the improvement of the transformation efficiency, which could severely affect the conversion efficiency due to blocking of the efficient entry of linear DNA into the cell and difficulty in the screening of transformants (Hattermann and Stacey, 1990; Yan et al., 2016). The longer recovery time in this study also showed lower efficiency mainly due to cell lysis (Yan et al., 2016).

The optimized SSCE method developed in this research showed unique advantages in gene deletion and heterologous gene expression in methanotrophs compared with the existing methods. A higher transformation frequency was observed when using PCR-generated fragments to delete the *glgA2* (0.37 kb) and *mmo* (0.83 kb) genes in methanotrophs through electroporation (Yan et al., 2016), which may be due to the shorter length of the selected genes compared with that of *fadE* (2.3 kb). Thus, the frequency of 719.0 ± 22.5 CFU/μg DNA obtained from this *fadE*-based SSCE was still high enough for most genetic manipulations, including gene deletion and heterologous gene expression in *M. buryatense* 5GBlS. Moreover, the antibiotic cassette used in the *fadE*-based SSCE method was less than 1 kb in comparison to the markerless counterselection cassettes *pheS* and *sacB* used in methanotrophs, which can facilitate the overlap step during PCR (Nguyen and Lee, 2020). Finally, the biosynthesis of isobutyraldehyde was conducted by heterologously expressing *kivd* in *M. buryatense* 5GB1S with deletion of the *fadE* gene. Favorably, better growth was achieved with a similar isobutyraldehyde titer from the SSCE method compared with the plasmid-based method because of the metabolic burden of the plasmid. Nevertheless, the yield of isobutyraldehyde on cell density from *M. buryatense* 5GBlSΔ*fadE*:Km^r:*kivd* (0.69 mg/L per OD_{600}) was lower than that of *M. buryatense* 5GBlS-pAWP89:*kivd* (0.89 mg/L per OD_{600}), which may be due to the higher copy number from a plasmid than a single copy of the inserted gene. Thus, optimization of the promoters or the ribosome-binding site (RBS) for this *fadE*-based SSCE method is required in future works in order to deliver a robust strategy for the genetic engineering of methanotrophs.

In this work, an efficient and rapid method was developed to delete the endogenous gene and complete the heterologous gene expression in *M. buryatense* 5GB1S simultaneously. The exogenous gene *kivd* was inserted into the genome of

TABLE 2 | Biosynthesis of isobutyraldehyde in the cultures of wild-type (*Methylomicrobium buryatense* 5GB1S) and mutant strains.

Strains	Titer (mg/L)			
	0 h	**24 h**	**48 h**	**72 h**
M. buryatense 5GBlS	0.00	0.00	0.00	0.00
M. buryatense 5GBlS-pAWP89:*kivd*	0.00	3.08 ± 0.18	3.53 ± 0.04	3.01 ± 0.24
M. buryatense 5GBlSΔ*fadE*:Km^r:*kivd*	0.00	2.94 ± 0.10	3.29 ± 0.07	2.89 ± 0.20

M. buryatense 5GBlS (*fadE*), forming an isobutyraldehyde producer. Moreover, the *fadE* site could be used as an effective and specific site for the exogenous expression, with better growth due to the plasmid-free system. Overall, this study not only provides a bright idea for gene deletion and expression but also enriches the scope of genetic tools for methanotrophs, which promotes the application of methanotrophs in the utilization of C1 substrates.

DATA AVAILABILITY STATEMENT

The original contributions presented in the study are included in the article/**Supplementary Material**, further inquiries can be directed to the corresponding author/s.

AUTHOR CONTRIBUTIONS

QF and LH conceived and designed the work and provided conceptual advice with inputs from all authors. LH planned and performed the experiments and analyzed the data. LH, SG, and QF wrote and revised the manuscript. TZ and JX helped to complete the work. SG and XY provided conceptual advice. All authors contributed to the data analyses and read, revised, and approved the final manuscript.

FUNDING

This work was supported by the National Key R&D Programs of China (2018YFA0901500), the National Natural Science Foundation of China (21878241), and the Key Research and Development Program of Shaanxi Province (2021SF-103).

ACKNOWLEDGMENTS

The authors would like to thank Mary Lidstrom from the University of Washington for providing *M. buryatense* 5GB1S for research purposes and the Instrument Analysis Center of Xi'an Jiaotong University for helping with GC analysis.

SUPPLEMENTARY MATERIAL

The Supplementary Material for this article can be found online at: https://www.frontiersin.org/articles/10.3389/fmicb.2021.717033/full#supplementary-material

REFERENCES

Alexey, G., Laurens, L. M., Puri, A. W., Frances, C., Pienkos, P. T., and Lidstrom, M. E. (2015). Bioreactor performance parameters for an industrially-promising methanotroph *Methylomicrobium buryatense* 5GB1. *Microb. Cell Fact.* 14:182. doi: 10.1186/s12934-015-0372-8

Atsumi, S., Wu, T.-Y., Eckl, E.-M., Hawkins, S. D., Buelter, T., and Liao, J. C. (2010). Engineering the isobutanol biosynthetic pathway in *Escherichia coli* by comparison of three aldehyde reductase/alcohol dehydrogenase genes. *Appl. Microbiol. Biotechnol.* 85, 651–657. doi: 10.1007/s00253-009-2085-6

Bjorck, C. E., Dobson, P. D., and Pandhal, J. (2018). Biotechnological conversion of methane to methanol: evaluation of progress and potential. *AIMS Bioeng.* 5, 1–38. doi: 10.3934/bioeng.2018.1.1

Conrado, R. J., and Gonzalez, R. (2014). Chemistry. Envisioning the bioconversion of methane to liquid fuels. *Science* 343, 621–623. doi: 10.1126/science.1246929

Demidenko, A., Akberdin, I. R., Allemann, M., Allen, E. E., and Kalyuzhnaya, M. G. (2016). Fatty acid biosynthesis pathways in *Methylomicrobium buryatense* 5G(B1). *Front. Microbiol.* 7:2167. doi: 10.3389/fmicb.2016.02167

Dower, W. J., Miller, J. F., and Rags Da Le, C. W. (1988). High efficiency transformation of *E. coli* by high voltage electroporation. *Nucleic Acids Res.* 16, 6127–6145. doi: 10.1093/nar/16.13.6127

Fei, Q., Guarnieri, M. T., Tao, L., Laurens, L. M. L., Dowe, N., and Pienkos, P. T. (2014). Bioconversion of natural gas to liquid fuel: opportunities and challenges. *Biotechnol. Adv.* 32, 596–614. doi: 10.1016/j.biotechadv.2014.03.011

Fei, Q., Puri, A. W., Smith, H., Dowe, N., and Pienkos, P. T. (2018). Enhanced biological fixation of methane for microbial lipid production by recombinant *Methylomicrobium buryatense*. *Biotechnol. Biofuels* 11:129. doi: 10.1186/s13068-018-1128-6

Fu, Y. F., Li, Y., and Lidstrom, M. E. (2017). The oxidative TCA cycle operates during methanotrophic growth of the type I methanotroph *Methylomicrobium buryatense* 5GB1. *Metab. Eng.* 42, 43–51. doi: 10.1016/j.ymben.2017.05.003

Hattermann, D. R., and Stacey, G. (1990). Efficient DNA transformation of *Bradyrhizobium japonicum* by electroporation. *Appl. Environ. Microbiol.* 56, 833–836. doi: 10.1128/Aem.56.4.833-836.1990

Holo, H., and Nes, I. F. (1989). High-frequency transformation by electroporation of *Lactococcus lactis* subsp. Cremoris grown with glycine in osmotically stabilized media. *Appl. Environ. Microbiol.* 55, 3119–3123. doi: 10.1128/aem.55.12.3119-3123.1989

Hu, B., and Lidstrom, M. E. (2014). Metabolic engineering of *Methylobacterium extorquens* AM1 for 1-butanol production. *Biotechnol. Biofuels* 7:156. doi: 10.1186/s13068-014-0156-0

Hu, L. Z., Yang, Y. F., Yan, X., Zhang, T. Q., Xiang, J., Gao, Z. X., et al. (2020). Molecular mechanism associated with the impact of methane/oxygen gas supply ratios on cell growth of *Methylomicrobium buryatense* 5GB1 through RNA-Seq. *Front. Bioeng. Biotechnol.* 8:263. doi: 10.3389/fbioe.2020.00263

Hur, D. H., Na, J. G., and Lee, E. Y. (2017). Highly efficient bioconversion of methane to methanol using a novel type I *Methylomonassp*. DH-1 newly isolated from brewery waste sludge. *J. Chem. Technol. Biotechnol.* 92, 311–318. doi: 10.1002/jctb.5007

Itoh, N., Kouzai, T., and Koide, Y. (1994). Efficient transformation of *pseudomonas* strains with pNI vectors by electroporation. *Biosci. Biotechnol. Biochem.* 58, 1306–1308. doi: 10.1271/bbb.58.1306

Li, S. Y., Li, Z. T., Shu, F. J., Xiong, H. R., Phillips, A. C., and Dynan, W. S. (2014). Double-strand break repair deficiency in NONO knockout murine embryonic fibroblasts and compensation by spontaneous upregulation of the PSPC1 paralog. *Nucleic Acids Res.* 42, 9771–9780. doi: 10.1093/nar/gku650

Liu, Y. C., Zhang, H. L., He, X. R., and Liu, J. (2021). Genetically engineered methanotroph as a platform for bioaugmentation of chemical pesticide contaminated soil. *ACS Synth. Biol.* 10, 487–494. doi: 10.1021/acssynbio.0c00532

Matsuda, F., Ishii, J., Kondo, T., Ida, K., Tezuka, H., and Kondo, A. (2013). Increased isobutanol production in *Saccharomyces cerevisiae* by eliminating competing pathways and resolving cofactor imbalance. *Microb. Cell Fact.* 12:119. doi: 10.1186/1475-2859-12-119

Mcintyre, D. A., and Harlander, S. K. (1989). Genetic transformation of intact *Lactococcus lactis* subsp. Lactis by high-voltage electroporation. *Appl. Environ. Microbiol.* 55, 604–610. doi: 10.1128/aem.55.3.604-610.1989

Miao, R., Xie, H., Ho, F. M., and Lindblad, P. (2018). Protein engineering of α-ketoisovalerate decarboxylase for improved isobutanol production in *Synechocystis* PCC 6803. *Metab. Eng.* 47, 42–48. doi: 10.1016/j.ymben.2018.02.014

Min, J. P., Park, M. S., and Ji, G. E. (2018). Improvement of electroporation-mediated transformation efficiency for a *Bifidobacterium* strain to a reproducibly high level. *J. Microbiol. Methods* 159, 112–119. doi: 10.1016/j.mimet.2018.11.019

Morales-Ruiz, E., López-Ceballos, A., and Maldonado-Mendoza, I. E. (2019). Transformation of the rhizospheric *Bacillus cereus sensu* lato B25 strain using a room-temperature electrocompetent cells preparation protocol. *Plasmid* 105:102435. doi: 10.1016/j.plasmid.2019.102435

Nguyen, A. D., and Lee, E. Y. (2020). Engineered methanotrophy: a sustainable solution for methane-based industrial biomanufacturing. *Trends Biotechnol.* 39, 381–396. doi: 10.1016/j.tibtech.2020.07.007

Nguyen, A. D., Hwang, I. Y., Lee, O. K., Kim, D., Kalyuzhnaya, M. G., Mariyana, R., et al. (2018). Systematic metabolic engineering of *Methylomicrobium alcaliphilum* 20Z for 2,3-butanediol production from methane. *Metab. Eng.* 47, 323–333. doi: 10.1016/j.ymben.2018.04.010

Pariatamby, A., Weng, Y. C., Shrizal, R., Thamlarson, N., Lim, B. T., and Barasarathi, J. (2015). Enhancement of landfill methane oxidation using different types of organic wastes. *Environ. Earth Sci.* 73, 2489–2496. doi: 10.1007/s12665-014-3600-3

Puri, A. W., Owen, S., Chu, F., Chavkin, T., Beck, D. A., Kalyuzhnaya, M. G., et al. (2015). Genetic tools for the industrially promising methanotroph *Methylomicrobium buryatense*. *Appl. Environ. Microbiol.* 81, 1775–1781. doi: 10.1128/AEM.03795-14

Rittich, B., and Španová, A. (1996). Electrotransformation of bacteria by plasmid DNAs: statistical evaluation of a model quantitatively describing the relationship between the number of electrotransformants and DNA concentration. *Bioelectrochem. Bioenerg.* 40, 233–238. doi: 10.1016/0302-4598(96)01915-0

Shimogawara, K., Fujiwara, S., Grossman, A. R., and Usuda, H. (1998). High-efficiency transformation of *Chlamydomonas reinhardtii* by electroporation. *Genetics* 148, 1821–1828.

Steele, C., Zhang, S., and Shillitoe, E. J. (1994). Effect of different antibiotics on efficiency of transformation of bacteria by electroporation. *Biotechniques* 17, 360–365.

Su, Z. L., Ge, X. M., Zhang, W. X., Wang, L. L., Yu, Z. T., and Li, Y. B. (2017). Methanol production from biogas with a thermotolerant methanotrophic consortium isolated from an anaerobic digestion system. *Energy Fuels* 31, 2970–2975. doi: 10.1021/acs.energyfuels.6b03471

Wang, J., Jian, X., Xing, X. H., Zhang, C., and Fei, Q. (2020). Empowering a methanol-dependent *Escherichia coli* via adaptive evolution using a high-throughput microbial microdroplet culture system. *Front. Bioeng. Biotechnol.* 8:570. doi: 10.3389/fbioe.2020.00570

Wu, S. X., and Letchworth, G. J. (2004). High efficiency transformation by electroporation of *Pichia pastoris* pretreated with lithium acetate and dithiothreitol. *Biotechniques* 36, 152–154. doi: 10.2144/04361DD02

Yan, X., Chu, F., Puri, A. W., Fu, Y., and Lidstrom, M. E. (2016). Electroporation-based genetic manipulation in type I methanotrophs. *Appl. Environ. Microbiol.* 82, 2062–2069. doi: 10.1128/AEM.03724-15

Yekta, A. A., Dalman, A., Sanati, M. H., Fatemi, N., and Gourabi, H. (2013). Optimization of the electroporation conditions for transfection of human factor IX into the goat fetal fibroblasts. *Cell J.* 14, 270–275.

Conflict of Interest: The authors declare that the research was conducted in the absence of any commercial or financial relationships that could be construed as a potential conflict of interest.

Publisher's Note: All claims expressed in this article are solely those of the authors and do not necessarily represent those of their affiliated organizations, or those of the publisher, the editors and the reviewers. Any product that may be evaluated in this article, or claim that may be made by its manufacturer, is not guaranteed or endorsed by the publisher.

Advantages of publishing in Frontiers

OPEN ACCESS
Articles are free to read for greatest visibility and readership

FAST PUBLICATION
Around 90 days from submission to decision

HIGH QUALITY PEER-REVIEW
Rigorous, collaborative, and constructive peer-review

TRANSPARENT PEER-REVIEW
Editors and reviewers acknowledged by name on published articles

Frontiers
Avenue du Tribunal-Fédéral 34
1005 Lausanne | Switzerland

Visit us: www.frontiersin.org
Contact us: frontiersin.org/about/contact

REPRODUCIBILITY OF RESEARCH
Support open data and methods to enhance research reproducibility

DIGITAL PUBLISHING
Articles designed for optimal readership across devices

FOLLOW US
@frontiersin

IMPACT METRICS
Advanced article metrics track visibility across digital media

EXTENSIVE PROMOTION
Marketing and promotion of impactful research

LOOP RESEARCH NETWORK
Our network increases your article's readership